IMPERIAL

The role of northern high latitude peat fires in shaping future atmospheric composition, the carbon cycle and climate

---

Katie Rose Blackford

August 2024

Imperial College London

Department of Physics

Submitted in part fulfilment of the requirements for the degree of Doctor of Philosophy (PhD) of Imperial College London

Statement of Originality

All work presented in this thesis is original and my own, with the exception of other work that has been appropriately referenced in text, with the original sources available in the bibliography. Part of this work has been previously published in the following article:

Blackford, K. R., Kasoar, M., Burton, C., Burke, E., Prentice, I. C., and Voulgarakis, A.: INFERNO-peat v1.0.0: a representation of northern high-latitude peat fires in the JULES-INFERNO global fire model, Geosci. Model Dev., 17, 3063–3079, https://doi.org/10.5194/gmd-17-3063-2024, 2024.

Copyright Declaration

The copyright of this thesis rests with the author. Unless otherwise indicated, its contents are licensed under a Creative Commons Attribution-Non Commercial 4.0 International Licence (CC BY-NC).

Under this licence, you may copy and redistribute the material in any medium or format. You may also create and distribute modified versions of the work. This is on the condition that: you credit the author and do not use it, or any derivative works, for a commercial purpose.

When reusing or sharing this work, ensure you make the licence terms clear to others by naming the licence and linking to the licence text. Where a work has been adapted, you should indicate that the work has been changed and describe those changes.

Please seek permission from the copyright holder for uses of this work that are not included in this licence or permitted under UK Copyright Law.

Acknowledgements

Firstly, and most importantly, I would like to thank my primary supervisor, Apostolos Voulgarakis. His insights, knowledge, and guidance throughout my PhD have been invaluable to this work and to myself. I would also like to thank my team of co-supervisors, Colin Prentice, Chantelle Burton and Matt Kasoar. They have been instrumental in this work, providing their expertise and offering guidance and advice. It has been a great privilege to work alongside them, and I hope we can continue to collaborate in the future.

I am thankful for not only the financial support provided to me through the Leverhulme Centre for Wildfires, Environment and Society, but also for the opportunities they have provided to me. A special thanks goes to Adriana Ford, for her endless guidance and friendship, and for helping to encourage my love of Arctic research. I would also like to thank all the past and present members of the centre for the numerous stimulating discussions and their friendship.

I am also grateful for the financial support provided to me by the Met Office, and also to all my colleagues at the Met Office who have provided advice, guidance, and JULES support during this work. In particular, I would like to acknowledge the contributions of Eleanor Burke towards this thesis. Her expertise on peatland modelling has been invaluable, and I am grateful for the JULES runs she provided me for use within this thesis.

I would also like to thank my partner, Alex, for his help, support and love over the last four years. For putting up with my endless talk about fires, discussing peat whenever we are hiking in the UK moorlands, and always providing IT support. This work would not have been possible without his support and encouragement.

Finally, I would like to acknowledge my parents, who throughout my life have encouraged my curiosity and taught me to follow my passions. My parents harnessed my love for nature and the environment, from weekends spent hiking and running across the UK, to all the places I have had the privilege of travelling too. I attribute this to my desire to understand and protect the world around us, which I am certain will continue for many years to come.

Abstract

The northern high latitude peatlands represent a crucial store of carbon that are being increasingly threatened by climate change and fires. Peat fires represent a major fire phenomenon, which burn prominently by smouldering combustion and emit vast amounts of long-term stored carbon to the atmosphere. Peat fires also emit a suite of aerosols, which degrade air quality and impact upon human health. However, despite the importance of peat fires to atmospheric composition, the carbon cycle, climate and air quality, they are not currently represented in most Earth system models. Additionally, Earth observation products tend to omit peat fires, and consequently little is known about the large-scale impacts of peat fires on atmospheric composition and air quality. Consequently, within this thesis I developed INFERNO-peat, a novel parameterisation of northern high latitude peat fires in the JULES-INFERNO fire model based on the latest laboratory and field studies on peat fires and their dynamics. Here I show that by explicitly incorporating peat fires in a fire model, the spatial representation of burnt area and interannual variability in burnt area and carbon emissions are greatly improved. Additionally, I show that peat fires have major impacts on atmospheric composition and air quality in the northern high latitudes, especially in terms of NO_2, CO, and $PM_{2.5}$ emissions. Finally, I show how under future climate change scenarios, peat fire burnt areas and carbon emissions are expected to increase, particularly under high emissions scenarios, thereby exacerbating the impacts peat fires have on atmospheric composition, climate, the carbon cycle and air quality. Overall, in this thesis I demonstrate the critical need for representing peat fires in our fire models, and the necessity for obtaining accurate peat fire observations in order to better quantify their impacts on the climate system.

Table of Contents

Statement of Originality **2**
Copyright Declaration **3**
Acknowledgements **4**
Abstract **5**
Table of Contents **6**
List of Figures **10**
List of Tables **18**
List of Acronyms **24**
Chapter 1: Introduction **28**
1. Significance of peatlands 28
1.1. High latitude peatlands 29
1.2. Changes in high latitude peatlands due to climate change and humans 30
2. Wildfires in the northern high latitudes 31
3. Peat fires and smouldering combustion 33
3.1. Effects of soil properties on the ignition and spread of peat fires 34
3.2. Depth of burn of peat fires 36
3.3. Controls on carbon and gaseous emissions from peat fires 37
4. Peat fires in the northern high latitudes 38
4.1. Impacts of peat fires on the carbon cycle, climate and air quality 40
4.2. Environmental impacts of peat fires 42
5. Tropical peat fires 44
6. Impacts of climate change on high latitude peat fires 46
7. Thesis outline 47
Chapter 2: Methodologies **50**
1. Fire modelling 50
1.1. Peat fire modelling 52
2. The INFERNO fire model 53
2.1. Current performance of INFERNO 55
3. INFERNO-peat 56
3.1. Peat fire ignitions (I_{peat}) 57
3.2. Peat probability of ignition ($ProbI_{peat}$) 57
3.3. Peat burnt area (BA_{peat}) 58
3.4. Depth of burn (BDpeat) 58
3.5. Carbon emissions 59
4. Experimental set up for simulating present day peat fires using INFERNO-peat 60
4.1. Model evaluation protocol 61

5. Future peat fire simulations 62
5.1. Future climate change scenarios 62
5.1.1. The Inter-Sectoral Impact Model Intercomparison Project (ISIMIP) 64
5.2. Modelling high latitude peat fires over then next century using INFERNO-peat 65
6. Observing fires from space 67
6.1. Remote sensing of peat fires 71
7. Remote sensing of atmospheric composition and air quality 74
8. Assessing the impact of fires on atmospheric composition and air quality in the high latitudes 78
8.1. Fire data 80
8.2. Atmospheric data 81
8.2.1. TROPOMI 81
8.2.2. CAMS reanalysis 83
8.2.3. Data processing 85
8.3. Data analysis 85
Chapter 3: Representing northern high latitude peat fires in the JULES-INFERNO global fire model 87
Abstract 87
1. Introduction 87
2. Methods 90
2.1. Model evaluation 94
3. Results 97
3.1. Burnt area 97
3.1.1. Subregion analysis 100
3.2. Depth of burn 108
3.3. Carbon emissions 110
3.3.1. Subregion analysis 112
4. Discussion 119
Chapter 4: Trends and impacts of fires in the northern high latitudes using satellite data 128
Abstract 128
1. Introduction 128
2. Methods 130
2.1. Data analysis 132
2.1.1. Correlation analysis 132
2.1.2. Burnt area size category analysis 133
2.1.3. Vegetation burning analysis 133
2.1.4. Comparisons to INFERNO-peat 133
3. Results 134

3.1. Eastern Siberia 134
3.1.1. Trends in wildfires and peat fires 134
3.1.2. Drivers of large fire years 136
3.1.3. Impacts of fires on atmospheric composition 137
3.1.4. Impacts of fires on air quality 142
3.2. Northwest Siberia 144
3.2.1. Trends in wildfires and peat fires 144
3.2.2. Drivers of large fire years 147
3.2.3. Impacts of fires on atmospheric composition 148
3.2.4. Impacts of fires on $PM_{2.5}$ 153
3.3. Alaska 155
3.3.1. Trends in wildfires and peat fires 155
3.3.2. Drivers of large fire years 157
3.3.3. Impacts of fires on atmospheric composition 158
3.3.4. Impacts of fires on $PM_{2.5}$ 164
3.4. Western Canada 166
3.4.1. Trends in wildfires and peat fires 166
3.4.2. Drivers of large fire years 168
3.4.3. Impacts of fires on atmospheric composition 169
3.4.4. Impacts of fires on $PM_{2.5}$ 174
3.5. Distinguishing between smouldering and flaming combustion in atmospheric composition data 176
3.6. Impact of the amount of peat fire BA on identifying atmospheric composition signals 177
3.7. Disentangling the effects of peat fires and vegetation fires 180
3.8. Comparisons of INFERNO-peat to GFED5 estimated peat fires and their impacts on atmospheric composition 184
4. Discussion 187
4.1. Trends in total and peat BA in the northern high latitudes 187
4.2. The impacts of fires on atmospheric composition in the high latitudes 191
4.3. The impacts of fires on air quality across the northern high latitudes 197
4.4. Conclusion 198
Chapter 5: Modelling future changes to peat fires using INFERNO-peat under differing climate change scenarios 200
Abstract 200
1. Introduction 200
2. Methods 204
3. Results 206
3.1. Peat burnt area 209

3.1.1. Peat fire ignitions 212
3.1.1.1. PFT fractions 214
3.1.1.2. PFT flammability 219
3.1.1.3. Temperature and precipitation 222
3.1.2. Peat probability of ignition 223
3.1.2.1. Soil moisture 225
3.1.2.2. Drivers of changes in soil moisture 227
3.2. Depth of burn 235
3.3. Carbon emissions 238
4. Discussion 241
4.1. Conclusions 254
Chapter 6: Discussion and conclusions 256
1. Summary of key findings 256
1.1. The importance of parameterising peat fires in global fire models 257
1.2. The influence of peat fires on atmospheric composition and air quality in the high latitudes 258
1.3. Future changes to peat fires with climate change 259
1.4. Challenges in observing peat fires 261
2. Future work 264
2.1. Improving observations of northern high latitude peat fires 264
2.2. Future INFERNO-peat development 266
2.2.1. Expansion of the INFERNO-peat scheme to the tropics 267
2.2.2. Representing gaseous and aerosol emissions from peat fires in INFERNO-peat. 268
2.2.3. Coupling INFERNO-peat to peatland models 268
2.2.4. Coupling of INFERNO-peat to the UKESM 270
3. Conclusions and wider implications 270
Bibliography 274
Appendices 331
1. Supplementary information for Chapter 3 331
2. Supplementary information for Chapter 4 334

List of Figures

Figure 1: The global distribution of peatlands, obtained from the Global Peatlands Initiative and the United Nations Environment Programme (2022a). 29

Figure 2: An example of the relationship between the probability of ignition and moisture content from Frandsen (1997). 34

Figure 3: The relationship between horizontal (or lateral) spread rate and moisture content from Christensen et al. (2020). Note, this figure additionally shows the impact of different wind directions on the horizontal spread rate. 35

Figure 4: Schematic demonstrating the key drivers of peat fires (blue), and the various atmospheric (orange), human (purple) and environmental (green) impacts of peat fires. Feedback effects are denoted by the thick dashed lines. The small, dashed line indicates the potential reaccumulation of carbon within the system. 39

Figure 5: Schematic of the INFERNO fire model from Mangeon et al. (2016). 53

Figure 6: Schematic summarising the new parameterisations introduced as part of INFERNO-peat, the input variables, and their sources. 56

Figure 7: Relationship between soil moisture and a) peat probability of ignition and b) critical temperature. 59

Figure 8: Maps of a) peatland fraction (%) and b) peatland soil organic carbon (kg/m^2) for north of 23° latitude from the Northern Peatland Dataset (Hugelius et al., 2020). 61

Figure 9: Comparisons of the 2010-2014 soil moisture content modelled by JULES in the high latitudes between a) mineral soils, b) organic soils and c) the mineral soil moisture scaled up based on the difference between mineral and organic soil moisture. 66

Figure 10: Annual total global burnt area over 1997 to 2020 from four commonly used EO fire products: GFED4s, GFED5, fireCCILT11 and fireCCI51. Dashed lines indicate the overall time series trends for each dataset. 69

Figure 11: Change in grid cell burnt area fraction from the 2001-2005 average, and the 2010-2014 average for a) GFED4s, b) GFED5, c) FireCCILT11 and d) FireCCI51. The time periods were chosen as they are the earliest and latest 5-year periods obtainable concurrently from all datasets. 70

Figure 12: Diagnostic plots from INFERNO-peat using mineral soil moisture, showing the relationship between peat fraction and a) probability of ignition, b) probability of ignition and peat burnt area, and c) organic moisture content. 92

Figure 13: Diagnostic plots from INFERNO-peat using organic soil moisture, showing the relationship between peat fraction and a) probability of ignition, b) probability of ignition and peat burnt area, and c) organic moisture content. 93

Figure 14: Sensitivity analysis of RMSE across maximum depth of burn and combustion completeness values. 94

Figure 15: Histogram of the average grid cell depth of burn between 2010 and 2014 for the INFERNO-peat simulation using BD_{max} = 0.4 and CC = 0.8. 94

Figure 16: The location of the seven subregions used to evaluate the performance of INFERNO-peat in the northern high latitudes. 96

Figure 17: The 2010 to 2014 average annual burnt area fraction for INFERNO (a), INFERNO-peat driven by LIS-OTD climatology (b), INFERNO-peat driven by WGLC timeseries (c), GFED4s (d), GFED5 (e) and fireCCILT11 (f). 98

Figure 18: The annual total burnt area across the high latitudes (<50o N) from 1997 to 2014 compared between the models (indicated by solid lines) and observations (indicated by dashed lines)..... 100

Figure 19: The average annual burnt area (2010-2014), from INFERNO, and INFERNO-peat driven by the LIS-OTD and WGLC lightning data, compared to the observations, in each subregion..... 102

Figure 20: Trends in BA from 2001 to 2014 in INFERNO and INFERNO-peat compared with the observational datasets in each of the subregions. Note that the WGLC INFERNO-peat runs are only for 2010 to 2014. Dashed lines indicate observations and solid lines represent models. 106

Figure 21: INFERNO-peat grid cell average depth of burn (m) between 2010 and 2014 across the northern high latitudes. 108

Figure 22: The average depth of burn modelled by INFERNO-peat in each of the 7 subregions. 109

Figure 23: Annual average peat fire depth of burn between 1997 and 2014 in the northern high latitudes. 109

Figure 24: The annual total carbon emissions from fires across the high latitudes (<50° N) from 1997 to 2014 compared between the models (indicated by solid lines) and observations (indicated by dashed lines)..... 110

Figure 25: The annual total carbon emissions from fires across the high latitudes (<50° N) from 1997 to 2014 compared between the GFED 500m products above and belowground burning, and INFERNO-peat emissions split to peat fires only and INFERNO only. 112

Figure 26: The average annual carbon emissions (2010-2014), from INFERNO, and INFERNO-peat driven by the LIS-OTD and WGLC lightning data, compared to the observations, in each subregion. 113

Figure 27: The average annual carbon emissions (2010-2014), from INFERNO, and peat fires only from INFERNO-peat driven by the LIS-OTD and WGLC lightning data, compared to the aboveground and belowground burning from the GFED 500m product, in each subregion. 114

Figure 28: 2010-2014 average dominant land fraction type in each grid cell modelled by the TRIFFID dynamic vegetation model in JULES..... 115

Figure 29: Carbon emissions timeseries graphs broken down by subregion, from 2003 to 2014. Note that the WGLC INFERNO-peat runs are only for 2010 to 2014. Dashed lines indicate observations and solid lines represent models. Comparisons against the GFED500m above and belowground burning can be found in Figure S1..... 117

Figure 30 Locations of the four regions of Alaska (-170,55, -140,75), western Canada (-140,50, -110,75), northwest Siberia (60,50, 90,80) and eastern Siberia (130,50, 180,80) for studying the affects of fires on atmospheric composition and air quality. 131

Figure 31: Fire trends over 2003-2022 for eastern Siberia. BA data covers the period from 2003 to 2020, and the FRP data continues up to 2022. The trends shown are a) average annual total BA and FRP and b) the seasonality in total BA and FRP (averaged over their respective time periods). Panel (c) shows the yearly timeseries trends in estimated peat BA and FRP and d) shows the seasonality in estimated peat BA and estimated peat FRP. Panel (e) shows the estimated peat BA as a percentage of total BA and the estimated peat FRP as a percentage of total FRP, and panel (f) shows the seasonality in estimated peat BA and FRP percentage. 135

Figure 32: Scatterplot of seasonal temperature anomalies vs seasonal BA anomalies for a) total BA and b) estimated peat BA, in E Siberia. 137

Figure 33: Time series plots for NO_2 (a) and its seasonality (b), CO (c) and its seasonality (d), and the ratio of NO_2/CO (e) and its seasonality (f), for the period 2003-2022 for CAMS reanalysis data (red) and 2018-2021 for the TROPOMI data (blue), in eastern Siberia. 139

Figure 34: Timeseries plot for $PM_{2.5}$ from 2003-2022 in eastern Siberia from the CAMS reanalysis data (a), and the 2003-2022 averaged eastern Siberia seasonality in $PM_{2.5}$ (b) 143

Figure 35: Relationships between monthly total CAMS $PM_{2.5}$ and monthly total BA (a), estimated peat BA (b), estimated peat fire percentage of BA (c), total mean FRP (d), estimated peat fire mean FRP (e) and estimated peat fire percentage of FRP (f) in eastern Siberia. 144

Figure 36: Fire trends over 2003-2022 for northwest Siberia. BA data covers the period from 2003 to 2020, and the FRP data continues up to 2022. The trends shown are a) average annual total BA and FRP and b) the seasonality in total BA and FRP (averaged over their respective time periods). Panel c) shows the yearly timeseries trends in estimated peat BA and FRP and panel d) shows the seasonality in estimated peat BA and estimated peat FRP. Panel e) shows the estimated peat BA as a percentage of total BA and the estimated peat FRP as a percentage of total FRP, and panel f) shows the seasonality in peat estimated BA and FRP percentage. 146

Figure 37: Correlations between seasonal BA anomalies and seasonal temperature anomalies for a) total BA and b) estimated peat BA in northwest Siberia..... 148

Figure 38: Time series plots for NO_2 (a) and its seasonality (b), CO (c) and its seasonality (d), and the ratio of NO_2/CO (e) and its seasonality (f), over 2003 to 2022 for CAMS reanalysis data (red) and 2018 to 2021 for the TROPOMI data (blue) in northwest Siberia. 150

Figure 39: Timeseries plot for $PM_{2.5}$ from 2003-2022 in eastern Siberia from the CAMS reanalysis data (a), and the 2003-2022 averaged northwest Siberia seasonality in $PM_{2.5}$ (b)..... 154

Figure 40: Relationships between monthly total CAMS $PM_{2.5}$ and monthly total BA (a), estimated peat BA (b), estimated peat fire percentage of BA (c), total mean FRP (d), estimated peat fire mean FRP (e) and estimated peat fire percentage of FRP (f) in northwest Siberia. 154

Figure 41: Fire trends over 2003-2022 for Alaska. BA data covers the period from 2003 to 2020, and the FRP data continues up to 2022. The trends shown are a) average annual total BA and FRP and b) the seasonality in total BA and FRP (averaged over their respective time periods). Panel c) shows the yearly timeseries trends in estimated peat BA and FRP and panel d) shows the seasonality in estimated peat BA and estimated peat FRP. Panel e) shows the estimated peat BA as a percentage of total BA and the estimated peat FRP as a percentage of total FRP, and panel f) shows the seasonality in peat estimated BA and FRP percentage. 157

Figure 42: Correlations between seasonal BA anomalies and seasonal temperature anomalies for a) total BA and b) estimated peat BA in Alaska. 158

Figure 43: Time series plots for NO_2 (a) and its seasonality (b), CO (c) and its seasonality (d), and the ratio of NO_2/CO (e) and its seasonality (f), over 2003 to 2022 for CAMS reanalysis data (red) and 2018 to 2021 for the TROPOMI data (blue) in northwest Siberia. 160

Figure 44: Timeseries plot for $PM_{2.5}$ from 2003-2022 in Alaska from the CAMS reanalysis data (a), and the 2003-2022 averaged Alaska seasonality in $PM_{2.5}$ (b) 165

Figure 45: Relationships between monthly total CAMS $PM_{2.5}$ and monthly total BA (a), estimated peat BA (b), estimated peat fire percentage of BA (c), total mean FRP (d), estimated peat fire mean FRP (e) and estimated peat fire percentage of FRP (f) in Alaska. 166

Figure 46: Fire trends over 2003-2022 for western Canada. BA data covers the period from 2003 to 2020, and the FRP data continues up to 2022. The trends shown are a) average annual total BA and FRP and b) the seasonality in total BA and FRP (averaged over their respective time periods). Panel c) shows the yearly timeseries trends in estimated peat BA and FRP and panel d) shows the seasonality in estimated peat BA and estimated peat FRP. Panel e) shows the estimated peat BA as a percentage of total BA and the estimated peat FRP as a percentage of total FRP, and panel f) shows the seasonality in peat estimated BA and FRP percentage. 167

Figure 47: Correlations between seasonal BA anomalies and seasonal temperature anomalies for a) total BA and b) estimated peat BA in western Canada. 169

Figure 48: Time series plots for NO_2 (a) and its seasonality (b), CO (c) and its seasonality (d), and the ratio of NO_2/CO (e) and its seasonality (f), over 2003 to 2022 for CAMS reanalysis data (red) and 2018 to 2021 for the TROPOMI data (blue) in western Canada. 171

Figure 49: Timeseries plot for $PM_{2.5}$ from 2003-2022 in western Canada from the CAMS reanalysis data (a), and the 2003-2022 averaged western Canada seasonality in $PM_{2.5}$ (b). 175

Figure 50: Relationships between monthly total CAMS $PM_{2.5}$ and monthly total BA (a), estimated peat BA (b), estimated peat fire percentage of BA (c), total mean FRP (d), estimated peat fire mean FRP (e) and estimated peat fire percentage of FRP (f) in western Canada. 176

Figure 51: Correlations between peat BA and CAMS NO_2 (a), CO (b) and NO_2:CO (c), for all subregions, grouped by the total monthly BA amount categories. No peat burning contains 325 datapoints, small contains 217, medium 280 and large 42 179

Figure 52: Annual peat burnt area estimated from GFED5 (red) and modelled by INFERNO-peat (blue) for eastern Siberia (a), northwest Siberia (b), Alaska (c) and western Canada (d). Dashed lines show the multiannual mean. 186

Figure 53: The location of the four subregions used to identify differences in changes in burnt area: northern Canada ((140°W, 51°N), (88°W, 73°N)), Fennoscandia ((4°E, 54°N), (42°E, 73°N)), northwest Siberia ((55°E, 51°N), (95°E, 80°N)) and eastern Siberia ((105°E, 51°N), (180°E, 78°N)). 205

Figure 54: Timeseries plots of a) average annual temperatures and b) average annual daily precipitation for the northern high latitudes (>50° N) under SSP126, SSP370 and SSP585..... 207

Figure 55: Changes in temperature from the 2015-2025 annual average to the 2090-2100 annual average for the northern high latitudes under a) SSP126, b) SSP370 and c) SSP585. 208

Figure 56: Changes in precipitation from the 2015-2025 annual average to the 2090-2100 annual average for the northern high latitudes under a) SSP126, b) SSP370 and c) SSP585. 208

Figure 57: Change in annual peat burnt area fraction from the 2015-2025 average to the 2090-2100 average across the northern high latitudes in a) SSP126, b) SSP370 and c) SSP585. 209

Figure 58: Annual peat burnt area (M km^2) above 50°N from 2015 to 2100 for each of the SSPs. The dashed lines indicate the quadratic trendline for the respective SSP..... 210

Figure 59: Change in peat burnt area from the 2015-2025 annual average to the 2090-2100 annual average the three SSP scenarios for four different subregions of the northern high latitudes. Panel a) shows the absolute change in peat BA in M km^2, and b) shows the percentage change in peat BA. . 212

Figure 60: Annual peat fire ignitions in the northern high latitudes from 2015 to 2100 under the three different SSPs..... 213

Figure 61: Change in annual total peat fire ignitions between the 2015-2025 average and the 2090-2100 average in SSP126 (a), SSP370 (b) and SSP585 (c). 214

Figure 62: Timeseries graph of the annual average total fraction of grid cells that are covered by vegetative land surface types from 2015 to 2100 under SSP126, SSP370 and SSP585. 215

Figure 63: Change in grid cell PFT fractional coverage across the high latitudes between the 2015-2025 average and the 2090-2100 average. 215

Figure 64: The dominant land cover type in each grid cell in a) 2015 and b) 2100 under SSP585. ... 216

Figure 65: Change in land cover type grid cell fraction from the 2015-2025 average compared to the 2090-2100 average over the high latitudes under the three SSP scenarios. Plots a-c show the C3 grass fraction change, d-f the Needleleaf tree evergreen fraction change, g-i the needleleaf tree deciduous fraction change and j-l show the bare soil fraction change. 217

Figure 66: Temporal trends in the annual fractional coverage of C3 grass, needleleaf tree evergreen, needleleaf tree deciduous and bare soil land cover types under SSP126 (a-c), SSP370 (d-f) and SSP585 (g-i), for 50-60° N (a, d, g), 60-70° N (b,e,h), and > 70° N (c, f, i)..... 218

Figure 67: Total annual number of peat fire ignitions plotted against the annual PFT fraction coverage under a) SSP126 ($r=0.741$, $p<0.001$), b) SSP370 ($r=0.952$, $p<0.001$) and c) SSP585 ($r=0.973$, $p<0.001$). 219

Figure 68: Timeseries graph of the annual average total PFT flammability from 2015 to 2100 under SSP126, SSP370 and SSP585. 220

Figure 69: Change in grid cell total PFT flammability across the high latitudes between the 2015-2025 average and the 2090-2100 average. 220

Figure 70: Changes in the flammability of C3 grasses from the 2015-2025 average to the 2090-2100 average under a) SSP126, b) SSP370 and c) SSP585. Additionally, plots d-f show the changes in needleleaf evergreen tree flammability from the 2015-2025 average to the 2090-2100 average under d) SSP126, e) SSP370 and f) SSP585. 221

Figure 71: Total annual number of peat fire ignitions plotted against the annual PFT flammability under a) SSP126 ($r=0.930$, $p<0.001$), b) SSP370 ($r=0.991$, $p<0.001$) and c) SSP585 ($r=0.995$, $p<0.001$). 222

Figure 72: Annual mean peat probability of ignition in the northern high latitudes from 2015 to 2100 under the three different SSP scenarios. 224

Figure 73: Difference in mean annual peat probability of ignition from the 2015-2025 average to the 2090-2100 average across the northern high latitudes in a) SSP126, b) SSP370 and c) SSP585. 225

Figure 74: Mean annual soil moisture percentage in the northern high latitudes from 2015 to 2100 under the three different SSP scenarios. 226

Figure 75: Change in mean annual soil moisture from the 2015-2025 average to the 2090-2100 average across the northern high latitudes in a) SSP126, b) SSP370 and c) SSP585. 227

Figure 76: The change in mean annual number of days below 0°C from the 2015-2025 average to the 2090-2100 average across the northern high latitudes in a) SSP126, b) SSP370 and c) SSP585.....228

Figure 77: The change in mean annual snow mass from the 2015-2025 average to the 2090-2100 average across the northern high latitudes in a) SSP126, b) SSP370 and c) SSP585. 229

Figure 78: The change in mean annual soil temperature from the 2015-2025 average to the 2090-2100 average across the northern high latitudes in a) SSP126, b) SSP370 and c) SSP585. 230

Figure 79: The change in mean annual number of months when average soil temperature is below 0°C from the 2015-2025 average to the 2090-2100 average across the northern high latitudes in a) SSP126, b) SSP370 and c) SSP585. 231

Figure 80: The change in various hydrological parameters from the 2015-2025 average to the 2090-2100 average across the northern high latitudes under SSP126 (a, d, g, j), SSP370 (g, e, h, k) and SSP585 (c, f, i, l). Plots a-c show the change in soil evapotranspiration and d-f show the change in canopy evaporation. Plots g-i show the change in surface moisture flux, and plots j-l show the change in runoff. 232

Figure 81: The change in mean annual water table depth (m) from the 2015-2025 average to the 2090-2100 average across the northern high latitudes in a) SSP126, b) SSP370 and c) SSP585. 233

Figure 82: Average annual peat depth of burn (m) above 50 degrees north from 2015 to 2100 for each of the SSPs. The dashed lines indicate the quadratic trendline for the respective SSP. 236

Figure 83: The change in mean depth of burn from the 2015-2025 average to the 2090-2100 average over the northern high latitudes under a) SSP126, b) SSP370 and c) SSP585. 237

Figure 84: Annual peat fire carbon emissions (Tg C) above 50°N from 2015 to 2100 for each of the SSPs. The dashed lines indicate the quadratic trendline for the respective SSP. 239

Figure 85: The change in mean carbon emissions (Tg C) from the 2015-2025 average to the 2090-2100 average over the northern high latitudes under a) SSP126, b) SSP370 and c) SSP585. 240

Figure 86: Schematic demonstrating the potential future developments of INFERNO-peat (red text), and the potential future couplings (red arrows). Black arrows indicate preexisting couplings. 266

List of Tables

Table 1: Descriptions of the three SSP scenarios used in Chapter 5. Information has been obtained from O'Neill et al., 2017; Riahi et al., 2017; van Vuuren et al., 2014 and van Vuuren et al., 2017. 63

Table 2: Summary of the input variables required for INFERNO-peat, and the source of these variables used in the future INFERNO-peat runs. 66

Table 3: A summary of the different global EO products available for detecting fires. 68

Table 4: A summary of the different remote sensing-based observations of atmospheric composition and air quality, in order of launch. Only the key measurements relevant to this section are included. 75

Table 5: Summary of the input variables required for INFERNO-peat, and the source of these variables used in the present-day INFERNO-peat runs. 91

Table 6: The different observational datasets used for model evaluation, the variables used from each and what evaluation was conducted using them. 95

Table 7: Summary of the seven subregions, their geographical coordinates, corresponding GFED region, and notable characteristics. Dominant landcover types are obtained from JULES-INFERNO. 96

Table 8: 2010 to 2014 average annual burnt area (M km^2) and statistics for the various models and observations. 97

Table 9: Values of M (RMSE adapted to consider that the observations underestimate BA) for the different models and observational datasets using the 2010 to 2014 average annual BA. 99

Table 10: 1997 to 2014 average annual burnt area, temporal standard deviation (std), coefficient of variation (cv) and temporal correlation (R), for models and observations. Correlation coefficients for the WGLC period (2010-2014) are available in Table S1 100

Table 11: 2010 to 2014 average annual burnt area (M km^2) and spatial statistics (Pearson's R and RMSE) for the various models and observations broken down into subregions. Note that the ABoVE-FED dataset is only for the three North American subregions. 102

Table 12: Burnt area averages, interannual variability metrics and temporal correlation broken down by each subregion for the 2001 to 2014 period. Results for the WGLC run are only available from 2010 onwards, therefore these runs are excluded from this table. ABoVE-FED correlations are only available for North America subregions. 106

Table 13: Average annual carbon emissions, standard deviation (std), coefficient of variation (cv) and temporal correlation R coefficients for models and observations over 2003 to 2014. Note, the INFERNO-peat WGLC run, is conducted from 2010 to 2014, and therefore not included in the temporal correlations. 111

Table 14: Carbon emission averages, interannual variability and temporal correlations between models and observations over 2003 to 2014, broken down by subregion. Results for the WGLC run are only available from 2010 onwards, therefore these runs are excluded from this table, and instead can be found in Table S2. 118

Table 15: Summary of the variables used in the analysis of the effects of fires on atmospheric composition and air quality. 132

Table 16: Annual values for BA from GFED5 and FRP from GFAS for eastern Siberia, and the summary statistics (mean, standard deviation (STD) and coefficient of variation (CV)) for the whole time series. Values in bold highlight years in which the value is at least one standard deviation greater than the mean. 135

Table 17: Annual values for NO_2, CO and their ratio from both TROPOMI and CAMS reanalysis data, and the summary statistics (mean, standard deviation (SD) and coefficient of variation (CV)) for the whole time series. Values in bold highlight years in which the value is at least one standard deviation above or below the mean. 138

Table 18: Correlations between the GFED5 and GFAS fire parameters, with NO_2, CO and their ratio in the TROPOMI and CAMS reanalysis datasets, on seasonal data (a), multi-year monthly data (b) and multi-year annual data (c) in eastern Siberia. Asterisks indicate significant p values (* = $p<0.05$, **=$p<0.001$, ***=$p<0.001$) 141

Table 19: Correlations between the yearly GFED5 and GFAS fire parameters, and the CAMS reanalysis $PM_{2.5}$ data, using annual totals, monthly totals and the seasonality (average monthly totals 2003-2020) in eastern Siberia. Asterisks indicate significant p values (* = $p<0.05$, **=$p<0.001$, ***=$p<0.001$) 143

Table 20: Annual values for BA from GFED5 and FRP from GFAS for northwest Siberia, and the summary statistics (mean, standard deviation (SD) and coefficient of variation (CV)) for the whole time series. Values in bold highlight years in which the value is at least one standard deviation greater than the mean. 146

Table 21: Annual values for NO_2, CO and their ratio from both TROPOMI and CAMS reanalysis data for northwest Siberia, and the summary statistics (mean, standard deviation (SD) and coefficient of

variation (CV)) for the whole time series. Values in bold highlight years in which the value is at least one standard deviation above or below the mean. 149

Table 22: Correlations between the GFED5 and GFAS fire parameters, and NO_2, CO and their ratio in the TROPOMI and CAMS reanalysis datasets, on seasonal data (a), monthly data (b) and yearly data (c) in northwest Siberia. Asterisks indicate significant p values (* = p<0.05, **=p<0.001, ***=p<0.001)..... 152

Table 23: Correlations between the yearly GFED5 and GFAS fire parameters, and the CAMS reanalysis $PM_{2.5}$ data, using annual totals, monthly totals and the seasonality (average monthly totals 2003-2020) in northwest Siberia. Asterisks indicate significant p values (* = p<0.05, **=p<0.001, ***=p<0.001)..... 155

Table 24: Annual values for BA from GFED5 and FRP from GFAS for Alaska, and the summary statistics (mean, standard deviation (SD) and coefficient of variation (CV)) for the whole time series. Values in bold highlight years in which the value is at least one standard deviation greater than the mean. 156

Table 25: Annual values for NO_2, CO and their ratio from both TROPOMI and CAMS reanalysis data for northwest Siberia, and the summary statistics (mean, standard deviation (SD) and coefficient of variation (CV)) for the whole time series. Values in bold highlight years in which the value is at least one standard deviation above or below the mean. 160

Table 26: Correlations between the GFED5 and GFAS fire parameters, and NO_2, CO and their ratio in the TROPOMI and CAMS reanalysis datasets, on seasonal data (a), monthly data (b) and yearly data (c) in Alaska. Asterisks indicate significant p values (* = p<0.05, **=p<0.001, ***=p<0.001)..... 163

Table 27: Correlations between the yearly GFED5 and GFAS fire parameters, and the CAMS reanalysis $PM_{2.5}$ data, using annual totals, monthly totals and the seasonality (average monthly totals 2003-2020) Alaska. Asterisks indicate significant p values (* = p<0.05, **=p<0.001, ***=p<0.001) 165

Table 28: Annual values for BA from GFED5 and FRP from GFAS for western Canada, and the summary statistics (mean, standard deviation (SD) and coefficient of variation (CV)) for the whole time series. Values in bold highlight years in which the value is at least one standard deviation greater than the mean. 168

Table 29: Annual values for NO_2, CO and their ratio from both TROPOMI and CAMS reanalysis data for western Canada, and the summary statistics (mean, standard deviation (SD) and coefficient of

variation (CV)) for the whole time series. Values in bold highlight years in which the value is at least one standard deviation above or below the mean. 170

Table 30: Correlations between the GFED5 and GFAS fire parameters, and NO_2, CO and their ratio in the TROPOMI and CAMS reanalysis datasets, on seasonal data (a), monthly data (b) and yearly data (c) in Alaska. Asterisks indicate significant p values (* = p<0.05, **=p<0.001, ***=p<0.001)..... 173

Table 31: Correlations between the yearly GFED5 and GFAS fire parameters, and the CAMS reanalysis $PM_{2.5}$ data, using annual totals, monthly totals, and the seasonality (average monthly totals 2003-2020) in western Canada. Asterisks indicate significant p values (* = p<0.05, **=p<0.001, ***=p<0.001)..... 175

Table 32: Correlation coefficient (r) between peat BA and CAMS NO_2, CO and NO_2:CO, for all subregions, grouped by the total monthly BA amount categories. Small contains 217 datapoints, medium 280 and large 42. 179

Table 33: Annual total BA and the relative percentages of peat fires and the 5 most commonly burnt land cover types in each of the 4 subregions, averaged over 2003-2020. 180

Table 34: Yearly and monthly correlations between the five most common land cover type BAs and the CAMS NO_2, CO and NO_2:CO ratio in the four different subregions. Asterisks indicate significant p values (* = p<0.05, **=p<0.01, ***=p<0.001) 181

Table 35: Yearly and monthly correlations between the five most common land cover type percentages of total BA and the CAMS NO_2, CO and NO_2:CO ratio in the four different subregions. Asterisks indicate significant p values (* = p<0.05, **=p<0.01, ***=p<0.001)..... 183

Table 36: Correlation coefficients for both yearly and monthly timescales in the four different regions between INFERNO-peat modelled peat BA and NO_2, CO and the NO_2:CO ratio from the CAMS reanalysis dataset. 187

Table 37: INFERNO-peat driving variables used to assess trends and changes seen in the future peat fire simulations, their sources and what variables they drive. 206

Table 38: The annual average burnt area (in M km^2) above 50°N averaged over the starting and ending decades of the model runs for each of the scenarios, and the absolute and percentage change between these two periods. 210

Table 39: Decadal average annual peat burnt area (M km^2), and decadal variability metrics standard deviation (std dev) and coefficient of variation (CV) for each SSP. 211

Table 40: The annual total peat fire ignitions above 50°N averaged over the starting and ending decades of the model runs for each of the scenarios, and the absolute and relative change between these two periods..... 213

Table 41: The annual mean peat probability of ignition above 50 degrees North averaged over the starting (2015-2025) and ending (2090-2100) decades of the model runs for each of the scenarios, and the change between these two periods. 224

Table 42: The annual mean soil moisture above 50°N averaged over the starting (2015-2025) and ending (2090-2100) decades of the model runs for each of the scenarios, and the change between these two periods..... 226

Table 43: The annual average soil moisture, and its driving parameters, above 50 degrees North averaged over the starting and ending decades of the model runs for each of the scenarios, and the change between these two periods. 233

Table 44: Pearsons's correlation coefficients (r) between the change in soil moisture from the 2015-2025 average and the 2090-2100 average with the change in numerous variables from the JULES land surface model. Asterisks indicate significant p values (*=p<0.05, **=p<0.01, ***=p<0.001). 234

Table 45: The mean peat depth of burn (m) above 50 degrees north averaged over the starting and ending decades of the model simulations for each of the scenarios, and the change between these two periods..... 235

Table 46: Pearsons's correlation coefficients (r) between the mean annual peat fire depth of burn and its three driving variables; soil moisture; soil temperature; and water table depth. Asterisks indicate significant p values (*=p<0.05, **=p<0.01, ***=p<0.001). 237

Table 47: Pearsons's correlation coefficients (r) between the change from the 2015-2025 average to the 2090-2100 average annual peat fire depth of burn and its three driving variables; soil moisture; soil temperature; and water table depth. Asterisks indicate significant p values (*=p<0.05, **=p<0.01, ***=p<0.001)..... 238

Table 48: The mean annual peat fire carbon emissions (Tg C) above 50°N, averaged over the starting (2015-2025) and ending (2090-2100) decades of the model simulations for each of the scenarios, and the change between these two periods 239

Table 49: Pearsons's correlation coefficients (r) between the mean annual peat fire carbon emissions and burnt area and depth of burn in the three SSP scenarios. Asterisks indicate significant p values (*=p<0.05, **=p<0.01, ***=p<0.001). 240

Table 50: Pearsons's correlation coefficients (r) between the change in mean annual peat fire carbon emissions and burnt area and depth of burn in the three SSP scenarios from the 2015-2025 average to the 2090-2100 average. Asterisks indicate significant p values (*=p<0.05, **=p<0.01, ***=p<0.001). 241

List of Acronyms

BA	Burnt area
FRP	Fire Radiative Power
FWI	Fire Weather Index
dNBR	difference Normalised Burn Ratio
NBR	Normalised Burn Ratio
NDMI	Normalised Difference Moisture Index
MCE	Modified Combustion Efficiency
PM	Particulate Matter
AOD	Aerosol Optical Depth
EO	Earth Observation
IR	Infrared
NIR	Near Infrared
SWIR	Short-wave infrared
VIS	Visible
UV	Ultraviolet
SCD	Slant Column Densities
DOAS	Differential Optical Absorption Spectroscopy
SICOR	Shortwave Infrared Carbon Monoxide Retrieval
PFT	Plant Functional Type
DGVM	Dynamic Global Vegetation Model
LSM	Land Surface Model
GCM	Global Climate Model
ESM	Earth System Model
CTM	Chemical Transport Model
INFERNO	INteractive Fire and Emission algoRithm for Natural envirOnments

JULES	Joint UK Land Environment Simulator
TRIFFID	Top-down Representation of Interaction of Foliage and Flora Including Dynamics
TRENDY	Trends in net land atmosphere carbon exchange model intercomparison project
UKESM	UK Earth System Model
CESM	Community Earth System Model
CLM	Community Land Model
CMIP	Coupled Model Intercomparison Project
ISIMIP	Inter Sectoral Impact Model Intercomparison Project
FireMIP	Fire Model Intercomparison Project
ESA	European Space Agency
NASA	National Aeronautics and Space Administration
ECMWF	European Centre for Medium-range Weather Forecasts
CEDA	Centre for Environmental Data Analysis
CAMS	Copernicus Atmospheric Monitoring Service
CAMSRA	Copernicus Atmospheric Monitoring Service Reanalysis
IFS	Integrated Forecasting System
GFED	Global Fire Emissions Database
GFAS	Global Fire Assimilation System
FireCCI	Fire Climate Change Initiative
MODIS	Moderate-Resolution Imaging Spectroradiometer
VIIRS	Visible Infrared Imaging Radiometer Suite
AVHRR	Advanced Very High Resolution Radiometer
IASI	Infrared Atmospheric Sounding Interferometer
TROPOMI	TROPOspheric Monitoring Instrument

GOME	Global Ozone Monitoring Experiment
SCIAMACHY	Scanning Imaging Absorption Spectrometer for Atmospheric Chemistry
OMI	Ozone Monitoring Instrument
TES	Tropospheric Emission Spectrometer
AIRS	Atmospheric Infrared Sounder
MOPITT	Measurements of Pollution in the Troposphere
AASTR	Advanced Along Track Scanning Radiometer
MISR	Multiangle Imaging Spectro Radiometer
LiDAR	Light Detection and Ranging
CALIOP	Cloud-Aerosol Lidar with Orthogonal Polarisation
CALIPSO	Cloud-Aerosol Lidar and Infrared Pathfinder Satellite Observation
ERS	European Remote Sensing satellite
EUMETSAT	European Organisation for the Exploitation of Meteorological Satellites
MetOP	Meteorological Operation satellites
MEGAN	Model of Emissions of Gases and Aerosols from Nature
MERRA	Modern-Era Retrospective Analysis for Research and Applications
MACC	Monitoring Atmospheric Composition and Climate
RCP	Representative Concentration Pathway
SSP	Shared Socioeconomic Pathways
BC	Black Carbon
BrC	Brown Carbon
OC	Organic Carbon
ABoVE	Arctic-Boreal Vulnerability Experiment
ABoVE-FED	Arctic-Boreal Vulnerability Experiment – Fire Emissions Database
NPD	Northern Peatland Dataset
ToPeCAI	Tropical Peatland Combustion Algorithm

IAV	Interannual variability
HDI	Human Development Index
RMSE	Root Mean Squared Error
STD	Standard deviation
CV	Coefficient of Variation

Chapter 1: Introduction

The high latitudes are undergoing rapid anthropogenically induced climate change. The Arctic is currently warming at twice the rate of the global average (Bruhwiler et al., 2021). Temperatures across the high latitudes have increased by 0.73°C per decade since 1979 (Rantanen et al., 2022), with extremes also increasing rapidly (Walsh et al., 2020). In addition to temperature, climate change is expected to induce changes in precipitation, and lightning across the high latitudes (Chen et al., 2021a). Simultaneously there are a range of huge environmental changes occurring in these latitudes, such as declining sea ice, permafrost thaw and degradation, vegetation changes including greening and woody expansion into the tundra, and increases in the frequency, extent, and severity of wildfires (Bruhwiler et al., 2021; Walsh et al., 2020).

Much of the high latitudes are underlain by peatlands, which store huge quantities of carbon (Hugelius et al., 2020a; Tarnocai, 2009). However, peatlands are being increasingly threatened by wildfires as a result of increasing temperatures, and the drying out of soils (Turetsky et al., 2015). Peat fires threaten to release vast amounts of long term stored carbon to the atmosphere, exerting strong positive feedback effects on the climate system and carbon cycle (Lasslop et al., 2019; Rein, 2015). Furthermore, peat fires release large amounts of radiatively active aerosols, including $PM_{2.5}$, which result in degraded air quality, with impacts on high latitude populations across the world (Turetsky et al., 2015; Hu et al., 2018). However, despite the importance of peat fires to climate, carbon cycles and air quality, peat fires are currently not represented in most Earth system models.

This thesis aims to address the necessity of parameterising peat fires in global fire models through the development of INFERNO-peat, a novel representation of northern high latitude peatland burning in the JULES-INFERNO fire model (Chapters 2 and 3). The impacts of present-day peatland burning on atmospheric composition and air quality using satellite-based data will also be explored in Chapter 4. Chapter 5 then examines how peat fires may change into the future through running INFERNO-peat using multiple climate change scenarios, and the associated emission changes than can impact atmospheric composition, climate, and the carbon cycle.

1. Significance of peatlands

Peatlands cover just 3% of the Earth's land surface, despite this they house one third of the world's soil carbon, representing a globally important store of carbon (Xu et al., 2018; Yu et al., 2010; UNEP, 2022a). Peat is defined as partially decomposed plant material that has accumulated in situ, when microbial decomposition of organic matter is incomplete due to waterlogged anaerobic conditions and low temperatures allowing for the build up of carbon rich organic matter within the soil (UNEP, 2022a). Anaerobic conditions within peatlands favour methanogenesis, therefore peatlands act as global sources of methane (Huang et al., 2021; Frolking et al., 2011). But undisturbed peatlands have very high carbon density and overall act as carbon sinks (Frolking et al., 2011). Therefore, peat-

dominated soils around the world act as net sinks of carbon, with Europe's peatlands storing five times more carbon than is stored in forests (Panagos et al., 2013; Swindles et al., 2019).

Peatlands are distributed across the world with notable deposits in the high latitudes, northern Europe, and the tropics (Figure 1; UNEP, 2022a). It is estimated that 11% of global peatland area is located in the tropics, 56% of which is in southeast Asia (Page et al., 2011). Other extensive tropical peatlands exist in western and central Amazonia and the Congo basin (Lahteenoja et al., 2013; Dargie et al., 2017). The Congo basin is home to the most extensive tropical peatland which covers 145,500 km^2, storing 30 billion tonnes of carbon (Dargie et al., 2017). However, the high latitudes make up the vast majority of global peatland area, of which ~50% is found in Canada and Russia alone (UNEP, 2022a), and 75-80% in all boreal and subarctic regions (Frokling et al., 2011). As the high latitudes are undergoing rapid climate and environmental change (Bruhwiler et al., 2021, Walsh et al., 2020; Chen et al., 2021a), this thesis will focus on the peat dominated soils of the high latitudes, defined here as anything north of 50° latitude.

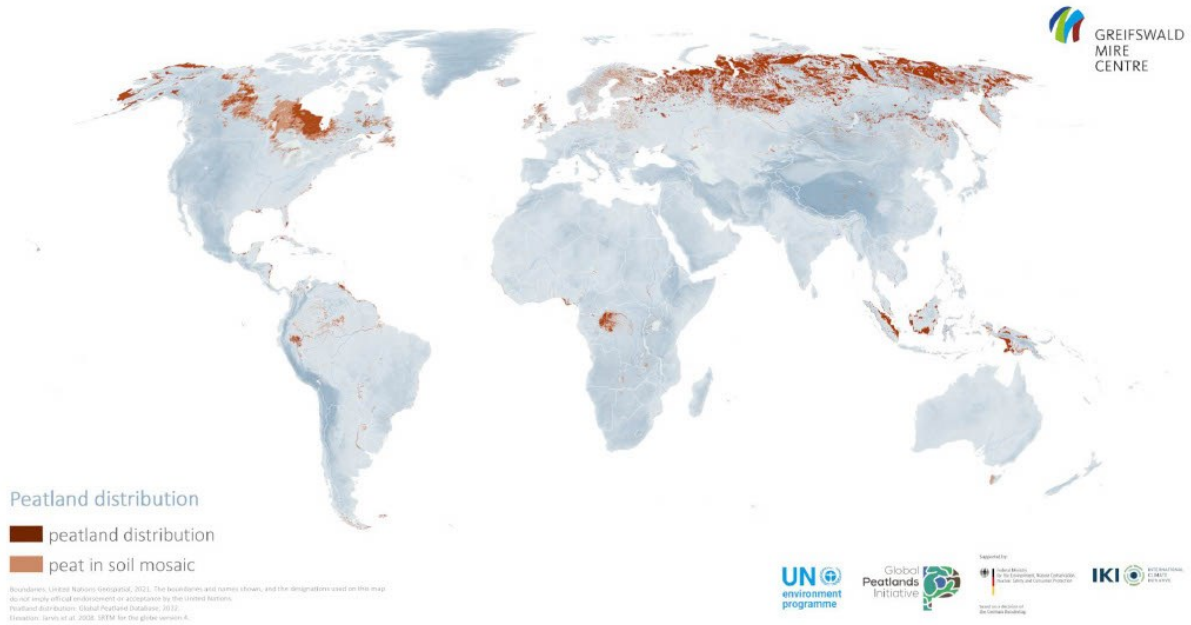


Figure 1: The global distribution of peatlands, obtained from the Global Peatlands Initiative and the United Nations Environment Programme (2022a).

1.1. High latitude peatlands

High latitude peatlands represent a globally important store of carbon, containing a total of 415 Pg of carbon and 10 Pg of organic nitrogen (Hugelius et al., 2020; Loisel et al., 2014), exerting a net cooling effect on the atmosphere (Frolking and Roulet, 2007). In Canada alone, peatlands contain 147 Gt of soil organic carbon whilst covering just 12% of the land area (Tarnocai, 2009). Approximately half of the northern high latitude peatlands are underlain by permafrost (Hugelius et al., 2020). Permafrost is any ground that remains frozen for two or more consecutive years and covers approximately 22% of

the Northern Hemisphere (Obu et al., 2019; Burke et al., 2020). Permafrost stores high amounts of organic carbon, with global estimates amounting to ~1300 Pg C (Hugelius et al., 2014; Schuur et al., 2015). Therefore, high latitude peat-dominated soils are a crucial store of carbon, and any degradation to these environments could cause vast carbon losses, with a positive feedback effect on the climate system.

1.2. Changes in high latitude peatlands due to climate change and humans

Peatlands are being increasingly threatened by both climate change and anthropogenic activity, with 54% of high latitude peatlands drying over the last 200 years (Zhang et al., 2022). Net losses in global peatland area and stored carbon are expected over the next century, with the northern high latitudes particularly at risk (Muller and Joos, 2021; Chaudhary et al., 2020). For example, areas of peat blanket bogs are expected to decline by 50% in the coming century (Gallego-Sala and Prentice, 2013). Rising temperatures are the main drivers of peatland loss (Muller and Joos, 2021; Gallego-Sala and Prentice, 2013), leading to enhanced decomposition and carbon loss (Loisel et al., 2021). Rising temperatures lead to higher levels of evapotranspiration, resulting in increased drying of peatlands and deeper water tables (Helbig et al., 2020; Tarnocai, 2009). In turn, deeper water tables can increase decomposition rates, and result in vegetation shifts from herbaceous to woody vegetation, leading to further carbon losses from peatlands (Zhao and Zhuang, 2023; Huang et al., 2021). A warming of 4°C has been shown to result in an 40-86% loss of soil organic carbon from peat in the northern high latitudes (Ise et al., 2008). Additionally, a peatland water table drawdown is expected to result in an increase in CO_2 emissions from peatlands by 1.13 Gt per year (Huang et al., 2021). There is also substantial anthropogenic pressure on peatlands from agriculture, forestry, industrial peat extraction and grazing, which all contribute to peatland loss (Loisel et al., 2021). Therefore, it is expected that Northern peatlands will switch to become sources of carbon of between 1.2 and 13.3 Pg C by around 2050, under RCP4.5 and 8.5, respectively (Zhao and Zhuang, 2023). Consequently, continued degradation of peatlands by both climate change and anthropogenic activities, may amplify carbon loss with the potential to switch peatlands from being sinks to sources of carbon, creating a positive feedback loop (Loisel et al., 2021; Swindles et al., 2019; Hugelius et al., 2020; Tarnocai, 2009; Zhao and Zhuang, 2023). Furthermore, the degradation of peatlands resulting from both humans and climate change is increasing the frequency and extent of wildfires in peatlands (Turetsky et al., 2015).

Permafrost degradation is primarily driven by warming temperatures (Zhang et al., 2018). Degradation of permafrost peatlands exposes perennially frozen carbon to thaw through a deepening of the active layer and subsidence (Nitzbon et al., 2020), resulting in increases in the emissions of CH_4 and CO_2 from permafrost peatlands and a positive feedback effect on the climate system (Schuur et al., 2015). Much of the high latitude peatlands are currently dominated by permafrost (Hugelius et al., 2020), reduction of these permafrost-dominated areas may result in carbon loss and ecosystem

shifts. Climate change in the high latitudes, such as in Northern Canada, is expected to result in widespread collapse of permafrost landscapes, resulting in degradation of peatlands (Tarnocai, 2009; Nitzbon et al., 2020). Furthermore, it is expected that all of Fennoscandia will become climatically unsuitable for permafrost peatlands by 2040 as a result of climate change (Fewster et al., 2022). It has been estimated that by 2100 there could be a twelve-fold increase in thaw-effected carbon under RCP8.5 (Nitzbon et al., 2020). Consequently, increased permafrost degradation with climate change further enhances the release of carbon from peatlands, resulting in a positive climate feedback loop.

2. Wildfires in the northern high latitudes

Wildfires are one of the largest natural disturbances in the world, with far reaching impacts on the Earth system. Around 4% of the Earth's ice-free land surface burns annually (Randerson et al., 2012; Giglio et al., 2013), emitting, on average, 1.6-1.7 Gt of carbon (Friedlingstein et al., 2023), roughly equivalent to 25% of anthropogenic fossil fuel CO_2 emissions (Hantson et al., 2016). Wildfires have substantial effects on vegetation, the carbon cycle and climate (Bowman et al., 2009; Bowman et al., 2011; Lasslop et al., 2019). Wildfires also have important implications on atmospheric composition and its interannual variability (Voulgarakis and Field, 2015; Voulgarakis et al., 2015). Interannual variability in carbon monoxide is almost entirely due to biomass burning emissions, particularly in the northern high latitudes (Voulgarakis et al., 2015). Over the last 20 years global burned area has declined as a result of agricultural expansion and anthropogenic activities (Andela et al., 2017; Giglio et al., 2013; Doerr and Santin, 2016). However, this pattern is not globally ubiquitous with much of this decline occurring in savanna ecosystems of sub-Saharan Africa (Andela et al., 2017). In particular, there are significant increases in burning happening in temperate and boreal forests especially in the Western US and Siberia (Yang et al., 2023; Descals et al., 2022). Increases in the frequency and extremity of fires are occurring around the world, as a result of climate change (Jones et al., 2022). Climate change drives increases in temperatures and in some areas decreases in relative humidity, causing increased fire danger, and consequently fires (Grillakis et al., 2022; Jain et al., 2022).

Across the high latitudes in recent years wildfires have become increasingly prominent in frequency and severity (Walsh et al., 2020; McCarty et al., 2021; York et al., 2020, Hu et al., 2015; Kharuk et al., 2021), so much so that fires are the dominant ecological disturbance in boreal regions (York et al., 2020; Nitze et al., 2018). Whilst historically, periodic fires in the northern high latitudes have supported ecosystem health and biodiversity, amplified fire frequency and a northward shift in fire regimes pose substantial threats to ecosystem stability (Kharuk et al., 2021). In such high latitudes, fires are largely driven by climatic variables (Chuvieco et al., 2021), and are primarily ignited by lightning (Stocks et al., 2002; Wendler et al., 2011; Hessilt et al., 2022). As high as 80% of large wildfires that occurred in Canada between 1959 and 1997, and 93% of fires in Alaska between 1955

and 2009 were lightning ignited (Stocks et al., 2002; Wendler er al., 2011). Human ignitions also occur in boreal regions, but are centred around population centres (Calef et al., 2008). Humans cause fire in high northern latitudes primarily through industrial activities, agriculture, and prescribed burning (McCarty et al., 2021). In some areas, such as Yakutia, Russia, up to 50% of wildfires can be caused by these human activities (Xu et al., 2022; Kirillina et al., 2020). Indigenous populations in the pan-Arctic region also use traditional fire practices, however, knowledge is limited in the prevalence of such burning, particularly in the Russian Arctic (McCarty et al., 2021).

Across the high latitudes, there are substantial amounts of land burning each year. In the Sakha Republic, Russia, on average 1.7 million hectares burn annually (Kirillina et al., 2020), and across Alaska and the Northwest Territories, Canada, approximately 13 million hectares burned between 2001 and 2018 (Hessilt et al., 2018). Fires in the high latitudes exhibit substantial interannual variability in burnt area and carbon emissions (Chuvieco et al., 2021; York et al., 2021). In Alaska there has been a large increase in burning over 1995 to 2009 (Wendler et al., 2011), with the 2007 Anaktuvuk river fire in Alaska alone burning over 1000km^2 and releasing 2.1 Tg of carbon to the atmosphere (Mack et al., 2011). In recent years fires in the Siberian Arctic have become increasingly prominent (Descals et al., 2022; Scholten et al., 2022; Yang et al., 2023). For example, in 2019 and 2020 fires in the Siberian Arctic burned 4.7 million hectares, accounting for almost 50% of all burned area between 1982 and 2020 and resulted in emissions of 90.4 Tg of carbon in 2020 alone (Descals et al., 2022). Furthermore, burning in Siberia has been shifting northward (Scholten et al., 2022), and the fire season has lengthened in parts of the region by more than 13 days (Kirillina et al., 2020). Overall, across the high latitudes fires are becoming more common, and burn larger areas, emitting vast amounts of carbon from forest and from carbon rich peat-dominated soils.

Fire regimes in the high latitudes are primarily driven by summer temperatures, precipitation, and relative humidity, which all effect fire weather (Young et al., 2017; Hessilt et al., 2022; Talucci et al., 2022). For example, Kharuk et al., (2021) showed that large fire years in Siberia, such as that of 2003, coincided with years, of anomalously high summer air temperatures and extreme weather events. Over the last 40 years, increasing air temperatures and fuel availability has resulted in fire weather conditions that are more favourable for fire spread, more intense burning and greater fuel consumption (York et al., 2020). Fire weather is the major driver in controlling how likely a fire is to result from a lightning strike in Alaska and the Northwest Territories of Canada (Hessilt et al., 2022). Increasing fire frequency and burnt area in the high latitudes may also be driven by earlier spring snow melt, which on average means that snow melt begins 10.2 days earlier in Siberia than it did 60 years ago (Scholten et al., 2022). Moisture availability in fuels, controlled by parameters such as plant water stress, has also been shown to influence the interannual variability in burnt area (Young et al., 2017; Descals et al., 2022). The recent large fire years in 2019, 2020 and 2021 in Siberia were driven by high summer temperatures and dry conditions (Descals et al., 2022; Scholten et al., 2022). In these

years there was a northward displacement of the polar arctic front jet, which resulted in blocking anticyclones which drove record high temperatures and dry conditions (Scholten et al., 2022). This arctic front jet pattern has become three times more frequent in the last 40 years, which combined with increasing lightning activity during blocking anticyclones, results in an increased likelihood for fires in the high latitudes (Scholten et al., 2022). Future climate change may exacerbate the climatic conditions that lead to large and impactful fires in the northern high latitudes. The effects of climate change on high latitude fires are already being seen with a rapid attribution study reporting that the extreme wildfires seen in Quebec in 2023 were made around 50% more likely due to climate change, and the likelihood of future fire seasons of this severity are around 7 times more likely as a result of climate change (Barnes et al., 2023). Furthermore, by 2100 under RCP6.0, there is expected to be a fourfold increase in the probability of fires occurring, especially in low flammability regions such as the tundra (Young et al., 2017).

3. Peat fires and smouldering combustion

Whilst in their natural, undisturbed state peatlands are resistant to wildfires, climatic induced drying or human driven degradation can lead to an increased vulnerability of these carbon rich environments to fire (Turetsky et al., 2015). Peat fires are some of the largest and most persistent wildfire phenomena on Earth (Rein, 2013). Fundamentally, peat fires are a different phenomenon to vegetation fires as they burn predominately by smouldering combustion (Akagi et al., 2011), which is slow, low temperature and flameless burning with incomplete combustion (Rein, 2013; Rein, 2015; Huang and Rein, 2017). Smouldering peat fires can persist under low temperatures, high moisture contents and low oxygen levels leading to fires which burn for extended periods of time, despite changes in the fire weather conditions (Turetsky et al., 2015; Rein, 2013). This means that peat fires have the potential to emit vast quantities of long term stored carbon to the atmosphere, with potentially significant positive feedback effects on the climate system (Lasslop et al., 2019; Rein, 2013).

Smouldering is a volumetric phenomenon meaning that peat fires not only spread laterally through the soil, but they also spread downwards within the soil (Rein, 2013; Huang and Rein, 2019; Santoso et al., 2019a). On average, smouldering fires spread at a rate of 3.1 cm per hour, however this is heavily dependent on the moisture content of peat with dry soils resulting in spread rate of 21.5 cm/hour (Santoso et al., 2019a). The lateral spread of peat fires is also heavily influenced by the microtopography of peatlands (Santoso et al., 2019a). In-depth spread is slower ranging from 0.5 to 2 cm/hour (Huang and Rein, 2017). However, smouldering can burn deep into the soil and persist for extend periods of time (Rein and Huang, 2021), making peat fires challenging to supress and firefighting highly water intensive (Rein, 2013; Lin et al., 2020; Santoso et al., 2021). Smouldering fires are most commonly initiated from a flaming vegetation fire, and in rare cases can transition back into flaming fires (Santoso et al., 2019b). The ignition and spread of peat fires are heavily influenced

by soil properties, most importantly soil moisture (Rein, 2015). There have been extensive laboratory studies into the dynamics of smouldering peat fires, which provide a useful insight into how and why these fires may occur, with implications for modelling peat fires. Below I present a summary of key literature on this topic.

3.1. Effects of soil properties on the ignition and spread of peat fires

Soil moisture is the single most important factor governing the ignition and spread of peat fires (Rein 2013; Rein 2015). Soil moisture levels are controlled by precipitation, evapotranspiration, and water table levels (Christensen et al., 2020; Schulte et al., 2019). Local heterogeneity in soil moisture will affect how a peat fire spreads and at what speed this occurs (Prat-Guitart et al., 2016). But, in general, drier soils with deep water tables facilitate greater and deeper burning with high fuel consumption (Purnomo et al., 2020; Lin et al., 2019; Benscoter et al., 2011; Turetsky et al., 2011b; Che Azmi et al., 2021). Frandsen (1997) showed that moisture content and the probability of burning exhibit a reverse sigmoid curve from high probability at low moisture contents to low probability at high moisture contents (Figure 2), but this relationship is altered by the bulk density and inorganic content of the soil. The lateral spread rate of smouldering peat fires shows a linear decrease with moisture content (Figure 3; Christensen et al., 2020). Therefore, increased likelihood of peat fires and a greater spread rate with lower moistures results in an inverse relationship between soil moisture and peat burnt area (Dadap et al., 2019). For example, droughts in boreal Canada have been shown to result in lower soil moistures and lead to a six-fold increase in fire activity (Thompson et al., 2019). Despite these relationships, fires can still be maintained at moisture contents as high as 160% (Rein, 2013; Hu et al., 2019b; Rein, 2015; Purnomo et al., 2020), indicating the high combustion potential of peatlands.

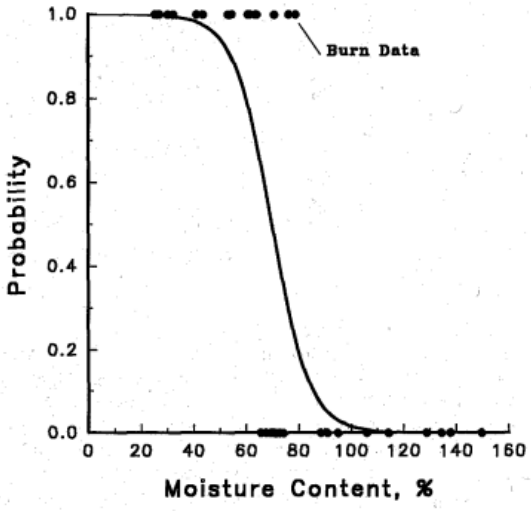


Figure 2: An example of the relationship between the probability of ignition and moisture content from Frandsen (1997).

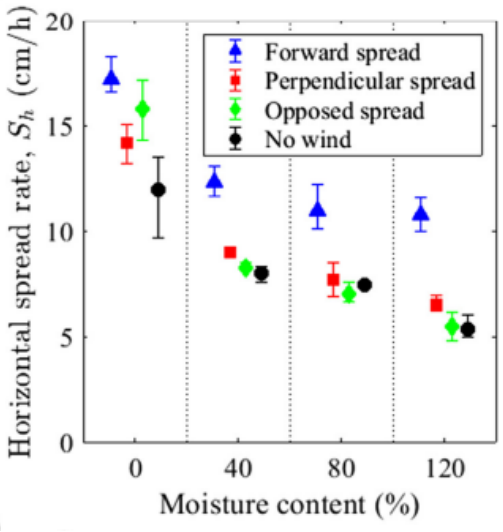


Figure 3: The relationship between horizontal (or lateral) spread rate and moisture content from Christensen et al. (2020). Note, this figure additionally shows the impact of different wind directions on the horizontal spread rate.

Inorganic content and bulk density also exert an important control on peat fire ignition and spread (Rein, 2013; Rein, 2015). Bulk density averages 0.12 g/cm^3 in the high latitudes with inorganic content averaging 9.3% (Loisel et al., 2014). Higher inorganic content levels in peat, results in a slower spread rate of peat fires (Yang and Chen, 2018; Christensen et al., 2020). Inorganic content also increases the critical moisture threshold for ignition, thereby affecting the likelihood of a peat fire starting (Santoso et al., 2019a). Bulk density describes the compactness of soil (Chaudhari et al., 2013, Keller and Hakansson 2010; Che Azmi et al., 2021). Increased peat bulk density is associated with increased fire spread (Huang and Rein, 2019). Furthermore, bulk density influences the maximum soil moisture at which combustion can occur (Benscotter et al., 2011), with soils with lower bulk densities able to smoulder at higher moisture contents (Schulte et al., 2019). Soils with high bulk densities can result in greater water table fluctuations, potentially leading to greater in-depth burning (Nelson et al., 2021). Soil temperature is also important, as a peat fire will continue to spread downward and laterally into the soil, existing and spreading underground for months, until it is too cold to maintain a fire (Lin et al., 2021).The minimum temperature required to sustain a smouldering fire is related to soil moisture, as soils with high moisture contents require warmer temperatures to be able to burn and visa versa, meaning that extremely dry soils can burn at temperatures below -35°C (Lin et al., 2021). On average peatlands have a moisture content of 82% (Smith et al., 2012), and therefore need temperatures of at least 6.5°C for fires to occur (Lin et al., 2021). However, soil moisture in peatlands has been shown to vary from as little as 24% to upwards of 98% (Smith et al., 2012), therefore the critical temperature for peat fires can also vary significantly. Consequently, soil properties play an important role in enhancing and limiting the occurrence and spread of peat fires.

Other environmental factors also play an important role in controlling the ignitions and spread of peat fires. For example, both wind and terrain slope have been shown to affect the lateral spread of peat

fires (Christensen et al., 2021). Wind that is perpendicular to the direction of spread enhances spread rates, whilst smouldering fires spread 21% faster up hill compared to a flat bed (Christensen et al., 2021). Antecedent precipitation and evapotranspiration also play an indirect role in the vulnerability of peatlands to fire through their effects on soil moisture levels (Schulte et al., 2019).

The microtopography and fragmentation of peatlands also play a key role in how peatlands burn. For example, shallow peat deposits have been shown to be more vulnerable to fires with peatlands deeper than 0.66m being more resistant to burning due to stronger water storage capacities and a tendency for water tables to be closer to the surface (Wilkinson et al., 2020). Furthermore, the fragmentation of peatlands alters peatland hydrological properties, modifying the vulnerability of peatlands to burning (Wilkinson et al., 2019). For example, there is often a disconnect from groundwater systems in small and fragmented peatlands, making them more vulnerable to fires (Wilkinson et al., 2019).

It is evident that there are many soil and environmental factors that alter peatland ignition probability and modify the spread rate of smouldering combustion. However, what many of these factors link back to is the moisture content of the soil, thereby highlighting soil moisture as the key influencer of peat fire ignition and spread.

3.2. Depth of burn of peat fires

On average, peat fires burn 12cm deep into the soil (Santoso et al., 2019a), but this depth of burn ranges from 5 to 30cm in many field studies (Turetsky et al., 2011b; Walker et al., 2020; Santoso et al., 2019a; Lukenbach et al., 2015; Hokanson et al., 2016; Wilkinson et al., 2018; Davies et al., 2013). However, laboratory experiments have shown that they can burn as deep as 50 – 100cm (Rein, 2015; Qin et al., 2023). Depth of burn and the downwards spread of peat fires, are also influenced by a range of soil properties, primarily linked to soil temperature and moisture. As previously mentioned, fires will burn downwards into the soil until it is too cold for that fire to be maintained, and this temperature threshold is altered by the moisture content of the soil, with drier soils being able to maintain a fire at lower temperatures (Lin et al., 2021). Soil moisture also directly influences the in-depth spread rate of peat fires, with increases in spread rate occurring alongside increases in soil moisture (Huang and Rein, 2017; Christensen et al., 2020). Christensen et al., (2020), observed a tripling in the rate of downward spread from 0-140% moisture content due to decreases in organic density with moisture, resulting in less fuel and consequently less time is required to consume this fuel. However, just because fires propagate downwards into the soil faster with high moisture contents, does not necessarily lead to greater burn depths, as wetter soils result in higher soil temperatures needed for burning (Lin et al., 2021), and tend to have higher water tables, thereby they are less likely to be ignited in the first place.

Depth of burn is strongly controlled by water table depth (Nelson et al., 2021; Wilkinson et al., 2020). Lower water tables result in lower soil moisture (Nelson et al., 2021). When water tables are high

there are stronger capillary forces within the peat that enable the transfer of water from the water table to the surface, maintaining higher moisture contents (Wilkinson et al., 2020). However, when the water table is deeper, the moisture content in the upper soil layers becomes disconnected from the water table, leading to drying and consequently deeper burning (Wilkinson et al., 2020). Therefore, the positioning of the water table controls the moisture content of the soil, and therefore indirectly effects the depth of burn through alterations to moisture content itself and the critical temperatures needed for burning to occur.

Microtopography and heterogeneity within peatlands also play an important role on the depth of burn as a result of changes to the hydrological connectivity within peatlands due to fragmentation (Nelson et al., 2021). In general, the more fragmented a peatland is the greater the depth of burn. Peatland margins often experience the greatest fluctuations in water table depth, which has been shown to result in depth of burn of up to 50cm at peatland margins (Hokanson et al., 2016). Congruent with this, Lukenbach et al., (2015) showed a five-fold increase in depth of burn from 8cm in peatland middles to 42cm in peatland margins, due to higher peat densities and low soil moisture at peatland margins. Additionally, the pre-fire management of a peatland affects the depth of burn, with heavily drained peatlands burning significantly deeper than undrained peatlands (Wilkinson et al., 2018; Turetsky et al., 2011b). Severe drainage results in extremely dry conditions and in severe cases can result in the combustion of the entire peat profile during a fire (Wilkinson et al., 2018). Consequently, the moisture content of peatlands, which is affected by numerous factors including water table position, fragmentation and microtopography, and soil temperature play a critical role in how deep peat fires burn.

3.3. Controls on carbon and gaseous emissions from peat fires

Peat fires are responsible for some of the highest emissions of carbon per area burned on Earth (Lasslop et al., 2019). On average, between 2.2 and 3.5 kg C/m^2 is burned during a peat fire (Turetsky and Weider, 2001; Benscoter and Wieder, 2003; Potter et al., 2023; Veraverbeke et al., 2021). However, severe fires can result in much greater carbon consumption. For example, during the 2011 Utikuma complex fire in Alberta, Canada, carbon release reached as high as 96 kg C/m^2 (Lukenbach et al., 2015). A peat fire in the Scottish Highlands in 2006 resulted in the loss of 396 tonnes of Carbon, equivalent to 9.6 kg C/m^2 (Davies et al., 2013). Carbon emissions from peat fires are directly proportional to the depth of burn (Lin et al., 2021; Che Azmi et al., 2021), meaning that deep peat burning that occurs as a result of low soil moistures and deep water tables can result in extremely high carbon loss, which may not be able to be recuperated post fire. Combustion during peat fires is often incomplete (Rein, 2013; Rein, 2015), with peat fires often having a combustion completeness of less than 0.9 (Urbanski, 2014; Wiggins et al., 2021). Values of combustion completeness in peat fires often

vary between 0.65 and 0.90 (Urbanski, 2014; Agaki et al., 2011), with an average of 0.87 reported from numerous field studies (Walker et al., 2020).

Smouldering peat fires emit different gas species and in different quantities compared to flaming fires. The predominant gas species emitted by peat fires include CO_2, CO, CH_4 and NH_3 (Hu et al., 2019a; Hu et al., 2018). Compared to flaming savanna fires, peat fires emit significantly more CO and CH_4, as a result of incomplete combustion (Hu et al., 2019a; Hu et al., 2018). This means that ratios of CO:CO_2 or NO_2:CO can be used to differentiate between smouldering and flaming combustion (Rein et al., 2009; Andreae, 2019; van der Velde et al., 2021). Emissions from peat fires can also be altered by the moisture content of the soil. For example, Hu et al. (2019b) showed that wet peat emitted less CO_2, CH_4 and NH_3, but more CO, HCN and coarse particles than dry peat. Therefore, the emissions from a peat fire are dominated by the products of incomplete combustion and can be affected by the soil moisture of the peat.

Peat fires are also a dominant source of aerosols and particulate matter across the globe, especially black carbon (BC) and organic carbon (OC). OC is the dominant component of PM2.5 emitted from peat fires (Hu et al., 2018; Kondo et al., 2011; Yokelson et al., 2011), contributing as much as 71% of $PM_{2.5}$ mass in peat fires in Indonesia (Fujii et al., 2014), and 91-95% of total carbon aerosols in peat fires in western Russia (Popovicheva et al., 2019). Chakrabarty et al., (2016) showed that aerosol emissions from Alaskan and Siberian peatlands are predominately brown carbon (BrC), with negligible amounts of BC. In general, it has been shown that smouldering peat fires have negligible contributions from BC (Conny and Slater, 2002; Hu et al., 2019b; Chakrabarty et al., 2016), with contributions of 1-5% of total aerosol mass in boreal North America, and Siberia (Kondo et al., 2011). OC is strongly emitted during peat fires relative to BC due to the lower combustion efficiency that occurs during smouldering combustion, which has been shown to be associated with higher levels of OC and lower BC compared to a flaming fire (Yokelson et al., 2011; Che et al., 2022; Christian et al., 2003)). BC is still present in small amounts in peat fire emissions (Hu et al., 2018), and when peat undergoes flaming combustion, BC can account for 92% of total carbon aerosols (Hu et al., 2019b). Flaming fires have also been shown to release 10 times more BC than smouldering fires relative to total particulate carbon (Conny and Slater, 2002). Therefore, peat burning has the potential to release large amounts of particulate matter, predominately as BC and OC, which may have impacts on air quality, human health, and radiative forcing (Randerson et al., 2006; Lelieveld et al., 2015; Bond et al., 2013; Oris et al., 2014).

4. Peat fires in the northern high latitudes

In the northern high latitudes, peat fires largely originate from lightning strikes (Wendler et al., 2011; McCarty et al., 2021; Xu et al., 2022). However, human activities such as timber and energy extraction, prescribed burning and tourism can also lead to fires (McCarty et al., 2021). Across the

high latitudes peat fires are becoming increasingly common, and they threaten to release vast amounts of legacy carbon to the atmosphere, alongside a suite of aerosols and particulates which can have detrimental effects on air quality (Lasslop et al., 2019; Rein, 2015). For example, Descals et al., (2022) showed that fires in the Siberian Arctic in 2020 damaged 0.71 M ha of carbon rich peatlands. Therefore, peat fires represent an important environmental disturbance in the high latitudes, with far reaching implications (Figure 4).

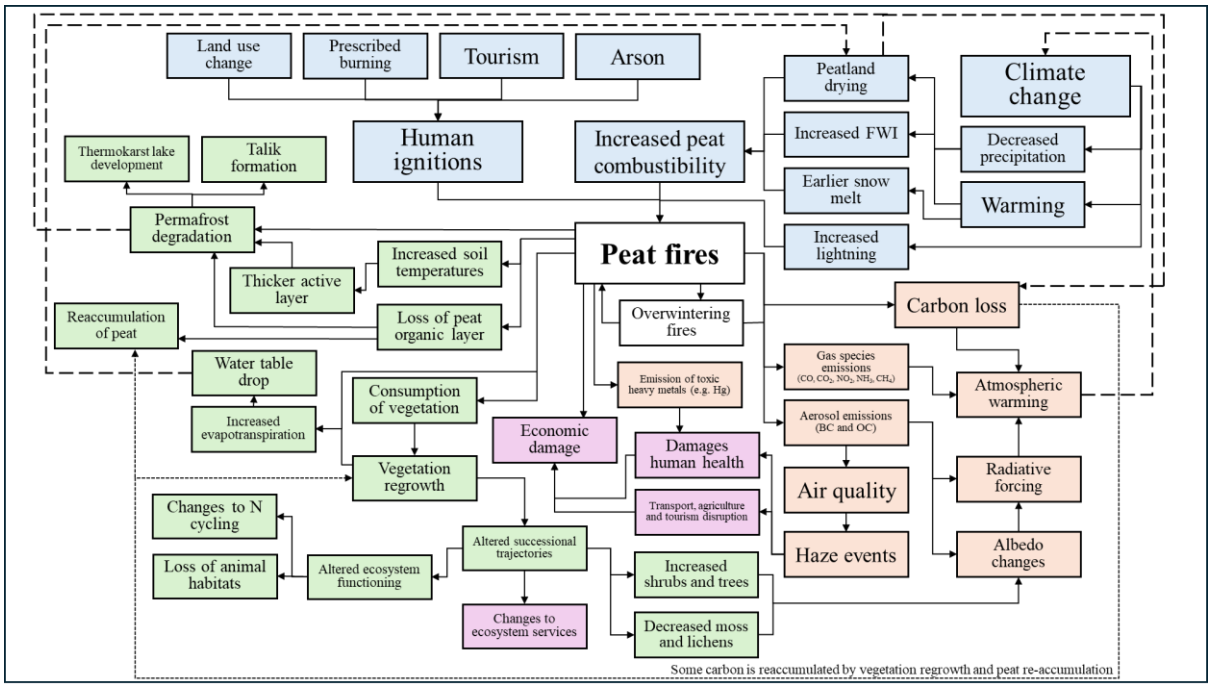


Figure 4: Schematic demonstrating the key drivers of peat fires (blue), and the various atmospheric (orange), human (purple) and environmental (green) impacts of peat fires. Feedback effects are denoted by the thick dashed lines. The small, dashed line indicates the potential reaccumulation of carbon within the system.

Peat fires are also of major concern as they can lead to overwintering fires. Overwintering, or 'zombie fires', are fires that continue to smoulder belowground after the end of the fire season throughout the winter, before re-emerging the following spring as flaming fires that can then burn additional areas (McCarty et al., 2020; Irannezhad et al., 2020; Scholten et al., 2021; Figure 4). Overwintering fires have been detected across Alaska, the Northwest Territories, Canada, and Eastern Siberia (Scholten et al., 2021; Xu et al., 2022). In Alaska and the Northwest Territories, between 2002 and 2018, overwintering fires made up 0.8% of burned area, and emitted 3.5 Tg of carbon (Scholten et al., 2021). However, 64% of this burning occurred in just two fire seasons (Scholten et al., 2021), indicating that whilst overwintering fires are rare, when they do occur, they can burn large areas and release large amounts of carbon. For example, in 2008 a single overwintering fire burned 13,700 ha in Alaska, 38% of the total burnt area in that year (Scholten et al., 2021). Similarly in Yakutia, Eastern Siberia, overwintering fires contributed to 3.2% of total burnt area between 2012 and 2020 (Xu et al., 2022). However, in 2020 overwintering fires burned much larger areas than in previous years, accounting for 7.2% of burned area and resulted in the fire season starting two months earlier than

usual (Xu et al., 2022; McCarty et al., 2020). Overwintering fires have been shown to be primarily driven by extreme summer temperatures and higher overnight temperatures (Scholten et al., 2021). Consequently, rising global temperatures may result in an increased occurrence of overwintering fires in peatlands, leading to greater burnt areas and subsequently higher carbon emissions, exacerbating the positive feedback loop on the climate system and resulting in substantial environmental change (Figure 4).

4.1. Impacts of peat fires on the carbon cycle, climate and air quality

Due to the large quantities of carbon sequestered in peatlands, peat fires can release vast amounts of carbon, estimated to be roughly equivalent to 15% of that of anthropogenic emissions (Lasslop et al., 2019; Loisel et al., 2021; Poulter et al., 2006; Rein, 2015). Carbon emissions from peat fires are heavily influenced by the depth of burn, as the deeper a peat fire burns the larger the pool of carbon that is exposed to combustion (Lin et al., 2021; Huang and Rein, 2017; Che Azmi et al., 2021). In the immediate aftermath of a fire, peatlands are net sources of carbon (Wieder et al., 2009). However, carbon can typically be reaccumulated within 10-30 years post fire, allowing peatlands to remain a net carbon sink (Wilkinson et al., 2023; Wieder et al., 2009; Ingram et al., 2019). Severe fires or fires on degraded peatlands may result in higher carbon emissions that may take up to 330 years to recover the lost carbon (Ingram et al., 2019; Wilkinson et al., 2023). Peat fires that occur specifically in the high latitudes have been shown to have fire return intervals of 15-60 years (Sizov et al., 2021), meaning that many peatlands would not have recovered the lost carbon from the initial fire before it burns again, resulting in a net loss of carbon. For example, Turetsky et al., (2011a) showed fire emissions between 2000 and 2009 to have exceeded decadal carbon uptake by peatlands by 86 Tg C in Alaska, consequently diminishing the carbon sink. In addition, in western Canada it has been shown that severe burning in drained peatlands triggers the loss of 450 years worth of peat accumulation, and with an average fire return interval of 120 years in this region it is highly unlikely that these severe carbon losses will be reaccumulated between fires (Turetsky et al., 2011b). Therefore, peat fires have the potential to cause catastrophic losses of long-term stored carbon, which cannot be reaccumulated, thus leading to positive climate feedback effects (Figure 4).

Smouldering peat fires also emit a range of gas species, including CO_2, CO, CH_4 and NH_3 alongside a suite of aerosols (Hu et al., 2019a; Voulgarakis and Field, 2015). For example, large fires in Russia in 2010 (of which 30% were peat fires) led to 10 Tg of CO being emitted, equivalent to 85% of the country's total annual anthropogenic emissions (Konovalov et al., 2011). Peat fires can also trigger the release of toxic heavy metals, such as mercury, that are stored within peatland soils (Kohlenberg et al., 2018). Consequently, peat fires are dominant in driving the interannual variability of global fire emissions and their consequent effects on global atmospheric composition (van der Werf et al., 2010; Voulgarakis et al., 2015).

The emission of aerosols from fires can have large implications on air quality as well a radiative forcing (Figure 4). In the high latitudes wildfires release more $PM_{2.5}$ than all anthropogenic sectors combined (McCarty et al., 2021), with a key species released being black carbon (BC) and organic carbon (OC). Black carbon emitted during wildfires represents more than half of all black carbon emissions north of 60 degrees latitude (McCarty et al., 2021). For example, during the 2002 fire season in Quebec, fires accounted for 80% of the annual BC emissions in that area (Lavoue and Stocks, 2011). BC and other aerosols, such as OC, can have impacts on atmospheric absorption and the Earth's reflectivity (surface albedo), both leading to radiative forcing of the climate system (Thomas et al., 2017; Bond et al., 2013; Evangeliou et al., 2019; Hao et al., 2016). Peat fires in western Greenland in summer 2017 resulted in the emission of 23.5t of BC and 731t of OC and the deposition of such aerosols over the Greenland ice sheet (Evangeliou et al., 2019). Deposition of aerosols, in particular BC, on glaciers, snow and sea ice may reduce surface albedo, leading to atmospheric warming and enhanced surface melting (Randerson et al., 2006). For example, the transport of aerosols from fires in Canada in summer 2013 led to large BC deposition over the Greenland ice sheet, resulting in a lowering of snow albedo (Thomas et al., 2017). Furthermore, the substantial release of aerosols from Siberian fires have been shown to result in a six-fold increase in aerosol optical depth, exerting a net cooling effect on the atmosphere (Zhuravleva et al., 2017, Jeong et al., 2008). Smouldering peat fires emit substantially more OC than BC (Fujii et al., 2014; Che et al., 2022; Conny and Slater, 2002). Whilst OC is made up in a large part of light scattering organic aerosols (Che et al., 2022), large amounts of light absorbing brown carbon (a type of OC) are also emitted, with the potential to result in a warming of the atmosphere (Chakrabarty et al., 2016). Therefore, emissions of aerosols from peat fires have a large potential effect on radiative forcing which could lead to atmospheric warming. However, there is also a substantial health burden from aerosols on human populations in fire affected areas (Lelieveld et al., 2015).

Fires are the main source of air pollution induced health burden in Canada and Siberia (Lelieveld et al., 2015), due to the release of aerosols during burning. Peat fire emissions of aerosols and particulates degrade air quality and cause haze events (Turetsky et al., 2015; Hu et al., 2018), consequently disrupting transport, tourism, agriculture, and human health (Hu et al., 2018; Heil and Goldammer, 2001; Figure 4). Haze events are common as the smoke produced during a peat fire is highly persistent and can accumulate close to the ground (Hu et al., 2019a). Haze contributes significantly to respiratory and cardiovascular problems (WHO, 2006; Hu et al., 2018). Consequently, $PM_{2.5}$ emissions attributed to wildfires in the Arctic have been estimated to have resulted in between 25,000 and 50,000 premature deaths (Silver et al., 2023). For example, fires surrounding Moscow in 2010 alone led to extreme air pollution and 11,000 additional deaths (Konovalov et al., 2011; Shaponshnikov et al., 2014). However, most of the health burden that results from fires in the Arctic falls upon nations outside of the Arctic (Silver et al., 2023) due to the trans-boundary transport of fire-

produced smoke. For example, fires in Siberia in 2003, 71% of which occurred on peatlands (Huang et al., 2008), resulted in enhancements in atmospheric PM_{10} and ozone in the Korean peninsula, with smoke plumes also reaching as far as Japan and the USA (Jeong et al., 2008; Huang et al., 2009). Additionally, smoke plumes from fires in Siberia in 2012 were transported to the Pacific northwest where, due to the presence of high pressure, the smoke settled and led to the exceedance of ozone and $PM_{2.5}$ health standards across British Columbia and Washington State (Teakles et al., 2017). Therefore, peat fires are of major concern for the climate and air quality.

4.2. Environmental impacts of peat fires

Peat fires also have widespread impacts on ecosystems through altered ecosystem composition and successional trajectories, and changes to moisture and nutrient dynamics including increased evapotranspiration, which may alter the functioning of peatlands and cause further carbon losses (Kettridge et al., 2015; Kettridge et al., 2019; Mekonnen et al., 2021; Figure 4). Peat fires lead to increases in post-fire evapotranspiration and trigger a drop in water table positioning (Kettridge et al., 2019; Kettridge et al., 2015). For example, severe burning has been shown to increase post-fire evapotranspiration by 410% in a feather moss peatland (Kettridge et al., 2019). In this example, fires triggered an overriding of the stability mechanisms within peat that would usually reduce post fire evaporation, consequently leading to extensive drying and exposure of carbon stocks to decomposition (Kettridge et al., 2019). Alterations to the hydrological conditions of peatlands can lead to vegetation changes and shifts in the successional trajectories of peatlands.

Peat burning commonly results in bare peat with thin moss layers following fires (Noble et al., 2019). Vegetation recovery post fire can be very slow, with forested peatlands taking upwards of 50 years to recover, and lichen cover taking 35 years to recover to pre fire levels (Gibson et al., 2018). However, the trajectory and speed of vegetation recovery following a peat fire depends on the severity of the fire and the status of the peatland pre-fire. Severe burning has been shown to result in the replacement of mosses with colonising species that thrive on bare soil in Alaska (Nossov et al., 2013). Low severity fires where the organic soil remains relatively intact allow for the re-establishment of preexisting vegetation (Nossov et al., 2013). Similarly, undrained pristine peatlands are more resilient to fires, allowing for the maintenance of a high water table and the reestablishment of moss dominated pre-fire vegetative communities (Kettridge et al., 2015). However, it has been shown that in moderately drained Canadian peatlands, fires can trigger a conversion from moss dominated peatlands, to a shrub or grass ecosystem which results in a loss of the carbon accumulation mechanism in peatlands (Kettridge et al., 2015). Due to the extensive drainage and degradation of northern high latitude peatlands (Zhang et al., 2022), vegetation shifts are common. Over multi-decadal timescales wildfires have resulted in the expansion of shrubs across tundra regions (Mekonnen et al., 2021). Additionally,

40-85% of the areas that have experienced burning in northwest Siberia have seen a vegetation shift from tundra to needleleaf forests in recent decades (Sizov et al., 2021).

Vegetation changes can alter the carbon balance of high latitude ecosystems through plant-soil-atmosphere interactions (Mekonnen et al., 2021). For example, the composition of plant communities influences processes such as nitrogen cycling, plant productivity, decomposition, active layer depths in permafrost environments, snow distribution and surface albedo (Elmendorf et al., 2011). Increased plant productivity, such as through the expansion of shrubs in fire-affected environments, can lead to substantial losses carbon from deep soil layers due to changes in rhizosphere processes, offsetting the carbon accumulated through increases in vegetation, leading to a net carbon loss to the atmosphere (Mack et al., 2004; Parker et al., 2021). The expansion of shrub and woody species, has also been shown to decrease albedo and increase evapotranspiration, leading to a positive feedback effect on climate (Sizov et al., 2021; Loranty and Goetz, 2012). Additionally, increased shrub coverage also has ecological implications such as altered animal habitats (Tape et al., 2016). Therefore, peat fires, through their alterations to hydrological processes, can trigger substantial vegetation changes, further exacerbating carbon loss and altering peatland ecosystem functioning.

In the high latitudes, 50% of peatlands are underlain by permafrost (Hugelius et al., 2020). Additionally, 71% off all fires that occurred in the Siberian Arctic between 1982 and 2020 occurred in regions of continuous permafrost (Descals et al., 2022). Therefore, a high proportion of peat fires in the high latitudes occur on permafrost affected peatlands, and lead to permafrost degradation (Zoltai, 1993; Li et al., 2021). Peat fires result in the direct loss of the organic layer from the soil, with five-fold decreases in the mean thickness of the organic layer being seen in Alaska (Nossov et al., 2013). Following a fire, thermal and geomorphic changes are initiated within permafrost that alter the hydrology and biochemistry of these landscapes (Holloway et al., 2020). For example, permafrost can be exposed to warming resulting in drying, degradation, thermokarst development and further carbon losses (Chen et al., 2021a; Nitze et al., 2018; Li et al., 2021). Post burning, soil temperatures rise, and the active layer thickens (Holloway et al., 2020; Li et al., 2021; Gibson et al., 2018; Smith et al., 2015; Kharuk et al., 2011). Soil temperatures rise as a result of increased ground thermal conductivity and soil heat input (Yoshikawa et al., 2002; Nossov et al., 2013). Consequently, warmer soils following a fire result in a thickening of the active layer by 60% (Gibson et al., 2018), which has been shown to average 0.5m over several years post fire in the Northwest Territories, Canada (Zhang et al., 2015).

Peat fires can also trigger other permafrost disturbances such as talik and thermokarst lake formation, and retrogressive thaw slump development (Nitze et al., 2018; Gibson et al., 2018). In the last 30 years approximately 25% of all thermokarst lake expansion in western Canadian permafrost peatlands can be attributed to wildfires (Gibson et al., 2018). Taliks (continuously thawed soil layers), are formed post fire due to enhanced heat flow through the active layer leading to permafrost thawing

(Brown et al., 2015; Yoshikawa et al., 2002). Increased thawing of permafrost can then lead to subsidence and thermokarst development (Holloway et al., 2020). For example, following the 2007 Anaktuvuk river fire, permafrost thaw subsidence was detected across 34% of the burnt area (Jones et al., 2015). Therefore, wildfires can trigger substantial landscape scale changes in permafrost peatlands, which result in more carbon being lost.

The effects of fires on peatland and permafrost landscapes have long lasting impacts on the CO_2 and CH_4 emissions from these environments. For example, Koster et al. (2018) show that fire effected permafrost peatlands are sources of CO_2, with elevated CO_2 emissions continuing for over 50 years following a fire. Additionally, it has been shown that wildfire effects on permafrost lead to long-term increases in thaw depth (Rocha et al., 2012), lasting upwards of 30 years (Gibson et al., 2018). Therefore, it can take decades to centuries for fire disturbed permafrost to return to pre-fire conditions (Li et al., 2021). With shortening fire return intervals and increasing fire severity as a result of climate change, it is expected that these impacts will only further be exacerbated (Li et al., 2021), accelerating permafrost thaw (Zhang et al., 2015).

From all the above, it is evident that peat fires and their impacts play a crucial role in the carbon balance within the Earth system, highlighting the importance of representing peat fire processes within Earth system models, to be able to assess their current and future impacts on both the climate and ecosystems.

5. Tropical peat fires

Whilst this thesis will focus on the peatlands and peat fires of the northern high latitudes, tropical peat fires provide useful knowledge on the extent and impacts of peatland burning and help in contextualising the global picture of peatland burning. Undisturbed tropical peatlands tend to have high soil moisture as a result of abundant rainfall, and understory microclimates (Kelly et al., 2014), and therefore they tend to be fire resistant (Turetsky et al., 2015). However, extensive human driven land use change including plantation development, logging, and agriculture have resulted in peatlands becoming more vulnerable to fires (Langner and Siegert, 2009; Turetsky et al., 2015; Loisel et al., 2020). Additionally, increasing presence of drought like conditions in the tropics increases the vulnerability of tropical peat to burning (Loisel et al., 2020; Dadap et al., 2019). For example, in southeast Asia, peat fires are driven by El Niño induced drought conditions which exacerbate favourable fire conditions, resulting in large burnt areas (Hirano et al., 2006; Atwood et al., 2016). In Borneo between 1997 and 2006, prolonged droughts because of El Niño resulted in annual burnt areas three times greater than in non-El Niño effected years (Langner and Siegert, 2009). For example, the 1997 El Niño event led to 2.44 M ha of peat burning in Indonesia, releasing between 0.81 and 2.57 Gt C, equivalent to 13-40% of global annual carbon emissions from fossil fuel burning at that time (Page

et al., 2002). Similarly, very strong ENSO conditions in 2015 led to large fires across Indonesia and southeast Asia (Atwood et al., 2016; Roulston et al., 2018).

Tropical peat fires tend to burn much larger areas than high latitude fires, with an average burnt area reported by Santoso et al., (2019a) from tropical peat fires being nearly 600% larger than boreal peat fires at 8378 km^2. Tropical peat fires have also been shown to burn much deeper than boreal, at 43cm compared to 12cm (Santoso et al., 2019a). The carbon emission flux from tropical peat fires is also much larger than high latitude peat fires, with Canadian boreal peatlands emitting on average 2.1 kg C m^{-2} (Benscoter and Wieder, 2003), whereas tropical peat fires are estimated to emit an average of 28 kg C m^{-2} (Santoso et al., 2019), but can be as much as 31.5 kg C m^{-2}, which was estimated from the 1997 Indonesian peat fires (Page et al., 2002). Combustion efficiency is similar between tropical and boreal peat fires; however, the relative amounts of different gaseous and particulate emissions vary significantly (Hu et al., 2018). Tropical peat fires emit approximately 42% more CO_2 compared to boreal and temperate peat fires, as well as emitting more CO, CH_4, HCN and NH_3 (Hu et al., 2018). Higher CO_2 emissions from tropical peat is due to tropical peat having a higher carbon content, at approximately 56% compared to a carbon content of 44% in boreal and temperate peat (Hu et al., 2018). In contrast boreal and temperate peat fires emit larger quantities of $PM_{2.5}$, and in particular organic carbon, than tropical peat fires (Hu et al., 2018).

Much like high latitude peat fires, emissions from tropical peat fires can have large effects on air quality across the tropics. In 1997, peat fires in Indonesia accounted for 17% of total annual global fire $PM_{2.5}$ emissions (Roulston et al., 2018). Smoke plumes from the 2015 southeast Asia peat fires resulted in persistent pollution across much of Asia in September and October (Field et al., 2016), leading to an estimated 100,000 premature deaths (Koplitz et al., 2016). The 2015 Indonesian peat fires also led to high $PM_{2.5}$ emissions, with an estimated 95% of Indonesia $PM_{2.5}$ emissions in 2015 due to peat burning (Wooster et al., 2018).

Future drivers of peat fires also vary significantly between tropical and high latitude peatlands. In the tropics, peatlands are being damaged and drained as a result of anthropogenic activities and are increasingly threatened by human ignitions (Turetsky et al., 2015). Whereas in higher latitudes peatland drying and increased lightning ignitions are driving increasing peat fire incidences (Turetsky et al., 2015). Modelling human fire use and processes is a challenge in global fire modelling (Perkins et al., 2022; Teixeria et al., 2023). Recent advancements have been made, such as through the introduction of agent-based models of human fire use (Perkins et al., 2022), but at present humans remain a challenge in accurately modelling fires. Therefore, by initially focusing on high latitude peat fires, where anthropogenic factors play a much smaller role, potential errors can be reduced.

6. Impacts of climate change on high latitude peat fires

Peatlands are becoming increasingly vulnerable to fires (York et al., 2020). The Arctic is currently warming at twice the rate of the global average (Bruhwiler et al., 2021). This alongside decreased precipitation can lead to earlier snow melt and increased water deficits, thus increasing peatland vulnerability to fires and larger burnt areas (Talucci et al., 2022). Land use change, drainage, agriculture, and logging are also increasing peatland vulnerability (Rein, 2015; Langner and Siegert, 2009). Coincidently, lightning frequency has increased substantially in the high latitudes (Veraverbeke et al., 2017), alongside an expansion of human populations and activities into the high latitudes (Bartsch et al., 2021). Increasing lightning and human ignitions, combined with amplified peatland vulnerability to wildfires is resulting in an increase in fire activity across the high latitudes (McCarty et al., 2021) and risks switching high-latitude peatlands from fire resistant systems to fire prone systems (Turetsky et al., 2015). For example, 2019, 2020 and 2021 saw the largest fire years on record in northeastern Siberia, driven by increased summer temperatures, earlier snow melt and greater plant water stress (Descals et al., 2022; Scholten et al., 2022).

Climate change is expected to amplify the vulnerability of peatlands to wildfires through rising temperatures, increased frequency, and intensity of droughts, and increases in fire weather (Thompson et al., 2019; Descals et al., 2022; Lund et al., 2023). Climatic warming of between 1 and 4°C is expected to lead to a doubling in the number of days with a moderate or higher fire weather index (FWI) across Canada (Lund et al., 2023). Lightning strikes in the high latitudes are expected to increase by 112% by 2100 (Chen et al., 2021a), giving rise to increases in burned area of more than 100% (Krause et al., 2014). In addition, increased frequency and intensity of droughts are expected to result in a six-fold increase in fire activity and a five-fold increase in fire size with fires occurring in previously fire-resistant environments (Thompson et al., 2019). Furthermore, under high emissions scenarios, it is estimated that fire spread days could increase by upwards of 50% (Wang et al., 2017). As a result, peat fires are expected to increase in frequency and severity (McCarty et al., 2021; Turetsky et al., 2015; Nelson et al., 2021). For example, a doubling in burnt area in the Alaskan tundra is expected by the end of the century (Hu et al., 2015). Additionally, increasing temperatures in the Siberian Arctic have been shown to substantially increase burnt area, with fires expected to be burning 2.5 M ha and releasing 37.8 Tg C each year by 2050 (Descals et al., 2022).

Peat fires result in a net loss of carbon (Lasslop et al., 2019). Therefore, increased fire occurrence and severity can lead to greater carbon emissions from fires and may result in a positive feedback loop with the climate system, and potentially a catastrophic loss of carbon from the northern high latitudes (Mack et al., 2011; Chen et al., 2021a; Turetsky et al., 2015; Nelson et al., 2021). Fire return intervals are expected to shorten as a result of climate change (Li et al., 2021). Even over the recent historical period, the duration of fire return intervals in northern Siberia has halved since the $16^{th}/18^{th}$ century

(Kharuk et al., 2011). If fire return intervals in Canada are reduced to 61 years, then peatlands would be converted to a net carbon source (Wieder et al., 2009). This means that by the end of the century, peatlands could switch from a carbon sink to source (Wilkinson et al., 2023; Walker et al., 2019). Current estimates suggest a reduction in the size of the peatland carbon sink by 57% by 2050, if current trends in burning continue, directly as a result of peatland burning (Wilkinson et al., 2023).

7. Thesis outline

This thesis aims to expand the current body of knowledge on the role of northern high latitude peat fires within the Earth system. This will primarily be achieved through a novel parameterisation of peat fires in the INFERNO global fire model, which allows for the assessment of present-day peat burnt area and carbon emissions and allows for the quantification of potential future changes to peat fires under different climate change scenarios. In addition, the impacts of northern high latitude wildfires and peat fires on atmospheric composition and air quality data will be assessed using the most up-to-date Earth observation products.

Chapter 2 will detail the experimental methodologies utilised throughout this thesis. Primarily chapter 2 details the development and recent progress in fire modelling, but highlights the current deficiencies in fire models, stemming from a lack of peat fire representation. Consequently, INFERNO and the new peat fire parameterisation I developed as part of this thesis are explained. Crucially, the development of a new peat fire model requires evaluation against state-of-the-art Earth observation products. Therefore, Chapter 2 also details the different observational datasets available for model evaluation and explains current limitations to these products. The experimental methodologies that utilise INFERNO-peat for simulating present day burning in Chapter 3 and future burning in Chapter 5 are briefly outlined. Finally, Chapter 2 explores the use of Earth observation products for assessing the impact of peat fires on atmospheric composition and air quality, and the current performance of these products.

The lack of representation of peat fires within fire models has been cited as a potential cause of the tendency of fire models to underestimate burning in the high latitudes and failure to capture the interannual variability (IAV) in carbon emissions (Mangeon et al., 2016; Teixeria et al., 2021; Li et al., 2013). Therefore, Chapter 3 utilises the newly developed INFERNO-peat to demonstrate the importance of explicitly representing northern high latitude peat fires within fire models, and the significant effect that peat fires have on burnt area and subsequent carbon emissions. INFERNO-peat is evaluated against a suite of Earth observation-based datasets. However, key deficiencies in Earth observation-based detections of peat fires are noted (McCarty et al., 2021), which provides challenges for the evaluation of peat fire models. The analysis presented throughout Chapter 3 and the development of INFERNO-peat detailed in Chapter 2 Section 3 is published in Blackford et al., (2024).

To date there is no global, or high latitude, dataset of observed peat fires, therefore, Chapter 4 explores the potential for detecting peat fires from the Global Fire Emissions Database v5 (GFED5: Chen et al., 2023b). Chapter 4 also capitalises on these potential peat fire observations to analyse the effects of peat fires on atmospheric composition and air quality, using measurements from the Tropospheric Monitoring Instrument (TROPOMI; Veefkind et al., 2012) onboard the Sentinel-5p satellite and the multiple satellite sensors assimilated into the Copernicus Atmospheric Monitoring Service (CAMS) reanalysis (CAMSRA) dataset (Innes et al., 2019). To date, many studies have analysed the atmospheric composition and air quality effects of specific high latitude fire events (e.g. Huang et al., 2009; Teakles et al., 2017; Konovalov et al., 2011; Lavoue and Stocks, 2011). However, minimal research on the large-scale trends and impacts has been undertaken. Therefore Chapter 4 aims to determine regional, broad time scale effects of peat fires on atmospheric composition and air quality, in order to lead to an improved representation of the effects of peat fires within global fire models. Primarily, the impacts of fires and peat fires on concentrations of NO_2 and CO are studied due to the dominance of smouldering combustion during peat fires which should result in higher emissions of CO relative to NO_2 (Andreae and Merlet, 2001; Rein et al., 2009; Andreae, 2019; van der Velde et al., 2021). Consequently, the impacts of burning on ratios of NO_2:CO are assessed, with the potential of being able to use differences in these emissions ratios to differentiate between peat vs non peat burning. Additionally, $PM_{2.5}$ concentrations and the influence fires have upon them are also studied within the context of air quality and human health.

The northern high latitudes are undergoing rapid anthropogenic climate change (IPCC, 2013; Bruhwiler et al., 2021), which is expected to increase the vulnerability of peatlands to wildfires (York et al., 2020; Talucci et al., 2022). Consequently, large increases in the frequency, extent, and severity of peat fires are anticipated over the coming century (McCarty et al., 2021; Turetsky et al., 2015; Nelson et al., 2021). Therefore, Chapter 5 explores the use of INFERNO-peat to simulate potential future peat fire trajectories under different climate change scenarios. Three SSP scenarios, which describe different potential socioeconomic pathways and their associated climatic changes over the 21st century are used. Under these scenarios the potential changes to peat burnt area and carbon emissions can be estimated and provide an insight into the devastating consequences of uncontrolled anthropogenic climate change.

Finally, Chapter 6 discusses the general summary and conclusions that can be taken from the body of work presented in this thesis. The importance of parameterising peat fires in global fire models is emphasised, both in terms of improving model abilities to simulate present day burning and providing more realistic estimates of future fire regimes in the northern high latitudes. The impacts peat fires have on atmospheric composition and air quality are also discussed in detail. Additionally, the lack of robust observation-based peat fire datasets is highlighted as a key issue in peat fire research both in terms of evaluating peat fire models and in being able to assess the impacts of peat fires. The potential

climate change induced changes in peat fires in the northern high latitudes are also discussed, alongside the potential implications this may have on the carbon cycle, atmospheric composition, air quality and climate. Finally, potential future avenues for further research are explored, including further INFERNO-peat model developments and the potential for developing observation-based peat fire datasets, based on the insights gained in this thesis.

Chapter 2: Methodologies

With the view to improving fire modelling capabilities and the scientific understanding of the impacts of peat fires on atmospheric composition, air quality, the carbon cycle and the climate system, this thesis is focused upon the development of INFERNO-peat (Section 3). INFERNO-peat is a novel peat fire parameterisation for the northern high latitudes, used to assess present day peat burning (Section 4) and potential future changes to peat fires (Section 5). Therefore, fire modelling fundamentally underpins this thesis, and consequently this chapter will begin by exploring the history and development of fire modelling, focusing on the INFERNO global fire model, and in particular the current deficiencies in many models, which could be improved through the representation of peat fires (Section 1 and 2). Subsequently, Sections 4 and 5 describe the experimental set up for using INFERNO-peat to model present day and future peat burnt area and carbon emissions. Accurate fire models rely heavily on the availability of robust observational datasets. Consequently, this chapter will also explore the use of Earth observation products to detect and monitor fires around the globe, and the limitations many of these products have in the northern high latitudes (Section 6). Finally, remotely-sensed data on atmospheric composition and air quality is also evaluated, and its use in being able to analyse the large scale impacts of peat fires in the high latitudes is assessed (Section 7 and 8).

Throughout this thesis the term "peat" is used to describe all organic fuel accumulated belowground that burns as smouldering. Common definitions of peatlands require 20-50cm of peat depth, however these were largely informed by agricultural considerations (UNEP, 2022a). However, it is thought that shallow peatlands are crucial for assessing the complete role of peatlands in the Earth system, due to the considerably larger peatland area which shallow peatlands cover globally (UNEP, 2022a). As climate impacts form a large part of this thesis, depth-based definitions of peat were not used, and instead all fuel that has accumulated belowground is considered peat and can potentially burn by smouldering combustion.

1. Fire modelling

Progress in representing fires in Dynamic Global Vegetation Models (DGVMs) and Land Surface Models (LSMs) have improved the ability to model not only present day burning but also fire regime changes in the future, allowing for predictions on the magnitude and geographical patterns of future fire impacts (Hantson et al., 2016). Modelling fires and their emissions within DGVMs began in the early 2000s and has rapidly progressed over the last two decades (Hantson et al., 2016; Li et al., 2019), a development partly driven by the need for representing fire in Earth system models used for understanding and predicting climate change. Globally, fire models have been used to aid fire management, estimate trends and patterns in burnt area and to help assess drivers of wildfire patterns (Yang et al., 2014a). Fire models have also been used to examine future changes to fire regimes under

global climate change (Rabin et al., 2017). In general, there are two types of global fire models, empirical top-down models and bottom-up process-based models (Hantson et al., 2016). Recent work has also shown the feasibility and efficiency of using ensemble machine learning models of fire, in understanding contemporary fire regimes (Zhang et al., 2023).

Empirical fire models are based on statistical relationships between environmental variables and fire regimes (Hantson et al., 2016). The Global FIRe Model (Glob-FIRM) was the first global fire model, which is commonly coupled with the LPJ-GUESS DGVM (Thonicke et al., 2001; Hantson et al., 2020). Glob-FIRM calculates daily fire probability using litter moisture and uses a statistical relationship between the length of the fire season and area burned to estimate annual burnt area (Thonicke et al., 2001; Rabin et al., 2017). Since the development of Glob-FIRM, other relatively simple empirical fire models have been developed, including INFERNO and SIMFIRE-BLAZE (Hantson et al., 2020). INFERNO (INteractive Fire and Emissions algOrithm for Natural envirOnments) is based on a calculation of PFT flammability utilising vapour pressure deficit, precipitation, soil moisture and fuel loads, combined with PFT average burnt area in order to estimate grid cell burnt areas and subsequent emissions (Mangeon et al., 2016). Meanwhile, SIMFIRE estimates annual burnt area based on fire weather, fuel continuity, human population density and PFT fire resistance (Rabin et al., 2017; Knorr er al., 2016a). Therefore, empirical models represent relatively simple ways of modelling global fire regimes, which have been shown to accurately diagnose burnt area and subsequent emissions around the world (Hantson et al., 2020).

Process-based models are more complex than empirical models, as they simulate small scale fire dynamics, which are then scaled up to get an overall picture of burning within a grid cell (Hantson et al., 2016). MC-FIRE was the first attempt to simulate fires globally, using a process-based rate-of-spread model coupled to a DGVM (Hantson et al., 2016; Lenihan et al., 1998). However, substantial further development of process-based models has occurred since then. For example, The SPread and InTensity of FIRE model (SPITFIRE) is a rate of spread based fire model, which has been coupled with numerous DGVMs including ORCHIDEE and LPJ-GUESS (Yue et al., 2014; Thonicke et al., 2010). SPITFIRE calculates daily potential ignitions based on lightning and human activity, which is combined with a fuel moisture derived fire danger index to get daily fire numbers (Yue et al., 2014; Thonicke et al., 2010). Fire size is then calculated as a product of fire spread rate, using the Rothermel equation (Rothermel, 1972), and active burning time (Yue et al., 2014; Thonicke et al., 2010). The Community Land Model (CLM) is also a process-based approach to modelling fires, focusing on fire occurrence, spread and impacts (Li et al., 2013). CLM is part of the Community Earth System Model (CESM) and differs to other fire modelling approaches as it also models agricultural, deforestation and peat burning (Li et al., 2013), processes which are commonly not accounted for in fire models. However, despite their added complexity, process-based models do not perform better than empirical models on a global scale (Hantson et al., 2020).

In general, fire models broadly reproduce, on a global scale, annual total burnt area and fire emissions. For example, fire models in the Fire Modelling Intercomparison Project (FireMIP) simulate total burnt area that largely falls within the range of observational uncertainty (Hantson et al., 2020). Additionally, most models also simulate present day global total fire emissions within the range of satellite-based products (Li et al., 2019). However, fire models do not completely reproduce observed patterns of burnt area (Jones et al., 2022), in particular in the high latitudes (Kantzas et al., 2013). Fire models also struggle to represent interannual variability in both burnt area and carbon emissions (Hantson et al., 2020; Li et al., 2019). Furthermore, they differ on how they represent trends in burning since the early 20th century, largely due to the representation of anthropogenic ignitions and suppressions (Teckentrup et al., 2019; Andela et al., 2017).

The failure of fire models to reproduce observed spatial patterns of burnt area and carbon emissions, and in particular the interannual variability in these, has been attributed to a lack of representation of peatland burning in them (Li et al., 2013; Mangeon et al., 2016; Teixeria et al., 2021). The necessity for accurately representing fire regimes is particularly important in the high latitudes, to be able to examine the links between permafrost and fire, in order to assess the consequences of fire-induced permafrost changes on climate change and ecosystems (Kantzas et al., 2013). Therefore, explicit parameterisation of peat fires in fire models may improve the representation of burning in the high latitudes, allowing for more accurate predictions of future changes to, and impacts of, high latitude fires.

1.1. Peat fire modelling

Despite the importance of peat fires, they are currently not explicitly incorporated into most fire models, meaning that important climate and carbon feedbacks cannot be accurately assessed. As previously mentioned, the absence of peat fires is a limiting factor in model ability to reproduce present day burning and capture interannual variability in burnt area and carbon emissions (Mangeon et al., 2016; Teixeria et al., 2021). Therefore, at present the capacity of fire models to predict future fire activity is limited (Jones et al., 2022). Peat fire representation in models is also key to accurately representing the northern peatland carbon balance in Earth system models (Wilkinson et al., 2023). As the Arctic is undergoing substantial climatic and environmental change, it is also crucially important that Earth system models are able to capture Arctic fires and their environmental and climatic drivers in order to assess the interactive effects between fires and climate in the Arctic (Irannezhad et al., 2020).

At present, the Community Earth System Model (CESM) is the only model to represent peatland burning through its fire / land surface model CLM-Li (Li et al., 2013). In the CESM approach, burnt area due to peat fires in both tropical and boreal environments is estimated through the fractional coverage of peat in a grid cell, a climatic effect (effected by long term precipitation and temperatures),

and the fraction of the grid cell with a water table at the surface or higher (Li et al., 2013). Whilst the CESM approach was a major step forward, it is limited by the fact that it does not consider the effects of soil properties on peat fires (Li et al., 2013). CLM estimates that approximately 6% of total global fire emissions are due to peat fires (Li et al., 2013).

Therefore, the main aim of this thesis is to develop a parameterisation of peat fires into the INFERNO fire model. This process will be detailed throughout Chapter 2 section 3and Chapter 3, with the goal of being able to simulate future changes in fires in the high latitudes (chapter 5).

2. The INFERNO fire model

The INteractive Fire and Emission algoRithm for Natural envirOnments (INFERNO) is a reduced complexity empirical fire model, that is part of the Joint UK Land Environment Simulator (JULES) land surface model (Mangeon et al., 2016; Burton et al., 2019). Put simply, INFERNO estimates burnt area for different plant functional types (PFT) through lightning and population density estimated ignitions, a calculation of PFT flammability, and heuristically determined average burnt areas for each PFT (Mangeon et al., 2016, Figure 5).

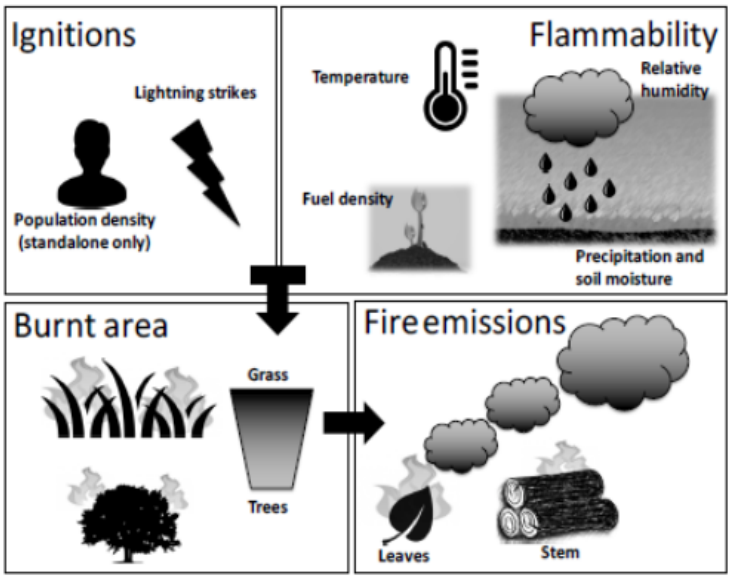


Figure 5: Schematic of the INFERNO fire model from Mangeon et al. (2016).

Burnt area is calculated per PFT in INFERNO through ignitions, PFT flammability and PFT average burnt area. Ignitions are calculated through one of three different modes (Mangeon et al., 2016). Firstly, mode 1 assumes constant ignitions of 1.67 ignitions km^{-2} $month^{-1}$, split into 1.5 ignitions km^{-2} $month^{-1}$ from human activities, and 0.17 ignitions km^{-2} $month^{-1}$ from cloud-to-ground lightning strikes. Alternatively, mode 2 continues to use constant human ignitions and suppressions, whilst natural lightning ignitions are allowed to vary through the use of a lightning climatology dataset (LIS-OTD). The final ignition mode (3) uses varying natural ignitions (I_N) and varying human ignitions. Anthropogenic ignitions (I_A) are calculated based on population density (Equation 1).

Equation 1

$$I_A = k(PD)PD\alpha$$

PD reflects population density in people km^{-2} and is obtained from the HYDE dataset (Hurtt et al., 2011). *k(PD)* is a function that represents the varying anthropogenic influence on fire ignitions in rural and urban environments as $6.8 \times PD^{-0.6}$. Parameter α is set as equal to 0.03 and represents the number of potential ignitions per person per month per km^2. The fundamental relationship underlying the calculation of human ignitions is based on the idea that increasing human population density increases fire frequency up to around 0.1 people per km^2, after which increasing population density results in decreases in fire frequency (Knorr et al., 2014). INFERNO also considers the capability for humans to supress both natural and anthropogenic ignitions with the fraction of fires not supressed calculated following Equation 2.

Equation 2

$$f_{NS} = 7.7(0.05 + 0.9 \times e^{-0.05PD})$$

A scaling factor of 7.7 calibrates the number of fires to MODIS observations (Pechony and Shindell, 2009; Mangeon et al., 2016). Total ignitions (I_T) are calculated by Equation 3.

Equation 3

$$I_T = (I_N + I_A)f_{NS}$$

How INFERNO treats human ignitions is likely overly simplistic, and improvements in the representation of humans are required, potentially through recent approaches that have accounted for the Human Development Index (HDI; Teixeria et al., 2023) or on agent-based modelling (Perkins et al., 2022).

Flammability is calculated from saturation vapour pressure (e^*) and its temperature (T) dependence following the Goff-Gratch equation (Goff and Gratch, 1946), fuel load index (FL), relative humidity (RH), precipitation (R), and soil moisture (θ) (Equation 4; Mangeon et al., 2016), and reflects an adaptation of the scheme proposed by Pechony and Shindell (2009). Fuel load index (FL_{PFT}) is estimated as the PFT-specific leaf carbon (aboveground) and the belowground soil carbon from the decomposable plant material (DPM) within JULES (Mangeon et al., 2016). Consequently, the PFT specific flammability (F_{PFT}) is calculated following Equation 4, depending on relative humidity (RH).

Equation 4

$$F_{PFT} = \begin{cases} e^* e^{-2R} FL_{PFT}(1-\theta) & for\ RH_{up} < RH \\ e^* \frac{RH - RH_{low}}{RH_{up} - RH_{low}} e^{-2R} FL_{PFT}(1-\theta) & for\ RH_{low} < RH < RH_{up} \\ 0 & for\ RH_{low} > RH \end{cases}$$

Low and high thresholds are used for RH (RH_{low} = 10%, RH_{up} = 90%) to allow for the influence of RH to scale between 0 and 1. Depending on RH, PFT flammability is calculated using the previously calculated saturation vapour pressure and fuel load index combined with soil moisture, which is here defined as the unfrozen soil moisture as a fraction of saturation.

Burnt area (BA) is then estimated based on PFT flammability and ignitions, alongside a heuristically determined average burnt area for each PFT ($\overline{BA_{PFT}}$) (Mangeon et al., 2016). Therefore, BA per PFT is calculated following Equation 5:

Equation 5

$$BA_{PFT} = I_T F_{PFT} \overline{BA_{PFT}}$$

Emitted carbon (Kg C m^{-2} s^{-1}) is then estimated based on total burnt area, the carbon stored in the PFTs' leaves or stems, the decomposable plant material and the resistant plant material, and combustion completeness (Equation 6; Mangeon et al., 2016).

Equation 6

$$EC_{PFT} = BA_{PFT} \sum_{leaf,stem}^{i} (CC_{min,i} + (CC_{max,i} - CC_{min,i})(1 - \theta)) C_i$$

CC_{min} and CC_{max} reflect the minimum and maximum combustion completeness for leaves and stems, which scale linearly with soil moisture. C_i represents the carbon stored in each PFT's leaves/stems. C stored within the decomposable plant material and resistant plant material soil pools is shared across the PFTs and included in the estimation of emitted carbon per PFT. PFT specific emissions factors are then used to convert total carbon emissions into emitted species including, CO_2, CO, CH_4, NO_x, SO_2, OC and BC.

More recent work by Burton et al. (2019) added a disturbance term from fire on the dynamic vegetation model within JULES (TRIFFID), allowing for feedback effects of fire on vegetation.

2.1. Current performance of INFERNO

INFERNO has been shown to accurately diagnose global burnt area compared to observational data from the Global Fire Emissions Database (GFED) (Mangeon et al., 2016), and compares well to other fire models on a global scale (Hantson et al., 2020). However, over the northern high latitudes INFERNO fails to capture a significant amount of burnt area, particularly in Canada, Alaska, and Siberia. INFERNO also underestimates carbon emissions and fails to capture the interannual variability in these emissions (Mangeon et al., 2016). Although overall INFERNO can reproduce observed present day fire emissions of CO and aerosols, it underestimates fire emissions in boreal regions (Teixeria et al., 2021). Mangeon et al. (2016) put these underestimates partly down to the lack of representation of peat fires in INFERNO.

Consequently, Chapter 3 explores the benefits of an addition of a peat fire parameterisation into INFERNO (INFERNO-peat).

3. INFERNO-peat

INFERNO-peat is a novel parameterisation of northern high latitude peat fires, which utilises the existing JULES-INFERNO framework, to add additional burnt area and carbon emissions from peatland burning (Blackford et al., 2024). INFERNO-peat is a simplified peat fire model, which is summarised in Figure 6. In summary, INFERNO-peat estimates the number of potential peat fire ignitions by utilising ignitions data from population density and lightning, alongside PFT flammability calculated by INFERNO and PFT fractions from JULES. The probability of those ignitions developing into a peat fire is represented by a parameterisation based on key relationships with soil moisture, inorganic content, and bulk density (Frandsen 1997). The depth of burn in peatlands is also parameterised using critical soil temperature (Lin et al., 2021) and water table depth, with the soil and hydrology simulated by JULES. A parametrisation of peatland carbon emissions was also implemented using calculated peat burnt area, depth of burn and the carbon content existing in the peat (Lin et al., 2021). In the sub-sections below, the individual steps of the peat fire simulation are presented in more detail.

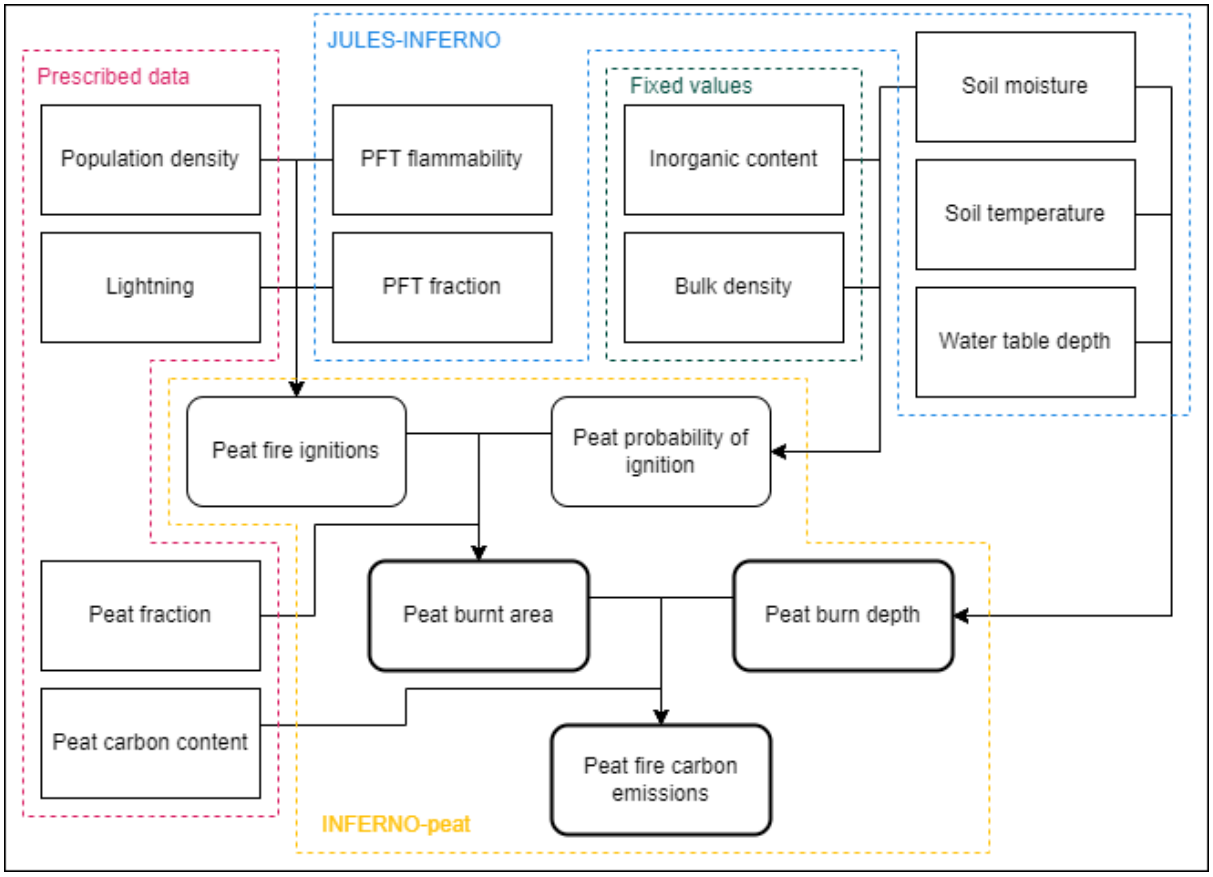


Figure 6: Schematic summarising the new parameterisations introduced as part of INFERNO-peat, the input variables, and their sources.

3.1. Peat fire ignitions (I_{peat})

The majority of peat fire ignitions result from a pre-existing flaming vegetation fire (Rein, 2013). To account for this, peat fire ignitions are based on the number of flaming vegetation fires in a grid cell identified from INFERNO (Equation 7). Here, the third ignition mode of INFERNO is used unchanged from Mangeon et al. (2016) (Equation 1-Equation 3). Total ignitions (I_T) are comprised of human ignitions and suppressions, based on population density, and varying natural ignitions, based on cloud-to-ground lightning strikes (see Section 2 for more details). The flammability of each of the 13 plant functional types (PFTs) represented in JULES is also calculated using the original equations from Mangeon et al. (2016) in INFERNO (Equation 4). Flammability of each PFT ($Flam_{PFT}$) (0-1) is based on key climatic drivers of fires such as temperature, relative humidity, and precipitation, alongside fuel density and soil moisture (Mangeon et al., 2016). From Equation 7, the number of peat fires (I_{peat}) in a particular PFT is given by the flammability ($Flam_{PFT}$) multiplied by the grid cell ignition rate (I_T) and the fraction of the grid cell occupied by that PFT ($Frac_{PFT}$):

Equation 7

$$I_{peat} = \sum_{PFT} I_T \cdot Flam_{PFT} \cdot Frac_{PFT}$$

3.2. Peat probability of ignition ($ProbI_{peat}$)

For each grid cell where peat is located, the probability of ignition of peat is calculated using Equation 8 based on that reported by Frandsen (1997) and used by Purnomo et al. (2020). However, the Frandsen (1997) probability expression, also shown in Figure 7a, was observed in laboratory experiments over 25 years ago and its expression has not been tested since, therefore its ability to capture the probability of a smouldering fire occurring may be limited. However, as it considers the three most important factors that control smouldering combustion: soil moisture, inorganic content and bulk density (Rein, 2013; Rein, 2015; Christensen et al., 2020); it is likely that it still accurately reflects probability of peat fire ignitions in natural peatlands.

Equation 8

$$ProbI_{peat} = \frac{1}{1+\exp(-(B_0+(B_1 \cdot SM)+(B_2 \cdot IC)+(B_3 \cdot \rho)))}$$

The probability of a peat fire igniting and spreading depends on the peatland soil moisture (*SM*) (dry moisture content %), inorganic content (*IC*) (%) and bulk density (ρ) (kg/m^3). Soil moisture is the most important variable affecting the ignition and spread of peat fires (Rein, 2013; Rein 2015). Here, soil moisture and probability of ignition exhibit a reverse sigmoid curve, where the likelihood of peat igniting is high at low SM and low at high SM (Frandsen, 1997; Figure 7a). For this initial approach, fixed values are utilised for *IC* and ρ of 9.4% and 222kg/m^3 respectively (Frandsen, 1997), due to a lack of robust observational datasets of peatland-specific IC and BD on a global scale, and to avoid adding additional sources of uncertainty into the model. The use of fixed values of IC and BD

represents a key limitation in INFERNO-peat as it is known that IC and BD vary greatly across northern high latitude peatlands (Loisel et al., 2014; Chambers et al., 2011). Therefore, average IC and BD values may not be representative of all peat in the northern high latitudes. Consequently, variations in peat ignition probability that stem from variable IC and BD are not being captured within INFERNO-peat at present. B values represent constants identified by Frandsen et al. (1997), where B_0 = -19.8198, B_1 = -0.1169, B_2 = 1.0414, B_3 = 0.0782.

3.3. Peat burnt area (BA_{peat})

Calculating burnt area from peat fires uses a similar approach to how PFT burnt areas are calculated in JULES (Mangeon et al., 2016; Equation 5). In INFERNO, average burnt area values for each PFT were heuristically determined (Mangeon et al., 2016). Here, an average peat burnt area ($\overline{BA_{peat}}$) was obtained from Santoso et al. (2019a), who estimated an average peat fire burnt area, depth, and emitted carbon for boreal peat fires reported from field studies between 1983 and 2015. For use in INFERNO-peat, anomalously large values reported from Santoso et al. (2019a) were omitted from the average. Therefore, an average peat burnt area of 381.7km^2 was used. The peat burnt area is then calculated following Equation 9, where BA_{peat} (peatland burnt area in km^2) results from combining I_{peat}, $Comb_{peat}$, $\overline{BA_{peat}}$ and grid cell peatland fraction ($Frac_{peat}$).

Equation 9

$$BA_{peat} = I_{peat} \cdot Comb_{peat} \cdot \overline{BA_{peat}} \cdot Frac_{peat}$$

3.4. Depth of burn (BDpeat)

Depth of burn (m) resulting from a peat fires is estimated through an adaptation of the scheme used by Lin et al. (2021). The critical soil temperature (T_{crit}) (°C), which represents the minimum environmental temperature that can sustain a smouldering fire in peatlands, is estimated from the moisture content (SM) (%) of the soil (Lin et al., 2021; Equation 10). Lin et al. (2021), identified a linear relationship between T_{crit} and SM, with increasing SM increasing the T_{crit}, which allows dry peat to burn at extremely low temperatures (Figure 7b). It is important to note that the calculation of depth of burn relies heavily on the expression of critical temperature as a function of soil moisture. Consequently, errors in this relationship would result in limitations in the ability of INFERNO-peat to model depth of burn in peatlands.

Equation 10

$$T_{crit} = (42 \times SM) - 28$$

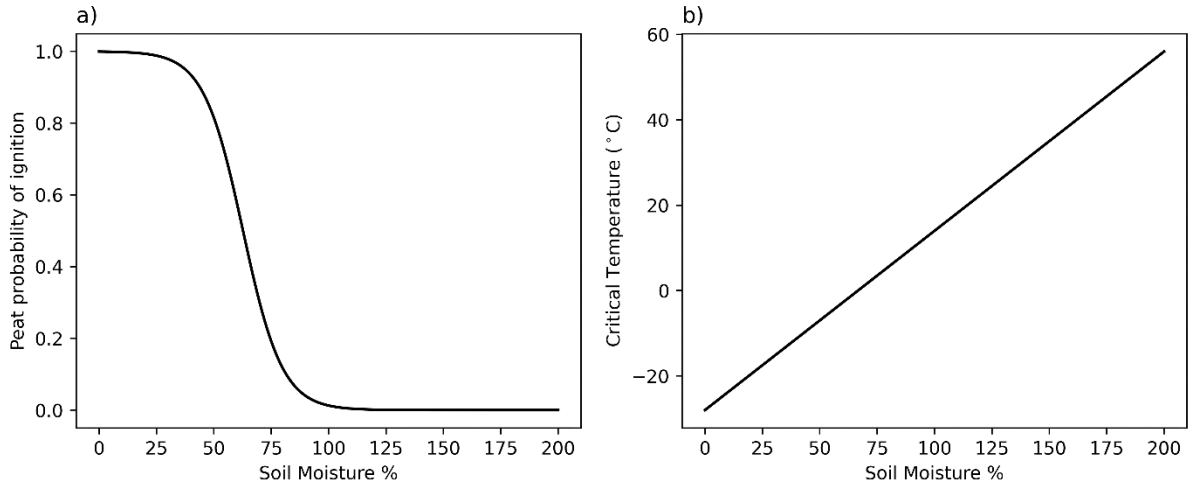


Figure 7: Relationship between soil moisture and a) peat probability of ignition and b) critical temperature.

INFERNO-peat uses outputs of soil temperature from JULES to then locate at what depth within the soil column T_{crit} is reached. We then assume that a peat fire will burn to this depth, or the depth of the water table (zw) if that is higher. A maximum depth of burn (BD_{max}) of 40cm is used in INFERNO-peat, meaning that no fire can burn deeper than 40cm into the soil. Field studies conducted across the high latitudes have shown that peat fires burn on average the top 5 to 20cm of the soil (Turetsky et al., 2011b; Walker et al., 2020; Santoso et al., 2019a; Lukenbach et al., 2015; Hokanson et al., 2016; Wilkinson et al., 2018; Davies et al., 2013). Although some lab-based studies have shown the possibility of peat burning up to 1m into the soil (Qin et al., 2023), only 7.4% of the 905 sites studied by Walker et al. (2020) showed burning deeper than 20cm, with the maximum value recorded being 34.2cm. Therefore, capping burn depth at 40cm, should still capture the variation seen in burning across the high latitudes whilst preventing unrealistically deep burning.

3.5. Carbon emissions

Total emitted carbon from a peatland burning is calculated using Equation 11, and reflects common carbon emission calculations (Lin et al., 2021; Che Azmi et al., 2021; Hu et al., 2018). Total emitted carbon from peat fires (EC_{peat}) is obtained from peat burnt area (BA_{peat}) the depth of burn (BD_{peat}), a combustion completeness (CC) value, and the carbon content of the peat in that grid box (C_{peat}). A combustion completeness of 0.8 is used here, which was selected through a sensitivity analysis (Chapter 3 section 2). On average, data from field studies collated by Walker et al. (2020), showed that on average the proportion of total C burnt that is attributed to below ground carbon is 0.866. Similarly, smouldering combustion is often cited as having a combustion completeness of less than 0.9 (Wiggins et al., 2021; Urbanski et al., 2014). Whilst the selected CC value is close to what is reported from field and lab studies, it may not actually reflect the proportion of carbon that gets released in the atmosphere during burning. Therefore the CC value acts as a calibration factor for the calculation of carbon emissions.

Equation 11

$$EC_{peat} = BA_{peat} \times BD_{peat} \times C_{peat} \times CC$$

4. Experimental set up for simulating present day peat fires using INFERNO-peat

For the results presented in Chapter 3, INFERNO-peat was run as an offline model using Python version 3.8, requiring output files from JULES and INFERNO, alongside prescribed datasets. A brief description of the experimental set up and evaluation protocol is outlined here, with a full justification in Chapter 3 Section 2. JULES-INFERNO calculated PFT fractions and flammabilities were obtained from a TRENDY (Trends in net land atmosphere carbon exchange model intercomparison project) JULES simulation, at JULES vn5.4 using the TRIFFID (Top-down Representation of Interaction of Foliage and Flora Including Dynamics) dynamic vegetation model. For the soil variables that are used in calculations of peat probability of ignition and depth of burn, an experimental JULES run, which utilises new peat module developments (JULES-peat; Chadburn et al., 2022), and assumes that all soils north of 50°N are organic (rather than mineral as in standard JULES) was used. JULES-peat therefore gives a better representation of northern peatland soil physics and dynamics. Full reasoning for the use of JULES-peat is detailed in Chapter 3 section 2. Static population density data from the HYDE dataset (Hurtt et al., 2011) were used to calculate human ignitions and suppressions of fires using Equation 1 and Equation 2. In order to estimate natural ignitions from lightning data, INFERNO-peat was run with two datasets. Firstly, as in the original INFERNO (Mangeon et al., 2016), I used a monthly lightning climatology from LIS-OTD (Lightning Imaging Sensor – Optical Transient Detector) (Christian et al., 2003). However, a lightning climatology does not represent year to year variation in lightning and therefore could contribute to inaccuracies in the model. Consequently, we also used the WGLC (Worldwide Lightning Location Network – WWLLN – Global Lightning Climatology and time series) lightning time series produced by WWLLN covering 2010–2020 for comparison (Kaplan and Lau, 2021).

As previously mentioned, fixed values were used for inorganic content and bulk density, of 9.4% and 222kg/m^3 respectively. These values were obtained from Frandsen (1997) and are representative of values recorded in field studies across the northern high latitudes (Chambers et al., 2011; Loisel et al., 2014). Similarly, prescribed values for maximum depth of burn and combustion completeness of 0.4m and 0.8 are used in INFERNO-peat. These values were selected through a sensitivity analysis, the results of which can be found in Chapter 3 Section 2.

Gridded peatland fractions and their respective carbon contents were prescribed to the model from the Northern Peatland Dataset (Hugelius et al., 2020). The Northern Peatland Dataset (NPD) was developed based on data from more than 7,000 peat cores and a machine learning approach for the

Northern Hemisphere (>23° latitude) (Hugelius et al., 2020). Hugelius et al. (2020), estimated that peatlands cover 3.7 million km^2 of the northern hemisphere, with large deposits in Canada and across Siberia (Figure 8a). This is similar in extent to that previously reported (Yu, 2012; Loisel et al., 2014), but over 1 million km^2 more than the PEATMAP dataset (Xu et al., 2018). NPD was used in the present-day simulations of peat fires in the current thesis, as it also contains information of peatland C and N stocks, peat depth, and the presence of permafrost. The NPD estimates that high latitude peat stores 415 Pg C, notably in northwest Canada, the Hudson Bay Lowlands, and the Great Vasyugan Mire (Figure 8b).

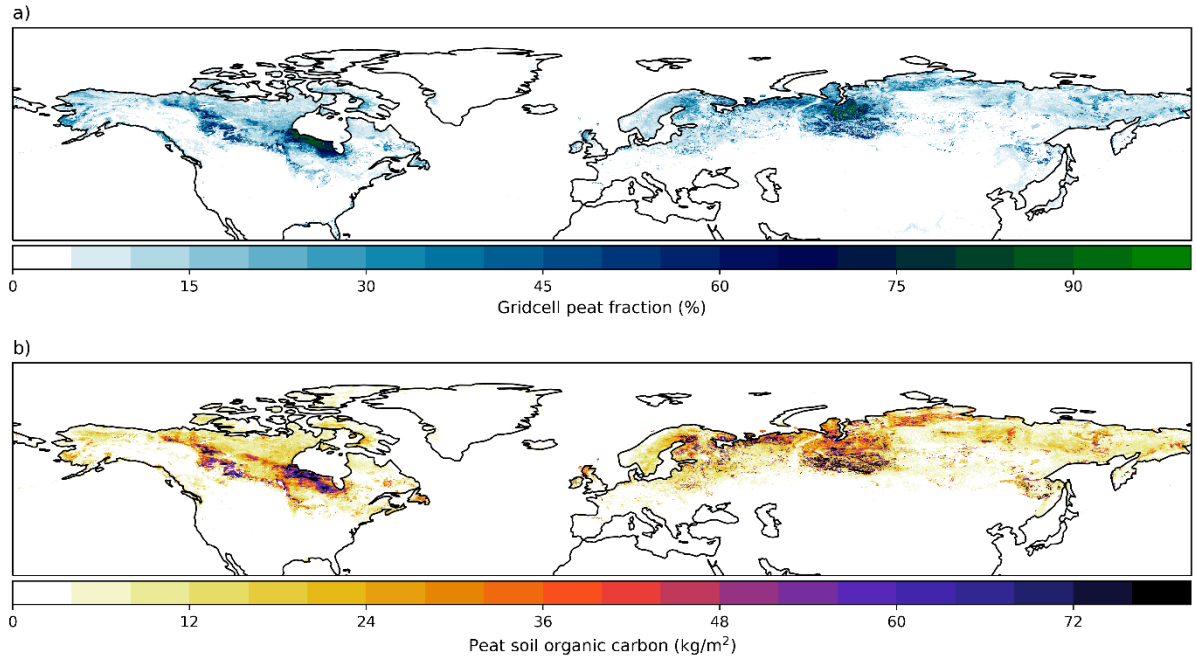


Figure 8: Maps of a) peatland fraction (%) and b) peatland soil organic carbon (kg/m^2) for north of 23° latitude from the Northern Peatland Dataset (Hugelius et al., 2020).

INFERNO-peat was run at N96 resolution (1.25° latitude X 1.875° longitude) at monthly time steps from 1997 to 2014 for the LIS-OTD lightning run and from 2010-2014 for the WGLC lightning run. Due to the availability of data from the organic soil moisture run, INFERNO-peat could only be run up to 2014.

4.1. Model evaluation protocol

To evaluate model performance, numerous datasets were utilised for different parameters. Burnt area was evaluated against BA data from GFED4s (van der Werf et al., 2017), GFED5 (Chen et al., 2023a; Chen et al., 2023b), FireCCILT11 (Otón et al., 2021) and ABoVE-FED (Potter et al., 2023). Multiple observational datasets were used for evaluation due to known deficiencies in the ability of remote sensing-based products, in particular MODIS which is used in GFED4s, in being able to detect peat fires in the high latitudes (McCarty et al., 2021). GFED5 was therefore used as the most up to date product which, on top of MODIS burned area, utilises high resolution observations from Landsat and

Sentinel-2, leading to a 61% increase in burned area globally compared to GFED4s (Chen et al., 2023b). Additionally, FireCCILT11 which is based off AVHRR images, was used as a non-MODIS based comparison (Otón et al., 2021). The ABoVE-FED dataset was also used to evaluate burnt area in Alaska and Canada, as this uses high resolution Landsat data to map burning, therefore providing an alternative data source for optimum model evaluation.

Modelled carbon emission estimates were evaluated against total carbon emissions from GFED4s (van der Werf et al., 2017), GFED500m (van Wees et al., 2022) and GFAS (Kaiser et al., 2012). Similar to burned area, multiple products were used in addition to GFED4s. GFED500m enhances the accuracy of carbon emissions estimations by increasing the spatial resolution to 500m, as well as differentiating between aboveground and belowground carbon emissions, allowing for enhanced analysis of INFERNO-peat's performance (Van Wees et al., 2022). GFAS (Kaiser et al., 2012), which is based on MODIS fire radiative power (FRP) observations, was used as an alternative to the GFED family of products. For more information on the aforementioned satellite-based products please see Section 6 and Table 3. Prior to use, all observational datasets were resampled to a N96 grid using linear interpolation. Additionally, a null model (Standard JULES-INFERNO vn5.4) without peat fires was used for comparison.

Burnt area was evaluated using spatial correlations on averaged maps of BA using Pearson's R. Additionally, the RMSE metric was used to diagnose spatial performance in BA. Temporal correlations were conducted for the whole timeseries for both BA and C emissions, again using Pearson's R, alongside comparisons of variation metrics such as standard deviation (STD) and the coefficient of variation (CV). These analyses were also conducted on 7 subregions of the northern high latitudes (Alaska; western Canada; eastern Canada; Fennoscandia; western Russia; central Russia and eastern Russia), in order to observe if there are any unique trends and patterns in peat burning happening in different regions of the high latitudes.

5. Future peat fire simulations

Successful development of INFERNO-peat allows for future changes in northern high latitude peat fires to be modelled over the 21st century under different climate change scenarios. The following section will detail the background to future climate change scenarios, and briefly describe the INFERNO-peat modelling protocol used to model changes to high latitude peat fires with climate change, which will be further expanded upon in Chapter 5.

5.1. Future climate change scenarios

Scenarios which combine alternative futures of climate and society have been developed over the last 10-15 years to facilitate climate change research and inform policy (O'Niell et al., 2020). Emissions scenarios, referred to as Representative Concentration Pathways (RCPs), have undergone rapid

development since 2010 (Moss et al., 2010; van Vuuren et al., 2011). The RCPs were published in 2011 and described multiple atmospheric concentration pathways that lead to varying levels of radiative forcing in 2100 (van Vuuren et al., 2011). Simultaneously, socio-economic scenarios were developed (Moss et al., 2010). The Shared Socioeconomic Pathways (SSPs) describe possible trajectories and narratives of human development and environmental change during the 21st century (van Vuuren et al., 2017). These socioeconomic scenarios are combined with the Representative Concentration Pathways (RCPs) in a scenario matrix (SSP-RCP combined scenarios) giving a level of radiative forcing reached in the climate system by 2100 along with and a trajectory of future global development, to be used in climate change research (van Vuuren et al., 2014; Riahi et al., 2017).

To assess future changes in peat fires, three SSP-RCP combined scenarios were used: SSP126, SSP370, and SSP585, which are described in detail in Table 1. Scenario SSP126 represents the lowest emissions scenario, under which radiative forcing reaches 2.6 W m^{-2} in 2100. Sustainable development drives lower emissions of key greenhouse gases, whilst global populations are low, with reductions in inequality (O'Neill et al., 2017). SSP370 sees increasing global populations and high inequalities alongside high fossil fuel consumption which leads to 7.0 W m^{-2} of radiative forcing in 2100 (O'Niell et al., 2017 Riahi et al., 2017). Finally, SSP585 features the highest end of century radiative forcing of 8.5 W m^{-2} due to rapid economic growth and fossil fuel consumption (O'Niell et al., 2017 Riahi et al., 2017).

Table 1: Descriptions of the three SSP scenarios used in Chapter 5. Information has been obtained from O'Neill et al., 2017; Riahi et al., 2017; van Vuuren et al., 2014 and van Vuuren et al., 2017.

Scenario	SSP narrative	Radiative forcing	Description
SSP126	SSP1 – Sustainability	2.6 W/m^2	This scenario is characterised by sustainable development focused on human well-being, achieving development goals, and reducing inequality, at the cost of slower economic growth (O'Neill et al., 2017). Global population is low but urbanised and educated (Riahi et al., 2017). There is also strong investment in renewable energy, environmental technology, and lower resource and energy intensity (O'Neill et al., 2017), resulting in low global emissions of CO_2, CH_4 and N_2O and a peak in energy demand in 2060, followed by a decline due to successful energy efficiency measures and behavioural changes (Riahi et al., 2017). Low population, sustainability incentives and high agricultural productivity leads to a gradual expansion in forest and other ecosystems (Riahi et al., 2017).
SSP370	SSP3 – Regional rivalry	7.0 W/m^2	High international fragmentation and resurgent nationalism, leads to slow economic development and high inequality (O'Neill et al., 2017). Global population increases, reaching 12.6 billion in 2100 with declines in education

			levels (Riahi et al., 2017). Population growth leads to increased food demand and consequently large scale losses of forests and natural land due to agricultural expansion (Riahi et al., 2017). There is high dependency on fossil fuels, and an increased contribution of coal to the energy mix (Riahi et al., 2017), fuelling environmental degradation (O'Neill et al., 2017) and high emissions of CO_2, CH_4 and N_2O (Riahi et al., 2017).
SSP585	SSP5 – Fossil-fuelled development	8.5 W/m^2	There is rapid economic growth and globalisation coupled with exploitation of fossil fuels, and resource and energy intensive lifestyles (O'Neill et al., 2017). Whilst global population is low, there is rapid urbanisation due to high income growth and over a tripling in energy demand (Riahi et al., 2017). High reliance on fossil fuels and increasing contributions from coal to the energy mix results in high CO_2 emissions (Riahi et al., 2017).

5.1.1. The Inter-Sectoral Impact Model Intercomparison Project (ISIMIP)

The Inter-Sectoral Impact Model Intercomparison Project (ISIMIP) is a climate impacts modelling initiative, aimed at examining the impacts, and associated uncertainties, of climate change (ISIMIP, 2018; Warszawski et al., 2013; Rosenzweig et al., 2017). As part of ISIMIP, multiple impact models' simulations are compared using a common simulation protocol. At present there have been five ISIMIP simulation protocols. Initially, a Fast Track protocol was developed which focused on producing cross-sectoral projections of the impacts of different levels of global warming on water, biomes, agriculture, coasts, and health (ISIMIP, 2018; Rosenzweig et al., 2017). Results from the ISIMIP Fast Track simulations highlighted the success of the protocol for assessing the current state of climate impacts research and climate risk analysis (Rosenzweig et al., 2017), and led to further development of the ISIMIP protocols. ISIMIP2a focused primarily on model validation with respect to extreme weather events and climate variability (ISIMIP, 2023). ISIMIP2b meanwhile focused on the impacts of 1.5°C of global warming, compared to low-emission pathways (Frieler et al., 2017; ISIMIP, 2021). Similarly to ISIMIP2a, ISIMIP3a focuses on the improvement and evaluation of impact models but additionally, ISIMIP3a looks at a counterfactual i.e. no climate change simulations with the aim to attribute impacts to climate change (ISIMIP3a simulation protocol, available from: https://protocol.isimip.org/#/ISIMIP3a/, last accessed: 17/05/2024). Finally ISIMIP3b, focuses on climate change impacts at different levels of climate change and socioeconomic development (SSP126, SSP370 and SSP585) using bias adjusted global climate models (GCMs) (ISIMIP3b simulation protocol, available from: https://protocol.isimip.org/#/ISIMIP3b/, last accessed:

17/05/2024). As the ISIMIP2 simulations do not have a fire impact protocol, ISIMIP3b protocols will be used here to assess the potential climate change induced changes in peat fires.

Whilst many model simulations under the ISIMIP3b protocol are still in progress, preliminary results have shown the capabilities for ISIMIP3b impact models to successfully assess climate impacts in the future. For example, ISIMIP3b climate forcings under the three SSP scenarios have been used to assess changes in Canadian wildfires over the next century, using the CLASSIC FWI fire module, showing that under SSP370 and SSP585, annual burnt area in Canada reaches 10.5 to 11.7 Mha in the 2090s (Curasi et al., 2024). Additionally, the ISIMIP3a protocol has been used to analyse present day trends in global burnt area, highlighting that between 2003 and 2019, climate change has increased global burned area by 16% (Burton et al., 2023). Consequently, the ISMIP3b protocols can be used for assessing future changes to fires and peat fires under different climate change scenarios.

5.2. Modelling high latitude peat fires over then next century using INFERNO-peat

INFERNO-peat (described in Section 3) can be used to simulate future changes to peat fires and their associated carbon emissions. Therefore, INFERNO-peat in its offline version was run in python version 3.8 under three climate change scenarios: SSP126, SSP370 and SSP585, from 2015 to 2100.

JULES-INFERNO model outputs were utilised, from a version 6.3 run which were conducted following the ISIMIP3b fire sector protocols for SSP126, SSP370 and SSP585 (available from: https://protocol.isimip.org/#/ISIMIP3b/fire, last accessed: 20/05/2024). The climate driving data used is UKESM 1-0-LL, which has undergone bias adjustment and statistical downscaling using the WFDE5 version 2 observational dataset over land and ERA5 over oceans (Lange et al., 2021). UKESM 1-0-LL is comprised of multiple components including an aerosol model (UKCA-GLOMAP-mode), atmosphere component (MetUM-HadGEM3-GA7.1), atmospheric chemistry model (UKCA-StratTrop), land surface model (JULES-ES-1.0), oceanic model (NEMO-HadGEM3-GO6.0), ocean biogeochemistry (MEDUSA2) and a sea ice model (CICE-HadGEM3-GSI8).

The outputs used from JULES-INFERNO to drive INFERNO-peat are described in Table 2. Much like the present-day simulations of burning (see Section 4), JULES-INFERNO calculated PFT fractions and flammabilities were obtained. Due to the absence of available JULES organic soil runs for the future climate scenarios, in contrast to the present day runs, soil variables including soil moisture, water table depth and soil temperature were obtained from the standard JULES run where soils are assumed to be mineral. However, a scaling factor to account for the differences between mineral and organic soils were used to help reduce biases in the model in terms of soil moisture (please see Chapter 3 Section 2). Consequently, a soil moisture scaling factor was estimated by calculating the difference in the 2010 to 2014 average soil moisture for the high latitudes between the mineral and organic soil present day JULES outputs. Scaled mineral soil variables were then

compared to the organic soil variables to ensure consistency and increase confidence in using these scaling factors for future simulations (Figure 9).

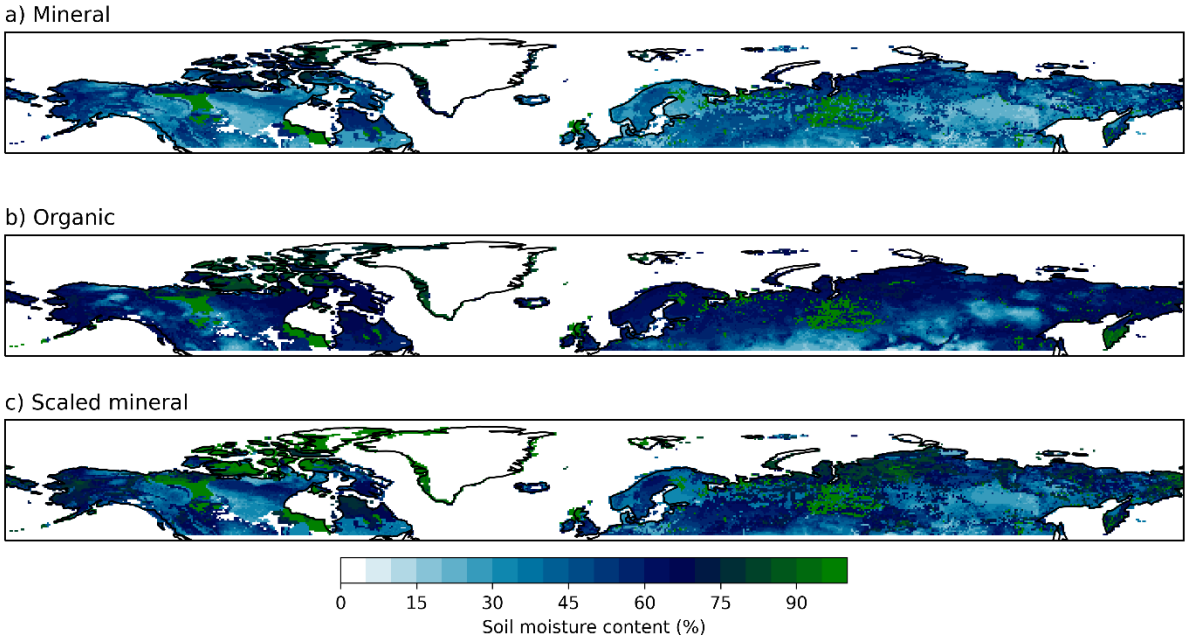


Figure 9: Comparisons of the 2010-2014 soil moisture content modelled by JULES in the high latitudes between a) mineral soils, b) organic soils and c) the mineral soil moisture scaled up based on the difference between mineral and organic soil moisture.

Due to a lack of available and verified datasets at the time, the same static climatology's as used in the present day runs for population density (HYDE: Hurtt et al., 2011) and lightning (LIS-OTD; Christian et al., 2003) were used. Again, much like the present day runs, the northern peatland dataset (Hugelius et al., 2020) was used to prescribe peatland fractions and carbon contents. Peatland fractions and carbon contents were assumed to remain static over the next century. Whilst this is not a realistic representation of potential future peatland dynamics, in which peatlands are expected to decline across the high latitudes (Zhao and Zhuang 2023; Loisel et al., 2021; Swindles et al., 2019), there is little data available at present that can be integrated into modelling efforts on how peatlands, and their stored carbon, may change with climatic changes.

Finally, a maximum depth of burn of 0.4m and a combustion completeness of 0.8 are used. These are the same values used for the present day runs, and their selection was via a sensitivity analysis, the details of which can bee seen in section 4.

Table 2: Summary of the input variables required for INFERNO-peat, and the source of these variables used in the future INFERNO-peat runs.

Variable	Abbreviation	Units	Source
Population density	PD	People/km^2	HYDE
Lightning	L	Flashes/km^2	LIS-OTD
PFT flammability	$Flam_{PFT}$	0-1	ISIMIP3b JULES
PFT fraction	$Frac_{PFT}$	0-1	ISIMIP3b JULES
Soil moisture	SM	%	ISIMIP3b JULES

Water table depth	zw	m	ISIMIP3b JULES
Soil temperature	tsoil	°C	ISIMIP3b JULES
Inorganic content	IC	%	Prescribed value
Bulk density	ρ	Kg/m^3	Prescribed value
Peat fraction	$Frac_{peat}$	%	Northern peatland dataset
Peat carbon content	C_{peat}	Kg/m^2	Northern peatland dataset
Maximum depth of burn	BDmax	m	Prescribed value
Combustion completeness	CC	0-1	Prescribed value

INFERNO-peat was run for the three scenarios at a 0.5° resolution on monthly time steps from 2015 to 2100 for north of 50°N latitude only. Outputs of peat burnt area, peat depth of burn and peat fire emitted carbon are generated.

6. Observing fires from space

Reliable modelling of global wildfires relies heavily on the existence of high quality remotely sensed data. Remotely sensed Earth observation (EO) data (Such as: MODIS, VIIRS and Sentinel products) are frequently used to derive burned area, active fires, fire size and severity on global scales, and are used in the evaluation of fire models. Over the last 15 years burned area detection algorithms have improved significantly (Chuvieco et al., 2019; Mouillot et al., 2014), with the latest GFED5 product now recording 93% more burning than the MODIS product MCD64A1 (Chen et., 2023b). These global fire products have a range of uses from modelling to land management (Mouillot et al., 2014), and more recently near-real time (NRT) EO data have allowed for rapid air quality forecasting during wildfire events (Wooster et al., 2021). Most global burned area products rely on satellite sensors that provide high temporal resolution and coarse spatial resolution, and detect changes in surface reflectance from NIR, SWIR and visible spectral regions, alongside detection of thermal anomalies (Chuvieco et al., 2019). Thermal anomalies indicate hotspots of burning and help to identify burning pixels, whilst the reflectance signals from charcoal and scorched vegetation cover the whole area affected by fires and help to map burned area (Chuvieco et al., 2019). This approach is used in both the MODIS product MCD64A1 and ESA's FireCCI50 (Chuvieco et al., 2019; Giglio et al., 2018; Chuvieco et al., 2018). Active fire detection is based on the signals detected from infrared radiation emitted during biomass burning and can be used to estimate measures of fire intensity and severity such as fire radiative power (FRP) (Wooster et al., 2021).

There are a wide variety of EO products currently in use (Table 3). Fire datasets are often either "bottom up" i.e. burned area based, such as GFED, or "top down", i.e. fire energy based such as GFAS (Liu et al., 2020). These different methods are useful for detecting different types of fires with burned area-based bottom-up detections better for larger more continuous fires, and top-down active fire detections better for small, fragmented fires (Liu et al., 2020). Furthermore, small fires often fail to be detected by coarse resolution sensors, such as MODIS (Liu et al., 2020). However, MODIS sensors form the basis of most burnt area (BA) products (Chuvieco et al., 2019; Mouillot et al., 2014).

For example, FireCCI products utilise 250m IR and NIR reflectance bands from MODIS (Chuvieco et al., 2018), and MCD64A1 is derived from 500m MODIS imagery (Giglio et al., 2018). In turn, the MCD64A1 product, alongside additional variables, forms the basis of the Global Fire Emissions Database (GFED) (Chuvieco et al., 2019; Randerson et al., 2012; van der Werf et al., 2017), which is the most commonly used observational dataset to evaluate fire model performance.

Table 3: A summary of the different global EO products available for detecting fires.

Dataset	Satellite/sensor	Spatial coverage	Time span	Spatial resolution	Temporal resolution	Fire parameters	Reference
MCD64A1	MODIS terra/aqua	Global	2000-present	0.25°x0.25°	Monthly	BA	Giglio et al. (2018)
GFED4s	MCD64A1	Global	1997-2016 (2017-present beta)	0.25°x0.25°	Monthly	BA, C emissions	van der Werf et al. (2017)
GFED5	MCD64A1 – adjusted using Landsat and Sentinel-2	Global	1997-2020	1.0°x1.0° (1997-2000) 0.25°x0.25° (2001-2020)	Monthly	BA	Chen et al. (2023b)
GFED500m	MODIS/ MCD64A1	Global	2002-2020	500m x 500m	Monthly	BA, C emissions	van Wees et al. (2022)
Fire Atlas	MCD64A1	Global	2003-2016	500m x 500m 0.25°x0.25°	Daily and monthly	Fire characteristics e.g. Size, duration, speed.	Andela et al. (2019)
GFASv1.2	MODIS terra/aqua	Global	2003-present	0.1°x0.1°	Daily	FRP, C emissions, and other emissions fluxes	Kaiser et al. (2012)
FireCCI51	MODIS terra/aqua	Global	2001-2017	0.25°x0.25°	Monthly	BA	Chuvieco et al. (2018)
FireCCILT11	AVHRR	Global	1982-2018	0.25°x0.25°	Monthly	BA	Oton et al. (2021)
FireCCISFD11	Sentinel-2	Sub-Saharan Africa	2016	0.05°x0.05°	Daily	BA	Roteta et al. (2019)
ABoVE-FED	Landsat	Alaska and Canada	2001-2019	500m x 500m	Annual	BA, emissions	Potter et al. (2023)

Overall, most EO fire products document a decline in global burned area over the last 20 years, primarily attributed to agricultural expansion and anthropogenic activities (Figure 10; Andela et al., 2017; Giglio et al., 2013; Chen et al., 2023b). The latest GFED5 burned area estimation suggests a decline of 24.2% in burned area between 2001 and 2020, largely occurring in savannas, grasslands, and croplands (Chen et al., 2023b). However, EO products show that portions of the high latitudes are seeing increases in BA (Figure 11; Chen et al., 2023b; Yang et al., 2023; Descals et al., 2022). For example, most EO products show increases in BA in central and western Canada, as well as parts of

western and central Siberia (Figure 11). The only area with consistent decreases in BA in the high latitudes is Southern Russia (Figure 11), where agricultural burning dominates the fire regimes (Hall et al., 2016).



Figure 10: Annual total global burnt area over 1997 to 2020 from four commonly used EO fire products: GFED4s, GFED5, fireCCILT11 and fireCCI51. Dashed lines indicate the overall time series trends for each dataset.

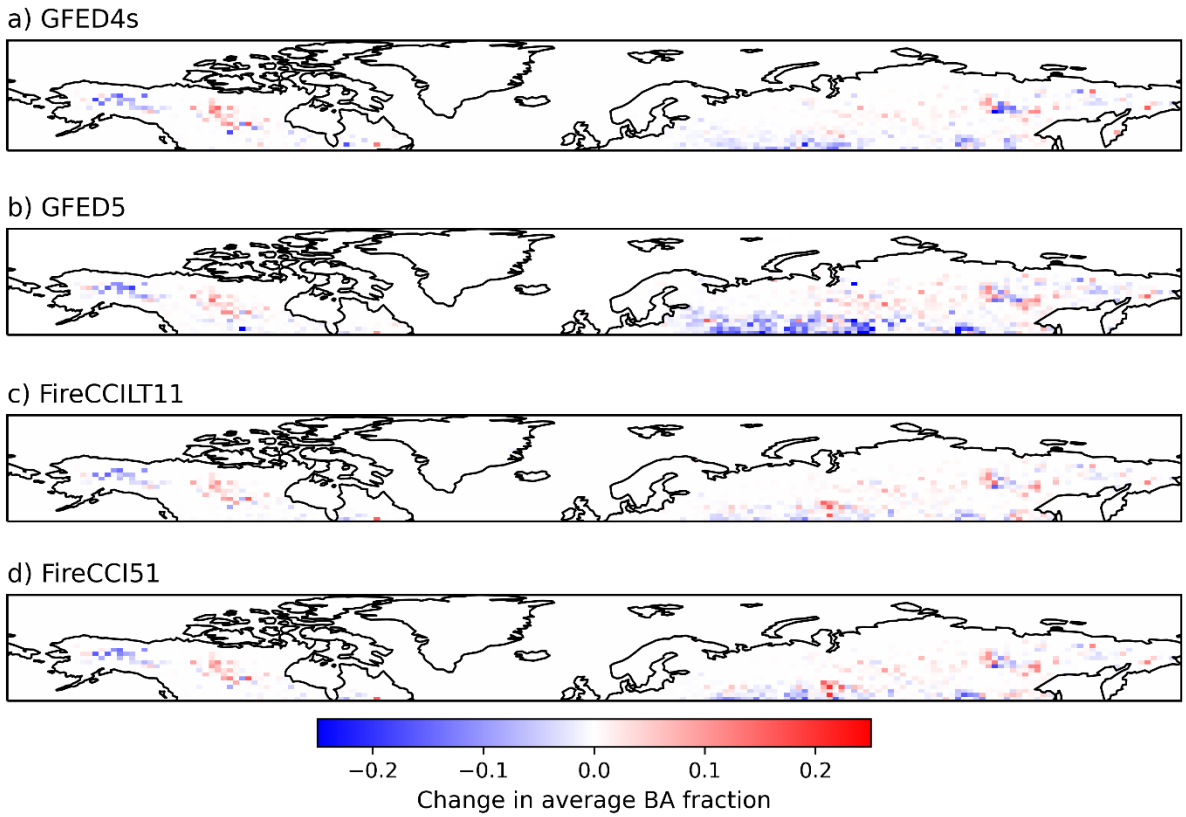


Figure 11: Change in grid cell burnt area fraction from the 2001-2005 average, and the 2010-2014 average for a) GFED4s, b) GFED5, c) FireCCILT11 and d) FireCCI51. The time periods were chosen as they are the earliest and latest 5-year periods obtainable concurrently from all datasets.

However, MODIS data and consequently other satellite-based products, suffer from significant omission errors. Whilst commission errors in MODIS hotspot data are rare, there are substantial omission errors, particularly associated with small fires (Hantson et al., 2013). Improved detection of small fires over sub-Saharan Africa using Sentinel-2 (FireCCISFD11) showed burned area to be 80% larger than previous MODIS estimations (Roteta et al., 2019). If that pattern holds true for the high latitudes, then MODIS-based products could be failing to capture a substantial amount of burning, and consequently carbon emissions. Sentinel-2 data also has been used to create a short-term fire dataset for Russia, which reported 5 times more burned area than MODIS (Glushkov et al., 2021). Therefore, it is highly likely that, at present, coarse resolution EO products are not capturing the full extent of burning globally. However, it is important to note that FireCCISFD11 still had an omission error of 26.5%, potentially owing to Sentinel-2's lower temporal resolution, leading to greater impacts of cloud coverage on fire detection (Roteta et al., 2019).

The high latitudes have been shown as a region when fires are often underestimated by global datasets (Chen et al., 2021b, McCarty et al., 2021; Yang et al., 2023). For example, MCD64A1 has high omission errors in boreal forest and tundra regions of North America, and FireCCI51 also misses 40% of the burned area's north of 60° (Chen et al., 2021b). In addition, many EO products underestimate carbon emissions in the boreal regions (Chen et al., 2021b; Stroppiana et al., 2010). For example,

Stroppiana et al. (2010) showed variations in CO emissions of over 1000 Tg between different datasets, with the largest difference seen in North America and Siberia. Furthermore, through the use of IASI CO measurements, MODIS FRP and AOD, and a chemistry transport model, Konovalov et al., (2014) found CO_2 emissions from Siberian wildfires in 2012 to be 73% larger than in GFAS. Using this method, over 2007-2012 carbon emissions were found to be a factor of 2.5 larger than GFED and 1.8 larger than GFAS (Konovalov et al., 2014). Therefore, the high latitudes represent a region of high uncertainty in our current burned area and emissions inventories.

Recent developments have been carried out on detecting fires in the high latitudes and boreal regions. For example, Potter et al., (2023), as part of the NASA Terrestrial Ecology Program's Arctic-Boreal Vulnerability Experiment (ABoVE), developed a novel burned area detection algorithm using high spatial resolution Landsat imagery for Alaska and Canada, known as the ABoVE Fire Emissions Database (ABoVE-FED). Here they differentiated between burned and unburned pixels using the difference Normalised Burn Ratio (dNBR) (Potter et al., 2023). Compared to GFED4s, ABoVE-FED shows 36% higher carbon emissions and 18% more burnt area (Potter et al., 2023). Landsat derived dNBR has also been used in Eastern Siberia to calculate fire perimeters and captured 48% more burned area than MODIS products (Talucci et al., 2022), suggesting that coarse resolution MODIS based products may be missing a significant amount of burning and carbon emissions in the high latitudes. Similarly, the Arctic Boreal Burned Area (ABBA) dataset, also developed as part of the ABoVE program, which uses pre and post fire surface reflectance data to map burned area, outperformed both MCD64A1 and FireCCI51, showing these products to miss nearly 75,000 km^2 of burning between 2001 and 2015 (Chen et al., 2021b). Furthermore, when MODIS burned area data were combined with VIIRS active fire products, and an additional overwintering fire detection algorithm for Yakutia, Russia, 44% more burned area was detected than MODIS alone (Xu et al., 2022). However, despite these advancements, many peat fires still go undetected (Chen et al., 2021b, McCarty et al., 2021; Yang et al., 2023).

6.1. Remote sensing of peat fires

Earth observation products have been shown to underestimate the extent of burning in peatland environments, particularly in the high latitudes (Chen et al., 2021b; McCarty et al., 2021; Yang et al., 2023). Satellite based products likely omit a large number of peat fires, as such fires tend to burn below ground and at low temperatures making them difficult to detect by remote sensing (McCarty et al., 2021; Yang et al., 2023). For example, Sirin and Medvedeva et al., (2022) showed MODIS alone to be insufficient for detecting the peat fires that occurred in the area surrounding Moscow in 2010, with differences in the moisture index pre- and post-fire showing the best results in detecting peat fires. Therefore, current remote sensing technologies cannot be applied unanimously to peat fires, as these were designed for flaming fires, which burn at much higher temperatures and predominately

aboveground (Hu and Rein, 2022; Rein 2013; Christensen et al., 2020; Sofan et al., 2019). In particular, this makes active fire detection difficult, as peat fires will result in lower thermal anomalies, that may not get detected by active fire algorithms. In addition, peat burning is often associated with thick haze, which can make satellite detection of burning during peat fires in both tropical and boreal environments challenging (Liu et al., 2020). As the Arctic is undergoing high levels of climatic change, there is a need for improved observations and data from satellites to aid in understanding the Arctic climate cycle and climate (Bruhwiler et al., 2021). Having better observations, and constraints upon these observations, of high latitude fires is essential to being able to predict future fire regimes (McCarty et al., 2021).

Whilst overall improvements to satellite-based fire detection on regional scales in the high latitudes will concurrently improve the detection of peat fires, without tailored peat fire detection algorithms many may still go undetected. Although only currently applied in a tropical environment, the Tropical Peatland Combustion Algorithm (ToPeCAI) uses shortwave infrared reflectance and thermal infrared reflectance to detect peat combustion, with an accuracy of 82% compared to ground-truthed data, 10% higher than the accuracy of VIIRS active fires in peatland areas (Sofan et al., 2019). In the high latitudes, the use of dNBR and the Normalised Difference Moisture Index (NDMI) have been shown to be able to map peatland burned areas with an accuracy of 93% (Sirin and Medvedeva, 2022). However, these parameters require high quality data for both the pre- and post-fire period, which is not always possible.

Peat fires also need to be considered explicitly in global fire emissions inventories. For example, inclusion of peat fire burned area and greenhouse gas emissions in FAOSTAT (UN Food and Agriculture Organisation Statistics Division) showed 30% higher fire emissions globally compared to GFED4s, largely in boreal Asia (Prosperi et al., 2020). Emphasising the importance of specifically parameterising peat fires in global fire emissions inventories. This can range from the inclusion of peat fire specific emission factors to different detection algorithms for peat fires. Proper representation is crucial, as common emissions inventories, such as GFED4s and GFASv1.2, have been shown to overestimate CH_4 emissions from tropical peatlands, but massively underestimate $PM_{2.5}$ emissions (Wooster et al., 2018). Therefore, if peat specific emission factors, based on in-situ field data and laboratory experiments, are used, the accuracy of estimations of the impacts of peat fires on atmospheric composition can be vastly improved.

Remotely sensed atmospheric composition data could be used as an alternative to traditional fire detection methods. Wildfires have been shown globally to have significant impacts on the interannual variability in trace gas emissions, in particular CO and aerosols in the peatland dominated environments of Equatorial Asia and the northern high latitudes (Voulgarakis et al., 2015). Furthermore, in the Arctic, biomass burning is the dominant driver of CO interannual variability,

which is also related to ENSO correlated reductions in precipitation (Monks et al., 2012). Peat fires also emit different quantities of gas species compared to flaming wildfires (see Section 4.3). Smouldering combustion releases more CO and CH_4 than flaming fires (Hu et al., 2019a; Hu et al., 2018), and emissions factors of NH_3 are 10-20 times larger for smouldering peat compared to flaming biomass combustion (Hu and Rein, 2022). At a site level, spectrometer data is able to detect wildfires from anomalously high CO coinciding with HCN and ethane in the high latitudes (Lutsch et al., 2020). At a larger scale different combustion behaviours have been able to be determined from large-scale emission ratios and patterns of CO_2, CO and NO_2 from satellite data (Parker et al., 2016; Silva and Arellano, 2017). Therefore, the signals of wildfires on atmospheric composition data should be detectable at large scales.

The Modified Combustion Efficiency (MCE), which is the ratio of $\Delta CO_2/(\Delta CO_2-\Delta CO)$, has been used as a key metric for representing the role of flaming vs smouldering combustion in vegetation fires (Andreae, 2019). Smouldering peat fires release greater quantities of CO, resulting in an average MCE of 0.77, compared to high CO_2-releasing flaming grassland fires with an average MCE of 0.98 (Andreae, 2019). Similar results have been identified in Indonesia, with smouldering peat having an MCE of 0.75-0.84 (Stockwell et al., 2016). Furthermore, when looking at the ratio of CO/CO_2, smouldering fires in the lab have shown a ratio that is 0.6 lower than in flaming combustion (Rein, 2015). However, despite these results, it has been suggested that MCE does not distinguish between combustion types with sufficient accuracy to be used as a fire regime indicator (Hu et al., 2019b).

Other alternative approaches have been suggested. For example, Hu and Rein (2022), showed the ratio of the emissions factors for CO_2 and CH_4 to be nearly 600% lower for smouldering combustion compared to flaming combustion. Furthermore, the CO_2/CH_4 ratio was found to be lower during the 2015 Indonesian peat fires compared to fires over the Amazon and southern Africa (Parker et al., 2016). However, there is limited evidence to show this as an effective determinant of peat fires in the high latitudes. Additionally, the ratio of NO_2/CO has also been identified as a proxy for combustion efficiency to differentiate between flaming and smouldering combustion (van der Velde et al., 2021). At a broad spatial scale, the ratio of NO_2/CO is lower in boreal environments, compared to savanna ecosystems and fires in boreal forests result in 3-6 times larger increases in CO relative to NO_2 than anywhere else in the world due to smouldering combustion (van der Velde et al., 2021).

However, being able to differentiate between peat burning and vegetation burning may be challenging due to the presence of smouldering combustion not in peat. Also, the co-existence of smouldering and flaming combustion may result in a masking of signals from either burning source and pose a challenge to using emission signatures for fire identification (Hu and Rein, 2022). Consequently, whilst there are many avenues for further research into detecting peat fire burnt area and estimating their emissions, at present this remains a limitation in global fire databases. Therefore, there is a need

to better understand the impacts that peat fires have on atmospheric composition in the high latitudes, in order to inform potential future peat fire detection algorithms. Consequently, Chapter 4 will focus on the impacts that both peat and non-peat fires have on atmospheric composition and air quality, with the view to these insights being able to inform future modelling efforts.

7. Remote sensing of atmospheric composition and air quality

Fires are among the largest sources of trace gas and aerosol emissions to the atmosphere globally (Andreae, 2019), with large impacts on the global carbon budget (Friedlingstein et al., 2023). Globally fires are estimated on average to emit 1.6-1.7 Gt C per year (Friedlingstein et al., 2023), with substantial interannual variability. For example, in 2023 carbon emitted from fires was higher than the average largely due to the extreme fires that burned in Canada, emitting 0.5-0.8 Gt C, over 500% greater than the regional average (Friedlingstein et al., 2023; Byrne et al., 2024). Additionally, peat fires also function as strong sources of carbon emissions at 0.3 Gt C per year (Friedlingstein et al., 2023). Fires are also major sources of greenhouse gas emissions, including CO_2, CH_4 and N_2O (Tian et al., 2016; Le Quere et al., 2018). However, two of the most important trace gas emissions from fires are carbon monoxide (CO) and nitrogen oxides (NO_x). It has been estimated that fires are responsible for between 33% and 50% of all global CO emissions, and 20% of global NOx emissions (Wiedinmyer et al., 2011; Olivier et al., 2005)). Therefore, it is highly important that reliable observations of these key trace gases exist for enabling effects of wildfires and peat fires on atmospheric composition to be studied.

Fires are also major sources of aerosol emissions worldwide (Wiedinmyer et al., 2011; Andreae and Rosenfeld, 2008), and, in particular, are dominant sources of black carbon (BC; Bond et al., 2013). BC exerts a direct radiative forcing effect of +0.7 W m^{-2}, making BC the second most important human emission in terms of its effect on climate forcing (Bond et al., 2013). Fires are estimated to emit 57-74% of global emissions of primary organic particulate matter and between 27 and 60% of global emissions of BC (Bond et al., 2004; Andreae and Rosenfeld, 2008; Wiedinmyer et al., 2011; Bond et al., 2013). Consequently, it is incredibly important that reliable and accurate observations of atmospheric composition and air quality exist, in order to be able to understand the effects of fires, and in particular their effect on human health.

A wide variety of remote sensing products are available and have been developed over the last two decades for assessing atmospheric trace gases and pollutants in the troposphere. These observations have been extensively used for air quality forecasting, tracking smoke plumes from power plants and wildfires, and identifying emissions sources (Kopacz et al., 2023). Table 4 summarises multiple satellite instruments that monitor atmospheric composition and air quality. There have been near-continuous global measurements of the atmosphere since 1995, undertaken by numerous space agencies and projects. Broadly speaking, most of these instruments rely on spectrometer

measurements of solar irradiance scattered and absorbed by the different constituents of the Earth's atmosphere (Levelt et al., 2006; Burrows et al., 1999; Bovensmann et al., 1999; Veefkind et al., 2012).

Table 4: A summary of the different remote sensing-based observations of atmospheric composition and air quality, in order of launch. Only the key measurements relevant to this section are included.

Instrument	Satellite	Time span	Global coverage	Spatial resolution	Key measurements	Reference
GOME	ERS-2	1995-2011	3 days	40x320 km	H_2O, NO_2, SO_2, aerosols	Burrows et al. (1999); ESA (1995)
MOPITT	Terra (NASA)	1999-present	3 days	22x22 km	CO, CH_4	Drummond et al. (2010); Drummond and Mand (1996)
MODIS	Terra and Aqua	2000 – present	Daily	250m, 500m or 1km	Aerosols	Remer et al. (2005); Levy et al. (2013)
SCIAMACHY	ENVISAT	2002-2012	3 days	30x120 km	CO, CH_4, CO_2, NO_2, O_3	Bovensmann et al. (1999); Buchwitz et al. (2004)
AATSR	Envisat	2002-2012	1-3 days	1 x 1 km	Aerosols	Kolmonen et al. (2016); ESA (2007)
AIRS	Aqua	2002-present	Daily	45x45 km	CO_2, CH_4, CO, O_3, SO_2	Aumann et al. (2003), Susskind et al. (2003)
TES	Aura	2004-2018	2 days	0.53 x 5.3 km	CO, O_3, CH_4, H_2O	Beer (2006)
OMI	Aura	2004-present	Daily	13x24 km	O_3, NO_2, SO_2, HCHO BrO and OC1O, Aerosol characteristics, cloud top heights, surface UV irradiance	Levelt et al. (2006)
CALIOP	CALIPSO	2006-2023	16 days	333 x 333 m	Aerosols and clouds	Winker et al. (2004)
IASI	MetOp-A, B and C	2006-present	Daily	12x12 km	CO_2, N_2O, H_2O, CH_4, O_3, CO, NH_3, SO_2, aerosols	Clerbaux et al. (2009); Turquety et al. (2004)
GOME-2	MetOp-A, B and C	2007-present	Daily	80 x 40 km	O_3, NO_2, SO_2	Munro et al. (2016); Chan et al. (2023)
OMPS	Suomi NPP	2011-present	Daily	50 x 50 km	O_3, NO_2, SO_2	Yang et al. (2014b)
TROPOMI	Sentinel 5p (ESA)	2018-2022	Daily	7x7 km	O_3, NO_2, CO, SO_2, CH_4, CH_2O, aerosols, clouds	Veefkind et al. (2012)

One of the first spectrometer instruments launched with the purpose of monitoring atmospheric composition was the Global Ozone Monitoring Experiment (GOME), which launched aboard the European Remote Sensing 2 (ERS-2) satellite in 1995 and was operational until 2011 (Burrows et al.,

1999). Subsequent development of the GOME instrument resulted in the launch of GOME-2 onboard EUMETSAT's Meteorological Operation satellites (MetOP) A, B and C in 2006, 2012 and 2018 respectively, with greater temporal coverage and spatial resolution than its predecessor (Munro et al., 2016). In 2002 the Scanning Imaging Absorption Spectrometer for Atmospheric Chemistry (SCIAMACHY) was launched onboard the Envisat satellite, which continued until 2012 (Bovensmann et al., 1999). Subsequently, the Ozone Monitoring Instrument (OMI) was launched in 2004 on NASA's Aura satellite (Levelt et al., 2006). With a spatial resolution of 13x24 km and daily global coverage (Levelt et al., 2006), this was a major step forward in atmospheric composition monitoring. Overall, OMI has been shown to agree well with ground-based measurements (Lamsal et al., 2008). Still, it has been found that its spatial resolution was too coarse for resolving urban NO_2 plumes (Kim et al., 2016). Therefore, with heritage to OMI and SCIAMACHY, the Tropospheric Monitoring Instrument (TROPOMI) was launched onboard the Sentinel 5 Precursor (S5P) satellite in 2017, which delivered significant improvements in the signal-to-noise ratio and provided daily global coverage and an unprecedented spatial resolution, three times higher than OMI (Veefkind et al., 2012; Van Geffen et al., 2022a).

Whilst all spectrometers, the instruments described above are capable of observing in different wavelengths to one another, allowing for extensive profiling of atmospheric composition or leading to the absence of certain wavelengths and consequently trace gases. For example, the GOME products are focused on monitoring ozone (O_3) concentrations and have spectral range of 240 to 790 nm, covering the ultraviolet (UV) and visible (VIS) wavelengths, allowing for the measurement of NO_2, SO_2 and H_2O (Munro et al., 2016; de Vries et al., 2009). OMI operates in a similar spectral range of 270-500 nm capturing the UV and some of the VIS wavelengths, and therefore monitors similar trace gases to GOME and GOME-2 (Buchwitz et al., 2004; de Vries et al., 2009). However, neither of these products measure in the near infrared (NIR) or short-wave infrared (SWIR) wavelengths, leading to the absence of key trace gases such as CO, CH_4 and CO_2.

Spectrometers that observe in the NIR and SWIR wavelengths include the Tropospheric Emission Spectrometer (TES; Beer, 2006), the Infrared Atmospheric Sounding Interferometer (IASI; Clerbaux et al., 2009) and the Atmospheric Infrared Sounder (AIRS; Aumann et al., 2003). Additionally, the Measurements of Pollution in the Troposphere (MOPITT) instrument, which is a cross-track scanning infrared radiometer launched onboard NASA's Terra satellite in 1999, measures in the SWIR wavelengths (Drummond and Mand, 1996; Drummond et al., 2010). These instruments all allow for the observation of trace gases such as CO, CH_4 and CO_2, and also show good agreement with each other. For example, MOPITT, AIRS, TES and IASI all show a decrease in total column CO of 1% per year in the Northern Hemisphere between 2000 and 2011 (Worden et al., 2013).

However, some products such as SCIAMACHY and TROPOMI operate with much larger spectral ranges allowing for a vast array of concurrent trace gas detections in UV, VIS and SWIR wavelengths. For example, SCIAMACHY has a spectral range of 240-2400 nm and TROPOMI a spectral range of 270-2385 nm (Veefkind et al., 2012; de Vries et al., 2009). Detecting in the SWIR wavelengths allows TROPOMI to additionally measure CO and CH_4, and SCIAMACHY to measure CO, CO_2 and CH_4 (de Vries et al., 2009), on top of the UV/VIS measurements of NO_2, O_3 and SO_2.

Many of the aforementioned satellite instruments are also capable of retrieving information on aerosols and their properties. Atmospheric aerosol particles can attenuate incoming solar radiation in the VIS, UV and SWIR spectral bands through scattering, reflection, and absorption, allowing spectrometers and radiometers to quantify aerosol optical properties (Zhang et al., 2021). For example, The Moderate Resolution Imaging Spectroradiometer (MODIS) onboard the NASA Terra and Aqua satellites has provided knowledge and understanding on the spatial and temporal variability of Aerosols on Earth over the last 20 years (Zhang et al., 2021; Levy et al., 2013; Remer et al., 2005). Of the previously mentioned products, IASI, OMI, GOME and TROPOMI all also measure aerosols and their properties. In addition, multi-angle sensors such as the Advanced Along Track Scanning Radiometer (AASTR; Kolmonen et al., 2016) and the Multiangle Imaging Spectro Radiometer (MISR; Diner et al., 1989) allow for the identification of different types of aerosols and cloud forms through changes in solar reflection under the different viewing angles provided (Zhang et al., 2021). LiDAR (Light Detection and Ranging) has been used to measure aerosols and their vertical profiles, the first instrument being the Cloud-Aerosol Lidar with Orthogonal Polarisation (CALIOP) onboard the Cloud-Aerosol Lidar and Infrared Pathfinder Satellite Observation (CALIPSO) satellite, which launched in 2006 (Winker et al., 2004).

Consequently, many Earth observation products exist that monitor and measure atmospheric composition and air quality and have provided substantial advances in scientific understanding on the atmosphere. However, these products share common sources of error including measurement noise, calibration errors, simplifications and inaccuracies in the radiative transfer models used in retrieval schemes, and errors in auxiliary data (von Clarmann et al., 2020). Furthermore, clouds are a common source of error in many satellite based atmospheric composition detections (Veefkind et al., 2012; Martinez-Alonso et al., 2020; Vidot et al., 2012). Clouds can disrupt measurements by creating very bright radiance scenes, leading to pixel saturation (Ludewig et al., 2020), and consequently areas of the world that suffer from extensive cloud coverage (e.g. the tropics) may suffer from a lack of high-quality remote sensing observations.

Satellite observations have been used on numerous scales to assess the impacts of fires on atmospheric composition and air quality (Lama et al., 2020; Margo et al., 2021; van der Velde et al., 2021). In particular, NO_2 and CO concentrations have frequently been used to quantify burning

efficiencies and emission factors (Lama et al., 2020; Hung et al., 2022; Wan et al., 2023; Peiro et al., 2022; Anderson et al., 2023). Emissions ratios between NO_2 and CO are a proxy for combustion efficiency, capable of distinguishing between flaming and smouldering combustion (Andreae and Merlet, 2001). For example, Wan et al., (2023) and Peiro et al., (2022) demonstrated that ratios of NO_2:CO can be used for large scale estimates of smouldering and flaming combustion. Furthermore, on a seasonal scale ratios of NO_2:CO have been shown to allow for the distinction of different fire types that occur at different points in the fire season (Hung et al., 2022). In addition, fire event monitoring from remote sensing, has shown that on a small-scale, shifts from flaming to smouldering combustion can be identified throughout the progression of a fire (Anderson et al., 2023).

Whilst numerous studies have explored the impacts of specific high-latitude fire events and peat fires on atmospheric composition, limited research has been undertaken on the large-scale influences of fires and peat fires in the northern high latitudes. Therefore, Chapter 4 will explore the impacts of fires, and peat fires, on atmospheric composition and air quality in the high latitudes, with Section 8 of the current chapter presenting the methodology used.

8. Assessing the impact of fires on atmospheric composition and air quality in the high latitudes

The impacts of fires and peat fires on atmospheric composition and air quality can be studied using NO_2, CO and $PM_{2.5}$ concentrations from remotely sensed products. NO_2 and CO represent important trace gases in the Earth's atmosphere that are heavily emitted by both wildfires in general and peat fires in particular (Wiedinmyer et al., 2011; Olivier et al., 2005). Changes to the atmospheric composition regarding both NO_2 and CO have a major effect on pollution levels felt by populations around the world. Outdoor air pollution is considered the biggest environmental risk to public health globally (WHO, 2016, WHO 2006). Furthermore, emissions of particulate matter (PM) also have a major impact on air quality, leading to perverse health outcomes. In particular, $PM_{2.5}$ have been shown to result in human respiratory and cardiovascular disease, which increases mortality risks across populations, especially because of long-term exposure (Dockery et al., 1993; Pope et al., 2002; Brook et al., 2010). Across the EU, PM are estimated to be responsible for 412,000 deaths per year, with an additional 71,000 deaths per year attributed to NO_2 pollution (EEA, 2019). Whilst other sources of PM and NO_2 exist, in the high latitudes in particular wildfires are the major source of $PM_{2.5}$, emitting more than all anthropogenic sectors combined (McCarty et al., 2021). Consequently, fires are the main source of air pollution-induced health burdens in Canada and Siberia (Lelieveld et al., 2015). Therefore, it is critically important that the impacts of fires and peat fires on atmospheric composition and air quality in the northern high latitudes are adequately understood, in order to better quantity the health impacts of wildfires.

Nitrogen oxides (NO_x), which are composed of nitrogen dioxide (NO_2) and nitrogen oxide (NO) are significant trace gases in the Earth's atmosphere. A photochemical process involving ozone (O_3) in the presence of sunlight rapidly converts NO into NO_2. Therefore, NO_2 can be regarded as a robust measure of atmospheric NO_x concentrations (Van Geffen et al., 2020). Natural sources of NO_2 emissions include lightning, fires, and soil microbial processes (Cerosimo et al., 2020). Additionally, anthropogenic activities such as traffic, biomass, and fuel combustion, are significant emission sources of NO_2 (Cersosimo et al., 2020). NO_2 is strongly reactive, particularly with OH, and triggers the formation of tropospheric ozone and aerosols which lead to positive radiative forcing and warming (Fuglestvedt et al., 1999; Shindell et al., 2009). Consequently, NO_2 also heavily influences the concentration of OH radicals, which shortens the lifetime of methane, leading to a negative radiative forcing and cooling effect (Fuglestvedt et al., 1999). Overall, NO_x has been shown to exert a net cooling effect (Shindell et al., 2009). Due to its reactive nature, the lifetime of NO_2 varies from hours to days (Fuglestvedt et al., 1999). However, in the high latitudes the lifetime of NO_2 can be longer due to slower photochemistry as a result of less intense sunlight (van Geffen et al., 2022b).

Tropospheric CO is primarily produced by incomplete combustion and biomass burning, although it can also be produced by the oxidation of methane and other hydrocarbons (Martinez-Alonso et al., 2020). The main sink of CO in the atmosphere are hydroxyl radicals (OH) (Spivakovsky et al., 2000; Lelieveld et al., 2016), with CO being shown to reduce the global OH burden by around 13% (Shindell et al., 2009). However, this reaction with OH produces greenhouse gases such as CO_2 and O_3 (Minschwaner et al., 2010). Therefore, CO emissions have an indirect positive radiative forcing of 0.23 W m^{-2}, and a warming effect (Myhre et al., 2013). CO has a much longer lifetime than NO_2 ranging from days to months (Minschwaner et al., 2010; Holloway et al., 2020; Martinez-Alonso et al., 2020), depending on the concentration of OH (Spivakovsky et al., 2000).

CO is most strongly emitted by incomplete combustion (Borsdorff et al., 2020). In contrast, NO_2 is primarily emitted during flaming combustion, with the amount of nitrogen emitted being heavily dependent on the type of fuel that is consumed (Griffin et al., 2021). Therefore, the emissions ratio between NO_2 and CO can be used as a proxy for combustion efficiency allowing for the differentiation between flaming and smouldering combustion (Andreae and Merlet, 2001; Rein et al., 2009; Andreae, 2019; van der Velde et al., 2021). Consequently, an additional benefit of studying NO_2 and CO in the context of peat fires is being able to potentially distinguish between the presence of flaming combustion that is dominant in vegetation fires and the smouldering combustion that is dominant in peat fires.

Therefore, this section, and Chapter 4, explores the use of remotely sensed data of the atmosphere and fires in being able to assess the impacts of fires on atmospheric composition and air quality. For this analysis, four focus regions were used; eastern Siberia; northwest Siberia; Alaska; and western

Canada. For each of these regions, trends in wildfire burnt area, and estimated peat burnt area from GFED5, and FRP and peat estimated FRP from GFAS were studied. Additionally, trends in atmospheric composition and air quality were examined from TROPOMI and CAMS reanalysis and correlations with the fire metrics were conducted. The details of these datasets and analyses will be covered in the following sections.

It is important to note that the following analyses are carried out from a global fire modelling perspective, where we are interested in large scale trends, patterns and relationships that can help to inform models and to aid in evaluating them. Consequently, this analysis is conducted on a regional scale, at monthly and annual time steps. As a result, singular fire events are not studied, and instead the whole overview of a region both during and out of the fire season is examined.

8.1. Fire data

Two datasets of different fire metrics were utilised within this work. Firstly, the Global Fire Emissions Database v5 (GFED5; Chen et al., 2023a), which measures global burnt area based on MODIS satellite detections. GFED5 is the latest iteration of MODIS based fire products and includes an additional novel calibration with Landsat and Sentinel-2, to increase the total burned area by more than 61% compared to GFED4s (Chen et al., 2023b). GFED5 is available from 1997 to 2020 at a 0.25° resolution (Chen et al., 2023b). In order to extend the temporal range of the fire products used up until present day and to obtain a metric of fire intensity, fire radiative power (FRP) was obtained from the Global Fire Assimilation System v1.2 (GFAS; Kaiser et al., 2012). GFAS is available from 2003 to present at a 0.1° resolution (Kaiser et al., 2012). FRP describes the rate at which fires are emitting thermal energy (Wooster et al., 2021). In GFAS, FRP is calculated from MODIS active fire detections (Kaiser et al., 2012). Additionally, I chose to use GFAS FRP as it has been hypothesized that FRP, due to its integration of all radiative energy emitted within a pixel, can provide better estimates of smouldering fires (Yang et al., 2023, Laurent et al., 2019). For example, FRP has been successfully used to assess particulate emissions from peat fires in Indonesia (Fisher et al., 2020).

Peat burnt area (BA_{peat}) was estimated from GFED5 by overlapping the northern peatland dataset (NPD) map of peatland fractional coverage (Hugelius et al., 2020), and calculating peat burnt area following Equation 12, where BA_{tot} is the grid cell total burnt area, and $peat_{frac}$ is the grid cell peatland fraction. Details of the NPD can be found in Section 4. Prior to calculations, the NPD was regridded using area weighted regridding to the GFED5 0.25° regular grid. Similarly, peat FRP (FRP_{peat}) was estimated by also overlapping GFAS and the NPD following Equation 13, where FRP_{tot} is the total grid cell FRP. However, for peat FRP the NPD was area-weighted regridded to the GFAS 0.1° grid prior to calculation.

Equation 12

$$BA_{peat} = BA_{tot} \times peat_{frac}$$

Equation 13

$$FRP_{peat} = FRP_{tot} \times peat_{frac}$$

These estimations of peat BA and FRP are likely oversimplistic and do not reflect heterogeneity in peatland environments. Equations 12 and 13 assume that BA, or FRP, is equally distributed among peat and non-peat fires. However, this is likely not realistic, as peatlands, due to their higher moisture environments, tend to be more resistant to wildfires than other areas of boreal landscapes (McCarty et al., 2021; Turetsky et al., 2015). Therefore, peat BA and FRP are likely overestimated within this analysis. However, for this preliminary analysis a simple estimation of peat BA and FRP was chosen, with future research to explore the potential for estimating maximum and minimum peat BA and FRP values and the associated uncertainty.

8.2. Atmospheric data

8.2.1. TROPOMI

TROPOMI is the spectrometer onboard the S5P satellite, which measures in the UV, VIS, NIR and SWIR wavelengths, allowing for the observation of multiple trace gases (including NO_2, SO_2, CO and CH_4), aerosols, and clouds (Veefkind et al., 2012; Babic et al., 2022). S5P is a near-polar sun-synchronous orbit satellite which flies at an altitude of 817 km (Veefkind et al., 2012). S5P forms part of the Global Monitoring of the Environment and Security (GMES) Space Component Program and aims to provide information and services on air quality, climate and the ozone layer (Veefkind et al., 2012). The TROPOMI instrument operates in a push-broom configuration, with a swath width of 2600km, and along-track of 7km providing unprecedentedly high resolution daily global coverage (Veefkind et al., 2012). Additionally, TROPOMI's stability, precision and spatial resolution mean that it is primed for studying weekly, monthly, and even annual atmospheric composition abundances (Goldberg et al., 2021).

Co-located retrievals of NO_2 and CO, were required for this analysis, in order to minimise potential errors arising from using multiple instruments. Therefore, TROPOMI, with its large spectral band range, was used as it simultaneously measures both NO_2 and CO. Additionally, TROPOMI, compared to previous iterations of atmospheric composition monitoring sensors, provides high signal-to-noise ratios, daily global coverage, and a high spatial resolution (van Geffen et al., 2022a; 2022b). The spatial resolution of TROPOMI is a factor of three higher than its predecessor OMI, which has allowed for variations in concentrations of trace gases to be distinguished within urban areas and better quantification of emission sources (Veefkind et al., 2012). Furthermore, the daily global

coverage provided by TROPOMI enables it to be able to capture the day-to-day evolution of atmospheric composition (Borsdorff et al., 2018).

Retrieval of NO_2 concentrations from TROPOMI are based on the TM5-MP chemistry transport model, the DOMINO system, which was previously developed for the OMI instrument, and QAECV processing systems (van Geffen et al., 2022b). NO_2 is retrieved in UV-VIS bands in the 405-465 nm wavelength range (Griffin et al., 2019). The retrieval is a three-step process (van Geffen et al., 2022b). Firstly, total NO_2 slant column densities (SCD) are calculated from Level-1b radiance and irradiance spectra using a Differential Optical Absorption Spectroscopy (DOAS) method (van Geffen et al., 2022b). Then the NO_2 SCD's are separated into a stratospheric and tropospheric part, before being converted into a tropospheric vertical column density using air mass factors (van Geffen et al., 2022b).

Total CO column values are obtained from measurements of reflected solar IR radiation in the 2305-2385 nm spectral range (Landgraf et al., 2016). TROPOMI CO retrievals are based on the Shortwave Infrared Carbon Monoxide Retrieval (SICOR) originally proposed by Vidot et al., (2012). Briefly, the CO retrieval employs a radiative transfer model which filters out optically thick clouds, and separates the atmosphere into a clear sky part, and a part that accounts for cloud and aerosol scattering (Vidot et al., 2012; Landgraf et al., 2016). Vertically integrated CO column densities are then determined from Tikhonov regularisation, utilising a prior estimate of methane abundance to characterise the light path and allow for cloud filtering (Vidot et al., 2012; Landgraf et al., 2016).

TROPOMI has been shown to perform well compared to airborne and local observations (Griffin et al., 2021; Cerosimo et al., 2020; Borsdorff et al., 2018; Bodah et al., 2022; Park et al., 2021). TROPOMI significantly improves the quality of air pollution monitoring of both NO_2 and CO (Savenets et al., 2022). Spatial and temporal patters of NO_2 are accurately observed by TROPOMI and have been shown to be capable of identifying the fine-scale heterogeneity in NO_2 emissions in urban areas (Goldberg et al., 2021). Additionally, Cersosimo et al., (2020) highlighted the capability of TROPOMI to reproduce lower troposphere NO_2 concentrations compared to ground-based data in the Po Valley, Italy. Furthermore, TROPOMI's ability to detect individual NO_2 plumes was demonstrated for mining activities in the Canadian Oil Sands, which also compared well to aircraft and surface in-situ observations (Griffin et al., 2019). Compared to ground-based observations, TROPOMI has been shown to be able to capture weekly cycles of NO_2 in Helsinki (Ialongo et al., 2020), as well as accurately detecting CO pollution hotspots, such as over Mexico City (Borsdorff et al., 2020), and specific events such as the air pollution event in India in November 2017 (Borsdorff et al., 2018). Therefore, NO_2 and CO measurements from TROPOMI are capable of accurately monitoring atmospheric composition over fine spatial and temporal scales, allowing for the analysis of pollution events, such as those caused by wildfires.

However, there are numerous potential sources of error and weaknesses with TROPOMI atmospheric composition measurements. In particular, TROPOMI has been shown to underestimate NO_2 over highly polluted areas (van Geffen et al., 2022a; Wang et al., 2020a). These underestimations may stem from biases in the cloud pressure retrieval, surface albedo climatology, errors within the TM5-MP chemistry model and air mass factors used in the NO_2 retrieval algorithms, and spectral fitting errors (van Geffen et al., 2022a; 2022b). Cloudiness is a major source of error in atmospheric composition retrievals and strongly affects NO_2 measurements, due to most tropospheric NO_2 occurring in the boundary layer, meaning that NO_2 retrievals are only reliable up to a certain cloud fraction (Veefkind et al., 2012). Additionally, clouds have been shown to cause significant errors in CO retrievals (Martinez-Alonso et al., 2020; Vidot et al., 2012). CO and NO_2 retrievals are also strongly affected by aerosol shielding, which is particularly significant when estimating fire emissions, as TROPOMI observations during fires will almost always be influenced by smoke (Griffin et al., 2021). Aerosol shielding occurs during wildfires due to higher aerosol densities produced by fires, which results in a reduction in the number of photons that can pass through the smoke plume and be detected by the satellite sensor (Anderson et al., 2023). Whilst TROPOMI does utilise an aerosol correction, which effectively assumes aerosols are clouds (van Geffen et al., 2020), observations in the UV/VIS wavelengths will still be affected (Griffin et al., 2021). For example, smoke can reduce NO_2 and other trace gas measurements by between a factor of 2 and 6 (Rowe et al., 2022; Anderson et al., 2023). Consequently, only high quality atmospheric composition data should be used, with knowledge of context-dependant possible limitations being key.

8.2.2. CAMS reanalysis

The Copernicus Atmospheric Monitoring Service (CAMS) reanalysis (hereafter referred to as CAMSRA) is the latest atmospheric composition dataset produced by the European Centre for Medium-Range Weather Forecasts (ECMWF). CAMSRA assimilates data from satellite retrievals of aerosols and chemical species (Inness et al., 2019). The dataset is produced using a 4DVar data assimilation in cycle 42R1 of ECMWF's Integrated Forecasting System (IFS; Remy et al., 2022). IFS is coupled to the Carbon Bond 2005 (Yarwood et al., 2005) tropospheric chemistry scheme implemented in the TM5 Chemical Transport Model (CTM). Numerous emissions datasets are used in the reanalysis including MACCity for anthropogenic emissions (Stein et al., 2014), GFAS v1.2 for biomass burning emissions (Kaiser et al., 2012), and biogenic emissions calculated from the Model of Emissions of Gases and Aerosols from Nature (MEGAN) using NASA's Modern-Era Retrospective Analysis for Research and Applications (MERRA) reanalysed meteorology (Sindelarova et al., 2014). CAMSRA is available from 2003 to 2022 at a spatial resolution of 0.7° x 0.7° every 3 hours (Inness et al., 2019). CO measurements are assimilated from MOPITT and NO_2 measurements are assimilated from SCIAMACHY, OMI and GOME-2 (Inness et al., 2019). CAMS also estimates particulate matter

based off air density, sea salt, desert dust, nitrate, organic matter, black carbon, ammonium and SO_4 (Ali et al., 2022; Remy et al., 2022).

CAMSRA was used as an additional dataset for atmospheric composition analysis as it has the benefit of assimilating data from multiple sources (Inness et al., 2019), meaning that trends and patterns seen in TROPOMI can also be verified by CAMSRA, to enable a more accurate assessment of the effects of wildfires on atmospheric composition. Furthermore, CAMSRA is a consistent long-term dataset, making it useful for trend analysis and comparisons of different regions over time (Inness et al., 2019). Additionally, CAMRA includes estimates of particulate matter, which allows for the additional analysis of wildfire effects on air quality. The accuracy and reliability of CAMSRA has also been extensively studied and demonstrated (Inness et al., 2019; Wagner et al., 2021; Wang et al., 2020b; Ali et al., 2022).

Due to higher temporal and spatial resolution, and an extensive range of chemical species included, CAMSRA outperforms previous reanalysis products such as the CAMS interim reanalysis, and the Monitoring Atmospheric Composition and Climate (MACC) reanalysis (Inness et al., 2019). Particular improvements, in terms of the magnitude of biases, have been identified over Arctic regions (Wagner et al., 2021). Global distribution of key trace gases, including O_3, CO and NO_2, are accurately represented, compared to independent observations, in CAMRA (Wagner et al., 2021). CO has been shown to be well represented in CAMSRA, with small biases of less than 20% and accurate seasonal cycles and interannual variability, particularly over Europe, the US, east Asia, and north Africa (Inness et al., 2019; Wagner et al., 2021; Wang et al., 2020b). The NO_2 measurements from CAMSRA also accurately capture the seasonality and magnitude of NO_2 observed from SCIAMACHY and GOME-2 satellite retrievals (Wagner et al., 2021). Furthermore, $PM_{2.5}$ from CAMSRA has been shown to produce similar spatial patterns compared to ground-based data across China (Ali et al., 2022). Consequently, CAMSRA provides an accurate and reliable alternative product to studying wildfire effects on atmospheric composition, with the benefit of assimilating data from multiple sources.

However, there are known underestimations and biases within CAMSRA. For example, CAMSRA underestimates tropospheric CO in the northern hemisphere when compared to aircraft measurements, potentially stemming from only one CO product being assimilated (Inness et al., 2019). In contrast overestimations of CO are commonly seen in the southern hemisphere (Wagner et al., 2021). CAMSRA further underestimates seasonal tropospheric NO_2 columns over east Asia and Europe (Inness et al., 2019). However, it is estimated that CAMSRA may overestimate NO_2 emissions from boreal fires in summer (Wagner et al., 2021). Across China, $PM_{2.5}$ and PM_{10} from CAMSRA are overestimated in urban and desert areas but are underestimated over the Tibetan Plateau (Ali et al., 2022). Inaccuracies in trace gas estimations in CAMSRA may stem from errors and uncertainties in

the individual satellite retrievals that are assimilated (Inness et al., 2019). Furthermore, uncertainties in the emissions inventories, such as GFASv1.2, used in CAMSRA, alongside assumptions in the underlying atmospheric models, may exacerbate biases and errors.

8.2.3. Data processing

For this analysis TROPOMI NO_2 and CO data was obtained from the Centre for Environmental Data Analysis (CEDA) archive from 2018 to 2021. I regridded the L2 TROPOMI tropospheric vertical column of NO_2 and total column CO to a common 0.5° x 0.5° grid using the HARP Python package v1.21. Prior to regridding, the data were filtered to only use the highest quality measurements, by restricting retrievals to those with a quality assurance (QA) flag of greater than 0.75, as recommended by Landgraf et al., (2023) and Eskes and Eichmann (2023). Restricting to this QA value removes cloud-cover scenes, partially snow- and ice-covered scenes, errors, and problematic retrievals. Once the regridding is completed, daily files were concatenated into a global monthly gridded dataset, from which regional monthly totals were calculated. Therefore, I created a monthly dataset of total NO_2 and CO in the 4 regions from 2018 to 2021.

CAMSRA NO_2, CO and $PM_{2.5}$ was obtained from the Copernicus Atmosphere Data Store (Available from: https://ads.atmosphere.copernicus.eu/cdsapp#!/dataset/cams-global-reanalysis-eac4, last accessed: 13/05/24) from 2003 to 2022. CAMSRA NO_2, CO and $PM_{2.5}$ is on a regular 0.75° x 0.75° grid and provided on a three hourly time step, from which regional monthly totals were calculated. Thereby generating a monthly dataset of total NO_2, CO, and $PM_{2.5}$ in the 4 regions of interest from 2003 to 2022.

8.3. Data analysis

Trends and patterns in monthly, annual, and seasonal fire variables were examined. Additionally, on the same timescales, trends in NO_2, CO and $PM_{2.5}$ were also studied. In addition, the ratio of NO_2:CO, calculated simply as regional total NO_2 over regional total CO, was also examined for both the TROPOMI and CAMSRA data. Large fire years were identified as those in which burnt area or FRP was greater than one standard deviation above the multi-annual mean. Similarly, greater, or less than average atmospheric composition years were identified in the data as those that were above or below one standard deviation of the multi-annual mean.

The role of temperature as a driver of large fire years was examined using 2m temperature data obtained from CAMSRA for each of the regions. CAMSRA estimates 2m temperature by assimilating data from weather stations and satellites, and through the ECMWF Integrated Forecasting System (ECMWF, 2024). CAMSRA monthly averaged 2m temperature was obtained from the Copernicus Atmosphere Data Store (Available from: https://ads.atmosphere.copernicus.eu/cdsapp#!/dataset/cams-global-reanalysis-eac4-monthly?tab=overview last accessed: 13/05/24) from 2003 to 2022.

Correlations were calculated using Spearman's Rank Correlation Coefficient, in order to determine the relationship between abnormal temperatures and extreme fire seasons.

As 2019 and 2020 are two years in which all four datasets recorded data, and they exhibit large differences in the amounts of fires between these years in all four regions, they were used to establish whether a distinction can be made between flaming and smouldering combustion. Primarily TROPOMI NO_2, CO and NO_2:CO data were used, alongside GFED5 estimated peat burnt area. Months were directly compared between these two years with months in which there was greater than a 0.1 M ha change in peat burnt area, or a greater that 5% change in estimated peat fire percentage of burnt area. Consequently, the concentrations of CO, NO_2 and the NO_2:CO ratios were compared between these months, to establish if there are any patterns in changes in atmospheric composition, with the hypothesis that more peat burning, and thus smouldering combustion, would lead to lower NO_2:CO ratios.

In order to establish potential relationships between fires and atmospheric composition and air quality, correlations were carried out using Spearman's rank correlation coefficients between all fire variables and all atmospheric variables on monthly, annual and seasonal timescales. Additionally, to assess the effects of the amount of BA on atmospheric composition, annual BAs were categorized based on their total amounts, with correlations calculated within each category between BA and atmospheric composition data. Furthermore, GFED5 differentiates burnt area in different land cover types and therefore correlations are also conducted on the different vegetation BAs with atmospheric composition, in order to assess if different vegetation burning has any effect on atmospheric composition.

Finally, modelled peat burnt areas from INFERNO-peat (see sections 3 and 4), were used to compare to the estimated peat burnt areas from GFED5 for each region, to allow for the effects of peat burning on atmospheric composition to be further understood and verified. Correlations were also conducted between INFERNO-peat peat BA and the atmospheric composition data and compared against the correlations using GFED5. Further details on the data analysis carried out can be found in Chapter 4 Section 2.1

Chapter 3: Representing northern high latitude peat fires in the JULES-INFERNO global fire model

This chapter contains work that was published in Geoscientific Model Development in April 2024 under the title “INFERNO-peat v1.0.0: a representation of northern high-latitude peat fires in the JULES-INFERNO global fire model”.

Abstract

Peat fires in the northern high latitudes have the potential to burn vast amounts of carbon rich organic soil, releasing large quantities of long-term stored carbon to the atmosphere. Due to anthropogenic activities and climate change, peat fires are increasing in frequency and severity across the high latitudes. However, at present they are not explicitly included in most fire models. Here I detail the development of INFERNO-peat, the first parameterisation of peat fires in the JULES-INFERNO fire model, built upon extensive knowledge from lab and field-based studies on peat fire ignition and spread to be able to model peat burnt area, burn depth and carbon emissions. INFERNO-peat improves the representation of burnt area in the high latitudes, with peat fires simulating on average an additional 0.305 M km^2 of burnt area each year, emitting 224.10 Tg of carbon. Compared to GFED5, INFERNO-peat captures ~20 % more burnt area, whereas INFERNO underestimated burning by 50 %. Additionally, INFERNO-peat substantially improves the representation of interannual variability in burnt area and subsequent carbon emissions across the high latitudes. Therefore, explicitly modelling peat fires shows a substantial improvement in the fire modelling capabilities of JULES-INFERNO, highlighting the importance of representing peatland systems in fire models.

1. Introduction

Northern high latitude peatlands represent globally important stores of carbon, containing approximately 415 Pg C (Hugelius et al., 2020), which have accumulated over millennia and exert a net cooling effect on the atmosphere (Frolking and Roulet, 2007). Consequently, peatlands represent a significant area of carbon sequestration, that if damaged could lead to vast carbon losses, with a positive feedback effect on the climate system (Loisel et al., 2021; Swindles et al., 2019; Hugelius et al., 2020; Tarnocai, 2009; Zhao and Zhuang, 2023). However, the northern high latitudes are undergoing rapid anthropogenic induced climate change and are increasingly threatened by human activities and land use change (Bruhwilder et al., 2021; Walsh et al., 2020; Zhang et al., 2022). Consequently, peatlands are becoming more vulnerable to wildfires (Turetsky et al., 2015; Dadap et al., 2019).

Peat fires are some of the largest and most persistent wildfires on Earth (Rein, 2013), which release vast amounts of long-term stored carbon, roughly equivalent to 15% of that of anthropogenic

emissions (Lasslop et al., 2019; Loisel et al., 2020; Poulter et al., 2006; Rein, 2015). The vast majority of fires in the northern high latitudes are ignited by lightning (Wendler et al., 2011; McCarty et al., 2021; Xu et al., 2022), but human activities such as timber and energy extraction, prescribed burning and tourism can also lead to fires (McCarty et al., 2021). In the high latitudes, wildfires and peat fires are becoming increasingly common (McCarty et al., 2021; Walsh et al., 2020; York et al., 2020). For example, 2020 was a severe wildfire season in Siberia, damaging an estimated 0.71 M ha of carbon rich peatlands (Descals et al., 2022). Therefore, peat fires are an important environmental disturbance in the high latitudes, and their increasing commonality is a concern for the peatland carbon sink. As a result, it is important that peat fires, and their effects, are understood, in order to gain insight into how they might change in the future and the implications this may have on the global climate system.

Peat fires burn predominantly through smouldering combustion, which is slow, low temperature and flameless burning with incomplete combustion (Rein, 2013; Huang and Rein, 2017; Rein, 2015). Smouldering is a volumetric phenomenon occurring within the peat itself, and is heavily influenced by soil properties (Rein, 2013; Rein, 2015; Archibald et al., 2018), the most important of which being soil moisture (Rein, 2013; Rein, 2015). Low soil moisture, which tends to coincide with deep water tables, facilitates greater and deeper burning of the peat, leading to greater fuel consumption (Purnomo et al., 2020; Lin et al., 2019; Benscoter et al., 2011; Turetsky et al., 2011a; Che Azmi et al., 2021). However, inorganic content, bulk density and soil temperature also exert an important control on the ignition and spread of peat fires (Rein, 2013; Rein, 2015; Lin et al., 2021). More information on how these properties influence the spread of peat fires can be found in Chapter 1 section 3).

How deep a peat fire propagates into the soil determines the amount of carbon that is exposed to combustion and that is consequently emitted to the atmosphere (Lin et al., 2021; Huang and Rein, 2017; Che Azmi et al., 2021). Immediately following a fire, peatlands are net source of carbon (Wieder et al., 2009). In an ideal world, over time this carbon can be reaccumulated through vegetation regrowth and peatland recovery, allowing peatlands to remain net carbon sinks (Wilkinson et al., 2023; Wieder et al., 2009; Ingram et al., 2019). However, carbon lost during a peat fire can be equivalent to as much as 330-450 years of carbon reaccumulation (Ingram et al., 2019; Turetsky et al., 2011b), but with fire return intervals averaging 15-120 years in the high latitudes (Sizov et al., 2021; Turetsky et al., 2011b), many peatlands will not be able to reaccumulate the lost carbon, resulting in a net loss to the atmosphere. Net losses of carbon from peat fires, could consequently lead to a positive feedback effect on the climate system.

Smouldering peat fires also emit a range of trace gases including CO_2, CO, CH_4 and NH_3, as well as aerosols (Hu et al., 2019a; Voulgarakis and Field, 2015). Emissions from peat fires are so strong that they are considered a dominant force in driving interannual variability of global fire emissions, especially CO, highlighting the considerable impacts peat fires have on global atmospheric

composition (van der Werf et al., 2010; Voulgarakis et al., 2015). The release of aerosols from peat burning is particularly concerning, as they can degrade air quality and lead to hazardous haze events (Turetsky et al., 2015; Hu et al., 2018). Haze can disrupt transport, tourism and agriculture (Hu et al., 2018; Heil and Goldammer, 2001), as well as leading to respiratory and cardiovascular problems (WHO, 2006; Hu et al., 2018). For example, in 2010 peat fires in the Moscow region of Russia severely degraded air quality and resulted in 11,000 additional deaths (Konovalov et al., 2011; Shaponshnikov et al., 2014). Consequently, peat fires are of major concern for the climate and air quality.

Peat fires also have widespread and major impacts on ecosystems. Peat fires can lead to altered ecosystem composition and successional trajectories, drive changes to soil moisture and nutrient dynamic and ultimately alter the functioning of peatlands leading to further carbon losses (Kettridge et al., 2015; Kettridge et al., 2019; Mekonnen et al., 2021). Approximately 50% of high latitude peatlands are underlain by permafrost (Hugelius et al., 2020). In these areas fires can result in permafrost warming, thawing, degradation, and thermokarst development, driving further carbon losses (Chen et al., 2021a; Nitze et al., 2018). Hence, peat fires have the potential to shift ecosystem functioning and further exacerbate carbon emissions from peatlands. More detailed information on the impacts of peat fires can be found in Chapter 1 section 4.

In recent decades peatlands have become more vulnerable to fires (York et al., 2020; Talucci et al., 2022) and climate change is expected to further amplify the vulnerability of peatlands to fires as a result of rising temperatures, increased frequency and intensity of droughts, and increases in fire weather (Thompson et al., 2019; Descals et al., 2022; Lund et al., 2023). Lightning strikes are also expected to increase in frequency (Chen et al., 2021a), which may help to drive increases in the frequency and severity of peat fires in the coming century (McCarty et al., 2021; Turetsky et al., 2015). This is of particular concern as increased peat fire occurrence, will result in greater carbon emissions, and potentially a positive feedback on the climate system, resulting in a catastrophic loss of carbon (Mack et al., 2011; Chen et al., 2021a; Turetsky et al., 2015), and potentially a switch from peatlands being a carbon sink to a source of carbon by 2100 (Wilkinson et al., 2023).

Despite the importance of peat fires, at present they are not explicitly incorporated into most fire models, meaning that the influence of peat fires on climate, the carbon cycle, air quality and ecosystems cannot be accurately assessed. It also means that most fire models fail to reproduce observed patterns of burnt area, especially in the high latitudes. Additionally, fire models tend to fail to simulate interannual variability in burnt area and carbon emissions, in part due to the lack of consideration of peat fires. Therefore, fire models are limited in their abilities to predict future fire activity, particularly in the northern high latitudes (Jones et al., 2022). Peat fires are also a crucial component for representing carbon balances in the northern high latitudes within Earth system models

(Wilkinson et al., 2023). Therefore, it is important that peat fires are included into fire models and ultimately Earth system models in order to better represent high latitude systems, and how they may change in the future. Currently only the Community Earth System Model (CESM), through its land surface model CLM-Li (Li et al., 2013), represents peatland burning. Details of the CLM-Li approach can be found in Chapter 2 section 1.1. Whilst the CLM-Li approach was a major step forward it does not consider the impacts of soil properties on peat fires (Li et al., 2013), and therefore its scope and accuracy are limited.

Therefore, this chapter details the development and evaluation of INFERNO-peat, a novel parameterisation of peat fires in the northern high latitudes in the INFERNO fire model. INFERNO (INteractive Fire and Emission algoRithm for Natural envirOnments) is a reduced complexity fire model that sits within the Joint UK Land Environment Simulator (JULES) land surface model (Mangeon et al., 2016). INFERNO is detailed in Chapter 2 section 2, but briefly, it estimates burnt areas from ignitions (from lightning and population density) and plant functional type (PFT) flammability (driven by climatic and vegetation variables). INFERNO is capable of accurately diagnosing global burnt area (Mangeon et al., 2016), and compares well to other fire models on a global scale (Hantson et al., 2020). However, in the high latitudes INFERNO fails to capture a large amount of burnt area compared to observations and does not capture the interannual variability in carbon emissions, thought to result from a lack of representation of peat fires (Mangeon et al., 2016). Therefore, INFERNO-peat was developed with the aim of filling this gap and allowing for more accurate representations of burning in the high latitudes. The remainder of this chapter aims to describe the development of INFERNO-peat and evaluate its performance over the recent historical observational period.

2. Methods

INFERNO-peat is a simplified peat fire model that simulates peat burnt area, depth of burn and carbon emissions. INFERNO-peat is an offline model which is run in python vn3.8 using outputs from JULES-INFERNO and numerous prescribed datasets (detailed below). The model, its inputs, and fundamental equations are described in detail in Chapter 2 section 3 and in Blackford et al., (2024). To summarise, INFERNO-peat is formed of 5 main equations. Firstly, 1) the number of potential peat fire ignitions are calculated (Equation 7) utilising lightning and population density to calculate total ignitions, as per INFERNO (Equation 1-Equation 3). Total ignitions are then scaled down using PFT flammability and fractions to effectively give the number of flaming vegetation fires which could potentially ignite a peat fire. 2) A calculation of peat probability of ignition (Equation 8) is based on key relationships with soil moisture, inorganic content and bulk density (Frandsen, 1997). For the simulations presented here, fixed values for inorganic content and bulk density of 9.4% and 222kg/m^3 respectively were used (Frandsen, 1997), in order to minimise potential sources of

additional error in the model. 3) peat burnt area is then estimated as the product of peat ignitions, peat ignition probability, average peat fire burnt area, and the grid cell fraction of peat (Equation 9). The use of an average peat fire burnt area directly replicates INFERNO, which uses average PFT burnt areas in its calculation of burnt area (Mangeon et al., 2016; Equation 5). 4) peat depth of burn is calculated as an adaptation of the scheme used by Lin et al., (2021), whereby the critical soil temperature is estimated based off the moisture content of the soil. But additionally, INFERNO-peat also uses water table depth to constrain the depth of burn. Finally, 5) carbon emissions resulting from peat fires are calculated from peat burnt area, depth of burn, the carbon content of the peat and combustion completeness (Equation 11).

Numerous driving variables are used in INFERNO-peat and are summarised in Table 5. Gridded peatland fractions and carbon contents were prescribed to the model from the Northern Peatland Dataset (NPD; Hugelius et al., 2020). More details on the NPD can be found in Chapter 2 Section 4. Ignitions are calculated using human population density from the HYDE dataset (Hurtt et al., 2011), and lightning data from the LIS-OTD (Lightning Imaging Sensor – Optical Transient Detector) lightning climatology (Christian et al., 2003), as well as the WGLC (Worldwide Lightning Location Network – WWLLN – Global Lightning Climatology and time series) lightning time series (Kaplan and Lau, 2021). PFT fractions and flammabilities are obtained from a JULES-INFERNO simulation, using JULES vn5.4 in the TRENDY set up using the TRIFFID dynamic vegetation model. Fixed values were used in INFERNO-peat for inorganic content, bulk density and combustion completeness in order to minimise potential additional sources of error.

Table 5: Summary of the input variables required for INFERNO-peat, and the source of these variables used in the present-day INFERNO-peat runs.

Variable	Abbreviation	Units	Source
Population density	PD	People/km^2	HYDE
Lightning	L	Flashes/km^2	LIS-OTD or WGLC
PFT flammability	$Flam_{PFT}$	0-1	TRENDY JULES
PFT fraction	$Frac_{PFT}$	0-1	TRENDY JULES
Soil moisture	SM	%	JULES-peat
Water table depth	zw	m	JULES-peat
Soil temperature	tsoil	°C	JULES-peat
Inorganic content	IC	%	Prescribed value
Bulk density	ρ	Kg/m^3	Prescribed value
Peat fraction	$Frac_{peat}$	%	Northern peatland dataset
Peat carbon content	C_{peat}	Kg/m^2	Northern peatland dataset
Maximum depth of burn	BDmax	m	Prescribed value
Combustion completeness	CC	0-1	Prescribed value

For the peat soil variables (SM, zw, tsoil), an experimental JULES run utilising new peat module developments (Chadburn et al., 2022), was used which assumes that from 50° north all soils are organic, therefore producing a better representation of the northern peatland soil physics and

dynamics. Standard JULES operates in a similar manner, but instead assumes that all soils are mineral. Within early INFERNO-peat testing I identified this to be causing a systematic bias in the model towards peatlands being drier than they should be, and consequently resulting in inflated burnt area estimates (Figure 12). When INFERNO-peat was run with mineral soil variables negative correlations were present between peat fraction and its probability of ignition, whereby grid cells with smaller peat fractions tend to be more likely to ignite (Figure 12a). This results in large peat burnt areas (Figure 12b) and a tendency towards a positive bias in the model compared to GFED5 observations. The inflation in the probability of ignition potentially results from using soil moisture which is more reflective of non-peat soils. For example, grid cells that have smaller peat fractions are biased towards lower moisture content values (Figure 12c), meaning that the moisture of peat soils (which should be higher than mineral soils) in particular in these grid cells where we have smaller peat fractions is not being well represented. Therefore, there is a fundamental bias in the model whereby smaller peat fractions are biased towards lower moisture content percentages, consequently inflating ignition probabilities and thus peat burnt area.

This issue was resolved when using organic soil moisture (Figure 13). Whilst using organic soil moisture there is still a negative correlation between peat fraction and peat ignition probability (Figure 13a), due to smaller peat fractions tending to have lower moisture contents (Figure 13c), these biases are significantly reduced compared to the standard JULES soil moisture. Therefore, the same burnt area inflations are no longer as commonly seen (Figure 13b). Consequently, for present day simulations of peat fires, INFERNO-peat was run using organic soil variables from JULES-peat.

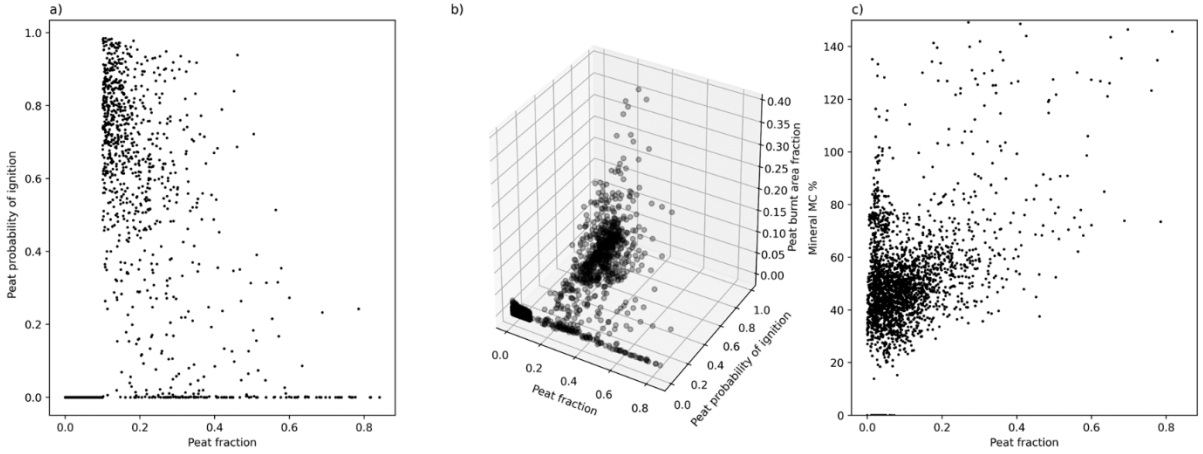


Figure 12: Diagnostic plots from INFERNO-peat using mineral soil moisture, showing the relationship between peat fraction and a) probability of ignition, b) probability of ignition and peat burnt area, and c) organic moisture content.

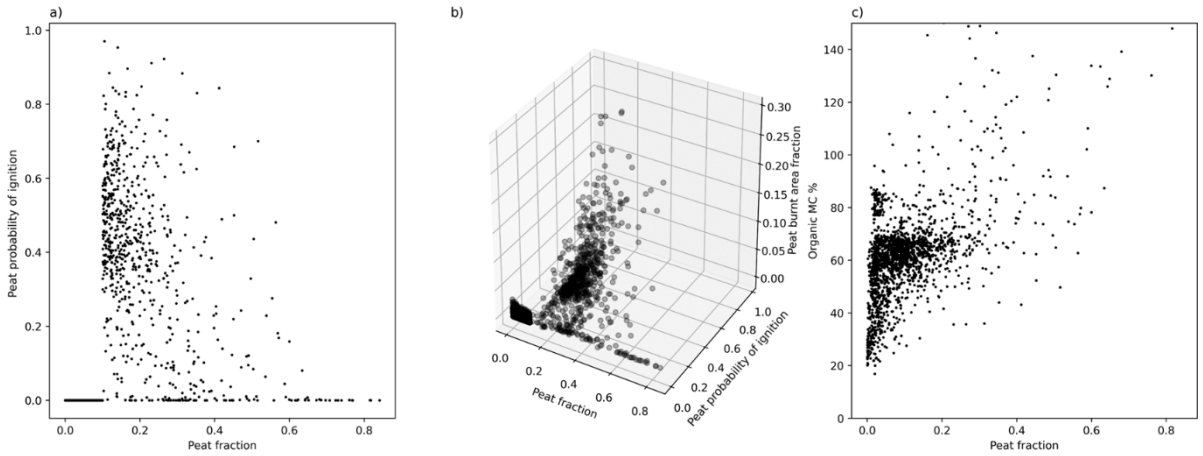


Figure 13: Diagnostic plots from INFERNO-peat using organic soil moisture, showing the relationship between peat fraction and a) probability of ignition, b) probability of ignition and peat burnt area, and c) organic moisture content.

Prescribed values for maximum depth of burn and combustion completeness of 0.4m and 0.8 were used in the simulations presented in this chapter and were selected through a sensitivity analysis. I carried out 16 unique runs using combinations of 4 different maximum depths of burn and 4 different combustion completeness values. The maximum depths of burn tested were 0.2m, 0.4m, 1m and 3m (entire soil column). Combustion completeness values of 0.4, 0.6, 0.8 and 1.0 were used. To evaluate model performance, Root Mean Squared Error (RMSE) was calculated between each of the runs and GFED500m belowground burning observations. Sensitivity analysis revealed the optimum combination of values to be 0.4m for maximum depth of burn, and 0.8 for combustion completeness (Figure 14), therefore these values were used in the model runs presented in Chapter 3. Furthermore, to ensure that the maximum depth of burn parameter was not effectively acting a as fixed depth of burn with the majority of grid cells hitting it, a histogram of simulated average values across the northern high latitudes between 2010 and 2014 was plotted (Figure 15). It is evident that the burn depth values are rarely reaching 40cm, with the majority of grid cells burning less that the top 4cm.

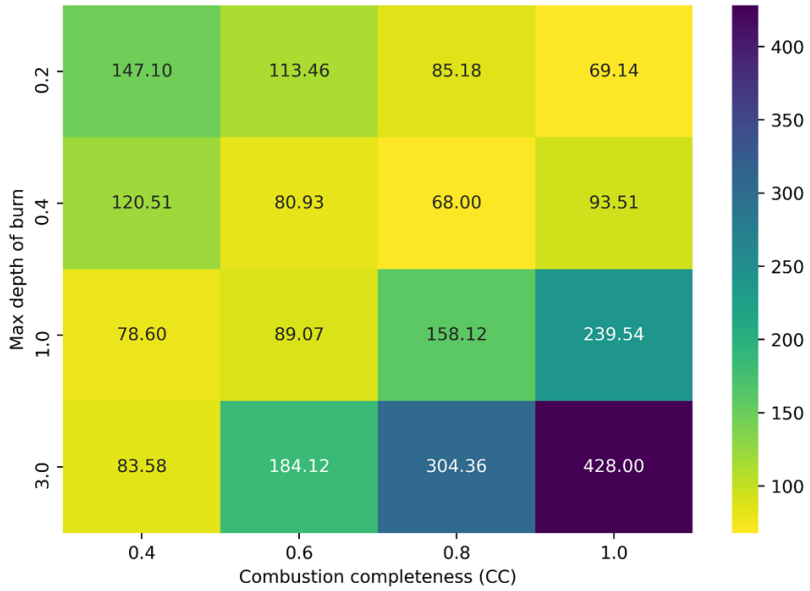


Figure 14: Sensitivity analysis of RMSE across maximum depth of burn and combustion completeness values.

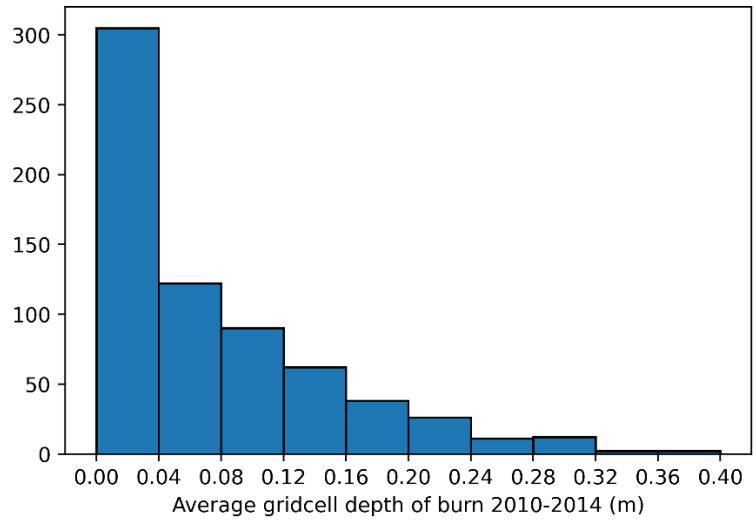


Figure 15: Histogram of the average grid cell depth of burn between 2010 and 2014 for the INFERNO-peat simulation using BD_{max} = 0.4 and CC = 0.8.

2.1. Model evaluation

In order to evaluate model performance, INFERNO-peat was run over the recent historical period which overlaps with multiple observational datasets from 1997 to 2014. INFERNO-peat in these simulations could not be run beyond 2014, as data from JULES-peat was only available up until 2014. Two different datasets for lightning were used to ascertain the impacts of using a lightning climatology compared to a time series in the model. Due to the length of the data, the run using WGLC lighting data could only be conducted for 2010-2014. INFERNO-peat was run at a N96 resolution (1.25° latitude X 1.875° longitude) at monthly time steps.

Model evaluation was conducted using numerous datasets for the different parameters (Summarised in Table 6). It is known that satellite-based products struggle to detect peat fires in the high latitudes (McCarty et al., 2021), therefore multiple products were used to try and mitigate this issue. For a detailed discussion on remote observations of fires and specifically peat fires, please see Chapter 2, Section 5. Peat BA was evaluated against BA data from GFED4s (van der Werf et al., 2017), GFED5 (Chen et al., 2023a; Chen et al., 2023b), and FireCCILT11 (Otón et al., 2021). The ABoVE-FED (Potter et al., 2023) dataset was also used to evaluate burnt area in Alaska and Canada. Carbon emissions were evaluated using GFED4s (van der Werf et al., 2017), GFED500m (van Wees et al., 2022) and GFAS (Kaiser et al., 2012).

Table 6: The different observational datasets used for model evaluation, the variables used from each and what evaluation was conducted using them.

Product	Variables used	Evaluation conducted	Reference
GFED4s	BA, emitted C	Spatial and temporal BA, temporal C	Van der Werf et al. (2017)
GFED5	BA	Spatial and temporal BA	Chen et al. (2023)
GFED500m	Emitted C (total, aboveground, and belowground)	Temporal C	Van Wees et al. (2022)
GFASv1.2	Emitted C	Temporal C	Kaiser et al. (2012)
FireCCILT11	BA	Spatial and temporal BA	Oton et al. (2021)
ABoVE-FED	BA	Spatial and temporal BA for North American subregions	Potter et al. (2023)

Spatial correlations using Pearson's R, alongside RMSE (Root Mean Squared Error) were used to diagnose spatial performance in burnt area. As satellite-based products are known to underestimate BA, and particularly peat BA, in the northern high latitudes (McCarty et al., 2021), an adaptation to RMSE was made to create a new metric (hereafter referred to as M), which considers that the observations likely underestimate BA. RMSE measures the difference between predicted and actual values, essentially meaning that any values that are not on a 1:1 line contribute towards the mean error of the model. However, what M does is neutralise any values that are above the 1:1 line i.e. where simulated values are greater than observed values, allowing for only underpredicting values to contribute towards the mean error of the model. Therefore, M is calculated following Equation 14 when the simulated values (*sim*) are less than the observed values (*obs*). However, when $sim \geq obs$, the contribution to the summation is taken as zero, rather than using the term $(sim_i - obs_i)^2$. N is the total number of values.

Equation 14

$$M = \sqrt{\frac{\sum_i^N (sim_i - obs_i)^2}{N}}$$

Temporal correlations, again using Pearson's R, were also conducted for the entire timeseries, alongside comparisons of variation metrics such as standard deviation (STD) and the coefficient of variation (CV) for both burnt area and carbon emissions.

Analysis was also carried out on subregions of the high latitudes, in order to examine any different trends and patterns in peat burning in and among different areas of the high latitudes. Seven subregions were selected, 3 for North America and 4 for Eurasia (Figure 16) to represent different geographic and ecological areas. Table 7 describes the naming conventions and latitudinal and longitudinal coordinates for each subregion used throughout Chapter 3, alongside information on the dominant landcover types and notable geographical features present in each subregion.

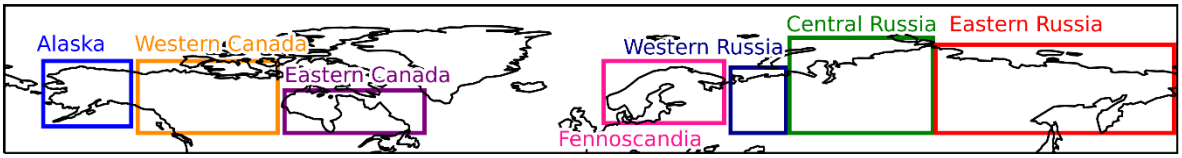


Figure 16: The location of the seven subregions used to evaluate the performance of INFERNO-peat in the northern high latitudes.

Table 7: Summary of the seven subregions, their geographical coordinates, corresponding GFED region, and notable characteristics. Dominant landcover types are obtained from JULES-INFERNO.

Subregion	Coordinates	GFED region	Dominant landcover types	Notable geographic features
Alaska	(167°W, 73°N), (140°W, 53°N)	Boreal North America	Needleleaf tree evergreen and deciduous, C3 grass and bare soil.	Split into three distinct geographic zones from mountainous in the south, intermontane basins and plateaus in the centre, and Arctic coastal plains in the North.
Western Canada	(140°W, 73°N), (95°W, 50°N)	Boreal North America	Needleleaf tree evergreen and deciduous, C3 grass and bare soil.	Includes part of the Canadian Rocky Mountains to the west, and plains, lowlands, and the Canadian Shield to the east.
Eastern Canada	(95°W, 64°N), (52°W, 50°N)	Boreal North America	Needleleaf tree evergreen.	Includes the Hudson Bay lowland peatlands and the Canadian Shield.
Fennoscandia	(4°E, 73°N), (42°E, 54°N)	Europe	Needleleaf tree evergreen.	Rough, mountainous terrain to the west and plains and lowlands to the east.
Western Russia	(42°E, 71°N), (60°E, 50°N)	Boreal Asia	Needleleaf tree evergreen.	Plains and lowlands, bounded by the Ural Mountains in the east.
Central Russia	(60°E, 80°N), (105°E, 50°N)	Boreal Asia	Needleleaf tree deciduous and bare soil.	Includes the Great Vasyugan Mire, the west Siberian plain and part of the central Siberian plateau.
Eastern Russia	(105°E, 78°N),	Boreal Asia	Needleleaf tree	Includes part of the central

(180°E, 50°N)	deciduous, bare soil and C3 grass.	Siberian plateau, the Yakutsk Basin and the eastern highlands including the Kolyma Mountains.

3. Results

3.1. Burnt area

The incorporation of peat fires into INFERNO results in an overall improvement in total BA compared to observations (Figure 17; Table 8). INFERNO-peat models that, on average, peat fires burn an additional 0.305 M km^2 each year across the high latitudes. This additional BA brings the total INFERNO-peat BA, of 0.520 M km^2, to within 0.09 M km^2 of the GFED5 observations (Table 8). However, when INFERNO-peat is driven by the WGLC lightning climatology, there is significantly less peat burning, with peat fires contributing only an additional 0.067 M km^2 per year across the high latitudes (Figure 17b, c; Table 8). Whilst the use of a lightning timeseries brings BA estimates close to that of the FireCCILT11 dataset, INFERNO-peat WGLC massively underestimates total BA compared to GFED5 (Table 8). It is also crucial to note that the INFERNO-peat LIS-OTD model runs estimate BA to be twice as large as is estimated from standard INFERNO, which may be an overestimation of BA from peat fires. It is possible that some of the additional BA modelled by INFERNO-peat may in reality not actually be peat burning, and instead is capturing northern high latitude vegetation fires that are missed by INFERNO.

Table 8: 2010 to 2014 average annual burnt area (M km^2) and statistics for the various models and observations.

		R			RMSE		
Model	BA	GFED4S	GFED5	FireCCILT11	GFED4S	GFED5	FireCCILT11
INFERNO	0.215	0.485	0.530	0.486	0.061	0.095	0.068
INFERNO-peat LIS-OTD	0.520	0.414	0.431	0.398	0.098	0.124	0.099
INFERNO-peat WGLC	0.282	0.475	0.510	0.467	0.071	0.099	0.076
GFED4s	0.172		0.820	0.868		0.068	0.028
GFED5	0.429	0.820		0.879	0.068		0.053
FireCCILT11	0.276	0.868	0.879		0.028	0.053	

INFERNO-peat allows for better representation of clusters of burning across the high latitudes compared to INFERNO, especially in western Canada, central Siberia and eastern Siberia (Figure 17). However, there are also clear regions of overestimation of BA compared to observations in western Russia and eastern Canada (Figure 17). Interestingly, these areas also see overestimations in BA in INFERNO, perhaps suggesting a driving force of these overestimations are underlying biases in JULES-INFERNO itself. Opposingly, INFERNO-peat underrepresents burning in Alaska compared to all the observations. There is also a notable area of southern Russia, where there is a high degree of

burning in all observational datasets, but minimal burning in both INFERNO and INFERNO-peat. JULES models this region of Russia as an area dominated by C3 crops (Figure 28). In addition, the Northern peatland dataset (Figure 8) indicates that there is minimal peatland coverage in southern Russia. Therefore, the underestimations seen in INFERNO and INFERNO-peat are likely a product of INFERNO failing to represent cropland burning and agricultural fire management, rather than peat fires.

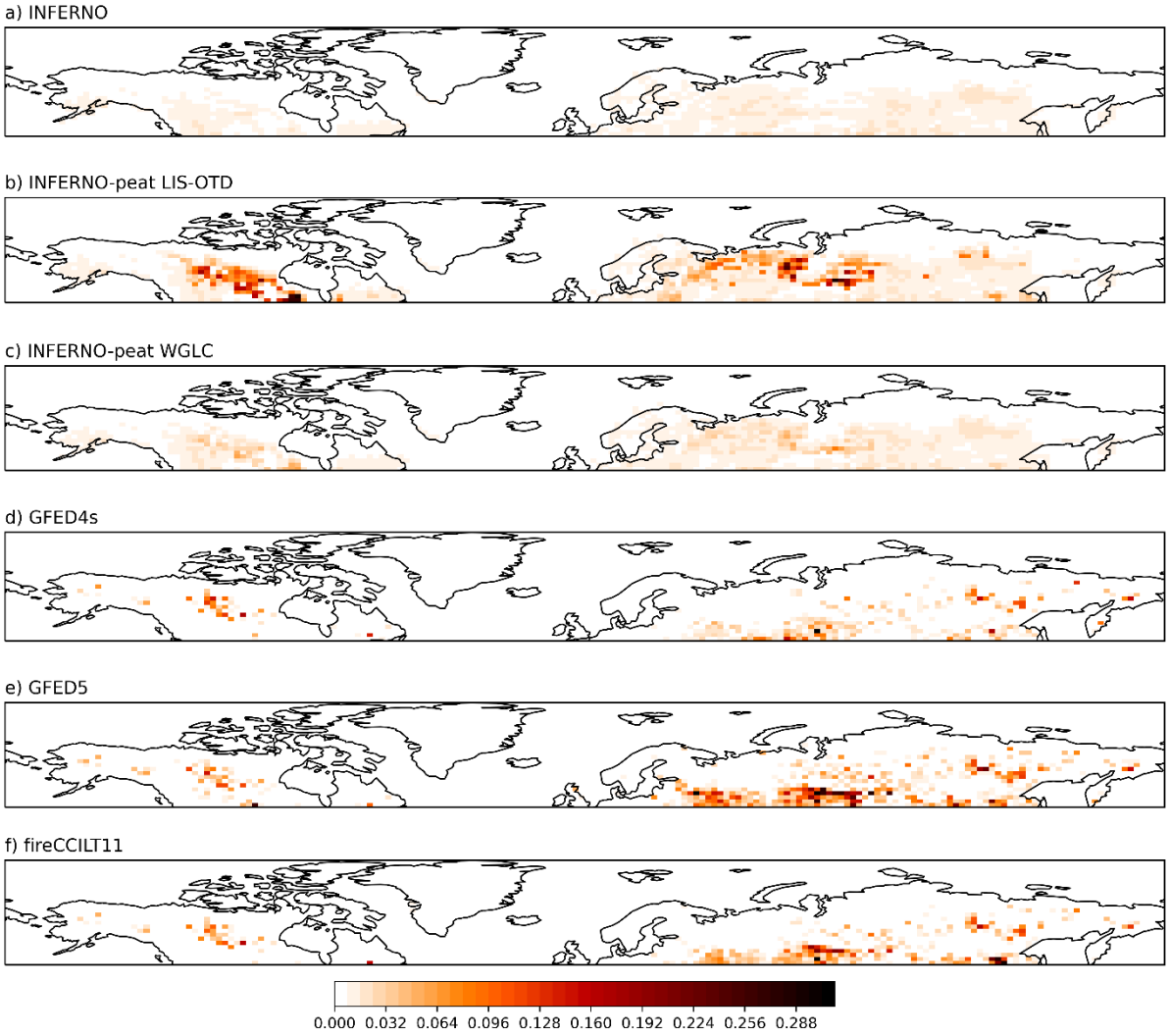


Figure 17: The 2010 to 2014 average annual burnt area fraction for INFERNO (a), INFERNO-peat driven by LIS-OTD climatology (b), INFERNO-peat driven by WGLC timeseries (c), GFED4s (d), GFED5 (e) and fireCCILT11 (f).

Across the high latitudes when compared to all observation datasets, despite INFERNO-peat capturing more BA, bringing it closer to total observation estimates, lower spatial correlations with all observational datasets are seen compared to standard INFERNO (Table 8). Similarly, both INFERNO-peat runs see higher RMSE values for the high latitudes as a whole, indicating poorer spatial agreement in BA in INFERNO-peat compared to INFERNO with the observations (Table 8). However, these statistics do not necessarily produce a true reflection of what is occurring within the

models and observations. As is shown in Figure 17, there are clear improvements in certain regions of the northern high latitudes such as western Canada, eastern Siberia, and central Siberia, therefore suggesting that in these regions the model is performing significantly better than INFERNO (see more in section 3.1.1). Additionally, satellite observations of peat fires are known to omit significant amounts of peat fires, as a result of the low temperature and below ground burning that occurs, making them difficult to be detected by standard procedures (Chen et al., 2021b; McCarty et al., 2021; Yang et al., 2023). Consequently, it is likely that all the observational products used here underestimate BA, particularly in peatlands. This makes evaluating a peat fire model difficult, as even the best observational products are likely still missing a large amount of burnt area, so a model is being evaluated against underestimated observations. Therefore, metrics such as R and RMSE may indicate that INFERNO-peat performs poorly as it is being penalised for overpredicting compared to the underestimated observations.

Consequently, a new metric (M) was developed that adapts the RMSE to take into account that the observations miss some fires. Consequently, INFERNO-peat shows improvements in M compared to INFERNO, for both lightning dataset runs (Table 9). For example, there is a large drop in M from 0.727 in INFERNO to 0.555 in INFERNO-peat LIS-OTD when compared against GFED5. Therefore, INFERNO-peat shows an improvement in the model's ability to replicate spatial patterns in burnt area in the northern high latitudes, when the fact that the observations likely underestimate BA is considered.

Table 9: Values of M (RMSE adapted to consider that the observations underestimate BA) for the different models and observational datasets using the 2010 to 2014 average annual BA.

	M		
Model	**GFED4s**	**GFED5**	**FireCCILT11**
INFERNO	0.471	0.727	0.785
INFERNO-peat LIS-OTD	0.306	0.555	0.550
INFERNO-peat WGLC	0.329	0.578	0.570

INFERNO-peat shows significant improvements across the entirety of the model run (1997 to 2014) in the representation of interannual variability (IAV) in burnt area compared to INFERNO (Figure 18). Significantly higher IAV is captured in INFERNO with an increase in standard deviation from 0.011 in INFERNO to 0.041 in INFERNO-peat, bringing the model closer to the magnitude of IAV seen in the observations (Table 10). Similarly, INFERNO-peat also has a higher coefficient of variation of 0.094 compared to just 0.058 in INFERNO, again a marked improvement compared to the observations (Table 10). On a temporal scale there are also improvements in the R value in INFERNO-peat across the observations, meaning that INFERNO-peat is more accurately capturing the timing of the IAV in BA than INFERNO (Table 10). However, when compared to GFED5 there are still noteworthy underestimations in BA IAV in INFERNO-peat, mainly between 2001 and 2011

(Figure 18). In particular, GFED5 shows large spikes in BA in 2003 and 2008, which are not as pronounced in INFERNO-peat, even though they are captured in a qualitative sense.

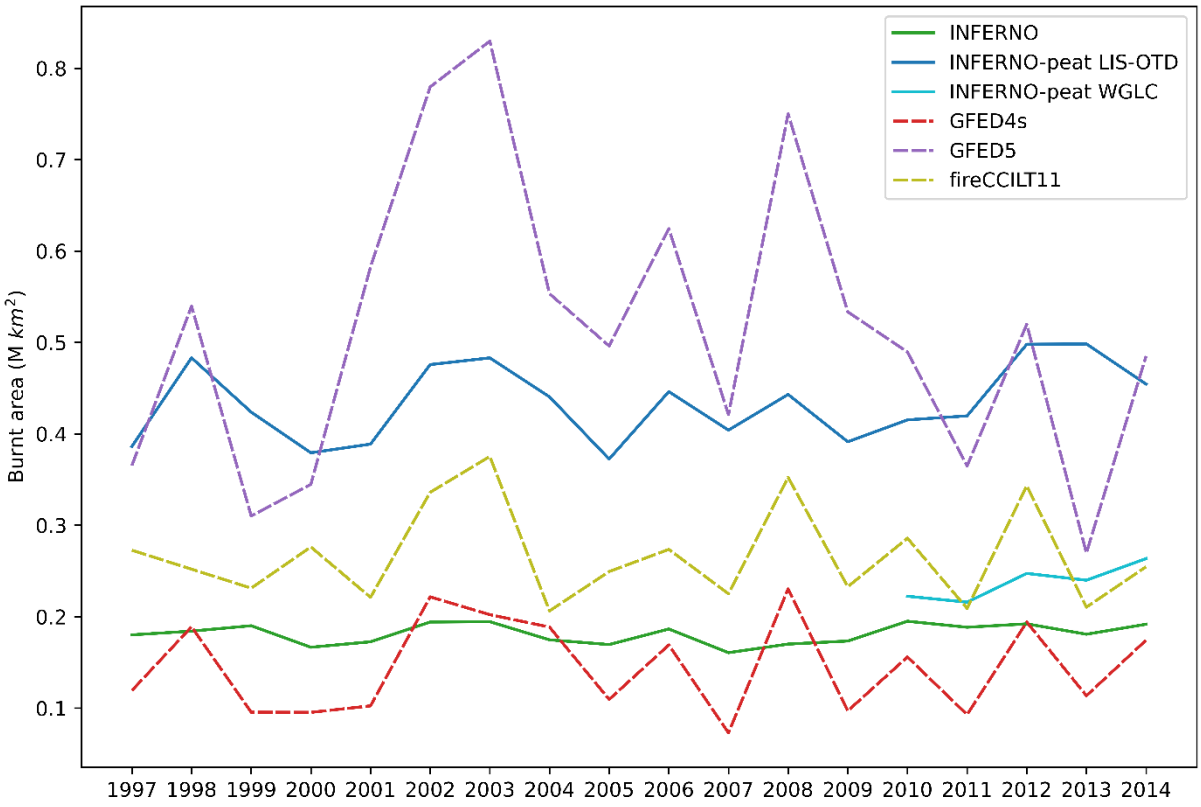


Figure 18: The annual total burnt area across the high latitudes (<50o N) from 1997 to 2014 compared between the models (indicated by solid lines) and observations (indicated by dashed lines).

Table 10: 1997 to 2014 average annual burnt area, temporal standard deviation (std), coefficient of variation (cv) and temporal correlation (R), for models and observations. Correlation coefficients for the WGLC period (2010-2014) are available in Table S1.

Model	Average annual BA (M km^2)	std	cv	R (GFED4s)	R (GFED5)	R (fireCCILT11)
INFERNO	0.181	0.011	0.058	0.463	0.206	0.370
INFERNO-peat LIS-OTD	0.434	0.041	0.094	0.676	0.323	0.394
GFED4s	0.146	0.050	0.340		0.759	0.709
GFED5	0.514	0.155	0.300	0.759		0.692
fireCCILT11	0.267	0.051	0.192	0.709	0.692	

3.1.1. Subregion analysis

Due to the prevalence of regional features and patterns in the northern high latitudes, seven subregions were examined in detail (Figure 16). On average, across all three North American subregions, INFERNO-peat overestimates burning compared to the observations, including the North American only dataset ABoVE-FED (Figure 19). Whilst the overestimation is only minor in Alaska, western Canada displays a significant pronounced overestimation, with INFERNO-peat LIS-OTD

estimated BA around 2.5 times greater than in GFED5. However, the estimated average annual BA in the WGLC INFERNO-peat run of 0.048 M km^2 is much closer to the GFED5 estimate of 0.047 M km^2. However, there is better spatial correlation in BA in western Canada in INFERNO-peat compared to INFERNO when correlated with GFED4s, FireCCILT11 and ABoVE-FED (Table 11), reflecting that in western Canada modelling peat fires significantly improves the ability of fire models to reflect spatial patterns in burnt area. Similarly in Alaska, INFERNO-peat outperforms INFERNO in terms of spatial correlations in BA with all the observations, and in particular shows strong correlations with the ABoVE-FED dataset (Table 11). Large overestimations in BA by INFERNO-peat LIST-OTD are also seen in eastern Canada, where INFERNO-peat estimates 0.074 M km^2 BA each year, 10 times higher than GFED5, and 7 times higher than ABoVE-FED (Figure 19). Consequently, INFERNO without peat fires has a higher correlation and smaller RMSE values with all datasets (Table 11).

In contrast in Fennoscandia the opposite is true, with both INFERNO-peat runs showing smaller average annual BA's than GFED5 (Figure 19). INFERNO-peat LIS-OTD does however show a significant improvement from INFERNO, capturing on average 0.035 M km^2 of BA each year compared to just 0.019 M km^2 in INFERNO. Much closer to the 0.048 M km^2 of BA each year estimated in GFED5. However, spatially, INFERNO shows better correlations and records lower RMSE values with all datasets (Table 11).

It is apparent that INFERNO-peat performs well in western Russia, regardless of the lightning dataset used in terms of total annual average BA (Figure 19). According to GFED5, approximately 0.040 M km^2 burns annually. In comparison, INFERNO-peat LIS-OTD models only 0.007 M km^2 more BA, and INFERNO-peat WGLC only 0.006 M km^2 less BA. However, in central and eastern Russia INFERNO-peat still underestimates burning, especially compared to GFED (Figure 19). In central Russia, INFERNO-peat LIS-OTD models 0.151 M km^2 of BA on average each year, 0.036 M km^2 short of the BA estimated by GFED5. However, compared to GFED4s and FireCCILT11, INFERNO-peat does capture more BA than these datasets estimate. However, the spatial pattens of burning in these regions show weaker correlations with all the observational datasets than standard INFERNO (Table 11). Therefore, whilst total burning in western and central Russia may be similar to the observations, the spatial pattern of BA is not being well modelled by INFERNO-peat.

In eastern Russia, whilst INFERNO-peat increases the amount of burning relative to INFERNO, it only captures, 0.065 M km^2 in the LIS-OTD run and 0.055 M km^2 in the WGLC run, significantly lower than is observed GFED5 and FireCCILT11 which both capture almost 0.100 M km^2 of BA each year on average. However, the small increases in BA resulting from modelling peat fires does help to improve the model's spatial performance, with high correlations with all observational datasets (Table

11). Additionally, eastern Siberia is the only subregion in which lower RMSE values are seen in the INFERNO-peat runs than the INFERNO runs (Table 11).

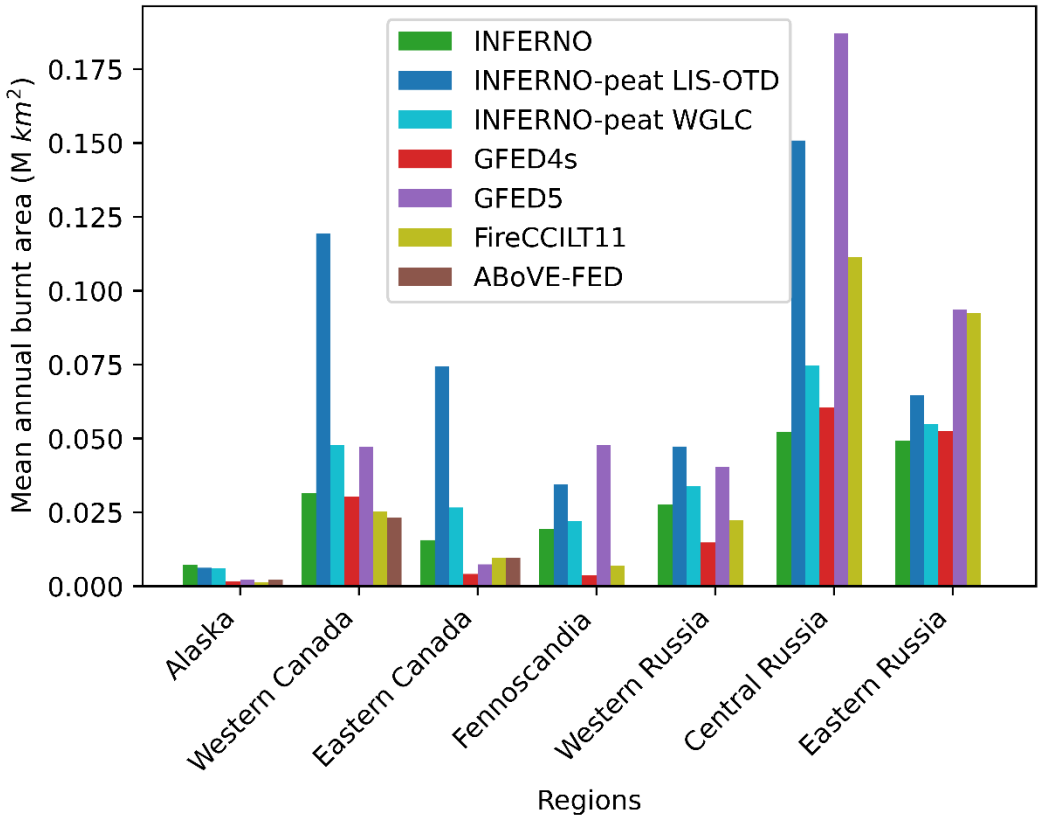


Figure 19: The average annual burnt area (2010-2014), from INFERNO, and INFERNO-peat driven by the LIS-OTD and WGLC lightning data, compared to the observations, in each subregion.

Table 11: 2010 to 2014 average annual burnt area (M km^2) and spatial statistics (Pearson's R and RMSE) for the various models and observations broken down into subregions. Note that the ABoVE-FED dataset is only for the three North American subregions.

		R				RMSE			
Model	BA	GFED4s	GFED5	FireCCILT11	ABoVE-FED	GFED4S	GFED5	FireCCILT11	ABoVE-FED
Alaska									
INFERNO	0.007	0.202	0.242	0.194	0.682	0.056	0.064	0.056	0.037
INFERNO-peat LIS-OTD	0.006	0.236	0.282	0.216	0.760	0.066	0.071	0.065	0.040
INFERNO-peat WGLC	0.006	0.224	0.272	0.203	0.763	0.066	0.071	0.065	0.040
GFED4s	0.002		0.884	0.959	0.376		0.022	0.007	0.028
GFED5	0.002	0.884		0.897	0.430	0.022		0.020	0.047
FireCCILT11	0.001	0.959	0.897		0.358	0.007	0.020		0.027
ABoVE-FED	0.002	0.376	0.430	0.358		0.028	0.047	0.027	
Western Canada									
INFERNO	0.032	0.331	0.384	0.310	0.570	0.074	0.084	0.071	0.048
INFERNO-peat LIS-OTD	0.119	0.353	0.307	0.379	0.654	0.130	0.135	0.129	0.105
INFERNO-	0.048	0.334	0.322	0.343	0.608	0.087	0.088	0.083	0.059

		R				RMSE			
Model	BA	GFED4s	GFED5	FireCCILT11	ABoVE-FED	GFED4S	GFED5	FireCCILT11	ABoVE-FED
peat WGLC									
GFED4s	0.030		0.759	0.948	0.665		0.052	0.020	0.049
GFED5	0.047	0.759		0.744	0.482	0.052		0.053	0.077
FireCCILT11	0.025	0.948	0.744		0.677	0.020	0.053		0.047
ABoVE-FED	0.023	0.665	0.482	0.677		0.049	0.077	0.047	
Eastern Canada									
INFERNO	0.016	0.330	0.379	0.295	0.630	0.065	0.079	0.072	0.048
INFERNO-peat LIS-OTD	0.074	0.256	0.285	0.132	0.467	0.148	0.183	0.133	0.118
INFERNO-peat WGLC	0.027	0.309	0.367	0.231	0.562	0.085	0.103	0.086	0.064
GFED4s	0.004		0.608	0.575	0.430		0.046	0.037	0.042
GFED5	0.007	0.608		0.909	0.548	0.046		0.024	0.051
FireCCILT11	0.009	0.575	0.909		0.566	0.037	0.024		0.042
ABoVE-FED	0.010	0.430	0.548	0.566		0.042	0.051	0.042	
Fennoscandia									
INFERNO	0.019	0.301	0.341	0.366		0.068	0.128	0.063	
INFERNO-peat LIS-OTD	0.035	0.235	0.216	0.270		0.105	0.150	0.100	
INFERNO-peat WGLC	0.022	0.238	0.266	0.285		0.083	0.141	0.078	
GFED4s	0.004		0.823	0.795			0.114	0.023	
GFED5	0.048	0.823		0.832		0.114		0.095	
FireCCILT11	0.007	0.795	0.832			0.023	0.095		
Western Russia									
INFERNO	0.028	0.397	0.324	0.243		0.084	0.108	0.096	
INFERNO-peat LIS-OTD	0.047	0.133	0.035	0.040		0.126	0.147	0.133	
INFERNO-peat WGLC	0.034	0.364	0.233	0.202		0.093	0.116	0.104	
GFED4s	0.015		0.675	0.685			0.090	0.057	
GFED5	0.040	0.675		0.894		0.090		0.058	
FireCCILT11	0.022	0.685	0.894			0.057	0.058		
Central Russia									
INFERNO	0.052	0.489	0.511	0.479		0.069	0.126	0.091	
INFERNO-peat LIS-OTD	0.151	0.274	0.272	0.236		0.127	0.154	0.132	
INFERNO-peat WGLC	0.075	0.403	0.397	0.362		0.083	0.131	0.101	
GFED4s	0.060		0.787	0.854			0.102	0.054	
GFED5	0.187	0.787		0.907		0.102		0.066	
FireCCILT11	0.111	0.854	0.907			0.054	0.066		
Eastern Russia									
INFERNO	0.049	0.480	0.502	0.478		0.068	0.089	0.082	
INFERNO-peat LIS-OTD	0.065	0.493	0.531	0.513		0.075	0.089	0.079	
INFERNO-peat WGLC	0.055	0.495	0.530	0.506		0.070	0.087	0.078	
GFED4s	0.052		0.846	0.826			0.056	0.044	
GFED5	0.094	0.846		0.864		0.056		0.044	

		R				RMSE			
Model	BA	GFED4s	GFED5	FireCCILT11	ABoVE-FED	GFED4S	GFED5	FireCCILT11	ABoVE-FED
FireCCILT11	0.092	0.826	0.864			0.044	0.044		

It is apparent that whilst INFERNO-peat shows an overall improvement in the ability of INFERNO to capture total amounts of burning across the high latitudes and within specific subregions, there are key differences in the ability of the model to capture spatial patterns in burning in different regions. For example, INFERNO-peat demonstrates notable improvements in modelling spatial patterns in burning in eastern Siberia, Alaska and western Canada. However, key deficiencies of INFERNO-peat are identified in eastern Canada, Fennoscandia and western Russia. Consequently, further model development may be required to help address these spatial biases. Nonetheless, it is also important to note that it is likely that many peat fires across the high latitudes are not being captured within the observational products.

The performance of INFERNO-peat can also be evaluated in the different subregions over time, and in terms of interannual variability (IAV) in BA. Across the majority of the subregions, increases in BA IAV are apparent with the addition of peat fires into INFERNO (Figure 20). For example, whilst in western and eastern Canada overall amounts of burning in INFERNO-peat are higher than the observations suggest, there are significant improvements in the representation of BA IAV compared to INFERNO (Figure 20b,c). In western Canada, INFERNO-peat shows an increase in standard deviation to 0.017 and an increase in the coefficient of variation to 0.145 compared to 0.002 and 0.068 respectively in INFERNO, much closer to the values seen in the observations (Table 12). On top of this, there are also higher temporal correlations in BA between INFERNO-peat and all observational datasets compared to standard INFERNO in western and eastern Canada (Table 12), suggesting that representing peat fires in INFERNO results in more accurate modelling of IAV and its timing across Canada. Similarly, in Fennoscandia, INFERNO-peat shows improvements in the models ability to represent IAV (Figure 20d), with increases in the coefficient of variation from 0.160 in INFERNO to 0.178 in INFERNO-peat (Table 12). However, this is still much below the IAV shown in the observations (Figure 20d; Table 12).

Across the three Russian subregions there are also notable improvements in the representation of IAV in BA in INFERNO-peat compared to INFERNO (Figure 20). The smallest improvements are seen in western Russia, where only a small increase in standard deviation is seen, which bring the models standard deviation closer to that of GFED4s and FireCCILT11, but no improvements are seen in terms of the coefficient of variation (Table 12). However, temporal correlations between INFERNO-peat and all observations are much stronger than INFERNO, suggesting improvements in the modelled timing of IAV. Similarly, central and eastern Siberia also show improvements in the IAV metrics compared to INFERNO, although variation is still lower than what is observed, especially in GFED5

(Table 12; Figure 20f, g). In contrast to the other regions, INFERNO-peat shows weaker temporal correlations with the observations than INFERNO in both central and eastern Russia (Table 12). The exception to this is in eastern Russia, where INFERNO-peat is more strongly correlated with GFED4s than INFERNO. Overall, this suggests that in central and eastern Russia the increases in IAV may not be occurring during the same years as the observations, creating a temporal mismatch in IAV. One example of this is 2013 in central Russia, where INFERNO-peat models and increase in BA compared to 2012, whereas all the observations capture a decrease in BA in 2013 relative to 2012 (Figure 20f).

INFERNO-peat overall captures higher amounts of IAV in BA compared to INFERNO bringing, making INFERNO-peat more representative of the observed IAV in BA in many of the subregions of the high latitudes, highlighting the importance of representing peat fires within fire models. However, it is important to note that there is substantial variability in the amounts of IAV captured in different regions of the high latitudes, with the greatest improvements seen across Canada. Canada also witnesses improvements in the temporal correlations in the timing of BA between INFERNO-peat and the observations. Consequently, it is important that peat fires are incorporated into fire models, as they significantly improve the model's ability to capture the IAV in burning, notably in Canada.

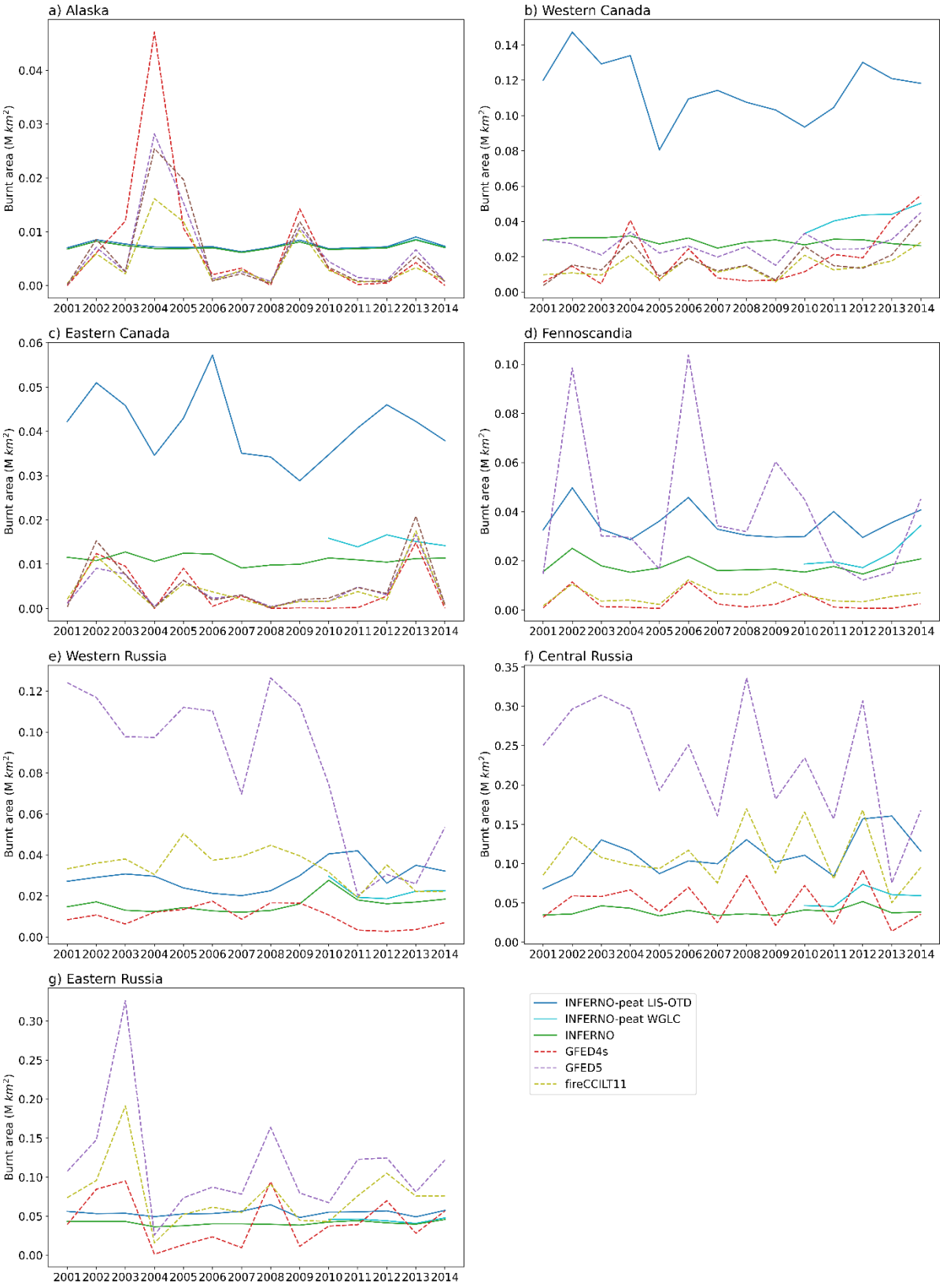


Figure 20: Trends in BA from 2001 to 2014 in INFERNO and INFERNO-peat compared with the observational datasets in each of the subregions. Note that the WGLC INFERNO-peat runs are only for 2010 to 2014. Dashed lines indicate observations and solid lines represent models.

Table 12: Burnt area averages, interannual variability metrics and temporal correlation broken down by each subregion for the 2001 to 2014 period. Results for the WGLC run are only available from 2010 onwards,

therefore these runs are excluded from this table. ABoVE-FED correlations are only available for North America subregions.

	Avg annual BA (M km2)	std	cv	R GFED4s	GFED5	fireCCILT11	ABoVE-FED
Alaska							
INFERNO	0.007	0.001	0.089	0.059	0.117	0.165	0.143
INFERNO-peat	0.007	0.001	0.097	0.082	0.141	0.180	0.162
LIS-OTD							
GFED4s	0.007	0.012	1.616		0.924	0.858	0.857
GFED5	0.006	0.007	1.261	0.924		0.967	0.980
fireCCILT11	0.004	0.005	1.125	0.858	0.967		0.988
ABoVE-FED	0.006	0.008	1.290	0.857	0.980	0.988	
Western Canada							
INFERNO	0.029	0.002	0.068	-0.022	-0.158	-0.170	-0.166
INFERNO-peat	0.115	0.017	0.145	0.288	0.201	0.130	0.149
LIS-OTD							
GFED4s	0.019	0.015	0.811		0.753	0.808	0.839
GFED5	0.027	0.007	0.261	0.753		0.873	0.845
fireCCILT11	0.015	0.006	0.414	0.808	0.873		0.940
ABoVE-FED	0.017	0.009	0.546	0.839	0.845	0.940	
Eastern Canada							
INFERNO	0.011	0.001	0.090	0.318	0.274	0.258	0.181
INFERNO-peat	0.041	0.007	0.177	0.411	0.360	0.429	0.360
LIS-OTD							
GFED4s	0.004	0.005	1.322		0.925	0.910	0.926
GFED5	0.004	0.004	1.026	0.925		0.970	0.974
fireCCILT11	0.004	0.005	1.118	0.910	0.970		0.985
ABoVE-FED	0.005	0.006	1.190	0.926	0.974	0.985	
Fennoscandia							
INFERNO	0.018	0.003	0.160	0.721	0.759	0.615	
INFERNO-peat							
LIS-OTD	0.035	0.006	0.178	0.691	0.660	0.478	
GFED4s	0.003	0.004	1.160		0.926	0.743	
GFED5	0.040	0.028	0.712	0.926		0.900	
fireCCILT11	0.006	0.003	0.536	0.743	0.900		
Western Russia							
INFERNO	0.016	0.004	0.244	-0.223	-0.349	-0.404	
INFERNO-peat	0.029	0.006	0.217	-0.482	-0.534	-0.727	
LIS-OTD							
GFED4s	0.010	0.005	0.489		0.808	0.640	
GFED5	0.084	0.037	0.436	0.808		0.716	
fireCCILT11	0.034	0.008	0.246	0.640	0.716		
Central Russia							
INFERNO	0.039	0.005	0.130	0.626	0.457	0.448	
INFERNO-peat	0.111	0.026	0.234	0.326	0.032	0.214	
LIS-OTD							
GFED4s	0.049	0.025	0.498		0.850	0.908	
GFED5	0.230	0.074	0.320	0.850		0.753	
fireCCILT11	0.109	0.036	0.329	0.908	0.753		
Eastern Russia							
INFERNO	0.041	0.003	0.063	0.534	0.469	0.483	
INFERNO-peat	0.054	0.004	0.074	0.587	0.311	0.272	
LIS-OTD							
GFED4s	0.043	0.031	0.717		0.810	0.810	
GFED5	0.115	0.068	0.592	0.810		0.968	
fireCCILT11	0.075	0.039	0.521	0.810	0.968		

3.2. Depth of burn

On average, peat fires are modelled by INFERNO-peat to burn 7.388cm deep into the soil. This is in accordance with numerous depths of burn reported by field studies across the northern high latitudes, which show that peat fires tend to burn the top 5-20cm of the soil (Turetsky et al., 2011b; Walker et al., 2020; Santoso et al., 2019a; Lukenbach et al., 2015; Hokanson et al., 2016; Wilkinson et al., 2018; Davies et al., 2013). There is significant spatial variability in peat fire depth of burn (Figure 21). Deeper burning tends to occur in western Canada, western Russia/eastern Europe and in the peatlands of the great Vasyugan mire. However, it is difficult to evaluate these results due to a lack of high latitude wide observational datasets on average peat fire depths of burn, with the majority of the literature focusing on specific fire events.

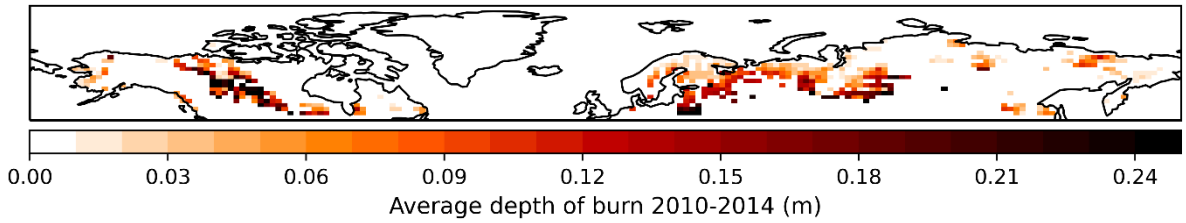


Figure 21: INFERNO-peat grid cell average depth of burn (m) between 2010 and 2014 across the northern high latitudes.

Across the 7 subregions there is substantial variation in the average depth of burn (Figure 22). Western Canada sees the deepest peat burning, with an average depth of burn of 13.231 cm. Meanwhile, peat fires in eastern Canada only burn on average 4.359 cm deep, nearly 9cm less than in western Canada. In contrast, Alaska sees the shallowest burning of just 3.953 cm. Peat fires in western Russia, according to INFERNO-peat, burn deeper than central Russia, and nearly twice as deep as in eastern Russia. Depth of burn is driven in INFERNO-peat by water table depth, soil moisture and soil temperatures. Therefore, the deeper burning in western Canada may be a product of deeper water tables and drier soils, which allow for burning at colder temperatures and deeper fire propagation into the soil. Opposingly, water tables may be higher and soil moisture greater in regions such as Alaska, eastern Canada and eastern Russia, resulting in shallower burning.

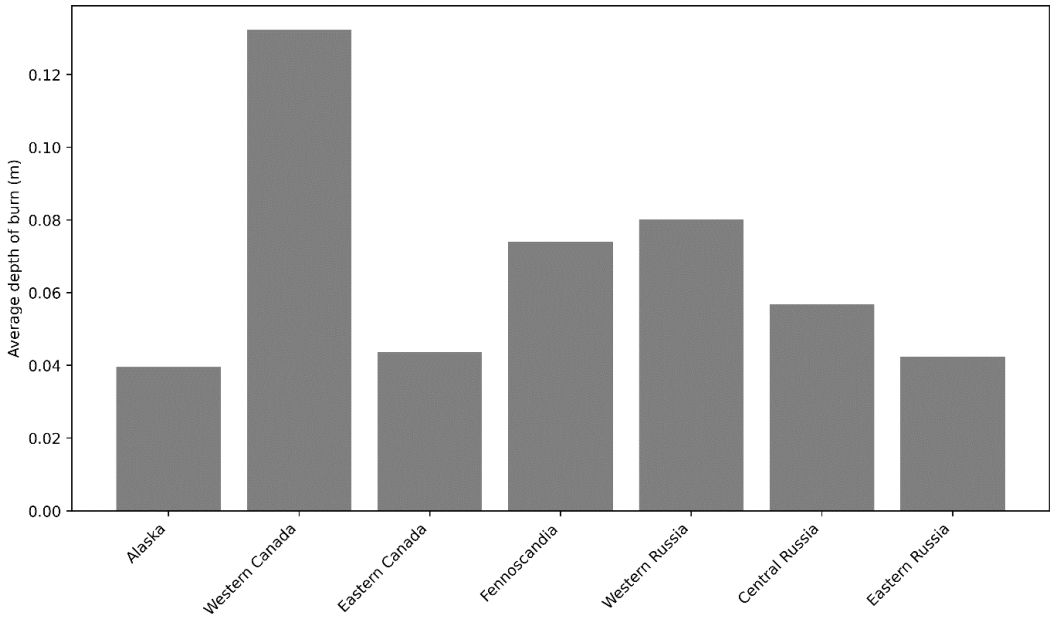


Figure 22: The average depth of burn modelled by INFERNO-peat in each of the 7 subregions.

There is considerable interannual variability in the average annual peat fire depth of burn across the time series (Figure 23). Notable years with deep burning are seen to occur in 2007, 2008 and 2009. Conversely, 1997, 2004 and 2010 are years in which depth of burn was notably shallow. Across the 18 years of the simulation there are not overall trends in the depth of burn across the high latitudes.

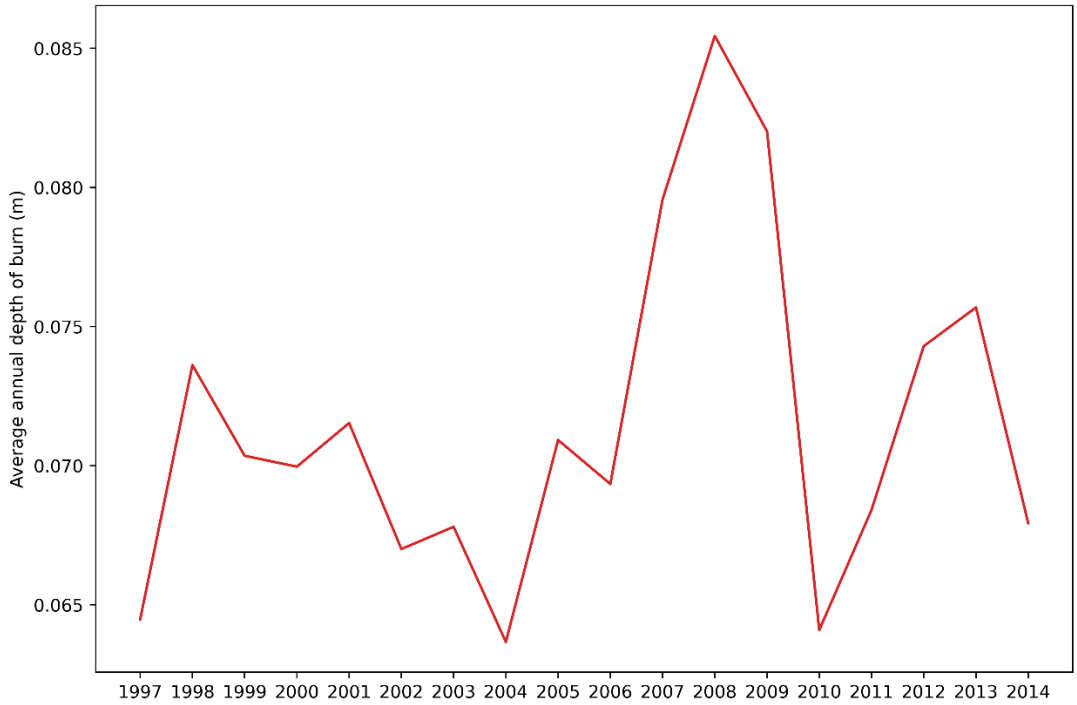


Figure 23: Annual average peat fire depth of burn between 1997 and 2014 in the northern high latitudes.

3.3. Carbon emissions

Peat fires emit on average an additional 204.5 Tg C per year in INFERNO-peat, significantly more than the 103.28 Tg C modelled by INFERNO (Figure 24; Table 13). This brings emissions estimates closer to the totals observed in GFED500m and GFAS at 305.35 Tg C and 248.57 Tg C respectively (Table 13). Not only does the additional representation of peat fires improve overall estimates of carbon emissions from fires in the northern high latitudes, but INFERNO-peat also allows for more accurate representation of the interannual variability in carbon emissions. INFERNO models a standard deviation of 7.341 and a coefficient of variation of 0.071. But the inclusion of peat fires increases these variability metrics to 48.663 and 0.158 in INFERNO-peat LIS-OTD and to 16.533 and 0.110 in INFERNO-peat WGLC. These values are much closer to the amounts of variability seen in the observational datasets (Table 13). In addition, there are also stronger temporal correlations between INFERNO-peat and the GFED500m and GFAS observations compared to INFERNO (Table 13). Therefore, the inclusion of peat fires also improves INFERNO's ability to accurately represent the timing of IAV in carbon emissions.

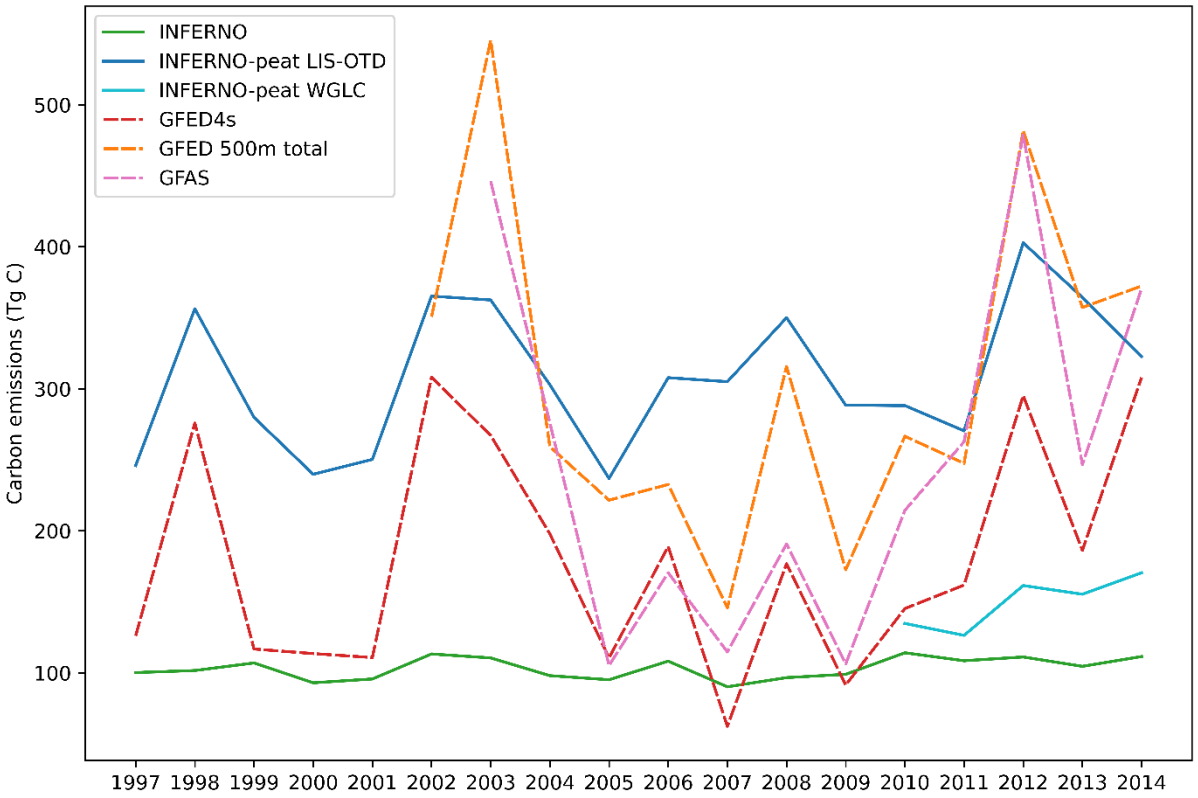


Figure 24: The annual total carbon emissions from fires across the high latitudes (<50° N) from 1997 to 2014 compared between the models (indicated by solid lines) and observations (indicated by dashed lines).

Table 13: Average annual carbon emissions, standard deviation (std), coefficient of variation (cv) and temporal correlation R coefficients for models and observations over 2003 to 2014. Note, the INFERNO-peat WGLC run, is conducted from 2010 to 2014, and therefore not included in the temporal correlations.

Model	Average annual C emissions (Tg)	std	cv	R GFED4s	GFED500m	GFAS
INFERNO	103.282	7.341	0.071	0.685	0.601	0.670
INFERNO-peat LIS-OTD	307.786	48.663	0.158	0.657	0.768	0.702
INFERNO-peat WGLC	149.731	16.533	0.110			
Peat only LIS-OTD	204.503	45.587	0.223			
GFED4s	180.192	77.259	0.429		0.858	0.914
GFED500m - total	305.350	111.106	0.364	0.858		0.912
GFED500m - aboveground	102.718	29.674	0.289			
GFED500m - belowground	202.632	86.844	0.429			
GFAS	248.574	121.469	0.489	0.914	0.912	

The GFED500m product is uniquely beneficial as it differentiates between aboveground and belowground carbon emissions. Belowground emissions come from the burning of organic matter within the soil, which occurs predominantly during peat burning. Therefore, the GFED500m belowground emissions can be compared to peat fire carbon emissions from INFERNO-peat. When compared to GFED500m, INFERNO-peat represents fire emissions and their sources well. From Figure 25, it is clear that INFERNO, which only represents vegetation fires, does an adequate job at capturing the aboveground burning, albeit not capturing the interannual fluctuations in burning. Emissions from peat fires in INFERNO-peat also quite accurately reflect emissions from GFED500m belowground burning, especially between 2010 and 2014. Furthermore, peat fire emissions from INFERNO-peat also capture similar levels of interannual variability as GFED500m belowground. Consequently, the inclusion of peat fires in INFERNO, is successful in capturing observed belowground burning emissions, highlighting the importance of parameterising peat fires into global fire models.

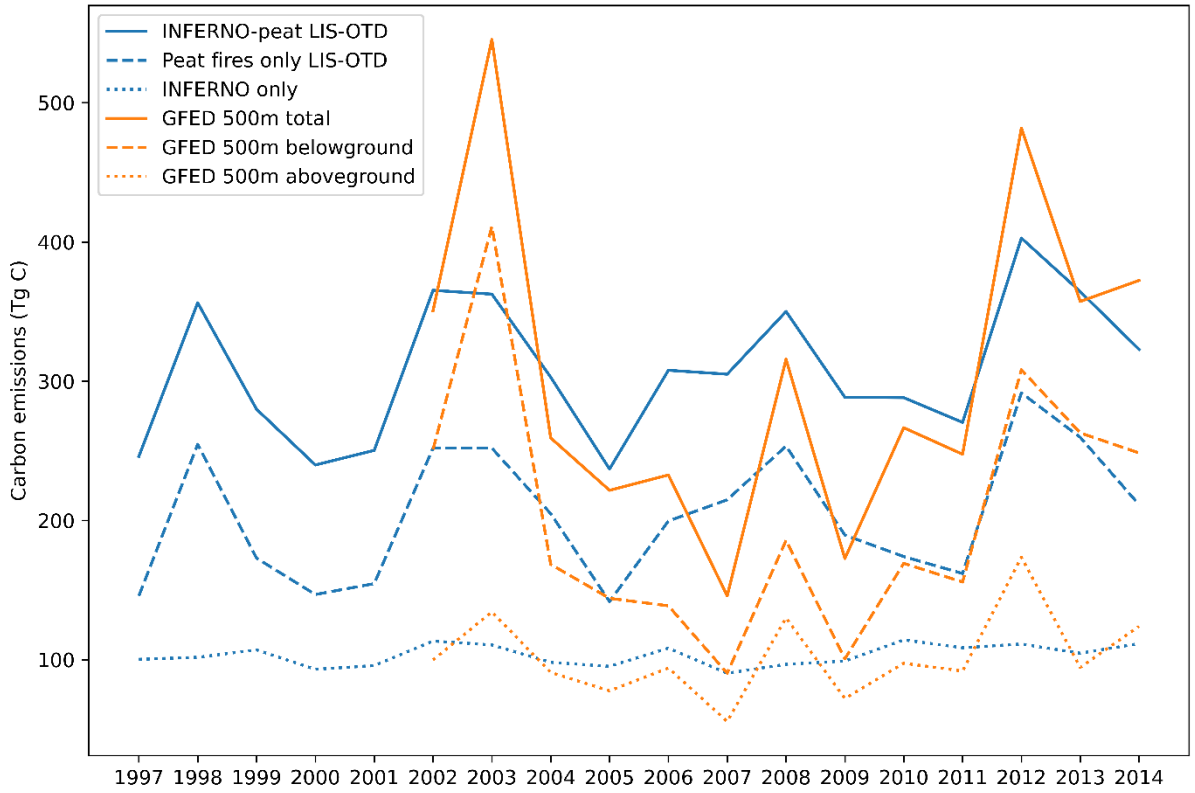


Figure 25: The annual total carbon emissions from fires across the high latitudes (<50° N) from 1997 to 2014 compared between the GFED 500m products above and belowground burning, and INFERNO-peat emissions split to peat fires only and INFERNO only.

3.3.1. Subregion analysis

Carbon emissions modelled by INFERNO-peat vary greatly between subregions (Figure 26). Much like BA, the modelled and observed carbon emissions in Alaska are very close, and there are only minor increases in carbon emissions associated with peat burning (Figure 26). In western Canada there are large contributions from peat fire carbon emissions especially in the LIS-OTD run. INFERNO-peat LIS-OTD annual average emissions of 83.674 Tg C fall within the range of carbon emissions from the observations of 70.783-99.386 Tg C per year. However, in the WGLC run emissions are much lower at 28.956 Tg C per year, likely a reflection of the lower burnt area seen in this run relative to the LIS-OTD run. In eastern Canada, emissions of 26.517 Tg C modelled by INFERNO-peat LIS-OTD are extremely close to the carbon emissions estimated from GFED500m, despite a large overestimation in BA. In both Fennoscandia and western Russia there are large overestimations in carbon emissions in both INFERNO-peat runs compared to GFED4s and GFED500m (Figure 26). However, in Fennoscandia emissions from INFERNO-peat WGLC of 15.485 Tg C are extremely close to the GFAS dataset which estimates emissions of 15.987 Tg C. Similarly in central Russia pronounced overestimations in carbon emissions are seen in INFERNO-peat LIS-OTD but INFERNO-peat WGLC emissions are very similar to those from GFED4s and GFAS. These results suggest that in term of carbon emissions, in both Fennoscandia and central Russia the use of timeseries lightning data to drive INFERNO-peat results in notable improvements in

model performance. In contrast, in eastern Russia emissions captured by the GFED500m product are over 6 times greater than the emissions modelled by INFERNO-peat, meaning that large amounts of carbon emissions in eastern Russia are still not being captured by the addition of peat fires into INFERNO.

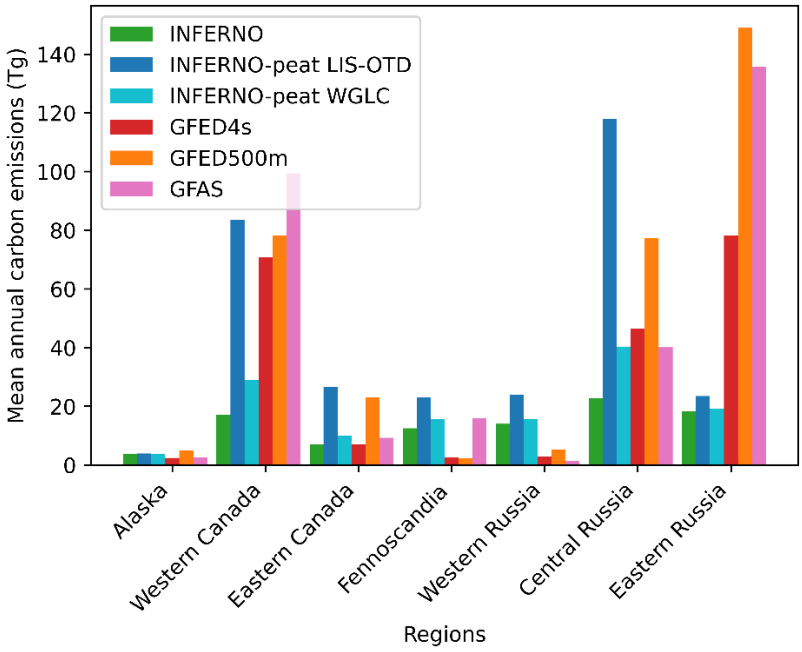


Figure 26: The average annual carbon emissions (2010-2014), from INFERNO, and INFERNO-peat driven by the LIS-OTD and WGLC lightning data, compared to the observations, in each subregion.

Differences in aboveground and belowground burning can be examined from the GFED500m product to understand how well the addition of peat fires into INFERNO is performing in subregions of the high latitudes. In Alaska, INFERNO is capturing the majority of GFED500m aboveground carbon emissions, but emissions from peat fires are negligible (Figure 27). This means that the small deficit in total carbon emissions estimates in Alaska are likely a result of not capturing the belowground burning that is shown to be occurring in GFED500m. Similarly, in western and eastern Canada INFERNO appears to capture the amount of aboveground burning seen in GFED500m well (Figure 27). Concurrently, peat only emissions from INFERNO-peat LIS-OTD in both regions are close to that of the GFED500m belowground emissions. For example, in eastern Canada INFERNO-peat LIS-OTD estimates that peat fires release 19.394 Tg C, compared to 16.573 Tg of C emissions from belowground sources in GFED500m. Therefore, it is clear that not only does INFERNO-peat represent total fire carbon emissions well in Canada compared to GFED500m, but it also accurately represents the division of burning from above and belowground sources.

However, INFERNO-peat performs less well across Eurasia. In Fennoscandia and western Russia, GFED500m estimates negligible amounts of carbon emissions from belowground burning. However, INFERNO-peat suggests that belowground emissions from peat fires are occurring in these regions,

resulting in the overall overestimation of carbon emissions from INFERNO-peat in Fennoscandia and western Russia (Figure 27). Similarly, in central Russia INFERNO-peat overestimates peat fire contributions to emitted carbon, modelling 95.354 Tg C emitted from peat fires compared to only 44.059 Tg C emitted from belowground fires in GFED500m (Figure 27). The opposite is true in eastern Russia where GFED500m estimates 107.002 Tg C from belowground burning, compared to just 5.127 Tg C from peat burning in INFERNO-peat LIS-OTD. Therefore, a large amount of peat and belowground burning in eastern Russia is not being captured in INFERNO-peat, despite being a marked improvement from INFERNO.

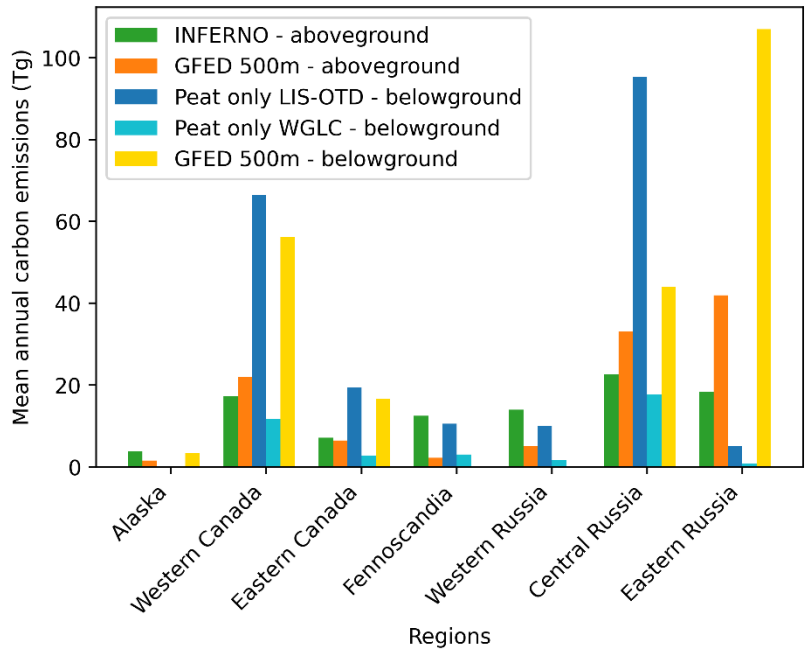


Figure 27: The average annual carbon emissions (2010-2014), from INFERNO, and peat fires only from INFERNO-peat driven by the LIS-OTD and WGLC lightning data, compared to the aboveground and belowground burning from the GFED 500m product, in each subregion.

In both central and eastern Russia, INFERNO underestimates carbon emissions compared to GFED500m aboveground burning. Failures of INFERNO to capture the aboveground vegetation fires in these regions has knock on effects on the ability of INFERNO-peat to represent peat fires due to lower peat fire ignition events in the model. Underestimations of both burnt area and carbon emissions from vegetation fires in Eastern Russia and Alaska may result from inherent biases within JULES-INFERNO. In these regions temperatures are low, which results in underestimations in the flammability of vegetation, consequently causing INFERNO-peat to underestimate the number of ignitions in these areas, resulting in underestimations in peat burnt area and emitted carbon. Furthermore, simulated vegetation bias in the TRIFFID dynamic vegetation model within JULES, results in a high proportion of the land surface being covered by non-vegetative surface types, predominately bare soil (~67% of the land surface north of 60°N is classed as non-vegetative) (Figure 28). Therefore, the number of possible ignition events in INFERNO-peat is further reduced. However,

the opposite may be true in central Russia and western Canada where there are large overestimations in both burnt area and carbon emissions. In these regions the most common PFT's, according to JULES, are needleleaf deciduous trees, whereas, in reality, these regions contain large amounts of herbaceous wetlands, a PFT which is not currently represented in JULES. This may be contributing to a possible inflation in the number of flaming vegetation fires in these regions, leading to overestimates in burnt area and consequently carbon emissions in INFERNO-peat. Therefore, it is also vital that improvements are made to how INFERNO performs in the high latitudes, to further benefit peat fire model development.

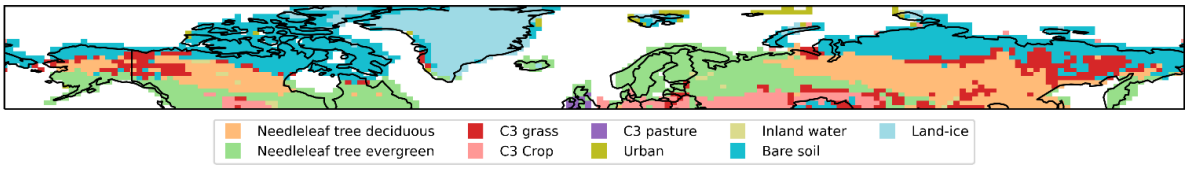


Figure 28: 2010-2014 average dominant land fraction type in each grid cell modelled by the TRIFFID dynamic vegetation model in JULES.

Trends in regional carbon emissions can also be examined over 2003 to 2014, the period of overlap between all observational datasets and the INFERNO-peat LIS-OTD run, in order to assess the effects of representing peat fires on interannual variability. As previously mentioned, INFERNO-peat models only minimal additional peat fires in Alaska and shows minimal change in IAV in carbon emissions (Figure 29a). On top of this, there are minimal differences in the temporal correlations between INFERNO and INFERNO-peat with all the observational datasets (Table 14). In contrast in the two Canadian subregions, there are increases in standard deviation and the coefficient of variation in INFERNO-peat compared to INFERNO (Table 14). Therefore, in Canada INFERNO-peat better captures the IAV seen in the observational datasets. In western Canada there are also increases in the strength of the temporal correlations between modelled carbon emissions and observations from GFED4s and GFAS from INFERNO to INFERNO-peat (Table 14), therefore the timing of variability in carbon emissions is more accurate in INFERNO-peat. In Fennoscandia, small increases in standard deviation and the coefficient of variation are seen in INFERNO-peat compared to INFERNO, more inline with the amount of IAV seen in all observational datasets (Table 14). However, temporal correlations are not improved from INFERNO to INFERNO-peat in Fennoscandia, except with the GFAS data, which is also the dataset which has the largest carbon emissions (Table 14). Finally, across all three of the Russian subregions there are increases in the IAV in carbon emissions in INFERNO-peat relative to INFERNO, bringing levels of variability closer to what is shown in the observations (Figure 29e-g; Table 14). However, crucially these changes in carbon emissions year to year do not appear to be occurring at the same time as they do in the observations (Figure 29e-g). For example, in 2013 in western Russia, carbon emissions are increased from their levels in 2012, whereas this does not occur in the observations. Therefore, in the Russian subregions there are weaker

temporal correlations between observed carbon emissions and those modelled by INFERNO-peat compared to INFERNO (Table 14). Consequently, whilst there are clear improvements in the overall ability of INFERNO-peat to capture carbon emissions, there is substantial variation among different regions and in particular a mismatch in the timing of variability in carbon emissions over Russia between INFERNO-peat and the observations.

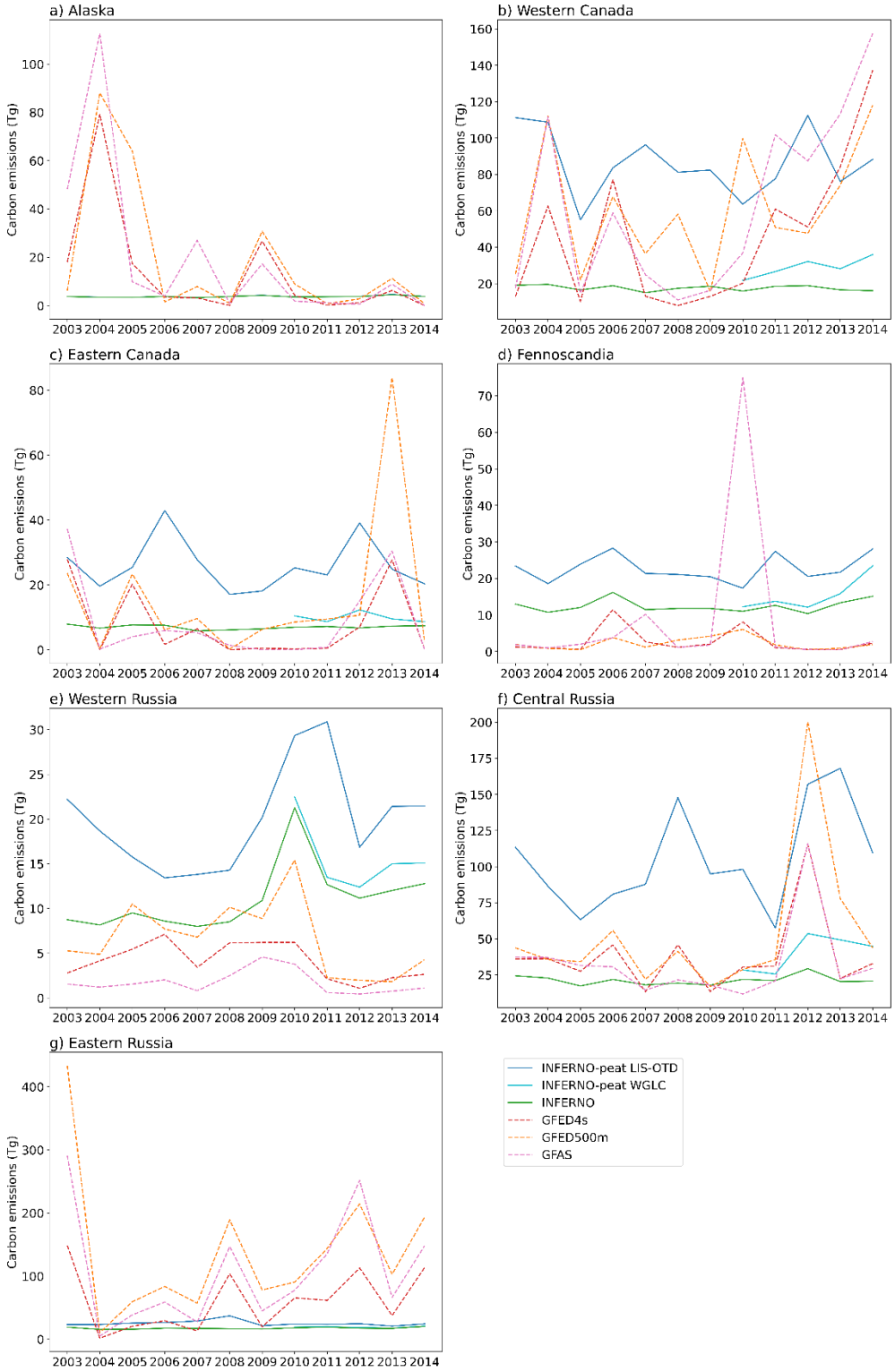


Figure 29: Carbon emissions timeseries graphs broken down by subregion, from 2003 to 2014. Note that the WGLC INFERNO-peat runs are only for 2010 to 2014. Dashed lines indicate observations and solid lines represent models. Comparisons against the GFED500m above and belowground burning can be found in Figure S1.

Table 14: Carbon emission averages, interannual variability and temporal correlations between models and observations over 2003 to 2014, broken down by subregion. Results for the WGLC run are only available from 2010 onwards, therefore these runs are excluded from this table, and instead can be found in Table S2.

Model	Avg annual C emissions (Tg)	std	cv	R GFED4s	GFED500m	GFAS
Alaska						
INFERNO	3.735	0.337	0.090	-0.165	-0.286	-0.278
INFERNO-peat	3.766	0.355	0.094	-0.143	-0.264	-0.254
LIS-OTD						
GFED4s	13.334	21.528	1.614		0.876	0.927
GFED 500m – total	18.657	27.291	1.463	0.876		0.721
GFAS	9.365	31.298	1.616	0.927	0.721	
Western Canada						
INFERNO	17.612	1.455	0.083	0.015	-0.123	0.066
INFERNO-peat	25.992	7.599	0.292	0.155	0.053	0.311
LIS-OTD						
GFED4s	45.913	38.696	0.843		0.681	0.930
GFED 500m - total	60.662	33.349	0.550	0.681		0.706
GFAS	62.659	47.740	0.762	0.930	0.706	
Eastern Canada						
INFERNO	6.987	0.607	0.087	0.513	0.328	0.437
INFERNO-peat	25.992	7.599	0.292	0.155	0.053	0.311
LIS-OTD						
GFED4s	7.700	10.562	1.372		0.790	0.868
GFED 500m – total	15.387	21.895	1.423	0.790		0.699
GFAS	8.350	12.176	1.458	0.868	0.699	
Fennoscandia						
INFERNO	12.449	1.676	0.135	0.464	0.119	-0.249
INFERNO-peat	22.688	3.482	0.153	0.179	-0.162	-0.452
LIS-OTD						
GFED4s	2.715	3.298	1.215		0.699	0.520
GFED 500m - total	2.224	1.659	0.746	0.699		0.691
GFAS	8.473	20.215	2.386	0.520	0.691	
Western Russia						
INFERNO	11.029	3.524	0.320	0.045	0.382	0.361
INFERNO-peat	19.860	5.463	0.275	-0.258	-0.023	0.117
LIS-OTD						
GFED4s	4.135	1.929	0.467		0.829	0.771
GFED 500m - total	6.658	3.926	0.590	0.829		0.766
GFAS	1.742	1.242	0.713	0.771	0.766	
Central Russia						
INFERNO	21.271	3.160	0.149	0.848	0.800	0.828
INFERNO-peat	105.394	34.132	0.324	0.448	0.601	0.408
LIS-OTD						
GFED4s	37.573	25.523	0.679		0.918	0.937
GFED 500m -	52.996	46.956	0.886	0.918		0.933

Model	Avg annual C emissions (Tg)	std	cv	R GFED4s	GFED500m	GFAS
total						
GFAS	32.612	26.374	0.809	0.937	0.933	
Eastern Russia						
INFERNO	17.476	1.356	0.078	0.666	0.596	0.581
INFERNO-peat	25.266	4.084	0.162	0.166	0.031	0.041
LIS-OTD						
GFED4s	0.607	46.239	0.763		0.914	0.943
GFED 500m - total	137.947	107.069	0.776	0.914		0.938
GFAS	107.550	86.069	0.800	0.943	0.938	

4. Discussion

The explicit representation of peat fires in INFERNO-peat has significantly improved INFERNO's ability to represent burning in the northern high latitudes. Most notably, INFERNO-peat improves simulated estimates of wildfire carbon emissions and their interannual variability, compared to the observations. Based on INFERNO-peat, on average peat fires account for 58% of burned area and 68% of carbon emissions north of 50°N latitude. In addition, the results presented here have also addressed noted deficiencies in the INFERNO fire model (Mangeon et al., 2016). Given that the lack of peat fire representation is also the norm in global fire models used in the scientific community, we highlight the critical need for representing peat burning in fire models, as this is shown to have a large impact on simulated model performance. The vast carbon emissions of over 200 Tg C per year on average represent a large perturbation to the carbon cycle and climate, consequently highlighting the need for representing peat fires and their emissions in studies of the carbon cycle, in order to simulate and quantify the release of vast amounts of long-term stored carbon to the atmosphere.

At present, the land surface component of the Community Earth System Model (CESM) is the only other model to incorporate a specific peat fire parameterisation (CLM-Li; Li et al., 2013). In contrast to the findings presented in this chapter, the inclusion of peat burning in CLM did not show substantial improvements in the simulation of fires in North America and eastern Siberia (Li et al., 2013). This was attributed to a wet simulation bias seen in CLM which results from an underestimation of the latent heat flux, thereby leading to an increase in the amount of water stored in the land in the model (Li et al., 2013). In INFERNO-peat, organic soil moisture was used, which allowed for a better representation of the hydrology of peatlands, which may explain why INFERNO-peat captures substantial increases in burned area, particularly in North America, compared to INFERNO. Consequently, it is apparent that accurate representation of peatland hydrology is critical to the performance of peat fire modelling. Similarly, Mortelmans et al. (2024) demonstrated the importance of using peatland specific hydrology for calculating peat FWI and peat fire occurrence.

Historically, few land surface models have simulated peat, let alone its specific hydrological processes, leading to poor representation of peatlands in Earth system models (Bechtold et al., 2019; Melton et al., 2013). However, recent progress in peat modelling has been made, with numerous parametrisations now developed, including JULES-PEAT (Chadburn et al., 2022); PEATCLSM (Bechtold et al., 2019); ORCHIDEE-MICT-PEAT (Guimberteau et al., 2018; Qiu et al., 2018; Qiu et al., 2019); LPJ-GUESS Peatland (Chaudhary et al., 2017; Chaudhary et al., 2020); and LPX-Bern (Muller and Joos, 2021; Muller and Joos, 2020; Stocker et al., 2014). All the aforementioned models have or are expected to contribute towards the ISIMIP3a and b simulation rounds with specific peatland experiments (available from: https://protocol.isimip.org/#/ISIMIP3a/peat, last accessed: 04/07/2024). These recent model developments have allowed for peat to be simulated across the world, with the accumulation, or loss, of carbon being able to be studied both historically and into the future. With the concurrent development of INFERNO-peat, it is possible in the future to use modelled peatland area, carbon, and hydrology in order to drive INFERNO-peat, potentially leading to further improvements in our fire modelling capabilities. In particular, a coupling between peat models and peat fire models would further improve modelling capabilities, allowing for dynamic feedbacks on carbon storage.

The CLM-Li approach also showed minimal peatland burning in Siberia (Li et al., 2013). Similarly, in INFERNO-peat whilst there are increases in estimations of burning in eastern Siberia, there is still considerably less modelled BA compared to what is observed. Li et al. (2013) attributed this to low fuel loads within CLM. Similarly, land cover fractions modelled in JULES show low levels of vegetation and a dominance of bare soil in Eastern Siberia (Figure 28). However, in reality much of these tundra ecosystems in eastern Siberia are dominated by grass, moss and lichen, PFT's which are not currently represented in JULES, resulting in a significant underestimation of burnable area in the model. Similarly, in other parts of the boreal regions, JULES has been shown to underestimate needleleaf tree presence compared to observations (Teixeria et al., 2023), which would also result in underestimations in fuel loads, and inaccuracies in fuel properties, hampering INFERNO's capability to replicate present-day burning. Biases in the underlying vegetation models have been shown to have significant impacts on modelled burned area (Teixeria et al., 2023). Therefore, improvements in the simulation of high latitude ecosystems within dynamic vegetation models are necessary for improving fire modelling in these regions.

There is significant regional variation in the performance of INFERNO-peat. One notable area of improvement is seen in the Northwest Territories region of Canada. Previously INFERNO has struggled to replicate observed patterns of burning in this region, but the addition of peat fires in INFERNO results in a 0.087 M km^2 increase in annual average BA in the western Canadian region. Accurate simulation of fires in this region is vitally important, due to the major climatic implications of wildfires in western Canada in recent years, and due to potential climate changes in the future. For

example, the summer of 2023 burned 4.16 M ha in the Northwest Territories alone, the largest burned area in the 44-year Canadian fire record (Thoman et al., 2023). Similar extreme fires burned in 2014, burning 3.39 M ha of the Northwest Territories (Kochtubajda et al., 2019). These extreme fire years can lead to large gaseous and aerosol emissions, with implications on human health and radiative forcing. For example, the 2023 Canadian wildfires resulted in dense smoke plumes and air quality warnings for much of Canada and the northern United States, with smoke even reaching western Europe (Barnes et al., 2023). Moreover, in 2013 Canadian fires emitted high levels of black carbon, which was deposited over the Greenland ice sheet, resulting in a lowered albedo and a warming effect on the climate (Thomas et al., 2017). Therefore, by incorporating peat fires into INFERNO, we are better able to model the severe wildfires seen in western and northern Canada, with the potential to aid in analysing the atmospheric and air quality impacts of such burning in the future.

INFERNO-peat also improves estimates of BA across Russia, where large peat fires are common. Mostly notably, INFERNO-peat improves the overall estimations of BA relative to GFED5 observations in central and eastern Russia compared to INFERNO (Figure 17). In eastern Siberia especially, INFERNO-peat results in a stronger spatial correlation and lower RMSE than INFERNO when compared with both GFED and FireCCILT11 observations (Table 12). Peat fires are common across Russia, as is seen in observations and also suggested in INFERNO-peat. For example, over 40,000 ha of peatland burned in 2010, in the Moscow region (Sirin and Medvedeva, 2022), and fires in the Siberian Arctic in 2020 burned approximately 0.71 M ha of peatlands (Descals et al., 2022). INFERNO-peat estimates that on average in central Russia peat fires contribute between 30.7 and 65.6% of the annual BA, and in eastern Russia between 10.9 and 24.6% of the annual BA. Therefore, the average contributions of peat fires to total burning seen in INFERNO-peat are likely representative of the true peat fire contributions in Russia. As shown in this chapter, peat fires in Russia can lead to large carbon emissions, supported by the findings of Kajii et al. (2002) who showed that peat and boreal forest fires in the summer of 1998 led to 11 million ha of burned area and 176 Tg C emitted (Kajii et al., 2002). Representing a substantial effect on the atmosphere and peatland carbon stores. Therefore, being able to accurately represent burning in Siberia is crucial to being able to quantify fire impacts on the atmosphere, air quality and the peatland carbon store, both at present and in the future.

However, INFERNO-peat performs less well in some other regions of the northern high latitudes. For example, it overestimates burning in eastern Canada and Fennoscandia. One potential cause of these overestimates is that they may be a result of how humans are represented in INFERNO. In comparison to other regions of the high latitudes, eastern Canada and Fennoscandia have higher population densities, and therefore the fire regimes in these areas are likely more influenced by human activities. At present, INFERNO, and many other fire models, use simplistic relationships of fire ignitions and suppression with population density or GDP, which fail to capture the highly complex

relationships between humans and fire (Perkins et al., 2022; Teckentrup et al., 2019). Fire is used as a land management tool around the world, resulting in altered fuel loads, the fragmentation of natural landscapes and land use change to agriculture, pasture or industry (Smith et al., 2022a; Perkins et al., 2022; Archibald, 2016). Recent INFERNO developments on the representation of human fire dynamics have included accounting for the Human Development Index (HDI) (Teixeria et al., 2023) and agent-based modelling of human fire use (Perkins et al., 2022), and have shown the importance of more realistic modelling of humans in fire models. Furthermore, recent analysis has shown that land fragmentation, through metrics such as road density, exerts a strong control on BA (Haas et al., 2022), and therefore represents possible future improvements that could be made to INFERNO, which may aid in the modelling of fires in more human-dominated landscapes.

In contrast, there is very little burning compared to the observations in southern Russia in both INFERNO and INFERNO-peat. This is likely the result of a dominance of agricultural burning in southern Russia (Hall et al., 2016; Van Wees et al., 2022), which is not being well represented in INFERNO. It is estimated that 80% of fires in southern Siberia originate from human causes (Kharuk et al., 2021). Furthermore, HDI, crops and livestock have been shown to be the most important explanatory variables of interannual fire variability in southern Russia (Chuvieco et al., 2021). Therefore, the inability of INFERNO to model observed fires in this region cannot be due to a lack of peat fire representation and is likely due to INFERNO underestimating global cropland burning and not representing region-specific agricultural fire management (Burton et al., 2021).

In Alaska, on average INFERNO and INFERNO-peat model more burning than what occurs in the observations. However, this is only by ~0.004 M km^2, and there are poor spatial correlations between the model and observed patterns of burning. Peatlands in boreal interior Alaska are more likely to experience more frequent fires than subarctic or coastal peatlands (Innes, 2015). For example, Wendler et al. (2011) estimate that 90% of fires in Alaska occur in interior Alaska. In INFERNO and INFERNO-peat burning is shown to occur in small amounts across southern and coastal Alaska, yet in all three observational datasets this burning occurs in interior Alaska (Figure 17). Therefore, INFERNO-peat is failing to capture the burning that is occurring in interior Alaska, whilst simultaneously overestimating burning in southern Alaska. Significant amounts of wildfires do occur across Alaska, estimated to average between 6785 and 7670 km^2 (Pastick et al., 2017; Kasischeke et al., 2010). Despite 95% of burned area in interior Alaska originating from lightning (Veraverbeke et al., 2017), there is still a large human influence on fires in the region. Humans have been shown to reduce BA and strongly influence fire regimes within 40km of settlements, an area which represents 31% of interior Alaksa (Calef et al., 2008). Consequently, a large portion of fires may be actively supressed or ignited by humans in interior Alaska. Therefore, by not accurately representing humans within INFERNO, fires in Alaska may not be well simulated. Some studies have suggested that fires are rare in peatlands in Alaska due to the presence of wet sphagnum moss (Yoshikawa et al., 2003),

and historically Alaskan tundras have been of low flammability (Young et al., 2016), therefore peat fires may not have been overly common over the period studied here, meaning that the inclusion of peat fires in INFERNO may not result in large model improvements. However, it is likely that these low flammability environments could become highly vulnerable to fires as a result of climate change (Young et al., 2016). Fires may also be inaccurately modelled in INFERNO and INFERNO-peat due to potential inaccuracies in the underlying hydrological and vegetation models within JULES. Therefore, it will be important in future efforts to improve the modelling of fires in Alaska for the present-day, in order to be able to model potential future changes.

Failures to accurately model burnt area in Alaska, have knock on effects on the ability of INFERNO to capture carbon emissions in the area, resulting in significant underestimations (Table 14). It is important that these carbon emissions are accurately simulated, as despite burning relatively small areas compared to the other regions, fires in Alaska release substantial quantities of carbon and aerosols which have impacts on atmospheric composition and air quality. For example, over 1.6 M ha of boreal forest and peatlands burnt in the summer of 2015 in Alaska, emitting 160 Tg C (Potter, 2018). This vast release of carbon from Alaskan peat and vegetation, has consequential effects on the current Alaskan carbon sink, with fire emissions in Alaska between 2000 and 2009 estimated to have exceeded decadal carbon uptake by 86 Tg C (Turetsky et al., 2011a). In addition, fires in Alaska can have large effects on air quality and radiative forcing. For example, fires that burned during the summer of 2004, of which 17% occurred on peatlands (Turquety et al., 2007), led to a 0.12 Tg enhancement of tropospheric $PM_{2.5}$ over the eastern US, emissions that were a factor of 8 larger than daily anthropogenic PM emissions in the US (Mathur, 2008). The release of aerosols in 2004 also led to a top-of-the-atmosphere radiative cooling effect due to the scattering of solar radiation by organic aerosols (Pfister et al., 2008). Therefore, it is important that fires are modelled accurately in Alaska, as they have been shown to have considerable effects on long term carbon storage in the region, as well as impacting air quality and radiative forcing.

The majority of fires models, including many of the FireMIP models, are deficient in their abilities to capture interannual variability (IAV) in fires (Li et al., 2019). However, this Chapter has shown that INFERNO-peat leads to a significant improvement in the representation of IAV in both burnt area and carbon emissions in the northern high latitudes. Crucially INFERNO-peat can also better represent the timing of IAV in BA than in standard INFERNO as well as capturing the magnitude of these changes. This means that INFERNO-peat is better able to capture notable large fire years in the observational record, for example in 1998, 2002, 2003, and 2012 (Figure 24). It is important to note that INFERNO-peat cannot replicate real life fire events, and instead essentially gives an overview of potential burning at any given time. Nonetheless, being able to capture large increases in burning in a fire season for a region overall in INFERNO-peat, that is inline with severe burning events and seasons in the observations, signifies a significant step forward in fire modelling capabilities. For example, over

22 million ha burned in Siberia in 2003, emitting 72 Tg of CO (Talucci et al., 2022). This is reflected well in INFERNO-peat with spikes in BA and C emissions occurring in 2003 in the central Russia subregion, which covers a large portion of Siberia (Figure 20f and Figure 29f). Haze and smoke plumes produced by these fires had major impacts on the health of Siberian populations as well as further afield (Huang et al., 2009). Similarly, in 2012, 17,000 wildfires burned in Siberia, emitting 48 Tg CO (Teakles et al., 2017), with a spike in BA and carbon emissions also seen in 2012 in central Russia in INFERNO-peat (Figure 20 and Figure 29). However, these large fire years are less well captured by INFERNO-peat in eastern Russia, potentially due to the aforementioned biases in the JULES vegetation simulation, leading to poor fuel representation in the model. Consequently, the ability to simulate large-scale fire events and their carbon emissions is highly important in assessing the impacts of wildfire, and therefore, INFERNO-peat presents a substantial improvement in this area of fire modelling capabilities.

A major challenge in modelling peat burning stems from an absence of robust observational datasets on peat fires, making model evaluation difficult (Blackford et al., 2024). GFED4s is the most commonly used observational dataset for fire model evaluation and is based off MODIS satellite data. However, as peat fires tend to burn belowground and at low temperatures, they are difficult for satellite products to detect (McCarty et al., 2021), leading to large number of peat fires likely being omitted from MODIS, and other satellite-based products. For example, Sirin and Medvedeva (2022) demonstrated MODIS to be insufficient in detecting the 2010 peat fires near Moscow. However, this issue does not just effect peat fires, as small fires around the world are also not well captured by satellite-based products. For example, high resolution Sentinel-2 satellite data over sub-Saharan Africa captured 80% more burnt area than MODIS due to improved detection of small fires (Roteta et al., 2019). If that pattern also holds true for the high latitudes, then many commonly used burned area products may not capture substantial amounts of burning. Conversely, in the high latitudes coarse resolution burned area products can overestimate burnt area due to the presence of water bodies which may not be accounted for in coarse pixels (Chen et al., 2021b; Hall et al., 2020). In this Chapter, data from the ABoVE-FED dataset was also used for evaluation over North America, as it also uses high resolution Landsat imagery to enhance the MODIS estimates, providing a more accurate estimate of burning across Canada and Alaska (Potter et al., 2022). However, similar more fine resolution products do not currently exist for Russia, nor is there a reliable national fire inventory (McCarty et al., 2021). Therefore, it is challenging to sufficiently evaluate INFERNO-peat performance, as evaluations are being conducted with datasets that are known to underestimate peat fires. Consequently, it is important that research efforts in the future are focused on improving satellite-based estimates of peat fires and identifying potential other novel methods of detecting peat fires such as through atmospheric perturbations in NO_2:CO ratios. As a result, Chapter 4 of this thesis will explore the use of GFED5 to estimate peat burning across the northern high latitudes and their

potential effects on atmospheric composition and air quality, with the view to be able to inform future peat fire modelling efforts.

Several limitations exist in INFERNO-peat, which can be improved with future model developments. One such limitation is that at present INFERNO-peat has no representation of sub grid cell level heterogeneity. Therefore, within a grid cell it is assumed that all peat is continuous and not fragmented. Similarly, PFTs within JULES-INFERNO are represented in the same way, meaning that landscape fragmentation is not captured. In terms of peat burning this becomes particularly important when modelling depth of burn. Numerous studies have shown that depth of burn varies between peatland margins and middles (Nelson et al., 2021; Lukenbach et al., 2015; Hokanson et al., 2016). For example, peat fire burn depth is estimated to average only 8cm in peatland middles, where water tables tend to be highest, but peat fires can burn 42cm deep in peatland margins (Lukenbach et al., 2015). Not accounting for the variability in depth of burn across a peat fire has been suggested to result in an underestimation of C loss from boreal peatlands (Nelson et al., 2021). Therefore, the C emissions presented in this chapter could be significantly altered if sub-grid scale heterogeneity was considered.

An additional limitation to INFERNO-peat is that at present there are no feedback effects of peat burning on the amount of carbon stored in the peat. For the results presented in this Chapter, fixed peatland carbon content from the Northern Peatland Dataset (Hugelius et al., 2020) was prescribed to the model, meaning that the carbon content of peatlands does not change over the simulation. Therefore, when INFERNO-peat simulates peat burning, carbon emissions are estimated based off the carbon available, but there is no effect on the amount of carbon stored in the peat prescribed to the model. Therefore, over long simulation periods if a grid cell is burning frequently enough and in large enough quantities, more carbon could be emitted than is stored in the peat, leading to unrealistically high carbon emissions. However, over the relatively short period of time presented in this Chapter, this is unlikely to be the case. In the future a feedback effect of peat burning on the peat carbon store could be incorporated into the model but would require an estimate of the rate at which carbon is reaccumulated by peat following a fire.

At present, the runs presented in this chapter used fixed values that are prescribed to the model for the whole of the high latitudes for inorganic content and bulk density. These values were obtained from Frandsen (1997) and broadly represent the average inorganic content and bulk densities seen across the northern high latitudes. However, these average values may not be representative of all peat in the northern high latitudes. Inorganic content is likely well represented with a value of 9.4%, as a study based on 268 peat cores across the northern high latitudes estimated an average organic content of 90.7%, therefore the inorganic component is likely to average 9.3% (Loisel et al., 2014). However, there seems to be large variation in peat bulk densities across the high latitudes, with values typically

ranging between 50 to 200 kg/m^3 (Chambers et al., 2011). Additionally, Loisel et al. (2014) estimated northern peat bulk densities to average 111kg/m^2, but with substantial variation. Based off these estimates, INFERNO-peat is using a bulk density on the upper end of the estimated range, and therefore having an influence on the accuracy of the calculated peat ignition probability. As higher bulk densities are associated with increased fire spread (Huang and Rein, 2019), overestimating peat bulk density could result in an overestimation of the probability of ignition of peat and consequently burnt area. Therefore, a series of INFERNO-peat runs should be conducted using different prescribed values of bulk density, and a sensitivity analysis performed in order to optimise this parameter. Additionally, Loisel et al. (2014) showed that across the high latitudes there are substantial variations in both inorganic content and bulk density depending on the vegetation composition and type of peat. For example, sphagnum peatlands were shown to have lower bulk densities and higher inorganic content compared to herbaceous peatlands, and even more so compared to humified peatlands. Therefore, if data on the vegetation make up of the northern high latitude peatlands was available this could be utilised within INFERNO-peat to provide peatland vegetation specific inorganic content and bulk density values. Ideally, gridded datasets of inorganic content and bulk density for northern high latitude peatlands would be prescribed to the model, such as through the use of the SoilGrids dataset (Poggio et al., 2021). The potential for this will be explored as a future INFERNO-peat development.

Further future developments to INFERNO-peat could include the estimation of gas species and aerosol emissions from peat fires. Peat specific emissions factors, such as those published by Hu et al. (2018), could be used to extend the present modelling scope to include emissions of species such as CO_2, CO, CH_4, and NO_2. This novel model development would allow for further analysis into the atmospheric composition and air quality impacts of peat fires. Additionally, the INFERNO-peat scheme could also be extended globally to incorporate temperate and tropical peatlands. Tropical peat fires are known to release vast quantities of carbon to the atmosphere. For example, peat fires in Indonesia in 1997 released 2.57 Gt C, equivalent to 40% of global fossil fuel burning C emissions in 1997 (Page et al., 2002). Therefore, modelling peat fires in tropical regions would represent another substantial step forward in fire modelling capabilities and may also help boost global representation of interannual variability in fire emissions.

INFERNO-peat has demonstrated the importance of parameterising northern high latitude peat fires into fire models, through improvements in high latitude-wide and region-specific estimates of burnt area and carbon emissions, improved representation of the spatial patterns of burning, and drastically improved abilities to represent the interannual variability in burnt area and carbon emissions. There is substantial regional variation in the performance of INFERNO-peat and areas of potential improvement have been discussed extensively in the preceding paragraphs. Despite potential future improvements, INFERNO-peat already performs well on the whole for the high latitudes and reproduces present day peatland burning. However, the high latitudes are undergoing rapid climatic

warming (Bruhwiler et al., 2021), and under continued climate changes peatlands are expected to dry out, becoming more vulnerable to fires, and lightning strikes are also anticipated to increase, overall resulting in an escalation of fire frequencies and severities (Talucci et al., 2022; McCarty et al., 2021; Turetsky et al., 2015; Chen et al., 2021). Increases in peat fires are of particular concern as they may amplify carbon losses, creating a positive feedback loop on the climate system (Rein, 2013; Hu et al., 2018; Turetsky et al., 2015) that risks shifting peatlands from sinks to sources of carbon by the end of the century (Swindles et al., 2019; Turetsky et al., 2015; Loisel et al., 2020). Therefore, INFERNO-peat can be used to model how peat fires may change over the coming century as a result of climate change (Chapter 5) and be able to anticipate potential future impacts on the climate system, air quality and the carbon cycle.

Chapter 4: Trends and impacts of fires in the northern high latitudes using satellite data

Abstract

Wildfires are important and large sources of gas and aerosol emissions, which have implications for atmospheric composition, global carbon cycles and air quality worldwide. Strong aerosol emissions from wildfires in the northern high latitudes exert a strong effect on air quality resulting in air pollution induced health burdens. Peat fires in particular have major impacts on atmospheric composition and air quality, due to the release of different amounts of trace gases and aerosols during smouldering combustion, such as higher CO and $PM_{2.5}$ emissions. However, minimal research has been carried out on assessing large scale trends and patterns of peat fires in the high latitudes, and the impacts these have on atmospheric composition. Here I show that peat fires, estimated from GFED5 burnt area observations, burn significant proportions of the northern high latitudes with substantial interannual variability. Additionally, peat fires and wildfires are shown to have major impacts on atmospheric composition, through elevations in NO_2 concentrations. Only peat fires in northwest Siberia exhibit the expected relationships of elevated CO emissions relative to NO_2, indicative of a strong presence of smouldering combustion. Fires, and specifically peat fires, are also shown to be positively associated with $PM_{2.5}$ concentrations. However, it remains difficult to be able to differentiate between peat and non peat burning in terms of their impacts on atmospheric composition and air quality. Therefore, this chapter presents a starting point for further analysis into the impacts of peat fires on atmospheric composition and air quality using large scale Earth observation data, which hopes to aid in the detection of peat fires in the northern high latitudes and inform global fire models.

1. Introduction

Globally wildfires are among the largest sources of trace gas and aerosol emissions to the atmosphere, with major impacts on atmospheric composition and the global carbon budget (Chuvieco, 2009; Sofiev, 2013; Andreae, 2019; Langmann et al., 2009; Friedlingstein et al., 2023). Whilst globally fires are estimated to emit 1.6-1.7 Gt C per year, peat fires also function as strong source of carbon emissions at around 0.3 Gt C each year (Friedlingstein et al., 2023). Fires are major sources of key greenhouse gas emissions including CO_2, CH_4, NO_2 and N_2O (Tian et al., 2016; Le Quere et al., 2018), as well as being a crucial source of aerosol emissions (Wiedinmyer et al., 2011; Andreae and Rosenfeld, 2008). For example, approximately 57-74% of global primary organic particulate matter emissions and 27-60% of black carbon (BC) emissions result from fires (Bond et al., 2004; Andreae and Rosenfeld, 2008; Wiedinmyer et al., 2011; Bond et al., 2013). The release of large amounts of aerosols, and in particular fine particulate matter, can have major implications on air quality and human health (Goldammer et al., 2008). Across Canada and Siberia, fires are the main source of air pollution induced health burdens (Lelieveld et al., 2015). Additionally, aerosols can have major

impacts on radiative forcing (Singh et al., 2010; Stone et al., 2008). Consequently, it is important that the impacts of fires and peat fires on key atmospheric constituents are studied and understood in order to better quantify potential effects on human populations and the climate system.

Carbon monoxide (CO) and nitrogen oxides (NO_x) are atmospheric pollutants, which are a major environmental risk to public health (WHO, 2016; WHO, 2003), and are heavily from fires. Wildfires are thought to be responsible for 33-50% of all global CO emissions, and 20% of global NO_x emissions (Wiedinmyer et al., 2011; Olivier et al., 2005), with peat fires in particular being a dominant driver of the interannual variability in global fire emissions (van der Werf et al., 2010; Voulgarakis et al., 2015). Additionally, high latitude peat fires also emit significant amounts of $PM_{2.5}$ with key species released being BC and organic carbon (OC) (McCarty et al., 2021; Hu et al., 2018; Kondo et al., 2011; Yokelson et al., 2011). Particulate emissions from peat fires can lead to haze events (Turetsky et al., 2015; Hu et al., 2018), which impacts upon transport, tourism, agriculture and human health through respiratory and cardiovascular problems (Hu et al., 2018; Heil and Goldammer, 2001; WHO, 2006). Over the last 2 decades, wildfire attributed $PM_{2.5}$ has resulted in between 25,000 and 50,000 premature death across the Arctic (Silver et al., 2023). Consequently, fires, and more specifically peat fires, result in degraded air quality which impacts populations throughout the high latitudes. Therefore, understanding how vegetation and peat fires differ in their emissions and the effects these emissions have is crucial to better representing these dynamics within Earth system models.

Atmospheric emissions from wildfires depend on fuel characteristics, burning efficiency, burning phase and fire type (Miranda et al., 2009). CO is most strongly emitted by incomplete combustion which is dominant during smouldering fires (Borsdorff et al., 2020; Miranda et al., 2009; Andreae and Merlet, 2001), whereas NO_2 is primarily emitted during flaming combustion when combustion is more complete (Miranda et al., 2009; Andreae and Merlet, 2001). Flaming combustion occurs at higher temperatures than smouldering, which increases the efficiency of N oxidation, leading to greater NO_x emissions during flaming fires (Mebust and Cohen, 2014). The amount of NO_x emitted during a fire depends heavily on the type of fuel being consumed and the amount of N it contains (Griffin et al., 2021; Andreae and Merlet, 2001). For example, savanna and cropland fires emit up to 3 times more NO_x than forests partially due to higher N content in these biomes compared to forests, and therefore there is more N available to be oxidised into NO_x (Fu et al., 2018; Schreier et al., 2014). However, compared to forest fires, cropland fires emit lower concentrations of aerosols and CO (Fu et al., 2018). Similarly, peat fires emit significantly more CO and CH_4 compared to flaming savanna fires (Hu et al., 2019a; Hu et al., 2018). The emission ratio (or concentration ratio) between NO_2 and CO can be used as a proxy for combustion efficiency and ultimately allow for the distinction between flaming and smouldering combustion (Andreae and Merlet, 2001; Rein et al., 2009; Andreae, 2019; van der Velde et al., 2021). Numerous studies have used NO_2:CO ratios to distinguish between

flaming and smouldering combustion on a range of spatial and temporal scales (Lama et al., 2020; Hung et al., 2022; Wan et al., 2023; Peiro et al., 2022; Anderson et al., 2023). Consequently, there is the potential for the NO_2:CO ratio to indicate the presence of smouldering vs flaming combustion during a wildfire (van der Velde et al., 2021), with lower ratios of NO_2:CO indicating smouldering and higher ratios indicating flaming fires.

There are large differences in the constituents and amounts of particulate matter (PM) emitted from peat fires compared to vegetation fires. During smouldering combustion, the amount of smoke particles emitted is over double than that emitted during flaming (Hardy et al., 2001). Therefore, it can be expected that peat fires would have larger air quality impacts due to a greater volume of harmful PM in the atmosphere. The composition of emitted PM is altered by combustion efficiency, with lower efficiency peat fires emitting more OC and negligible amounts of BC compared to flaming fires (Yokelson et al., 2011; Che et al., 2022; Christian et al., 2003; Conny and Slater, 2002; Hu et al., 2019b; Chakrabarty et al., 2016). Subsequently, differences in the amounts and impacts of PM emissions between peat and non peat fires are also highly important for gaining a better understanding of the impacts of different types of fire on air quality across the northern high latitudes.

However, despite the importance of peat fire emissions of CO and $PM_{2.5,}$ particularly in the context of their differences to flaming fires, trends and impacts of peat fires on atmospheric composition and air quality have not been extensively studied, especially in the northern high latitudes. Numerous studies have explored the impacts of specific high latitude fire and peat fire events on atmospheric composition (e.g. Huang et al., 2009; Teakles et al., 2017; Konovalov et al., 2011; Lavoue and Stocks, 2011), but this has not been conducted on large spatial scales over extended time periods. Consequently, little is understood about the large-scale effects of peat fires on atmospheric composition and air quality in a general climate context. This means that across fire modelling efforts and observational datasets, emissions from peat fires may be inaccurately represented due to an absence of information on peat fire emissions. Consequently, studies looking to assess the health implications of wildfires, may be missing crucial peat fire emissions, potentially leading to underestimations of the air quality impacts of wildfires. Therefore, this chapter aims to examine the trends in wildfires and atmospheric composition on monthly and yearly time scales across broad regions of the northern high latitudes. Furthermore, relationships between fires and atmospheric composition will be examined, and crucially compared between peat and non peat burning in order to gauge any differences in the impacts of these different fire types, with the ultimate aim of being able to inform peat fire modelling efforts.

2. Methods

To study the trends in fires in the northern high latitudes and their impacts on atmospheric composition, four focus regions were used: eastern Siberia, northwest Siberia, Alaska, and western

Canada (Figure 30). These four regions were chosen because each contains a significant presence of peat dominated soils (Figure 8a), and experience regular burning (Figure 17). Within each region this chapter explores trends in wildfires, atmospheric composition and air quality using remotely sensed observations and assesses the influence of wildfires on both atmospheric composition and air quality.



Figure 30 Locations of the four regions of Alaska (-170,55, -140,75), western Canada (-140,50, -110,75), northwest Siberia (60,50, 90,80) and eastern Siberia (130,50, 180,80) for studying the affects of fires on atmospheric composition and air quality.

Fire metrics were obtained from the Global Fire Emissions Database v5 (GFED5: Chen et al., 2023a and 2023b) and the Global Fire Assimilation System v1.2 (GFAS; Kaiser et al., 2012). More details of these two datasets are available in Chapter 2 section 8.1. Both BA and FRP were studied as both are useful descriptors of fire regimes, with BA representing the overall amounts of burning seen in a given area, and FRP reflecting the amount of thermal energy emitted from a fire and thus indicates fire intensity (Wooster et al., 2021). Additionally, the use of GFAS allows for a longer time period to be studied as this dataset runs until present day. As shown in more detail in Chapter 2 section 8.1, estimated peat burnt area and estimated peat FRP are calculated from their respective datasets by overlapping a map of peatland fractional coverage (The Northern Peatland dataset; Hugelius et al., 2020). A similar procedure was conducted by Turquety et al., (2007) in order to estimate peat fire contributions during the 2004 fire season in Alaska and Canada.

NO_2, CO and their ratio were used to quantify the atmospheric composition component of this study. TROPOMI was used as it is the most recently launched spectrometer that measures in a range of spectral bands allowing the simultaneous observation of multiple trace gases (Veefkind et al., 2012; Babic et al., 2022). More details on TROPOMI can be found in Chapter 2 section 8.2.1. Additionally, The CAMS reanalysis (CAMSRA) was used for the analysis of atmospheric composition, as it assimilates data from multiple sources, allowing for a more accurate estimate of atmospheric trace gas concentrations (Inness et al., 2019). Furthermore, CAMSRA is a long-term dataset currently available from 2003 to 2022, which significantly extends the 2018-2021 time range of TROPOMI. $PM_{2.5}$ from CAMSRA was used to assess trends in air quality across the regions of the high latitudes, as well as to estimate relationships between wildfires and $PM_{2.5}$ concentrations. Data processing of both TROPOMI and CAMSRA was conducted to ensure high quality data, and to create a monthly dataset of NO_2, CO and $PM_{2.5}$ for the four regions of the northern high latitudes. Details of this preprocessing can be found in Chapter 2 section 8.2.3.

2.1. Data analysis

Trends and patterns in monthly, annual and seasonal fire and atmospheric composition variables were examined. Here 'monthly' refers to the monthly total BA, NO_2 and CO or monthly mean FRP and 'annual' refers to the annual total BA, NO_2 and CO or annual mean FRP. 'Seasonal' refers to the mean total BA, NO_2 and CO or mean FRP that occurs each month averaged over the entire length of the dataset. In addition, the ratio of NO_2:CO, calculated simply as regional total NO_2 over regional total CO, was also examined. A summary of the variables used in this chapter can be seen in Table 15. Large fire years, and years with greater or less than average NO_2 and CO, were identified as those greater than one standard deviation above or below the multi-annual mean. Drivers of these large fire year were examined using 2m temperature data from CAMSRA (see Chapter 2 section 8.3 for further details). Temperatures and BA anomalies were calculated as the difference between the multi-annual seasonal average temperature and burnt area in winter (DJF), spring (MAM), summer (JJA) and autumn (SON) and the observed monthly temperature or burnt area. Using these anomalies, Spearman's rank correlation coefficients were calculated to assess the relationship between abnormally high or low temperatures on unseasonably large or small burnt areas. Comparisons were also directly made between 2019 and 2020 due to all four datasets recording data in these years.

Table 15: Summary of the variables used in the analysis of the effects of fires on atmospheric composition and air quality.

Variable	Units	Data source	Time range
Total burnt area	M ha	GFED5	2003-2020
Estimated peat burnt area	M ha	GFED5	2003-2020
Estimated peat fire percentage of burnt area	%	GFED5	2003-2020
Total FRP	W m^{-2}	GFASv1.2	2003-2022
Estimated peat FRP	W m^{-2}	GFASv1.2	2003-2022
Estimated peat FRP percentage of total FRP	%	GFASv1.2	2003-2022
NO_2	Kg or mol	TROPOMI/	2018-2021
		CAMSRA	2003-2022
CO	Kg or mol	TROPOMI/	2018-2021
		CAMSRA	2003-2022
NO_2:CO	-	TROPOMI/	2018-2021
		CAMSRA	2003-2022
$PM_{2.5}$	Kg	CAMSRA	2003-2022
2m temperature	°C	CAMSRA	2003-2022

2.1.1. Correlation analysis

Correlations using Spearman's rank correlation coefficient were used to assess the monotonic relationship between fire variables and atmospheric variables, due to non-normal distributions in the data. All fire variables, on monthly, annual, and seasonal scales were correlated with NO_2, CO, and NO_2:CO from both TROPOMI and CAMSRA, and with $PM_{2.5}$ from CAMSRA. Due to differences in

the observation periods for all four products, correlations with TROPOMI data were conducted using data from 2018-2020 for GFED5 and 2018-2021 from GFASv1.2. Correlations using the longer timespan CAMS data were conducted using data from 2003-2020 for GFED5 and for 2003-2022 for GFASv1.2.

2.1.2. Burnt area size category analysis

Peat fires across the high latitudes may be too small for their effects to be detected on atmospheric composition. In order to assess this affect, annual burnt areas for all regions were divided into 4 different categories based on the total amount of peat burning within a year. These classes are: no peat burning, low peat burnt area (<0.005 M ha), medium peat burnt area (0.005-0.15 m ha) and high peat burnt area (>0.15 M ha). These categories were chosen to ensure an even distribution of data across the categories. Correlations using Spearman's rank correlation coefficient were conducted for each class between estimated peat burnt area from GFED5 and NO_2, CO and the NO_2:CO ratio from CAMSRA.

2.1.3. Vegetation burning analysis

Smouldering and flaming combustion often occur simultaneously and as a result individual signals may be difficult to identify. Therefore, a short analysis of the effects of different vegetation fires on atmospheric composition was conducted. GFED5 splits BA into 17 land cover types, including boreal, tropical and temperate forests, tundra, shrublands and grasslands. GFED5 obtains burning in different land cover types through the use of the Collection 6 MODIS land cover type product (MCD12Q1) and fractional tree cover from the MODIS Collection 6 Vegetation Continuous Fields product (MOD44B) (Chen et al., 2023b). For each region, the dominant types of vegetation burning are identified, and the percentage of total burning attributed to each vegetation type is additionally calculated. Spearman's rank correlation coefficients were calculated for vegetation type burnt area and vegetation burning percentages of total burnt area, with NO_2, CO and NO_2:CO from CAMSRA on both monthly and annual scales.

2.1.4. Comparisons to INFERNO-peat

Modelled peat fire burnt areas from INFERNO-peat, generated using the experimental set up described in Chapter 2 Sections 3 and 4, can provide additional insights into the effects of peat fires on atmospheric composition and air quality. Furthermore, INFERNO-peat and GFED5 estimated peat burnt area can help to validate one another, allowing for detected signals of peat burning on atmospheric composition to be verified and understood. For each region, monthly and annual modelled estimates of peat burnt area from INFERNO-peat were compared to what is estimated from GFED5, and key differences were identified. Overall trends and interannual variability in peat burnt area from INFERNO-peat were also examined with respect to GFED5 estimated peat burnt area.

Correlations between annual and monthly INFERNO-peat peat burnt area and NO_2, CO and NO_2:CO from CAMSRA were conducted using Spearman's rank correlation coefficient. Correlations were only conducted with the CAMSRA data as INFERNO-peat was only run from 1997 to 2014, therefore having no overlap with the TROPOMI observation period (2018-2021). Consequently, correlation analysis was conducted using INFERNO-peat burnt areas and CAMSRA atmospheric composition data from 2003 to 2014.

3. Results

3.1. Eastern Siberia

3.1.1. Trends in wildfires and peat fires

On average 2.7 M ha burn each year in eastern Siberia (E Siberia) with a mean FRP of 78.8 W/m^2, which largely occurs during the summer months of June, July and August (Figure 31b). In E Siberia the largest fire years occurred in 2003, 2012 and 2020 (Figure 31a) in which 5.7, 5.8 and 8.4 M ha were burned respectively (Table 16), in agreement with Bondur et al., (2023). Large burned area (BA) years occur alongside the largest FRP years (Figure 31a), with the exception of 2010, where the FRP in this year is close to that of 2003, despite burning 2.2 M ha less area. 2020 is the largest fire year at 8.5 M ha. During 2020 over 90% of this burning occurred during June-August. There are minimal changes in burnt area and FRP across the timeseries, with total BA increasing by 0.728 ± 5.058 M ha per decade. Therefore, there are minimal trends detected here, partly due to the large interannual variability.

Of this 2.7 M ha of annual burning, 8.6% was found to overlap with peat-dominated soils, and therefore I estimate that on average 0.2 M ha of peat burns each year, with an average estimated FRP of 10.7 W/m^2 (Table 16). The majority of peatland burning, much like overall burning, occurs during the summer months (Figure 31d), most notably July where on average an estimated 0.08 M ha of peat burns (1/3rd of the annual estimated peat burning total). Notable estimated peat burning years occur concurrently with large fire years in 2003, 2012 and 2020. However, estimated peat burning also spikes in 2010, whereas total vegetation burning does not, meaning peat fires are estimated to have been responsible for 12.5% of the total BA which is the highest annual percentage recorded between 2003 and 2020 (Figure 31e). The 2010 peak of 0.4 M ha of estimated peat BA coincides with a large spike in estimated peat FRP of 30 W/m^2. As previously reported, the overall FRP in 2010 was equivalent to that of 2003 but burned significantly less area overall. Therefore, it is likely that in 2010 the large peat fires that are estimated here, may have burned at a higher severity, with a large influence on the whole regions annual mean FRP. The largest estimated peat BA occurred in 2020, burning an estimated 0.8 M ha with an estimated peat FRP of 38.9 W/m^2. The seasonality of estimated peat BA percentage of total BA shows elevated percentages over the entire burning season from March to October, with estimated peat FRP percentage showing a similar result (Figure 31f). Due to

the stochasticity of peat burning in E Siberia, there are no clear trends in estimated peat BA, FRP or their percentage contributions over the time period examined.

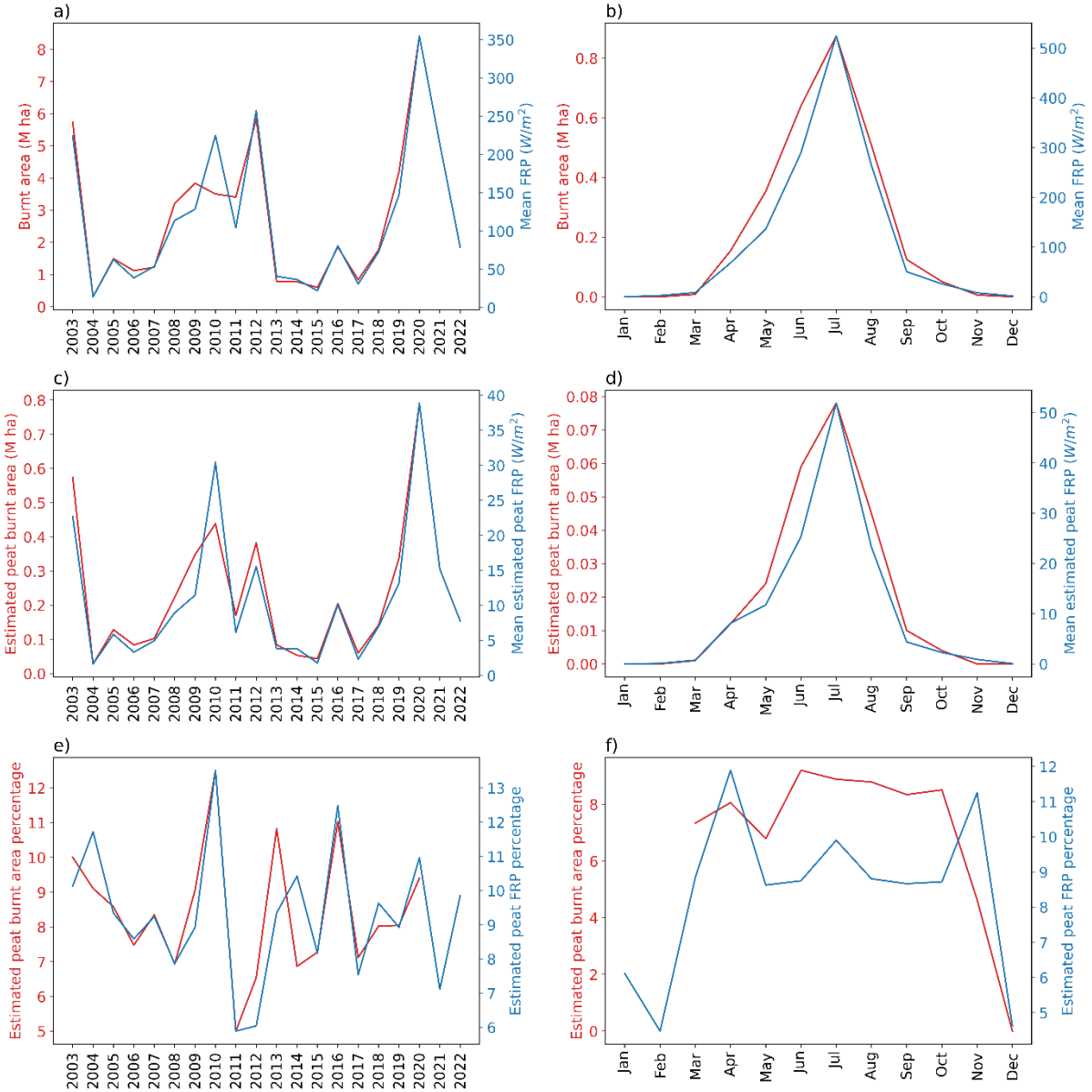


Figure 31: Fire trends over 2003-2022 for eastern Siberia. BA data covers the period from 2003 to 2020, and the FRP data continues up to 2022. The trends shown are a) average annual total BA and FRP and b) the seasonality in total BA and FRP (averaged over their respective time periods). Panel (c) shows the yearly timeseries trends in estimated peat BA and FRP and d) shows the seasonality in estimated peat BA and estimated peat FRP. Panel (e) shows the estimated peat BA as a percentage of total BA and the estimated peat FRP as a percentage of total FRP, and panel (f) shows the seasonality in estimated peat BA and FRP percentage.

Table 16: Annual values for BA from GFED5 and FRP from GFAS for eastern Siberia, and the summary statistics (mean, standard deviation (STD) and coefficient of variation (CV)) for the whole time series. Values in bold highlight years in which the value is at least one standard deviation greater than the mean.

	GFED5			GFAS		
Year	Total BA (M ha)	Peat BA (M ha)	Peat BA percentage	Total FRP (W/m^2)	Peat fire FRP (W/m^2)	Peat fire FRP percentage
2003	**5.743**	**0.575**	10.006	**224.281**	**22.721**	10.131
2004	0.309	0.028	9.107	14.071	1.649	**11.719**

2005	1.494	0.128	8.577	62.747	5.859	9.337
2006	1.121	0.084	7.476	38.694	3.322	8.586
2007	1.230	0.103	8.348	53.784	4.968	9.238
2008	3.215	0.223	6.930	113.751	8.944	7.862
2009	3.840	0.348	9.057	128.490	11.465	8.923
2010	3.506	**0.438**	**12.508**	**225.019**	**30.417**	**13.517**
2011	3.408	0.170	5.001	104.274	6.141	5.889
2012	**5.846**	0.382	6.543	**257.370**	15.547	6.041
2013	0.778	0.084	**10.827**	40.752	3.809	9.348
2014	0.777	0.053	6.865	36.643	3.819	10.422
2015	0.598	0.044	7.273	21.980	1.796	8.170
2016	1.855	0.205	**11.023**	80.694	10.072	**12.482**
2017	0.841	0.060	7.120	30.793	2.322	7.542
2018	1.771	0.142	8.025	72.747	7.006	9.630
2019	4.197	0.338	8.041	147.497	13.162	8.924
2020	**8.415**	**0.791**	9.401	**354.764**	**38.880**	10.960
2021				213.772	15.198	7.110
2022				78.847	7.768	9.852
Mean	2.719	0.233	8.572	115.048	10.743	9.284
STD	2.242	0.209	1.842	93.770	9.897	1.962
CV	0.825	0.897	0.215	0.815	0.921	0.211

3.1.2. Drivers of large fire years

In E Siberia there are significant positive correlations between seasonal temperature anomalies and seasonal BA, as well as estimated peat BA (Figure 32; $r=0.388$, $p<0.001$; $r=0.351$, $p<0.001$). Therefore, months in which temperatures are higher than the seasonal average tend to be associated with months with higher than seasonal BA (Figure S3). For example, during the 2003 fire season, which was the large fire season on record in Siberia (Talucci et al., 2022), GFED5 estimates that BA in July and August is greater than 1 M ha higher than the summer average BA, and temperatures from CAMSRA in July 2003 were 1.2°C higher than the seasonal average. Balzter et al., (2005) demonstrated that positive phases of the Arctic Oscillation index and high summer temperatures drove the large 2003 Siberian fires. Similarly, 1.5 M ha more BA occurred in July 2012 than the seasonal average, concurrent with the seasonal average temperatures being 0.6°C warmer. Additionally, large fires throughout June, July and August of 2020 show larger than average temperatures, particularly in July. 2020 was a particularly large fire season in northeast Siberia, as well as being the largest fire season on record in the Chukchi Peninsula in far eastern Siberia (Talucci et al., 2022). Much like the results shown here, this extreme fire season resulted from high summer temperatures and dry conditions produced as a result of blocking anticyclones (Scholten et al., 2022; Descals et al., 2020)

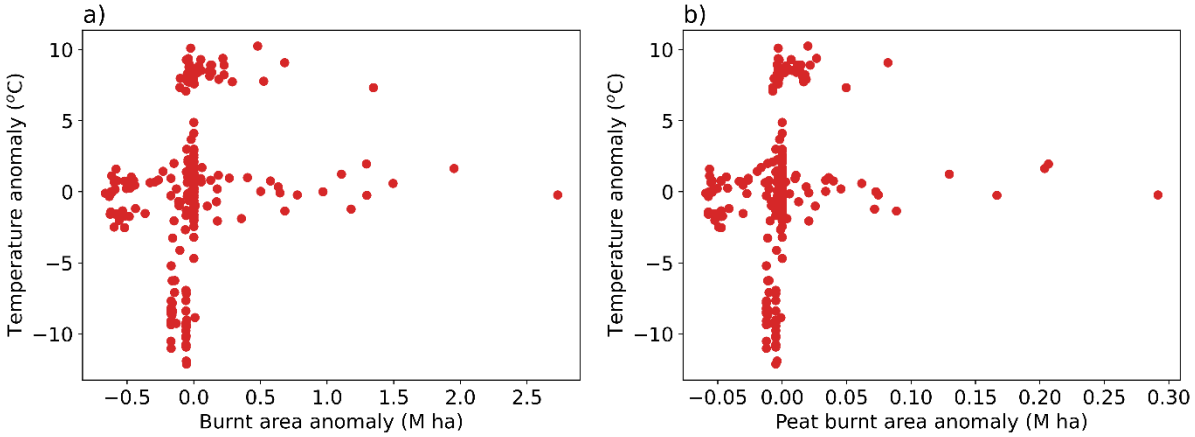


Figure 32: Scatterplot of seasonal temperature anomalies vs seasonal BA anomalies for a) total BA and b) estimated peat BA, in E Siberia.

3.1.3. Impacts of fires on atmospheric composition

Over the period 2003 to 2022 from the CAMS reanalysis data there are increases in NO_2 (Figure 33a) and decreases in CO (Figure 33c), which is driving an overall increase in the annual NO_2:CO ratio (Figure 33e). The largest NO_2 levels occur in 2003, 2012 and 2020, all of which are the years with the highest BAs and FRPs. However, when looking at CO there are peaks in both 2003 and 2012 but not in 2020. This perhaps suggests a dominance of flaming combustion in 2020, which is supported by 2020 having the second largest NO_2:CO ratio, indicating a higher combustion efficiency occurring. Data from TROPOMI also shows 2020 to have a large value of NO_2, and a relatively low NO_2:CO ratio. Comparison of 2003 to 2020 in the CAMS reanalysis data revealed that NO_2 levels are relatively similar, but CO in 2020 was 1657.8 kg lower than 2003. Consequently, in 2003 the NO_2:CO ratio was nearly 25% lower than in 2020. A lower NO_2:CO ratio indicates a high dominance of incomplete combustion which is associated with smouldering peat burning, therefore suggesting that 2003 may have seen more peat burning than 2020. This is somewhat reflected in the GFED5 data with peat fires being responsible for 10.0% burning in 2003, compared to 9.4% in 2020. However, this difference is small, and it is important to recall that these are estimates of peat burning based on a fire happening in an area where there is peat and there may have been more (or less) peat burning. Similarly, in the TROPOMI data, 2020 can be compared to 2019, as 2020 had over double the amount of burning than 2019. However, there is a less pronounced effect of this doubling on the NO_2 and CO levels observed in TROPOMI. There is a moderate increase in the NO_2:CO ratio in 2020 compared to 2019 (0.00014 vs 0.00012), however the peat fire percentage stays very similar. Therefore, the increase in the NO_2:CO ratio seen in 2020 is more likely to be indicative of the increase in flaming vegetation fires in 2020, rather than of a decrease of smouldering peat fires.

Both CAMS reanalysis and TROPOMI show a peak in NO_2 during summer (Figure 33b). However, the CAMS data shows a much wider period of elevated NO_2 from March through to October, concurrent with the elevated BA from March to October, whereas TROPOMI shows a much sharper

peak in July. Overall, the elevated NO_2 values over this period indicate that fires may be a driving force in the intra-annual variability in NO_2. CO in the TROPOMI data shows elevated levels from March to October, but also shows an early burning season peak in March, and a summer peak in August, with a drop in June and July (Figure 33d). However, this is not the case in the CAMS reanalysis data with large fluctuations in CO happening throughout the year, with the largest values occurring between March and May. As a result, in the CAMS data NO_2:CO ratios are lowest over winter, and peak during the summer months of June to October. In contrast, NO_2:CO ratios according to TROPOMI show peaks over winter (December and January) as well as a summer peak. The differences in the seasonalities between CAMS and TROPOMI may be a result of the different averaged time periods, with TROPOMI having significantly less data available. However, even when calculating the monthly seasonality for CAMS over the TROPOMI period (2018-2021), patterns in the seasonality of NO_2, CO and their ratio remain similar to the longer timeseries seasonality (Figure S2). The high winter NO_2:CO ratios being seen in TROPOMI may also be the result of poor data quality or poor satellite coverage over winter. As the CAMS reanalysis data is combined from multiple different sources, such data quality impacts may be reduced.

Table 17: Annual values for NO_2, CO and their ratio from both TROPOMI and CAMS reanalysis data, and the summary statistics (mean, standard deviation (SD) and coefficient of variation (CV)) for the whole time series. Values in bold highlight years in which the value is at least one standard deviation above or below the mean.

	CAMS reanalysis				TROPOMI		
Year	NO_2 (kg)	CO (kg)	Ratio NO_2:CO	$PM_{2.5}$	NO_2 (mol)	CO (mol)	Ratio NO_2:CO
2003	**6.287**	**8521.891**	**0.00074**	**0.063**			
2004	**5.211**	7197.940	**0.00072**	**0.029**			
2005	**5.426**	7418.242	**0.00073**	0.035			
2006	**5.200**	7362.542	**0.00071**	0.035			
2007	5.599	7271.349	0.00077	0.033			
2008	5.908	7591.117	0.00078	0.053			
2009	5.786	6951.668	0.00083	0.052			
2010	6.182	7181.739	0.00086	0.044			
2011	5.918	6878.692	0.00086	0.047			
2012	**6.337**	**7795.823**	0.00081	**0.064**			
2013	**5.501**	6827.816	0.00081	0.035			
2014	6.043	6915.125	0.00087	0.035			
2015	**5.478**	6866.813	0.00080	**0.032**			
2016	5.833	6942.206	0.00084	0.036			
2017	6.069	**6565.220**	**0.00092**	0.035			
2018	6.073	7013.887	0.00087	0.039	0.214	1239.529	0.00017
2019	5.979	6726.968	0.00089	0.056	0.250	2016.426	0.00012
2020	**6.688**	6864.049	**0.00097**	**0.069**	0.275	2020.569	0.00014
2021	6.335	7548.774	0.00084	0.059	0.249	2159.916	0.00012
2022	6.394	**6211.047**	**0.00103**	0.038			
Mean	5.912	7132.645	0.00083	0.044	0.247	1859.110	0.00014
SD	0.410	496.305	0.00008	0.012	0.025	418.403	0.00003
CV	0.069	0.070	0.10021	0.279	0.000	0.225	0.18373

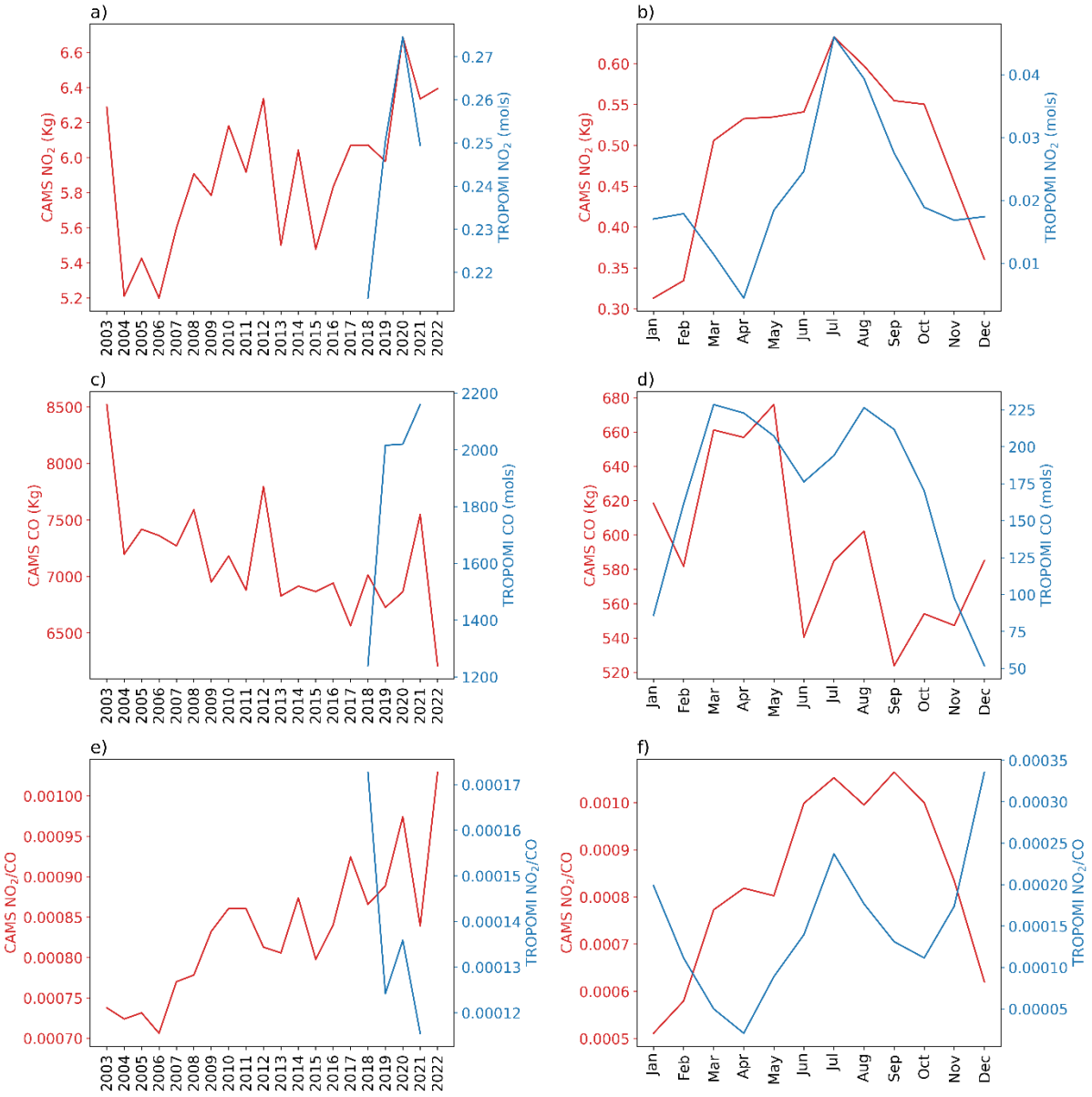


Figure 33: Time series plots for NO_2 (a) and its seasonality (b), CO (c) and its seasonality (d), and the ratio of NO_2/CO (e) and its seasonality (f), for the period 2003-2022 for CAMS reanalysis data (red) and 2018-2021 for the TROPOMI data (blue), in eastern Siberia.

As identified earlier, 2010 saw the largest peat fire percentage of BA. Despite this, the 2010 NO_2:CO ratio was not significantly different from the multiannual average (Table 17). By comparison 2004 has the lowest estimated peat BA at just 0.028 M ha but has a lower NO_2:CO ratio than 2010, despite 2010 burning over 90% more BA. Furthermore, 2020 sees the largest estimated peat BA (0.791 M ha) but compared to 2004, both years have comparable percentages of peatland burning (9.1% compared to 9.4%) (Table 17). Comparing these two years, 2004 has a ratio of 0.00072, compared to 0.00097 in 2020 (Table 17). This suggests that in 2020 much of the signal of burning in the atmospheric composition data is being dominated by flaming fires compared to 2004. The total CO in 2004 was 4.6% higher than 2020, but NO_2 was 28.3% lower. This perhaps indicates that the peat fires that

occurred in 2004 had more of an impact on atmospheric composition that those in 2020. When we look at FRP, we see that in 2004 11.7% of FRP could be attributed to peat fires, compared to 9.8% in 2020, suggesting a larger impact of peat fires on the severity of the total burning in 2004 compared to 2020. Alternatively, the large flaming fires in the record breaking 2020 fire season may have overridden the signal from smouldering fires in that year.

2003 also sees high levels of estimated peat BA, of 0.575 M ha, which coincides with the fourth lowest yearly NO_2:CO ratio of 0.00074, significantly below the multiannual mean, and the highest annual CO levels (Table 17). This suggests that 2003 did see a significant amount of peat burning, driving the strong increases in CO relative to smaller fire years, and therefore a lower NO_2:CO ratio. 2012 also shows a large amount of peat BA at 0.382 M ha, and has the second highest CO levels, as well as a lower NO_2:CO ratio compared to the prior year, which saw around 0.2 M ha less peat BA. This year again reflects the pattern of increased peat burning being associated with higher CO emissions compared to years with more flaming fires.

2013 and 2016 see the 2nd and 3rd highest peat fire percentages in E Siberia. However, these years show no significant deviation from the multiannual average NO_2:CO ratio (Table 17). This is likely a reflection of that fact that these years only feature very small absolute peat BAs of 0.084 M ha and 0.205 M ha, respectively, perhaps indicating that these BAs are too small to be able to produce a signature on the atmospheric composition.

When it comes to the seasonal cycle, there are relatively strong positive correlations between GFED5 total BA and TROPOMI NO_2 ($r=0.613$, $p=0.034$), and CAMS reanalysis NO_2 ($r=0.866$, $p<0.001$), suggesting that months with high BA are associated with high concentrations of NO_2 in the atmosphere (Table 18a). According to the TROPOMI data, there are also positive correlations between total BA and CO ($r=0.592$, $p=0.043$). However, there is no relationship between total BA and CAMS CO. Whilst there are no significant correlations between total BA and TROPOMI NO_2:CO ratios, there are strong positive correlations between total BA and the CAMS NO_2:CO ratio on a seasonal scale ($r=0.711$, $p=0.009$), indicating that over a large time series, the presence of more burning in E Siberia is correlated with increases in the ratio of NO_2:CO in the atmosphere. Similar results are seen when looking at estimated peat burning, where estimated peat BA and peat % are positively correlated with NO_2 from both TROPOMI and CAMS (Table 18a). There is no relationship between estimated peat burning in the GFED5 data on the TROPOMI NO_2:CO ratio, but there are positive correlations between the CAMS NO_2:CO ratio and estimated peat BA ($r=0.666$, $p=0.018$), and estimated peat fire percentage ($r=0.733$, $p=0.016$), opposite to what might be expected. The GFAS FRP data shows similar positive correlations to that of GFED5 BA, with total FRP and estimated peat fire FRP positively correlated with NO_2 and CO from TROPOMI (Table 18a). Furthermore, when looking at total FRP and estimated peat FRP there is no relationship with the TROPOMI NO_2:CO

ratio, but there are positive correlations with the CAMS NO_2:CO ratio. Estimated peat fire % of FRP shows no significant relationships with atmospheric composition quantities.

Correlations between multi-year annual data have only been conducted between GFED5 and GFAS annual values against the CAMS reanalysis, as the TROPOMI timeseries is too short for this correlation analysis. There are positive correlations between total BA and NO_2 (r=0.682, p=0.002), and peat BA and NO_2 (r=0.678, p=0.002). However, there is no correlation with CO or the NO_2:CO ratio (Table 3c). The same pattern is seen when looking at GFAS FRP with a positive correlation between total and peat FRP with NO_2, but no relationships with CO or the ratio. Peat fire percentage of BA shows a weak and non-significant negative correlation with NO_2 (r=-0.042, p=0.868), and the NO_2:CO ratio (r=-0.094, p=0.711). Given that these relationships are statistically insignificant and very weak, although they follow the expected patterns (increases in peat burning resulting in decreasing ratios between NO_2 and CO), no conclusions can be taken from these results.

Correlating multi-year monthly values of BA and atmospheric composition variables showed positive correlations between total BA and TROPOMI CO (r=0.627, p<0.001) and estimated peat BA with TROPOMI CO (r=0.599, p<0.001). However, the longer time series CAMS data shows no relationship between monthly BA and CO (Table 18b). Similarly, there are positive correlations between total FRP (r=0.611 p<0.001) and estimated peat FRP (r=0.587, p<0.001) with TROPOMI CO, but no relationship with CAMS CO. However, there are strong positive correlations between BA, FRP, estimated peat BA and estimated peat FRP with both TROPOMI NO_2 and CAMS NO_2 Table 18b). There are positive correlations of the ratio of NO_2:CO from CAMS with total BA, with estimated peat BA, with total FRP, and with estimated peat FRP (Table 18b). This shows that regardless of whether burning is due to peat fires or not, larger BAs result in larger ratios of NO_2:CO. There are no significant relationships between the TROPOMI NO_2:CO ratio and any of the fire parameters. Additionally, there are no significant relationships between estimated peat fire percentage of BA or FRP with any of the atmospheric composition variables.

Table 18: Correlations between the GFED5 and GFAS fire parameters, with NO_2, CO and their ratio in the TROPOMI and CAMS reanalysis datasets, on seasonal data (a), multi-year monthly data (b) and multi-year annual data (c) in eastern Siberia. Asterisks indicate significant p values (* = p<0.05, **=p<0.001, ***=p<0.001)

		TROPOMI			CAMS		
		NO_2	CO	NO_2:CO Ratio	NO_2	CO	NO_2:CO Ratio
a) Seasonality data							
GFED5	Total BA	0.613 *	0.592 *	-0.049	0.866 ***	-0.035	0.711 **
	Peat BA	0.641 *	0.591 *	-0.043	0.854 ***	0.007	0.666 *
	Peat BA percentage	0.697 *	0.445	0.209	0.830 **	-0.358	0.733 *
GFAS	Total FRP	0.622 *	0.601 *	-0.091	0.867 ***	-0.063	0.713 **
	Peat FRP	0.629 *	0.538 *	-0.049	0.860 ***	-0.119	0.734 **

	Peat FRP percentage	-0.182	0.391	-0.091	0.282	0.100	0.327
b) Monthly data							
GFED5	Total BA	0.523 **	0.627 ***	-0.167	0.812 ***	0.034	0.633 ***
	Peat BA	0.535 **	0.599 ***	-0.118	0.759 ***	0.062	0.572 ***
	Peat BA percentage	0.073	0.020	0.068	-0.005	0.089	-0.030
GFAS	Total FRP	0.616 ***	0.611 ***	-0.040	0.757 ***	0.039	0.583 ***
	Peat FRP	0.624 ***	0.587 ***	-0.024	0.748 ***	0.051	0.572 ***
	Peat FRP percentage	-0.159	-0.040	-0.164	0.022	0.064	0.024
c) Yearly data							
GFED5	Total BA				0.682 **	0.199	0.319
	Peat BA				0.678 **	0.232	0.286
	Peat BA percentage				-0.042	-0.003	-0.094
GFAS	Total FRP				0.681 **	0.275	0.277
	Peat FRP				0.716 ***	0.248	0.332
	Peat FRP percentage				0.054	-0.126	0.120

Overall, in E Siberia years and months with larger BAs tend to be associated with larger concentrations of NO_2, and often result in positive correlations between BA and the NO_2:CO ratio. However, large-scale impacts of peat fires on atmospheric composition in this region are less clear. When comparing monthly GFED5 and GFAS with TROPOMI there are positive correlations between CO and peat BA. There are also positive correlations between peat BA and total BA with NO_2 emissions, often resulting in elevated NO_2:CO ratios, suggesting that peat burning in E Siberia is not having a clear signature on atmospheric composition, outside of the effects seen for total burning.

3.1.4. Impacts of fires on air quality

CAMS reanalysis data shows substantial interannual variability in $PM_{2.5}$ (Figure 34a). There are large spikes in $PM_{2.5}$ in E Siberia in 2003, 2008, 2009, 2012 and 2019-2021. 2020 is the year with the largest $PM_{2.5}$ concentration of 0.069 kg across the E Siberia region. These years match up well with the largest fire years both in terms of BA and FRP, suggesting a strong connection between fires and atmospheric $PM_{2.5}$ concentrations in E Siberia. On a seasonal cycle, $PM_{2.5}$ peaks in June, July, and August. There are slightly elevated spring values (April, May), and the lowest values occur over winter (Figure 34b). This matches up well with the seasonalities seen in BA and FRP.

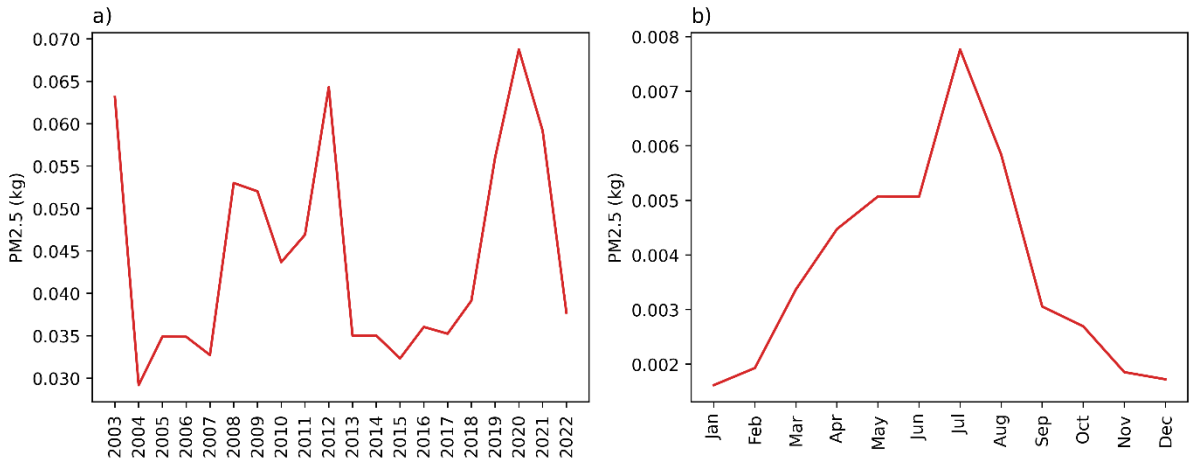


Figure 34: Timeseries plot for $PM_{2.5}$ from 2003-2022 in eastern Siberia from the CAMS reanalysis data (a), and the 2003-2022 averaged eastern Siberia seasonality in $PM_{2.5}$ (b)

There are significant strong positive correlations between multi-year annual, multi-year monthly and multi-year average monthly (seasonal cycle), $PM_{2.5}$ and BA, with estimated peat BA, FRP and estimated peat FRP (Figure 35, Table 19). In particular, the monthly totals exhibit significant strong positive correlations with both BA ($r=0.869$ $p<0.001$) and estimated peat BA ($r=0.860$, $p<0.001$), as well as weaker (but still significant) positive correlations between monthly total $PM_{2.5}$ and estimated peat fire BA percentages, with the higher the contribution of peat fires, the higher the $PM_{2.5}$ concentrations (Figure 35a-c). Similar results are seen when correlating with the GFAS FRP variables (Figure 35d-f). Additionally, there are also strong positive correlations between $PM_{2.5}$ seasonality and yearly data with total BA, estimated peat BA, total FRP and estimated peat FRP (Table 19). In contrast, the positive correlations seen between estimated peat fire percentage of BA and $PM_{2.5}$ are not seen in the annual data. This likely suggests that on a yearly time step the impact of the contribution of peat burning relative to total burning is minimal, but on a month-to-month basis, months that potentially burn significantly more peat correlate with increases in $PM_{2.5}$.

Table 19: Correlations between the yearly GFED5 and GFAS fire parameters, and the CAMS reanalysis $PM_{2.5}$ data, using annual totals, monthly totals and the seasonality (average monthly totals 2003-2020) in eastern Siberia. Asterisks indicate significant p values (* = $p<0.05$, **=$p<0.001$, ***=$p<0.001$)

		CAMS $PM_{2.5}$ Annual totals	Monthly totals	Seasonality
GFED5	Total BA	0.925 ***	0.869 ***	0.937 ***
	Peat BA	0.894 ***	0.860 ***	0.940 ***
	Peat BA percentage	-0.014	0.245 **	0.648 *
GFAS	Total FRP	0.918 ***	0.839 ***	0.951 ***
	Peat FRP	0.887 ***	0.842 ***	0.923 ***
	Peat FRP percentage	-0.167	0.217 **	0.469

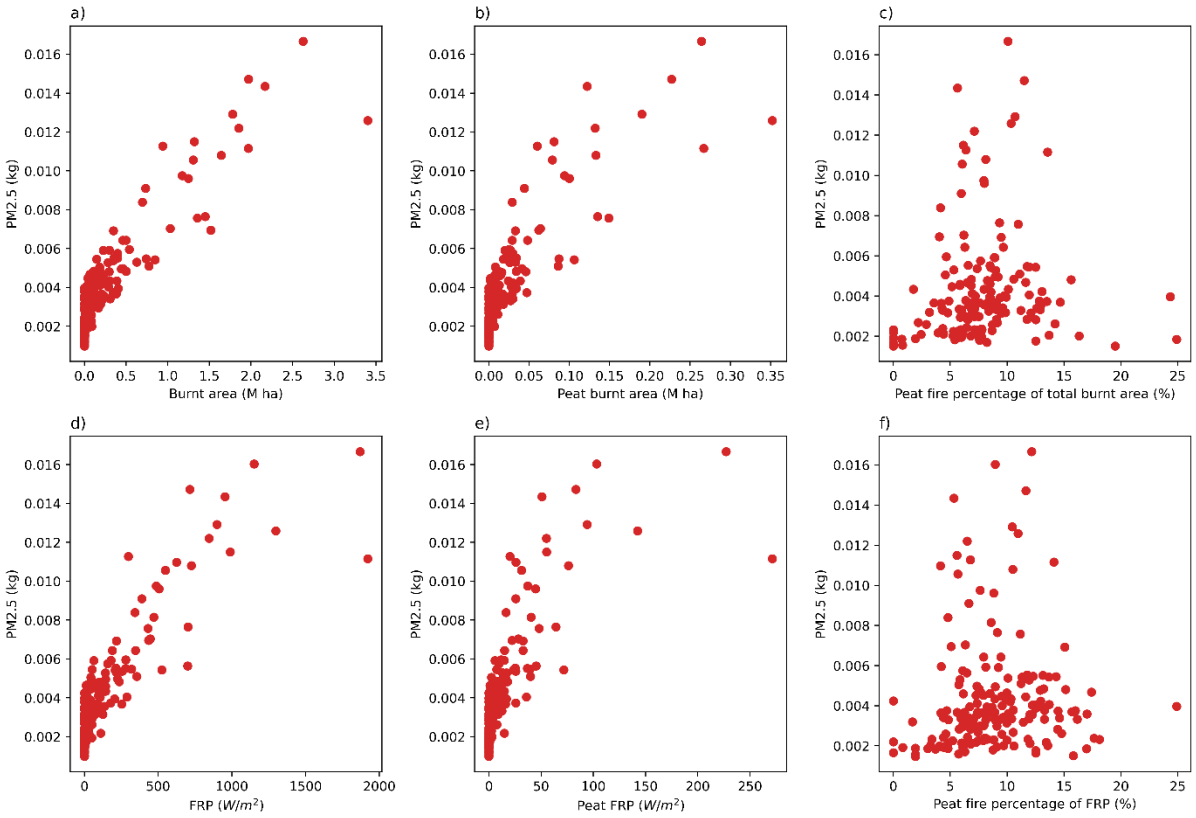


Figure 35: Relationships between monthly total CAMS $PM_{2.5}$ and monthly total BA (a), estimated peat BA (b), estimated peat fire percentage of BA (c), total mean FRP (d), estimated peat fire mean FRP (e) and estimated peat fire percentage of FRP (f) in eastern Siberia.

3.2. Northwest Siberia

3.2.1. Trends in wildfires and peat fires

On average, 15.4 M ha burns each year in northwest Siberia (NW Siberia), the largest amount seen in any of the subregions studied here. There is large interannual variability seen across the timeseries (Figure 36a) both in terms of BA and FRP (Table 20). There is a marked change in fire activity from 2013 onwards, where there is both a drop in annual average BA (from 20.8 M ha per year pre-2013, to 8.7 M ha post 2013) and interannual variability. The exact cause of this decline is unknown; however, as this signal is present in both the GFED5 BA and the GFAS FRP data, it indicates that this is not an erroneous feature. A similar signals was also detected in an area of western Siberia by Tomshin and Solovyev (2024), who also showed much of the burning to occur in spring. A reduction in spring burning perhaps suggests that post 2013 there may be a shift in fire and land management in the region towards smaller and less intense prescribed burning. Another potential cause may be due to wetter and cooler weather during this time period, as fires in western Siberia have been shown to be highly related to the presence of positive geopotential height anomalies, creating regions of high pressure and warm dry weather (Tomshin and Solovyev, 2024). Therefore, the lack of these conditions between 2013 and 2020 may have resulted in lower burnt areas in NW Siberia. Notable peaks in BA in NW Siberia occur in 2003, 2004, 2008 and 2012 (Figure 36a). During these years annual BA

exceeded 25 M ha, with average FRP greater than 300 W/m^2. The majority of burning in E Siberia occurs in the early fire season in April and May (Figure 36b), burning then remains elevated over summer and autumn relative to winter.

NW Siberia is also the region that sees the greatest amounts of estimated peat BA, of 0.9 M ha on average. However, on average peat fires are estimated to only account for 6% of the annual total BA, the lowest of all the regions studied here. In general, estimated peat BA and peat FRP do not change much on a year-to-year basis. There is a notable departure from the general estimated peat fire trend in 2012 both in terms of BA and FRP (Figure 36c). This year sees a total estimated peat BA of 2.7 M ha (192% greater than the average annual estimated peat BA), with peat fires estimated to be responsible for 10% of the total annual BA. In contrast, 2013 saw just 0.9 M ha of estimated peat BA, but in 2013 this accounted for nearly 20% of the annual total BA (Table 20). Other notable years in which peat fires are estimated to have contributed a large percentage of burning and FRP include 2005, 2016 and 2020 (Figure 36e).

The majority of estimated peat BA and FRP takes place in two peaks throughout the year (Figure 36d). Firstly, peat estimated BA and FRP peak in the early burning season in April and May, much like total BA, with a secondary peak in July (Figure 36d). However, the seasonality of estimated peat fire percentage of BA and FRP show only one peak in July (Figure 36f), meaning that burning that occurs in July involves a larger proportion of peat burning compared to other months. The early season (April/May) peak that is seen in the estimated peat BA is therefore not seen in the estimated peat fire percentage of BA due to large total BA during these months. However, in the GFAS FRP data there is also a secondary winter peak in peat fire attributed FRP (Figure 36f). Although total and peat estimated BA is low over winter (Figure 36b, d), these results suggest that any burning that is occurring in this season is more likely to be peat fires, compared to other times of year.

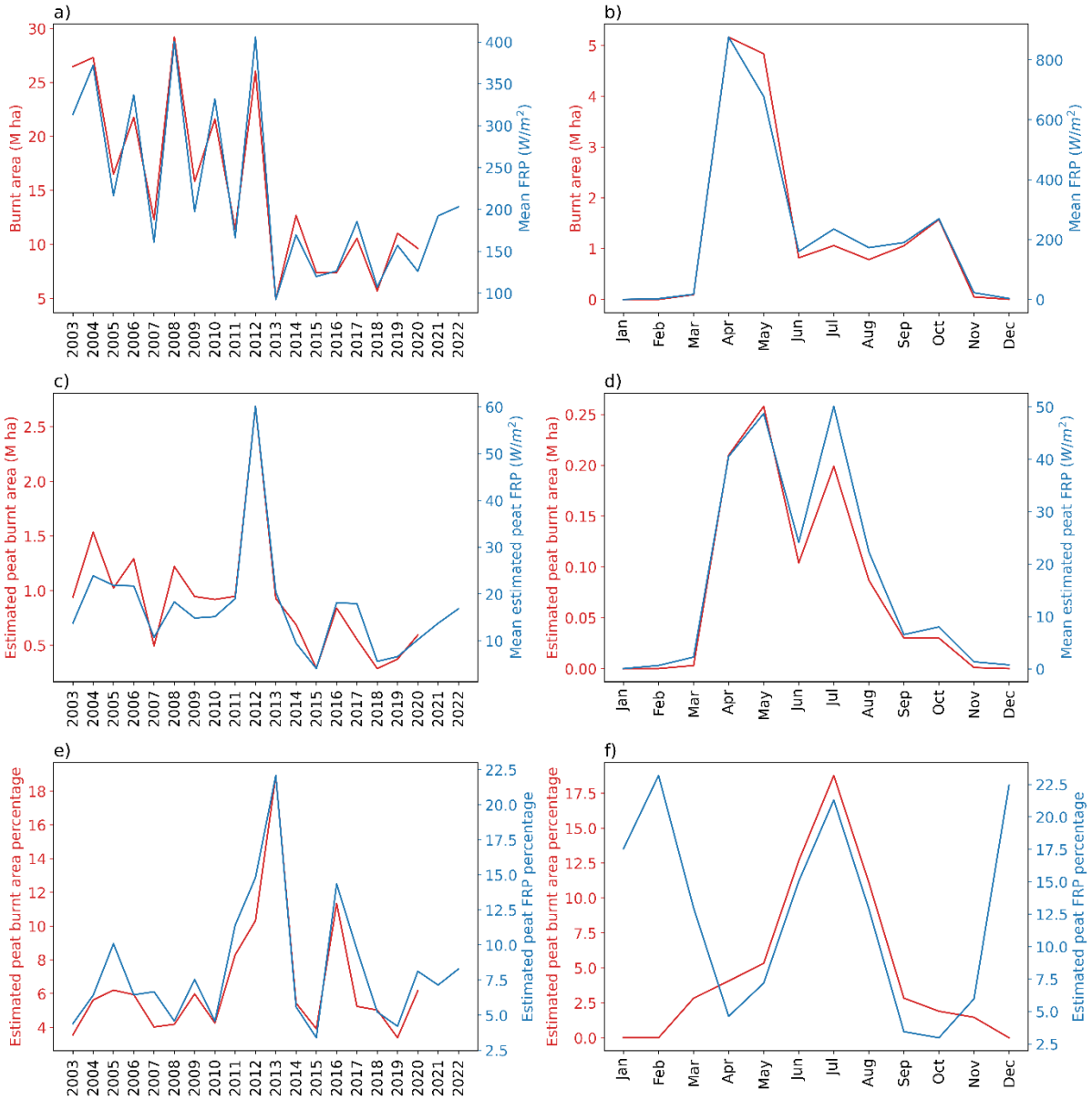


Figure 36: Fire trends over 2003-2022 for northwest Siberia. BA data covers the period from 2003 to 2020, and the FRP data continues up to 2022. The trends shown are a) average annual total BA and FRP and b) the seasonality in total BA and FRP (averaged over their respective time periods). Panel c) shows the yearly timeseries trends in estimated peat BA and FRP and panel d) shows the seasonality in estimated peat BA and estimated peat FRP. Panel e) shows the estimated peat BA as a percentage of total BA and the estimated peat FRP as a percentage of total FRP, and panel f) shows the seasonality in peat estimated BA and FRP percentage.

Table 20: Annual values for BA from GFED5 and FRP from GFAS for northwest Siberia, and the summary statistics (mean, standard deviation (SD) and coefficient of variation (CV)) for the whole time series. Values in bold highlight years in which the value is at least one standard deviation greater than the mean.

Year	GFED5 Total BA (M ha)	Peat BA (M ha)	Peat BA percentage	GFAS Total FRP (W/m^2)	Peat fire FRP (W/m^2)	Peat fire FRP percentage
2003	**26.469**	0.941	3.557	313.543	13.788	4.397
2004	**27.303**	**1.535**	5.621	**372.152**	23.897	6.421
2005	16.499	1.024	6.207	216.536	21.849	10.090
2006	21.766	1.292	5.937	**336.813**	21.729	6.451
2007	12.319	0.495	4.020	160.988	10.737	6.669
2008	**29.193**	1.221	4.181	**400.274**	18.323	4.578

2009	15.823	0.946	5.979	197.328	14.876	7.539
2010	21.600	0.919	4.257	**331.875**	15.163	4.569
2011	11.428	0.948	8.298	166.475	19.004	11.415
2012	26.030	**2.687**	**10.323**	**405.741**	**60.110**	**14.815**
2013	4.903	0.928	**18.923**	92.603	20.447	**22.080**
2014	12.675	0.689	5.437	169.502	9.478	5.591
2015	7.383	0.289	3.912	119.898	4.063	3.389
2016	7.405	0.840	**11.346**	126.555	18.158	**14.348**
2017	10.558	0.553	5.241	185.444	17.924	9.665
2018	5.693	0.286	5.028	107.266	5.609	5.229
2019	11.031	0.373	3.382	157.153	6.617	4.211
2020	9.629	0.594	6.167	126.045	10.248	8.131
2021				192.355	13.751	7.149
2022				203.136	16.839	8.290
Mean	15.428	0.920	5.964	221.455	17.334	8.310
SD	8.003	0.560	3.786	101.871	11.577	4.564
CV	0.519	0.608	0.635	0.460	0.668	0.549

3.2.2. Drivers of large fire years

In northwest Siberia there are relatively strong positive correlations between total and estimated peat BA anomalies with temperature anomalies ($r=0.434$, $p<0.001$; $r=0.477$ $p<0.001$). This suggests that higher than average BA years tend to coincide with warmer than average temperatures (Figure 37; Figure S3). 2003 featured abnormally high BA in May, 4.3 M ha greater than the spring average, coinciding with temperatures that were 8.8°C warmer than the seasonal average. Similarly, in May 2004, BA was 11 M ha larger than the seasonal average with temperatures 8°C warmer than average. Bondur et al., (2023), showed that large fire seasons in Siberia, like seen here in 2003 and 2004 are liked to the presence of large stationary anticyclones that produce abnormally hot and dry weather that is highly conducive to wildfires. In contrast to other regions, we see lower than average BA and temperatures over June and July, before then returning to higher-than-average temperatures in August-October, with larger than average BA. For example, September 2003 is 8.6°C warmer than the seasonal average, with 2.2 M ha of BA greater than average. In October 2003, there was 7.6 M ha more burning than average, although temperatures were only 0.2°C warmer than average. This may suggest that the high temperatures in the previous two months resulted in a drying out of fuels, allowing for this late season surge in burning. Kuhn-Regnier et al., (2021), highlighted that the antecedent vegetation conditions in the weeks and months prior to fires, especially in areas that are fuel limited such as tundra ecosystems which dominate in NW Siberia, exert an important influence on burnt area. Therefore, warmer and drier weather in the months preceding a fire, like are seen in 2003 may help to fuel large late season burnt areas.

Abnormal early season burning occurred in NW Siberia in 2008 and 2012. In April 2008, 13 M ha more burned area occurred than the seasonal average, with 1.4 M ha more BA than average in May. In May 2008, temperatures were almost 7°C warmer than average, however, in April temperatures were 1.7°C colder than average. Still, winter temperatures in 2008 were above average, for example February 2008 was 1.8°C warmer than average, meaning that that the antecedent weather conditions

may have had an influence on the April/May fire season of 2008 alongside other factors such as precipitation and fuel moisture. Similarly, April 2012 was 2.1°C warmer than average, with burned area over 9 M ha greater than average. In contrast to other years, temperatures in June and July 2012 were 2–3°C warmer than average, coinciding with 2 M ha greater than average BA in June and 4 M ha greater than average BA in July. It is also worth noting that May 2012 saw 8 degree warmer than average temperatures, but less burning than normal, perhaps suggesting the build up of dry fuels that led to the larger than normal summer burning.

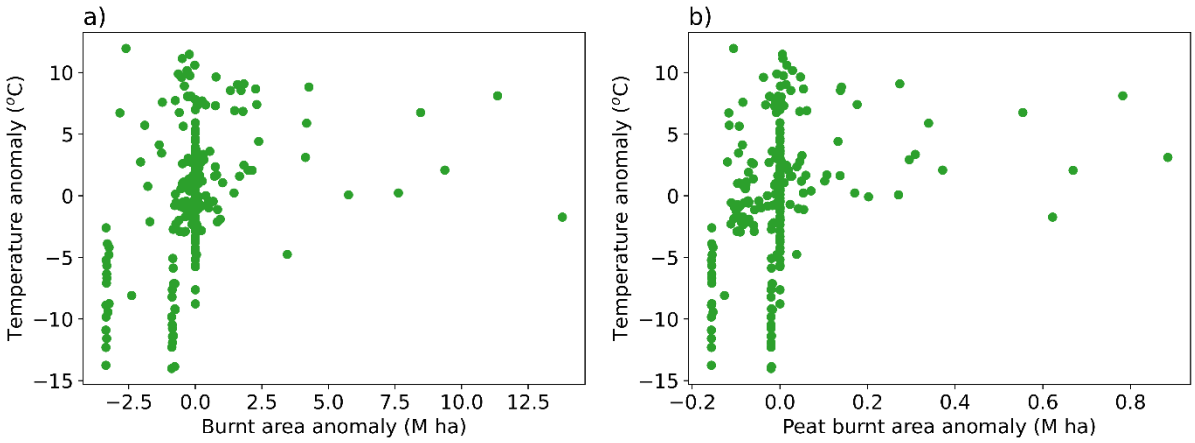


Figure 37: Correlations between seasonal BA anomalies and seasonal temperature anomalies for a) total BA and b) estimated peat BA in northwest Siberia

3.2.3. Impacts of fires on atmospheric composition

Between 2003 and 2022, according to the CAMS reanalysis data, NO_2 and CO levels exhibit substantial interannual variability (Figure 38a, c). NO_2 exhibits large peaks in 2003, 2012, 2016 and 2022, all of them being years that featured high levels of burning, especially 2003 and 2012. NO_2 levels in the atmosphere of northwest Siberia show a winter peak, and strong declines over summer (Figure 38b), opposite to the seasonality in estimated peat BA (Figure 36d). CO also exhibits peaks in 2003 and 2012, indicative of the large fire years that occurred. There are also large amounts of CO measured in 2021. CO levels peak over winter and in spring, with the highest CO being recorded in March and the lowest levels seen in June/July and September (Figure 38d). Overall, the ratio of NO_2:CO appears to be increasing across the CAMS reanalysis timeseries, but with substantial interannual variability (Figure 38e). The largest NO_2:CO ratio occurs in 2022 as a result of very low atmospheric CO. Especially low NO_2:CO ratios are seen in 2006, a year with relatively large peat BA. The seasonality of NO_2:CO ratios follow a similar pattern to that of NO_2, with the greatest ratios occurring in December, and the lowest in March-May (Figure 38f).

Over the four available years of TROPOMI data, the largest levels of NO_2 occur in 2020, although all years are very similar. TROPOMI NO_2 exhibits a high degree of intra-annual variability. In agreement with CAMS reanalysis data, the lowest NO_2 values occur in June and July (Figure 38b), which are the months where there are the largest values of estimated peat BA and estimated peat fire percentage of

burned area (Figure 36d,f). However, in contrast to CAMS, the TROPOMI data shows the highest levels of NO_2 occurring in spring (April) and autumn (September/October), concurrent with peaks in total BA. This suggests that flaming vegetation fires tend to occur over spring and autumn in NW Siberia, resulting in elevated NO_2 levels, and then when peat fires occur in summer, NO_2 levels are lower. The TROPOMI data shows the highest CO levels in 2021, which coincides with the year with the lowest NO_2:CO ratio (Figure 38c, e). TROPOMI CO exhibits a bimodal seasonality with peaks occurring in spring and autumn, with a slight fall in June/July (Figure 38d). The decrease in CO in summer occurs alongside a fall in total BA in these months, but perhaps the size of the decrease in summer is being limited by the increase in peat BA during these months. The highest NO_2:CO ratios are seen in winter, possibly due to the lowest levels of CO occurring in December and January (Figure 38f).

Table 21: Annual values for NO_2, CO and their ratio from both TROPOMI and CAMS reanalysis data for northwest Siberia, and the summary statistics (mean, standard deviation (SD) and coefficient of variation (CV)) for the whole time series. Values in bold highlight years in which the value is at least one standard deviation above or below the mean.

	CAMS reanalysis				TROPOMI		
Year	NO_2 (kg)	CO (kg)	Ratio NO_2:CO	$PM_{2.5}$	NO_2 (mol)	CO (mol)	Ratio NO_2:CO
2003	**6.423**	**4636.614**	0.00139	0.027			
2004	5.808	**4321.442**	0.00134	0.026			
2005	5.766	4296.676	0.00134	0.025			
2006	5.382	4293.662	**0.00125**	0.026			
2007	5.446	4208.527	**0.00129**	0.022			
2008	5.381	4160.564	**0.00129**	0.027			
2009	**5.350**	3888.551	0.00138	0.025			
2010	5.362	4151.911	**0.00129**	0.026			
2011	5.740	3960.024	0.00145	0.026			
2012	**6.021**	**4470.313**	0.00135	**0.049**			
2013	**5.272**	4046.730	0.00130	0.030			
2014	5.470	3960.353	0.00138	0.022			
2015	5.423	3951.186	0.00137	**0.021**			
2016	**6.115**	4017.121	**0.00152**	0.032			
2017	5.784	3845.894	**0.00150**	0.024			
2018	5.512	**3796.156**	0.00145	0.023	**0.223**	**746.607**	**0.00030**
2019	5.402	**3823.151**	0.00141	0.031	0.332	1198.368	0.00028
2020	5.736	3856.738	**0.00149**	0.027	0.337	1214.651	0.00028
2021	5.667	4198.359	0.00135	0.028	0.323	1295.781	**0.00025**
2022	5.944	**3638.447**	**0.00163**	0.023			
Mean	5.633	4093.645	0.00138	0.027	0.297	1053.208	0.00028
SD	0.306	250.066	0.00009	0.006	0.054	248.509	0.00002
CV	0.054	0.061	0.06867	0.221	0.182	0.236	0.07133

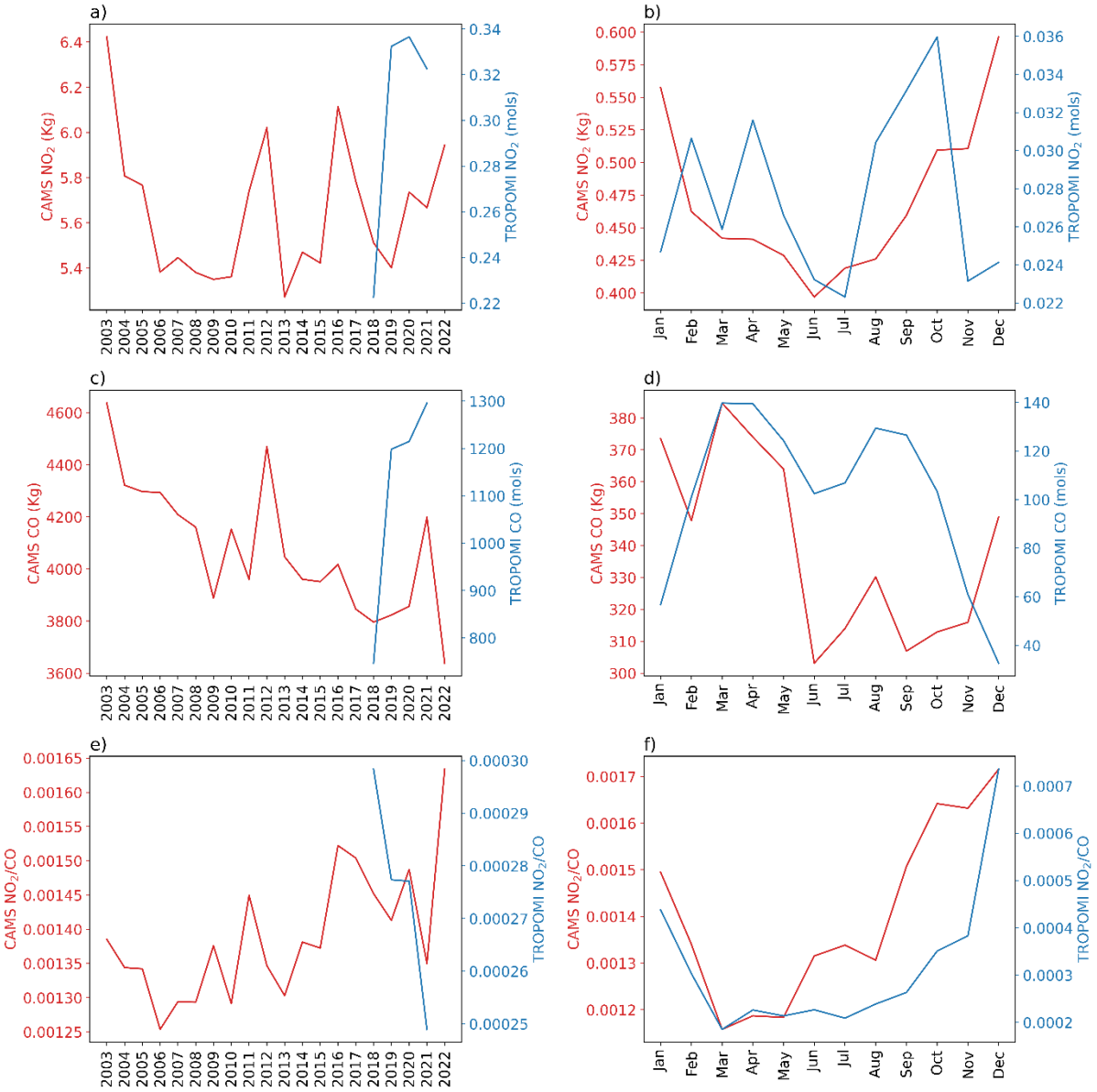


Figure 38: Time series plots for NO_2 (a) and its seasonality (b), CO (c) and its seasonality (d), and the ratio of NO_2/CO (e) and its seasonality (f), over 2003 to 2022 for CAMS reanalysis data (red) and 2018 to 2021 for the TROPOMI data (blue) in northwest Siberia.

In NW Siberia, the years with the largest overall BAs (2003, 2004, 2006, 2008 and 2012) feature, in general, higher than average NO_2 and CO concentrations (Table 21). For example, 2003 has a total BA of 26.5 M ha and has the highest yearly totals of NO_2 and CO (Table 21). Similarly, 2004 sees even higher BA at 27.3 M ha, and an increase of almost 0.6 M ha in estimated peat BA compared to 2003, meaning that approximately 2/3^{rds} of the increase in BA between 2003 and 2004 is due to peat fires. Potentially as a result of this there are significantly higher than average CO levels, and consequently the ratio of NO_2:CO is lower in 2004 compared to 2003 (0.00134 vs 0.00139), likely due to a larger contribution of peat burning. 2006 is the year with the fourth largest total BA and the third largest estimated peat fire BA at 1.292 M ha. This year also has one of the highest FRP values. It has the lowest NO_2:CO ratio of 0.00125, largely due to lower levels of NO_2. This supports our

hypothesis that peat fires result in lower NO_2:CO ratios, as in this year in particular we see that NO_2 is lower than average despite the elevated BA, suggesting that smouldering combustion was likely a dominant process in 2006. 2012 in NW Siberia saw the largest estimated peat BA of 2.7 M ha, with peat burning estimated to be responsible for 10.5% of total BA, resulting in a NO_2:CO ratio of 0.00135, comparable with the low values of 2004, suggesting that peat burning in both of those years has contributed to a lower NO_2:CO ratio, despite also having large amounts of flaming vegetation fires. The results for 2008 also strongly support this idea, where we see an estimated peat BA of 1.2 M ha, and one of the lowest recorded NO_2:CO ratios of 0.00126, due to lower-than-average NO_2 levels, despite the 29.2 M ha of total BA.

In contrast, 2013 is the year with the lowest total BA and FRP but it has the greatest peat BA percentage of 19%, resulting in one of the lowest NO_2:CO ratios of 0.00130 (Table 20 and Table 21). This means that the increased amounts of peat burning in this year are resulting in lower NO_2:CO ratios, compared to years which see less peat burning. For example, the lowest peat fire percentage occurs in 2019, at 3.4%, with a much higher ratio of 0.00141. The highest NO_2:CO ratio occurs in 2022, a year in which there is lower than average total FRP and estimated peat FRP. Furthermore, significantly higher than average NO_2:CO ratios are seen in 2016 and 2017 (Table 21). Again, in both these years we see lower than average total and estimated peat BA, although, 2016 does see a higher-than-average peat fire percentage of burning. Therefore, there is a general trend emerging of lower NO_2:CO ratios in years in which we see larger than expected estimated peat BA.

Correlations of yearly values from CAMS reanalysis and GFED5 and GFAS revealed no significant relationships with NO_2 (Table 22c). Additionally, we see no relationships between estimated peat fire percentages of BA and FRP with any of the atmospheric composition measurements (Table 22c). But there are strong positive correlations between CO and total BA, estimated peat BA, total FRP and estimated peat FRP (Table 22c). There are also significant negative relationships between NO_2:CO ratios and total BA ($r=-0.521$, $p=0.027$), and a non-significant negative relationship with peat BA ($r=-0.483$, $p=0.053$). Overall, on a yearly basis, increased estimated peat BA is associated with increases in levels of CO in the atmosphere and lower ratios of NO_2:CO as a result of smouldering combustion.

On a seasonal cycle, there are no relationships between total or estimated peat BA and TROPOMI NO_2 (Table 22a). However, in the longer timeseries CAMS reanalysis data there is a non-significant but strong negative relationship with total BA, but a significant strong relationship negative correlation with estimated peat BA ($r=-0.811$, $p=0.001$, Table 22a). There are significant positive correlations between TROPOMI CO and total BA ($r=0.609$, $p=0.035$) and estimated peat BA ($r=0.624$, $p=0.030$), but no significant relationships with CAMS CO (Table 22a). Indicating that months in which more peat is burning, there are also increases in CO levels, and decreases in NO_2, highlighting the effects of fire emissions on overall atmospheric composition of NO_2 and CO. As a

result of these relationships, there is a non-significant negative correlation between TROPOMI NO_2:CO ratios with total BA (r=-0.571, p=0.053) and a strong significant negative correlation with peat BA (r=-0.727, p=0.007) and peat fire percentage (r=-0.754, p=0.005). Similarly, there is a nonsignificant negative correlation between the CAMS NO_2:CO ratio and total BA but a significant correlation with estimated peat BA (r=-0.593, p=0.042). However, there are no significant correlations between any of the GFAS FRP variables and CAMS NO_2:CO ratio (Table 22a). Overall, peat fires have significant potential effects on the intra-annual variability in NO_2, CO and the ratio of NO_2:CO in NW Siberia. In general, in months where we see large peat BAs, we see decreases in amounts of NO_2 and increases in CO, which ultimately result in declines in the ratio of NO_2:CO. We also see that in NW Siberia, more so than the other regions, peat fires influence the trend in relationships of atmospheric composition quantities with total BA.

On a monthly timescale, total BA is positively correlated with TROPOMI CO (r=0.641, p<0.001), and correlated negatively with CAMS NO_2 (r=-0.387, p<0.001) (Table 22b). Therefore, total BA is negatively correlated with both TROPOMI and CAMS NO_2:CO ratios (r=-0.637, p<0.001; r=-0.356, p<0.001). Estimated peat BA exhibits a positive correlation with TROPOMI CO (r=0.648, p<0.001). There is no relationship with TROPOMI NO_2, but there is a negative correlation with CAMS NO_2 (r=-0.448, p<0.001). There is also a negative correlation between estimated peat FRP and CAMS NO_2 (r=-0.825, p=0.001). Furthermore, there are strong positive correlations between peat BA and the TROPOMI NO_2:CO ratio (r=-0.712, p<0.001), and the CAMS ratio (r=-0.397, p<0.001). There are also negative correlations of peat fire percentage with CAMS NO_2 (r=-0.340, p<0.001) and with CAMS NO_2:CO ratio (r=-0.213, p=0.005). Additionally, estimated peat FRP is strongly negatively correlated with the TROPOMI NO_2:CO ratio (r=-0.519, p<0.001) and the CAMS NO_2:CO ratio (r=-0.358, p<0.001). Overall, it is evident that peat fires may have a strong influence on the presence of CO and NO_2 in the atmosphere, whereby the months in which more peat burns, and peat occupies a greater percentage of total burning, cooccur with months with larger values of CO and smaller values of NO_2, leading to the lower ratios of NO_2:CO that are indicative of smouldering combustion.

Table 22: Correlations between the GFED5 and GFAS fire parameters, and NO_2, CO and their ratio in the TROPOMI and CAMS reanalysis datasets, on seasonal data (a), monthly data (b) and yearly data (c) in northwest Siberia. Asterisks indicate significant p values (* = p<0.05, **=p<0.001, ***=p<0.001)

		TROPOMI			CAMS		
		NO_2	CO	NO_2:CO Ratio	NO_2	CO	NO_2:CO Ratio
a) Seasonality data							
GFED5	Total BA	0.329	0.609 *	-0.571	-0.557	-0.151	-0.354
	Peat BA	0.081	0.624 *	-0.727 **	-0.811 **	-0.131	-0.593 *
	Peat BA percentage	-0.155	0.585 *	-0.754 **	-0.944 ***	-0.338	-0.563
GFAS	Total FRP	0.350	0.587 *	-0.510	-0.524	-0.175	-0.301
	Peat FRP	-0.028	0.566	-0.727 **	-0.825 **	-0.224	-0.503
	Peat FRP percentage	-0.552	-0.469	0.091	0.042	0.196	0.000

b) Monthly data							
GFED5	Total BA	0.069	0.641 ***	-0.637 ***	-0.387 ***	-0.067	-0.356 ***
	Peat BA	-0.051	0.648 ***	-0.712 ***	-0.448 ***	-0.067	-0.397 ***
	Peat BA percentage	0.023	-0.062	-0.046	-0.340 ***	-0.105	-0.213 **
GFAS	Total FRP	0.219	0.588 ***	-0.519 ***	-0.336 ***	-0.060	-0.318 ***
	Peat FRP	0.078	0.519 ***	-0.534 ***	-0.381 ***	-0.055	-0.358 ***
	Peat FRP percentage	0.053	-0.026	0.022	-0.099	0.030	-0.143 *
c) Yearly data							
GFED5	Total BA				0.137	0.725 **	-0.521 *
	Peat BA				0.133	0.730 **	-0.463
	Peat BA percentage				0.141	0.121	0.102
GFAS	Total FRP				0.189	0.603 **	-0.441
	Peat FRP				0.227	0.549 *	-0.346
	Peat FRP percentage				0.293	0.042	0.191

In NW Siberia, there is evidence for a strong interconnection between fires and atmospheric composition in both the TROPOMI and CAMS reanalysis data. In particular, peat burning has been shown to be heavily associated with elevated CO, lower NO_2 relative to CO and therefore a lower NO_2:CO ratio that would be expected with the smouldering combustion that dominates peat fires.

3.2.4. Impacts of fires on $PM_{2.5}$

Year-to-year variations in $PM_{2.5}$ are minimal in NW Siberia, with an average annual $PM_{2.5}$ of 0.027 kg, and a coefficient of variation of 0.221 (Table 21; Figure 39a). The notable exception is 2012, which sees 0.049 kg of $PM_{2.5}$, 0.017 higher than the next largest year (2016), and almost double the annual average. Other notable years in terms of $PM_{2.5}$ include 2013, 2016, and 2019. However, these years do not feature especially large BAs, whereas 2012 sees the fourth largest BA and the largest peat BA by more than 1 M ha (Table 20), perhaps suggesting an increased influence of peat burning in this year to $PM_{2.5}$. Other pronounced fire years in NW Siberia are 2003, 2004 and 2008, which do not stand out in terms of their $PM_{2.5}$ levels. This may perhaps be due to these years all having low potential percentage contributions from peat fires (all below 6%). Supporting this, $PM_{2.5}$ concentrations were high in both 2013 and 2016, years in which there were also high peat fire percentages of BA of 19% and 11%, respectively. However, 2019 does not follow this pattern, with peat fires potentially contributing just 3% to total BA.

Seasonally, there are two peaks in $PM_{2.5}$ levels. First in spring (April/May) and then followed by a second higher peak in July (Figure 39b). Interestingly, total BA sees an early spring peak, but no peak in July, whereas there is a July peak in estimated peat burning and percentage of total burning. Estimated peat BA also shows an early season peak. This suggests that in NW Siberia, variations in $PM_{2.5}$ on both a yearly and monthly scale may be being driven by peat burning.

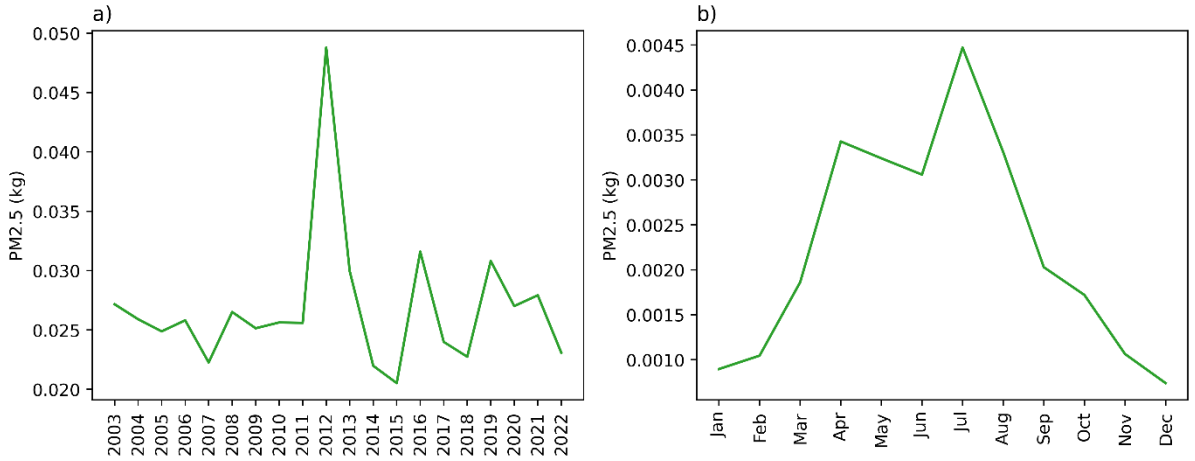


Figure 39: Timeseries plot for $PM_{2.5}$ from 2003-2022 in eastern Siberia from the CAMS reanalysis data (a), and the 2003-2022 averaged northwest Siberia seasonality in $PM_{2.5}$ (b).

Correlations between all fire variables and $PM_{2.5}$ on a monthly timescale are strongly positive (Table 23; Figure 40), suggesting that higher BAs and estimated peat BAs are associated with higher $PM_{2.5}$. The strong positive correlations between $PM_{2.5}$ and the estimated peat fire percentage of BA and FRP also suggest that the larger the contribution of peat fires to the total picture of burning, the larger the $PM_{2.5}$ concentrations. Therefore, this suggests that peat burning in NW Siberia is driving increases in $PM_{2.5}$ which would consequently result in a decline in air quality in this region during fire events.

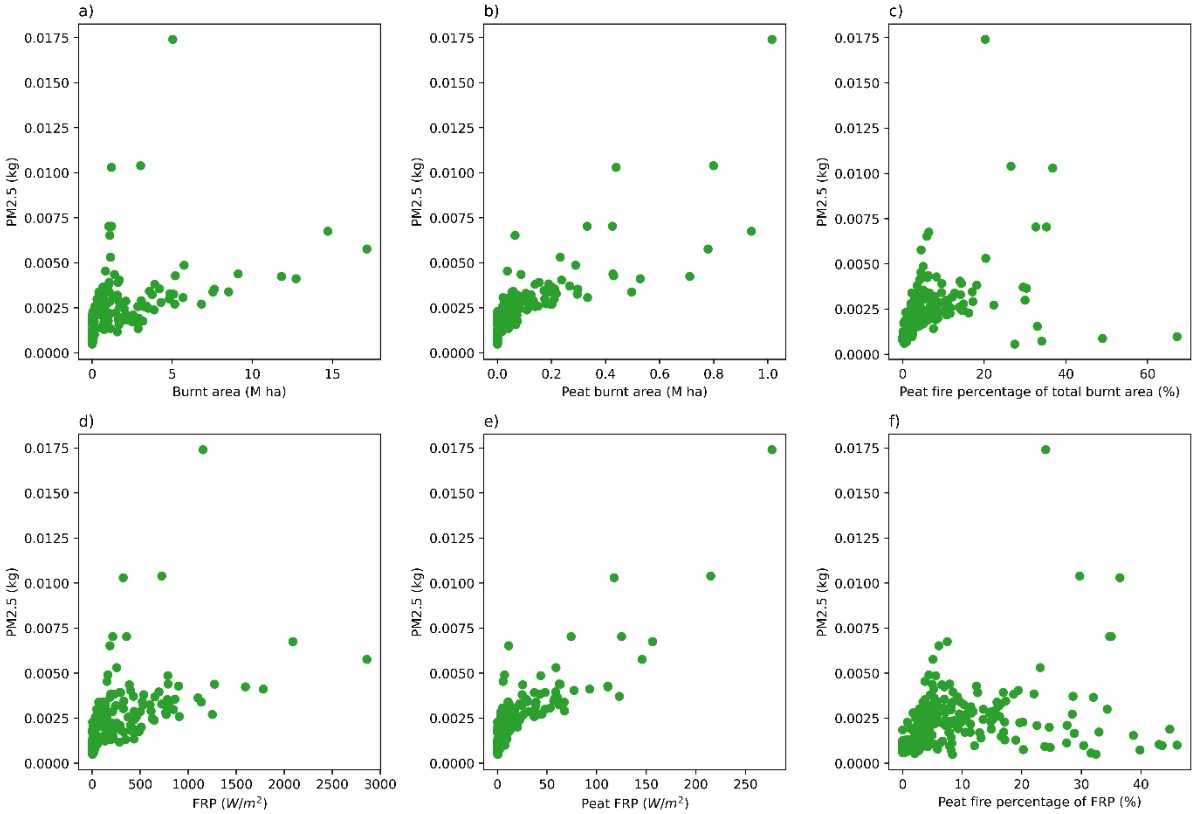


Figure 40: Relationships between monthly total CAMS $PM_{2.5}$ and monthly total BA (a), estimated peat BA (b), estimated peat fire percentage of BA (c), total mean FRP (d), estimated peat fire mean FRP (e) and estimated peat fire percentage of FRP (f) in northwest Siberia.

When looking just at the seasonality data, there are similar results, with strong positive correlations of total BA and estimated peat BA with $PM_{2.5}$, as well as between estimated peat FRP and total FRP with $PM_{2.5}$ (Table 23). There are also strong positive correlations between estimated peat fire percentage of total BA and $PM_{2.5}$ ($r=0.930$, $p<0.001$), again suggesting a strong connection between peat burning and $PM_{2.5}$. However, estimated peat fire percentage of FRP has a non-significant negative correlation ($r=-0.301$, $p=0.342$), perhaps suggesting that the severity of a peat fire doesn't have as much influence on $PM_{2.5}$ as the total area burnt does.

In contrast to these results, there are no significant correlations between the annual fire variables and annual $PM_{2.5}$ (Table 23). Whilst there are no significant correlations, there are positive relationships emerging, such as between $PM_{2.5}$ and estimated peat BA ($r=0.418$, $p=0.084$). Therefore, there appears to be a disconnect between fires and $PM_{2.5}$ on an annual scale, i.e. high fires years are not always high $PM_{2.5}$ years, but on a monthly scale high BAs are correlated with higher $PM_{2.5}$.

Table 23: Correlations between the yearly GFED5 and GFAS fire parameters, and the CAMS reanalysis $PM_{2.5}$ data, using annual totals, monthly totals and the seasonality (average monthly totals 2003-2020) in northwest Siberia. Asterisks indicate significant p values (* = $p<0.05$, **=$p<0.001$, ***=$p<0.001$)

		CAMS $PM_{2.5}$ Annual totals	Monthly totals	Seasonality
GFED5	Total BA	0.187	0.796 ***	0.774 **
	Peat BA	0.418	0.897 ***	0.917 ***
	Peat BA percentage	0.327	0.630 ***	0.930 ***
GFAS	Total FRP	0.185	0.800 ***	0.776 **
	Peat FRP	0.394	0.875 ***	0.923 ***
	Peat FRP percentage	0.280	0.309 ***	-0.301

3.3. Alaska

3.3.1. Trends in wildfires and peat fires

On average, 0.6 M ha burn each year in Alaska, with a mean FRP of 51.0 W/m^2 (Table 24). Alaska is the region studied here with the lowest amounts of burning. However, there is substantial interannual variability in BA with a coefficient of variation of 1.2, the largest of all the regions (Figure 41a; Table 24). Notable burning years occur in 2004, 2005, 2009, 2015 and 2019 (Figure 41a). 2004 sees the largest annual BA of 2.8 M ha, 350% larger than the annual average, with a mean FRP of 212.5 W/m^2. The majority of burning in Alaska occurs in summer between June and August (Figure 41b). Across the timeseries there is a slight tendency towards a decline in BA of -0.384 M ha per decade. However, due to large interannual variability there is a high uncertainty (+/- 1.668 M ha per decade) in this trend. In contrast there is also a suggestion of increasing estimated percentages of BA due to peat fires over 2003-2020 of 2.459% per decade, but with an uncertainty of +/-5.605% no clear trend can be observed.

Peat fires are estimated to burn, on average, 0.047 M ha each year, with a mean FRP of 3.773 W/m^2 representing an estimated 7.5% of total BA and 8.1% of total FRP (Table 24). Much like total BA, there is substantial interannual variability in estimated peat BA and FRP (Figure 41c). Estimated peat BA is shown to spike in 2004, 2005, 2009, 2015 and 2019, which coincide with spikes in estimated peat FRP. In contrast, the estimated peat fire percentage of BA shows much less interannual variability (coefficient of variation of 0.370 compared to 1.103 for estimated peat BA) (Figure 41e). However, the estimated peat fire percentage of BA is substantially higher in 2020, where 18% of total burning is estimated to have been attributed to peat burning. The majority of estimated peat BA and FRP occurs during the summer months of June, July and August (Figure 41d). However, in terms of peat fire percentage of total BA, there is a more extended peak from May to September (Figure 41f).

Table 24: Annual values for BA from GFED5 and FRP from GFAS for Alaska, and the summary statistics (mean, standard deviation (SD) and coefficient of variation (CV)) for the whole time series. Values in bold highlight years in which the value is at least one standard deviation greater than the mean.

	GFED5			GFAS		
Year	Total BA (M ha)	Peat BA (M ha)	Peat BA percentage	Total FRP (W/m^2)	Peat fire FRP (W/m^2)	Peat fire FRP percentage
2003	0.255	0.019	7.502	25.955	1.942	7.481
2004	**2.818**	**0.155**	5.487	**212.496**	**11.067**	5.208
2005	**1.540**	**0.125**	8.129	**131.964**	**10.872**	8.239
2006	0.124	0.013	10.058	9.822	0.875	8.906
2007	0.263	0.022	8.413	36.911	3.882	**10.517**
2008	0.077	0.006	8.342	4.012	0.329	8.192
2009	1.073	0.072	6.738	**133.228**	**8.412**	6.314
2010	0.447	0.033	7.274	34.457	2.465	7.154
2011	0.152	0.010	6.602	13.108	0.793	6.051
2012	0.099	0.007	7.484	6.888	0.465	6.758
2013	0.665	0.042	6.367	49.541	2.949	5.953
2014	0.080	0.009	**11.539**	12.401	1.298	**10.463**
2015	**1.756**	**0.164**	9.331	**109.146**	**10.427**	9.554
2016	0.234	0.023	10.006	30.335	2.460	8.109
2017	0.307	0.025	8.260	22.824	1.751	7.673
2018	0.187	0.015	7.892	13.738	1.029	7.492
2019	1.092	0.087	7.992	72.483	5.866	8.093
2020	0.087	0.016	**18.097**	5.813	0.788	**13.564**
2021				9.037	0.721	7.974
2022				85.973	7.079	8.234
Mean	0.625	0.047	7.500	51.007	3.773	8.096
SD	0.756	0.052	2.777	56.546	3.757	1.893
CV	1.210	1.103	0.370	1.109	0.996	0.234

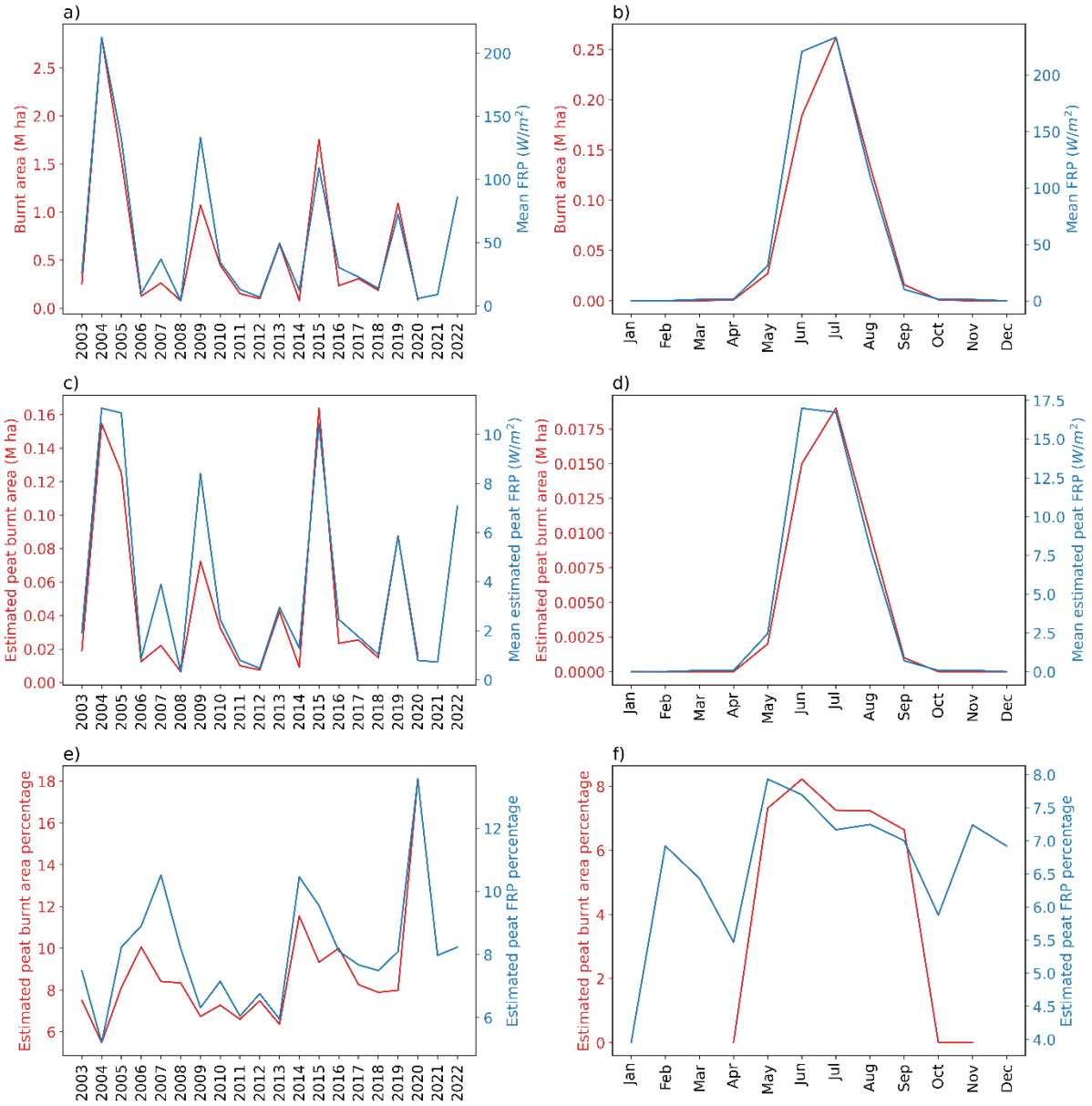


Figure 41: Fire trends over 2003-2022 for Alaska. BA data covers the period from 2003 to 2020, and the FRP data continues up to 2022. The trends shown are a) average annual total BA and FRP and b) the seasonality in total BA and FRP (averaged over their respective time periods). Panel c) shows the yearly timeseries trends in estimated peat BA and FRP and panel d) shows the seasonality in estimated peat BA and estimated peat FRP. Panel e) shows the estimated peat BA as a percentage of total BA and the estimated peat FRP as a percentage of total FRP, and panel f) shows the seasonality in peat estimated BA and FRP percentage.

3.3.2. Drivers of large fire years

There are significant positive correlations between total BA and estimated peat BA anomalies and temperature anomalies ($r=0.329$ $p<0.001$; $r=0.283$, $p<0.001$), suggesting that higher-than-average BA is related to higher-than-average temperatures (Figure 42; Figure S3). As identified earlier, 2004 is the largest fire season in Alaska in which greater than average BA occurred from June to September. Extreme fire activity coincided with 1.2°C warmer than average temperatures in July, 1.4°C warmer temperatures in August and 4.9°C warmer temperatures in September. The exceptionally warm and dry conditions seen in Alaska in 2004, have been shown to have contributed to the intense burning

seen across the region (Turquety et al., 2007; Shulski et al., 2005; Madani et al., 2021). Similarly, the summer of 2005 also sees higher than average temperatures in July, August, and September, which coincide with higher-than-normal burning in Alaska in these months. For example, August 2005 was 0.714°C warmer than average, and saw 0.6 M ha more burning than average. Following 2004, 2015 was the second largest fire season on record in Alaska (Partain et al., 2016). Here, June and July 2015 saw higher than the seasonal average BA of more than 0.6 M ha. In July this elevated burning coincided with 0.7°C warmer than usual temperatures, whereas in June, temperature was almost 1°C cooler than the seasonal average. However, May 2015 saw temperatures over 9°C warmer than average, which may have resulted in the drying out of fuels, leading to large fires in June 2015, highlighting the influence of antecedent conditions on burned area (Kuhn-Regnier et al., 2020). The large 2015 fire season has been attributed to warmer temperatures as a result of human induced climate changes (Partain et al., 2016), supporting the results presented here. However, during June 2015 there was also unprecedented amounts of lightning in Alaska, which resulted in 36,000 lightning strikes in just 3 days (Partain et al., 2016), which would have also influenced the number of fires that occurred.

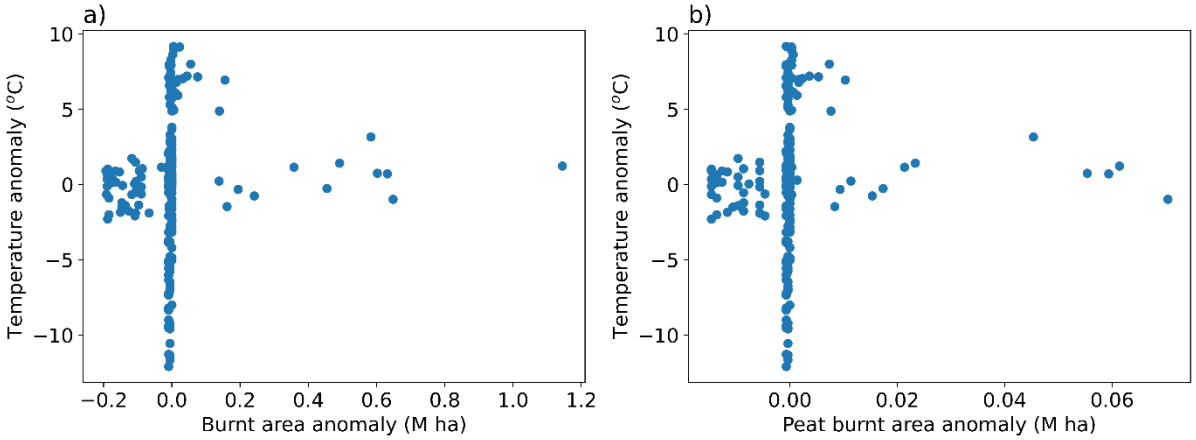


Figure 42: Correlations between seasonal BA anomalies and seasonal temperature anomalies for a) total BA and b) estimated peat BA in Alaska.

3.3.3. Impacts of fires on atmospheric composition

There is substantial interannual variability in NO_2 concentrations recorded in the CAMS reanalysis dataset, with average annual NO_2 concentrations of 2.521 kg over Alaska (Table 25, Figure 43a). The largest years in terms of NO_2 levels are 2004, 2005 and 2022. NO_2 levels, on a seasonal cycle, are elevated from March to October, reaching a peak in summer, specifically in July (Figure 43b). In contrast, CO concentrations from CAMS exhibit much less interannual variability and over the timeseries show a 13% decrease in CO (Figure 43c). The largest CO values are therefore seen at the start of the timeseries, most notably in 2003, and the lowest CO is recorded in 2022. On a seasonal basis, CO peaks in the spring from March to May, with the lowest values found in the summer (Figure 43d). Consequently, the NO_2:CO ratio shows large interannual variability and a tendency to be

increasing across the timeseries (Figure 43e). The lowest ratios of NO_2:CO are seen in 2003, 2006 and 2012, with the highest ratios occurring in 2022, 2017 and 2019. The NO_2:CO ratio peaks over the summer months, as well as early autumn (September/October) (Figure 43f), matching up well with when we see the highest NO_2 and lowest CO values.

Over the four years of TROPOMI data, the largest NO_2 values occur in 2019, which is also the case according to CAMS (Figure 43a). The seasonality of NO_2 shows an increase during summer with a peak from July to September, and the lower values occurring from November to January, following the same general pattern in seasonality as CAMS NO_2 (Figure 43b). CO peaks in 2021, according to TROPOMI but this is only a small increase from 2019 and 2020 (Figure 43c). CO seasonality from TROPOMI shows two peaks, firstly in spring (March-April) and secondly in late summer/early autumn (August-October) (Figure 43d). The spring peak in CO is also captured in the CAMS time series, however the autumn peak is not found in it. This difference between datasets is likely a result of the differing timeframes of data for which the seasonalities are calculated, as calculating the monthly averages using the TROPOMI years for the CAMS reanalysis data does reveal the early autumn peak in CO (Figure S2).

Across the four years there is a decline in the NO_2:CO ratio from TROPOMI, with the largest ratio occurring in 2018, and the lowest in 2021, broadly following the pattern seen in the CAMS data during these years (Figure 43e). Much like in E Siberia, there is a peak in the NO_2:CO ratio over the winter (December/January), and a secondary peak in July (Figure 43f), when we also see a peak in BA. The TROPOMI data does not feature the winter peak in the NO_2:CO ratio, and further analysis showed that this is not due to the differing years of data available for calculating monthly averages for TROPOMI and CAMS (Appendix Fig. X). Therefore, TROPOMI may be erroneously detecting NO_2 and CO over winter months because of poor-quality satellite observations over the high latitudes in that season (Goa et al., 2023).

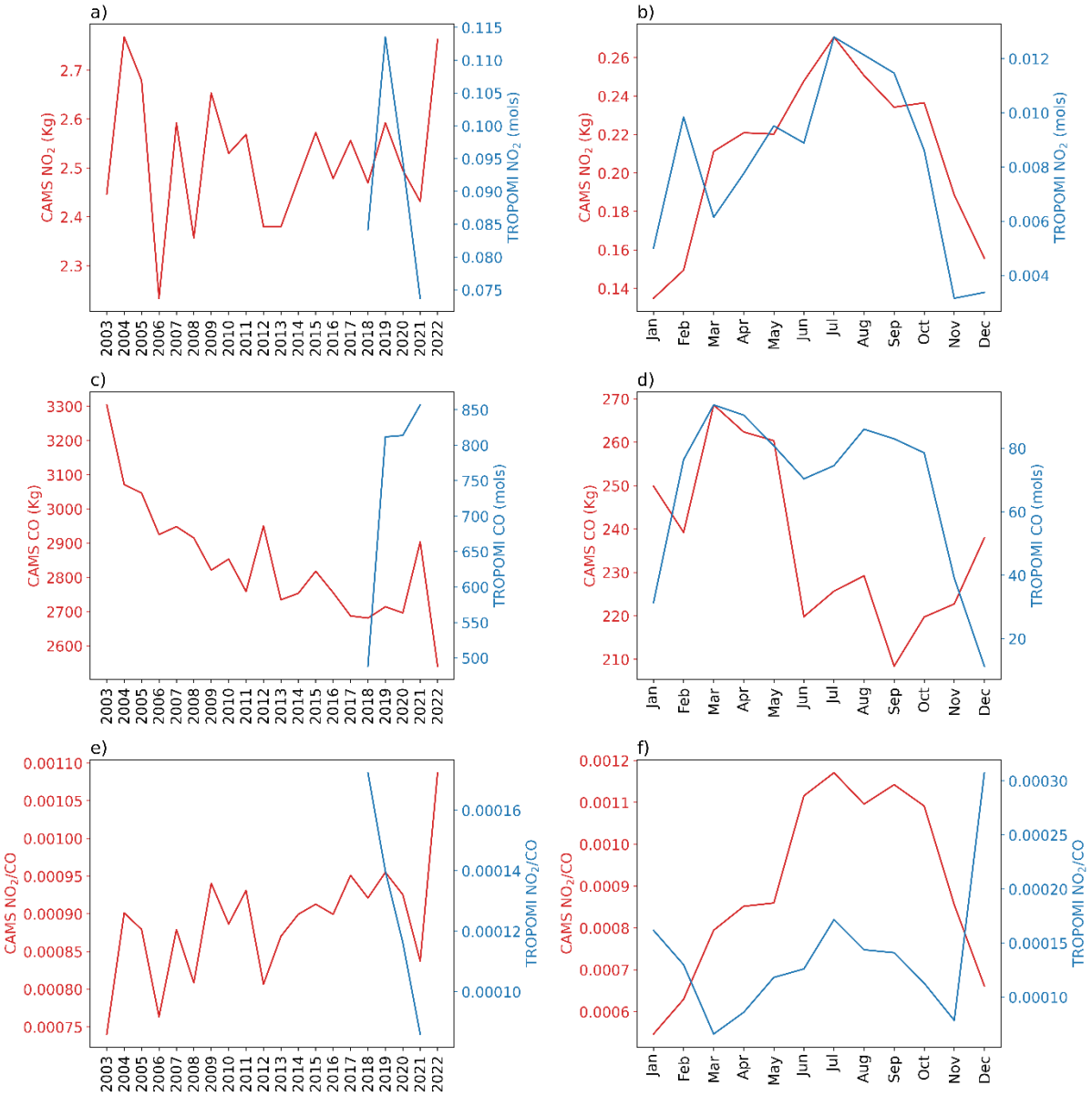


Figure 43: Time series plots for NO_2 (a) and its seasonality (b), CO (c) and its seasonality (d), and the ratio of NO_2/CO (e) and its seasonality (f), over 2003 to 2022 for CAMS reanalysis data (red) and 2018 to 2021 for the TROPOMI data (blue) in northwest Siberia.

Table 25: Annual values for NO_2, CO and their ratio from both TROPOMI and CAMS reanalysis data for northwest Siberia, and the summary statistics (mean, standard deviation (SD) and coefficient of variation (CV)) for the whole time series. Values in bold highlight years in which the value is at least one standard deviation above or below the mean.

	CAMS reanalysis				TROPOMI		
Year	NO_2 (kg)	CO (kg)	Ratio NO_2:CO	$PM_{2.5}$	NO_2 (mol)	CO (mol)	Ratio NO_2:CO
2003	2.447	**3303.995**	**0.00074**	0.016			
2004	**2.768**	**3071.128**	0.00090	**0.033**			
2005	**2.679**	**3046.480**	0.00088	**0.027**			
2006	**2.233**	2925.226	**0.00076**	0.014			
2007	2.592	2948.297	0.00088	0.015			
2008	**2.357**	2915.179	**0.00081**	0.015			
2009	**2.653**	2821.118	0.00094	**0.026**			
2010	2.530	2853.561	0.00089	0.014			

2011	2.568	2758.612	0.00093	0.015			
2012	**2.380**	2950.166	**0.00081**	0.014			
2013	**2.379**	2734.556	0.00087	0.016			
2014	2.477	2753.438	0.00090	0.014			
2015	2.572	2818.069	0.00091	0.022			
2016	2.478	2755.494	0.00090	0.013			
2017	2.556	**2687.490**	**0.00095**	0.015			
2018	2.469	**2681.104**	0.00092	0.015	0.084	**488.382**	**0.00017**
2019	2.592	2714.168	**0.00096**	**0.024**	**0.114**	811.769	0.00014
2020	2.496	**2696.437**	0.00093	0.014	0.095	813.741	0.00012
2021	2.431	2903.657	0.00084	0.015	**0.074**	856.826	**0.00009**
2022	**2.762**	**2540.662**	**0.00109**	0.020			
Mean	2.521	2843.942	0.00089	0.018	0.092	742.679	0.00013
SD	0.135	171.651	0.00008	0.006	0.017	170.802	0.00004
CV	0.054	0.060	0.08530	0.317	0.185	0.230	0.28418

Alaska's largest fire year was 2004, during which 2.818 M ha burned. However, in this year peat burning only accounted for an estimated 5.5% of the total annual burned area despite burning the second largest estimated peat BA of 0.155 M ha (Table 24). In contrast, 2014 saw the lowest total BA of 0.080 M ha, with just 0.009 M ha of estimated peat BA, accounting for an estimated 11.5% of the total (Table 24). However, both 2004 and 2014 had the same NO_2:CO ratio according to the CAMS reanalysis data of 0.00090 (Table 25), suggesting that we may not be able to detect a signal of peatland burning in 2004 because peat fires only represent a small fraction of burning, and therefore their effects on atmospheric composition are being masked by surrounding flaming fires. 2005 sees an above average peat BA of 0.125 M ha, making up 2.6% more of the annual total BA than in 2004. The NO_2:CO ratio in 2005 is lower than that of 2004, suggesting that the increased peat burning percentage in this year is likely resulting in a lower ratio of NO_2:CO relative to 2004.

2020, 2016 and 2006 are the three years with the largest estimated peat burning percentages of 18.1, 10.0 and 10.1%, respectively (Table 24). 2006 also features the lowest NO_2:CO ratio of 0.00076, which is occurring due to the lower-than-average NO_2 levels and higher-than-average CO levels, potentially indicating the increased presence of smouldering combustion in 2006. However, lower-than-average NO_2:CO ratios are not seen in either 2020 or 2016, with NO_2 levels marginally below average and CO levels below the annual average, suggesting minimal signatures of peat fires on atmospheric composition in these years.

Comparisons can be made between the impacts of burning on atmospheric composition from TROPOMI between 2019 and 2020. In 2019, significantly more burning is seen than in 2020, at 1.1 M ha in 2019 compared to just 0.1 M ha in 2020 (Table 24). However, in 2020, 18.1% of the total burned area is estimated to result from peat fires, compared to just 8.0% in 2019. 2020 then also sees a lower NO_2:CO ratio in the TROPOMI data of 0.00012 compared to 0.00014 in 2019, as a result of increased CO levels and decreased NO_2 levels in 2020 compared to 2019 (Table 25). Similarly, the CAMS data also shows 2020 to have a lower NO_2:CO ratio compared to 2019, suggesting that the

increase in the occurrence of peat burning in 2020 may have had a role in shaping the atmospheric composition over Alaska. Furthermore, the lower relative estimated peat fire percentage of total burned area seen in 2019, may mean that any signal from peat burning may be being masked by the presence of larger surrounding flaming vegetation fires. This idea will be discussed in more detail in section 3.5.

Correlations of yearly totals of all fire parameters showed no relationship with yearly CAMS CO or the CAMS NO_2:CO ratio (Table 26c). However, there were significant positive correlations of CAMS NO_2 with total BA ($r=0.719$, $p=0.001$), with estimated peat BA ($r=0.713$, $p=0.001$),with total FRP ($r=0.773$, $p<0.001$), and with estimated peat FRP ($r=0.780$, $p<0.001$), suggesting that increased burning in Alaska tends to cooccur with increased NO_2 levels regardless of whether peat is burning or not. Although non-significant, there is a weak negative correlation between annual estimated peat fire percentages of total burned area and NO_2 ($r=-0.232$, $p=0.354$), giving an indication that when peat fires occupy more of the total picture of BA, there are small effects on atmospheric composition, such as lower NO_2 levels.

On seasonal timescales, there are strong positive correlations between total burned area in a month and TROPOMI NO_2 ($r=0.759$, $p=0.004$) and CAMS NO_2 ($r=0.901$, $p<0.001$) (Table 26a). There are also significant positive correlations between TROPOMI and CAMS NO_2 with estimated peat BA, total FRP and estimated peat fire FRP (Table 26a). However, CAMS CO shows negative correlations with all the fire variables, whereas there are positive correlations between total and estimated peat BA and FRP and TROPOMI CO (Table 26), highlighting the benefit of also using the CAMS data to look at longer-term trends, which can cause a significant difference in the direction of the relationships. However, these correlations are all not statistically significant. Significant strong positive correlations are present between the CAMS NO_2:CO ratio with total BA ($r=0.875$, $p<0.001$), estimated peat BA ($r=0.811$, $p=0.001$), total FRP ($r=0.874$ $p<0.001$), and estimated peat FRP ($r=0.881$, $p<0.001$). There are no relationships between estimated peat fire percentage of BA or FRP with neither TROPOMI nor CAMS variables. But we do see non-significant positive correlations between estimated peat fire BA percentage of total BA and the TROPOMI NO_2:CO ratio ($r=0.610$, $p=0.108$) and the CAMs NO_2:CO ratio (0.537, $p=0.170$).

Overall, these results show that the seasonality in NO_2 and its ratio with CO is potentially heavily influenced by the seasonality of fires, with more burning associated with increases in NO_2 and consequently increases in NO_2:CO ratios. The presence of this relationship even with peat burning metrics suggests that perhaps there are not actually as many peat fires occurring as estimated here, or that they are occurring alongside flaming fires that are masking the signal.

Monthly total BA in Alaska is positively, but not significantly, correlated with TROPOMI NO_2 ($r=0.331$, $p=0.064$) and significantly correlated with CAMS NO_2 ($r=0.692$, $p<0.001$). Total BA is also

negatively correlated with CAMS CO (r=-0.254, p<0.001), resulting in a positive correlation with the CAMS NO_2:CO ratio (r=0.669, p<0.001) (Table 26b). In fact, all fire variables, on a monthly basis, show positive correlations with the CAMS NO_2:CO ratio (Table 26b), suggesting that increased BA and FRP is causing increases in the NO_2:CO ratio. Estimated peat BA and FRP both show a positive correlation with TROPOMI NO_2 (r=0.293, p=0.104; r=0.539, p<0.001) and with CAMS NO_2 (r=0.583, p<0.001; r=0.681, p<0.001). Furthermore, estimated peat BA and FRP exhibit a negative relationship with CAMS CO (r=-0.179, p=0.008; r=-0.259, p<0.001), resulting in the positive correlations seen with the CAMS NO_2:CO ratio (Table 26b). However, there are no significant relationships between the TROPOMI CO and NO_2:CO ratio with any of the fire parameters. Estimated peat fire percentage of total BA, shows weak and non-significant relationships with TROPOMI NO_2 (r=-0.369, p=0.132) and the NO_2:CO ratio from TROPOMI (r=-0.284, p=0.254). This perhaps suggests that when monthly percentages of peat fires increase, there starts to be a stronger influence of peat burning on atmospheric composition through lower NO_2 and lower NO_2:CO ratios.

Table 26: Correlations between the GFED5 and GFAS fire parameters, and NO_2, CO and their ratio in the TROPOMI and CAMS reanalysis datasets, on seasonal data (a), monthly data (b) and yearly data (c) in Alaska. Asterisks indicate significant p values (* = p<0.05, **=p<0.001, ***=p<0.001)

		TROPOMI			CAMS		
		NO_2	CO	NO_2:CO Ratio	NO_2	CO	NO_2:CO Ratio
a) Seasonality data							
GFED5	Total BA	0.759 **	0.218	0.299	0.901 ***	-0.374	0.875 ***
	Peat BA	0.749 **	0.070	0.359	0.772 **	-0.343	0.811 **
	Peat BA percentage	0.586	-0.195	0.610	0.415	-0.073	0.537
GFAS	Total FRP	0.699*	0.357	0.028	0.902 ***	-0.287	0.874 ***
	Peat FRP	0.580*	0.182	-0.028	0.825 **	-0.448	0.881 ***
	Peat FRP percentage	0.350	-0.450	0.383	0.117	-0.067	0.317
b) Monthly data							
GFED5	Total BA	0.331	0.083	-0.002	0.692 ***	-0.254 ***	0.669 ***
	Peat BA	0.293	0.095	-0.028	0.583 ***	-0.179 **	0.549 ***
	Peat BA percentage	-0.369	-0.044	-0.284	0.117	-0.139	0.185 *
GFAS	Total FRP	0.549 ***	0.171	0.206	0.678 ***	-0.240 ***	0.659 ***
	Peat FRP	0.539 ***	0.170	0.200	0.681 ***	-0.259 ***	0.669 ***
	Peat FRP percentage	0.096	-0.218	0.147	0.125	-0.144	0.186 *
c) Yearly data							
GFED5	Total BA				0.719 **	0.166	0.292
	Peat BA				0.713 **	0.053	0.352
	Peat BA percentage				-0.232	-0.238	-0.049
GFAS	Total FRP				0.773 ***	0.062	0.385
	Peat FRP				0.780 ***	0.066	0.367
	Peat FRP percentage				-0.002	-0.144	0.000

Overall, across the datasets, Alaska shows strong positive correlations between NO_2, from both TROPOMI and CAMS, with total and estimated peat BA and FRP. This indicates that fires are associated with elevated amounts of NO_2, regardless of whether they coincide with peat burning. This may indicate that in Alaska, it is less common for the peat to burn compared to other regions, and a lot of the signals detected here are from flaming vegetation fires. For example, Turquety et al., (2007) estimated that 17% of the burnt area in the 2004 summer wildfires may have occurred on peatlands, whereas during the 2010 summer Russian fires, 30% were estimated to be peat fires (Konovalov et al., 2011) and between 1982 and 2020 an estimated 71% of all fires that occurred in the Siberian Arctic occurred on permafrost (Descals et al., 2022). Therefore, this indicates that peat burning in Alaska may be less prevalent than in other regions of the world. Furthermore, total BA in Alaska is low, with some years having an estimated peat BA of less than 0.01 M ha (Table 24). This also is supported by the GFED500m product which captures relatively small amounts of belowground burning compared to other regions (See Chapter 3 section 3.3.1). There are also strong positive correlations between the CAMS NO_2:CO ratio and fires in both the monthly and seasonal data, suggesting that fires in Alaska tend to be associated with higher NO_2:CO ratios, and therefore smouldering peat fires, which are expected to result in lower NO_2:CO ratios, may not be having a large influence in this area. However, there are suggestions of an effect of peat fires on atmospheric composition in the data, such as the negative, although non-significant, correlations between TROPIMI NO_2 and the NO_2:CO ratio with estimated peat fire percentage of BA, and through comparing specific years such as 2020 vs 2019 and 2005 vs 2006. This suggests that when peat fires do occur in Alaska, and they occupy a significant percentage of total BA, their effect on atmospheric composition can start to be detected.

3.3.4. Impacts of fires on $PM_{2.5}$

Across Alaska, $PM_{2.5}$ averages 0.018 kg per year, with strong interannual variability (Figure 44a). Large peaks in $PM_{2.5}$ occur in 2004, 2005, 2009, 2015, 2019 and 2022. In all these years $PM_{2.5}$ is greater than 0.020 kg. 2004 sees the largest $PM_{2.5}$ levels of 0.033 kg. In general, these large $PM_{2.5}$ years match up well with the years in which the largest BAs are seen. For example, 2004, also sees the largest annual BA in the GFED5 data for Alaska (Table 24). $PM_{2.5}$ levels show high values from April to August, with a peak occurring in July (Figure 44b), matching up well with the July peak in BA and FRP (Figure 41b).

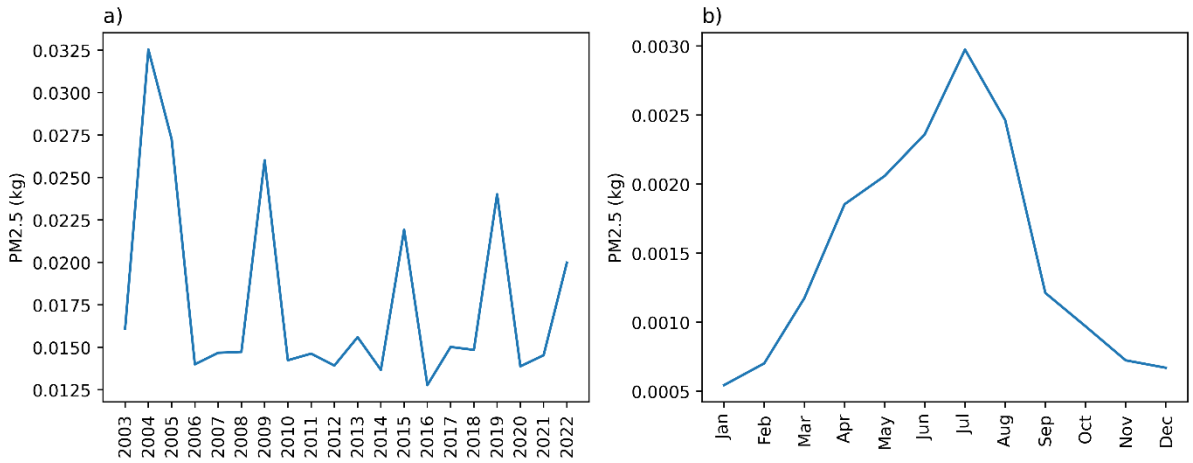


Figure 44: Timeseries plot for $PM_{2.5}$ from 2003-2022 in Alaska from the CAMS reanalysis data (a), and the 2003-2022 averaged Alaska seasonality in $PM_{2.5}$ (b)

There are strong positive correlations between total BA, estimated peat BA, and total FRP on all timescales, showing that in years and months where there are greater amounts and severities of burning there are higher levels of $PM_{2.5}$ (Figure 45, Table 27). The contribution of estimated peat BA to total BA shows much weaker relationships with $PM_{2.5}$ compared to total BA. For example, monthly estimated peat fire percentage of total BA is only weakly positively correlated to $PM_{2.5}$ (r=0.240, p=0.010. Furthermore, annual estimated peat fire percentage of total BA actually shows a negative correlation with $PM_{2.5}$ (r=-0.527, p=0.025). A similar negative correlation is seen between the annual estimated peat fire percentage of FRP and $PM_{2.5}$ (Table 27). There is therefore a disparity between the signals from the relative contribution of peat fires to the total picture of burning on annual compared to monthly timescales.

Table 27: Correlations between the yearly GFED5 and GFAS fire parameters, and the CAMS reanalysis $PM_{2.5}$ data, using annual totals, monthly totals and the seasonality (average monthly totals 2003-2020) Alaska. Asterisks indicate significant p values (* = p<0.05, **=p<0.001, ***=p<0.001)

		CAMS $PM_{2.5}$ Annual totals	Monthly totals	Seasonality
GFED5	Total BA	0.800 ***	0.707 ***	0.919 ***
	Peat BA	0.715 **	0.647 ***	0.858 ***
	Peat BA percentage	-0.527 *	0.240 *	0.732 *
GFAS	Total FRP	0.771 ***	0.675 ***	0.958 ***
	Peat FRP	0.729 ***	0.667 ***	0.860 ***
	Peat FRP percentage	-0.301	0.151	0.601 *

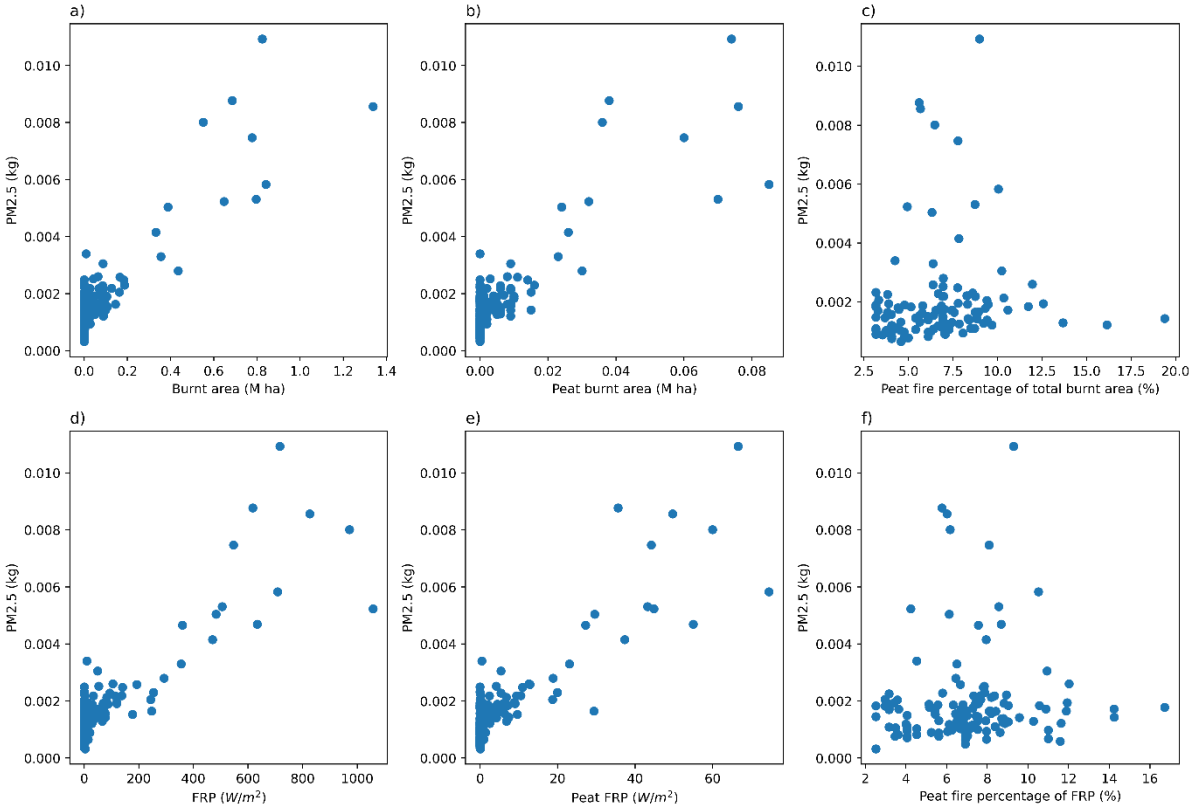


Figure 45: Relationships between monthly total CAMS $PM_{2.5}$ and monthly total BA (a), estimated peat BA (b), estimated peat fire percentage of BA (c), total mean FRP (d), estimated peat fire mean FRP (e) and estimated peat fire percentage of FRP (f) in Alaska.

3.4. Western Canada

3.4.1. Trends in wildfires and peat fires

Western Canada (W Canada), on average, sees 1.306 M ha burn annually, with a mean FRP of 177.727 W/m^2 (Table 28). There is some degree of interannual variability in BA in W Canada particularly towards the end of the timeseries (Figure 46a). However, there is also a period of relative stability in annual BA between 2005 and 2013. Large annual BAs do occur however, in 2004, 2014, 2015 and 2017, all of which have an annual burnt area of 2 M ha or more. These years also see large spikes in FRP, especially in 2014 (Figure 46a). The majority of burning occurs during the summer months in W Canada, with a peak in July (Figure 46b). The seasonality of FRP shows a similar pattern, however, there is also a secondary peak in FRP that occurs in October and November (Figure 46b).

On average 14.3% of the annual BA is estimated to be due to peat fires which burn an estimated 0.187 M ha per year on average (Table 28). In comparison to total BA, estimated peat BA exhibits more interannual variability across the timeseries (Figure 46c), with a coefficient of variation of 0.768 compared to 0.562 for total BA. The largest amount of estimated peat BA occurs in 2014 when 0.580 M ha of peat is estimated to have been burnt, approximately 20% of the annual total BA (Table 28). Other years with large estimated peat BA and FRP are 2004, 2012 and 2015. 2012 is also the year

with the highest estimated peat fire percentage of total BA, at 25%. Estimated peat fire percentages of total BA also show a period of elevated peat fire contribution to both BA and FRP between 2011 and 2015, in which peat fires contributed at least 15% of BA and over 10% of FRP (Figure 46e). There is also a large percentage of BA estimated to be coming from peat fires in 2017 at 17.8%, despite this year only burning a below-average amount of peat. Peat burning tends to occur during the summer, with the highest peat fire estimated FRPs also occurring over June to August (Figure 46d). Estimated peat fire percentage of total BA and FRP show a more extended period of burning occurring between May and September (Figure 46f).

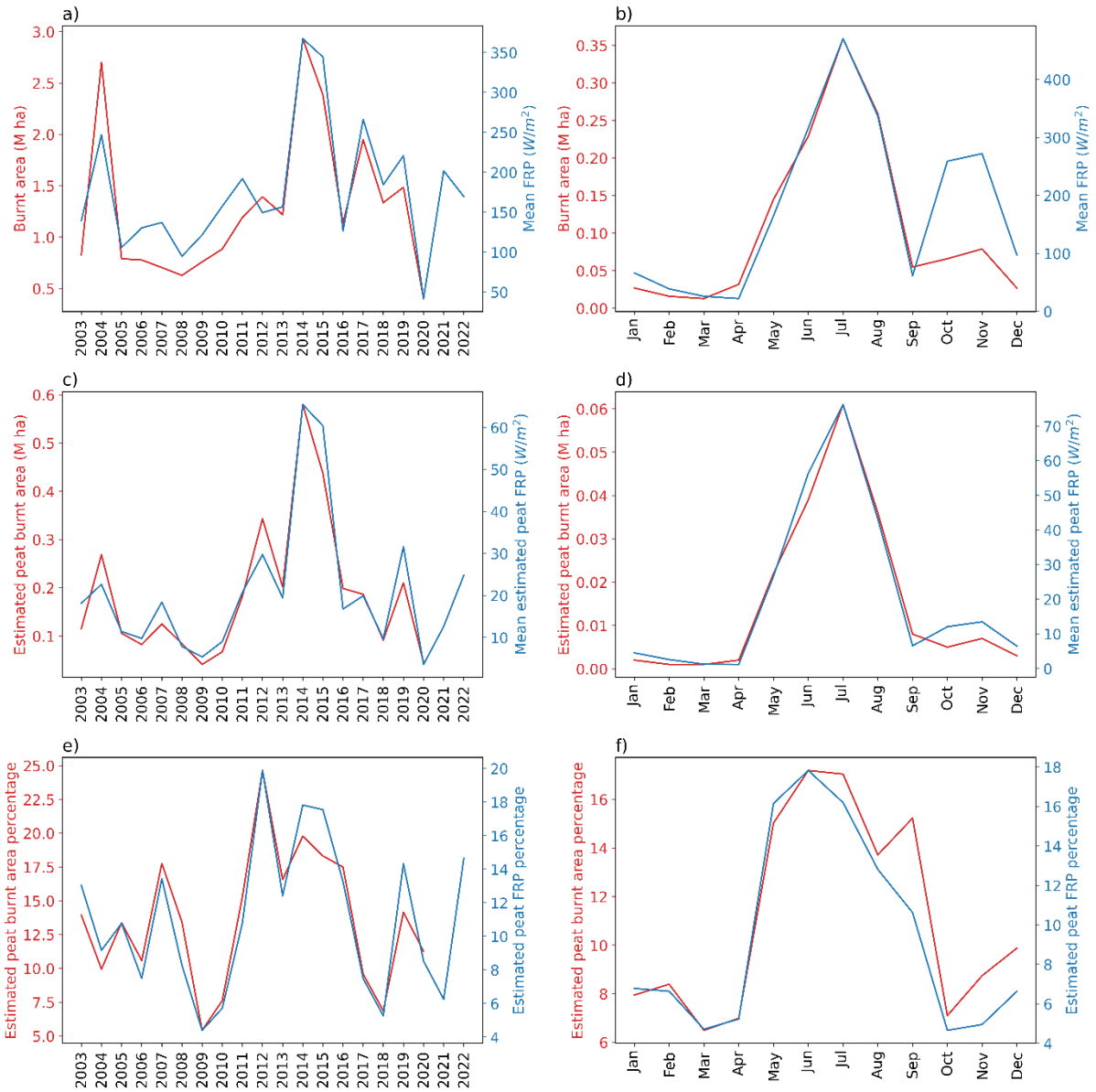


Figure 46: Fire trends over 2003-2022 for western Canada. BA data covers the period from 2003 to 2020, and the FRP data continues up to 2022. The trends shown are a) average annual total BA and FRP and b) the seasonality in total BA and FRP (averaged over their respective time periods). Panel c) shows the yearly timeseries trends in estimated peat BA and FRP and panel d) shows the seasonality in estimated peat BA and estimated peat FRP. Panel e) shows the estimated peat BA as a percentage of total BA and the estimated peat FRP as a percentage of total FRP, and panel f) shows the seasonality in peat estimated BA and FRP percentage.

Table 28: Annual values for BA from GFED5 and FRP from GFAS for western Canada, and the summary statistics (mean, standard deviation (SD) and coefficient of variation (CV)) for the whole time series. Values in bold highlight years in which the value is at least one standard deviation greater than the mean.

	GFED5			GFAS		
Year	Total BA (M ha)	Peat BA (M ha)	Peat BA percentage	Total FRP (W/m^2)	Peat fire FRP (W/m^2)	Peat fire FRP percentage
2003	0.829	0.116	13.938	139.327	18.152	13.028
2004	**2.701**	0.269	9.948	247.039	22.646	9.167
2005	0.790	0.106	13.375	105.823	11.402	10.774
2006	0.778	0.082	10.579	130.334	9.769	7.496
2007	0.705	0.125	17.763	137.122	18.419	13.433
2008	0.628	0.084	13.418	94.857	7.849	8.274
2009	0.760	0.041	5.418	121.539	5.346	4.399
2010	0.884	0.067	7.615	157.440	9.001	5.717
2011	1.193	0.182	15.283	192.092	20.727	10.790
2012	1.393	**0.343**	**24.639**	149.542	29.731	**19.881**
2013	1.219	0.202	16.577	156.652	19.467	12.427
2014	**2.932**	**0.580**	**19.775**	**367.383**	**65.471**	**17.821**
2015	**2.386**	**0.437**	18.318	**344.354**	**60.412**	**17.544**
2016	1.136	0.199	17.491	126.563	16.770	13.250
2017	1.948	0.187	9.577	**266.199**	19.923	7.484
2018	1.336	0.092	6.867	184.399	9.713	5.268
2019	1.486	0.210	14.153	220.658	31.602	14.322
2020	0.403	0.045	11.267	41.851	3.568	8.525
2021				201.805	12.612	6.250
2022				169.569	24.825	14.640
Mean	1.306	0.187	14.325	177.727	20.870	11.024
SD	0.733	0.144	4.965	80.263	16.311	4.461
CV	0.562	0.768	0.347	0.452	0.782	0.405

3.4.2. Drivers of large fire years

In W Canada there is a positive correlation between total BA and temperature anomalies ($r=0.278$, $p<0.001$), suggesting that elevations in BA relative to their seasonal average are likely to occur concurrently with elevations in temperature compared to their seasonal average (Figure 47a and Figure S3). Additionally, there is a positive correlation between estimated peat BA anomalies and temperature anomalies ($r=0.267$, $p<0.001$) (Figure 47b). For example, during 2004 there is higher than average summer burning, particularly in July, which saw 0.9 M ha more burning than the seasonal average, alongside temperatures that were 1.2°C warmer than average. Similarly, in summer 2014, BA was higher than average, with July 2014 burning over 1 M ha more than average, coinciding with 1.8°C warmer than average temperatures. May 2015 saw 0.362 M ha more than average BA, which coincided with temperatures being nearly 10°C warmer than average. The 2014 Canadian wildfires particularly in the Northwest Territories have been attributed to hot and dry weather conditions, associated with a dominant mid tropospheric ridging pattern (Kochtubajda et al., 2019; Gaboriau et al., 2022). However, the largest BA anomaly occurred in June, but during this month, temperatures were 0.9°C colder than average, suggesting that the warm temperatures in the preceding month may have contributed to a larger period of burning in June. Additionally, studies have shown that the breakdown of the ridging pattern led to thunderstorm and lightning formation

(Kochtubajda et al., 2019), resulting in a record number of lightning ignitions in 2014 (Veraverbeke et al., 2017). These results highlight the importance of both direct effects of warmer temperatures and also indirect effects that occur alongside high temperatures such reduced precipitation, humidity, and fuel moisture, which may have a large influence on the amounts of burning seen during a fire season.

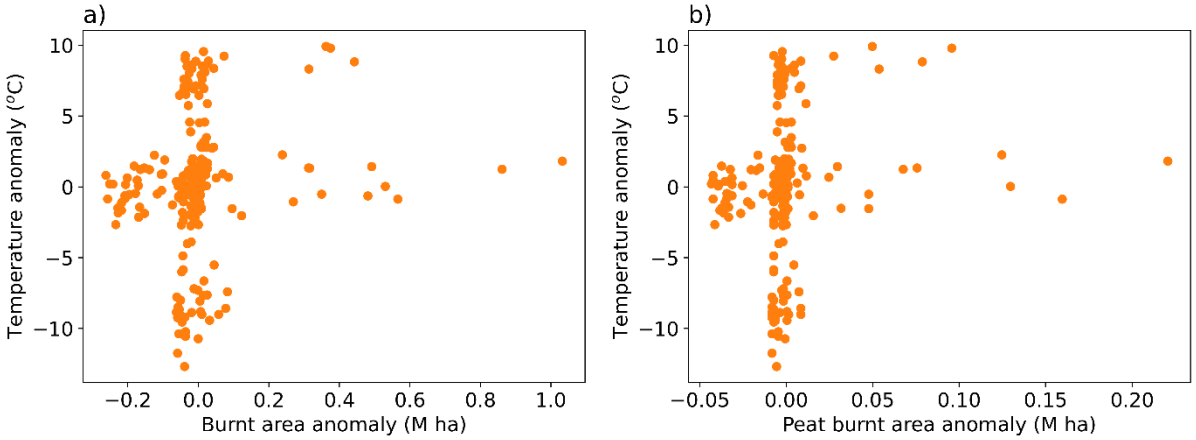


Figure 47: Correlations between seasonal BA anomalies and seasonal temperature anomalies for a) total BA and b) estimated peat BA in western Canada.

3.4.3. Impacts of fires on atmospheric composition

There is considerable interannual variability in annual NO_2 concentrations from the CAMS reanalysis data across W Canada, with the peak year being 2014 (Figure 48a), coinciding with the year with the largest BA. Large NO_2 values are also present in 2003, 2010, 2011, 2017 and 2022. NO_2 levels are elevated over March to November on average, with the higher values occurring in July and October, and the lowest values over winter (Figure 48b). Atmospheric concentrations of CO over W Canada appear to decline over the time series (Figure 48c), with a decrease of 392.9 kg between the 2003-2007 average and the 2018-2022 average. The largest CO values occur in 2003, and the lowest in 2022. There is a period from 2009 to 2015 during which CO concentrations are more level in terms of their overall trend, with minor interannual variability (Figure 48c). Compared to NO_2, CO exhibits a more complex seasonal pattern. The highest CO values occur in spring from March to May (Figure 48d), However, CO is also elevated over winter, most notably in December and January, with the lowest values occurring over summer and autumn and a notable drop in September, when there is also a drop in total BA.

The ratio of NO_2:CO from the CAMS reanalysis data shows an increase across the timeseries, but with significant interannual variability (Figure 48e). The highest NO_2:CO ratio occurs in 2022, closely followed by a large spike in the NO_2:CO ratio in 2014, the year with the largest BA. The lowest NO_2:CO ratios occur in 2005 and 2006, years in which there was lower than average BA. The ratio of NO_2:CO peaks in October, with high values seen from June to October (Figure 48f), with the lowest ratios occurring over December-February, when CO is relatively high and NO_2 is at its lowest.

Levels of NO_2 and CO from the three full years of data (2018-2020) from TROPOMI are relatively consistent (Figure 48a, c). 2020 sees the highest NO_2 levels, conversely CAMS over the same three years shows 2020 to have the lowest NO_2. Highlighting key differences between the two datasets. CO reaches its peak in the TROPOMI data in 2021, in agreement with the CAMS data over the TROPOMI period. In terms of the NO_2:CO ratio seen in the TROPOMI data, the lowest value is recorded in 2021, when there is the highest level of CO, in agreement with the CAMS data over the same period (Figure 48e). Overall, the seasonalities from the TROPOMI data are very similar to that of the CAMS reanalysis data (Figure 48b, d, f). TROPOMI NO_2, shows an extended peak in NO_2 from March to October, with the highest values being recorded in August. TROPOMI CO, like CAMS, shows a spring peak in CO. However, it does not then exhibit the same drop in CO that is seen in the CAMS data over the summer and autumn, and instead shows a secondary CO peak in August to October (Figure 48d). When the TROPOMI seasonalities are calculated over the same period, there is a similar secondary peak in August, suggesting that this feature may be a product of the averaging years used here (Figure S2). Much like the CAMS data, the NO_2:CO ratio derived from TROPOMI shows a peak from June to October, with the lowest values occurring over the winter (Figure 48f).

Table 29: Annual values for NO_2, CO and their ratio from both TROPOMI and CAMS reanalysis data for western Canada, and the summary statistics (mean, standard deviation (SD) and coefficient of variation (CV)) for the whole time series. Values in bold highlight years in which the value is at least one standard deviation above or below the mean.

	CAMS reanalysis				TROPOMI		
Year	NO_2 (kg)	CO (kg)	Ratio NO_2:CO	$PM_{2.5}$	NO_2 (mol)	CO (mol)	Ratio NO_2:CO
2003	3.729	**3792.615**	**0.00098**	0.023			
2004	3.678	**3584.704**	0.00103	**0.037**			
2005	3.481	**3555.712**	**0.00098**	0.020			
2006	**3.338**	3428.043	**0.00097**	0.021			
2007	3.591	3437.330	0.00104	0.021			
2008	3.457	3376.856	0.00102	0.022			
2009	**3.395**	3240.688	0.00105	0.026			
2010	3.733	3389.048	0.00110	0.023			
2011	3.777	3270.521	0.00115	0.023			
2012	3.614	3464.307	0.00104	0.026			
2013	**3.376**	3238.411	0.00104	0.024			
2014	**4.101**	3353.837	**0.00122**	**0.043**			
2015	3.722	3333.997	0.00112	**0.032**			
2016	3.535	3266.310	0.00108	**0.020**			
2017	3.780	3185.029	**0.00119**	0.030			
2018	3.611	3189.043	0.00113	0.026	**0.101**	**629.282**	**0.00016**
2019	3.483	3204.646	0.00109	0.029	0.145	1009.396	0.00014
2020	**3.346**	**3096.750**	0.00108	**0.017**	0.148	991.089	0.00015
2021	3.509	3356.603	0.00105	0.026	0.139	1057.460	**0.00013**
2022	**3.796**	**2986.828**	**0.00127**	0.024			**0.00016**
Mean	3.602	3337.564	0.00108	0.026	0.133	921.807	0.00015
SD	0.191	181.741	0.00008	0.006	0.022	197.015	0.00001
CV	0.053	0.054	0.07391	0.237	0.162	0.214	0.08420

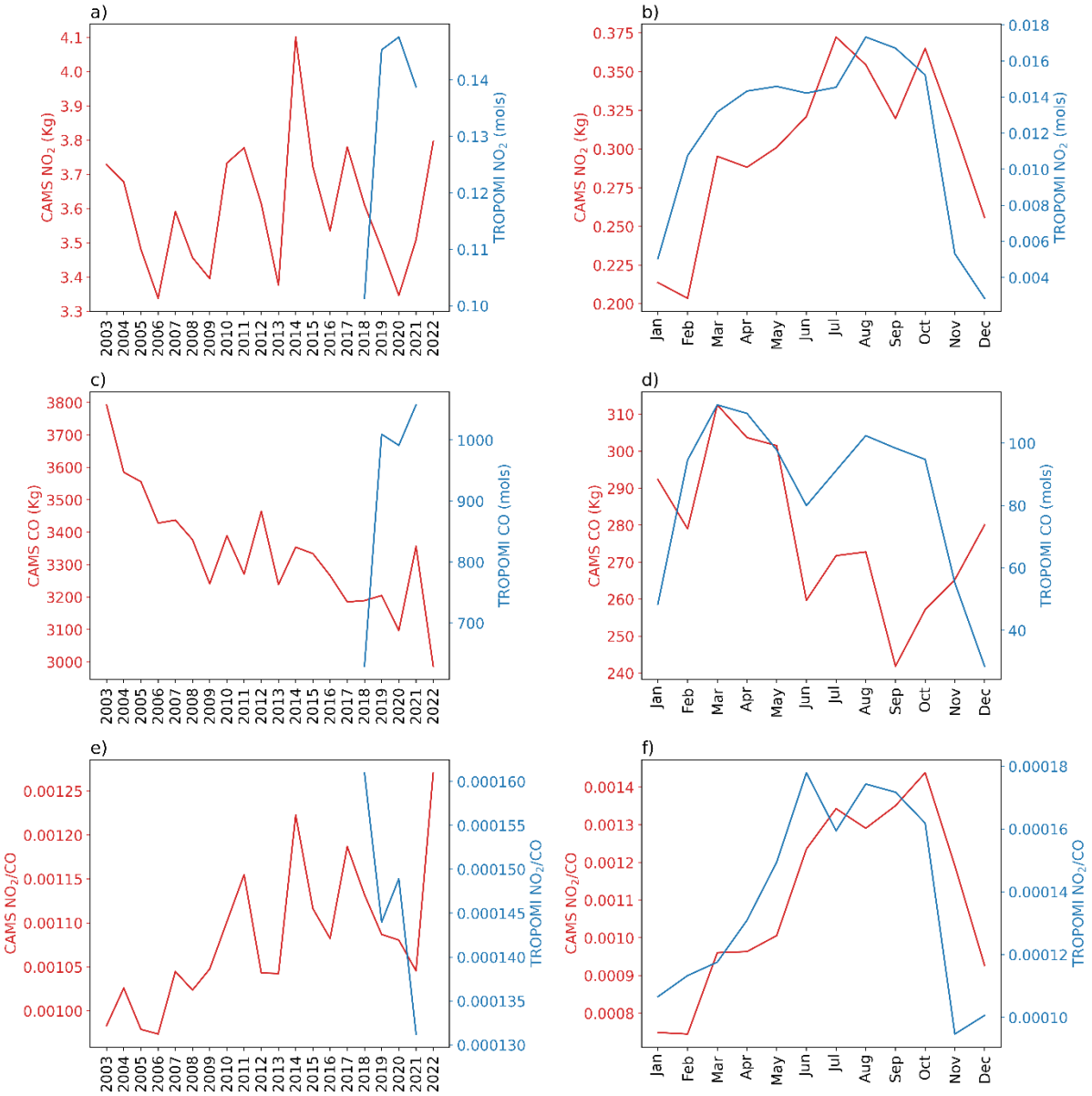


Figure 48: Time series plots for NO_2 (a) and its seasonality (b), CO (c) and its seasonality (d), and the ratio of NO_2/CO (e) and its seasonality (f), over 2003 to 2022 for CAMS reanalysis data (red) and 2018 to 2021 for the TROPOMI data (blue) in western Canada.

Across W Canada, we see a tendency for years with the largest BAs to result in greater levels of NO_2 and CO. For example, 2014 burnt the largest area at 2.932 M ha, compared to 2020, which was the lowest BA year at just 0.403 M ha (Table 28). Consequently, NO_2 concentrations are 23% higher in 2014 than 2020 and the CO concentrations are 8% higher, with both the NO_2 and CO levels in 2020 being significantly below the multiannual mean (Table 29). Consequently, the NO_2:CO ratio derived from CAMS in 2020 is close to the multiannual mean, whereas the NO_2:CO ratio in 2014 is significantly greater than the multiannual mean. Therefore, large BA years tend to result in higher concentrations of NO_2 and higher NO_2:CO ratios. 2014 also sees the largest estimated peat BA of 0.580 M ha, however there is no effect of this high peat BA on the NO_2:CO ratio. This may suggest

that either our method for estimating peat fires is resulting in an overestimation in 2014 in W Canada, or that the sheer size and intensity of the 2014 fire season when it comes to flaming fires in W Canada may be overriding any signal we may be able to observe for peat fires on these timescales.

However, there is some suggestion of an effect of peat burning on atmospheric composition in W Canada. For example, in 2019 W Canada saw three times more burning than in 2020, and considerably more peatland burning. 2019 saw an estimated 0.165 M ha more peat BA than 2020, making up 14% of the total burned area compared to 11% (Table 28). The TROPOMI NO_2:CO ratio in 2019 is 7% lower than 2020 at 0.00014 (Table 29), suggesting that the increased peat burning in 2019 may have resulted in a low NO_2:CO ratio. However, the CAMS reanalysis derived NO_2:CO ratios are very similar in these two years, and both are close to the multiannual average. Thereby suggesting that the effect of peat burning may be smaller than what is observed by TROPOMI. Furthermore, 2004 saw the second largest fire year, and also burnt an estimated 0.269 M ha of peat (almost 10% of the annual total). Potentially as a result, 2004 has a lower-than-average ratio of NO_2:CO in the CAMS data and is significantly smaller than the 2014 ratio. Additionally, in 2012, peat fires are estimated to have been responsible for nearly 25% of the annual total BA, and in 2007 peat fires accounted for an estimated 17.8% of BA. Both these years saw a lower-than-average ratio of NO_2:CO in the CAMS data. Crucially, the NO_2:CO ratios in 2004, 2007 and 2012 were lower than the ratios seen in years with minimal peat burning such as 2010 and 2020 (Table 28 and Table 29), suggesting that high peat burning may be leading to lower ratios of NO_2:CO. As previously identified, there is a period of elevated estimated peat fire percentages of total burned area from 2011 to 2016. However, there is no clear lowering of the NO_2:CO ratios during this period, with an average NO_2:CO ratio of 0.00111, higher than the multiannual mean. Therefore, whilst there is some indication that peat fires may be impacting atmospheric composition in W Canada, there is not clear pattern and limited conclusions can be taken.

BA and FRP are significantly positively correlated with CAMS NO_2 on a yearly basis, along with peat fire estimated BA and peat fire estimated FRP (Table 30c). Despite exhibiting weak non-significant negative relationships between total BA and CAMS CO, the NO_2:CO ratio is significantly positively correlated with total BA ($r=0.511$, $p=0.030$). Similarly, there is a positive correlation between total FRP and the NO_2:CO ratio ($r=0.580$, $p=0.007$). In contrast, peat fire estimated BA shows a small positive correlation with CO ($r=0.127$, $p=0.616$), although this is not statistically significant. As a result, unlike total BA, the correlation between estimated peat BA and the NO_2:CO ratio is not significant ($r=0.292$, $p=0.240$). There are no significant correlations between yearly estimated peat fire percentage and any of the atmospheric composition variables (Table 30c). Therefore, these results suggest that years which have larger peat burned areas see elevated NO_2 levels, however, they are not associated with higher CO or lower NO_2:CO ratios. Whereas total BA does show a significant positive association with the NO_2:CO ratio, suggesting that a high proportion of the estimated peat fires may

be occurring simultaneously with flaming fires, masking the detectable signal on atmospheric composition from peat fires.

On a seasonal cycle, there are positive correlations between TROPOMI NO_2 and the various fire variables, however, none of these are significant (Table 30a). There are significant positive correlations between CAMS NO_2 with total BA (r=0.816, p=0.001), estimated peat BA (r=0.800, p=0.002), FRP (r=0.748, p=0.005) and estimated peat FRP (r=0.776, p=0.003). There are non-significant negative correlations between TROPOMI CO and CAMS CO with the fire variables, indicating a tendency for fires in W Canada to be correlated with lower atmospheric CO levels (Table 30a). Consequently, there are positive correlations between total BA with the TROPOMI NO_2:CO ratio (r=0.592, p=0.043), and the CAMS ratio of NO_2 to CO (r=0.704, p=0.011). There are also positive correlations between peat BA with the TROPOMI ratio (r=0.632, p=0.028), and the CAMS ratio (r=0.709, p=0.010). These results suggest that, on average, months that have higher BAs (regardless of whether it is peat burning or not) also have higher levels of NO_2, and therefore higher NO_2:CO ratios.

On a monthly scale there are no significant correlations between any of the fire variables and the TROPOMI atmospheric composition data, except for a negative correlation between TROPOMI CO and the estimated peat fire percentage of total burned area (r=-0.371, p=0.037) (Table 30b). However, the CAMS data exhibits significant correlations with all fire variables except estimated peat fire percentage of FRP (Table 30b). For example, there are strong negative correlations between CO with total BA (r=-0.219, p=0.001), estimated peat BA (r=-0.258, p<0.001), estimated peat fire percentage of BA (r=-0.213, p=0.002), total FRP (r=-0.169, p=0.009) and estimated peat FRP (r=-0.204, p=0.002). Positive correlations are also present between the aforementioned fire variables, NO_2 and the NO_2:CO ratio (Table 30b). This means that across W Canada increased BA or fire severity, regardless of whether they are peat fires or not, are associated with lower levels of CO and higher levels of NO_2 in the atmosphere resulting in higher ratios of NO_2:CO which is anticipated to occur with flaming combustion. The lack of a different atmospheric signal from peat fires may be due to either inaccurate detection of peat burning in W Canada, or the presence of flaming vegetation fires alongside smouldering peat fires.

Table 30: Correlations between the GFED5 and GFAS fire parameters, and NO_2, CO and their ratio in the TROPOMI and CAMS reanalysis datasets, on seasonal data (a), monthly data (b) and yearly data (c) in Alaska. Asterisks indicate significant p values (* = p<0.05, **=p<0.001, ***=p<0.001)

		TROPOMI			CAMS		
		NO_2	CO	NO_2:CO Ratio	NO_2	CO	NO_2:CO Ratio
a) Seasonality data							
GFED5	Total BA	0.564	-0.060	0.592 *	0.816 **	-0.480	0.704 *
	Peat BA	0.526	-0.130	0.632 *	0.800 **	-0.544	0.709 *
	Peat BA percentage	0.294	-0.308	0.503	0.483	-0.538	0.427

GFAS	Total FRP	0.280	-0.371	0.385	0.748 **	-0.531	0.566
	Peat FRP	0.406	-0.266	0.524	0.776 **	-0.559	0.629 *
	Peat FRP percentage	0.273	-0.161	0.524	0.280	-0.189	0.168
b) Monthly data							
GFED5	Total BA	0.289	-0.136	0.284	0.644 ***	-0.219 **	0.593 ***
	Peat BA	0.211	-0.201	0.251	0.605 ***	-0.258 ***	0.582 ***
	Peat BA percentage	-0.113	-0.371 *	0.071	0.243 ***	-0.213 **	0.276 ***
GFAS	Total FRP	0.071	-0.241	0.222	0.597 ***	-0.169 **	0.525 ***
	Peat FRP	0.014	-0.251	0.194	0.561 ***	-0.204 **	0.511 ***
	Peat FRP percentage	-0.208	-0.212	0.016	0.119	-0.078	0.116
c) Yearly data							
GFED5	Total BA				0.633 **	-0.051	0.511 *
	Peat BA				0.482 *	0.127	0.292
	Peat BA percentage				0.191	0.218	0.075
GFAS	Total FRP				0.674 **	-0.134	0.580 **
	Peat FRP				0.594 **	0.020	0.374
	Peat FRP percentage				0.340	0.108	0.146

Overall, W Canada does not show any indication of peat fires resulting in a lower NO_2:CO ratio. Like for Alaska, this may be due to not many peat fires happening or being small and occurring simultaneously with flaming vegetation fires, meaning that the signal of peat fires is hard to detect at this scale. Supportive of this hypothesis is also the fact that we do see significant increases in NO_2 with BA, indicating the presence of flaming vegetation fires having an impact on the NO_2 monthly budgets. We do see that in some years such as 2019 compared to 2020, more peat burning results in a marginally lower NO_2:CO ratio. However, this is not always the case, with large peat fire percentages occurring between 2011-2016 and exhibiting mixed NO_2:CO ratios (Table 29).

3.4.4. Impacts of fires on $PM_{2.5}$

On average, $PM_{2.5}$ totals 0.026 kg annually, but with substantial interannual variability (CV=0.237). The largest spikes in annual $PM_{2.5}$ occur in 2004 and 2014, whereas 2020 shows extremely low $PM_{2.5}$ (Figure 49a). In 2014, over 2.9 M ha burnt, with 0.6 M ha of estimated peat burning, and coincided with the largest recorded annual $PM_{2.5}$ for this region at 0.043 kg. Similarly, 2004 features the second highest $PM_{2.5}$ levels and the second largest annual BA. In contrast, 2020 sees the lowest $PM_{2.5}$ levels at 0.017 kg, and the smallest burned area of just 0.4 M ha that year, suggesting that fires may be driving interannual variability of $PM_{2.5}$ in this region. Additionally, fires may also be driving intra-annual variability in $PM_{2.5}$, with the highest $PM_{2.5}$ occurring in the summer months (Figure 49b), which co-occurs with the months with the largest BAs and FRPs. Furthermore, there is a slight secondary peak in $PM_{2.5}$ levels in October and November, which is also seen in the FRP seasonalities (Figure 46b).

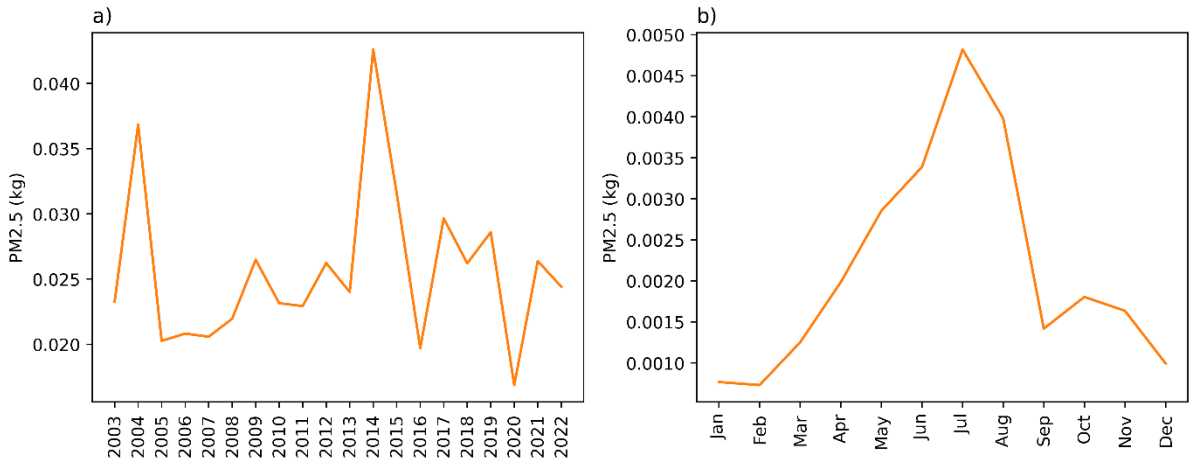


Figure 49: Timeseries plot for $PM_{2.5}$ from 2003-2022 in western Canada from the CAMS reanalysis data (a), and the 2003-2022 averaged western Canada seasonality in $PM_{2.5}$ (b).

There are strong positive correlations between yearly totals of BA, estimated peat BA, FRP and estimated peat FRP with $PM_{2.5}$ (Table 31). Additionally, there are similarly strong positive correlations with monthly and seasonal $PM_{2.5}$ data (Table 31). In particular, on a monthly timescale, there are strong positive correlations of $PM_{2.5}$ with BA ($r=0.778$, $p<0.001$) and estimated peat BA ($r=0.715$, $p<0.001$) (Figure 50a, b). Estimated peat fire percentage of total BA and FRP do not show any significant correlations with $PM_{2.5}$ on neither an annual nor seasonal scale. However, there are significant positive correlation on a monthly timescale ($r=0.307$, $p<0.001$). This suggest that on a monthly timescale, the greater the contribution of peat burning, the greater the levels of $PM_{2.5}$, potentially as a result of the fact that peat fires emit more $PM_{2.5}$ than flaming fires (Figure 50c, f).

Table 31: Correlations between the yearly GFED5 and GFAS fire parameters, and the CAMS reanalysis $PM_{2.5}$ data, using annual totals, monthly totals, and the seasonality (average monthly totals 2003-2020) in western Canada. Asterisks indicate significant p values (* = $p<0.05$, **=$p<0.001$, ***=$p<0.001$)

		CAMS $PM_{2.5}$ Annual totals	Monthly totals	Seasonality
GFED5	Total BA	0.822 ***	0.778 ***	0.907 ***
	Peat BA	0.593 **	0.715 ***	0.839 **
	Peat BA percentage	0.038	0.307 ***	0.524
GFAS	Total FRP	0.820 ***	0.519 ***	0.685 *
	Peat FRP	0.605 **	0.572 ***	0.748 **
	Peat FRP percentage	0.134	0.310 ***	0.517

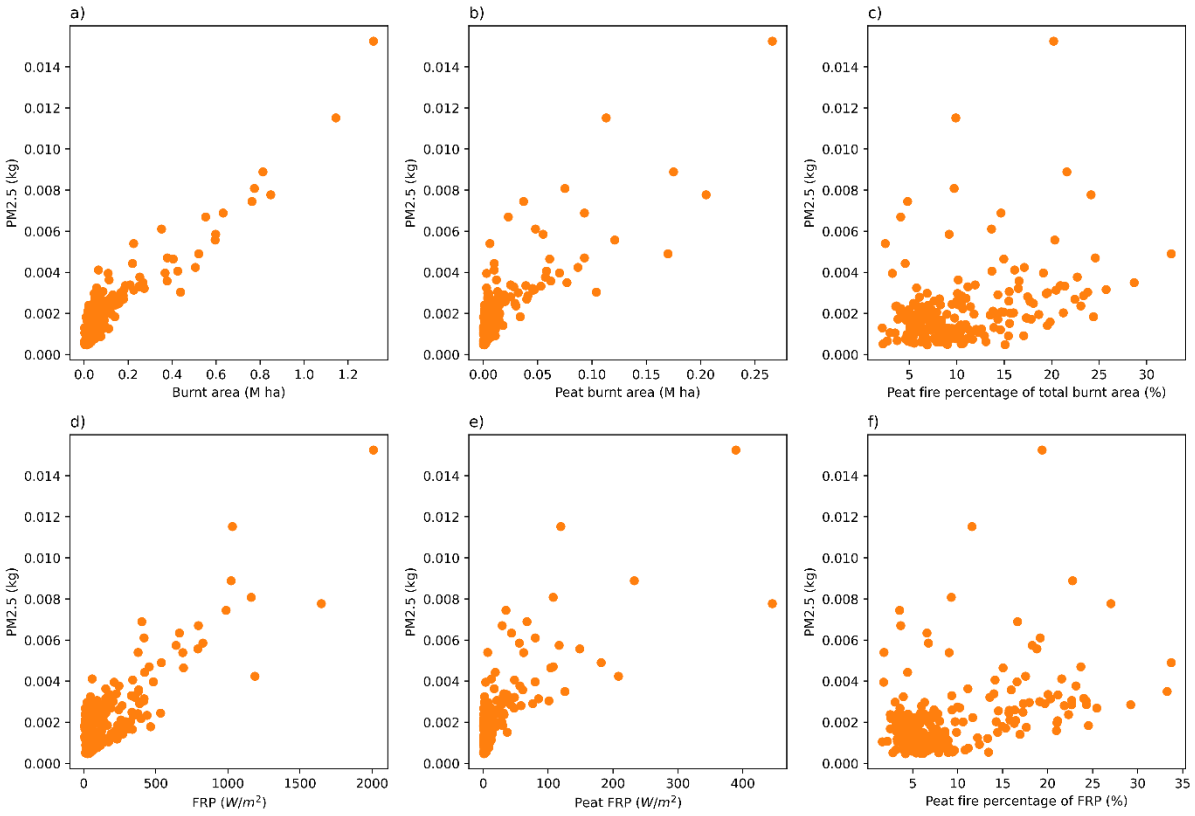


Figure 50: Relationships between monthly total CAMS $PM_{2.5}$ and monthly total BA (a), estimated peat BA (b), estimated peat fire percentage of BA (c), total mean FRP (d), estimated peat fire mean FRP (e) and estimated peat fire percentage of FRP (f) in western Canada.

3.5. Distinguishing between smouldering and flaming combustion in atmospheric composition data

In general, it is apparent that smouldering peat fires do have an effect on atmospheric composition in the high latitudes, which is to some extent distinguishable from that of flaming vegetation fires. In particular the preceding sections have highlighted that in NW Siberia, greater amounts and severities of estimated peat burning are associated with greater monthly levels of CO and lower NO_2:CO ratios, indicative of smouldering combustion. However, these signatures are less clear in the other regions. As mentioned throughout the prior sections, it is apparent that the detectable effect of peat fires on atmospheric composition may be being hampered by the typically small total BAs from peat fires (See Section 3.6) and simultaneous flaming vegetation fires (See section 3.7). However, being able to distinguish peat from non-peat burning using atmospheric composition observations may be crucial in creating a reliable peat fire dataset, which can potentially inform future peat fire modelling efforts. Therefore, this section explores the potential for distinguishing smouldering vs flaming combustion from TROPOMI observations and the aid of GFED5 data.

By looking at the changes in TROPOMI NO_2, CO and NO_2:CO along with BA, estimated peat BA and estimated peat fire percentage of BA between 2019 and 2020, months which have significantly greater or smaller amounts of peat burning can be identified. Across the regions, 14 data points were found in which the estimated peat fire percentage of BA changed by more than 5% from 2019 to 2020 (Table S3). Of these, 8 show months where the NO_2:CO ratio either increases with a decrease in peat fire percentage or visa versa, indicating smouldering combustion. For example, in W Canada there was a 10% decline in estimated peat fire percentage of total BA between August 2019 and 2020, coinciding with a 0.00009 higher NO_2:CO ratio. In Alaska, an 11% increase in estimated peat fire percentage of total BA occurred alongside a 0.00003 decrease in NO_2:CO in June between 2019 and 2020.

There are only 3 months in which estimated peat BA increased by more than 0.1 M ha between 2019 and 2020. These are June and July in E Siberia, in which estimated peat BA increased by 0.217 and 0.164 M ha respectively, and April in NW Siberia in which estimated peat BA increased by 0.223 M ha. In all three of these cases there are increases in atmospheric levels of CO according to TROPOMI. There are also minor increases in NO_2 levels and increases in the NO_2:CO ratio, the opposite to what would be expected with smouldering combustion. This potentially results from large increases also occurring in terms of total BA (including flaming fires) at the same time in the region of 1.4-2.2 M ha. This overall increase in burning may be masking the effect of peat fires on atmospheric composition.

3.6. Impact of the amount of peat fire BA on identifying atmospheric composition signals

Signals of peat burning on atmospheric composition may not be able to be adequately detected because the total amounts of burning occurring in many of the regions are small. For example, across W Canada, maximum monthly estimated peat BA is 0.266 M ha (July 2014), but the monthly average is just 0.016 M ha or 160 km^2. Similarly, the monthly average estimated peat BA in Alaska is just 0.004 M ha (40km^2), with the month with the largest estimated peat BA across the whole dataset occurring in June 2015 with just 0.085 M ha, despite being ~50% of the annual total for 2015 in Alaska. In comparison, NW Siberia is the only region in which we see statistically significant negative correlations between estimated peat BA and the NO_2:CO ratio and has significantly larger estimated peat fire monthly and annual total BAs than any other region. For example, NW Siberia averages an annual estimated peat BA of 0.920 M ha, 0.3 M ha larger than the largest single year of estimated peat BA in W Canada. Furthermore, the smallest annual estimated peat BA in NW Siberia is 0.286 M ha, which is larger than the largest year in Alaska by 0.104 M ha. E Siberia shows consistently higher estimated peat BA than the North American regions, however these are still much smaller than NW Siberia, with an annual average of 0.233 M ha. However, in E Siberia there are significant positive correlations between estimated peat burning and TROPOMI CO, and negative, but non-significant, correlations with TROPOMI NO_2:CO. Therefore, these results suggest that the

overall amounts of estimated peat BA may determine whether a signal can be detected in atmospheric composition data.

Four estimated peat BA amount classes were used to examine the effects of total amounts of burning on correlations with atmospheric composition metrics. These classes were no peat burning, low peat BA (<0.005 M ha), medium peat BA (0.005-0.15 M ha) and high peat BA (>0.15 M ha), which contained 325, 217, 280 and 42 datapoints respectively.

In general, there are weak positive correlations between estimated peat BA in the three BA categories and CAMS NO_2 (Table 32; Figure 51a). The strongest, and only significant relationship with NO_2 is seen in the medium class ($r=0.283$, $p<0.001$). However, the relationship in the high peat BA class is of a similar magnitude, but not significant ($r=0.273$, $p=0.081$). In the low peat BA class, there is a weak non-significant negative correlation with CO ($r=-0.085$, $p=0.211$). But there are significant positive correlations between peat BA in the medium and high BA classes and CO (Figure 51, ($r=0.244$, $p<0.001$; $r=0.410$, $p=0.007$). When looking at the ratio between NO_2 and CO, we see a positive correlation between peat BA and NO_2:CO in the small BA category ($r=0.142$, $p=0.037$) and the medium BA category ($r=0.156$, $p=0.009$). However, this switches to a non-significant but negative relationship in the large category ($r=-0.151$, $p=0.339$) (Figure 51c).

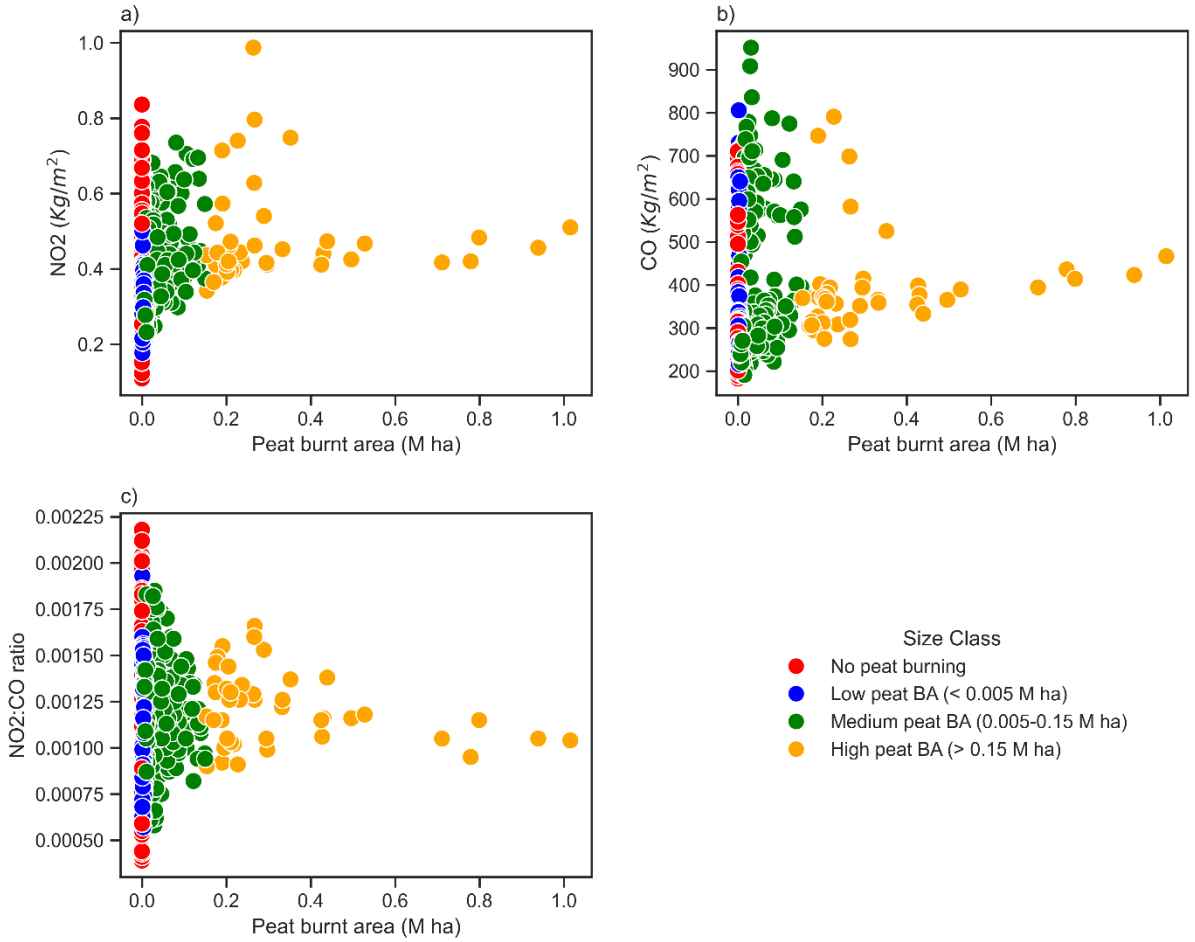


Figure 51: Correlations between peat BA and CAMS NO_2 (a), CO (b) and NO_2:CO (c), for all subregions, grouped by the total monthly BA amount categories. No peat burning contains 325 datapoints, small contains 217, medium 280 and large 42.

Table 32: Correlation coefficient (r) between peat BA and CAMS NO_2, CO and NO_2:CO, for all subregions, grouped by the total monthly BA amount categories. Small contains 217 datapoints, medium 280 and large 42.

BA amount class	CAMS NO_2	CAMS CO	CAMS NO_2:CO
Low (<0.005 M ha)	0.104	-0.085	0.142 *
Medium (0.005-0.15 M ha)	0.283 ***	0.244 ***	0.156 **
High (>0.15 M ha)	0.273	0.410 **	-0.151

Therefore, these results suggest that NO_2, increases with peat BA in all amount categories (though more so in the 'medium' and 'high' categories), but that CO may decrease - or have no relationship - with peat BA when the total peat BA is smaller than 0.005. Larger than this peat BA has a positive correlation with CO and gets stronger in the high BA category. Consequently, in the low and medium categories there is positive correlation between peat BA and NO_2:CO, suggesting that when peat BA is greater than 0.15 M ha this association switches to being negative, and therefore peat BA is associated with lower NO_2:CO ratios, as theoretically expected. From Fig. 21c, it appears that this relationship would be more prominently negative if we only looked at fires larger than 0.4 M ha, but this is not possible due to a smaller sample size. Therefore, it appears that there may be a threshold of

monthly BA of ~0.1 – 0.4 M ha needed to be crossed in order to see the effects of peat burning on atmospheric composition.

3.7. Disentangling the effects of peat fires and vegetation fires

It is likely that smouldering peat fires and flaming vegetation fires are occurring simultaneously. This means that flaming vegetation fires may potentially be masking the signal that can be detected by smouldering peat fires on atmospheric composition. GFED5 splits BA into 20 land cover types, the most prevalent in the high latitudes being boreal forest, sparse boreal forest and tundra. In W Canada, boreal forests account for on average 47% of the total BA, and on average 27% of BA occurs in sparse boreal forests (Table 33). Also, on average 95% of burning in Alaska and 86% in E Siberia happens in either boreal forests or sparse boreal forests (Table 33). In contrast, in NW Siberia, only 10% of burning on average occurs in boreal forests or sparse boreal forests, with the majority of burning in temperate mosaic (22%) and temperate grassland (30%) environments (Table 33). Burning in NW Siberia therefore occurs in very different vegetation types, which may also partly help to explain why there are different correlations of fire variables with NO_2 and CO, compared to other regions.

Table 33: Annual total BA and the relative percentages of peat fires and the 5 most commonly burnt land cover types in each of the 4 subregions, averaged over 2003-2020.

Region	Annual total BA	Peat BA %	Boreal forest BA %	Sparse boreal forest BA %	Tundra BA %	Temperate mosaic BA %	Temperate grassland BA %
Eastern Siberia	2.719	8.572	26.431	59.722	10.615	2.166	0.227
Northwest Siberia	15.428	5.964	4.184	5.945	1.325	22.202	29.524
Alaska	0.625	7.500	49.465	45.736	4.313	0.004	0.001
Western Canada	1.306	14.325	46.994	26.845	5.532	7.489	0.581

There are strong positive correlations of boreal forest, sparse boreal forest and tundra BA with NO_2 concentrations across E Siberia, Alaska and W Canada on an annual and monthly scale (Table 34). There are also positive correlations in NW Siberia for the yearly data, but these are much weaker and not significant (Table 34). However, on a monthly timescale in NW Siberia there are significant strong negative correlations between all land cover types and NO_2. In contrast to the other regions, on a yearly basis, NW Siberia sees significant positive correlations between CO and BA in all land cover types. However, on a monthly basis there are no relationships between BA and CO in all land cover types except for temperate grasslands which show a weak negative correlation. In the other regions, in general, on yearly scales these relationships are weaker and non-significant. But on a monthly basis, there are significant positive correlations between CO and BA in temperate mosaic and temperature grassland land cover types. Furthermore, on a monthly basis, there are significant negative correlations between CO and BA in boreal forests, sparse boreal forest and tundra environments in

Alaska. Similarly, in W Canada there are also significant negative correlations between CO and BA in sparse boreal forests and tundra, suggesting that on a monthly basis increased burning in these vegetation types is associated with lower atmospheric CO. There is the potential that lower atmospheric CO may occur during sunnier periods, despite being more conducive to wildfires, because of greater amounts of photolysis in the atmosphere, therefore leading to higher OH concentrations and consequently CO destruction (Atkinson, 2000; Lelieveld et al., 2016).

There are positive correlations between annual total BA and the NO_2:CO ratio in all regions and all land cover types expect temperate mosaic in eastern Canada and all land covers in NW Siberia. In NW Siberia there are relatively strong and statistically significant negative correlations between the NO_2:CO ratio and BA in tundra, temperature mosaic and temperate grassland, where the majority of burning occurs, suggesting that more smouldering combustion may be occurring. Similarly, on a monthly basis, there are significant strong positive correlations between NO_2:CO and BA in all landcover types in W Canada, and in boreal forests, sparse boreal forests and tundras in Alaska and E Siberia. Again, NW Siberia is considerably different to the other regions with strong negative correlations between monthly NO_2:CO and monthly BA in all land cover types.

In general, across all subregions there is a tendency for monthly BA in boreal forests, sparse boreal forests and tundras to exhibit either no relationship or a negative relationship with monthly CO, but a positive relationship with monthly NO_2, and consequently a positive relationship on the monthly NO_2:CO ratio. In contrast, with the exception of W Canada, temperate mosaic and temperate grassland vegetation BA shows negative correlations or no correlations with the NO_2:CO ratio. Furthermore, the significant negative relationships seen in these landcover types occur in NW Siberia where there are large amounts of burning in these vegetation types, potentially suggesting that burning in these environments tends to be more heavily dominated by smouldering combustion compared to boreal forest burning in other regions.

Table 34: Yearly and monthly correlations between the five most common land cover type BAs and the CAMS NO_2, CO and NO_2:CO ratio in the four different subregions. Asterisks indicate significant p values (* = $p<0.05$, **=$p<0.01$, ***=$p<0.001$)

Region	Land cover type	Yearly data			Monthly data		
		NO_2	CO	NO_2:CO	NO_2	CO	NO_2:CO
Eastern Siberia	Boreal forest	0.445	0.335	0.063	0.785 ***	0.065	0.595 ***
	Sparse boreal forest	0.614 **	0.176	0.286	0.796 ***	0.010	0.638 ***
	Tundra	0.606 **	0.344	0.197	0.774 ***	-0.044	0.642 ***
	Temperate mosaic	0.094	0.327	-0.166	0.422 ***	0.300 ***	0.168 *
	Temperate grassland	0.203	-0.428	0.517 *	0.350 ***	0.275 ***	0.093
Northwest Siberia	Boreal forest	0.185	0.719 **	-0.430	-0.479 ***	-0.024	-0.453 ***
	Sparse boreal	0.197	0.622 **	-0.276	-0.502 ***	-0.092	-0.430 ***

	forest						
	Tundra	0.193	0.835 ***	-0.505 *	-0.499 ***	-0.056	-0.445 ***
	Temperate mosaic	-0.082	0.478 *	-0.505 *	-0.368 ***	-0.083	-0.314 ***
	Temperate grassland	0.150	0.653 **	-0.484 *	-0.400 ***	-0.138 *	-0.309 ***
Alaska	Boreal forest	0.705 **	0.205	0.249	0.737 ***	-0.271 ***	0.713 ***
	Sparse boreal forest	0.635 **	0.123	0.261	0.692 ***	-0.211 **	0.650 ***
	Tundra	0.707 **	0.179	0.273	0.643 ***	-0.176 **	0.597 ***
	Temperate mosaic	0.499 *	0.021	0.295	0.038	0.034	0.034
	Temperate grassland	0.493 *	0.027	0.316	0.103	0.067	0.070
Western Canada	Boreal forest	0.416	-0.055	0.430	0.345 ***	-0.085	0.280 ***
	Sparse boreal forest	0.567 *	0.207	0.263	0.570 ***	-0.166 *	0.543 ***
	Tundra	0.672 **	0.020	0.478 *	0.623 ***	-0.165 *	0.578 ***
	Temperate mosaic	0.410	-0.003	0.265	0.444 ***	-0.054	0.400 ***
	Temperate grassland	0.420	-0.049	0.265	0.559 ***	-0.151 *	0.539 ***

There are however limited significant correlations between the annual percentage BA attributed to the various landcover types and the annual atmospheric composition of the four subregions (Table 35). There are negative correlations between the annual tundra BA percentage and NO_2 in all subregions, however none of these are significant. In line with this, there are also negative correlations between the annual tundra BA percentage and the NO_2:CO ratio in all regions expect NW Siberia. In E Siberia there is a significant negative correlation between the annual percentage of BA in temperate mosaic vegetation and NO_2. Concurrently, there is a significant negative correlation with the NO_2:CO ratio and percentage of BA in temperate mosaic vegetation in eastern Canada, suggesting higher proportions of burning in these landscapes is associated with lower ratios of NO_2:CO. However, in direct contrast to this, BA percentage in temperate mosaic and temperate grassland vegetation in Alaska is significantly positively correlated with NO_2, and positively, albeit not significantly, correlated with the NO_2:CO ratio (Table 35). This suggests that differences exist between the different regions, and the effect of vegetation burning on NO_2 and CO depends heavily on the region in which it is occurring.

On a monthly basis in E Siberia, much like the annual data, there are significant negative correlations between monthly percentage of BA in temperate mosaic and temperate grassland vegetation and the NO_2:CO ratio, alongside significant positive correlations with CO. A similar result can be seen in the temperate mosaic vegetation in NW Siberia and, albeit not significantly, in Alaska. In both E Siberia and W Canada there are significant positive correlations between BA percentage in sparse boreal

forests and NO_2, and the NO_2:CO ratio. In contrast in NW Siberia there are significant negative correlations between the percentage of BA in boreal forests and sparse boreal forests and NO_2 and the NO_2:CO ratio. Similarly, W Canada shows a strong negative correlation between monthly boreal forest BA percentage and NO_2 and the NO_2:CO ratio, as well as a positive correlation with CO. These correlations suggest that in W Canada and NW Siberia increased contributions from fires in boreal forests is associated with lower NO_2 and higher CO, and consequently a lower NO_2:CO ratio. Tundra-attributed BA percentages in NW Siberia and Alaska also exhibit negative correlations with both NO_2 and the NO_2:CO ratio.

Crucially there appear to be substantial differences in the direction of effects on atmospheric composition when looking at vegetation burning as a percentage of total burning, compared to absolute BA. For example, the BA data tends to show positive correlations with the NO_2:CO ratio in sparse boreal forests, but the opposite is true when looking at the vegetation percentage of BA. These discrepancies suggest that the interactions between BA in different vegetation types and their relative sizes to one another may be highly important to understanding the different atmospheric signals from fires.

Table 35: Yearly and monthly correlations between the five most common land cover type percentages of total BA and the CAMS NO_2, CO and NO_2:CO ratio in the four different subregions. Asterisks indicate significant p values (* = $p<0.05$, **=$p<0.01$, ***=$p<0.001$)

		Yearly data			Monthly data		
Region	Land cover type	NO_2	CO	NO_2:CO	NO_2	CO	NO_2:CO
Eastern Siberia	Boreal forest	-0.077	-0.026	-0.028	0.027	0.154	-0.130
	Sparse boreal forest	0.096	-0.061	0.075	0.292 ***	-0.103	0.311 ***
	Tundra	-0.379	0.404	-0.410	-0.047	-0.228 **	0.125
	Temperate mosaic	-0.655 **	-0.013	-0.472 *	-0.065	0.316 ***	-0.316 ***
	Temperate grassland	-0.075	-0.445	0.317	0.074	0.334 ***	-0.270 **
Northwest Siberia	Boreal forest	0.261	0.379	-0.022	-0.337 ***	0.168 *	-0.413 ***
	Sparse boreal forest	0.327	0.092	0.240	-0.382 ***	-0.064	-0.282 ***
	Tundra	-0.022	-0.185	0.232	-0.324 ***	-0.044	-0.236 **
	Temperate mosaic	-0.412	0.026	-0.335	-0.031	0.242 **	-0.188 *
	Temperate grassland	0.129	-0.245	0.185	-0.062	-0.324 ***	0.228 **
Alaska	Boreal forest	0.240	-0.022	0.261	0.049	-0.107	0.113
	Sparse boreal forest	0.053	0.044	-0.086	0.111	0.114	0.009
	Tundra	-0.395	-0.061	-0.195	-0.254 *	0.153	-0.262 **
	Temperate mosaic	0.496 *	0.004	0.320	-0.152	0.094	-0.135
	Temperate grassland	0.493 *	0.027	0.316	-0.018	0.174	-0.084

Western Canada	Boreal forest	-0.245	-0.117	0.005	-0.484 ***	0.202 **	-0.535 ***
	Sparse boreal forest	0.430	0.342	0.018	0.453 ***	-0.155 *	0.458 ***
	Tundra	-0.181	0.026	-0.160	0.090	-0.065	0.138 *
	Temperate mosaic	0.028	-0.125	0.030	0.092	0.058	0.070
	Temperate grassland	-0.106	-0.092	-0.137	0.130	-0.027	0.147 *

Overall, these results suggest that the signals from fires seen on atmospheric composition in NW Siberia may be being driven by substantially different types of vegetation burning in higher amounts compared to the other regions. The dominance of burning in temperate mosaic and temperate grassland vegetation in NW Siberia, is highly correlated with lower ratios of NO_2:CO, pointing towards smouldering combustion. Therefore, it is possible that belowground smouldering peat fires in these regions are occurring within these vegetation types and less of the actual vegetation is burning, leading to the lower NO_2:CO ratios. Burning in boreal forest vegetation types tends to be associated with higher NO_2:CO ratios. These results suggest that a greater amount of flaming combustion is occurring, and that any smouldering combustion is small and hard to detect within these vegetation types. Therefore, the effects of peat burning may be difficult to detect in regions that are heavily dominated by boreal forest vegetation such as Alaska and E Siberia.

3.8. Comparisons of INFERNO-peat to GFED5 estimated peat fires and their impacts on atmospheric composition

Modelled peat BA from INFERNO-peat (see Chapter 2 section 3) can be used to cross compare the peat fire BA estimated from GFED5 (and visa versa), providing more insights on the impacts of peat fires on atmospheric composition. It is important to note that INFERNO-peat only models a general expected peat BA and does not aim to capture actual fire events. Across E Siberia INFERNO-peat captures a similar amount of burning overall compared to GFED5-estimated peat BA (Figure 52a). On average, from 2003-2014 INFERNO-peat models 0.317 M ha per year compared to 0.218 M ha estimated from GFED5. However, some years have a larger mismatch. For example, INFERNO-peat models over ten-fold more BA than is estimated from GFED5 in 2004. The NO_2:CO ratio in 2004, is similar to the preceding and following year, despite GFED5 capturing more burning in these years than in 2004. Therefore, GFED5 in 2004 may be missing a significant amount of peat burning. From the modelled peat fire BA, 2003-2006 all have similar amounts of peat burning, which is reflected in the similar NO_2:CO ratios in these years (Table S4). Therefore, based on INFERNO-peat and the NO_2:CO ratios, this may suggest that in certain years the method used here for estimating peat fires from GFED5 is insufficient, or GFED5 itself is not detecting the peat burning that is happening in these years.

In NW Siberia, INFERNO-peat captures significantly greater annual peat BA compared to GFED5 estimated peat fires (Figure 52b). For example, over 2003-2014 INFERNO-peat captures seven times more peat BA than is estimated from GFED5. Relative to their respective multiannual means, the largest fire year occurs in 2012 in GFED5 compared to 2013 in INFERNO-peat. However, neither of these years sees an NO_2:CO ratio that is significantly above or below the multiannual average. Whilst still over 4 times larger than estimated from GFED5, peat BA modelled by INFERNO-peat in 2011 is significantly below the average, and this year is the only year in NW Siberia in which the NO_2:CO ratio is significantly higher than average, likely suggesting that the relative lack of peat burning in 2011 is driving the high NO_2:CO ratio.

Overall, INFERNO-peat tends to capture a similar amount of peat BA to what is estimated from GFED5 in Alaska (Figure 52c). Both data sources suggest that peat burning is uncommon in Alaska, and only occurs in small amounts. There are some large discrepancies between individual years such as 2004 and 2005. In 2004 and 2005, the ratio of NO_2:CO is relatively high with 2004 having the joint 3rd highest ratio and 2005 being above the average of 0.00086. During these years INFERNO-peat models 0.126 and 0.102 M ha less peat BA than GFED5 estimates. The high ratios in these years, combined with a lack of peat burning identified in INFERNO-peat may suggest that the GFED5 estimates may be over-estimating the amount of peat burning. Alternatively, 2004 and 2005 were significant overall fire years in Alaska, and the strong burning of vegetation in these years may be disrupting any signal from peat burning. The latter is likely more accurate as even in other large peat BA years such as 2009 and 2013, we still see elevated NO_2:CO ratios relative to the multiannual mean, suggesting that even in other years we cannot easily distinguish an atmospheric impact from peat fires.

In W Canada, INFERNO-peat captures almost 3 M ha more peat BA per year on average, suggesting either an overprediction of peat BA from INFERNO-peat, or an underestimation of peat BA from GFED5 (Figure 52d). However, there are no clear differences in terms of BA relative to their respective multiannual means between the two datasets, and no clear impacts on the NO_2:CO ratio.



Figure 52: Annual peat burnt area estimated from GFED5 (red) and modelled by INFERNO-peat (blue) for eastern Siberia (a), northwest Siberia (b), Alaska (c) and western Canada (d). Dashed lines show the multiannual mean.

Correlations between modelled peat BA from INFERNO-peat and the atmospheric composition data can be studied to investigate if there are effects that may be being missed in the GFED5 estimated peat BA data. Correlations between NO_2, CO and NO_2:CO from CAMS and modelled INFERNO-peat peat BA revealed very similar results to that of GFED5 in terms of their relationship with atmospheric composition metrics. Across all regions there were no significant correlations between INFERNO-peat modelled peat BA and neither NO_2, CO nor NO_2:CO at an annual scale (Table 36). On a monthly basis, INFERNO-peat modelled peat BA shows strong positive correlations with CAMS NO_2 and the NO_2:CO ratio in E Siberia (Table 36), similar to the correlations seen when using the GFED5 estimated peat BA. Similarly, W Canada also shows strong positive correlations between INFERNO-peat modelled peat BA and NO_2 and NO_2:CO, as well as a significant negative correlation with CO (Table 36), again reflecting the GFED5 estimated peat BA correlations, despite changes in the magnitudes of BA between the datasets. INFERNO-peat modelled peat BA is positively correlated with both NO_2 and CO in Alaska but exhibits no significant relationship with the NO_2:CO ratio (Table 36). This positive correlation with CO is not seen in the GFED5 analysis, and instead there is a significant negative correlation between GFED5 estimated peat BA and CO, as well as a significant

positive correlation with the NO_2:CO ratio. Finally, NW Siberia shows significant negative correlations between INFERNO-peat estimated peat BA and NO_2 and the NO_2:CO ratio (Table 36). These again are the same relationships as seen with the GFED5 estimated peat BA. Overall, apart from the correlation with CO in Alaska, INFERNO-peat peat BA has very similar impacts on atmospheric composition as the GFED5 peat BA, suggesting that these relationships may be reflective of the "real" impacts of peat fires on atmospheric composition in these regions.

Table 36: Correlation coefficients for both yearly and monthly timescales in the four different regions between INFERNO-peat modelled peat BA and NO_2, CO and the NO_2:CO ratio from the CAMS reanalysis dataset.

	Yearly data			Monthly data		
Region	NO_2	CO	NO_2:CO	NO_2	CO	NO_2:CO
Eastern Siberia	0.217	0.406	-0.021	0.732 ***	-0.140	0.687 ***
Northwest Siberia	-0.049	0.217	-0.007	-0.594 ***	-0.291 ***	-0.362 ***
Alaska	0.133	-0.081	0.147	0.264 **	0.261 **	0.131
Western Canada	0.042	0.217	-0.014	0.575 ***	-0.272 **	0.577 ***

4. Discussion

4.1. Trends in total and peat BA in the northern high latitudes

Fires are the dominant ecological disturbance in boreal regions (York et al., 2020; Nitze et al., 2018), and this chapter has shown that total BA varies greatly across the four regions of the high latitudes studied here, with each displaying significant interannual variability. The region with the lowest average annual burnt area is Alaska, with just 0.625 M ha burning each year. This is very close to the 0.767 M ha of burning estimated to occur in Alaska each year during the 2000s (Kasischke et al., 2010), suggesting that GFED5 is likely accurately capturing burning in Alaska. Despite having the smallest annual BA, Alaska displays the largest IAV in BA of all the regions studied, with a standard deviation of 0.756. Large fire years in Alaska are present in the GFED5 data in 2004 and 2005, which were the first and third largest BA years during 1956-2010 (Farukh and Hayasaka, 2012). Similarly, GFED5 accurately captures burning in 2009 and 2019 at 1.073 M ha and 1.092 M ha respectively, close to the 1.13 M ha and 1.05 M ha reported by the Alaska Interagency Coordination Centre (AICC 2009; AICC 2020). More BA is captured on average in western Canada, at 1.306 M ha per year, only 0.3 M ha short of that estimated by Coops et al. (2018). Western Canada comprises the majority of burning across the country, with an estimated 2 M ha of burnt area each year over the whole of Canada (Stocks et al., 2002). Large IAV is also present in western Canada (Coops et al., 2018), with notable large fire years identified in this chapter as 2004, 2014 and 2015, similar to what is reported in the literature (e.g. Coogan et al., 2019; Gaboriau et al., 2022).

GFED5 also reliably captures burnt area across Siberia. In northwest Siberia, an estimated 15.428 M ha burns each year, with substantial IAV. In contrast just 2.7 M ha burns each year in eastern Siberia, but with more IAV than in northwest Siberia. Across Siberia, fires are estimated to have burnt a total

of 200 M ha of land between 1999 and 2019 (Kharuk et al., 2021), averaging 10 M ha per year, considerably lower than the combined annual average BA from eastern and northwest Siberia in GFED5. However, when looking just at northeast Siberia, Garcia-Lazaro et al. (2018) estimates that 0.78 M ha burn each year, which is within the range estimated by GFED5 for the whole of Siberia. Similarly in the Sakha republic 1.7 M ha burn each year (Kirillina et al., 2020), which is well reflected in the GFED5 data. The GFED5 analysis presented in this paper identified 2003 as a notable large fire year in both Siberian regions, as identified by Talucci et al., (2022). In eastern Siberia, 2020 was also identified as a large fire year in the GFED5 data and was observed to be a large fire year in the Siberian Arctic (Descals et al., 2022). Therefore, quantities and variability in burning is being well captured by GFED5 compared to other observations.

Across the four regions of the northern high latitudes, there are also considerable amounts of peat burning estimated from GFED5 observational data, with peat fires contributing on average 7-14% of total BA each year. Western Canada has the largest estimated peat fire contributions, of 14.3% per year on average, equating to 0.187 M ha of peat BA each year. This figure is extremely close to that estimated by Turetsky et al. (2004) of 0.185 M ha of peat burnt area each year in western Canada. Consequently, it is likely that the methodology for extracting peat burnt area from GFED5 is doing an adequate job of representing observed peat BA in western Canada. BA is larger in both eastern and northwest Siberia, where each year 0.2 M ha and 0.9 M ha of peat burn annually. However, in eastern Siberia peat fires only account for 8.6% of total BA, and 6% of total BA in northwest Siberia. Alaska sees the smallest estimated peat BAs of 0.047 M ha per year on average, or 7.5% of total BA. These figures represent the first estimates of annual peat burnt area in each of these regions over 2003-2020. Whilst at present there are no similar peat fire burnt area datasets to compare to, these GFED5 estimated peat BA's fall within the range of what is calculated during specific fire seasons. For example, in 2020 it was estimated that in Arctic Siberia peat fires burned 0.71 M ha (Descals et al., 2022), within the range estimated here from GFED5 for two regions of Siberia. However, as mentioned in Chapter 2 section 8.1, it is likely that the methodologies used result in an overestimation of peat BA from GFED5 due to the assumption that BA is equally distributed among peat and non peat fires, despite known differences in the fire resilience between peatlands and other boreal ecosystems. Consequently, further analysis is required to assess the accuracy of peat BA calculations, and it is possible that maximum and minimum peat BA could be calculated in the future.

As noted throughout this chapter, there is large interannual variability in peat burnt area over the time period studied. Consequently, no clear trends over 2003-2020 can be identified, despite some visible indications that peat burning may be increasing. The large IAV also highlights the years in different regions which see more extreme fire seasons in terms of peat burning. In both Alaska and western Canada, large peat burnt areas occurred in 2004, burning 0.155 M ha in Alaska and 0.269 M ha in western Canada. However, these years also saw large overall burning, and consequently from GFED5

we estimate that only 5.48% of total BA is due to peat fires in Alaska in 2004, and only 9.95% in western Canada. However, according to Turquety et al. (2007), 17% of burned area in Alaska and western Canada in 2004 occurred on peatlands. Therefore, our peat fire estimates may be underrepresenting peat burning in 2004. Peat fires are responsible for large proportions of burnt areas in other years, such as in 2012 in western Canada where peat fires represent 25% of total BA. However, there is little evidence in the literature of large peat fires during this year.

Large IAV in peat fire BA is also evident across Siberia, with notable fire years including 2003, 2012 and 2020. 2012 was a record large fire year in northwest Siberia where 2.687 M ha of peat is estimated here to have burned, representing 10% of the annual total BA. 2012 is recognised to be a large fire year across the whole of Russia (Bondur et al., 2023), yet little research has been undertaken to quantify the peat fire contribution to this record year. Therefore, this Chapter presents the first work attempting to quantify peatland contributions towards total BA in 2012. In Eastern Siberia, 2003 was, at that time, the largest fire season on record (Talucci et al., 2022; Balzter et al., 2005), which is also found to be a large fire year in the GFED5 data. 2003 also saw a large amount of peat burning at 0.575 M ha, making up 10% of the annual total BA. However, this figure may be significantly underestimated as it is thought that across the entirety of Siberia 71% of the 2003 fires occurred on peatlands (Huang et al., 2009). Therefore, the methods used here to estimate peat BA from GFED5 may be insufficient at detecting peat fires in certain years.

Across all subregions, total BA and peat BA largely occurs during the summer months of June, July, and August. Supporting this, in northwest Canada, large wildfires have been found to predominately occur between the end of June and the middle of July (Gaboriau et al., 2022), explaining why GFED5 may see the bulk of BA occurring over the summer months. The only exception to this is in northwest Siberia, in which total BA only peaks in the early season in April/May, whereas peat burning peaks in both April/May and again in July. Human activity has been shown to supress wildfires and shift the peak in fire activity from summer to spring (Campos-Ruiz et al., 2018). Therefore, fires in northwest Siberia may be more effected by human activities, resulting in a spring peak in burning. For example, in the Sakha republic, Russia, spring burning has been shown to be associated with traditional agricultural burning (Kirillina et al., 2020). Consequently, it is evident that humans likely have a more influential role in determining the fire regimes in northeast Siberia. In addition, the fact that peat fires are also dominant in summer in northeast Siberia, suggests that these peat fires likely originate from natural sources and dominate summer burning in northeast Siberia.

It is evident that peat fires burn significant areas across all four regions of the northern high latitudes and contribute large amount of BA to the annual totals, but with significant interannual variability. Whilst there are some discrepancies between the estimated peat burnt areas presented in this chapter, and estimates of peat burning in specific years, this chapter presents the first attempt to quantify peat

burning from observations on a large scale across the high latitudes in the 21st century. This information may help to inform modelling efforts by providing a simplistic estimate of peat burning from observation-based datasets.

Consequently, GFED5 estimated peat BA was compared with modelled peat BA from INFERNO-peat. It is important to note that INFERNO-peat cannot be evaluated using the GFED5 estimated peat BA presented in this chapter, as it is just an estimate and, as mentioned in the preceding paragraphs, may not reflect true patterns of peat burning. The opposite is also true, INFERNO-peat is a model of potential peat burning in the high latitudes and cannot be said to reflect the true patterns and trends in peat fires. Therefore, whilst comparisons can be carried out, INFERNO-peat cannot be used to validate the estimations of peat BA from GFED5. Comparisons between the two products are still valuable as agreements, or disagreements, give indications as to how peat fires burn in the high latitudes. Results showed that both GFED5 and INFERNO-peat capture similar amounts of burning in eastern Siberia and Alaska, suggesting that there is a higher likelihood that both the model and peat fire estimates from GFED5 may be reflecting actual trends in peat fires. However, there are still notable mismatches in certain years. For example, in eastern Siberia in 2004, INFERNO-peat estimates a ten-fold higher peat BA than is estimated from GFED5. However, recent analysis has not revealed 2004 to be a large fire year in eastern Siberia (Natole et al., 2021; Talucci et al., 2022). But neither of these studies distinguished between peat and non peat burning, therefore, it is challenging to validate both INFERNO-peat and the GFED5 estimated peat burning. In both northwest Siberia and western Canada, INFERNO-peat captures much more peat BA than is estimated from GFED5. This large disparity indicates a poor understanding of peat fires in these regions, and the lack of other studies quantifying peat burning on these scales makes it challenging to identify the “true” state of peat burning in the northern high latitudes.

Large fire years are largely driven by temperature, whereby warmer than average temperatures tend to coincide with larger than average BA. This relationship was present across all regions. Numerous studies have highlighted the influence of high temperatures on extreme fire events across the northern high latitudes (Abatzoglou and Kolden, 2011; Bondur et al., 2023; Descals et al., 2022; Farukh and Hayasaka, 2012; Fazel-Rastgar and Sivakumar, 2022; Gaboriau et al., 2022; Kochtubajda et al., 2019; Konovalov et al., 2011; Ponomarev et al., 2016; Scholten et al., 2022; Talucci et al., 2022; Turetsky et al., 2004). Strong correlations between BA and temperatures have been demonstrated across Siberia (Talucci et al., 2022), and in the peatlands of western Canada (Turetsky et al., 2004), supporting the findings presented in this chapter. For example, I find that in western Canada in July 2014, over 1 M ha more BA than average occurred, coinciding with 1.8°C warmer than average temperatures, and these extreme fires in the Northwest Territories, Canada in 2014 have been shown to be caused by the presence of hot and dry weather (Kochtubajda et al., 2019).

High temperatures are not the sole drivers of extreme fire years. Drought conditions and low precipitation have also been shown to have an important influence on BA. For example, strong correlations between BA and drought indices were shown to occur in Siberian Larch forests (Ponomarev et al., 2016). It has also been shown that the 2004 Alaskan wildfires coincided with summer precipitation 38% of that of normal conditions (Shulski et al., 2005). Dry conditions can lead to lower fuel moisture levels and consequently, fuel moisture has also been shown to be a key driver of extreme wildfires in Canada (Gaboriau et al., 2022). Similarly, dry conditions induce plant water stress, which has been shown to have contributed to the extreme fires that occurred in Siberia in 2019 and 2020 (Descals et al., 2022). The presence of dry conditions in the weeks and months preceding a fire, has an important control on the dynamics of fuel accumulation and consequently the occurrence of extreme wildfires (Kuhn-Regnier et al., 2020). Dry conditions are particularly influential in driving extreme peat burning (Turetsky et al., 2004). For example, under moderate droughts, fire activity increases as much as 6-fold within peatlands (Thompson et al., 2019). Additionally, the timing of snow melt over the high latitudes has a major impact on the dynamics of a fire season, with earlier snow melt associated with longer fire seasons and increased BA (Gaboriau et al., 2022; Talucci et al., 2022). Consequently, it is highly important that antecedent weather and fuel conditions are considered for their effects on extreme fire events.

Another key driver of wildfire activity that was not considered in the analysis presented in this chapter is lightning. Fires in the northern high latitudes are primarily ignited by lighting (Stocks et al., 2002; Wendler et al., 2011; Hessilt et al., 2022), with 80% of large wildfires in Canada between 1959 and 1997, and 93% of fires in Alaska between 1955 and 2009 being ignited by lightning (Stocks et al., 2002; Wendler et al., 2011). Record numbers of lightning strikes have been shown to coincide with large fire years in the Northwest Territories, Canada, and Alaska (Veraverbeke et al., 2017). Consequently, it is estimated that lightning strikes can explain 55% of the interannual variability in BA (Veraverbeke et al., 2017). Therefore, it is likely that further analysis into what is driving large fire years in the GFED5 data would show a large influence from lightning activity. However, lightning activity is strongly correlated with temperature and precipitation (Veraverbeke et al., 2017), meaning that the correlations seen in this chapter between BA and temperature, may also be reflective of the increased number of lightning strikes that can coincide with warmer temperatures.

4.2. The impacts of fires on atmospheric composition in the high latitudes

Fires represent a major perturbation to the Arctic atmosphere, in terms of atmospheric composition, air quality and radiative forcing (Singh et al., 2010; Shindell et al., 2007; Langmann et al., 2009). Biomass burning has been shown to be the dominant driver of surface CO interannual variability in the Arctic (Monks et al., 2012). Consequently, this chapter explored potential relationships between total BA and peat BA with key components of the atmosphere: NO_2, CO and their ratio. It was

demonstrated that across the high latitudes' fires are significantly correlated with concentrations of NO_2 and CO in the atmosphere. On the whole, annual and monthly BAs were positively correlated with NO_2, suggesting that fires emit large quantities of NO_2 in the high latitudes. In northwest Siberia there are positive correlations with CO, however, these relationships are much weaker in the other regions. Consequently, total BA was shown on both annual and monthly scales to tend to be associated with higher ratios of NO_2:CO in Alaska, W Canada and E Siberia, indicating that fires emit relatively more NO_2 compared to CO. It has been shown that fires are responsible for 30-50% of global CO and 20% of global NO_x emissions (Olivier et al., 2005; Wiedinmyer et al., 2011), and it is evident that in the high latitudes' fires are having a large impact on the emissions of CO and NO_2. These results are supported by studies which have shown fires in Canada to be responsible for considerable percentages of annual greenhouse gas emissions, particularly in sparsely populated areas such as the Yukon territory (Lavoue and Stocks, 2011).

This chapter also examined the impacts of peat burning specifically on atmospheric composition, with the view to identifying differences in emissions of NO_2 and CO compared to vegetation fires. However, analysis has shown that large-scale impacts of peat fires are challenging to disentangle from that of vegetation burning. Often, in regions such as eastern Siberia, peat BA tends to exhibit the same relationships with NO_2, CO and NO_2:CO as total BA, indicating a minimal effect of peat fires. Similarly in Alaska, increased total BA is associated with increased NO_2 concentrations, regardless of whether peat is burning or not. Alaska experiences very small peat BAs, and therefore peat fires may be too small to exert a significant influence on atmospheric composition but could also indicate a strong masking of the peat fire signal from vegetation fires. However, there are some suggestions of an effect of peat fires on atmospheric composition in the data presented here, such as the negative (but non-significant) correlations between TROPOMI NO_2 and the NO_2:CO ratio with peat fire percentage of BA. Additionally, comparisons of specific years in which peat fires not only burn but are responsible for a large proportion of total BA, such as 2020 vs 2019, show that when peat fires occupy a larger percentage of total burnt area (Such as in 2020 relative to 2019), ratios of NO_2:CO are lower. Similarly, in western Canada there are suggestions of a distinguishable peat fire effect on atmospheric composition. For example, years such as 2004, 2012 and 2007 which all see relatively high peat burnt areas and percentage contributions of peat BA to total BA, tend to coincide with lower-than-average NO_2:CO ratios. This is what would be expected, as peat fires are dominated by smouldering combustion, which burns at a lower combustion efficiency resulting in higher emissions of CO relative to NO_2 (Andreae and Merlet, 2001; Rein et al., 2009; Andreae, 2019; van der Velde et al., 2021).

Unlike the other subregions, significant effects of peat fires on atmospheric composition are found in NW Siberia, where years and months with larger peat BAs and percentage contributions to total BA are associated with elevated CO and lower ratios of NO_2:CO. These results indicate that in NW

Siberia, peat fires result in higher emissions of CO compared to vegetation burning, which has major impacts on atmospheric composition. Smouldering combustion that dominates peat burning has been shown to produce high concentrations of CO (Akagi et al., 2011). For example, fires that burned predominately on peatlands in Siberia in 2003 contributed significantly to atmospheric concentrations of CO (Huang et al., 2009), and fires in Siberia in 2012 emitted approximately 48 Tg CO (Teakles et al., 2017). The reason why peat fires are shown to have the expected effects on atmospheric composition in northwest Siberia may stem from the fact that the amount of area burned by peat fires in this region tend to be significantly greater than the other regions.

Analysis of the effect of total amounts of peat BA on atmospheric composition revealed the presence of a threshold of monthly BA of ~0.1-0.4 M ha needed to be surpassed in order to see the effects of peat burning on atmospheric composition. Fundamentally, carbon emissions from peat fires are proportional to depth of burn and burnt area (Lin et al., 2021; Che Azmi et al., 2021; Hu et al., 2018), meaning that when only small areas of peat are burnt, the emissions are relatively lessened, and therefore a signal on atmospheric composition may not be detected. Whereas large total peat BA, results in greater emissions and consequently a greater perturbation to atmospheric composition. However, these results only indicate a tendency towards this pattern and therefore further research, encompassing more of the high latitudes is needed to fully examine the potential effects of the total amounts of BA on altering atmospheric composition.

Another potential cause of a lack of distinguishable peat fire effect on atmospheric composition in the northern high latitudes is the cooccurrence of flaming vegetation fires alongside smouldering peat fires, leading to mixed effects on atmospheric composition. Analysis revealed that the majority of BA in northwest Siberia is in temperate mosaic or grassland vegetation, which is highly correlated with lower ratios of NO_2:CO indicating that smouldering combustion dominates in these vegetation types. Across all other subregions on a monthly basis, all vegetation types, and in particular forests, are associated with higher NO_2:CO ratios, suggesting that a greater amount of flaming combustion is occurring, and that any smouldering combustion is small and hard to detect within these vegetation types. Therefore, the effects of peat burning may be difficult to detect in regions that are heavily dominated by boreal forest vegetation. Differences in emissions between different vegetation types in different regions is tied to the nutrient composition of the vegetation (Langmann et al., 2009; Andreae and Merlet, 2001). NO_x emissions from fires have been shown to be heavily dependent on the type of fuel and how much nitrogen it contains (Griffin et al., 2021; Andreae and Merlet, 2001). For example, on a global scale, savannas and croplands tend to have higher N content compared to forests and therefore fires in these environments tend to emit more NO_2 due to greater availability of N for oxidisation during combustion (Fu et al., 2018; Schreier et al., 2014). Following this, it is likely that the temperate mosaic or grassland vegetation in northwest Siberia may also be nitrogen limited, which would contribute to the lower emissions of NO_2 from fires in this region. Further analysis into the

composition of vegetation in each of the subregions is required to fully understand differences in fire emissions in different vegetation types in different regions.

A potential use case of the analysis presented in this chapter was the potential to be able to detect peat fires from ratios of NO_2:CO. Peat fires burn predominately by smouldering combustion which emits high quantities of CO relative to NO_2 as a result of incomplete combustion (Borsdorff et al., 2020). In contrast flaming fires burn at higher temperatures and with higher efficiency, leading to more effective oxidisation of N (Mebust and Cohen, 2014). Therefore, NO_2:CO ratios can be used as a proxy for combustion efficiency allowing for the differentiation between flaming and smouldering combustion (Andreae and Merlet, 2001; Rein et al., 2009; Andreae, 2019; van der Velde et al., 2021). Numerous studies have utilised NO_2:CO ratios to distinguish between flaming and smouldering combustion around the world (e.g. Lama et al., 2020; Hung et al., 2022; Wan et al., 2023; Peiro et al., 2022; Anderson et al., 2023; van der Velde et al., 2021). In general, fires in boreal regions of North America and Siberia tend to have lower NO_2:CO ratios compared to savanna fires (van der Velde et al., 2022; Wan et al., 2023), thought to be due to a dominance of smouldering combustion in the high latitudes (van der Velde et al., 2022). Furthermore, NO_2:CO ratios have been successfully used to track the progression of combustion from flaming to smouldering over the course of a wildfire (Anderson et al., 2023), and to differentiate between different fire types within a fire season in the United States (Hung et al., 2022). However, to date emissions ratios of NO_2:CO have not been used to attempt to distinguish between peat burning and non-peat burning in the high latitudes. The analysis presented in this chapter suggest that on broad timescales and on a regional basis TROPOMI is unlikely to be able to identify peat fires from the NO_2:CO ratios. The work carried out here has several limitations which may be affecting our ability to distinguish signals from peat burning, which will be discussed in more detail below. It is however possible that on smaller scales, looking at specific fire events, differences in emissions ratios may be detectable, but this is out of the scope of this thesis, and would have limited benefits from a global fire modelling perspective.

A key issue in trying to distinguish between peat and non peat burning, is that smouldering and flaming frequently occur simultaneously during fires (Akagi et al., 2011; Hu and Rein, 2022). It is possible that peat is burning through smouldering combustion, at the same time as a flaming fire on the vegetation above it, and therefore a mixture of low and high combustion efficiency species will be emitted. In addition, throughout the lifetime of a fire the combustion phase develops and tends to progress from more flaming to more smouldering (Anderson et al., 2023). Therefore, on a coarse temporal scale, like is used in this study, signals from smouldering and flaming may become entangled and result in being unable to distinguish specific smouldering signatures of burning.

Another source of error could be found in the relatively simplistic determination of peat BA. A map of peatland fraction is simply overlain over the map of BA, and it assumed that the amount of peat BA in

a grid cell is proportional to the amount of peat. However, in reality, within a grid cell fires may be occurring entirely within the peat, or not burning any peat at all. Also, because peat BA is estimated purely through the colocation of peat and BA, it does not necessarily mean that the peat itself is burning, and only the surface vegetation may be burning. The GFED5 data is on a 0.25° resolution grid, meaning that substantial sub grid cell variation may be occurring within this data. Consequently, a finer resolution satellite product may be able to better identify peatland fires, and even more so fire perimeter and peatland perimeter datasets would be beneficial for identifying high latitude peat fires. However, at present, GFED5 likely represents the best observations of fires due to its improved detection of small fires (Chen et al., 2023b), and therefore, these further refinements cannot be made until improvements are made to current fire inventories. On top of this, satellites struggle to detect peat fires and therefore, GFED5 may still be omitting a large number of peat fires, leading to underestimations of peatland BA. Consequently, being able to use measures of atmospheric composition such as NO_2 and CO to differentiate between peat and non peat burning presents an avenue for bypassing issues with fire observations. However, this chapter has shown that it is difficult to differentiate between peat and non peat burning in the high latitudes using the NO_2:CO ratios.

Difficulties in differentiating between the impacts of peat and non peat burning on atmospheric composition may also be a product of the timescales studied in this chapter. The coarsest time step used is a month, however NO_2 is a reactive gas, with its lifetime varying from hours to days (Fuglestvedt et al., 1999), due to reactions with OH that form O_3 (Fuglestvedt et al., 1999; Shindell et al., 2009). Whilst the lifetime of CO is longer, ranging from days to months (Minschwaner et al., 2010; Holloway et al., 2020; Martinez-Alonso et al., 2020), it is also reactive with OH producing CO_2 and O_3 (Minschwaner et al., 2010). Therefore, on a monthly time step emissions of NO_2 and CO from fires may not be as distinguishable as they would be if singular fire events were studied. This also raises issues when there are other notable sources of NO_2 and CO, which may mask the signal of fires on atmospheric concentrations of NO_2 and CO. Other than fires sources of NO_2 include lightning, soil microbial processes, traffic, and fossil fuel combustion (Cerosimo et al., 2020). In Canada the largest sources of CO also include transportation and the wood and aluminium industries (Government of Canada, 2013). Therefore, attributing NO_2 and CO emissions to wildfires on large spatial and temporal scales may not be possible.

Issues may also arise from errors and limitations in the atmospheric composition datasets, TROPOMI and CAMSRA, used. It has been shown that the presence of aerosols in dense smoke plumes, can strongly affect NO_2 retrieval from TROPOMI (Rowe et al., 2022), due to less photons being able to pass through the smoke plume and be reflected to the satellite sensor with higher aerosol optical depth, resulting in an underestimation in the NO_2 retrieval (Anderson et al., 2023). This is particularly important in the context of wildfires as trace gas retrievals over wildfires will almost always be affected by smoke (Griffin et al., 2021). Similarly cloud cover has been shown to strongly effect NO_2

and CO measurements in TROPOMI (Veefkind et al., 2012; Martinez-Alonso et al., 2020; Vidot et al., 2012). TROPOMI does utilise aerosol and cloud corrections (van Geffen et al., 2018), and the TROPOMI data used here has also been filtered to include only high-quality retrievals, therefore these effects should be minimised. Similarly, CAMSRA also has limitations that may affect the quality of data used in this chapter. For example, CO is known to be underestimated in the high latitudes compared to aircraft measurements (Inness et al., 2019). On the other hand, CAMSRA is thought to overestimate NO_2 emissions from boreal fires in summer (Wagner et al., 2021). This could have large implications on the results in this chapter, as an underestimation of CO and overestimation of NO_2 in the high latitudes may result in unrealistically high NO_2:CO ratios, leading to the assumption that signals from peat fires on atmospheric composition cannot be detected in the high latitudes.

As there are no clear differentiating signals from peat compared to non-peat fires in the high latitudes, future work could potentially explore using alternative trace gas measurements. For example, Lutsch et al., (2020) showed the ability to detect wildfires in the Arctic from anomalously high CO which coincided with high HCN and ethane concentrations. However, this study did not consider the identification of peat fires separate to that of general wildfires. But there is evidence to suggest that more HCN is strongly emitted from peat fires, particularly when the peat is wet (Hu et al., 2019b). Additionally, smouldering peat fires have been shown to emit 10 times higher emissions factors for HCN than flaming savanna fires (Hu et al., 2018), suggesting that perhaps anomalously high HCN concentrations could indicate the presence of smouldering peat fires. Alternative emissions ratios such as CO_2:CO, have been shown to be capable of differentiating between flaming and smouldering combustion (Andreae, 2019; Urbanski, 2014; Stockwell et al., 2016; Rein, 2015). However, the ratio of CO_2 to CH_4 has been recently identified as the best signature of smouldering peat, with emissions ratios being in excess of 500% lower in peat fires compared to savanna and grassland fires (Hu and Rein, 2022). Crucially, the ratio of CO_2:CH_4 has also been shown to be significantly lower in a purely smouldering peat fire compared to forest fires and mixed burning peat fires (Hu and Rein, 2022). Therefore, this ratio may help to eliminate some of the sources of error seen in this chapter, as clear peat fire signals should be distinguishable from other vegetation types. Furthermore, CO_2:CH_4 ratios are thought to be independent from fuel composition (Hu and Rein, 2022), and consequently the effects demonstrated in this chapter of different vegetation types on the NO_2:CO ratio would be eliminated by studying CO_2:CH_4 instead. CAMS greenhouse gas global reanalysis (Ramonet et al., 2021) contains data on both CO_2 and CH_4, from 2003 to 2020 which could be used in the future to study the effects of peat fires on atmospheric composition, and potentially lead to developments in identifying peat burning from perturbations to atmospheric composition.

4.3. The impacts of fires on air quality across the northern high latitudes

Biomass burning is a major source of aerosols, including black carbon and organic carbon, worldwide (Andreae, 2019; Andreae and Rosenfeld, 2008). Peat fires have been shown to release significant amounts of pollutants such as $PM_{2.5}$ (Black et al., 2016), and in the high latitudes wildfires emit more $PM_{2.5}$ than all anthropogenic sectors combined (McCarty et al., 2021). All regions studied in this chapter show significant positive correlations between fires and peat fires with $PM_{2.5}$ concentrations. For example, wildfires in Alaska and western Canada in the summer of 2004 resulted in a factor of 8 larger than normal enhancements in $PM_{2.5}$ (Mathur, 2008). Similarly, in the GFED5 data 2004 is a notable fire year in both Alaska and western Canada, which coincides with the highest annual average $PM_{2.5}$ recorded by CAMSRA in Alaska, and the second highest $PM_{2.5}$ recorded by CAMSRA in western Canada. However, the relationship between peat fire percentage of total BA and $PM_{2.5}$ was shown to vary across the regions. In northwest Siberia and western Canada, peat fire percentage of total BA is strongly correlated with $PM_{2.5}$, suggesting that peat fires may emit more $PM_{2.5}$ than flaming fires, as time steps with higher peat fire contributions are associated with higher $PM_{2.5}$ concentrations. In contrast, there is less of an effect of peat fire percentage of total BA on $PM_{2.5}$ in eastern Siberia and Alaska, suggesting that there is no difference between peat and non peat burning in terms of impacts on $PM_{2.5}$ in these regions.

Although all subregions show that peat fires influence atmospheric $PM_{2.5}$ concentrations, the minimal correlations between peat fire percentage of total BA and $PM_{2.5,}$ except in northwest Siberia, make being able to differentiate between peat and non peat burning difficult. In theory particulate emissions should be greater during smouldering combustion compared to flaming (Hardy et al., 2001), and consequently peat fires should have a larger effect on $PM_{2.5}$ concentrations. Therefore, further work is needed to disentangle the effects of peat fires on air quality in the high latitudes.

One such avenue is through the different components of $PM_{2.5}$ released during flaming and smouldering combustion. Peat fires, and smouldering combustion, have been shown to emit substantial amounts of OC and negligible amounts of BC (Fujii et al., 2014; Che et al., 2022; Conny and Slater, 2002; Hu et al., 2018; Kondo et al., 2011; Yokelson et al., 2011). OC is strongly emitted, and BC weakly emitted during smouldering peat fires due to lower combustion efficiencies compared to flaming fires (Yokelson et al., 2011; Che et al., 2022; Christian et al., 2003). For example, in western Russia, OC makes up over 90% of total carbon aerosols from peat fires (Popovicheva et al., 2019). Whereas, in smouldering peat fires in boreal North America and Siberia, only 1-5% of total aerosol mass is from BC (Kondo et al., 2011). In contrast, flaming fires release up to 10 times more BC than smouldering fires (Conny and Slater, 2002). Therefore, relative contributions of BC and OC could be used to better differentiate between peat and non peat burning. However, BC is still present

in small amounts in peat fire emissions, and if flaming combustion occurs within the peat or alongside it, BC can account for 92% of aerosol emissions (Hu et al., 2019b).

Understanding the effects of fires on atmospheric concentrations of $PM_{2.5}$ is crucial due to the detrimental effects they have on air quality and consequently human health. In Canada and Siberia fires are the main source of air pollution induced health burdens (Lelieveld et al., 2015), with $PM_{2.5}$ resulting in human respiratory and cardiovascular disease, and ultimately raises mortality risks (Dockery et al., 1993; Pope et al., 2003; Brook et al., 2010). The impacts of $PM_{2.5}$ emissions from fires are so great that they have been attributed to as many as 50,000 premature deaths across the Arctic over the last 20 years (Silver et al., 2023). Additionally, the release of aerosols from Siberian fires has been shown to result in six-fold increases in aerosol optical depth, exerting a net cooling effect on the atmosphere (Zhuravleva et al., 2017, Jeong et al., 2008). For example, top of atmosphere cooling was found to occur in the summer of 2004 in Alaska, as a result of the scattering of radiation on organic aerosols emitted from fires (Pfister et al., 2008). However, brown carbon (BrC) emitted from peat fires in Alaska and Siberia (Chakrabarty et al., 2016), has been shown to have a positive radiative forcing of as much as 17 W m^{-2} due to its light absorbing nature (Oris et al., 2014; Randerson et al., 2006; Chakrabarty et al., 2016). Additionally, the deposition of BC from fires onto glaciers, snow and sea ice can reduce surface albedo, leading to atmospheric warming and enhanced surface melting (Randerson et al., 2006; Thomas et al., 2017). Consequently, it is important that the effects of fires, and peat fires, on atmospheric aerosol concentrations are understood, in order to accurately incorporate these emissions into global fire models and allow for impacts on human health and radiative forcing to be assessed.

4.4. Conclusion

In conclusion, this chapter has highlighted the substantial interannual variability in BA from peat and vegetation fires across the northern high latitudes and presents the first estimates of northern high latitude peat fire BA from the GFED5 observational dataset. However, analysis has highlighted the difficulties in differentiating between peat and non peat fires in terms of their impacts on atmospheric composition and air quality. There is a tendency for peat fires to impact atmospheric composition and air quality in much the same way as wildfires in general, through increased $PM_{2.5}$ and NO_2 concentrations. However, peat fires, due to the presence of incomplete smouldering combustion should release substantially more CO and $PM_{2.5}$ and less NO_2 than flaming vegetation fires (Andreae and Merlet, 2001; Rein et al., 2009; Andreae, 2019; van der Velde et al., 2021). However, this result was only found in northwest Siberia, where peat BA was strongly negatively correlated with NO_2:CO ratios. However, as evidenced throughout this chapter, wildfires across the northern high latitudes, regardless of whether peat burning is occurring, likely undergo a degree of smouldering combustion, with smouldering and flaming often occurring simultaneously, and the composition of the vegetation

having a large impact on trace gas emissions, meaning that differentiating between the impacts of peat and non peat burning on atmospheric composition at broad spatial and temporal scales is challenging. There is the potential that if alternative emissions ratios, that are more independent of fuel composition, such as CO_2:CH_4 (Hu and Rein, 2022), are studied then peat fires may be found to have a distinguishable impact on atmospheric composition compared to flaming vegetation fires.

It is critically important that further research is carried out on assessing the impacts of peat fires on atmospheric composition due to climate change driving increases in the frequency, severity and extent of peat fires (McCarty et al., 2021; Turetsky et al., 2015; Nelson et al., 2021; Thompson et al., 2019; Li et al., 2021), which may result in large trace gas emissions which could have a positive feedback effect on the climate system (Mack et al., 2011; Chen et al., 2021a; Turetsky et al., 2015; Nelson et al., 2021). Consequently, it would be imperative that this knowledge is assimilated into global fire models to improve estimations of future changes to atmospheric composition with climate change. Furthermore, understanding the impacts that peat fires have on air quality across the high latitudes is also crucial in quantifying the potential peat fire impacts on the health of populations across the high latitudes, both at present and into the future. Finally, if clearly distinguishable signals from peat fires can be detected in atmospheric composition or air quality data, this could be used to aid in the detection of peat fires across the high latitudes, allowing for improved observation-based datasets of peat fires for fire model evaluation.

Chapter 5: Modelling future changes to peat fires using INFERNO-peat under differing climate change scenarios

Abstract

The northern high latitudes are witnessing rapid anthropogenically-induced climate change, with substantial warming, altered precipitation patterns and environmental degradation already seen across the region. The frequency, extent and severity of wildfires and peat fires have increased in the past decades and are anticipated to increase in the future. However, peat fires have commonly been excluded from fire models and consequently future projections of fires in the high latitudes may be missing large sources of burning and carbon emissions. Consequently, the recently developed INFERNO-peat model of northern high latitude peat fires was used to simulate potential future trajectories of change under multiple climate change scenarios. Here I show that peat fires and their emissions are expected to increase over the 21st century under all climate change scenarios. The largest changes are seen under the highest emissions scenario, under which annual peat fire carbon emissions are projected to exceed 1 Gt C by 2100, alongside a 270% increase in annual peat burnt area. These changes are driven by climate change induced warming which influences evapotranspiration, soil moisture, water table depths, fuel loads and fuel flammabilities, ultimately increasing the number of peat fire ignitions, the probability of those peatlands igniting, peat burnt area and carbon emissions. The losses of carbon projected by INFERNO-peat would have vast implications for the peatland carbon store, and risks switching peatlands to sources of carbon which would exert a positive feedback effect on the climate system, with major implications on the future of these crucial northern high latitude ecosystems. However, the benefits of following a trajectory like that of SSP126 (the lowest emissions scenario used in this chapter) is highlighted for its potential to limit climate change induced increases in peat burnt area, halving the amount of potential carbon emissions from peat fires at the end of the century compared to the highest emission scenario.

1. Introduction

Chapter 3 has demonstrated the effectiveness of including a representation of northern high latitude peat fires within a fire model, and in particular has highlighted the capabilities of INFERNO-peat to reproduce present-day observed patterns of burning across the high latitudes. Furthermore, explicit representation of peat fires in INFERNO-peat also led to improved abilities to model the interannual variability in carbon emissions from fires across the high latitudes. Consequently, as INFERNO-peat can accurately reproduce present day burning, it provides the unique opportunity to simulate future changes to peat fires in the northern high latitudes as a result of climate change.

The northern high latitudes are undergoing rapid anthropogenically-induced climate and environmental change, with the Arctic experiencing substantial warming since the mid 20th century

(IPCC, 2013). Since 1979, the high latitudes, north of 60°N, have warmed on average at a rate of 0.5°C per decade (IPCC, 2013). However, these temperature rises are not equal across the high latitudes. For example, temperatures across Scandinavia, Europe, Eastern Siberia and Alaska have risen by 0.5-1.5°C between 1916 and 2007, whereas in Canada, temperatures have increased by 2°C between 1976 and 2007 alone (Panin et al., 2009). Warming in the Arctic is happening at an unprecedented rate, approximately twice that of the global average (Winton, 2006; Meredith et al., 2019), a phenomenon known as Arctic Amplification (Serreze and Barry, 2011). More recent studies have estimated that over the last 43 years temperatures in the Arctic may have increased at a rate of 0.73°C per decade, almost four times faster than the global average (Rantanen et al., 2022). Arctic Amplification occurs as a result of albedo feedback effects that occur when snow and ice cover melts, exposing darker surfaces which absorb solar radiation, leading to further warming (Serreze and Barry, 2011; IPCC, 2013; Koenigk et al., 2020). Additionally, Arctic Amplification is influenced by changes in sea ice extent, which alter heat fluxes and transport between and within the atmosphere and oceans, alterations to cloud cover and water vapor as well as changes to aerosols including black carbon (Serreze and Barry, 2011; IPCC, 2013; Koenigk et al., 2020).

Climate change has resulted in record warm temperature across the high latitudes in recent years, with the 8 warmest years on record in the Arctic all having occurred since 2016 (Ballinger et al., 2023), and with 2023 recording the warmest summer Arctic temperature on record (Thoman et al., 2023). Additionally, evidence for the occurrence of extreme warm events appears to be increasing (Walsh et al., 2020), with particularly strong warming occurring over winter (Koenigk et al., 2015). Throughout the remainder of the 21st century, temperatures in the high latitudes are projected to continue to rise alongside strengthening of Arctic Amplification, particularly in winter (Serreze and Barry, 2011; Koenigk et al., 2020; Koenigk et al., 2015; IPCC, 2013). For example, following RCP8.5, temperature increases of up to 15°C may occur over parts of the Arctic during autumn and winter in 2080-2099 compared to 1980-1999 (Koenigk et al., 2015).

Rising temperatures and climatic change in the high latitudes is also intensifying the hydrological cycle in the northern high latitudes (Bintanja, 2018; McCrystall et al., 2021), primarily through increased precipitation (Box et al., 2021, IPCC, 2013; Biglake and Walsh, 2022). Arctic precipitation, in general, increases linearly with Arctic temperature change (Koenigk et al., 2015; Ye et al., 2021), because changes in precipitation are driven largely by thermodynamic processes (Yu and Zhong, 2021). Furthermore, expanding open water areas created via sea ice loss enhances evaporation, which, alongside poleward moisture transport, also increases precipitation in the high latitudes (McCrystall et al., 2021; Bintanja, 2018; Bintanja and Selten, 2014; Zhang et al., 2013). However, there is strong regional and seasonal variability in changes in precipitation (Walsh et al., 2023; Ye et al., 2021; Yu and Zhong, 2021). By the end of the century, an increase in precipitation of more than 50% is expected in the Arctic (IPCC, 2013; Bintanja and Selten, 2014). Increases are expected to be largest in

areas where sea ice disappears, highlighting the importance of increased evaporation for precipitation changes (Koenigk et al., 2020). In addition to the overall increase in precipitation, the Arctic is expected to shift from snow-dominated to rain-dominated precipitation, with a decrease in the snowfall ratio from 0.7 at the start of the century to 0.3 at the end of it (McCrystall et al., 2021). Furthermore, snow extent has declined over the northern hemisphere between 1981 and 2018 (Mudryk et al., 2020). With climatic change, there is expected to be an 8% reduction in snow cover relative to the 1995-2014 average for every 1°C of surface air temperature increase (Mudryk et al., 2020), resulting in reductions in snow cover over the majority of land area north of 55°N (Biglake and Walsh, 2022). However, there is strong regional variability in snowfall patterns, as a result of the opposing effects of warming and increased precipitation (Biglake and Walsh, 2022). For example, mild regions such as southern Alaska and Europe experience decreases in snowfall, whereas colder regions such as boreal northern Alaska and Canada and Siberia see increased snowfall (Biglake and Walsh, 2022; McCrystall et al., 2021) due to increased atmospheric water vapour with warming, but with the maintenance of sub-zero temperatures over much of the winter months, allowing for precipitation to fall as snow (Biglake and Walsh, 2022). Despite the overall increase in precipitation across much of the high latitudes, periods of dry weather and droughts are still prevalent, with notable droughts occurring in recent years such as in Fennoscandia in 2018, western Canada in 2015 and SE Alaska in 2018 and 2019 (Walsh et al., 2020).

Climate change is also increasing the likelihood of conditions that are inducive to wildfires, through rising temperatures, droughts and fire weather (Thompson et al., 2019; Descals et al., 2022; Lund et al., 2023). Already, across Canada, burnt area has increased 11% per year from 2006 to 2015 (Coops et al., 2018). Similarly, increases of 1.28 million ha/decade in burnt area have occurred over the last 40 years in northeast Siberia (Garcia-Lazaro et al., 2018). Furthermore, Siberian larch forests have seen increases in BA since 1996, which are strongly correlated with increasing temperatures and drought indicators (Ponomarev et al., 2016). 2023 was a notably extreme wildfire season in Canada, the severity of which was made 7 times more likely and 50% more intense due to climate change (Barnes et al., 2023). By October 2023, wildfires had burned 4.61 million hectares in North America mostly in the Northwest Territories of Canada - the largest area burned in Canada's 44-year record (Thoman et al., 2023). Large fire years have primarily been driven by prolonged periods of record breaking warm and dry weather (Abatzoglou and Kolden, 2011; Kirchmeier-Young et al., 2019; Coogan et al., 2019). For example, droughts across Alberta Canada resulted in 880,000 ha of burning in the spring of 2019 (MNP LP, 2020). High temperatures increase the atmospheric water demand, which in turn results in decreases in soil moisture, resulting in the increased probability of wildfires occurring (Madani et al., 2021). Furthermore, warmer temperature in the high latitudes can also cause a weaking of the polar front jet stream (Coogan et al., 2019; Walsh et al., 2020), allowing for large stationary anticyclones to develop, consequently leading to extreme weather and wildfire events

(Coogan et al., 2019; Bondur et al., 2023). Therefore, under a changing high latitude climate, wildfires are expected to increase due in part to rising temperatures and extreme heat events.

Climate change is expected to result in more frequent and intense fires over the next century in the northern high latitudes (UNEP, 2022b; de Groot et al., 2013; Moritz et al., 2012). In the Siberian Arctic, rising temperatures may result in substantial increases in burnt area, with fires expected to burn 2.5 million hectares and release 37.8 Tg of C each year by 2050 (Descals et al., 2022). Similarly, in Alaska, a doubling of burnt area is expected by 2100 (Hu et al., 2015), and shorter fire return intervals are predicted across much of the boreal forests (Li et al., 2021). Furthermore, Young et al. (2017) modelled a significant increase in fire probability in Alaskan boreal forest and tundra ecosystems above a July temperature of 13.4°C, with some regions displaying a fourfold increase in the 30-year probability of wildfires by 2100. In addition, carbon emissions from wildfires in the northern high latitudes are expected to increase (Kloster and Lasslop, 2017).

Climate change is also altering the vulnerability of peatlands to wildfires. In recent years there has been a notable increase in fire activity in peatlands in the high latitudes (McCarty et al., 2021) as peatlands have become more vulnerable to wildfires (York et al., 2020; Talucci et al., 2022). In the high latitudes, rising temperatures lead to higher levels of evapotranspiration, resulting in drier peat and deeper water tables (Helbig et al., 2020; Tarnocai, 2009). Not only does drying of peat lead to an increased vulnerability to fires but it also leads to large losses of carbon. Warming of 4°C in the high latitudes has been shown to result in a 40-86% loss of soil organic carbon from northern high latitude peat, as a result of warming induced increases in decomposition rates (Ise et al., 2008). Degraded peatlands are more vulnerable to wildfires and consequently in recent years there have been notable peat fire events. For example, 0.71 million hectares of Siberian peatland burnt in 2020 alone (Descals et al., 2022). Consequently, rising temperatures, increased fire ignitions and fire events and peatland vulnerability, result in an expected increase in peat fire frequency and severity in the high latitudes (McCarty et al., 2021; Turetsky et al., 2015; Nelson et al., 2021). It is estimated that if current burning trends were to continue, there could be a reduction in the peatland carbon sink by 57% by 2050 (Wilkinson et al., 2023), therefore highlighting the importance of understanding potential future changes to peat fires for the carbon cycle.

Climate change induced changes to peat fires have numerous potential impacts on the climate system, air quality and the carbon cycle. Peat fires emit a range of greenhouse gases including CO_2, CH_4, and CO, alongside aerosols, which can alter atmospheric composition and degrade air quality (Hu et al., 2019a; Voulgarakis and Field, 2015). Reductions in air quality lead to considerable health burdens in the northern high latitudes (Lelieveld et al., 2015). The emission of aerosols from peat fires also have direct and indirect effects on radiative forcing, and consequently the climate system. For example, the deposition of black carbon from fires over snow and ice lower surface albedo, leading to atmospheric

warming and enhanced surface melting (Randerson et al., 2006). However, the emission of light scattering aerosols, such as sulphate and organic carbon, from Siberian fires have been shown to result in increased aerosol optical depth, and a net cooling effect on the atmosphere (Zhuravleva et al., 2017, Jeong et al., 2008). Aerosols can also act as cloud condensation nuclei and alter microphysical properties of clouds, which not only can result in changes in temperature but can also lead to altered precipitation patterns (Richardson et al., 2018; Jiang et al., 2020; Tian et al., 2022). Therefore, increased frequency and severity of peat fires as a result of climate change, may result in an exacerbated health impact of wildfires in the northern high latitudes, alongside further climatic changes induced by aerosol emissions.

Climate change risks switching peatlands from fire resistant to fire prone systems (Turetsky et al., 2015), with substantial net losses of long-term stored carbon to the atmosphere (Lasslop et al., 2019). Consequently, increases in peat fire occurrence and severity leads to greater carbon emissions and may create a positive feedback loop with the climate system, resulting in a catastrophic loss of carbon from the high latitudes (Mack et al., 2011; Chen et al., 2021a; Turetsky et al., 2015; Nelson et al., 2021). However, despite these major potential impacts of peat fires in the future, currently no study so far has attempted to model the potential future changes of peat fires in the high latitudes, nor examined their impacts. INFERNO-peat represents the second global fire model to incorporate a peat fire parameterisation, which can be utilised for the first simulations of change to future peat fire burnt area and carbon emissions in the northern high latitudes with climatic change. Therefore, this chapter will explore the use of INFERNO-peat to simulate future peat fires, focusing on changes to burnt area, depth of burn and carbon emissions over the 21st century.

2. Methods

INFERNO-peat, which is described in detail in Chapter 2 Section 3, was used here to simulate future changes to peat fires in JULES ISIMIP3b simulations over the 21st century, under differing scenarios of change. INFERNO-peat was run from 2015 to 2100 under three different socio-economic and climate change scenarios; SSP126, SSP370 and SSP585. For further information on the SSP scenarios see Chapter 2 Section 5.1.

JULES-INFERNO model outputs of PFT fractions and flammabilities, soil moisture, soil temperature and water table depth, which follow the ISIMIP3b fire protocol, were used to drive INFERNO-peat alongside data from the Northern Peatland Dataset on peatland fractions and carbon content. UKESM 1-0-LL bias adjusted climate driving data (Lange et al., 2021) was used in the JULES-INFERNO simulations used in this analysis. Ignitions are calculated using population density (HYDE: Hurtt et al., 2011) and lightning (LIS-OTD; Christian et al., 2003) data. However, due to a lack of available and verified datasets at the time of analysis, static climatology's were used for both of these datasets,

and therefore no changes in lightning with climate change, or population density over time are considered. For more details on the driving data used please see Chapter 2 Section 5.2. INFERNO-peat was run using a 0.5° resolution on monthly time steps for above 50°N latitude only.

In order to assess future changes to peat fires, peat burnt area, depth of burn and carbon emissions were analysed from INFERNO-peat under the three scenarios. Temporal trends were examined for peat BA, depth of burn and C emissions. Changes in grid cell peat BA, depth of burn and C emissions between the present-day (2015-2025 average) and end-of-century (2090-2100 average) were also examined to get an impression of the changes in peat fires in different areas of the high latitudes. For each of these three variables, decadal averages, standard deviations and coefficients of variation were also calculated, in order to assess changes in mean annual metrics over time, as well as to assess potential interannual variability changes. Four subregions which see substantial changes in the data were selected (Figure 53), in order to assess any differences in changes in burnt area seen in different regions.

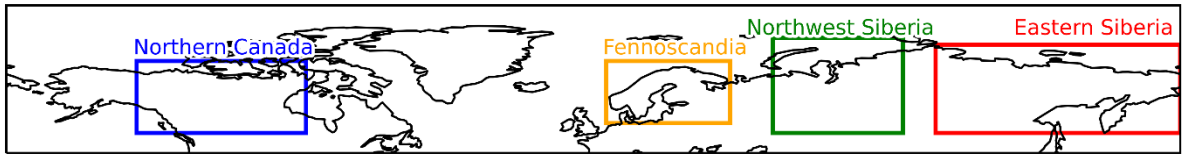


Figure 53: The location of the four subregions used to identify differences in changes in burnt area: northern Canada ((140°W, 51°N), (88°W, 73°N)), Fennoscandia ((4°E, 54°N), (42°E, 73°N)), northwest Siberia ((55°E, 51°N), (95°E, 80°N)) and eastern Siberia ((105°E, 51°N), (180°E, 78°N)).

As in this chapter I am simulating potential future changes to high latitude peat fires, the model output, after present day, cannot be evaluated or compared against observational data. As such, all variance that is occurring within BA, depth of burn and C emissions calculated in INFERNO-peat should be explained by the model's driving variables. The climate data driving INFERNO-peat has been bias-adjusted and therefore there should be minimal biases within this data (Lange et al., 2021). Therefore, the drivers of each of the calculated peat fire metrics will also be examined. Correlations, using Pearson's R were conducted between all driving variables and their respective peat fire metric. Details of the different driving variables are explained below and in Table 37.

Peat burnt area is estimated from calculated peat fire ignitions, and the probability of ignition of the peat (Equation 9). In turn, peat fire ignitions are calculated through known relationships between lightning and population density with ignition events, and the fuel loads and flammabilities of different PFTs (above-ground vegetation) as modelled by JULES. As static datasets are used for lightning and population density, PFT fractions and PFT flammabilities will be examined for their effects on peat fire ignitions. In turn, the effects of temperature and precipitation on PFT fractions and flammabilities will also be examined. Peat ignition probability is driven by inorganic content, bulk density and soil moisture, but due to fixed values being used in this model run for the former two

variables, soil moisture is the sole driving factor for peat ignition probability. Drivers of soil moisture will also be examined, including climatic and hydrological variables. Depth of burn is calculated using soil moisture, water table depth and soil temperatures (Chapter 2, Section 3.4). Therefore, correlations between depth of burn and soil moisture, soil temperature and water table depth were also carried out. Lastly, peat fire carbon emissions are directly a result of peat burnt area, depth of burn and the carbon content of peat. As a static dataset is used for peatland carbon content, peat fire carbon emissions are being solely driven by BA and depth of burn, and indirectly through the respective drivers of those two variables.

Table 37: INFERNO-peat driving variables used to assess trends and changes seen in the future peat fire simulations, their sources and what variables they drive.

Variable	Units	Source	What is it driving?
Temperature	°C	UKESM 1-0-LL	PFT fraction, PFT flammability, soil moisture
Precipitation	Kg m^{-2} s^{-1}	UKESM 1-0-LL	PFT fraction, PFT flammability, soil moisture
PFT fraction	0-1	ISIMIP3b JULES	Peat fire ignitions, soil moisture
PFT flammability	0-1	ISIMIP3b JULES	Peat fire ignitions
Soil moisture	%	ISIMIP3b JULES	Peat probability of ignition, depth of burn
Snow mass	Kg m^{-2}	ISIMIP3b JULES	Soil moisture
Soil temperature	°C	ISIMIP3b JULES	Soil moisture, depth of burn
Soil evapotranspiration	Kg m^{-2} day^{-1}	ISIMIP3b JULES	Soil moisture
Canopy evaporation	Kg m^{-2} day^{-1}	ISIMIP3b JULES	Soil moisture
Surface moisture flux	Kg m^{-2} day^{-1}	ISIMIP3b JULES	Soil moisture
Runoff	Kg m^{-2} day^{-1}	ISIMIP3b JULES	Soil moisture
Water table depth	m	ISIMIP3b JULES	Soil moisture, depth of burn
Peat fire ignitions	Ignitions $month^{-1}$	INFERNO-peat	Peat burnt area
Peat probability of ignition	0-1	INFERNO-peat	Peat burnt area
Peat burnt area	M km^{-2}	INFERNO-peat	Carbon emissions
Peat depth of burn	m	INFERNO-peat	Carbon emissions

3. Results

As mentioned earlier, the high latitudes are undergoing rapid anthropogenic climate change. The UKESM modelled climate data that drives INFERNO, and consequently INFERNO-peat shows increases in temperature and precipitation throughout the northern high latitudes in the 21st century (Figure 54). The smallest temperature and precipitation increases are seen under SSP126, which predicts average annual temperatures north of 50° to increase from -3.0°C in 2020-2029 to 0.7°C by 2090-2099. However, under SSP370 and SSP585, temperatures are projected to increase even further and up to 6.8°C and 8.7°C, respectively, on average by 2090-2099 (Figure 54a). Precipitation under SSP370 and SSP585 is predicted to increase in the high latitudes more so than SSP126 (Figure 54b). Under SSP126, precipitation increases by 11.8% from the 2015-2025 average to the 2090-2100

average, but changes are much greater between the same two periods in SSP370 and SSP585, at 31.7% and 37.2%, respectively.

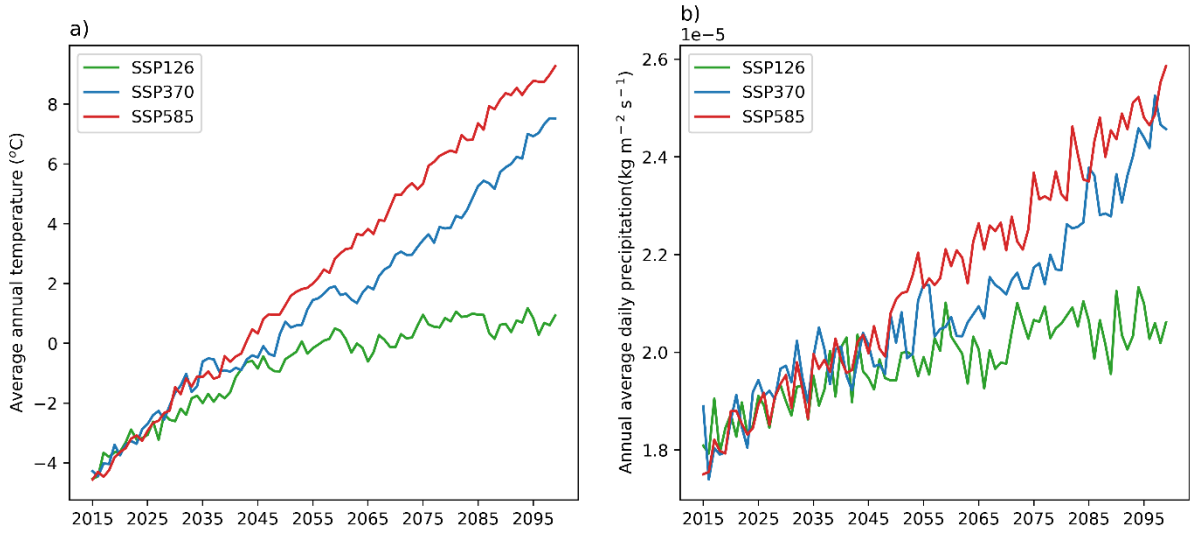


Figure 54: Timeseries plots of a) average annual temperatures and b) average annual daily precipitation for the northern high latitudes (>50° N) under SSP126, SSP370 and SSP585.

In terms of spatial structure, temperature increases are seen across the northern high latitudes to varying degrees (Figure 55). In general, under all scenarios, the largest increases in temperature occur in the northernmost areas, with more than 13°C of warming by the end of the century under SSP585 in parts of Arctic Canada and Siberia. SSP126 shows temperature changes of less than 3°C across much of the lower portions of the high latitudes, which is not seen under the higher emissions scenarios. Precipitation shows a patchier response to climate change, though the majority of high-latitude regions see increases (Figure 56). Across western Europe under all scenarios, precipitation is predicted to decrease by 2090-2100 compared to 2015-2025. Similarly, decreases, or minimal changes in precipitation are found in southern Canada under all scenarios. In contrast, the northernmost latitudes and most of Siberia see increases in precipitation by the end of the century. Interestingly, from Figures 2 and 3 it can be seen that the areas where precipitation increases the most often co-occur with the areas where the largest temperature increases are also found.

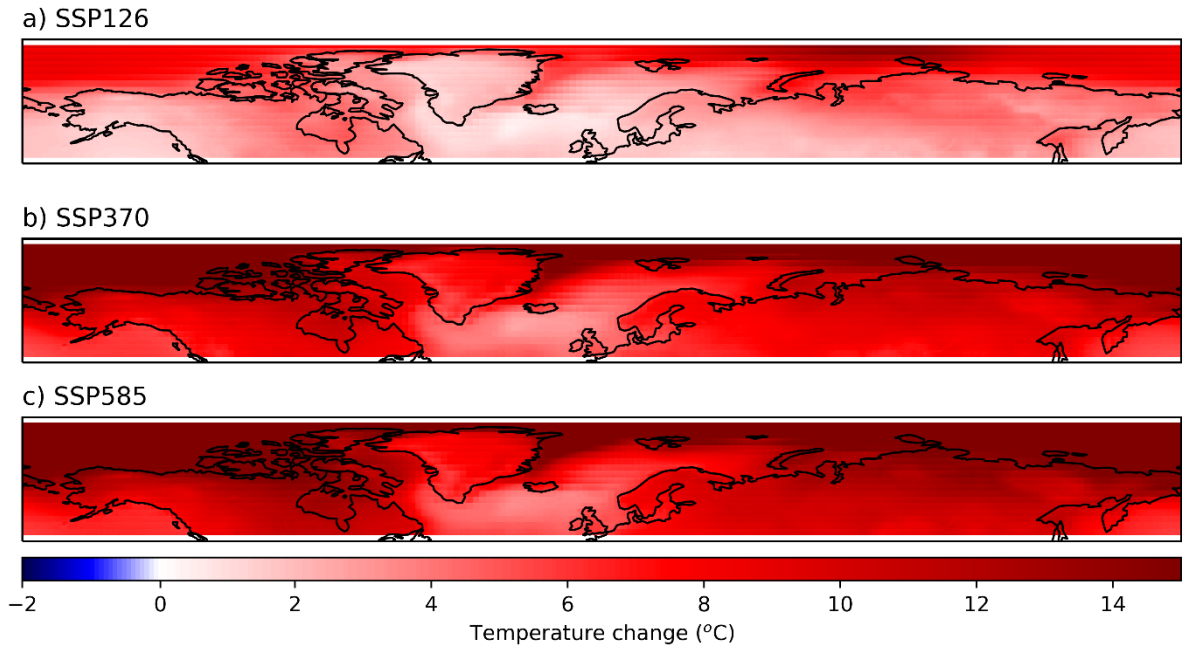


Figure 55: Changes in temperature from the 2015-2025 annual average to the 2090-2100 annual average for the northern high latitudes under a) SSP126, b) SSP370 and c) SSP585.

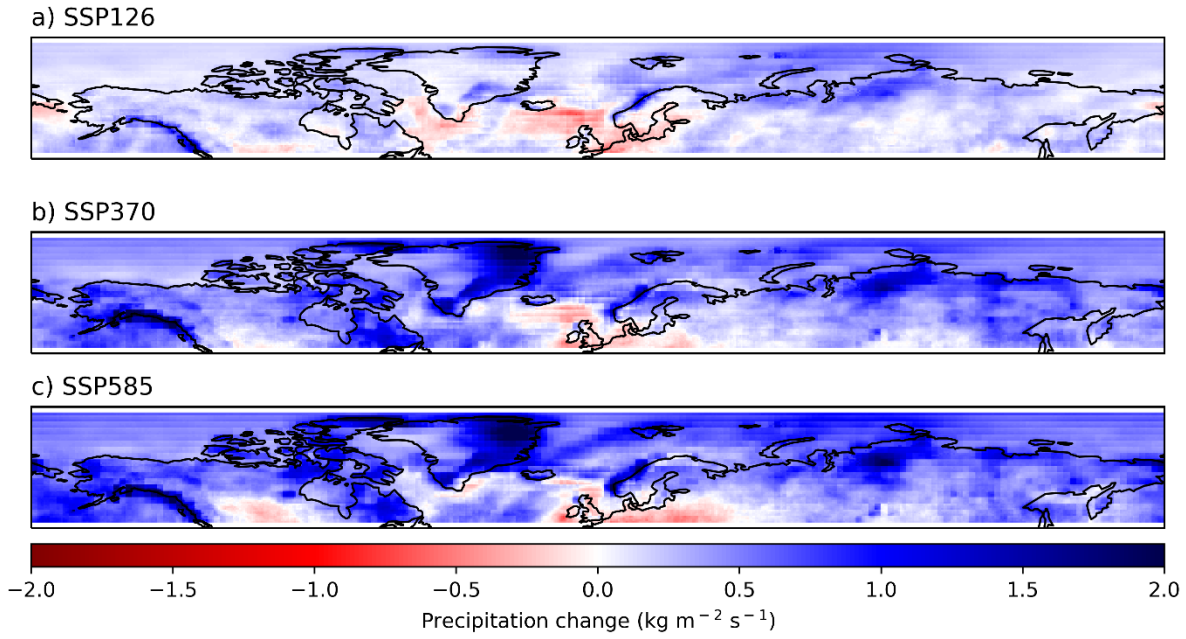


Figure 56: Changes in precipitation from the 2015-2025 annual average to the 2090-2100 annual average for the northern high latitudes under a) SSP126, b) SSP370 and c) SSP585.

Changes in temperature are highly correlated with changes in precipitation. There are significant positive correlations between temperature change and precipitation change from the 2015-2025 annual average to the 2090-2100 annual average across the northern high latitudes under SSP126 ($r=0.396$, $p<0.001$), SSP370 ($r=0.132$, $p<0.001$) and SSP585 ($r=0.206$, $p<0.001$). Additionally, there are significant positive correlations between the annual average temperatures and annual average

precipitation across the entirety of the northern high latitudes under SSP126 ($r=0.877$, $p<0.001$), SSP370 ($r=0.968$, $p<0.001$) and SSP585 ($r=0.985$, $p<0.001$). Therefore, there is a clear connection between temperature and precipitation, whereby increases in temperature are associated with increased precipitation. This is supported by the work of Koenigk et al., (2015) who showed a linear relationships between precipitation change and temperature change in the Arctic. This occurs as higher temperatures result in greater thermodynamic energy in the atmosphere, leading to greater evaporation and consequently more rainfall (Oki and Kanae 2006; Pan et al., 2014; Allen et al., 1998). Increasing temperatures can also lead to a northward shift in storm tracks (Harvey et al., 2020), resulting in higher levels of precipitation further north.

3.1. Peat burnt area

Across all scenarios, peat burnt area is projected to increase across the northern high latitudes (Figure 57). The largest increases in burnt area are seen in central and western Canada, more specifically the area southwest of the Hudson Bay, and in northwest Siberia, particularly to the west of the Great Vasyugan mire complex. Sizeable increases are also found in Eastern Europe. As expected, the largest changes are seen in SSP585, and the smallest under SSP126. On average, annual peat burnt area increases by 46% in SSP126 to burning an average of 0.489 M km^2 per year by the end of the century (Table 38). On the other end, there is an over 270% increase in peat burnt area under SSP585 to 1.218 M km^2 per year by the end of the century (Table 38).

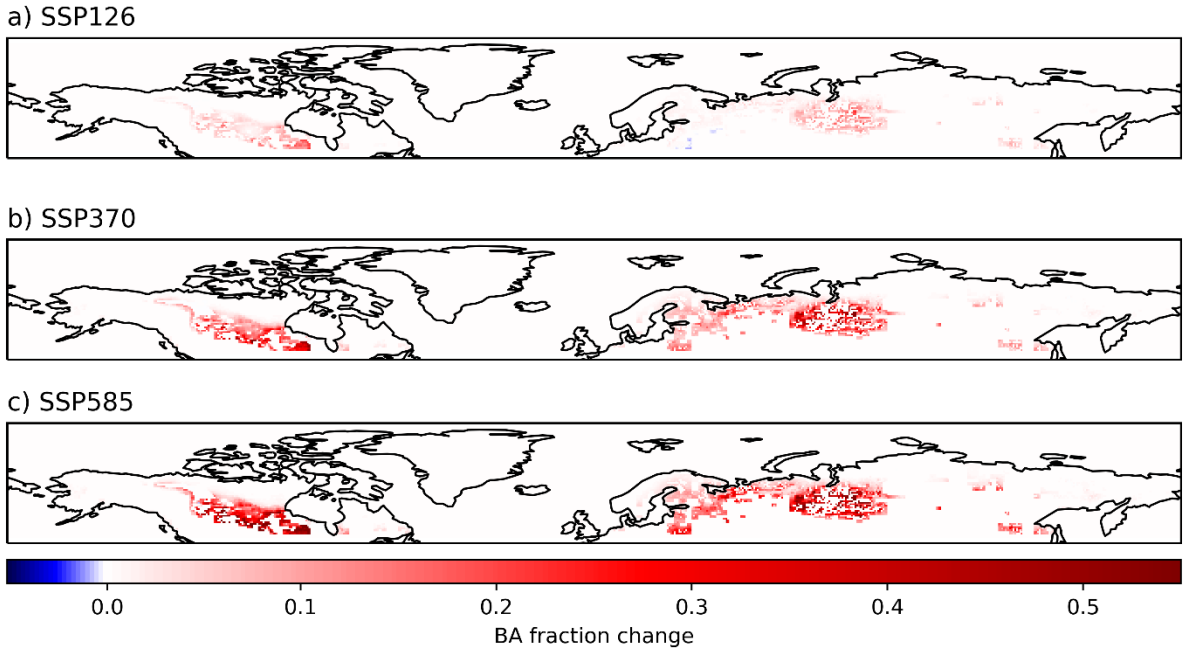


Figure 57: Change in annual peat burnt area fraction from the 2015-2025 average to the 2090-2100 average across the northern high latitudes in a) SSP126, b) SSP370 and c) SSP585.

Table 38: The annual average burnt area (in M km^2) above 50°N averaged over the starting and ending decades of the model runs for each of the scenarios, and the absolute and percentage change between these two periods.

Scenario	2015-2025 average annual BA (M km^2)	2090-2100 average annual BA (M km^2)	Change	% Change
SSP126	0.336	0.489	0.153	45.649
SSP370	0.329	0.889	0.559	169.896
SSP585	0.327	1.218	0.891	272.565

All three scenarios follow similar trajectories for the first 15 years of the simulation, before trends start to diverge from around 2030 (Figure 58). Initially, peat burnt area is greatest in SSP126, but is overtaken by the other SSPs by ~2030. Peat burnt area continues to increase under SSP126 until ~2060 when it appears to level off. SSP370 shows an increase in burnt area across the whole simulation period. SSP585 starts off with the lowest annual peatland burnt area, but undergoes rapid increases after 2030, resulting in burning over 1 M km^2 of peat per year by the end of the century. This 1 million km^2 threshold is otherwise only breached in SSP370 in 2095, whereas this threshold is breached for the first time over 20 years earlier in SSP585 (in 2072).

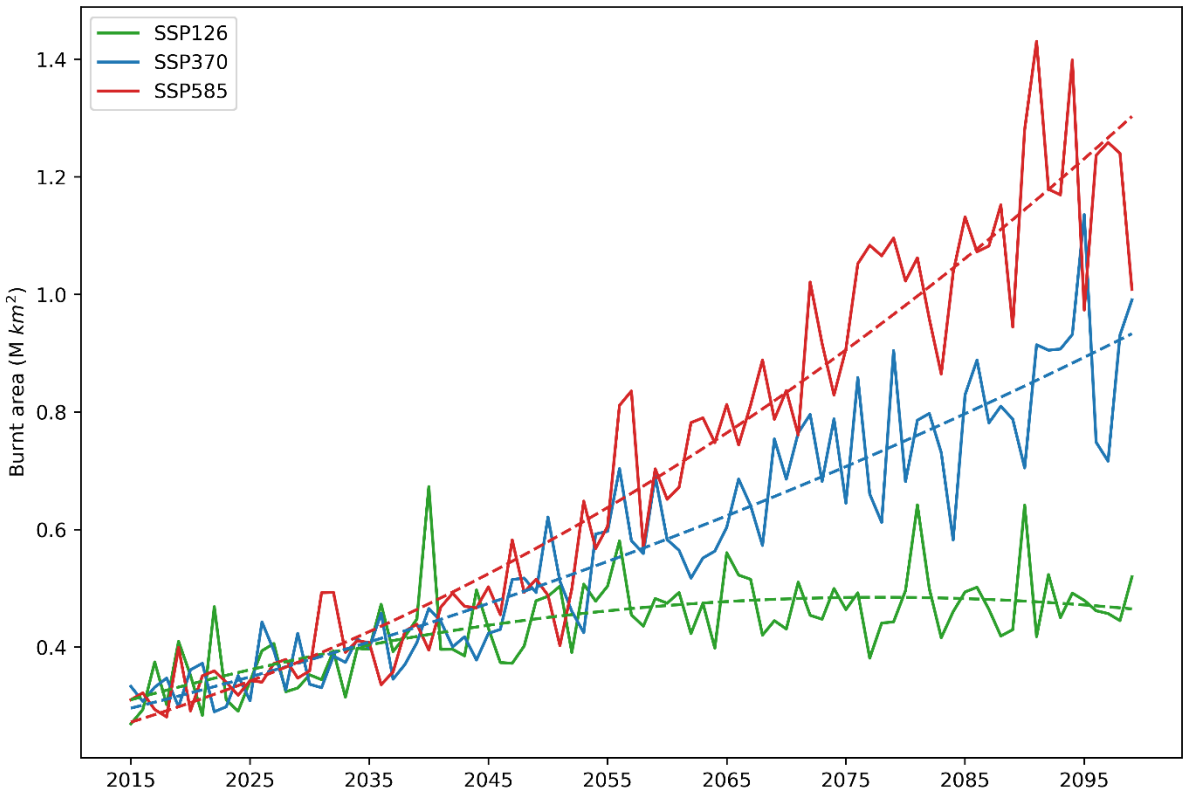


Figure 58: Annual peat burnt area (M km^2) above 50°N from 2015 to 2100 for each of the SSPs. The dashed lines indicate the quadratic trendline for the respective SSP.

There are some increases in interannual variability in peat burnt area with time in the scenarios. In particular, there are greater standard deviations in the later decades in SSP370 and SSP585 compared to the earlier decades, indicating that there is larger variability in annual peat burnt area towards the

end of the century (Table 39). However, there are no significant changes in the coefficient of variation. When focusing on the data pre- and post-2050, there is a similar trend. Standard deviation increases from 0.082 pre-2050, to 0.137 post-2050 in SSP370, and from 0.089 to 0.201 in SSP585. However, there are no significant changes in the coefficient of variation pre- and post-2050 for SSP370 (20.081% to 18.588%) or SSP585 (21.304% to 20.695%), which suggests that in relative terms, interannual variability of burnt area does not actually increase in the future in those scenarios. In contrast, post-2050 there is a large fall in the coefficient of variation in SSP126 from 19.696% pre-2050 to just 11.421% post-2050, indicating a drop in interannual variability in peat burnt area, which occurs at around the same time when the burnt area trend starts to level off (Figure 58).

Table 39: Decadal average annual peat burnt area (M km^2), and decadal variability metrics standard deviation (std dev) and coefficient of variation (CV) for each SSP.

Decade	SSP126			SSP370			SSP585		
	Mean	Std Dev	CV (%)	Mean	Std Dev	CV (%)	Mean	Std Dev	CV (%)
2020-2029	0.350	0.055	15.57	0.357	0.050	13.87	0.344	0.024	6.974
2030-2039	0.393	0.045	11.402	0.382	0.037	9.736	0.412	0.051	12.373
2040-2049	0.441	0.087	19.833	0.448	0.045	10.127	0.484	0.045	9.399
2050-2059	0.482	0.047	9.840	0.574	0.085	14.842	0.613	0.132	21.575
2060-2069	0.473	0.049	10.351	0.604	0.067	11.167	0.769	0.066	8.551
2070-2079	0.456	0.036	7.885	0.740	0.092	12.485	0.957	0.116	12.088
2080-2089	0.482	0.062	12.867	0.768	0.081	10.512	1.033	0.084	8.143
2090-2099	0.489	0.060	12.23	0.889	0.126	14.214	1.218	0.139	11.378

As is evident in Figure 57, different subregions of the northern high latitudes undergo different changes in peat burnt area in the different SSP scenarios. Four regions that all undergo different levels of changes to peat burning include northern Canada, Fennoscandia, northwest Siberia, and eastern Siberia (Figure 53). Of these four regions, eastern Siberia sees the smallest increases in peat BA of up to 0.043 M km^2 by the end of the century under SSP585 (Figure 59a). In contrast, regions such as northern Canada and northwest Siberia undergo much larger projected increases in peat BA of 0.348 M km^2 and 0.304 M km^2, respectively, by the end of the century under SSP585 (Figure 59a). However, when considering theses changes as percentage increases, all regions within each scenario see similar levels of increase, with all regions under SSP585 expected to see a greater than 200% increase in peat BA (Figure 59b). Eastern Siberia shows the largest percentage increase of 315% by 2100, despite having relatively low peat burnt area, perhaps suggesting a larger shift in fire regimes away from present conditions in this region.

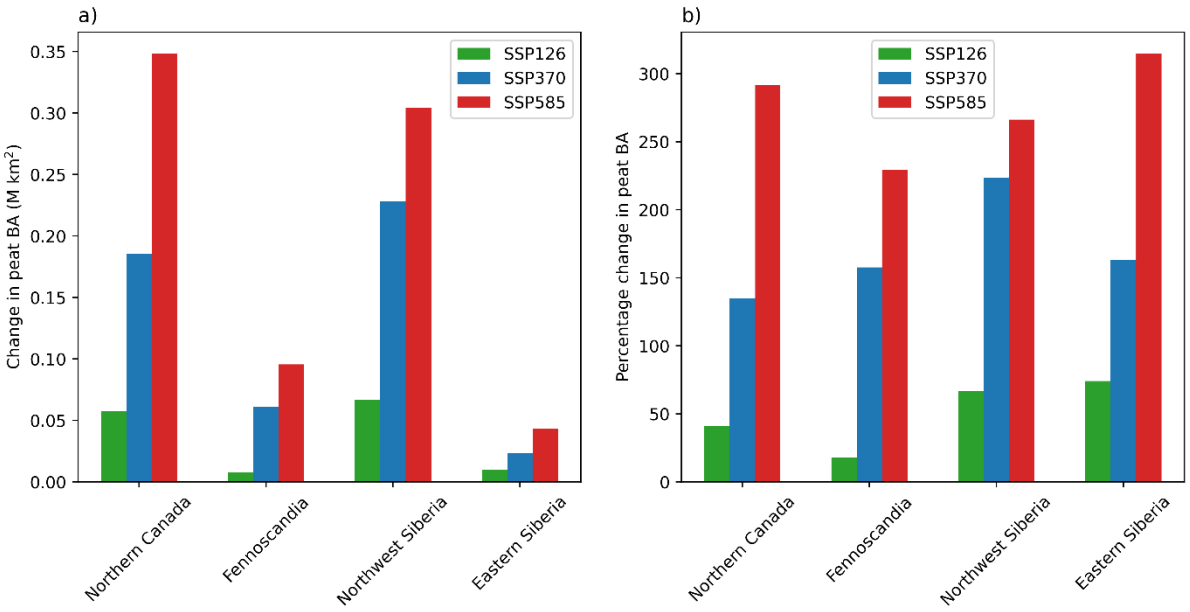


Figure 59: Change in peat burnt area from the 2015-2025 annual average to the 2090-2100 annual average the three SSP scenarios for four different subregions of the northern high latitudes. Panel a) shows the absolute change in peat BA in M km^2, and b) shows the percentage change in peat BA.

Trends and changes in burnt area shown here are a direct product of peat ignitions, peat probability of ignition, peat fraction and average peat burnt area (Equation 9). As peat fraction is prescribed to the model by a static dataset, and a fixed value is used for average peat burnt area in INFERNO-peat, the simulated peat burnt area changes are driven by peat ignitions and the probability of ignition. The following sections will examine the changes in peat fire ignitions and peat probability of ignition and their respective drivers for the high latitudes.

3.1.1. Peat fire ignitions

Peat fire ignitions increase under all three SSP scenarios (Figure 60). Similarly to the burnt area results, initially all scenarios show similar trajectories until ~2050, but after this point they start to diverge. From 2050 onwards, peat fire ignitions under SSP126 start to level off (Figure 60). In contrast, peat fire ignitions under SSP370 and SSP585 continue to grow, with the largest levels of growth seen in SSP585, which sees a 281% increase in ignitions between the beginning and ending decadal averages (Table 40).

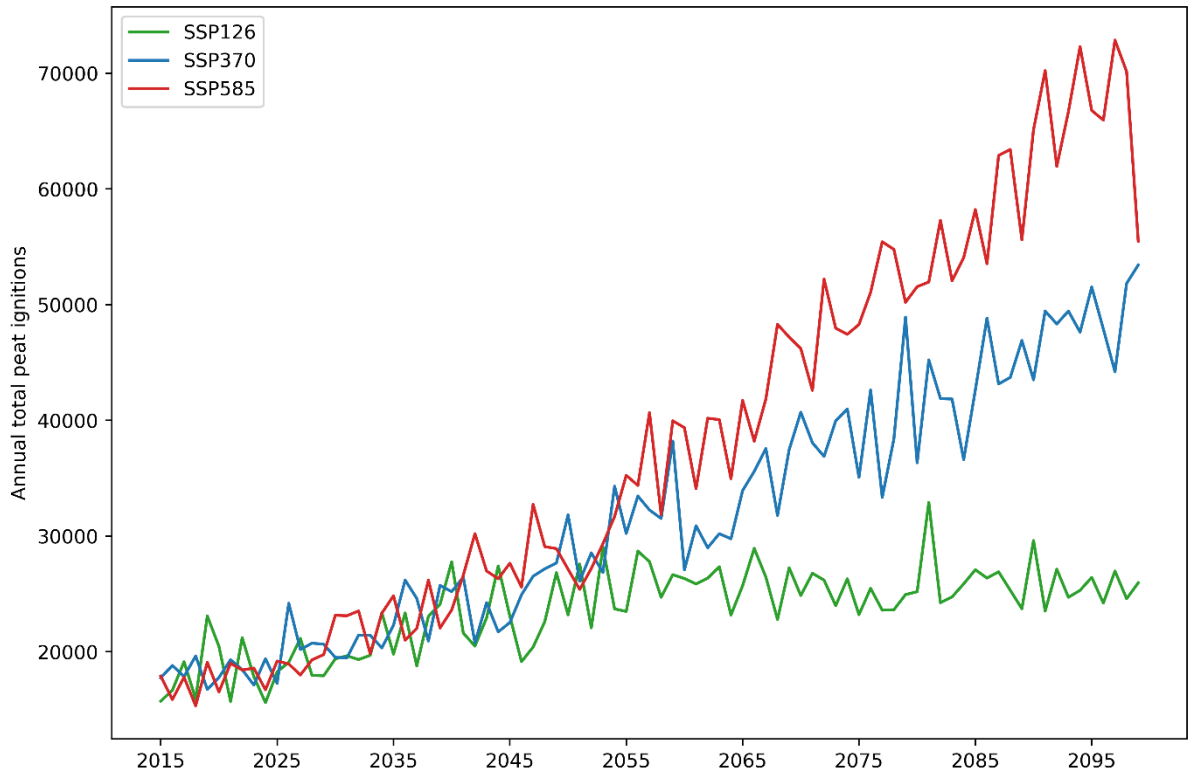


Figure 60: Annual peat fire ignitions in the northern high latitudes from 2015 to 2100 under the three different SSPs.

Table 40: The annual total peat fire ignitions above 50°N averaged over the starting and ending decades of the model runs for each of the scenarios, and the absolute and relative change between these two periods.

Scenario	2015-2025 average annual total peat fire ignitions	2090-2100 average annual total peat fire ignitions	Change	% Change
SSP126	18148.017	25849.520	7701.503	42.437
SSP370	18294.005	48726.076	30432.071	166.350
SSP585	17528.125	66750.799	49222.675	280.821

Ignitions increase almost everywhere under all scenarios (Figure 61). The exception to this is western Russia/eastern Europe in SSP126 which sees small decreases in peat fire ignitions. However, this feature does not occur in the higher emissions scenarios. Under all scenarios, the largest changes in the number of peat fire ignitions occur across central Canada, western Russia, and the lower latitudes of central Siberia. Smaller increases occur in the far northern latitudes of these regions, and in particular in Alaska and eastern Siberia. The most pronounced changes are seen under SSP370 and SSP585.

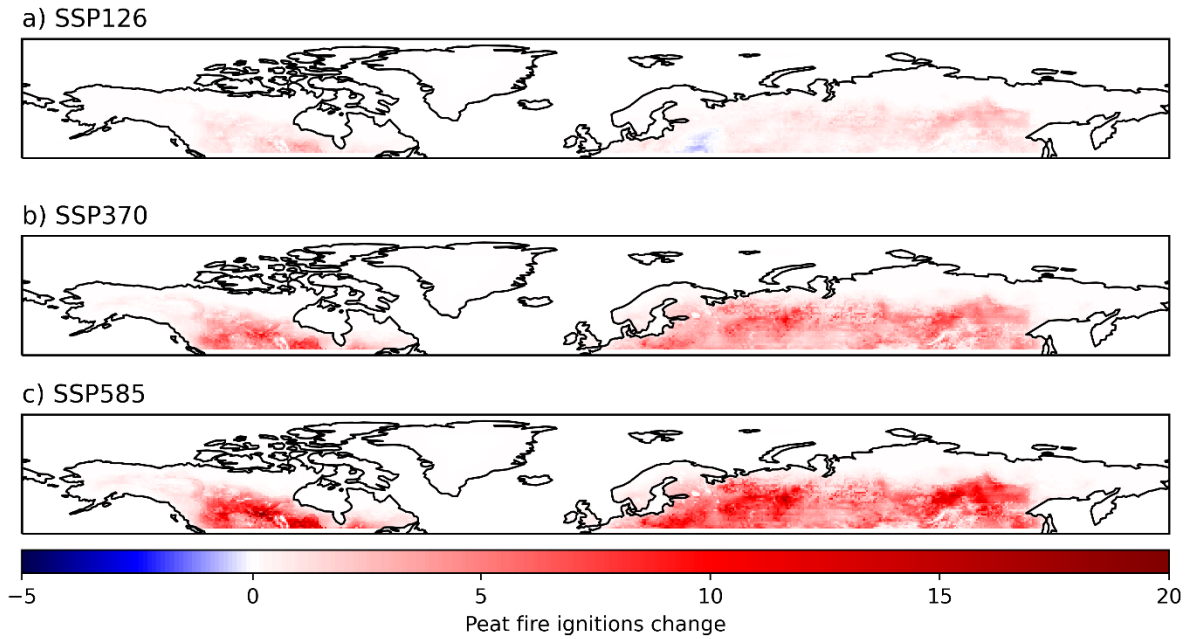


Figure 61: Change in annual total peat fire ignitions between the 2015-2025 average and the 2090-2100 average in SSP126 (a), SSP370 (b) and SSP585 (c).

Peat fire ignitions are treated in INFERNO-peat as the total number of flaming vegetation fires, which are assumed to be the cause of ignition of peat fires (Chapter 2 Section 3.1). Therefore, they are influenced by human and natural vegetation fire ignitions, which are driven respectively by prescribed population density and lightning, as well as plant functional type (PFT) fraction and flammability, which are ultimately a product of the JULES vegetation model (TRIFFID) and driven by UKESM climate data. INFERNO-peat in the setup used here utilises non-time varying datasets for lightning and population density, and therefore these parameters are not influencing the trends in ignitions seen here. Consequently, PFTs exert an important influence on peat fire ignitions in these model simulations.

3.1.1.1. PFT fractions

Increases in the fraction of grid cells covered by PFTs (i.e. vegetative land surface types) are seen across all scenarios by 2100 (Figure 62). On average, at the start of the simulation (2015-2025) vegetative surface types cover 54.6% of each grid cell. SSP126 shows the lowest increase in PFT fractional coverage at just 3.3% by 2100, with SSP585 and SSP370 showing similar increases in PFT fractions of 11.2% and 13.1% respectively. These increases are seen across the high latitudes, but most prominently in northern and eastern Siberia and northern Canada and Alaska (Figure 63). The greatest changes occur under SSP370 and SSP585. There are some regions of decrease in all simulations, but most notably in southern central Siberia, southern Alaska and parts of western Canada in SSP126. From Figure 63, broadly speaking there appears to be a band of decreases/minimal changes in PFT fractions across the middle of the region, i.e. the sub-Arctic region.

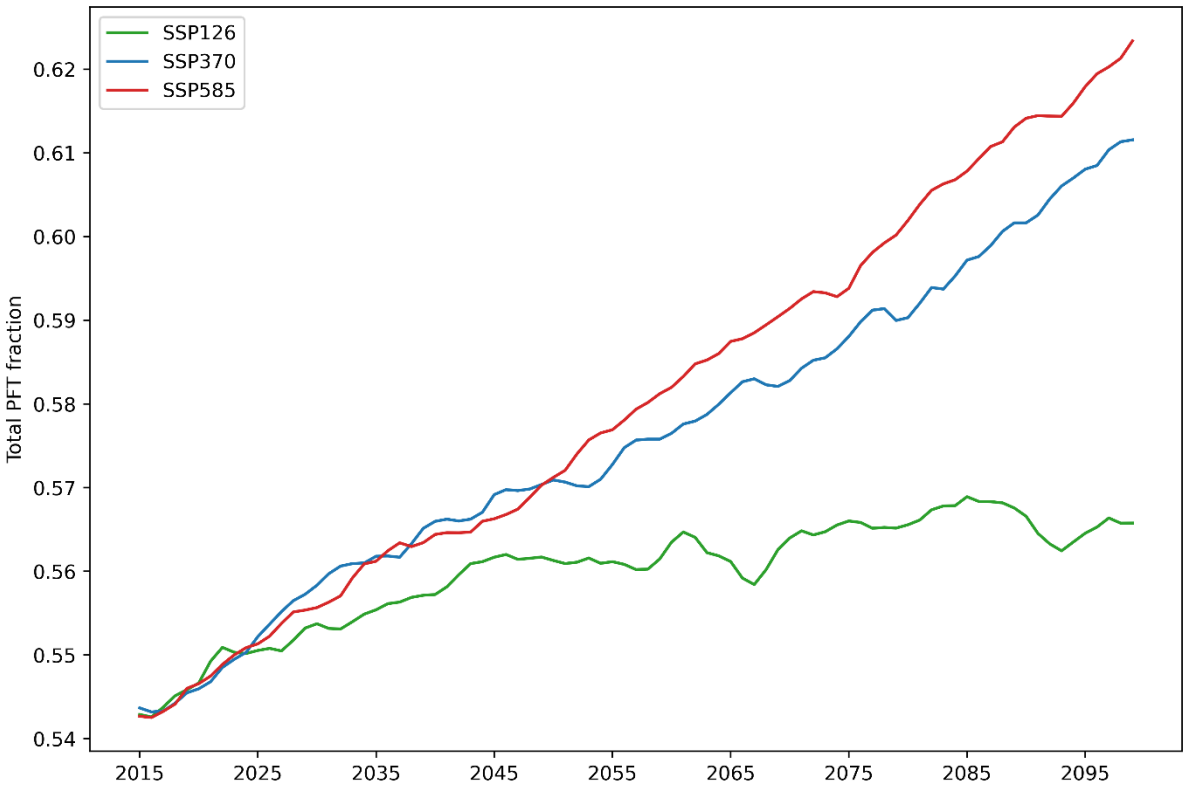


Figure 62: Timeseries graph of the annual average total fraction of grid cells that are covered by vegetative land surface types from 2015 to 2100 under SSP126, SSP370 and SSP585.

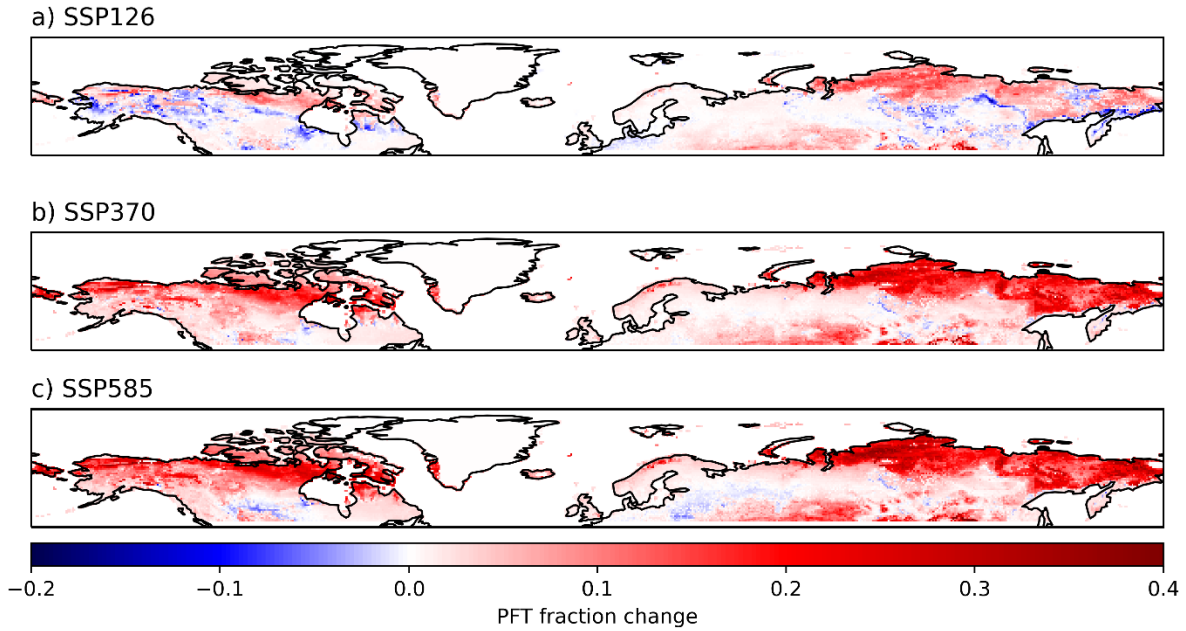


Figure 63: Change in grid cell PFT fractional coverage across the high latitudes between the 2015-2025 average and the 2090-2100 average.

Much of the northern high latitudes, according to the land cover type modelled by JULES, is covered in C3 grasses, needleleaf evergreen trees, needleleaf deciduous trees or bare soil (Figure 64).

However, over the course of the simulation period, the dominant land cover types in the high latitudes change substantially by the end of the century (Figure 64).

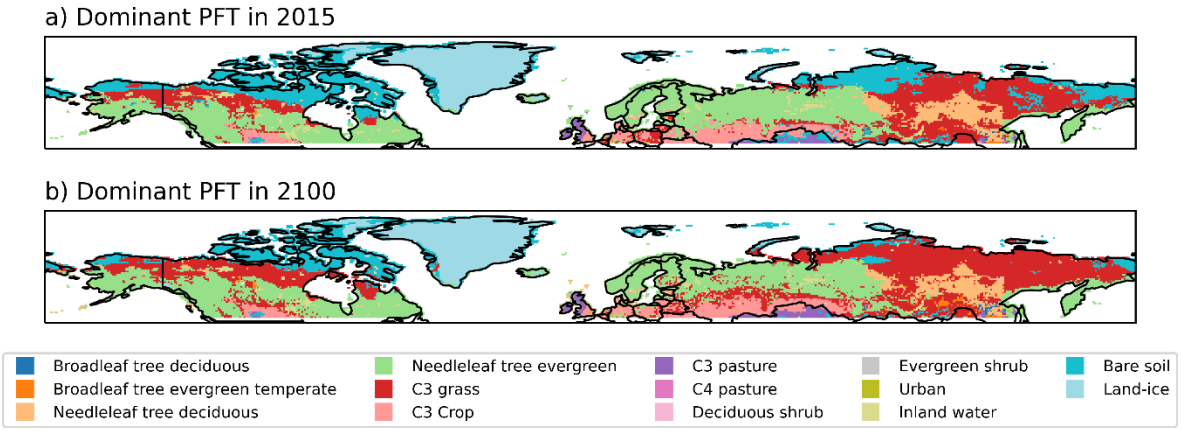


Figure 64: The dominant land cover type in each grid cell in a) 2015 and b) 2100 under SSP585.

The overall increase in PFT fraction is attributable to an overall decline in bare soil coverage in all three scenarios (Figure 65j-l). Most prominently we see a fall in bare soil coverage in the far north of the high latitudes, as well as in northern and eastern Siberia. In eastern and northern Siberia, the decrease in bare soil occurs alongside a rise in the fraction of C3 grasses across the region (Figure 65a-c), and to a lesser extent increases in needleleaf evergreen and deciduous trees (Figure 65d-i). There appears to be a Northward shift in C3 grasses, consequently leading to declines in C3 grasses seen across the subarctic region of the high latitudes. However, in place of these C3 grasses there is an increase in needleleaf evergreen and deciduous trees (Figure 65d-i). This may partially explain why there are minimal overall modelled changes in the sub-arctic region (Figure 63). Conversely, in the southernmost areas of the high latitude regions we see declines in needleleaf evergreen and deciduous trees but increases in C3 grasses.

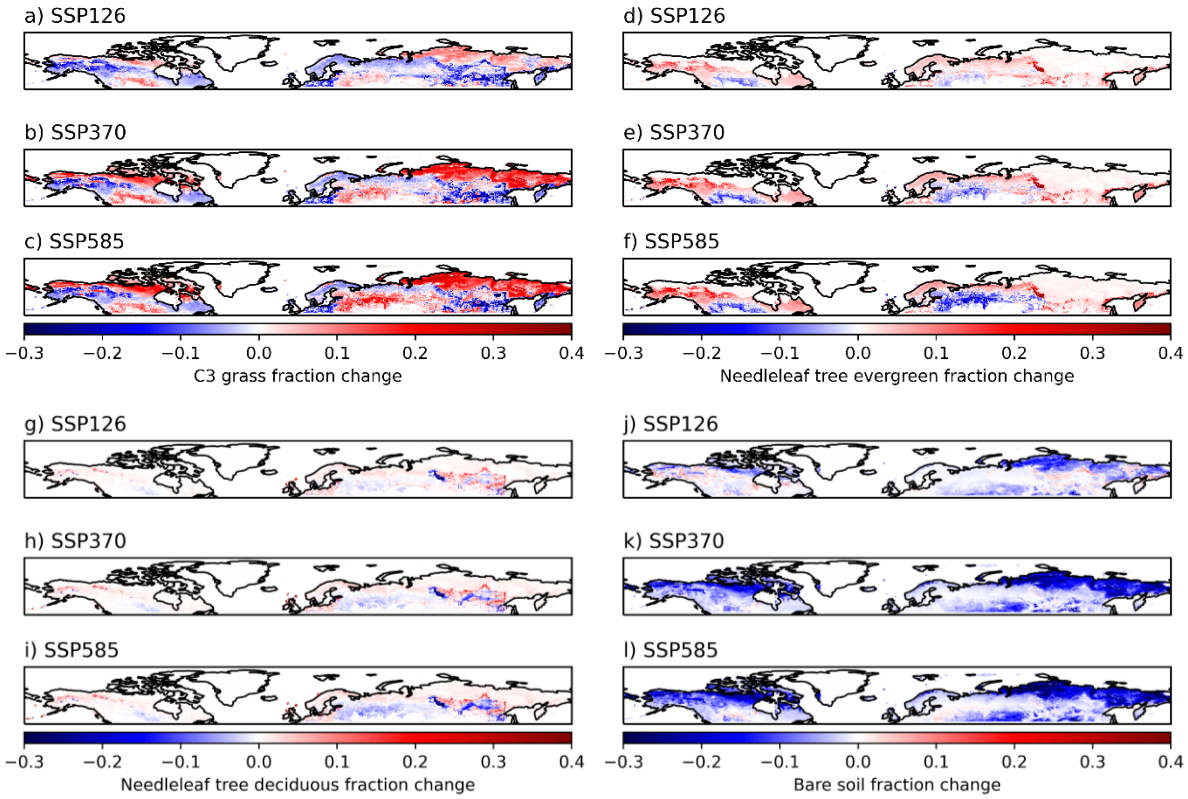


Figure 65: Change in land cover type grid cell fraction from the 2015-2025 average compared to the 2090-2100 average over the high latitudes under the three SSP scenarios. Plots a-c show the C3 grass fraction change, d-f the Needleleaf tree evergreen fraction change, g-i the needleleaf tree deciduous fraction change and j-l show the bare soil fraction change.

Temporal trends in the fraction of C3 grasses, needleleaf evergreen and deciduous trees, and bare soil across three latitudinal bands of the high latitudes (50-60° N, 60-70° N, and >70° N) can reveal further insights into shifting vegetation patterns in the high latitudes (Figure 66). Overall, across all latitudinal bands, there are small changes in land cover types under SSP126 and a notable decline in bare soil coverage and increases in needleleaf tree coverage (Figure 66a-c). In contrast, C3 grasses under SSP126 are declining in the 50-60°N and 60-70°N bands but increasing in the >70°N band. Under SSP370 and SSP585 in the lower latitude band, there is an initial decline in C3 grasses over the first 50-60 years of the simulation, followed by small increases up to the end of the century, co-occurring with a levelling off of the increase in needleleaf evergreen trees (Figure 66d, g). Trends in land cover types show more significant changes under SSP370 and SSP585 in the 60-70°N and >70°N band (Figure 66e, f, h, i). In these bands there are drastic declines in bare soil coverage, compensated for by an increase in C3 grasses, and in the 60-70°N band also by increasing needleleaf evergreen tree coverage. Overall, there are minimal changes in tree coverage above 70°N, with this region broadly remaining above the northern tree line.

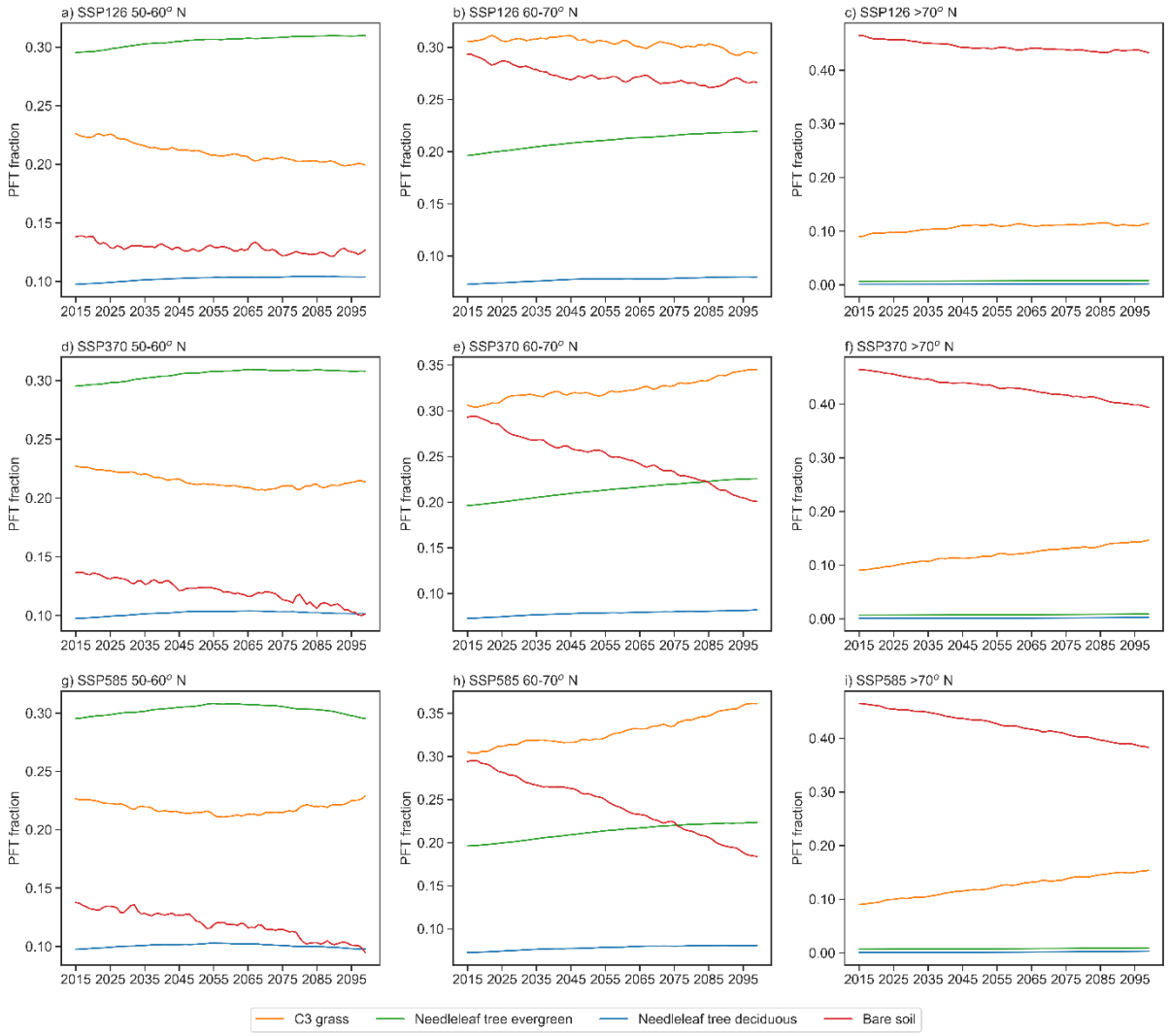


Figure 66: Temporal trends in the annual fractional coverage of C3 grass, needleleaf tree evergreen, needleleaf tree deciduous and bare soil land cover types under SSP126 (a-c), SSP370 (d-f) and SSP585 (g-i), for 50-60° N (a, d, g), 60-70° N (b,e,h), and > 70° N (c, f, i).

Overall, these results suggest a northward movement of C3 grass into the Arctic, replacing bare soil, with needleleaf trees replacing the C3 grasses, and in turn, C3 grasses then replacing the needleleaf trees. Some of these changes could stem from the repopulation of bare soil by vegetation, alongside warmer temperatures and CO_2 fertilisation, driving a northward movement of the tree line (Boisvert-Marsh et al., 2014; Harsch et al., 2009; Grace et al., 2002). Despite the changes in individual PFT dynamics, overall, there is an expansion of vegetative surface types over time, and with scenarios in the model. Therefore, there is an elevated fuel load, meaning that there is more vegetation available to burn across the high latitudes, and especially in the far north. Consequently, there are significant positive correlations between the fraction of grid cells covered in vegetative land cover types and the total number of peat fire ignitions in all scenarios (Figure 67). Therefore, elevated fuel loads may lead to greater amounts of fuel available to burn and consequently lead to a larger number of flaming wildfires that can then become peat fire ignitions.

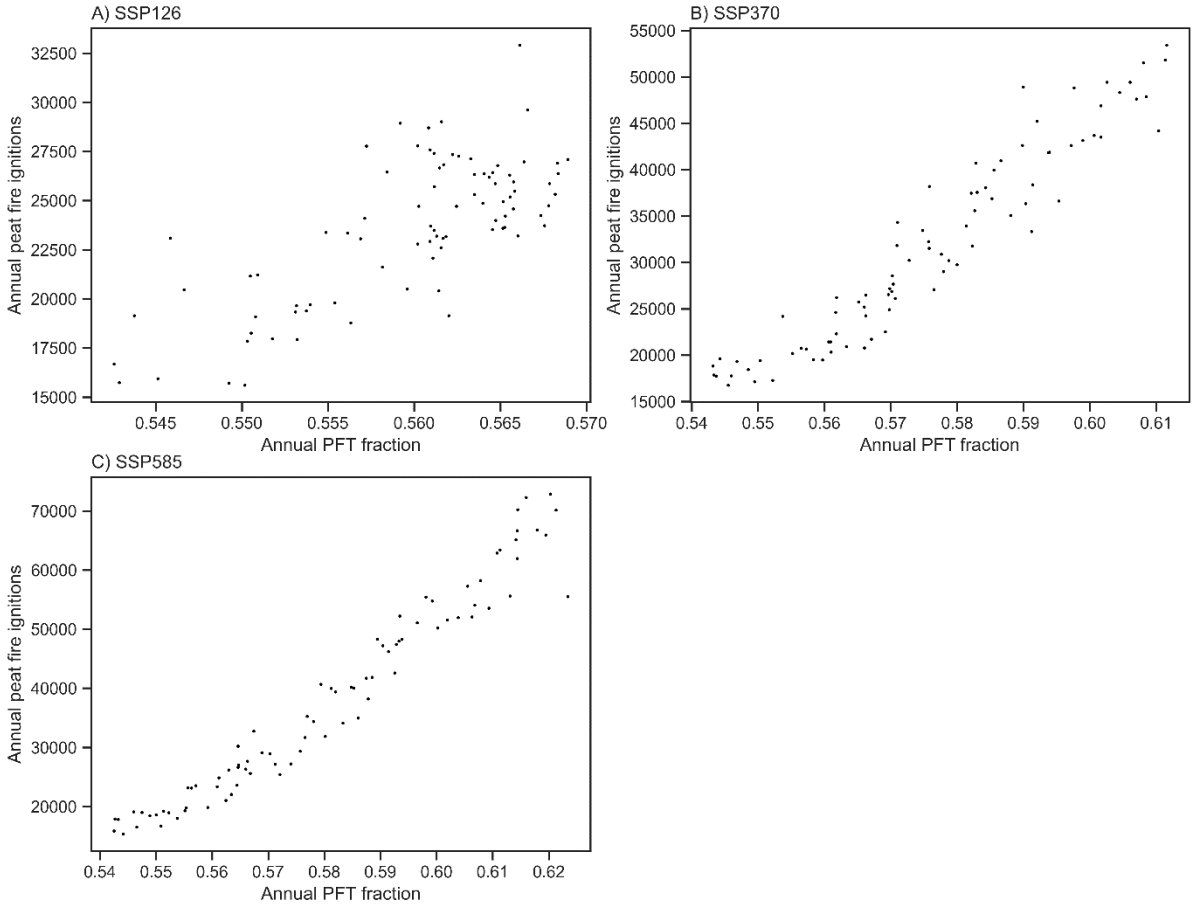


Figure 67: Total annual number of peat fire ignitions plotted against the annual PFT fraction coverage under a) SSP126 (r=0.741, p<0.001), b) SSP370 (r=0.952, p<0.001) and c) SSP585 (r=0.973, p<0.001).

3.1.1.2. PFT flammability

Not only does INFERNO model an increase in fuel loads, but these vegetation types are becoming more flammable. Overall, PFT flammability increases in all scenarios over the remainder of the century (Figure 68). All scenarios follow similar trajectories up until around 2050, where PFT flammability in SSP126 starts to level off, but still with an overall increase in PFT flammability of 46.7% by 2100 compared to 2015 in this scenario. In contrast, overall PFT flammability under SSP370 and SSP585 continues to increase by 153.4% and 240.9% by 2100, respectively. Total PFT flammability increases across the vast majority of the northern high latitudes to varying degrees (Figure 69). Under SSP126, increases in PFT flammability are lower than the other scenarios, with the largest areas of increased flammability in central Siberia and southern Canada (Figure 69a). Additionally, in SSP126 there is an area of decreased flammability in eastern Europe/western Russia, which is not seen in the other scenarios. Larger increases are seen further north in both SSP370 and SSP585, most notably across much of Canada, western Russia, and central Siberia (Figure 69b, c).

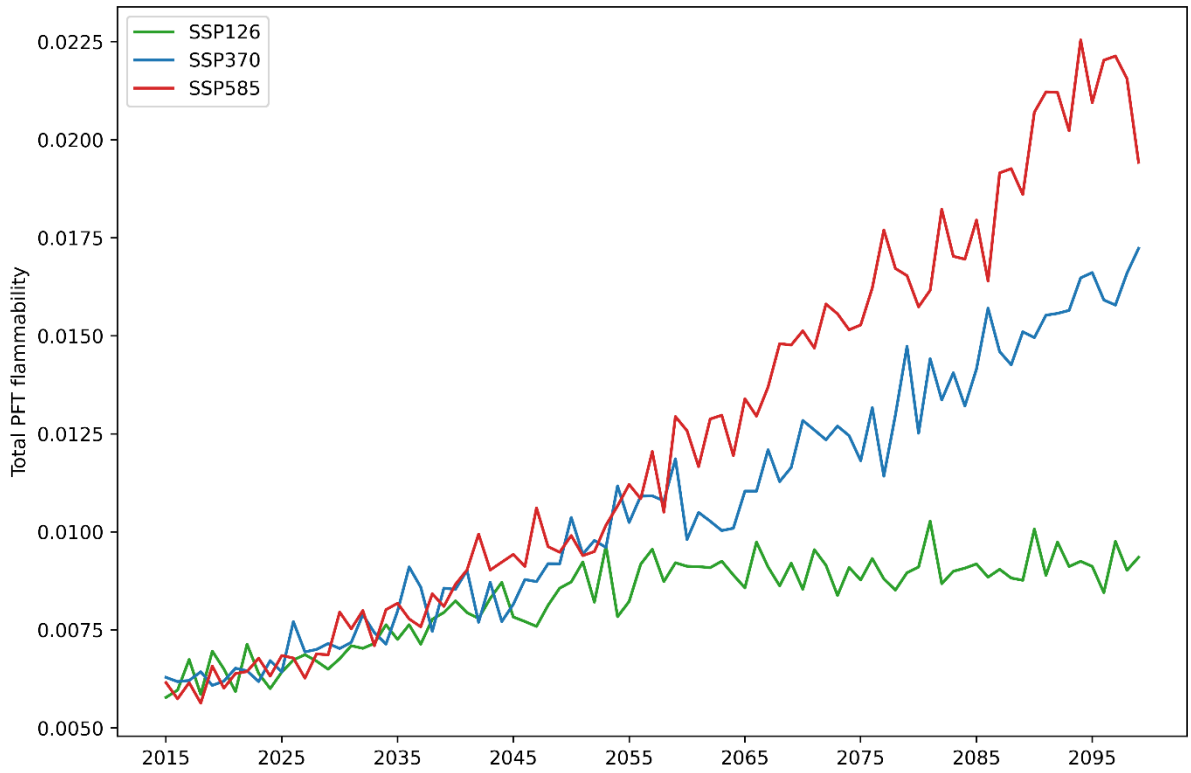


Figure 68: Timeseries graph of the annual average total PFT flammability from 2015 to 2100 under SSP126, SSP370 and SSP585.

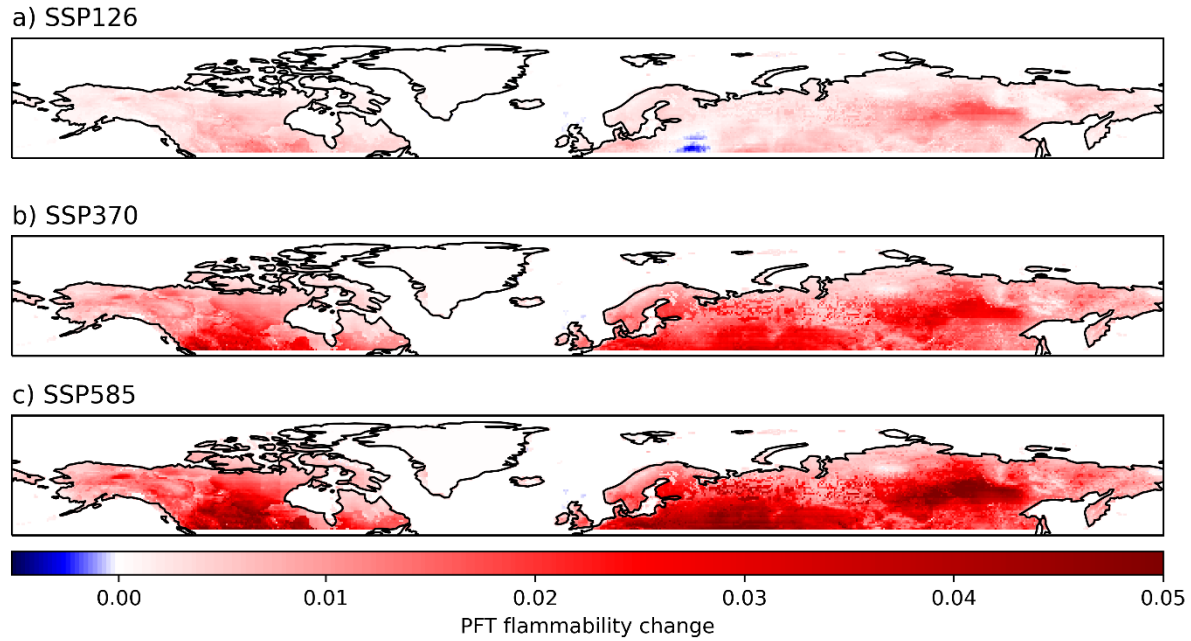


Figure 69: Change in grid cell total PFT flammability across the high latitudes between the 2015-2025 average and the 2090-2100 average.

As previously shown, C3 grasses and needleleaf evergreen trees are the dominant PFTs in the high latitudes, which also both show strong increases in their flammability across the remainder of the 21st

century (Figure 70). It is apparent that the total PFT declining flammability in western Russia/Eastern Europe in SSP126 is being more strongly driven by decreases in the flammability of needleleaf evergreen trees (Figure 70d). Additionally, a small area of decrease in C3 grass flammability is seen in southern Canada in SSP126 (Figure 70a), a trend that is not seen in the overall patterns of PFT flammability. Much like total PFT flammability, C3 grass and needleleaf evergreen tree flammability increase more strongly under SSP370 and SSP585. For example, C3 grass flammability increases by over 200% by 2100 under SSP585, compared to just 32.2% under SSP126. The largest increases in C3 grass flammability are seen in central and southern Canada and across sub-Arctic Russia and eastern Europe. Similar trends are seen in needleleaf evergreen tree flammability. However, there are additional strong increases in needleleaf evergreen tree flammability further north in central and eastern Siberia, than are seen with C3 grasses.

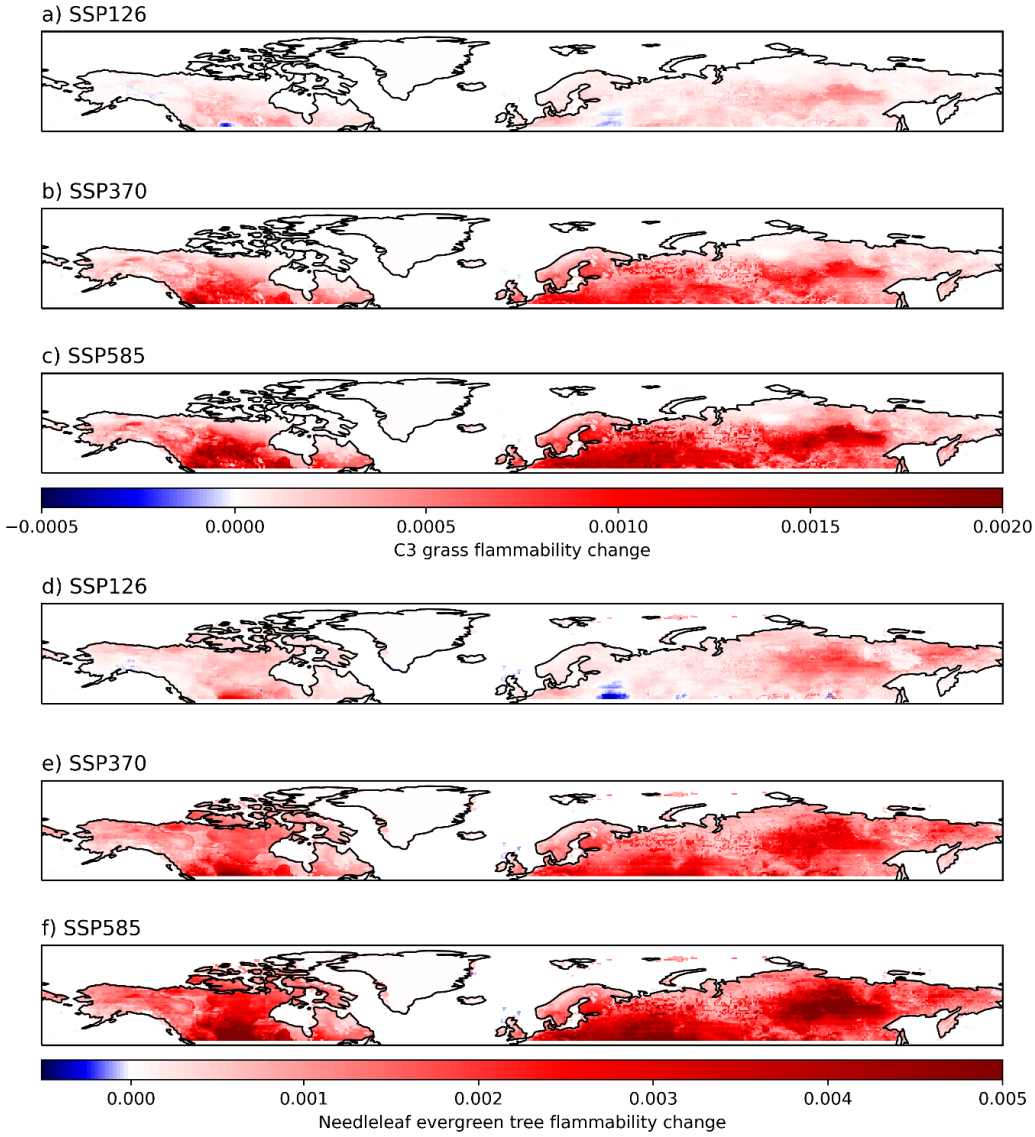


Figure 70: Changes in the flammability of C3 grasses from the 2015-2025 average to the 2090-2100 average under a) SSP126, b) SSP370 and c) SSP585. Additionally, plots d-f show the changes in needleleaf evergreen

tree flammability from the 2015-2025 average to the 2090-2100 average under d) SSP126, e) SSP370 and f) SSP585.

There are strong positive correlations between annual total PFT flammability and the annual number of peat fire ignitions for the northern high latitudes under all SSP scenarios (Figure 71). Consequently, increased flammability of vegetation in the northern high latitudes is associated with greater amounts of flaming vegetation fires, which in turn results in increases in the number of potential peat fire ignitions.

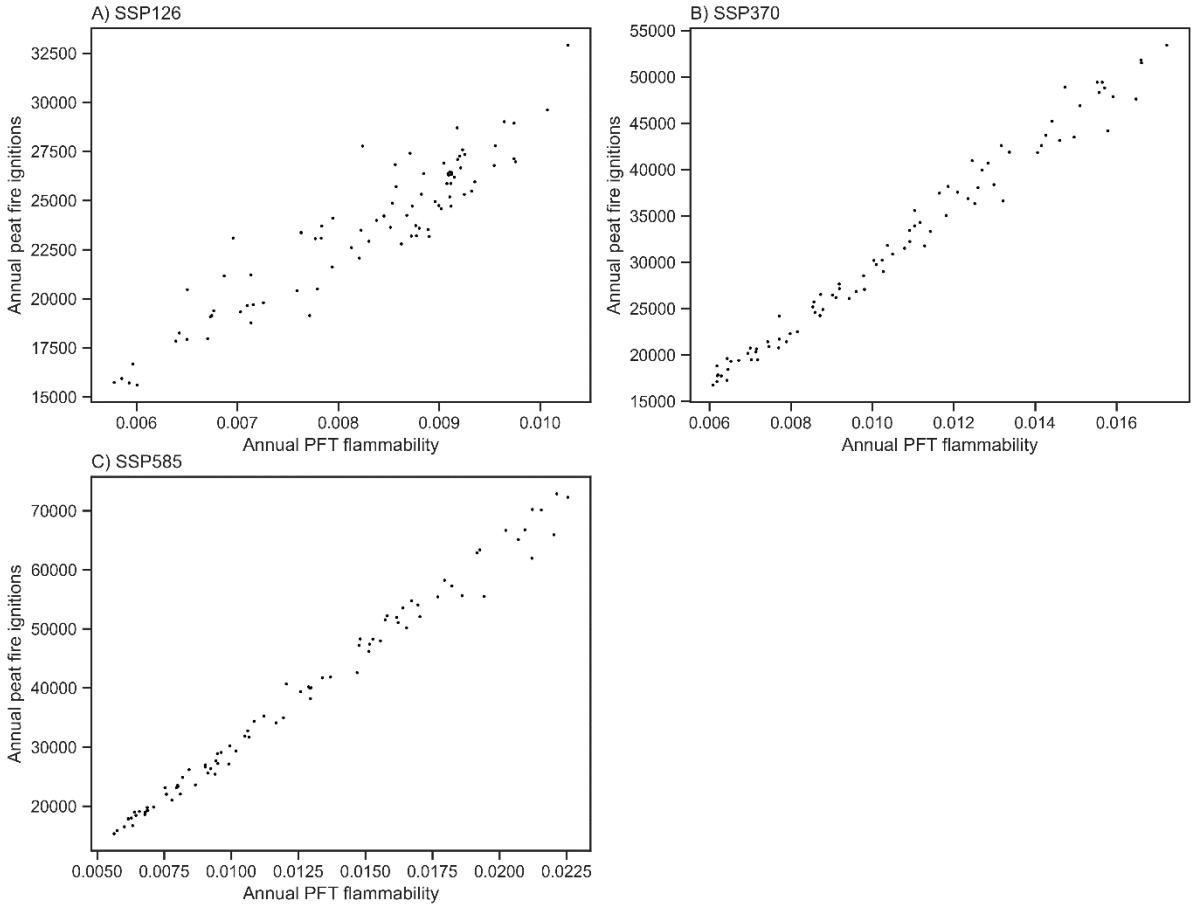


Figure 71: Total annual number of peat fire ignitions plotted against the annual PFT flammability under a) SSP126 (r=0.930, p<0.001), b) SSP370 (r=0.991, p<0.001) and c) SSP585 (r=0.995, p<0.001).

3.1.1.3. Temperature and precipitation

Climatic factors such as temperature and precipitation likely play an important indirect role in influencing peat fire ignitions, through driving changes in fuel loads and flammability. Increases in PFT fractions may be being driven by the increases in temperature and precipitation seen across the high latitudes (Figure 54). There are strong positive correlations between annual total PFT fractional coverage and annual average temperatures in the northern high latitudes under SSP126 (r=0.962, p<0.001), SSP370 (r=0.995, p<0.001) and SSP585 (r=0.996, p<0.001). Similarly, there are also strong positive correlations between average annual precipitation rates and annual total PFT fractional coverage in SSP126 (r=0.845, p<0.001), SSP370 (r=0.960, p<0.001) and SSP585 (r=0.996, p<0.001).

Therefore, there is a suggestion that the warmer and wetter environments expected by the end of the century favour the expansion of vegetative land surface types in the high latitudes, through improved growing conditions.

Furthermore, there are strong positive correlations between mean annual temperatures and total PFT flammability under SSP126 ($r=0.922$, $p<0.001$), SSP370 ($r=0.983$, $p<0.001$), and SSP585 ($r=0.977$, $p<0.001$). Additionally, there are also strong positive correlations with average annual precipitation rates under SSP126 ($r=0.821$, $p<0.001$), SSP370 ($r=0.956$, $p<0.001$), and SSP585 ($r=0.963$, $p<0.001$). Consequently, there are strong interconnections between flammability, temperature, and precipitation whereby a warmer and wetter climate, on the timescales studied here, in the northern high latitudes is associated with higher vegetation flammability. It is important to note that on finer timescales e.g. weeks within a fire season, precipitation may be negatively correlated with flammability, through temporary increases in fuel moisture (Cho et al., 2024; Holden et al., 2018).

Consequently, peat fire ignitions are expected to increase over the 21st century under all scenarios, but most strongly under SSP585. These increases are driven by increasing fuel loads and an increasing flammability of this fuel, which in turn are related to increasing temperatures and precipitation, which results in elevated numbers of flaming vegetation fires that can act as ignition events for peat fires.

3.1.2. Peat probability of ignition

Peat probability of ignition describes the likelihood of an ignition turning into a smouldering peat fire because of soil properties. Across the high latitudes the probability of peat igniting is expected to increase across the next century under all scenarios (Figure 72). All scenarios demonstrate similar trajectories of change for the first 40 years of the simulation, after which, increases in SSP126 start to slow and level off (Figure 72). However, peat ignition probability continues to grow at a similar rate as earlier in the century in both SSP370 and SSP585, with increases in the probability of peat igniting of 26.3% by 2100 under SSP585 compared to 2015-2025 (Table 41).

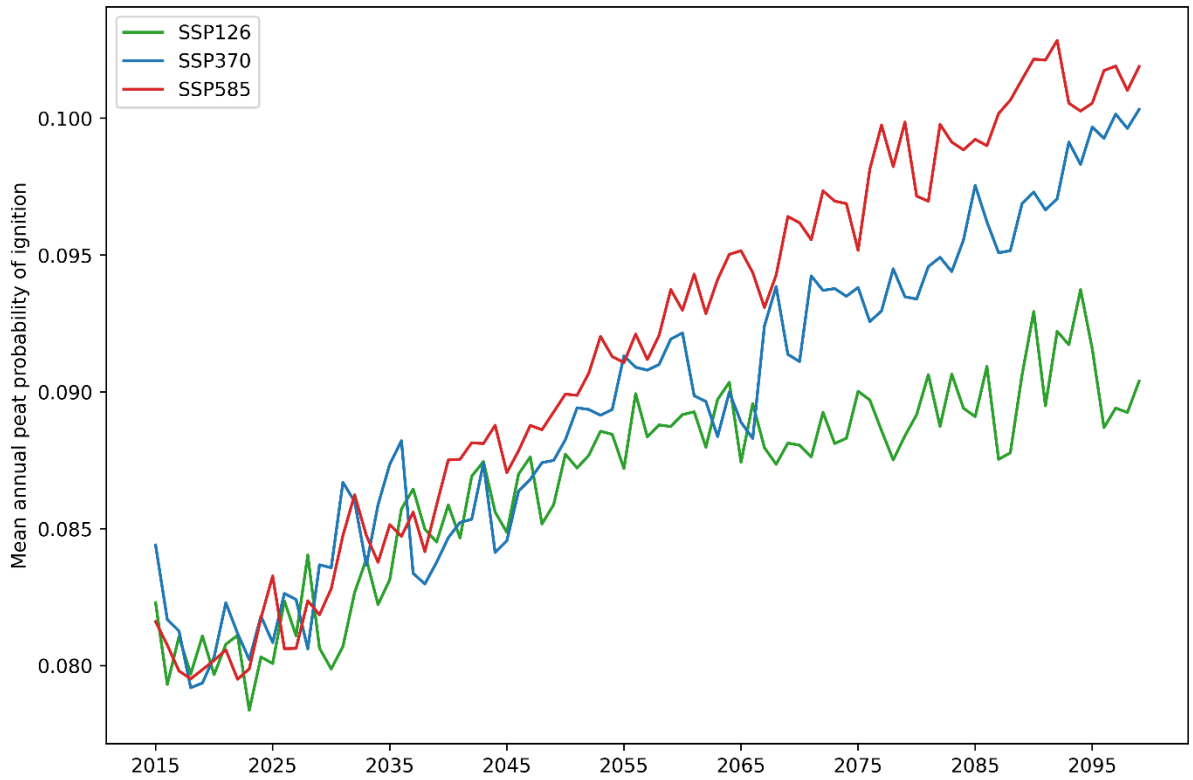


Figure 72: Annual mean peat probability of ignition in the northern high latitudes from 2015 to 2100 under the three different SSP scenarios.

Table 41: The annual mean peat probability of ignition above 50 degrees North averaged over the starting (2015-2025) and ending (2090-2100) decades of the model runs for each of the scenarios, and the change between these two periods.

Scenario	2015-2025 average annual peat **probability of ignition**	2090-2100 average annual peat **probability of ignition**	Change	% Change
SSP126	0.080	0.091	0.011	13.161
SSP370	0.081	0.099	0.018	21.661
SSP585	0.080	0.102	0.021	26.348

Increased peat ignition probabilities are seen for almost all the high latitude peatlands (Figure 73). These increases are most severe under SSP585, whilst the smallest increases are seen in SSP126. Broadly speaking, the largest increases in ignition probabilities are seen in the northernmost areas, in particular, in the Nunavut territory of Canada and the northern Siberian coast. However, there are also small areas of decreasing peat ignition probabilities which are seen most strongly in SSP370 and SSP585 (Figure 73b, c). The most prominent area of declining peat ignition probability is in the lowlands east of the Rocky Mountains in northwest Canada, where decreases in the probability of ignition of as much as 0.3 can be seen by the end of the century. Other areas of decrease also occur in northern Russia, and in parts of eastern Siberia, particularly in SSP370.

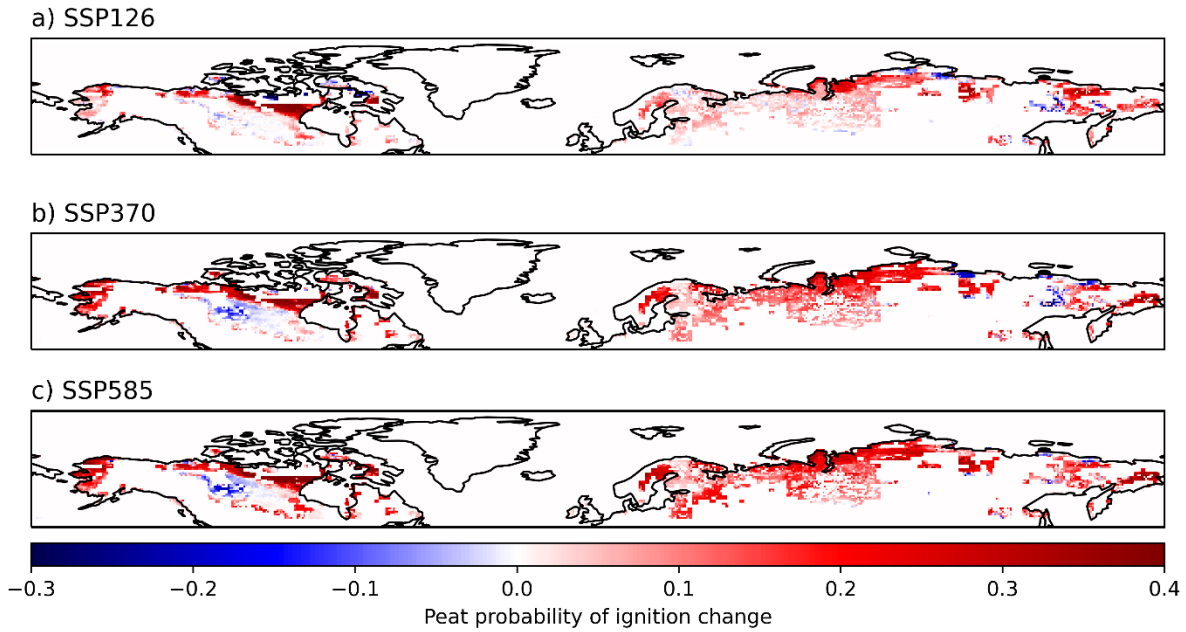


Figure 73: Difference in mean annual peat probability of ignition from the 2015-2025 average to the 2090-2100 average across the northern high latitudes in a) SSP126, b) SSP370 and c) SSP585.

Regions of increasing and decreasing probability of ignition are likely driven by the changing soil moisture in the northern high latitudes. Peat ignition probability is calculated as a product of known relationships between the likelihood of peat fire ignition with soil moisture, bulk density, and inorganic content. Within the simulations used here, temporally and spatially static values of bulk density and inorganic content are used. Therefore, soil moisture is the sole driver of variability in the probability of peat igniting.

3.1.2.1. Soil moisture

Across the high latitudes, on average, soil moisture declines over the next 85 years under all climate change scenarios (Figure 74). For the first 15 years of the simulation, there are minimal changes to the average soil moisture in all scenarios. However, beyond 2030, all scenarios begin to show similar levels of declining soil moisture. Soil moisture begins to level off in SSP126 in around 2055. Due to this levelling off, SSP126 sees only a 3.7% decrease in soil moisture by the end of the century (Table 42). In contrast, soil moisture continues to decline past 2055 in SSP370 and SSP585, resulting in overall decreases in soil moisture of 8.3% and 10.5% respectively by 2100 (Table 42).

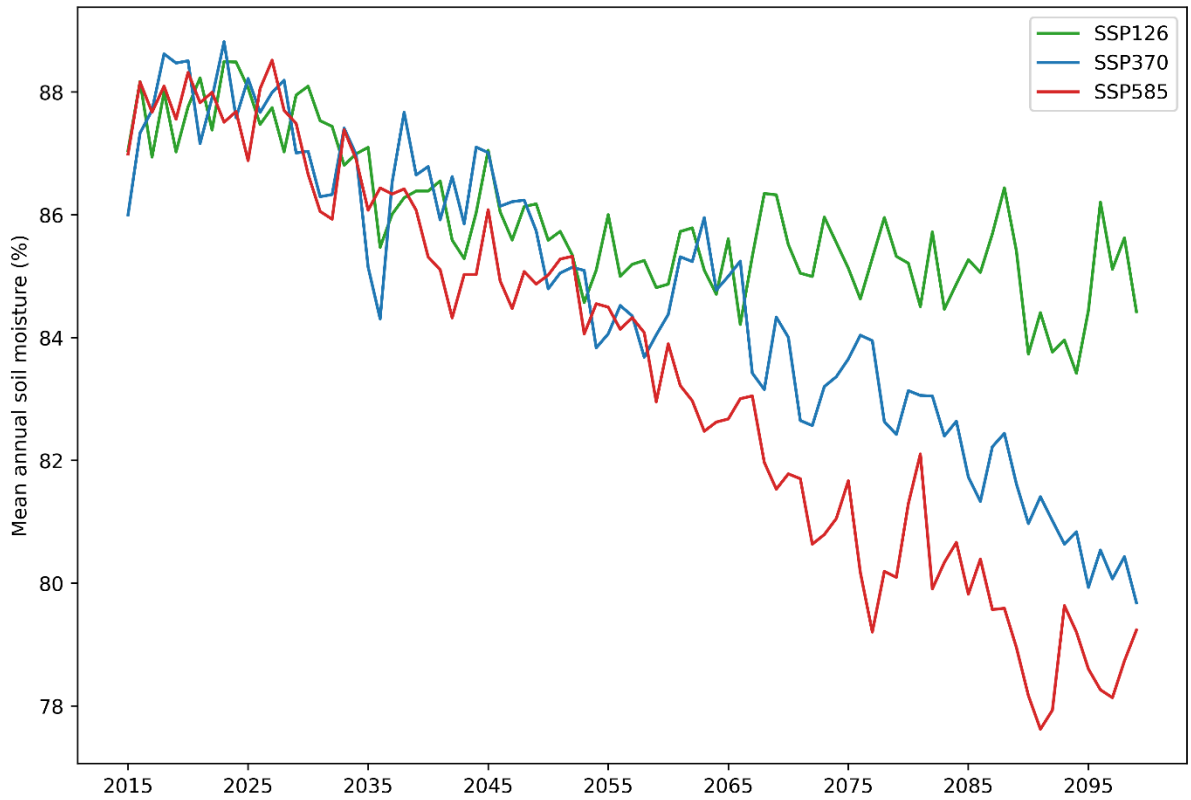


Figure 74: Mean annual soil moisture percentage in the northern high latitudes from 2015 to 2100 under the three different SSP scenarios.

Table 42: The annual mean soil moisture above 50°N averaged over the starting (2015-2025) and ending (2090-2100) decades of the model runs for each of the scenarios, and the change between these two periods.

Scenario	2015-2025 average annual peat soil moisture	2090-2100 average annual peat soil moisture	Change	% Change
SSP126	87.753	84.509	-3.244	-3.697
SSP370	87.810	80.552	-7.258	-8.266
SSP585	87.780	78.553	-9.227	-10.512

Decreases in soil moisture are seen across much of the high latitudes, with the largest declines seen in SSP585 (Figure 75). The strongest declines are seen in northern Canada, as well as parts of the Hudson Bay lowlands in Canada, and the Great Vasyugan Mire in Russia. Increases in soil moisture are also seen in all three scenarios. In SSP126 increases in soil moisture occur in southern Eurasia, whereas much of these areas experience decreases in SSP370 and SSP585 (Figure 75). Large areas of increasing soil moisture are also seen in northwest Canada and eastern Siberia, in line with the areas where there are decreases in peat ignition probability (Figure 75).

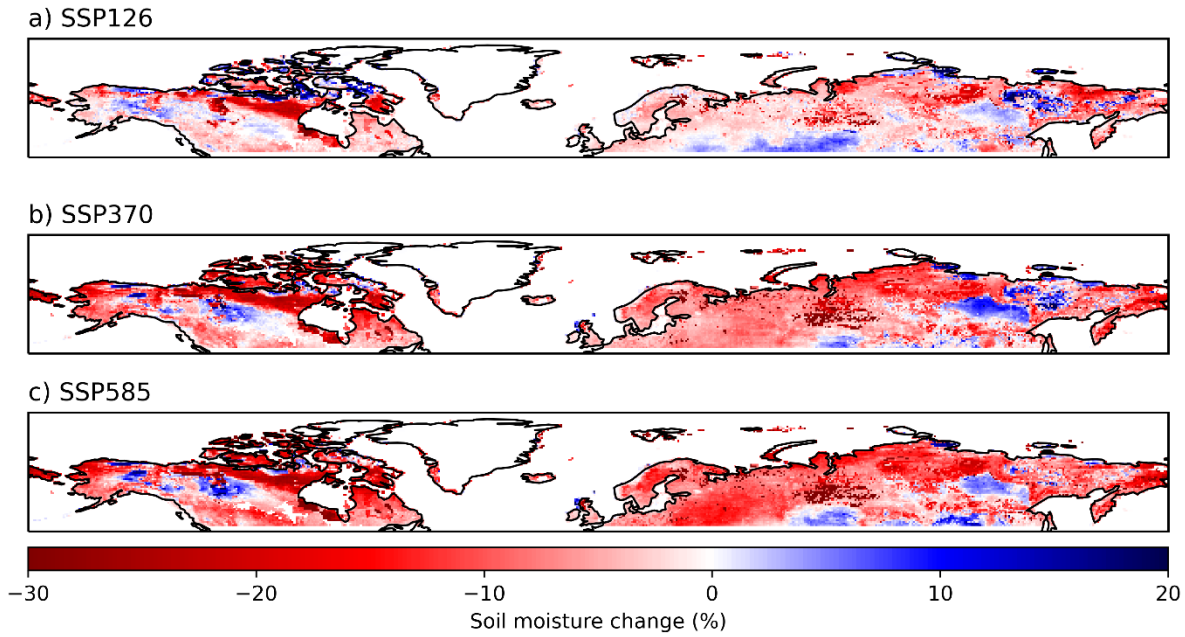


Figure 75: Change in mean annual soil moisture from the 2015-2025 average to the 2090-2100 average across the northern high latitudes in a) SSP126, b) SSP370 and c) SSP585.

There are strong large negative correlations between annual mean soil moisture and annual peat probability of ignition for the high latitudes under SSP126 ($r=-0.950$, $p<0.001$), SSP370 ($r=-0.984$, $p<0.001$) and SSP585 ($r=-0.983$, $p<0.001$), as expected due to soil moisture being the sole driver of peat ignition probability. This highlights that the overall trend towards drier soils in the high latitudes is resulting in higher probabilities of peat igniting, consequently leading to a greater number of peat fires, and greater burnt area. Additionally, spatially, the change from the starting and ending decade of the simulation in peat probability of ignition is negatively correlated with changes in soil moisture content under SSP126 ($r=-0.388$, $p<0.001$), SSP370 ($r=-0.253$, $p<0.001$) and SSP585 ($r=-0.183$, $p<0.001$). Therefore, areas of the northern high latitudes which see decreases in soil moisture commonly also show increases in the probability of peat igniting, and visa versa.

3.1.2.2. Drivers of changes in soil moisture

Within the JULES land surface model, soil moisture is influenced by numerous variables, ranging from climatological variables such as temperature and precipitation to hydrological factors such as evaporation and runoff. In order to better understand the driving forces behind the increasing probability of ignition of peat, the effects of 12 parameters on soil moisture changes between the starting and ending decades of the simulation are examined.

As seen in Figure 54a and Figure 55, modelled air temperature features increases over the 21st century, the magnitude of which are influenced by the different SSP scenarios. For example, under SSP126 temperature is expected to increase by 121% by the end of the century, but by 336% under SSP585 (Table 43). In general, in the high latitudes there is a tendency for increases in temperature to be associated with decreases in soil moisture (Table 44), thereby a warmer climate in the high latitudes is

associated with drier soils, potentially as a result of warmer temperatures driving higher evapotranspiration from the soil. Additionally, the number of days in a year in which temperatures are below freezing (0°C) decreases across the majority of the high latitude areas under all scenarios (Figure 76; Table 43). On average, under SSP126, at the start of the simulation 182 days per year see below freezing temperatures (i.e. almost half of the year). However, by the end of the simulation, the number of days below 0°C falls to 137 days under SSP126, 75 days under SSP370 and just 62 days under SSP585. The most prominent declines in days below freezing occur in the highest latitudes, and in particular in western Russia and Fennoscandia (Figure 76). It is expected that the presence of below-freezing temperatures results in soils with higher moisture contents, with freeze-thaw processes also playing an important role in driving soil moisture (Chen et al., 2022; Wang and Hu, 2023), due to known inverse relationships between soil temperature and soil moisture (Zhang et al., 2020). Therefore, there are significant positive correlations between changes in the number of days in a year below 0°C and changes in soil moisture (Table 44), suggesting that smaller declines in the number of days below freezing tend to lead to either increases or minimal changes in soil moisture, and that the largest declines in soil moisture occur in areas with the largest decreases in the number of days below freezing.

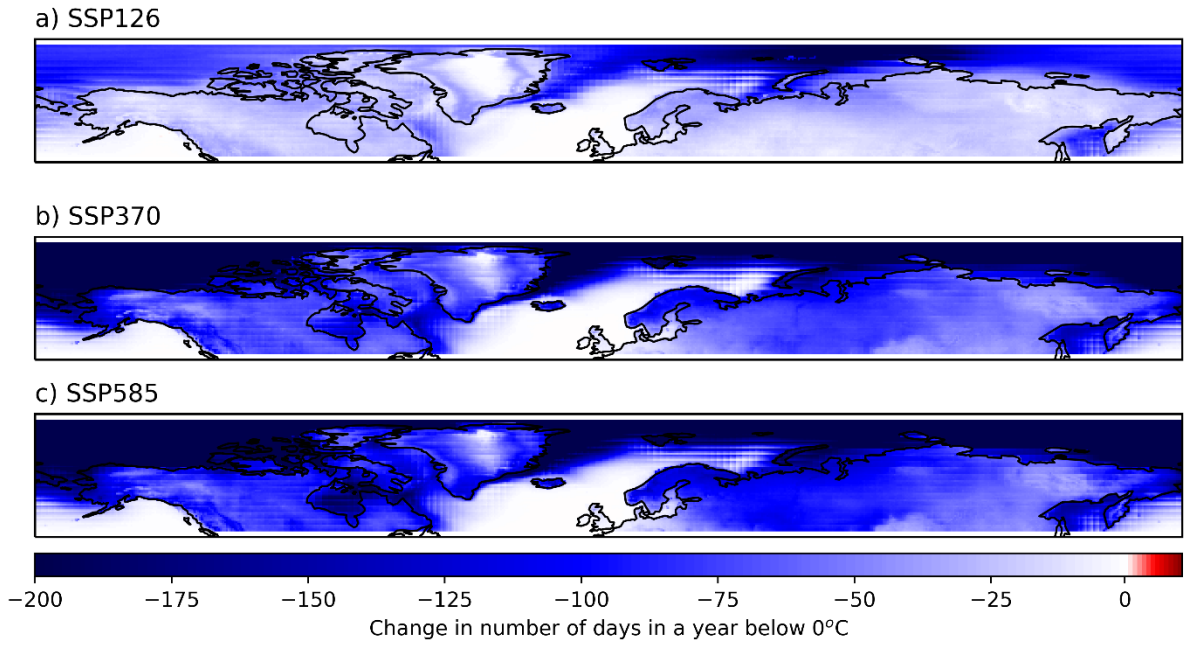


Figure 76: The change in mean annual number of days below 0°C from the 2015-2025 average to the 2090-2100 average across the northern high latitudes in a) SSP126, b) SSP370 and c) SSP585

Precipitation is expected to increase across all scenarios over much of the high latitudes by 2100 (Figure 54b and Figure 56). However, there is no relationship between the change in precipitation over the 21st century and the change in soil moisture (Table 43 and Table 44). It might have been expected that increases in precipitation would result in wetter soils. However, as higher precipitation

is significantly associated with higher temperatures, it may be possible that the effect of increased temperatures may be overriding that of increased precipitation, leading to the drying of soils seen in JULES.

Across much of the high latitudes, precipitation falls as snow, and therefore changes in snow mass fractions can be examined, with potential impacts on soil moisture. Also, across much of the high latitudes, snow mass declines between the 2015-2025 average and the 2090-2100 average under all scenarios (Figure 77; Table 43). However, there are some regions such as northwest Canada, eastern Alaska, eastern Siberia, and Greenland which feature increases in snow mass, particularly in SSP370 (Figure 77b). Changes in snow mass may be being driven by a combination of changes in precipitation and temperature, whereby decreases in snow mass may be due to warmer temperatures leading to snow melt, and precipitation falling as rain rather than snow. The increases in snow mass seem to occur in regions where there are smaller declines in the number of days below 0°C (Figure 76), but also where there are some of the larger increases in precipitation (Figure 56). Therefore, in these areas, due to higher precipitation and relatively cooler environments, snow mass may increase. On the other hand, there are no relationships between changes in snow mass and changes in soil moisture (Table 44).

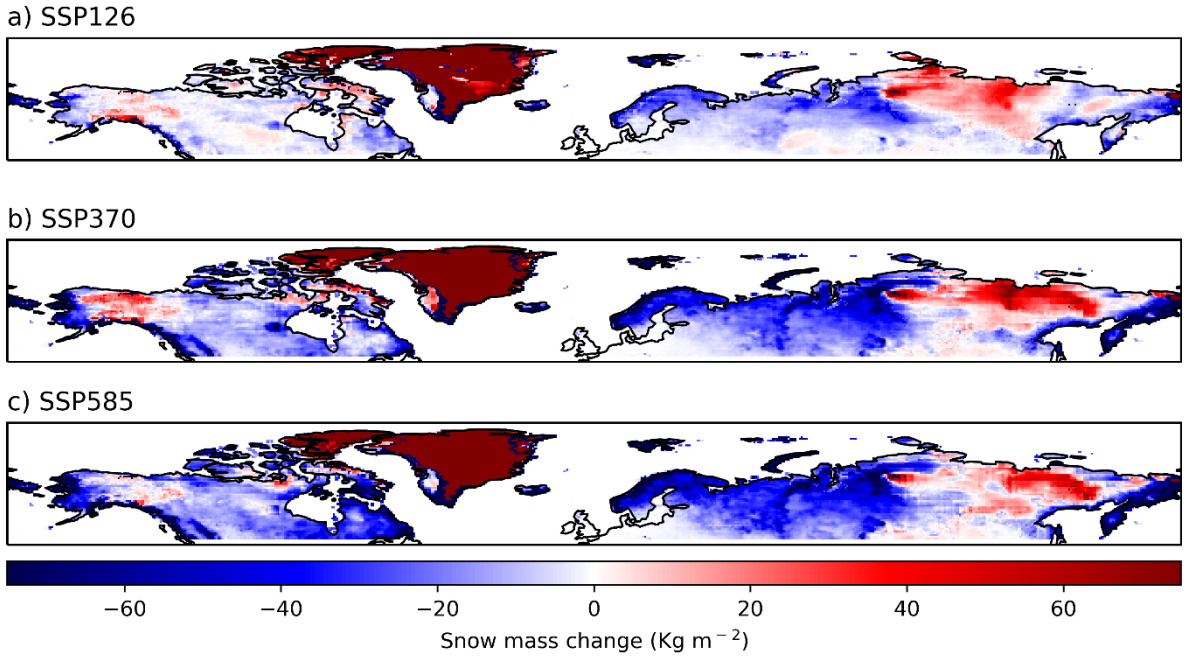


Figure 77: The change in mean annual snow mass from the 2015-2025 average to the 2090-2100 average across the northern high latitudes in a) SSP126, b) SSP370 and c) SSP585.

In addition to surface air temperatures, soil temperatures are also increasing across the whole of the northern high latitudes under all scenarios (Figure 78). The largest increases are seen under SSP585, and in areas of eastern Siberia and northern Canada (Figure 78c). On average across the high latitudes, soil temperatures are projected to increase from an average of -0.6°C in 2015-2025, to 6.9°C

in 2090-2100 under SSP585 (Table 43). Similarly, the mean annual number of months with an average soil temperature below 0°C decreases across the high latitudes and under all simulations, with average declines of 43% under SSP585 (Figure 79; Table 43). Like for air temperature, under SSPs 370 and 585 there are significant, albeit weak, negative correlations between the change in soil temperature and the change in soil moisture (Table 44). Therefore, in these scenarios higher soil temperatures are associated with drier soils. In contrast, under SSP126 there is a significant weak positive correlation (Table 44), suggesting that in SSP126 areas with higher soil temperatures also experience higher soil moisture. However, under all scenarios there are significant positive relationships between the number of months in a year with temperatures below freezing and soil moisture (Table 44). Consequently, areas where there are large reductions in the number of months below freezing, also see the largest declines in soil moisture, possibly due to a large shift in the climatic conditions of there area.

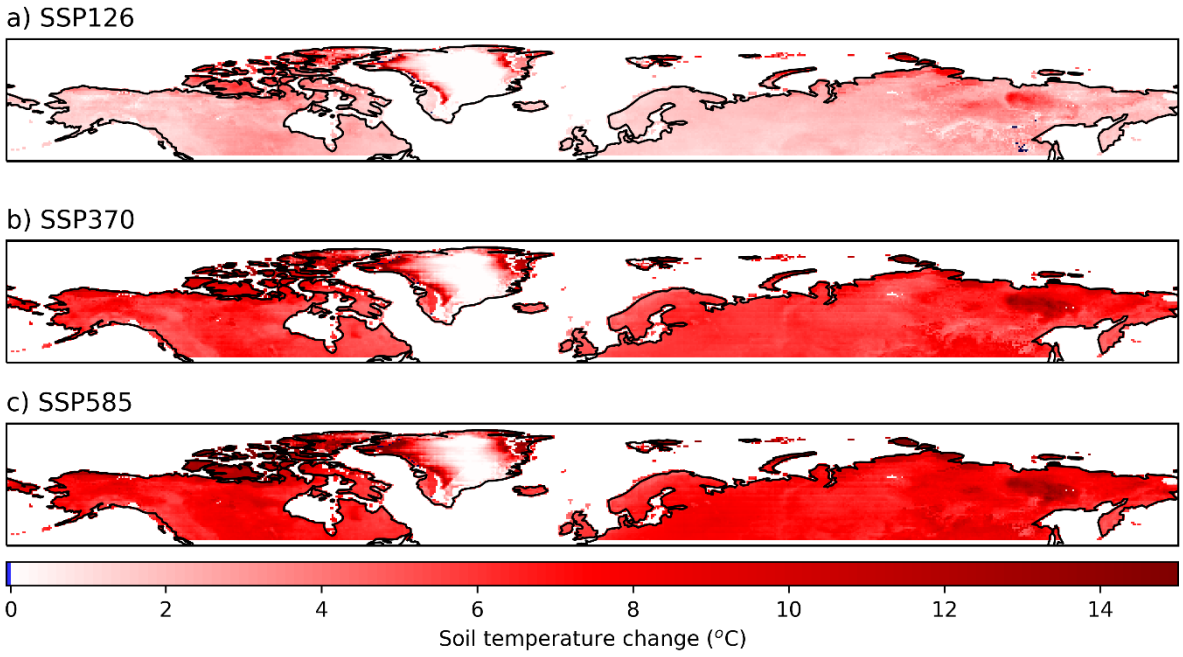


Figure 78: The change in mean annual soil temperature from the 2015-2025 average to the 2090-2100 average across the northern high latitudes in a) SSP126, b) SSP370 and c) SSP585.

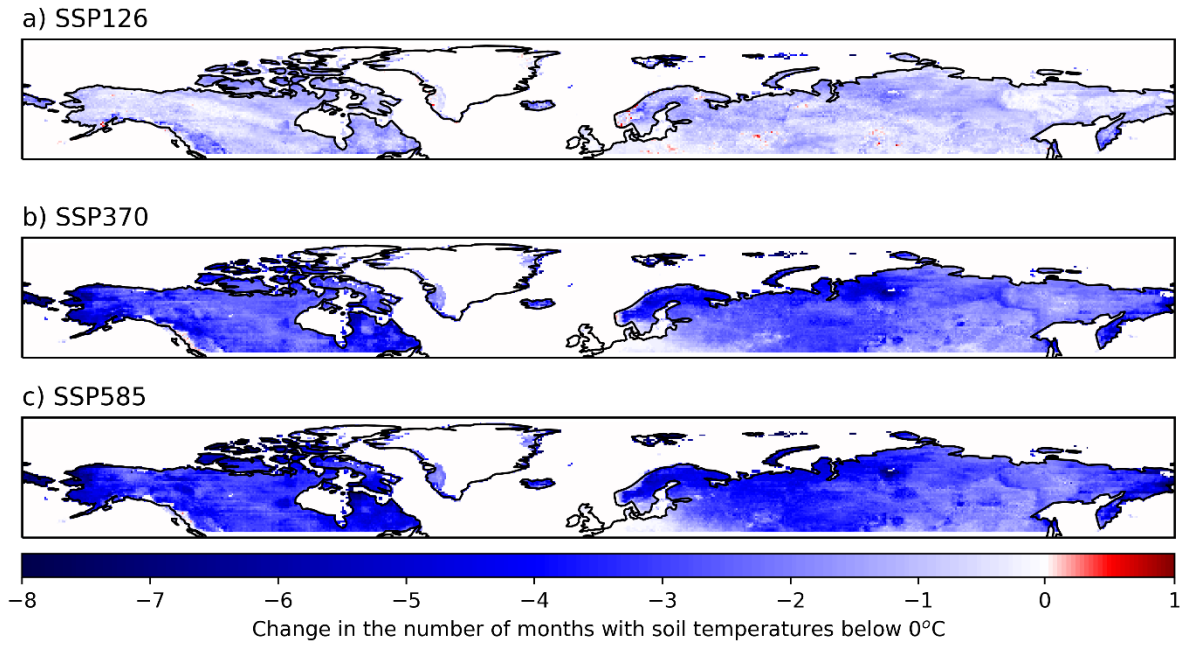


Figure 79: The change in mean annual number of months when average soil temperature is below 0°C from the 2015-2025 average to the 2090-2100 average across the northern high latitudes in a) SSP126, b) SSP370 and c) SSP585.

Changes to hydrological processes are also anticipated over the remainder of the 21st century (Figure 80; Table 43). Soil evapotranspiration is expected to increase across the high latitudes under all scenarios and most prominently in the northernmost regions (Figure 80a-c). However, under SSP370, and more prominently SSP585, there are areas of decreasing evapotranspiration across northern Europe, southern Canada and parts of Siberia (Figure 80c). Similarly, evaporation from the canopy layer across the high latitudes is also modelled to increase under all scenarios and across the high latitudes (Figure 80d-f), by as much as 78% by the end of the century under SSP585 (Table 43). The surface moisture flux describes the cumulative effect of evaporation and transpiration from the vegetative and soil moisture stores. Consequently, the average annual surface moisture flux is expected to increase by the ending decade of the simulation relative to the starting decade (Figure 80g-i), with average increases of 15-23% depending on the SSP scenario (Table 43). Changes in surface moisture fluxes exhibit very similar spatial patterns to both soil evapotranspiration and canopy evaporation, and also show declines in northern Europe and southern Canada (Figure 80g-i). These areas of decreasing surface moisture flux align well with areas where decreases in precipitation are seen (Figure 56), suggesting a general trend towards drier surface environments in these regions by the end of the century than are seen at present.

Finally, on average, runoff is predicted to increase across the high latitudes by as much as 80% under SSP585 (Table 43). However, there is substantial spatial variation (Figure 80j-l). For example, large increases in run off are seen in the Arctic regions of the high latitudes, but large decreases are seen under SSP126 across northern Europe and southern Fennoscandia, as well as across Canada and

eastern Siberia (Figure 80j). However, these decreases are less pronounced in the high emissions scenarios, with decreases confined to northern Europe and southern Canada (Figure 80i).

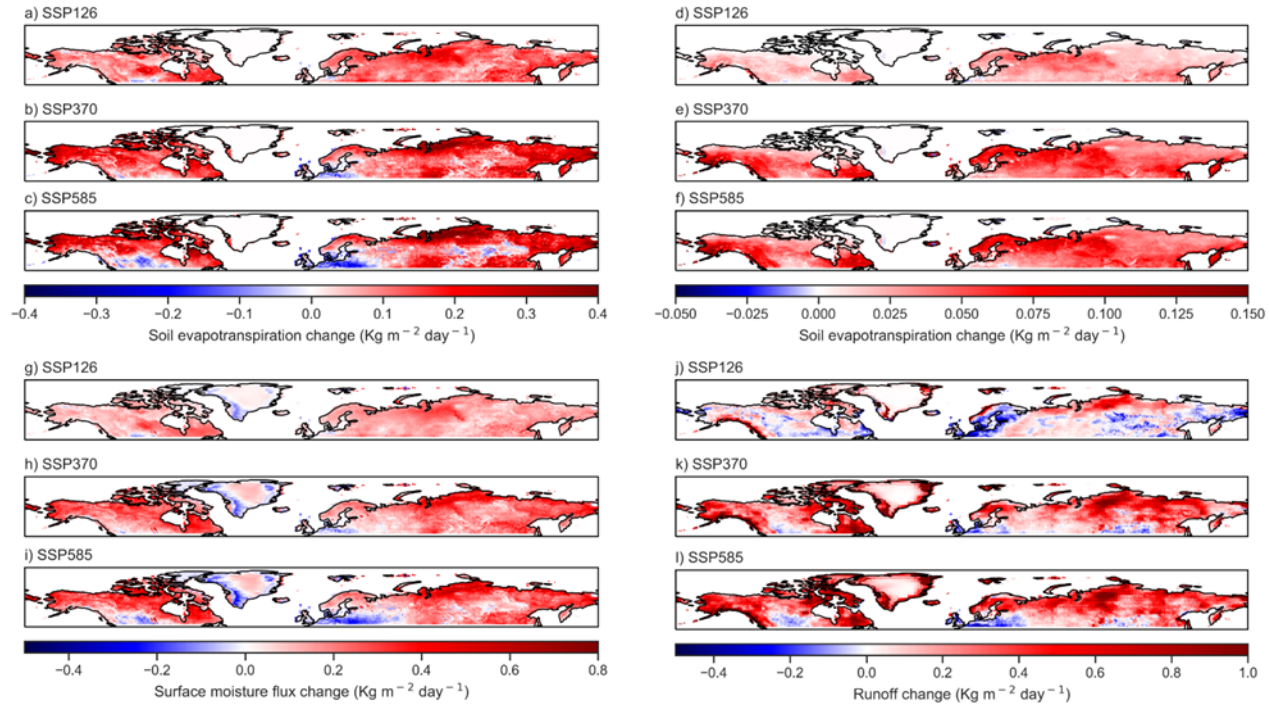


Figure 80: The change in various hydrological parameters from the 2015-2025 average to the 2090-2100 average across the northern high latitudes under SSP126 (a, d, g, j), SSP370 (g, e, h, k) and SSP585 (c, f, i, l). Plots a-c show the change in soil evapotranspiration and d-f show the change in canopy evaporation. Plots g-i show the change in surface moisture flux, and plots j-l show the change in runoff.

Changes in the four hydrological variables exhibit contrasting correlations with changes in soil moisture. Most strongly, there are significant negative correlations between changes in soil evapotranspiration and soil moisture, and changes in surface moisture flux and soil moisture under SSPs 370 and 585 (Table 44). However, there are only weak relationships between canopy evaporation and soil moisture regardless of scenario (Table 44). There are weak, but significant, positive correlations between changes in runoff and changes in soil moisture (Table 44). Consequently, these results suggest that the increased flux of moisture into the atmosphere, primarily in the form of soil evapotranspiration, is associated with decreases in soil moisture over the high latitudes, whilst increases in runoff, may be contributing to wetter soils in some areas.

Changes to the depth of the water table are also expected as a result of climate change and anthropogenic activities. As water table depth and soil moisture are highly linked, with higher water tables supporting wetter peat soils due to strong capillary forces within the soil (Nelson et al., 2021; Wilkinson et al., 2020), changes in soil moisture are likely to be strongly affected by changes in water table depth. On the whole, water table depths in the northern high latitudes are increased by the end of the century compared to the 2015-2025 average by as much as 29.3% under SSP585 (Table 43), meaning that water tables tend to move deeper into the soil column. However, spatially there is a

distinct contrast between areas of decreases and areas of increases, particularly under SSP370 and SSP585 (Figure 81). The northernmost regions exhibit strong increases in water table depth, especially in eastern Siberia. However, across much of western and central Russia, and southern Canada there are decreases in water table depths, indicating that the water table is moving closer to the surface in these areas, potentially driving the wetter soils seen in some of these areas. Especially under SSP126, there are significant negative correlations between the change in water table depth and soil moisture over the 21st century (Table 44), indicating that where there are large increases in water table depths, there tends to be large decreases in soil moisture.

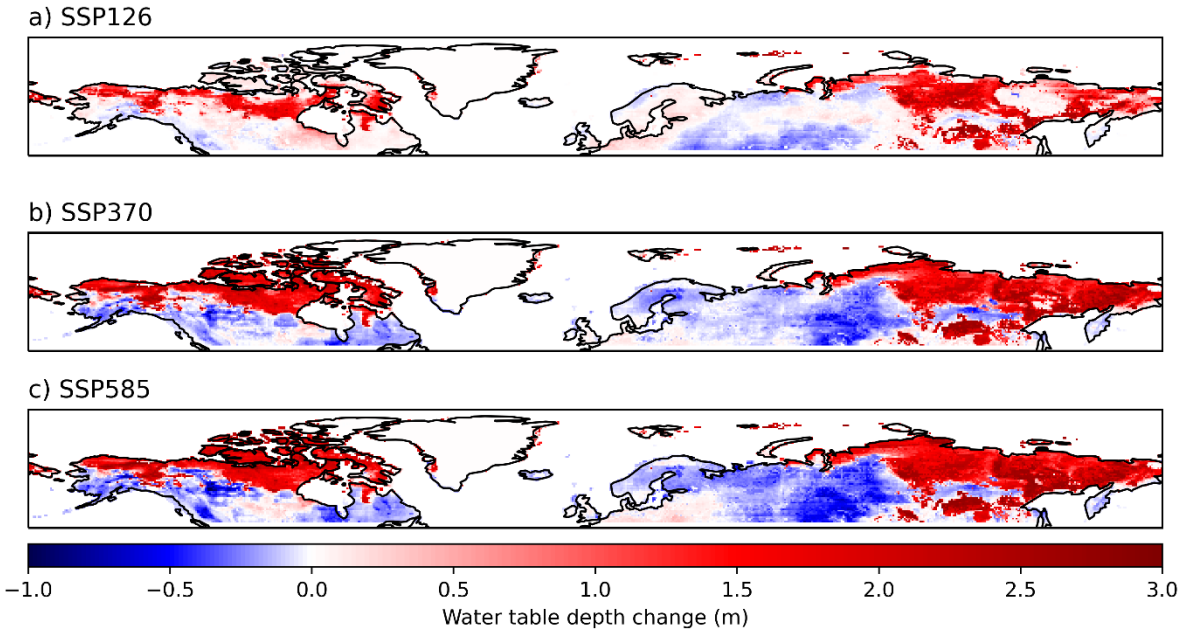


Figure 81: The change in mean annual water table depth (m) from the 2015-2025 average to the 2090-2100 average across the northern high latitudes in a) SSP126, b) SSP370 and c) SSP585.

As previously mentioned, the fraction of grid cells covered by vegetative land surface types is expected to increase by 2100 under all SSP scenarios (Table 43 and see Section 3.1.1.1. for more information). Increasing vegetation cover may alter soil moisture through changes in the vegetative water demand. However, there is no relationship between changes in PFT fractions and changes in soil moisture (Table 44), suggesting that the overall increase in vegetation is not associated with changes in soil moisture. As previously described (section 3.1.1.1.), the relative composition of different PFTs is also changing, which perhaps may also be having an influence on the changing soil moisture.

Table 43: The annual average soil moisture, and its driving parameters, above 50 degrees North averaged over the starting and ending decades of the model runs for each of the scenarios, and the change between these two periods.

Variable	SSP126			SSP370			SSP585		
	2015-	2090-	%	2015-	2090-	%	2015-	2090-	%

	2025 average	2100 average	Change	2025 average	2100 average	Change	2025 average	2100 average	Change
Soil moisture	87.753	84.509	-3.697	87.810	80.552	-8.266	87.780	78.553	-10.512
Air temperature (°C)	-3.450	0.723	120.954	-3.501	6.680	290.795	-3.624	8.540	335.619
Days air temperature below 0°C	181.630	137.241	-24.439	182.523	75.436	-58.671	185.512	61.776	-66.700
Precipitation (Kg m^{-2} s^{-1})	1.623	1.808	11.426	1.617	2.119	31.030	1.603	2.184	36.230
Snow mass (Kg m^{-2})	54.094	49.186	-9.074	53.435	38.051	-28.791	53.906	31.974	-40.686
Soil temperature (°C)	-0.489	1.859	479.946	-0.618	5.587	1003.656	-0.653	6.939	1162.965
Months soil temperature below 0°C	3.546	3.116	-12.146	3.569	2.300	-35.567	3.595	2.049	-43.010
Soil evapotranspiration (Kg m^{-2} day^{-1})	0.539	0.631	17.036	0.534	0.667	24.861	0.535	0.664	24.205
Surface evaporation (Kg m^{-2} day^{-1})	0.056	0.072	29.785	0.054	0.093	71.525	0.054	0.096	78.177
Surface moisture flux (Kg m^{-2} day^{-1})	0.761	0.875	14.946	0.755	0.932	23.477	0.757	0.930	22.935
Runoff (Kg m^{-2} day^{-1})	0.740	0.868	17.282	0.722	1.189	64.648	0.715	1.287	79.920
Water table depth (m)	1.968	2.341	18.974	1.952	2.506	28.370	1.949	2.521	29.309
PFT fraction	0.547	0.565	3.302	0.546	0.607	11.182	0.546	0.618	13.058

Table 44: Pearsons's correlation coefficients (r) between the change in soil moisture from the 2015-2025 average and the 2090-2100 average with the change in numerous variables from the JULES land surface model. Asterisks indicate significant p values (*=p<0.05, **=p<0.01, ***=p<0.001).

Soil moisture driver	SSP126	SSP370	SSP585
Air temperature	-0.126***	-0.212***	-0.235***
Days air temperature below 0°C	0.170***	0.369***	0.359***
Precipitation	0.044***	-0.038***	-0.030***
Snow mass	0.034***	0.024***	0.019**
Soil temperature	0.118***	-0.014*	-0.118***
Months soil temperature below 0°C	0.232***	0.401***	0.404***
Soil evapotranspiration	0.026***	-0.208***	-0.214***
Canopy evaporation	0.041***	0.068***	0.104***
Surface moisture flux	0.015*	-0.180***	-0.194***
Runoff	0.022***	0.023***	0.035***
Water table depth	-0.393***	-0.150***	-0.141***
PFT fraction	0.091***	-0.008	-0.009

Patterns and changes in soil moisture are likely a result of a combination of the different aforementioned interacting factors. It is apparent that increasing high latitude temperatures are associated with declining high latitude soil moisture, through increases in thermodynamic energy, which may lead to increases in moisture fluxes from the surface and especially evapotranspiration from soils. Additionally, deeper water tables across the high latitudes, which may be partially caused by higher temperatures, also appear to be contributing towards drier and more combustible soils. The freezing threshold also appears to be critical in controlling soil moisture in the high latitudes, with areas which retain more days below 0°C occurring alongside the smallest declines and increases in soil moisture. Therefore, declining soil moisture driven by increased temperatures and increased evapotranspiration, is resulting in increases in the probability of ignition of peatland environments across the northern high latitudes.

3.2. Depth of burn

The depth of burning into peatland environments is expected to increase by 2100 across the northern high latitudes under all SSP scenarios (Figure 82). All scenarios follow a similar trajectory for the first 30 years of the simulation. However, after around 2045, increases in depth of burn under SSP126 begin to slow down, and eventually begin to level off after ~2080 (Figure 82). By the end of the simulation, peat fires burn on average 2.4cm deeper into the soils under SSP126 compared to the 2015-2025 average, an increase of 11.8% (Table 45). Depth of burn continues to increase over the 21st century under SSP370 and SSP585, overall by 22.8% and 26.0%, respectively, by the end of the century; equating to, on average, 5.8cm of additional burnt soil under SSP585 (Figure 82; Table 45).

Table 45: The mean peat depth of burn (m) above 50 degrees north averaged over the starting and ending decades of the model simulations for each of the scenarios, and the change between these two periods

Scenario	2015-2025 average depth of burn (m)	2090-2100 average depth of burn (m)	Change	Percentage change
SSP126	0.223	0.249	0.026	11.799
SSP370	0.224	0.275	0.051	22.811
SSP585	0.222	0.280	0.058	25.994

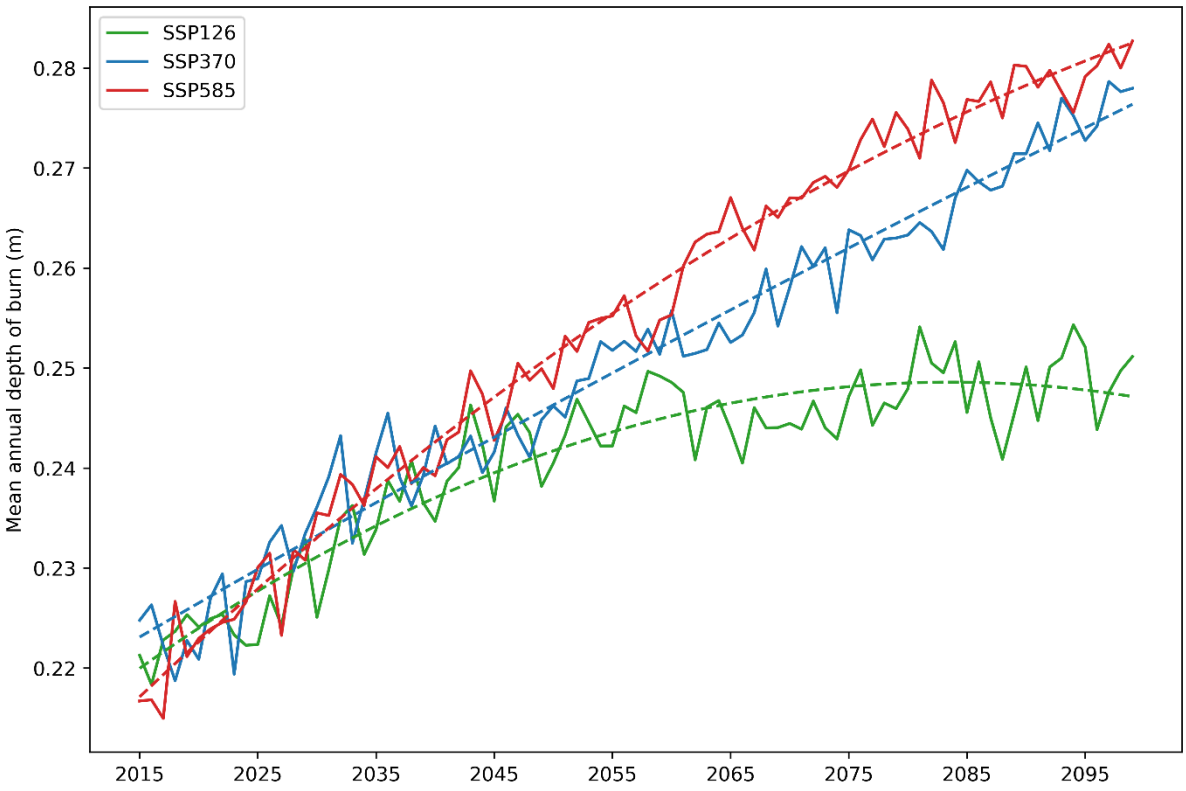


Figure 82: Average annual peat depth of burn (m) above 50 degrees north from 2015 to 2100 for each of the SSPs. The dashed lines indicate the quadratic trendline for the respective SSP.

Changes in depth of burn are seen across the majority of high latitude peatlands with notable large increases in the depth of peat burning by the end of the century, compared to the 2015-2025 average, in the far northern, Arctic regions of Alaska, Canada and Siberia, getting progressively larger with each climate change scenario (Figure 83). There are small patches of declines in depth of burn under SSP126 in far eastern Siberia, western Canada, and Fennoscandia (Figure 83). However, under SSPs 370 and 585 these reductions in depth of burn occur in more constrained areas and to a much lesser extent.

Depth of burn is calculated in INFERNO-peat as a function of soil moisture, soil temperature and water table depth (Chapter 2 Section 3.4), and consequently changes in depth of burn can be explained by changes in these factors.

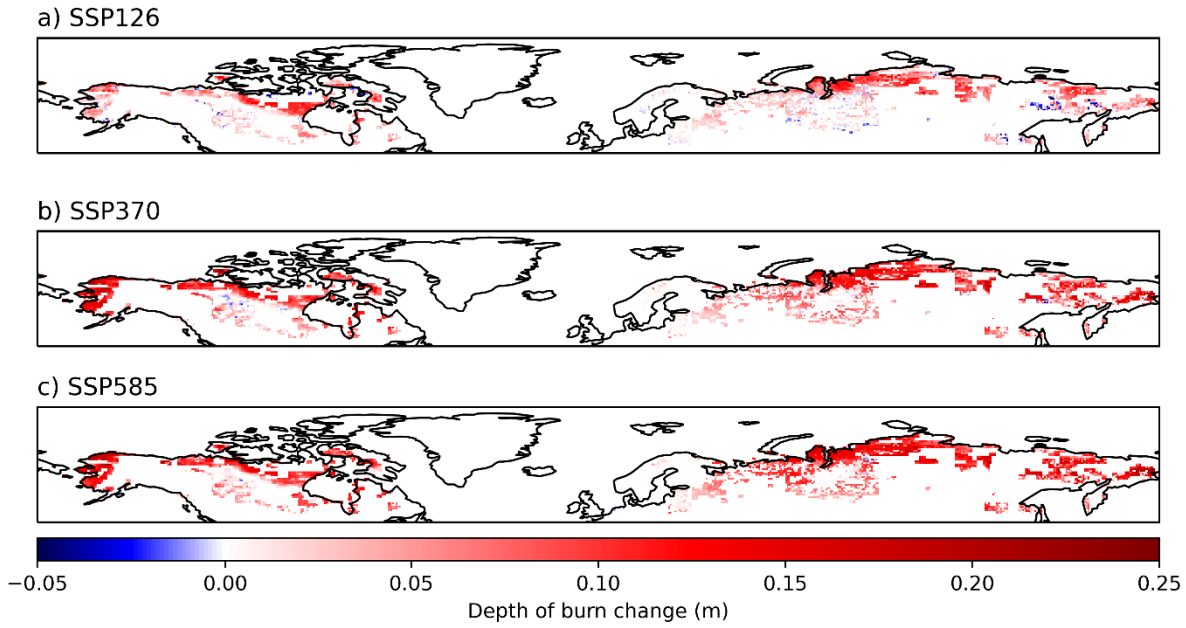


Figure 83: The change in mean depth of burn from the 2015-2025 average to the 2090-2100 average over the northern high latitudes under a) SSP126, b) SSP370 and c) SSP585.

Temporally, there are significant strong correlations in the northern high latitude average annual depth of burn with annual average soil moisture, soil temperature and water table depth (Table 46). There are strong negative correlations between mean annual depth of burn and mean annual soil moisture, indicating that wetter soils are associated with shallower burning, and that drier soils see much deeper burning. Positive correlations exist between average annual depth of burn and soil temperatures (Table 46), indicating that warmer soils may facilitate greater vertical burning of the soil column. Similarly, there are also strong positive correlations between water table depth and depth of burn on an annual basis (Table 46), with deeper water tables occurring alongside deeper burning into the soil. Therefore, shallower water tables, which are associated with wetter soils, see shallower burning of the soil.

Table 46: Pearsons's correlation coefficients (r) between the mean annual peat fire depth of burn and its three driving variables; soil moisture; soil temperature; and water table depth. Asterisks indicate significant p values (*=p<0.05, **=p<0.01, ***=p<0.001).

	SSP126	SSP370	SSP585
Soil moisture	-0.896***	-0.961***	-0.966***
Soil temperature	0.962***	0.987***	0.984***
Water table depth	0.943***	0.960***	0.977***

Spatially, changes in depth of burn are also driven by changes in soil moisture, soil temperature and water table depth. Changes in soil moisture, soil temperature and water table depth between the starting and ending decades can be seen in Figures Figure 75, Figure 78, and Figure 81, all showing increases across much of the high latitudes. There is a significant negative correlation between the change in soil moisture and depth of burn under SSP126 (Table 47), suggesting that drier soils are

associated with deeper burning. However, under SSP370 and SSP585 these relationships are much weaker and indicate no correlation between changes in soil moisture and changes in depth of burn (Table 47). In contrast there are significant and strong positive correlations between both changes in soil temperature and changes in water table depth with changes in depth of burn (Table 47). This suggests that warmer soils and deeper water tables contribute towards deeper peat burning into the soil, and visa versa.

Table 47: Pearsons's correlation coefficients (r) between the change from the 2015-2025 average to the 2090-2100 average annual peat fire depth of burn and its three driving variables; soil moisture; soil temperature; and water table depth. Asterisks indicate significant p values (*=p<0.05, **=p<0.01, ***=p<0.001).

	SSP126	SSP370	SSP585
Soil moisture	-0.235***	-0.025*	0.065***
Soil temperature	0.315***	0.336***	0.354***
Water table depth	0.541***	0.537***	0.562***

Overall, across the high latitudes, INFERNO-peat simulates an increase in peat depth of burn under all three scenarios, but most severely under SSP585. This increase in depth of burn is likely most strongly driven by increases in water table depth and rising soil temperatures, which both contribute towards drier soils, which can better facilitate the spread of smouldering peat fires deeper within the soil column. Deeper peat burning is of concern as it exposes a larger amount of long-term stored carbon within the peat to combustion, consequently resulting in greater carbon emissions and possible feedback effects on the atmosphere.

3.3. Carbon emissions

Annual carbon emissions from peat fires increase through the simulation period under all scenarios (Figure 84). Up until around 2030 all three scenarios remain similar, but from this point onwards there is a large increase in carbon emissions in SSP370 and SSP585 (Figure 84); whereas, under SSP126 there is a smaller increase, followed by a levelling off and eventual decline from ~2080 onwards (Figure 84). This means that annual peat fire carbon emissions appear to settle at around 490 Tg of carbon by the end of the simulation in SSP126, up 50.6% compared to the 2015-2025 average (Table 48). Peat fire carbon emissions undergo much larger increases across the northern high latitudes as a whole under the higher emissions scenarios, with SSP370 projecting a 170.1% increase and SSP585 a 269.3% increase in annual emitted carbon by 2100 (Table 48). This equates to an emission of more than 1 Gt of carbon every year from peat burning alone by 2100 under SSP585, potentially exerting a large forcing effect on the climate system.

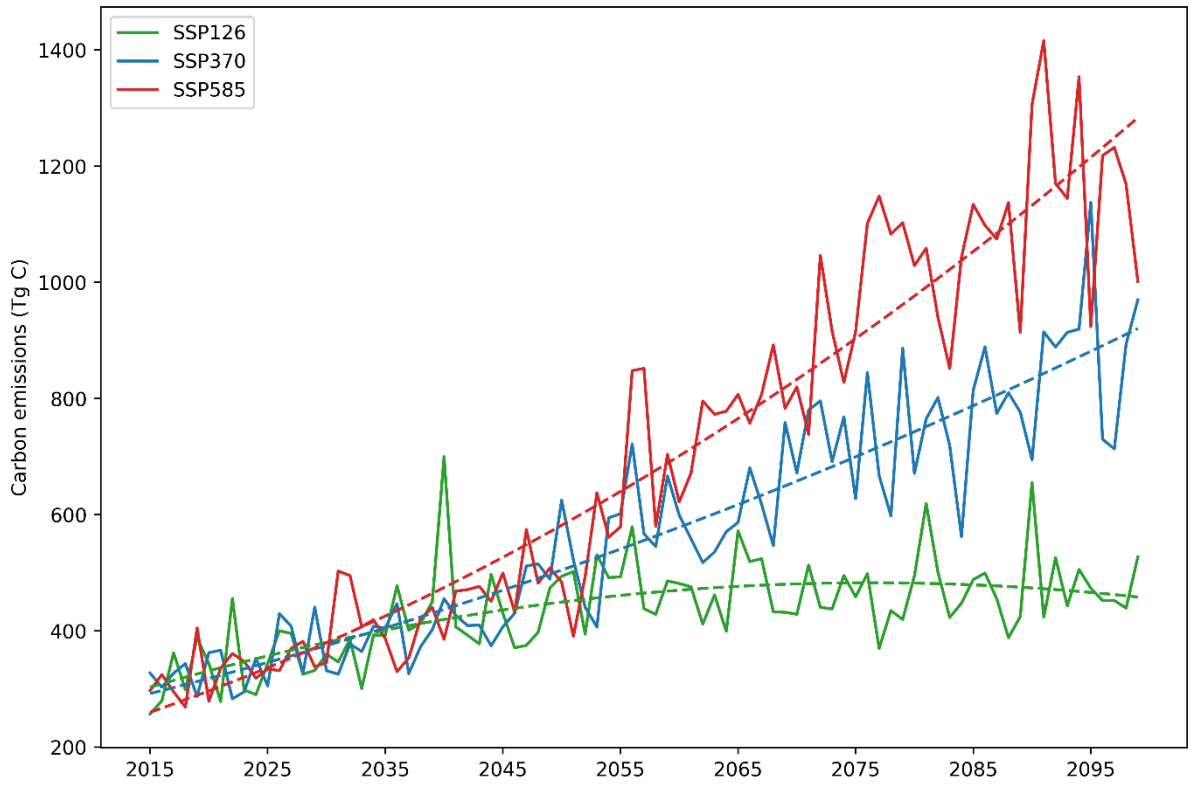


Figure 84: Annual peat fire carbon emissions (Tg C) above 50°N from 2015 to 2100 for each of the SSPs. The dashed lines indicate the quadratic trendline for the respective SSP.

Table 48: The mean annual peat fire carbon emissions (Tg C) above 50°N, averaged over the starting (2015-2025) and ending (2090-2100) decades of the model simulations for each of the scenarios, and the change between these two periods

Scenario	2015-2025 average carbon emission (Tg)	2090-2100 average carbon emission (Tg)	Change	Percentage change
SSP126	325.233	489.817	164.584	50.605
SSP370	324.853	877.528	552.676	170.131
SSP585	323.183	1193.603	870.420	269.327

Under all scenarios, carbon emissions from peat fires increase everywhere across the northern high latitudes, but most strongly over northwest Siberia and Canada (Figure 85). The areas which see the largest increases in peat fire carbon emissions occur in the same areas in which large increases in peat burnt area are seen, namely northwest Siberia surrounding the Great Vasyugan Mire, and in western and central Canada. Smaller increases in peat fire carbon emissions are found across eastern Siberia, western Russia and Fennoscandia.

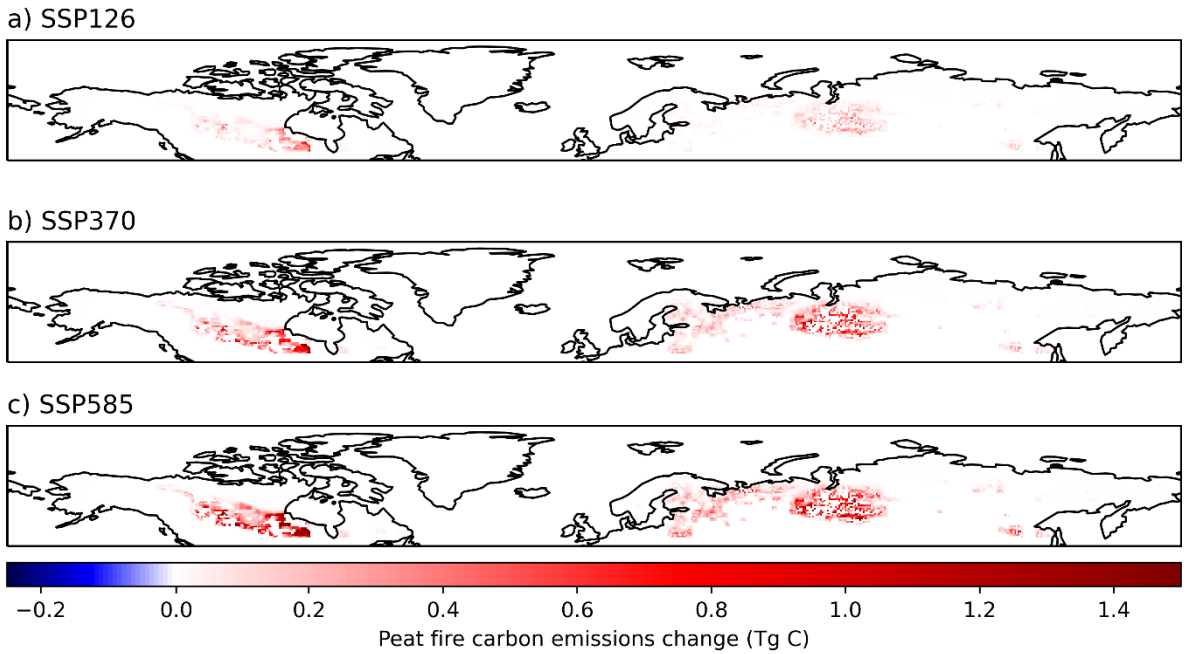


Figure 85: The change in mean carbon emissions (Tg C) from the 2015-2025 average to the 2090-2100 average over the northern high latitudes under a) SSP126, b) SSP370 and c) SSP585.

Within INFERNO-peat, peat fire carbon emissions are estimated as a product of peat burnt area, depth of burn, combustion completeness and the carbon content of the peat (Equation 11). As a non time varying dataset is used for peatland carbon content, and a fixed value is used for combustion completeness in these simulations, modelled peat fire carbon emissions are being driven by changes in burnt area and depth of burn. As previously mentioned, both peat burnt area and depth of burn increase throughout the simulation period across the majority of the high latitudes, consequently driving increases in the amount of carbon emitted from peat fires. As evidenced in Table 49, there are strong positive correlations between the mean annual burnt area and carbon emissions under all scenarios, indicating that burning larger areas within a year is associated with large carbon emissions. Additionally, there are strong positive correlations between mean annual depth of burn and carbon emissions (Table 49), highlighting that when peat fires burn deeper in the soil, a greater amount of carbon is exposed to combustion, consequently resulting in increases in carbon emissions from peat fires.

Table 49: Pearsons's correlation coefficients (r) between the mean annual peat fire carbon emissions and burnt area and depth of burn in the three SSP scenarios. Asterisks indicate significant p values (*=p<0.05, **=p<0.01, ***=p<0.001).

	SSP126	SSP370	SSP585
Burnt area (M km^2)	0.993***	0.999***	0.998***
Depth of burn (m)	0.636***	0.902***	0.922***

Spatially, changes in peat fire carbon emissions between the starting and ending decades of the simulation are strongly positively correlated with changes in burnt area (Table 50), indicating that strong increases in carbon emissions from peat fires are heavily associated with increases in peat burnt area. However, in contrast to the average annual correlations, there is a weak negative correlation between changes in carbon emissions and changes in depth of burn (Table 50). This would suggest that increases in carbon emissions would be associated with decreases in the depth of burn, contrary to what is theorised and opposite to what is shown in Table 49. This result is potentially occurring as a result of no areas seeing a decline in carbon emissions, and therefore, the areas which do see declining depths of burn, still see increases in carbon emissions (likely due to greater burnt areas) influencing the correlations seen here.

Table 50: Pearsons's correlation coefficients (r) between the change in mean annual peat fire carbon emissions and burnt area and depth of burn in the three SSP scenarios from the 2015-2025 average to the 2090-2100 average. Asterisks indicate significant p values (*=p<0.05, **=p<0.01, ***=p<0.001).

	SSP126	SSP370	SSP585
Burnt area (M km^2)	0.904***	0.895***	0.888***
Depth of burn (m)	-0.147***	-0.217***	-0.196***

Overall, large increases in carbon emissions are expected under all scenarios, but especially under SSP585, by the end of the century. These increases in carbon emissions occur largely due to greater peat burnt areas and deeper depths of burn. This means that more long-term stored carbon is exposed to combustion, either due to peat fires becoming more widespread, or peat fires burning deeper into the peat. Loss of long-term stored peat may have major implications of the climate system and has the possibility create strong positive feedback loops.

4. Discussion

INFERNO-peat suggests a rapid and large increase in the amount of northern high latitude peat burnt area over the 21st century, reaching as high as 1.218 M km^2 per year under SSP585. Concurrently, the increases in peat burnt area and depth of burn shown in Section 3 will drive large increases in the amount of carbon emitted from peat fires, with emissions reaching in excess of 1 Gt of carbon per year across the high latitudes. The largest increases in burnt area, and subsequently their carbon emissions, are witnessed across Canada, northwest Siberia and western Russia. Section 3.1 has demonstrated that in INFERNO-peat, increases in peat burnt area are driven by increasing numbers of peat fire ignitions from flaming vegetation fires, fuelled by higher fuel loads and greater vegetation flammability, alongside increases in the probability of ignition of peat as a result of drier soils across much of the high latitudes.

At present, no other fire models have simulated future changes in peat burnt area in the high latitudes, with only a few simulating changes in vegetation fires in the high latitudes with climate change. The

LPJ-GUESS-SIMFIRE fire model has been used to project future burnt area and carbon emissions changes (Knorr et al., 2016a; Knorr et al., 2016b). However, there has been no focus on the northern high latitudes. Despite this Knorr et al., (2016b) do show significant increases in wildfire emissions across the northern high latitudes under RCP4.5 and RCP8.5, largely as a direct result of climatic changes, in agreement with the large increase in carbon emissions from peat burning presented here as modelled by INFERNO-peat.

Overall, the increases in peat burnt area modelled by INFERNO-peat are supported in the literature. It has been stated that boreal regions are expected to experience larger and more frequent fires (Jia et al., 2019). Additionally, fires are expected to increase in the Arctic and in tundra ecosystems (McCarty et al., 2021; Pastick et al., 2017; Young et al., 2017; Moritz et al., 2012; Flannigan et al., 2005; Wang et al., 2017; Hu et al., 2015). Young et al. (2017) estimated a fourfold increase in the 30-year probability of wildfire occurrence in tundra ecosystems by 2100. Additionally, the length of the fire season is expected to increase in the northern high latitudes (McCarty et al., 2021; Wang et al., 2015). This would consequently increase the frequency of fires in general, as well as peat fires, which is evidenced in the INFERNO-peat simulations presented in Section 3.

INFERNO-peat highlights Canada in particular as a region which sees large increases in peat fires and their associated carbon emissions. Potentially because of an observed increase in extreme fire events in Canada in recent years, there have been numerous studies estimating potential changes to Canadian fire regimes as a result of climate change. Recently, a new Canadian wildfire module was developed within the Canadian Land Surface Scheme Including Biogeochemical Cycles (CLASSIC) land surface model (Curasi et al., 2024). Whilst this model does not explicitly represent peat fires, it is a notable step forward in the modelling of general fire trends within Canada (Curasi et al., 2014). Curasi et al. (2024) model an increase in burnt area in Canada in the region of 297-414% by 2100 under SSP370 and SSP585. Similarly, for northern Canada, INFERNO-peat simulates an approximately 290% increase in peat burnt area by the end of the century under SSP585, therefore showing a similar magnitude of change in burnt area between the two models, with the disparities likely accounted for by only modelling peat fires in the INFERNO-peat simulations presented here. Importantly, similar spatial patterns in burnt area are seen in Canada for the two models, with the largest increases in burnt area estimated by Curasi et al. (2024) occurring in the provinces of Saskatchewan, Manitoba and Ontario, as also in INFERNO-peat. In addition, Wang et al. (2017) showed that under RCP8.5 the number of fire spread days in Eastern Canada could increase as much as 3-fold, most notably in Alberta and Saskatchewan, supporting the large increases in burnt area in these regions in INFERNO-peat. Similarly, using a $3xCO_2$ scenario, Flannigan et al. (2005) estimated burnt area in Canada to increase by 74-118% by 2100. Differences between the aforementioned studies can be partially attributed to the use of different emissions scenarios. Whilst INFERNO-peat and CLASSIC both use the SSP scenarios, Flannigan et al. (2005) uses idealised increased CO_2 forcings, whereas Wang et al.

(2017) uses the RCP scenarios. The use of RCP scenarios alone, may limit potential future fire estimations as they only project changes in greenhouse gas emissions and do not represent the socioeconomic pathways that drive these changes. Still, whilst all these studies show different percentage changes in fire activity, they all agree on the direction of change towards an environment in Canada conducive to greater amounts of burning.

Ultimately climatic changes in the future underpin many of the changes in fire regimes expected in the northern high latitudes primarily due to increased temperatures and changes to precipitation. Predicted temperature changes from the UKESM modelled data that drive INFERNO-peat suggest that temperatures may increase by as much as 9-12°C over the high latitudes, with the largest changes occurring in the northernmost regions. These estimates are in line with numerous predictions from climate models over the Arctic. For example, based on CMIP5 models, the Arctic is expected to see 13°C increases in late autumn temperatures by 2100 under RCP8.5 (Overland et al., 2013). Similarly, in the latest round of coupled climate model intercomparisons (CMIP6), a warming rate of 0.83°C per decade is expected in the Arctic under SSP585, resulting in an increase in mean surface temperatures of 10.4°C by the end of the century (Cai et al., 2021). Therefore, elevated temperatures are likely to occur across the high latitudes (Koenigk et al., 2020), alongside increases in the occurrence of extreme warm events and droughts (Walsh et al., 2020). Increases in temperatures have been shown in this chapter to contribute towards high peat fire burnt areas through their effects of vegetation fuel loads and flammabilities, peat fire ignitions and the probability of ignition of peatlands.

In the recent historical period, rising temperatures have been shown to promote increased levels of burning across the high latitudes (Box et al., 2021). For example, Balzter et al. (2005) showed that higher temperatures in the high latitudes contributed towards the extreme burnt areas seen in 2002 and 2003 in central Siberia. More recently, strong positive correlations have been shown between burnt area and air temperatures across Siberia, indicating that warmer temperatures may be exacerbating fire frequency and severity (Ponomarev et al., 2016). Furthermore, results presented in Chapter 4, also highlight the strong connectivity between higher temperatures and extreme fire events. Therefore, the warmer temperatures predicted with climate change in the high latitudes may result in increased burnt area. For example, Descals et al. (2022) estimated that under RCP4.5 and RCP8.5, increased temperatures, may result in 2.5 million ha of burning in the Siberian Arctic each year by 2050, which would equate to mean annual carbon emissions of 37.8 Tg per year. These results are also realised in INFERNO-peat, where we see large increases in burnt area across Siberia, totalling 0.347 M km^2 per year by 2100, but most notably in the northwest (Figure 59), partially driven by rising temperatures.

A key implication of rising global temperatures which has been shown to result in extreme fire activity is the increasing presence of atmospheric blocking events (Sharma et al., 2022; Scholten et al., 2022). Atmospheric blocking events are large-scale quasi-stationary high-pressure systems which

can persist for extended periods (e.g. weeks) of time altering the positioning of and disrupting the jet stream, often resulting in prolonged extreme weather events such as summer heatwaves (Woolings et al., 2018). Between 1979 and 2020, the number of days during May-September in which blocking systems have been present over western North America has increased by 8 days, and most significantly between 60 and 75°N (Sharma et al., 2022). During these periods there are strong positive anomalies in mid-tropospheric geopotential height, surface air temperature, vapour pressure deficit (VPD) and the fire weather index (FWI), as well as negative precipitation anomalies, which result in a 7 times increase in the likelihood of large fire events (Sharma et al., 2022). In recent years, a connection between intense wildfires and the presence of large stationary anticyclones which create hot and dry weather, ideal for rapid wildfire spread, has been highlighted (Bondur et al., 2023). For example, in 2014, fires the Northwest Territories burned a record, at that time, area of 3.39 M ha (Kochtubajda et al., 2019). Simultaneously, there was a dominant mid tropospheric ridging pattern, which resulted in warm and dry conditions, drying out available fuels, and therefore thunderstorms that formed in the breakdown of these ridges resulted in a high number of lightning ignitions, causing the extreme burning that occurred in 2014 (Kochtubajda et al., 2019). Similarly, in northeast Siberia, the extreme fire activity that occurred in 2019, 2020 and 2021 has been shown to be driven by a blocking event which caused the displacement of the Arctic front jet, promoting warm and dry surface conditions, proceeded by anonymously high lighting activity and consequently wildfires (Scholten et al., 2022). The northward displacement of the Arctic front jet during the summer has shown a tripling in the frequency of occurrence between 1980 and 2020 (Scholten et al., 2022), indicating that the blocking conditions triggering large fire years are becoming more common.

Rising global temperatures are increasing the likelihood of blocking events such as high-pressure systems and ridges, as a result of thermal expansion of the lower troposphere with warming (Sharma et al., 2022; Scholten et al., 2022). Additionally, warming alters planetary wave resonance, which has been shown to result in an increase in persistent weather extremes in boreal regions in summers (Mann et al., 2017). Changes may also be occurring due to changing equator-to-pole temperature gradients (Scholten et al., 2022). Consequently, climate change is expected to substantially increase the spatial extent, duration and frequency of blocking events (Lyon et al., 2019; Nabizadeh et al., 2019; Horton et al., 2015), inevitably leading to increased frequencies of fire events and greater fire severities, such as those seen in recent years in Siberia and Canada.

Climate change is also expected to result in significant alterations to precipitation regimes across the high latitudes. Precipitation, according to the UKESM, is expected to increase across much of the high latitudes by 31-37% under SSP370 and SSP585 over the 21st century. Figure 56 suggests that the largest increases in precipitation will be seen in the Arctic regions of the high latitudes, with areas of decreasing precipitation over western Europe. This is in line with predictions from the literature of precipitation increases in the range of 40-60% in the Arctic by 2100 (Bintanja, 2018; IPCC, 2013;

Bintanja and Andry, 2017), and overall increases in precipitation across the high latitudes (Koenigk et al., 2020; Box et al., 2021). Arctic precipitation is expected to increase due to global warming, poleward moisture transport and sea ice loss (McCrystall et al., 2021; Bintanja, 2018; Bintanja and Selten, 2014). As demonstrated in Section 3, warmer temperatures are strongly correlated to increased precipitation, as is also found across the Arctic over the recent historical period (Koenigk et al., 2015; Ye et al., 2021). This relationship occurs due to intensified surface evaporation as warmer air temperatures increase the air moisture holding capacity through greater thermodynamic energy (Oki and Kanae 2006; Pan et al., 2014; Allen et al., 1998).

The overall increase in precipitation in the high latitudes is expected to occur concurrently with a shift from snow-dominated to rain-dominated precipitation due in part to warmer temperatures (McCrystall et al., 2021; Bintanja and Andry, 2017; Box et al., 2021). Under present-day Arctic climates 65% of precipitation falls as snow, however, under RCP8.5 by 2100 60% of precipitation will instead fall as rain (Bintanja and Andry, 2017). However, this trend is not ubiquitous across the high latitudes, with the coldest areas of the Arctic expected to see increases in snowfall in the future, due in part to the maintenance of sub-zero temperatures along with the increases in overall precipitation (McCrystall et al., 2021; Biglake and Walsh, 2022). Reductions in snowfall alongside increases in temperature may result in reductions in spring snow cover in the northern high latitudes, with Mudryk et al. (2020) predicting an 8% reduction in spring snow extent for every 1°C of warming. Reductions in snow cover, and, crucially, earlier snow melt, will have knock on effects on summer soil moisture levels and consequently the likelihood and severity of peat fires (Bruhwiler et al., 2021). For example, Scholten et al. (2022), showed earlier snow melt to be strongly correlated with summer fire activity and extreme fire events in Siberia, whilst Hessilt et al. (2024) identified connections between earlier snowmelt and large fires in boreal North America. Therefore, changes in snowfall and consequently snow cover in a warmer future climate may result in intensified summer fire seasons across the high latitudes.

Even with increases in precipitation in areas of the high latitudes, climate change may result in longer and warmer summers that result in drier vegetation and peat alongside droughts and increased fire weather, consequently increasing the likelihood of extreme wildfire seasons (Walsh et al., 2020). Between 1979 and 2019, the frequency and extremity of fire weather have increased with climate change (Jones et al., 2022), with increases in mean FWI and its variability, which are expected to continue to increase in the northern high latitudes with future climate change (Lund et al., 2023). Large increases in FWI with climatic change are expected across Canada (Coogan et al., 2019; Wang et al., 2015; Lund et al., 2023). For example, with between just 1 and 4°C of warming, the number of days with an FWI that is moderate or higher is doubled in Canada as a result of increases in air temperature and decline in relative humidity (Lund et al., 2023). Increased FWI was found to contribute to increases in the number of fire spread says, by as much as 400% by 2050 across Canada

(Wang et al., 2015), further supporting our findings of significantly increased future burnt area in Canada in INFERNO-peat. Additionally, de Groot et al. (2013) showed increases in the severity of fire weather in central Russia as a result of climate change, suggesting that the large increases in peat burnt area witnessed in central Russia in INFERNO-peat, may be due to climate change-induced changes to fire weather severity. Therefore, climate change-induced temperature increases and the consequent effects on the presence of blocking events, snow cover and fire weather are expected to have large effects on fire frequency and severity across the high latitudes, much like is captured in the future INFERNO-peat simulations which model significant increases in burnt area.

Increasing fuel loads across the high latitudes was shown to be a key driver in the increase in peat fire ignition events in the same areas under future climate change. Within INFERNO-peat, higher fuel loads, represented as fractional coverage of PFTs, result in greater numbers of flaming vegetation fires, which can then act as ignition sources for peatland fires. The land surface model, JULES, which drives INFERNO-peat simulates increases in the fractional coverage of vegetative land surface types across much of the high latitudes, but particularly in the northmost areas, where bare soil is shown to be replaced by grasses, indicating Arctic greening. Arctic greening describes the positive trends in vegetation indices seen across the Arctic region (Myers-Smith et al., 2020). Between 1982 and 2019, Arctic greenness has increased by 10%, which is highly correlated with melt season air temperatures (Box et al., 2021). Additionally, greening of the northern high latitudes is also driven by longer growing seasons and warmer temperatures that allow for more productive plant communities (Bruhwiler et al., 2021; Ernakovich et al., 2014; Berner et al., 2020). However, this trend has not been observed across all regions of the Arctic (Myers-Smith et al., 2020), with some regions displaying browning trends, particularly between 1999 and 2015 (Bhatt et al., 2017). Browning may occur because of extreme climatic events, disease, and altered hydrology or fires (Myers-Smith et al., 2020). However, much of the browning trend is occurring in forest ecosystems, whereas greening dominates in tundra and grassland areas (Bunn et al., 2007) that are pervasive in the most northernly regions of the high latitudes.

With climate change, greening and increased vegetation productivity in the northern high latitudes is expected to continue (Pearson et al., 2013; Madani et al., 2021; Ito et al., 2016). This is partially due to warmer temperatures, which provide more favourable conditions for vegetation growth (Madani et al., 2021). Ito et al. (2016) modelled gradual increases in vegetation productivity with climate change in the northern high latitudes due to longer growing seasons, as well as elevated CO_2 concentrations. CO_2 fertilisation will help to enhance vegetation growth across much of the high latitudes (Qian et al., 2010). Not only is vegetation productivity expected to increase with climate change, but shifts in vegetation communities are also anticipated. It has been estimated that approximately half of vegetated areas in the Arctic will shift to a different vegetation type by 2050 (Pearson et al., 2013). The key trend identified in section 3.1.1.1 is the replacement of bare soils by C3 grasses, a trend that

was already anticipated by Callaghan and Jonasson (1995). Furthermore, in Alaska, the coverage of deciduous forests is expected to increase by 223-620%, and shrub tundra by 4-21%, with climatic warming by 2100 (Pastick et al., 2017). These trends are also captured by JULES, with large increases in needleleaf evergreen trees expected under all climate change scenarios in Alaska (Figure 65d-f). JULES also shows signs towards an increasing dominance of woody vegetation in regions that used to be dominated by grasses. Pearson et al. (2013) estimated a similar future tendency, with trees and shrubs predicted to cover 24-52% of the present-day tundra area by 2050. Therefore, based on the current work and in agreement with earlier studies, large shifts in vegetation are expected under future climate change, which may alter fuel loads and fuel flammability across the high latitudes, altering fire regimes.

The large increases in peat burnt area modelled by INFERNO-peat are also a product of increasing peat probability of ignition with climate change. The regions with the largest increases in probability of ignition are seen in the far north of the high latitudes in Siberia and Canada, as well as in western Alaska and Fennoscandia. It was shown that these large increases in peat ignition probability are being driven by declining soil moisture across much of the high latitudes, supporting the findings of Turetsky et al. (2015) who suggested that drier soils are one of the most important factors increasing the likelihood of peat fires. Peatland hydrology plays the most important role in controlling the probability of ignition and peat fire depth of burn and burnt area (Frandsen, 1997; Rein et al., 2009; Hokanson et al., 2016; Lukenbach et al., 2015). Over the last 100 years, peatlands have been drying out across the world (Zhang et al., 2018). Consequently, this has increased the likelihood of fires. For example, peatland fire activity is increased 6-fold during moderate droughts (Thompson et al., 2019), alongside increases in burning intensity, and a nine-fold increase in carbon losses (Turetsky et al., 2011b). Therefore, continued drying of peatlands may result in increased burned area, fire frequency and fire size (Thompson et al., 2019).

Soil moisture is expected to continue to reduce with future climate change, along with anthropogenic activities such as drainage (Carrol et al., 2011). Despite the increases in precipitation that are projected across the northern high latitudes, these increases are expected to be offset by increased evapotranspiration under warmer climates (Muller and Joos, 2021), resulting in drier peatlands. For example, across much of Europe, soil moisture is predicted to decrease under climate change scenarios, with increasing incidences of severe and extreme drought events (Grillakis, 2019). These changes are seen in the JULES modelled soil moisture, with large reductions in soil moisture across Europe, as well as much of Russia and northern Canada (Figure 75). Consequently, INFERNO-peat shows strong increases in the probability of ignition of northern high latitude peatlands, especially under high emissions scenarios.

Whilst the analysis in Section 3.1.2.2 highlights that many factors influence future changes in northern high latitude soil moisture, it is apparent that rising global temperatures play a key role, through their induced changes in evapotranspiration. As previously mentioned, rising temperatures are expected to increase evaporation due to higher thermodynamic energy in the atmosphere which drives increases in the air moisture holding capacity (Oki and Kanae 2006; Pan et al., 2014; Allen et al., 1998). These rising temperatures are expected to induce increases in vapour pressure deficit, which has been proposed to significantly increase evapotranspiration from peatlands (Helbig et al., 2020). JULES models a 24.2% increase in soil evapotranspiration by the end of the century under SSP585 in the northern high latitudes. Similar increases in evapotranspiration have been predicted under high climate change scenarios in past studies. For example, Pan et al. (2014) estimated that 60% of global land area will see increase in evapotranspiration rates, with the largest increases occurring in the Arctic. Evapotranspiration from peatlands partially controls water losses from peatlands, therefore greater evapotranspiration from peatlands with climate change will make them more prone to drying (Helbig et al., 2020; Berg and Sheffield, 2018). As a result of these relationships, INFERNO-peat simulates strong correlations between evapotranspiration and soil moisture in the high latitudes under all climate change scenarios.

Depth to the water table was also identified in Section 3.1.2.2 as a key determinant of soil moisture. Studies have indicated that under future climate change, water table depths in northern peatlands are expected to significantly increase, particularly in summer (Bertrand et al., 2021; Roulet et al., 1992). JULES models nearly a 30% increase in water table depth, with water tables moving on average 57cm deeper into the soil under SSP585. Roulet et al. (1992) estimated that temperature increases of 3°C will result in drops in water tables of 14-22cm in the region. The UKESM driving data predicts an air temperature increase of on average 12°C across the high latitudes, which following the result of Roulet et al. (1992) would suggest an increase in water table depth of 56-88cm, with the JULES estimated increase in water table depth also falling within this range. There are strong connections between water table depths and soil moisture, with deeper water tables facilitating drier peatlands and visa versa (Wilkinson et al., 2020; Nelson et al., 2021). Deeper water tables, increase the likelihood of desiccation, thereby increasing soil moisture deficits in the future (Moore and Waddington, 2015). Therefore, changes in water table depths can be expected to exert a strong influence on soil moisture, as is seen in the INFERNO-peat analysis which reveals strong correlations between water table depth and soil moisture.

Deeper water tables and consequently drier peatlands also have effects on the carbon storage of peat. Deeper water tables allow for deeper anoxic layers in the peat which increases soil respiration rates and decomposition and consequently increases CO_2 emissions (Helbig et al., 2022; Trettin et al., 2006; Holden et al., 2007). Higher rates of decomposition, drier peatlands, and slower peat growth may result in peatlands switching from carbon sinks to sources, even in the absence of fire (Wu, 2011;

Salimi et al., 2011). Consequently, reductions in peatland water table depths as a result of climate change may result in fundamental changes in the carbon accumulation mechanisms of peatlands, resulting in large carbon emissions. At present JULES does not explicitly represent peatlands and their carbon accumulation, therefore there are potential large feedback effects that are not being captured or represented in the model, which would influence the amount of carbon available for combustion in INFERNO-peat. This may result in overestimations of the amount of carbon available to be burnt in the future.

It is apparent that changing global temperatures also have a large effect on peat soil moisture and consequently probability of ignition through the reduction of the extent of areas in high latitudes that experience sub-freezing temperatures. The presence of sub-freezing temperatures is crucial in the maintenance of permafrost peatlands. JULES models a significant increase in soil temperatures, particularly under the highest emission scenarios, with notably a 43% reduction in the number of months with soil temperatures below 0°C. A lack of freezing temperatures, in conjunction with hydrological changes may lead to permafrost thaw (Zhang et al., 2018). Thawing permafrost is expected to have numerous effects on peatland hydrology, such as through deeper water tables, but also through temporary increases in soil moisture as a result of melting (Zhao and Zhuang, 2023; Zhang et al., 2018). However, temporary increases in wetness from melting are expected to be offset by the increases in evapotranspiration (Zhang et al., 2018), shifting towards drier peat overall. INFERNO-peat shows regions of decreasing probability of ignition in northwest Canada and eastern Siberia, regions where JULES tends to show smaller reductions in the number of months with soil temperatures below 0°C, and in eastern Siberia also increases in snow cover. This suggests the maintenance of permafrost peatlands in these areas as a result of cooler temperatures, which may result in increases in probability of ignition . Consequently, there are strong positive correlations seen between the change in number of months with soil temperatures below 0°C and changes in soil moisture, suggesting that when peatlands see large declines in months with temperatures below 0°C, there are large declines in soil moisture, and consequently increases in probability of ignition and visa versa.

INFERNO-peat not only simulates large increases in peat burnt area with climate change, but it also estimates that depth of burn into the peat may also increase. Under the highest emissions scenario (SSP585) average depth of burn increases by 26%, representing 5.8cm of additional burning into the peat soil column. Increases in depth of burn in INFERNO-peat are driven by decreasing soil moisture, increasing soil temperatures and increasing water table depths with climate change, as discussed in the above paragraphs. Warmer, drier soils, facilitate greater vertical spread of fires into the soil column (Lin et al., 2021). Water table depth is inherently linked to soil moisture, with wetter soils having higher water tables (Wilkinson et al., 2020; Nelson et al., 2021). Numerous lab and field experiments have shown that drier soils lead to deeper burning (Benscotter et al., 2011; Wilkinson et al., 2018;

Christensen et al., 2020; Huang and Rein, 2017). Therefore, drier soils, as a result of climate change, may lead to deeper burning in the future, as is shown in INFERNO-peat. Soil moisture has also been shown to be linked to the minimum temperature required to sustain a smouldering fire, with drier soils allowing burning to occur at much lower temperatures (Lin et al., 2021). Consequently, drier soils, allow for greater amounts of burning, but additionally warmer temperatures would be conducive to burning of wetter soils, meaning that overall, burning may occur deeper into peat soil columns with climate change.

Increasing burnt area and depth of burn modelled by INFERNO-peat results in increased carbon emissions from peat fires under all climate change scenarios over the 21st century. Under SSP585 carbon emissions from peat fires are estimated to increase by 269.3%, with emissions expected to top 1 Gt of carbon per year by 2100. This figure is significantly higher than the 0.54 Gt C emitted from peat fires by 2100 as estimated by Lin et al. (2021). However, the figure was obtained using a fixed burn probability (Lin et al., 2021), which may result in an underestimation of carbon emissions, due to the fact that the probability of ignition of peat is expected to increase, as demonstrated in this chapter.

Other models have simulated global fire carbon emissions under climate change scenarios, for example CMIP5 simulations estimated a 58% increase in global fire carbon emissions by 2100 under RCP8.5 (Kloster and Lasslop, 2017). These estimates, like also the estimates of the majority of other global fire models, do not consider peat fires, and crucially they do not account for the increased soil carbon stored within peatlands. Therefore, it is likely that they underestimate global fire emissions and their future changes. More generally, the simulated fire occurrence in CMIP5 Earth system models has several deficiencies in a range of key regions, also resulting in underestimations (Kloster and Lasslop, 2017; Jones et al., 2022). Therefore, current global model estimates of future carbon emissions are likely underestimated. Consequently, peat fires and their carbon emissions represent a critical component of land surface and Earth system models that is currently excluded, but as shown in INFERNO-peat, have the potential to exert a large effect on the carbon cycle and the climate.

Hugelius et al. (2020) estimated the peatland carbon store at present as 415 Gt C. Here, over the whole 2015-2100 simulation, peat fires emit a total 37.08, 48.70 and 59.57 Gt of carbon under SSP126, SSP370 and SSP585, respectively. Therefore, future peat fires are estimated to consume 8.93-15.35% of the total northern high latitude carbon store. Under SSP585, this would result - when only considering fire induced losses of carbon and not allowing for any additional peatland carbon accumulation - in a reduction in the northern high latitude carbon store to 355 Gt C. If future fire carbon emissions remained at 1 Gt C per year beyond 2100, assuming no other peat carbon losses or gains, this would result in the total loss of the peatland carbon store by the year 2455. However, this dramatic a loss of peatland carbon solely from peat fires is unlikely, due to some reaccumulation of carbon during post fire vegetation and peat recovery (Wieder et al, 2009; Poulter et al., 2006).

However, whether peatlands remain a sink or source of carbon depends upon how well peat and vegetation can recover, on top of the frequency and severity of future peat fires. The rate of recovery of peatlands and vegetation is highly dependent upon the hydrological status of that peatland (Ingram et al., 2019; Kettridge et al., 2015). For example, peatlands which prior to burning had been exposed to moderate drainage and drying resulted in lower rates of carbon reaccumulation due to shifts in the vegetation composition of the peatland (Kettridge et al., 2015).

There is a tendency for peat fires to result in a net loss of carbon to the atmosphere (Lasslop et al., 2019). Peat fires have been shown to be capable of releasing 0.32 Gt C in a singular year at present (Poulter et al., 2006). Wieder et al. (2009) found that in Canada, peat fires are net sources of carbon in the immediate years following the fire, but after 13 years begin to reaccumulate carbon due to the recovery of vegetation. However, due to slow carbon accumulation rates, the time to recover all the lost carbon can take hundreds of years. For example, combustion of 20cm of peat, is estimated to be equivalent to approximately 280 years of peat accumulation (Trettin et al., 2006). Therefore, if the same peatland experiences another fire within this time, then there will be a net loss of carbon. More frequent wildfires due to climate change would decrease the amount of time available for a peatland to recover post-fire (Ingram et al., 2019). For example, Wieder et al. (2009) estimated that a drop in the fire return interval from 123 to 61 years would convert the peatlands of Alberta, Canada, to a net source of carbon. In addition, whilst not in the high latitudes, peatlands in North Carolina were found to need a fire return interval of greater than 80 years in order to maintain a carbon sink (Poulter et al., 2006). Increased wildfire carbon emissions and reduced fire return intervals are estimated to diminish the northern high latitude peatland carbon sink by 57% by 2050, compared with a no-fires scenario, potentially switching peatlands to source of 0.4 Gt C by 2100 (Wilkinson et al., 2023). Therefore, under future climate change, increasing peat fire frequency and burnt areas may consequently contribute towards switching peatlands from sinks to sources of carbon by the end of the century.

At present, JULES has no representation of peatlands and their dynamics, therefore peat carbon cannot be lost or reaccumulated within JULES and INFERNO-peat. Consequently, the consumption of peat carbon in INFERNO-peat has no effect on the amount of carbon available to be consumed in the next time step. Furthermore, peat carbon cannot be reaccumulated within JULES, so the overall change in peatland carbon storage as a result of peat fires cannot be evaluated here. This is a key limitation to the current INFERNO-peat parameterisation used in this chapter. A simple reduction of the peat carbon store at each time step according to the amount of carbon emitted by peat fires within a grid cell in the previous time step could be applied. However, this would likely result in an underestimation of the peat carbon pool due to the lack of consideration for the reaccumulation of carbon. Development of a peatland scheme within JULES, which would allow peat soils to accumulate carbon, is currently being undertaken (Chadburn et al., 2022). This could, in the future, be coupled with INFERNO-peat. Therefore, changes in peatland carbon storage could be simulated in the

future, allowing for the direct inclusion of climate change-induced effects on peatlands, alongside a feedback effect of burning on the stored carbon, leading to a more realistic representation of future carbon sources and sinks under future climate change.

Peat fire carbon emissions, due to causing a net loss of carbon to the atmosphere, may enhance climatic warming and result in positive feedback effects on the climate system (Nelson et al., 2021). A positive feedback effect will fuel further peat fires, potentially resulting in a catastrophic loss of carbon from the northern high latitudes (Mack et al., 2011; Chen et al., 2021a; Turetsky et al., 2015; Nelson et al., 2021). Oris et al. (2014) predicted that forest fires in the boreal regions will have a positive feedback on global warming, with a radiative forcing effect of 0.37 W m^{-2} $decade^{-1}$. Therefore, as carbon emissions from peat fires are higher than those from forest fires, a larger radiative effect can be expected. Consequently, a further development of INFERNO-peat could involve coupling with the UKESM, allowing for the quantification of a radiative forcing effect of peat fires and allowing for the emissions from peat fires to fully feed back on the atmosphere and climate, including also variables beyond temperature (e.g. precipitation, cloudiness, circulation, amongst others).

In addition to carbon emissions, peat fires may also have a myriad of effects on ecosystems and air quality in the future, which have not been explored in this chapter, but have the potential to be incorporated into INFERNO-peat and JULES in the future. For example, at present, peat fires are known to degrade air quality through emissions of aerosols such as organic and black carbon (leading to increases in $PM_{2.5}$), which have been shown to have numerous health impacts on high latitude populations (Turetsky et al., 2015; Hu et al., 2018; Silver et al., 2023). If the global population continues to grow and the movement of populations further north also continues (Bartsch et al., 2021), then increasing amounts of peat burning is likely to have even larger effects on the health of nearby populations. Through the use of peat-specific emission factors for various gas and particulate species, atmospheric burdens of key pollutants under future climate change could be studied.

Furthermore, atmospheric aerosols have also been shown to impact global and regional climate through altered precipitation patterns and temperature changes (Liu et al., 2018). Aerosols, such as black carbon, can absorb solar radiation thus having a positive radiative forcing effect, or, like sulphate and organic carbon, scatter radiation resulting in negative radiative forcing (Xu et al., 2021; Thornhill et al., 2021). The scattering or absorbing of radiation, leads to altered energy budgets, and consequently temperature changes (Liu et al., 2018; Fiedler et al., 2024). Aerosols also act as cloud condensation nuclei and alter the microphysical properties of clouds such as cloud droplet size, lifetime and reflectance (Tian et al., 2022; Xu et al., 2021; Baro et al., 2017a). Additionally, aerosol deposition over land surfaces can induce changes in albedo, and consequently temperature changes (Tian et al., 2022; Randerson et al., 2006). It is estimated that globally, fire emitted aerosols have a net

negative radiative forcing in the range of -0.78 to -2.3 W m^{-2} (Thornhill et al., 2021; Clark et al., 2015; Xu et al., 2021; Jiang et al., 2020; Ward et al., 2012). Consequently, fire emitted aerosols are estimated to reduce global temperatures by 0.17 to 0.64°C (Xu et al., 2021; Jiang et al., 2020; Tian et al., 2022), and result in a global reduction in precipitation over land by ~0.180 mm per month (Tian et al., 2022; Jiang et al., 2020). However, the effect of aerosols on temperature and precipitation can vary greatly based on the region and type of aerosols emitted (Liu et al., 2018). For example, aerosol emissions from Africa, result in a northward shift of the intertropical convergence zone (ITCZ), and enhanced local rainfall (Wells et al., 2023). In contrast, the emissions of sulphate aerosols in Asia, has been shown to result in a decrease in precipitation over Asia and in downwind regions (Liu et al., 2018). Fire emitted aerosols have also been shown to reduce windspeeds during fires in Russia in 2010 (Baro et al., 2017b). Therefore, if aerosol emissions from peat fires increase in the future, there may be large impacts upon global and regional temperatures and precipitation, with feedback effects on fires themselves. Consequently, it is important that aerosol emissions from peat burning are also quantified within fire models, in order to allow for their feedback effects on the climate system to studied, particularly in the context of global climate change.

Increased peat burning, in combination with increased high latitude populations may result in larger infrastructure damages and consequently costs. For example, Melvin et al., (2017) predict that increased burnt area in Alaska by 2100 under RCP8.5 may result in an estimated cumulative response costs of $1.2-2.1 billion. Furthermore, peat fires have been shown over the recent historical period to drive changes in vegetative communities and alter successional trajectories (Noble et al., 2019; Gibson et al., 2018; Nossov et al., 2013). For example, wildfires have been shown to result in shrub expansion over tundra regions (Mekonnen et al., 2021). Peat fire-induced changes to vegetation are currently not represented in INFERNO-peat. However, future implementation of these mechanisms may aid in accurately representing future vegetation communities which will have additional feedbacks on the likelihood of peat fire ignitions.

A further key feedback effect not currently incorporated in INFERNO-peat is the effect of fires on permafrost. At present this is not included due to a lack of permafrost representation within JULES. However, fires have been shown to result in permafrost degradation, thawing and the development of thermokarst landscapes (Brown et al., 2015; Chen et al., 2021a; Nitze et al., 2018; Li et al., 2021). Consequently, degraded permafrost results in large emissions of carbon (Chen et al., 2021a; Nitze et al., 2018; Li et al., 2021), which on top of peat fire-emitted carbon may further deplete the northern high latitude peatland carbon store, with a positive feedback on the climate system. Climate change itself is already estimated to exacerbate permafrost thaw in the high latitudes, potentially resulting in the emission of 12.5-64.4 Gt C directly from permafrost thaw by 2100 under RCP8.5 (Nitzbon et al., 2020). Therefore, future incorporation of fire effects on permafrost are crucial to being able to accurately simulate potential changes to permafrost peatlands, and their stored carbon.

Another current limitation of INFERNO-peat is the lack of use of a future projection of lightning to drive the model, as at present lightning is fixed at the present-day level. This may be significantly limiting the number of potential peat fire ignitions, as lightning is known to be the primary disturbance agent in boreal forests (Hessilt et al., 2022), and is expected to increase with climate change (Krause et al., 2014; Chen et al., 2021a). Summer lightning in the Arctic is predicted to increase by 112% by the end of the century under RCP8.5 (Chen et al., 2021a). Increases in lightning occur in the high latitudes with climate change due to increases in convection available potential energy of up to 100% in the arctic tundra and 70% in boreal forests by 2100 under RCP8.5 (Chen et al., 2021a). Projected increases in lightning are expected to equate to a 100-158% increase in burnt area and subsequent carbon emissions in the northern high latitudes (Chen et al., 2021a; Krause et al., 2014). Therefore, the estimates of future peat burnt area here may be significantly underestimated. Recently, a future global lightning strikes dataset has been developed (Kaplan et al., 2023) with the specific purpose of being used in ISIMIP and FireMIP simulations. However, due to a lack of evaluation of this dataset at the time of this analysis, present-day observations were used instead. Consequently, future developments of INFERNO-peat could incorporate this, or other datasets of future lightning, which may improve the accuracy of peat fire ignitions within the model and potentially further increase burnt area and carbon emissions.

4.1. Conclusions

Overall, INFERNO-peat represents the first peat fire model to simulate future changes to peat fires over the coming century across the northern high latitudes. Climate change is expected to significantly increase peat burnt area in the northern high latitudes, alongside increases in depth of burn and subsequent carbon emissions. Under the most severe climate change scenario, annual burnt area in the high latitudes reaches in excess of 1.2 M km^2, emitting over 1Gt C per year. The drivers of these increases in burnt area and carbon emissions have been extensively discussed, with climate change-induced changes to temperatures, and consequently evapotranspiration, soil moisture, water table depths, fuel loads and fuel flammabilities, exerting significant influences on peat fire ignitions and the probability of ignition, therefore altering future peat burnt areas, depths of burn and carbon emissions. The possibility of peat fires emitting 1 Gt C each year by the end of the century, represents a substantial threat to the vital high latitude peatland carbon store, and threatens to accelerate the expected switch in peatlands from sources to sinks of carbon by the end of the century. However, if future global socioeconomic development follows a lower emissions scenario, similar to that of SSP126, there is great potential for limiting the effects of climate change on peat fires. Consequently, strong climate mitigation efforts would help to avoid the worst impacts of peat fires. Under SSP126, much smaller temperature increases are seen, meaning that whilst soils still become drier, changes are minimal, meaning that smaller increases in the probability of ignition of peat are seen. Keeping global emissions and temperatures to the levels projected under SSP126 would allow for peat burnt areas to

increase by just 45.6% to 0.489 M km^2 per year by 2100, keeping annual average peat fire carbon emissions to below 0.5 Gt C.

To conclude, INFERNO-peat simulates significant increases in peat burnt area in the future, particularly under high climate change scenarios, which may result in net carbon losses from northern high latitude peatlands, with likely severe positive feedbacks on the climate system, ultimately resulting in a catastrophic loss of carbon to the atmosphere. However, the successful implementation of climate change mitigation strategies by global governments would significantly reduce these potential effects, helping to preserve the crucial high latitude carbon stores.

Chapter 6: Discussion and conclusions

1. Summary of key findings

The northern high latitude peatlands represent a crucial store of carbon, which has accumulated over millennia (UNEP, 2022a; Frolking et al., 2011; Hugelius et al., 2020; Frolking and Roulet, 2007). The northern high latitudes are facing rapid anthropogenic climate and environmental change (Bruhwiler et al., 2021, Walsh et al., 2020; Chen et al., 2021a), which is threatening peatlands, and the carbon stored within them (Muller and Joos, 2021; Chaudhary et al., 2020). It is estimated that climate change, drying, and human driven peatland degradation may switch peatlands to sources of carbon in the future (Zhao and Zhuang, 2023), potentially creating a positive feedback loop on the climate system (Loisel et al., 2021; Swindles et al., 2019; Hugelius et al., 2020a; Tarnocai, 2009; Zhao and Zhuang, 2023), and negatively impacting air quality. Additionally, the degradation of peatlands in the northern high latitudes by both climate change and humans, is increasing the frequency and extent of peat fires (Turetksy et al., 2015). Therefore, being able to accurately model peat fire activity, both historically and in the future, is of the upmost importance to be able to quantify potential future impacts of peat fires.

However, peat fires have not historically been incorporated into global fire models, which has contributed to fire models inadequately reproducing patterns of burned area in the high latitudes (Jones et al., 2022; Kantzas et al., 2013). Additionally, a lack of representation of peat burning is frequently cited as a cause of the inability of fire models to capture the interannual variability in burnt area and carbon emissions (Mangeon et al., 2016; Teixeria et al., 2021). Consequently, this thesis developed INFERNO-peat, a novel parameterisation of peat fires in the northern high latitudes (Chapter 2 Section 3), which has been used to simulate present day peat fire activity (Chapter 3), as well as potential future trajectories of change (Chapter 5). Crucially, INFERNO peat was shown to perform well across the northern high latitudes and represents a substantial step forward in global fire modelling capabilities. The development of INFERNO-peat, and the evaluation of its performance (Chapter 3) also reiterates the importance of parameterising peat fires within fire models in terms of being able to estimate the impacts of peat fires on atmospheric composition, air quality, the carbon cycle and climate. The impacts that peat fires impose upon atmospheric composition and air quality in the high latitudes is also assessed using the latest observational products (Chapter 4), demonstrating the importance of representing peat fires within global models. As a result of the key role that peat fires play and the impacts they exert on the climate and northern high latitude ecosystems, I explored the use of INFERNO-peat to simulate future changes to northern high latitude peat fires using three emission scenarios (Chapter 5). This work highlights how fire regimes could evolve in the future, and therefore, to be able to accurately model how carbon budgets will change we need to be able to simulate changes in peat burnt area and subsequent carbon emissions under different trajectories of

climate change. Crucially, peat fires are likely to dramatically alter fire regimes in the northern high latitudes in the coming century, with major implications on the global carbon cycle, air quality and ecosystems. The following sections will summarise in more detail the key findings of this thesis that have resulted from the development of INFERNO-peat, as well as the impacts that peat fires have on atmospheric composition, air quality, the carbon cycle and climate.

1.1. The importance of parameterising peat fires in global fire models

The development of INFERNO-peat is a notable output from this thesis, which has highlighted the importance of representing peat fires within fire and Earth system models. INFERNO-peat utilises the extensive body of knowledge on peat fires, and how they ignite and spread from numerous lab and field-based studies (e.g. Frandsen, 1997; Purnomo et al., 2020; Rein, 2013; Rein, 2015; Santoso et al., 2019a; Christensen et al., 2020; Lin et al., 2021), to develop equations for calculating peat fire ignitions, peat probability of ignition , peat burnt area, peat depth of burn and peat fire carbon emissions within the INFERNO fire model framework. INFERNO-peat also builds upon the first parameterisation of peat fires into a global fire model (CLM-Li; Li et al., 2013), by considering the role of peatland hydrological factors and soil properties on the probability of ignition of peatlands. The process of the development of INFERNO-peat was outlined in Chapter 2 section 3 and was successfully used for the assessment of present-day peat burning (Chapter 3) and future peat burning (Chapter 5).

It has been shown that fire models that do not include peat fire representation (the norm in current Earth system models) do not adequately reproduce patterns of burnt area, particularly in the high latitudes (Jones et al., 2022; Kantzas et al., 2013). I have shown that parameterising peat fires in the INFERNO global fire model, which is the fire modelling scheme of the UK Earth system model (UKESM) improves the capabilities of INFERNO to represent present-day burning across the northern high latitudes, including the representation of interannual variability (Chapter 3). INFERNO-peat estimates that peat fires, on average, account for 58% of annual burnt area north of 50°N latitude, emitting in excess of 200 Tg C annually. In comparison to the only other fire model that represents peat fires (CLM-Li; Li et al., 2013), INFERNO-peat captures substantially more burning in the northern high latitudes, much more in line with what is seen in satellite observations. In CLM-Li, the underrepresentation of peat burning is thought to stem partially from a wet simulation bias and partially from low fuel loads within CLM (Li et al., 2013). As explained in Chapter 3, INFERNO-peat utilises organic soil variables, resulting in a more realistic representation of soil moisture. Consequently, there is a better performance against observations in INFERNO-peat, which highlights the benefits of using peatland specific soil properties in fire modelling. However, low fuel loads appear to be an issue in INFERNO-peat as I show that JULES simulates a dominance of bare soil in the most northernly high latitude regions and in western Canada (Chapter 3). Underestimating fuel

loads within JULES results in an underestimation of the number of potential peat fire ignitions from flaming vegetation fires, ultimately resulting in an underestimation of peat fire burnt area.

There is substantial spatial variation in the performance of INFERNO-peat compared against observations (Chapter 3). Notable improvements in the representation of present-day high latitude fires are seen in western Canada, and in particular in the provinces of Saskatchewan, Manitoba, Nunavut and the Northwest Territories. This area of Canada is estimated by INFERNO-peat to experience an average of 0.087 M km^2 of peat burnt area each year. Improvements are also seen across Russia, and in particular in eastern Siberia. It is also important to note that INFERNO-peat performs less well in eastern Canada and Fennoscandia, where, compared to the observations, INFERNO-peat overestimates peat burning. I highlighted a variety of reasons for this overestimation, largely stemming from the poor representation of humans in fire models and a lack of consideration of landscape fragmentation (Chapter 3).

Fire models historically have also struggled to represent interannual variability in burnt area and carbon emissions (Hantson et al., 2020; Li et al., 2019). INFERNO-peat largely resolves this common issue and shows drastic increases in IAV across the high latitudes compared to INFERNO. There are also improved temporal correlations in INFERNO-peat against observations, indicating that peaks and troughs in fire activity and carbon emissions are more accurately represented over time. INFERNO-peat is capable of capturing the large fire years seen in 1998, 2002, 2003 and 2012 in the high latitudes. Consequently, I have shown that explicit representation of peat fires in fire models improves the capability of fire models to represent present day burnt area and carbon emissions in the high latitudes, and crucially allows for better representation of IAV (Chapter 3). Therefore, it is a recommendation of this thesis that high latitude peat fires are incorporated into the next generation of fire models.

1.2. The influence of peat fires on atmospheric composition and air quality in the high latitudes

The development of INFERNO-peat has revealed the substantial carbon emissions that are produced by peat burning in the northern high latitudes (Chapter 3), as well the potential vast increases in peat fire carbon emissions under climate change (Chapter 5). These emissions, whilst not dissected into their gas and aerosol species within this thesis, can be expected to have major implications for atmospheric composition and air quality in the northern high latitudes. It has long been understood that fires have major impacts on the atmosphere of the northern high latitudes both in terms of atmospheric composition and air quality (Singh et al., 2010; Shindell et al., 2007; Langmann et al., 2009). This work has demonstrated that peat fires have large impacts on aerosol, NO_2, and CO concentrations generally in the high latitudes, but most significantly in northwest Siberia (Chapter 4). For example, fires and peat fires in the northern high latitudes were significantly positively correlated

with concentrations of NO_2 in the atmosphere. In northwest Siberia, there are also significant positive correlations with CO. Smouldering combustion has been shown to produce high concentrations of CO (Akagi et al., 2011), therefore there is the possibility that the large peat fires that occur in northwest Siberia are having a major impact on atmospheric composition. For example, fires, which in a large part burned peatlands in Siberia in 2012, emitted 48 Tg CO, exerting a significant effect on atmospheric composition in the region (Teakles et al., 2017). Consequently, the results suggest that fires in the northern high latitudes result in higher concentrations of NO_2 and CO. Relatively more NO_2 is emitted compared to CO during these fires, as Chapter 4 also demonstrated that burnt area tends to be associated with higher ratios of NO_2:CO. However, the large-scale impacts of peat fires are challenging to disentangle from that of vegetation burning (Chapter 4). Results showed that peat burnt area tended to exhibit similar relationships with NO_2, CO and their ratio as total burnt area, potentially stemming from inaccurate estimations of peat burnt area from GFED5, or the concurrent burning of peat and vegetation that blurs the potential signals of lower NO_2:CO ratios, which peat fires are associated with.

Wildfires are also a major source of aerosols worldwide (Andreae, 2019; Andreae and Rosenfeld, 2008). In the high latitudes, peat fires have been shown to emit more $PM_{2.5}$ than all the anthropogenic sectors combined (McCarty et al., 2021). Black carbon emissions from wildfires have been shown to represent greater than 50% of all BC emissions north of 60° latitude (McCarty et al., 2021). For example, during the 2002 fire season in Quebec, fires accounted for 80% of the total annual BC emissions in the region (Lavoue and Stocks, 2011). Similarly, the analysis presented in Chapter 4 showed that burnt area and FRP are positively correlated with surface $PM_{2.5}$ concentrations. Peat fires have been shown to result in higher $PM_{2.5}$ emissions compared to flaming vegetation fires (Hu et al., 2018). I show that across the four regions of the high latitudes studied, there are suggestions from the observations that peat fires indeed contribute more to $PM_{2.5}$ concentrations than flaming fires, as evidenced by the significant positive correlations between peat fire percentage of burnt area and FRP with $PM_{2.5}$ concentrations, particularly on monthly timescales. Therefore, it is evident that peat fires have major impacts on $PM_{2.5}$ concentrations in the high latitudes, which may result in major impacts on air quality and human health.

1.3. Future changes to peat fires with climate change

It has been hypothesized that under global climate change, peatlands in the northern high latitudes would become more susceptible to wildfires, resulting in an increase in peat fire frequency, burnt area and emissions (McCarty et al., 2021; Turetsky et al., 2015; Nelson et al., 2021; Thompson et al., 2019; Li et al., 2021). However, due to the lack of peat parameterisation in most global fire models, there are currently no model quantifications of projected future changes to peat fires under different climate change scenarios. The development of INFERNO-peat (Chapter 2 Section 3) and its improved

modelling capabilities shown in Chapter 3, allowed for its use in Chapter 5 to conduct future projections of peat fires and their carbon emissions over the 21st century, under three different climate change scenarios.

Across the northern high latitudes, it is expected that burnt areas will increase, alongside a lengthening of the fire season and greater fire frequencies, particularly under high emissions scenarios (Wang et al., 2017; Flannigan et al., 2005; Curasi et al., 2024). In line with this, INFERNO-peat projects rapid and large increases in peat burnt area across the high latitudes by the end of the century. Changes are greatest under SSP585, with peat burnt areas reaching as high as 1.218 M km^2 per year by 2100 (Chapter 5). Different regions are projected to undergo different trajectories and magnitudes of change. For example, Canada is shown to undergo considerable changes, particularly in the provinces of Saskatchewan, Manitoba, and northern Ontario. Similarly, northwest Siberia is projected to undergo significant increases in peat burnt area and carbon emissions. Additionally, I show that peat fires under the highest emissions scenario are estimated to emit in excess of 1 Gt C each year across the high latitudes by 2100 (Chapter 5), representing a substantial perturbation to the climate system, and to carbon storage and sequestration in the northern high latitudes.

Large carbon loss as a result of peat fires is modelled by INFERNO-peat to result in the consumption of 9-15% of the total northern high latitude carbon store. Peat fires consequently result in the net loss of carbon to the atmosphere (Lasslop et al., 2019; Nelson et al., 2021), due to reduced fire return intervals and larger more severe fire events in the future, which mean that carbon cannot be reaccumulated fast enough and effectively enough to maintain peatlands as a net sink of carbon (Wilkinson et al., 2023; Li et al., 2021; Turetsky et al., 2015). It has been estimated that increased wildfire events could dimmish the peatland carbon sink by 57% by 2050 compared to a no-burn scenario, resulting in a switch of peatlands to a source of carbon by the end of the century (Wilkinson et al., 2023). A net loss of carbon due to peat fires, may enhance climatic warming, creating a positive feedback effect on the climate system (Nelson et al., 2021). Therefore, this thesis emphasises the need to understand and quantify potential changes to peatland carbon storage in the northern high latitudes as a result of the increased occurrence of peat fires. Research is consequently needed on linking peat fire and peatland models, in order to predict future changes to the peatland carbon store, and any impacts this may have on the climate system (see Section 2.2.3 for more information).

I also demonstrated the role of key drivers in shaping future peat fire burnt area and carbon emissions (Chapter 5). Increased burnt area was shown to be driven by increasing ignitions as a result of higher fuel loads and vegetation flammability leading to a greater number of flaming vegetation fires that can ignite peat fires, alongside increases in peat ignition probabilities due to drier soils across the high latitudes. Ultimately these changes are underpinned by climatic changes, such as increased temperature and precipitation. I show that temperature changes of as much as 12°C are anticipated by

the end of the century under SSP585 in the northern high latitudes. Warmer temperatures are strongly correlated with increased precipitation in the northern high latitudes (Chapter 5 Section 3; Koenigk et al., 2015; Ye et al., 2021), as a result of increases in the air moisture holding capacity with warmer temperatures, fuelling greater thermodynamic energy and intensified evaporation (Oki and Kanae 2006; Pan et al., 2014; Allen et al., 1998). However, the effects of increased precipitation on soil moisture are expected to be offset by greater evapotranspiration with warmer temperatures (Muller and Joos, 2021). Therefore, greater evaporation was shown to be associated with reduced soil moisture across much of the high latitudes, consequently increasing the probability of ignition of peatlands. Climate change and warmer temperatures have also been shown to drive increases in fire weather (Lund et al., 2023; Coogan et al., 2019; Wang et al., 2015), resulting in increases in the probability of ignition of peatlands and the flammability of vegetation, ultimately resulting in greater burnt areas. Furthermore, increased fuel loads are seen across the high latitudes stemming from increased vegetation productivity in warmer temperatures and the CO_2 fertilisation effect (Pearson et al., 2013; Madani et al., 2021; Ito et al., 2016). Additionally, a 112% increase in lightning strikes is projected by 2100 (Chen et al., 2021a), resulting in further vegetation fire ignition events. Lightning is expected to increase under warmer climates as a result of increases of up to 70-100% in convective available potential energy in Arctic tundra and boreal forests by 2100 under RCP8.5 (Chen et al., 2021a). I show that all these factors combine together to produce an environment that is highly conducive to peat fires in the future as a result of anthropogenically-induced climatic warming, which is particularly pronounced in the northern high latitudes.

1.4. Challenges in observing peat fires

A major challenge identified throughout this thesis is the lack of robust observational datasets of peat fire burnt area and carbon emissions. A lack of reliable observation-based data has been shown to influence our ability to evaluate peat fire models (Chapter 3), and to affect how well peat fire impacts on atmospheric composition and air quality can be determined (Chapter 4). Earth observation products are known to underestimate the quantity and spatial patterns of burning in peatland environments, notably in the northern high latitudes (Chen et al., 2021b; McCarty et al., 2021; Yang et al., 2023). Traditional EO methods fail to detect the majority of peat fires, as they tend to burn belowground and at lower temperatures (McCarty et al., 2023; Yang et al., 2023). For example, Sirin and Medvedeva et al. (2022) studied the 2010 fires in the Moscow region and showed MODIS hotspot fire detections to be insufficient to detect peat fires compared to ground-truthed data. Having reliable observations, and crucially constraints upon these observations, is essential for being able to predict future fire regimes (McCarty et al., 2021). As shown in Chapter 3, new peat fire models can only be evaluated on imperfect data and consequently may not be fully accurate and reliable in representing present-day burning. Therefore, when these models are used to simulate future trajectories of change, such as in Chapter 5, results may not be fully reflective of true changes that may occur to peat fires. It

is therefore essential that the detection of peat fires from remote sensing is rapidly improved, and conducted on a scale which can be useful to the wider fire modelling community.

The absence of observational datasets on peatlands themselves is also a key limitation in both observing and modelling peat fires. Until recently, accurate and reliable datasets on the distribution and extent of peatlands globally have been lacking (Melton et al., 2022). However, the development of recent datasets such as the Northern Peatland Dataset (Hugelius et al., 2020b) and Peat-ML (Melton et al., 2022) represent a substantial improvement in mapping peatlands. However, both approaches utilise in-situ peatland data and machine learning (Hugelius et al., 2020a; Melton et al., 2022). Meaning that these datasets may not represent the true distribution and extent of peatlands, which would have knock-on effects on the observation and modelling of peat fires. Stemming from the challenges to mapping global peatlands, obtaining global maps of peatland soil properties such as inorganic content and bulk density is challenging. As a consequence, fixed values of inorganic content and bulk density were used in INFERNO-peat within Chapters 3 and 5. It has been demonstrated that across the high latitudes inorganic content and bulk density vary significantly depending on the vegetation composition and type of peat (Loisel et al., 2014). Therefore, using fixed values likely results in inaccuracies in the calculation of peat ignition probability, with knock-on effects on peat burnt area and carbon emissions. However, there are at present no global datasets of peatland soil properties. Consequently, not only does the lack of observational data on peat fires effect our ability to accurately model and observe peat fires, but so does the lack of data on peatland distribution and soil properties.

It is also crucial to consider carbon and other trace gas and aerosol emissions from peat fires in global fire emissions inventories. For example, it was shown that the inclusion of peat fire burned area and greenhouse gas emissions in FAOSTAT (Food and Agriculture Organisation of the United Nations Statistics) resulted in 30% higher global fire emissions compared to GFED4s, thought to largely stem from peat fires in boreal Asia (Prosperi et al., 2020). Although mainly examined in tropical peatlands, emissions inventories such as GFED4s and GFASv1.2 have been shown to overestimate CH_4 emissions, and underestimate $PM_{2.5}$ emissions from peat fires (Wooster et al., 2018). In Chapter 3 it was shown that peat fires can result in emissions in excess of 200 Tg C each year in the northern high latitudes, and consequently represent a significant perturbation to the climate system. Additionally, Chapter 4 highlighted the major impacts peat fires have on atmospheric composition in terms of NO_2, CO and $PM_{2.5}$, particularly in northwest Siberia. Therefore, accurate representation of high latitude peat within global fire emissions inventories is vital in terms of quantifying present-day patterns and impacts of burning.

As wildfires in general, and peat fires in particular, have been shown to be dominant drivers of spatial and temporal variability in atmospheric composition in the northern high latitudes, there is the

possibility of using remotely sensed atmospheric composition data as an alternative to traditional fire detection methods. Smouldering combustion, which dominates during peat fires, is known to release more CO, NH_3 and CH_4 compared to that of flaming fires (Hu et al., 2019a; Hu et al., 2018; Hu and Rein, 2022). Consequently, ratios of NO_2:CO can be used as a proxy for combustion efficiency, which allows for differentiation between flaming and smouldering combustion (Andreae and Merlet, 2001; Rein et al., 2009; Andreae, 2019; van der Velde et al., 2021). Numerous studies have used NO_2:CO ratios from TROPOMI to distinguish between flaming and smouldering combustion (Lama et al., 2020; Hung et al., 2022; Wan et al., 2023; Peiro et al., 2022; Anderson et al., 2023; van der Velde et al., 2021). For example, van der Velde et al. (2022) examined differences in NO_2:CO ratios between biomes, and showed that boreal forests and tropical peatlands had lower ratios compared to savannas as a result of smouldering combustion. Additionally, Anderson et al. (2023) demonstrated how throughout the course of a fire, the relative contributions of flaming and smouldering can be quantified. However, to date no studies have looked at trying to use these ratios to identify peat burning in the northern high latitudes.

Chapter 4 consequently presented the first attempt to distinguish between peat and non-peat burning using NO_2:CO ratios from TROPOMI and CAMSRA across broad timescales in large regions of the northern high latitudes. However, analysis suggested TROPOMI is unlikely, on these scales, to be able to identify peat fires from the NO_2:CO ratios. Across all regions, except for northwest Siberia, peat fires tend to be associated with higher CAMSRA NO_2:CO ratios in our analysis, directly opposing what has been demonstrated in theory and laboratory studies. Expected perturbations to atmospheric composition from peat fires may not be being seen in Chapter 4 due to smouldering and flaming combustion occurring simultaneously in many environments (Akagi et al., 2011; Hu and Rein, 2022), potentially resulting in a masking of the signal from smouldering combustion. Additionally, Chapter 4 used relatively coarse temporal scales, yet NO_2 and CO are both reactive gases, particularly with OH (Fuglestvedt et al., 1999; Minschwaner et al., 2010); this means that NO_2 has a short lifetime ranging from hours to days (Fuglestvedt et al., 1999), and the lifetime of CO varies from days to weeks (Minschwaner et al., 2010; Holloway et al., 2020; Martinez-Alonso et al., 2020). Therefore, on the time steps studied here, emissions and signals of NO_2, CO, and indeed their ratio may not be as distinct compared to if singular fire events were studied.

In contrast, over northwest Siberia, Chapter 4 identifies that months and years which see larger peat burnt areas and percentage contributions of peat fires to total burnt area are positively associated with elevated CO and lower NO_2:CO ratios. Therefore, in northwest Siberia there is some suggestion that peat fires result in higher emissions of CO relative to flaming vegetation fires, supporting the findings of Hu et al. (2019a). Consequently, there is the potential for peat fires to be able to be distinguished from flaming vegetation fires in the northern high latitudes based on their impacts on atmospheric

composition. However, further research is required to fully determine the feasibility of using atmospheric composition impacts to identify peat fires on large spatial and temporal scales.

2. Future work

2.1. Improving observations of northern high latitude peat fires

As previously highlighted, a lack of robust observational datasets on peat fires and their emissions is a major challenge for the evaluation of peat fire models, and the quantification of the impacts of peat fires on atmospheric composition and air quality on large spatial and temporal scales. Therefore, a focus of future research should be on developing reliable and accurate datasets of peat fire burnt area and emissions. Tailored peat fire detection algorithms are likely to be highly beneficial for peat fire identification. For example, the Tropical Peatland Combustion Algorithm (ToPeCAI), used shortwave infrared and thermal infrared reflectance to detect peat fires (Sofan et al., 2019). ToPeCAI was shown to capture peat fires with an accuracy of 82% compared to ground-truthed data, higher than the accuracy of VIIRS active fire measurements in peatland environments (Sofan et al., 2019). However, this methodology has only been used for the tropics, and therefore its reliability for the high latitudes has yet to be assessed. Within the high latitudes specifically, the difference Normalised Burn Ratio (dNBR) and Normalised Difference Moisture Index (NDMI) have been shown to be capable of mapping peatland burned areas with an accuracy of 93% (Sirin and Medvedeva, 2022). However, this method would require high quality data both pre- and post-fire, which is not always possible. Consequently, further research is required into novel ways to detect and differentiate peat burning in the northern high latitudes using remote sensing.

Chapter 4 briefly explored the potential for alternative methods of peat fire detection using remotely sensed atmospheric trace gas emissions. Whilst within the analysis presented in Chapter 4 it still remains unclear whether the ratio of NO_2:CO inferred from satellite measurements could be used to distinguish peat fires from vegetation fires in the northern high latitudes on large spatial and temporal scales, a multitude of alternative options require further research to assess their viability. In addition to NO_2 smouldering peat fires are known to release substantially less CO_2 compared to flaming combustion (Hu and Rein, 2022). Therefore, emissions ratios of CO_2:CO or CO_2:CH_4 can potentially be used to identify peat burning in the high latitudes. The ratio of CO_2:CO has been used as a proxy for combustion efficiency and has been shown to be capable of differentiating between flaming and smouldering combustion (Andreae, 2019; Urbanski, 2014; Stockwell et al., 2016; Rein, 2015). However, the ratio of CO_2:CH_4 has been shown to be nearly 600% lower during smouldering combustion compared to flaming combustion (Hu and Rein, 2022). Consequently, CO_2:CH_4 is thought to be the best emissions signature for detecting peat burning (Hu and Rein, 2022). The ratio of CO_2:CH_4 has been shown to be significantly lower in smouldering peat fires, compared to that of

flaming savanna, grassland, and forest fires (Hu and Rein et al., 2022). Similarly, Parker et al. (2016) showed that emissions ratios of CO_2:CH_4, detected by satellite observations from GOSAT, were significantly lower during the 2015 Indonesia peat fires, compared to flaming vegetation fires in the Amazon and southern Africa. Therefore, there is the potential that remotely sensed data of CO_2 and CH_4 can be used to identify peat burning. Future work should therefore be undertaken using remotely sensed data of CO_2 and CH_4 in the northern high latitudes to firstly test if peat fires do produce different signals of CO_2:CH_4 compared to non-peat fires, likely using a methodology similar to what is presented in Chapter 4. Secondly, if different signals can be differentiated between peat and non-peat fires, then potential undetected peat fires could be identified through anomalous CO_2:CH_4 ratios. Whilst TROPOMI does record CH_4 concentrations, it does not detect CO_2 and therefore would not be able to be used for this purpose. CAMS (Inness et al., 2019) however does contain data on both CO_2 and CH_4 and therefore could be used in this future research. Additionally, other Earth observation products such as GOSAT (Kuze et al., 2009), which was used by Parker et al. (2016) to assess CO_2:CH_4 ratios during peat fires, IASI (Clerbaux et al., 2009), and AIRS (Aumann et al., 2003) do simultaneously measure by CO_2 and CH_4, and therefore could be used in this further research.

Chapter 4 also identified the potential for detecting peat fires through the ratios of different components of aerosol emissions. Peat fires have been shown, in both field and laboratory studies, to emit substantial quantities of organic carbon, and negligible amounts of black carbon (Fujii et al., 2014; Che et al., 2022; Conny and Slater, 2002; Hu et al., 2018; Kondo et al., 2011; Yokelson et al., 2011), as a result of lower combustion efficiency during smouldering fires (Yokelson et al., 2011; Che et al., 2022). Meanwhile, flaming fires are estimated to release ten times more black carbon than smouldering fires (Conny and Slater, 2002). Therefore, the relative contributions of BC and OC, perhaps in the form of emissions ratios, could potentially be used to distinguish between peat and non-peat fires. However, to date the use of these aerosol emissions components to identify peat burning has not been tested. Therefore, a further avenue for research could examine the possibility of using ratios of BC:OC to detect peat fires. A key issue, however, is the lack of remotely sensed data that differentiates between different components of aerosol emissions. Many satellite sensors such as AASTR (Kolmonen et al., 2016), CALIOP (Winker et al., 2004) and MODIS (Levy et al., 2013) just detect aerosol optical depth and aerosol size parameters. However, recent work has implemented retrieval algorithms to assess black and brown carbon concentrations from satellite sensors (e.g. Bao et al., 2019; Gogoi et al., 2023; Konovalov et al., 2022). There is consequently the potential for future research into the emissions of BC and OC from peat fires, and whether this can be used to aid peat fire detection.

2.2. Future INFERNO-peat development

This thesis has demonstrated the importance of parameterising high latitude peat fires within a fire model, with improvements seen in the representation of present day burning and the ability of the model to capture interannual variability. Additionally, such a development provides the opportunity for studies of peat fire driven feedbacks on atmospheric composition, the carbon cycle, and climate, for the past, present and future. However, further model developments are necessary to improve the representation of peat fires globally, and to improve our future estimations of peat fires and their impacts under anthropogenic climate change. Concurrent INFERNO and JULES model developments are also vital for improving INFERNO-peat. For example, the further development of a peatland scheme within JULES alongside additional permafrost representation will aid INFERNO-peat through more accurate representation of peatland hydrology and dynamics. Additionally, improvements in how humans are represented in INFERNO, such as through the modelling of human fire use or incorporation of HDI (Perkins et al., 2022; Teixeria et al., 2023), would result in improved estimations of ignitions in human-dominated landscapes. Furthermore, improvements to the TRIFFID dynamic vegetation model within JULES, to better represent the vegetation of the high latitudes, such as through the addition of a moss PFT, would aid in improving INFERNO's ability to capture high latitude vegetation fires, with implications for peat fire modelling. Couplings with other models, such as peat models and Earth system models, are also crucial to further quantify the large-scale effects of peat fires in the Earth system. Primarily, the incorporation of INFERNO-peat into JULES-INFERNO is essential for future model developments. The potential developments and couplings to INFERNO-peat are shown in Figure 86 and described in detail in the following sections.

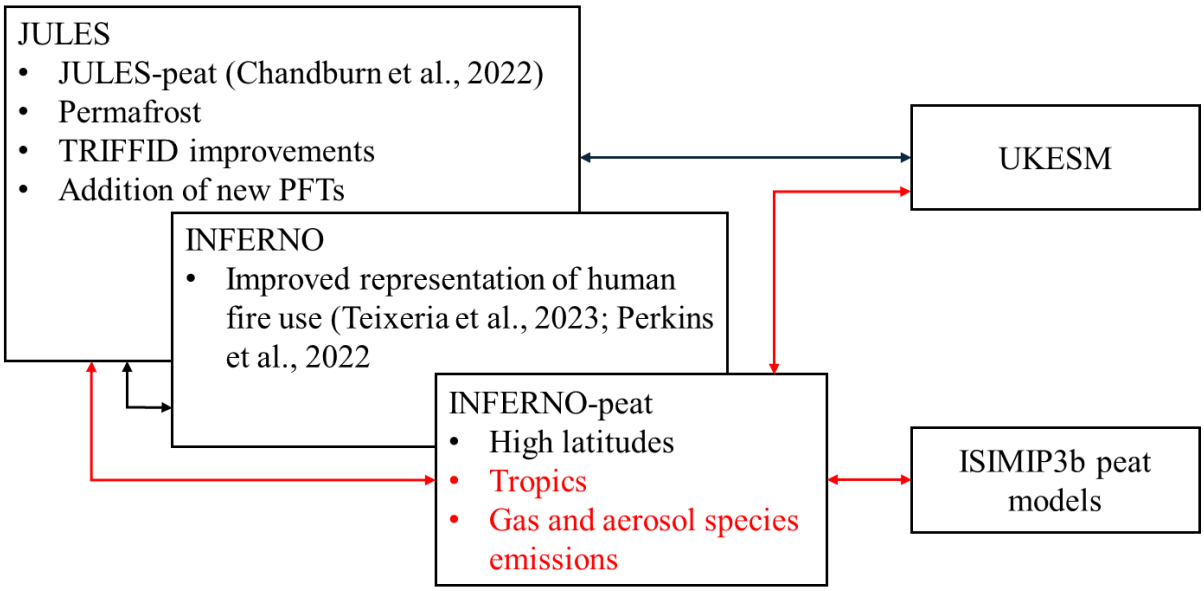


Figure 86: Schematic demonstrating the potential future developments of INFERNO-peat (red text), and the potential future couplings (red arrows). Black arrows indicate preexisting couplings.

2.2.1. Expansion of the INFERNO-peat scheme to the tropics

This thesis chose to focus on the northern high latitude peatlands, as they make up the vast majority of global peatland area (UNEP, 2022a; Frokling et al., 2011), and are undergoing rapid environmental and climatic change (Bruhwiler et al., 2021, Walsh et al., 2020; Chen et al., 2021a). However, the tropics also contain large areas dominated by peatlands, i.e. 11% of the global peatland area, with significant deposits in southeast Asia, the Amazon, and the Congo basin (Page et al., 2011; Lahteenoja et al., 2013; Dargie et al., 2017). The tropics are also undergoing extensive land use changes, such as plantation development, logging, and agriculture, which are increasing the vulnerability of peatlands to fires (Langner and Siegert, 2009; Turetsky et al., 2015; Loisel et al., 2020). Furthermore, climate change is increasing the presence of drought conditions in much of the tropics, further exacerbating the vulnerability of peatlands to fires (Loisel et al., 2020; Dadap et al., 2019). Large peat fires in the tropics have occurred frequently throughout the observational period and are often exacerbated by El Niño events. For example, peat fires in Indonesia in 1997 released an estimated 2.57 Gt C, equivalent to 40% of global fossil fuel burning emissions in 1997 (Page et al., 2002). In addition, these fires accounted for 17% of total annual global fire $PM_{2.5}$ emissions (Roulston et al., 2018), with dramatic impacts on air quality and human health. Large peat fires also occurred in southeast Asia in 2015 (Atwood et al., 2016; Roulston et al., 2018), which resulted in vast $PM_{2.5}$ emissions that were responsible for 95% of Indonesian $PM_{2.5}$ emissions in 2015 (Wooster et al., 2018). The smoke plumes from these fires led to extensive and persistent pollution across southeast Asia (Field et al., 2016), leading to 100,000 premature deaths (Koplitz et al., 2016).

Therefore, modelling tropical peat fires is crucial in being able to accurately represent fire emissions from the tropics, both in terms of the impacts on the carbon cycle and climate system, but also in terms of their air quality impacts and the devastating effects on human health and well-being, given the large human populations that reside in tropical areas. Additionally, peat fires in the tropics are heavily affected by El Niño conditions (Hirano et al., 2006; Atwood et al., 2016), and consequently their inclusion could help simulate better the regional and global interannual variability in burnt area and carbon emissions. Therefore, the INFERNO-peat scheme should also be extended to the tropics. The present scheme could be easily scaled up to the tropics using an alternative peatland fraction dataset such as Peat-ML (Melton et al., 2022), or PEATMAP (Xu et al., 2018). However, alterations to the calculations of peat probability of ignition, burnt area and depth of burn would need to be implemented due to the known differences between tropical and high latitude peat fires.

Tropical peat fires burn approximately 600% larger areas than high latitude fires, with an average peat fire size in the tropics of 8378km^2 (Santoso et al., 2019a). Therefore, the average BA value used in Chapter 2, Equation 9, would need to be adapted for tropical peat fires. Additionally, tropical peat fires have been shown to burn much deeper into the soil than boreal peat fires, with an average depth of burn of 43cm compared 12cm (Santoso et al., 2019a). Therefore, the maximum value used to cap

depth of burn (See Chapter 2 section 3.4) would need to be increased, and an additional sensitivity analysis (such as that detailed in Chapter 3, Section 2) would need to be conducted. Similarly, carbon emissions fluxes from tropical peat fires have been shown to be much larger than those of boreal peat fires, averaging 28 kg C m^{-2} (Santoso et al., 2019a), while they can be as much as 31.5 kg C m^{-2} (Page et al., 2002). Therefore, this would likely need to be accounted for by increasing the prescribed combustion completeness value used in Chapter 2, Equation 11. It is also crucial to consider that peatlands, and peat fires, in the tropics are greatly affected by human activity (Turetsky et al., 2015), whereas the majority of fires in the high latitudes are ignited by lightning (Wendler et al., 2011; McCarty et al., 2021; Xu et al., 2022). Therefore, tropical peat fires are more likely to be inaccurately represented by fire models if the human component is not accurately represented within a fire model. Consequently, it is important that the human components of INFERNO are improved, such as accounting for the Human Development Index in the parameterisation of human fire ignitions (Teixeria et al., 2023), or through the coupling of INFERNO with an agent-based model of human fire use (Perkins et al., 2022). Both these efforts are activities that are currently undertaken as part of the Leverhulme Centre for Wildfires, Environment and Society, with our team being centrally involved in their materialisation. Such efforts will allow for more accurate human fire use representations, allowing for more accurate modelling of tropical peat fires.

2.2.2. Representing gaseous and aerosol emissions from peat fires in INFERNO-peat

At present, INFERNO-peat simply assesses the total emitted carbon from peat fires. Chapter 4 however, highlighted the importance of knowledge on the impacts of peat fires on atmospheric composition and air quality being assimilated into global fire models in order to improve estimations of future changes to atmospheric composition and air quality with climate change. Therefore, further development of INFERNO-peat should include the estimation of trace gas and aerosol emissions from peat fires. Published peat fire specific emissions factors (such as those from Hu et al. (2018)) could be used to extend the present modelling scope to include emissions of key species such as CO_2, CO, NO_2, CH_4, non-methane VOCs, BC, and OC. The addition of these peat fire gas and aerosol emissions would allow for further analysis on the impacts of fires on atmospheric composition and air quality, as well as allowing for quantifications of the air quality impacts from peat fires across the world. Crucially, gas and aerosol emissions from peat fires would also be able to be simulated under future climate change scenarios, allowing for potential future changes to atmospheric composition and air quality to be assessed. Ultimately, through the additional coupling to the UKESM (See Section 2.2.4), feedback effects of these peat fire emissions on the climate system and their radiative forcing can be assessed.

2.2.3. Coupling INFERNO-peat to peatland models

As mentioned in Chapter 3, INFERNO-peat is limited by the lack of feedback effects of peat burning on peatland carbon storage and functioning. Fundamentally this was not implemented because at

present JULES has no representation of peatlands and their dynamics, meaning that peat carbon cannot be lost or accumulated dynamically in INFERNO-peat and JULES. Therefore, a future development to INFERNO-peat should involve coupling with a peatland model, in order to dynamically simulate the feedbacks and effects of peat fires on peatlands. Ideally, with the concurrent development of JULES-peat (Chadburn et al., 2022), this can be implemented within the JULES-INFERNO framework allowing for a fully coupled model. However, numerous other peatland models have been developed in recent years that form part of the ISIMIP3a and 3b simulation rounds for simulating peatlands in land surface models (available from: https://protocol.isimip.org/#/ISIMIP3a/peat, last accessed: 04/07/2024). These models, which include PEATCLSM (Bechtold et al., 2019), ORCHIDEE-MICT-PEAT (Guimberteau et al., 2018; Qiu et al., 2018; Qiu et al., 2019), and LPJ-GUESS Peatland (Chaudhary et al., 2017; Chaudhary et al., 2020), allow for peat accumulation, loss and carbon storage to be simulated over the recent historical period and into the future. Therefore, outputs from these models could be used to drive INFERNO-peat, potentially leading to a more accurate representation of peatland soil properties. Also, a more complete coupling can be carried out, in which peat fires would result in the loss of carbon immediately following a fire, with gradual reaccumulation of carbon post-fire. Peat fire effects on soil hydrological properties, such as increased soil evapotranspiration and deeper water tables post-fire (Kettridge et al., 2019; Kettridge et al., 2015), could also be implemented. These couplings would lead to further improvements in our fire modelling capabilities, particularly by allowing for dynamic feedbacks on carbon storage.

Approximately half of all high latitude peatlands are underlain by permafrost (Hugelius et al., 2020), meaning that many peat fires occur in permafrost peatlands. For example, 71% of all fires that occurred in the Siberian Arctic between 1982 and 2020 occurred in regions of continuous permafrost (Descals et al., 2022). Therefore, the effects of peat fires on permafrost peatlands are another important feedback that could be incorporated into INFERNO-peat if coupled with a peatland model. Some of the aforementioned models, including JULES, have begun to simulate permafrost dynamics in the northern high latitudes (Burke et al., 2017; Burke et al., 2020; Smith et al., 2022b). Consequently, feedbacks of fires on permafrost properties and disturbances can potentially be incorporated into INFERNO-peat. For example, fires have been shown to result in a direct loss of the organic layer from the soil (Nossov et al., 2013), increased soil temperatures and result in the thickening of the active layer (Holloway et al., 2020; Li et al., 2021; Gibson et al., 2018; Smith et al., 2015; Kharuk et al., 2011). In the Northwest Territories, Canada, the active layer has been shown to thicken by as much as 50cm in the years following a fire (Zhang et al., 2015). Peat fires can also lead to talik and thermokarst karst lake formation (Nitze et al., 2018; Gibson et al., 2018), so much so that 25% of all thermokarst lake expansion in western Canada over the last 30 years has been attributed to wildfires (Gibson et al., 2018). Permafrost thaw and degradation leads to large losses of long term

stored carbon to the atmosphere (Turetsky et al., 2020; Serikova et al., 2019). On top of this, fires in permafrost peatlands have been shown to result in elevated carbon emissions for many years following a fire, taking decades to centuries for disturbed permafrost to return to pre-fire conditions (Koster et al., 2018; Li et al., 2021). Under global climate change, Chapter 5 showed peat fires to increase, and therefore, the impacts that fires have on permafrost in the future could also be substantial. Therefore, the feedback effects between peat fires and permafrost are important to also consider in future model developments, due to the vast amounts of long-term stored carbon that could be emitted following these fires.

2.2.4. Coupling of INFERNO-peat to the UKESM

All of the model developments detailed in the preceding sections link back to the carbon and other emissions produced by peat fires, and the impacts they may have on the atmosphere, climate and the carbon cycle. Therefore, in order to fully quantify the scale of these effects on the atmospheric system and to estimate the potential radiative forcing of peat fires, INFERNO-peat should also be coupled with the UKESM. Additionally, this coupling would allow for a feedback effect of peat fires and their relevant emissions on the atmosphere and climate. In particular, it is critical that aerosol emissions from peat fire be considered as they have been shown to have large impacts on radiative forcing in the northern high latitudes. For example, the release of aerosols from Siberian fires, was shown to increase aerosol optical depth by six-fold, resulting in a net cooling effect on the atmosphere (Zhuravleva et al., 2017, Jeong et al., 2008). Similarly, cooling effects due to fire aerosol emissions were found in the summer of 2004 over Alaska (Pfister et al., 2008). However, emissions of light-absorbing aerosols such as brown carbon can have a positive radiative forcing effect, with estimates estimating this forcing to be 17 W m^{-2} after a flaming boreal vegetation fire (Oris et al., 2014; Randerson et al., 2006; Chakrabarty et al., 2016). Furthermore, the deposition of dark aerosols such as black carbon onto light coloured surfaces such as glaciers, snow and sea ice result in a lower surface albedo and consequently warming and surface melting (Randerson et al., 2006; Thomas et al., 2017). Therefore, a future iteration of INFERNO-peat which simulates aerosol and trace gas emissions and is coupled with the UKESM, would allow for a dynamic fire-atmosphere model in which fires create a feedback loop with the atmosphere, and allow for the quantification of the net effect of peat fires on the climate system. This would then be highly beneficial in the modelling of the impact of future climate change scenarios on peat fires, potentially exacerbating the amount of carbon emissions projected in Chapter 5.

3. Conclusions and wider implications

This thesis has highlighted, throughout its chapters, the importance of northern high latitude peat fires, both in terms of the importance of parameterising peat fires in global fire models and also the effect of peat fires upon atmospheric composition and air quality. Including a specific parameterisation of peat fires in the northern high latitudes in the INFERNO fire model was shown in Chapter 3 to result in a

much-improved capability of the model to represent present day patterns of burning and subsequently, carbon emissions from fires. Accurately capturing present day burning in the high latitudes is of the upmost importance for being able to project potential future changes to peat fires under different climate change scenarios. Without parameterising peat fires, the results of Chapter 5 indicate that major increases in burnt area and carbon emissions would be omitted, leading to an unrealistic representation of future fire regimes. It is therefore a key recommendation of this thesis that peat fires are integrated into all fire models and included in the next generation of fire and Earth system models.

This thesis, and in particularly Chapter 4, has also highlighted the major implications of peat fires on atmospheric composition and air quality across the high latitudes. It is well known that across the northern high latitudes, fires are the main source of air pollution-induced health burdens (Lelieveld et al., 2015). Elevated levels of $PM_{2.5}$, which are shown in Chapter 4 to be strongly associated with increased peat burnt area, result in respiratory and cardiovascular disease (Dockery et al., 1993; Pope et al., 2002; Brook et al., 2010). $PM_{2.5}$ emissions from fires have been attributed to 21,000 excess deaths each year in the Arctic, with Russia seeing the largest health impacts (Silver et al., 2024). However, the trans-boundary transport of fire-produced smoke often results in impacts upon health of populations far away from the source of the fire (Silver et al., 2023; Silver et al., 2024). For example, in 2003, large fires burned predominately upon peatlands in Siberia, which resulted in enhancements in PM_{10} and smoke plumes reaching as far away as the Korean Peninsula, Japan and the USA (Jeong et al., 2008; Huang et al., 2009). Similarly, in 2012 ozone and $PM_{2.5}$ health standards were exceeded in British Columbia, Canada, and Washington State, USA, as a result of the transportation of smoke plumes from fires in Siberia (Teakles et al., 2017). Consequently, it has been estimated that of the 21,000 excess deaths that occur each year due to Arctic wildfires, 8,000 occur in countries outside of the Arctic (Silver et al., 2024). It is therefore critical that fire models accurately represent burning in the northern high latitudes, in order to better understand the health impacts of degraded air quality produced by wildfires, and the additional representation of peat fires is a notable step forward in this modelling capability.

Crucially, the ideas and results presented in this thesis become particularly pertinent in the context of anthropogenic global climate change. The northern high latitudes are warming at double the rate of the global average (Bruhwiler et al., 2021), consequently driving, alongside other climatic and environmental changes, increases in the frequency and extent of peat fires (McCarty et al., 2021; Turetsky et al., 2015; Nelson et al., 2021; Thompson et al., 2019; Li et al., 2021). Chapter 5 highlighted that under all the climate change scenarios examined, INFERNO-peat predicts increases in peat burnt area over the next century, with those increases being rapid and large especially in the more severe climate change scenarios. This has been shown to occur, both in Chapter 5 and by McCarty et al. (2021), as a result of rising temperatures, which increase the vulnerability of peat to wildfires, as well as raising the likelihood of natural fire ignitions. Climatic warming of just 1-4°C

could result in a doubling of days with a moderate or higher fire weather index in the northern high latitudes (Lund et al., 2023), and, consequently, with the 12°C of warming anticipated by the UKESM under SSP585 (Chapter 5), the incidences of extreme fire weather will be further increased, resulting in amplified likelihood of peat fires. Warmer temperatures also result in an increased number of lightning strikes (Chen et al., 2021a), elevating the number of potential fire ignitions. Furthermore, increases in the frequency and intensity of droughts are expected with climatic change, which may drive declines in soil moisture and have been shown to potentially result in a six-fold increase in fire activity in the high latitudes (Thompson et al., 2019). All these factors combine, creating an environment that is highly vulnerable to wildfires, and with increasing numbers of ignitions, ultimately fuel the large increases in peat fires that are both expected and modelled to occur over the remainder of the 21st century.

Increasing likelihood of peat fires risk switching what was once a fire-resistant ecosystem, to a fire prone ecosystem (Turetsky et al., 2015), with potentially vast impacts on the long-term stored carbon sequestered within high latitude peatlands. Over millennia, peatlands have accumulated carbon, making them one of the most important stores of carbon within the Earth system (Yu et al., 2010; Gallego-Sala et al., 2018; Loisel et al., 2014). It has been estimated that globally peatlands are a carbon sink of approximately 142 Tg C per year, equivalent to a total millennial sink of 33 ppm CO_2 (Gallego-Sala et al., 2018). Consequently, any disturbance to this crucial carbon store could have major implications for the global carbon cycle and climate system. Peat fires are thought to release carbon equivalent to approximately 15% of that of anthropogenic emissions (Lasslop et al., 2019; Loisel et al., 2021; Poulter et al., 2006; Rein, 2015). Depending on the recovering times of peat and the fire return intervals, this could result in a net loss of carbon. For example, Turetsky et al. (2011a) showed that fire emissions between 2000 and 2009 exceeded the decadal carbon uptake by peatlands in Alaska. Furthermore, severe burning in western Canadian peatlands has been shown to potentially result in the loss of 450 years' worth of peat accumulation (Turetsky et al., 2011b). Therefore, peat fires have the potential to result in large net losses of carbon to the atmosphere, and particularly under climate change, these emissions could lead to major shifts in the carbon and climate systems. INFERNO-peat estimates under SSP585 that peat fires may result in the release of over 1 Gt C each year by 2100. This huge emission of long-term stored carbon from peatlands, could result in a positive feedback effect on the climate system, and ultimately a catastrophic loss of carbon from the high latitude soils into the atmosphere (Mack et al., 2011; Chen et al., 2021a; Turetsky et al., 2015; Nelson et al., 2021). Unless action is taken to preserve and restore peatlands across the high latitudes, and effective climate change policies are implemented to tackle rising global temperatures, it is inevitable that significant amounts of carbon from high latitude peatlands will be lost.

However, if future global socioeconomic development follows a low emission pathway similar to that of SSP126, there is great potential for limiting the effects of climate change on peat fires. Chapter 5

demonstrated that under SSP126, much smaller temperature increases are expected to occur, meaning that there are minimal changes to soil moisture and the probability of ignition of peatlands, resulting in smaller increases in peat burnt area seen across the northern high latitudes, compared to higher emissions scenarios. Under SSP126, peat burnt area is modelled to increase by 45.6% by 2100, with annual carbon emissions remaining below 0.5 Gt C. The SSP126 scenario follows a pathway that is focused on sustainable development, which drives lower greenhouse gas emissions (O'Neill et al., 2017). This sustainable development comes at the cost of slow economic growth, but instead focuses on achieving global development goals, and reducing global inequalities, alongside investment into renewable energy, and increased energy efficiency (O'Neill et al., 2017; Riahi et al., 2017). These social and economic changes in SSP126 ultimately result in a peak in CO_2, CH_4 and N_2O emissions in 2060, followed by a decline, and result in a global radiative forcing of 2.6 W m^{-2} in 2100 compared to the preindustrial era (Riahi et al., 2017). Therefore, policy and societal change towards a lower emissions trajectory is necessary for reducing the impacts of climate change and preventing large-scale losses of carbon as a result of northern high latitude peat fires.

To conclude, this thesis has demonstrated throughout its chapters the importance of peat fires within the Earth system, and the critical need for understanding their dynamics and historical trends of burning, alongside the impacts they inflict upon atmospheric composition, air quality, climate, and carbon cycles. Crucially, peat fires and their impacts need to be represented within our fire and Earth system models. This thesis has presented the first step in doing so, by the development of INFERNO-peat, which is capable of accurately representing present day burning at the northern high latitudes and capturing the interannual variability in both burnt area and carbon emissions. Further model developments are needed in order to better represent the impacts of peat fires, such as through the addition of peat fire trace gas and aerosol emissions and coupling with peatland models to capture the feedback effects on the carbon cycle. Furthermore, this thesis has highlighted the severe potential future scenarios of peat burning in the high latitudes and has emphasised the possible impacts of large-scale carbon emissions from peat burning later in the 21st century. In conclusion, it is imperative that peat fires are accounted for in fire models and understood in terms of their global impacts on atmospheric composition, air quality, ecosystems and the carbon cycle, with the view to preventing the large-scale impacts of peat fires on the planet and protecting the vital peatland ecosystems over the coming centuries.

Bibliography

Abatzoglou, J. T., and Kolden, C. A.: Relative importance of weather and climate on wildfire growth in interior Alaska, Int. J. Wildland Fire, 20, 479-486, https://doi.org/10.1071/WF10046, 2011.

AICC: Alaska fire season 2009: Wildland fire summary and statistics annual report, Alaska Interagency Coordination Centre, available from: https://fire.ak.blm.gov/content/aicc/stats/archive/2009.pdf, last access: 01/08/2024, 2009.

AICC: Alaska Fire Numbers 2019, Alaska Interagency Coordination Centre, available from: https://fire.ak.blm.gov/content/aicc/Statistics%20Directory/Previous%20Years%20Data%20and%20FFR%20Handouts/2019%20Fire%20Data/Alaska%20Fire%20Season%202019%20Presentation.pdf, last access: 01/08/2024, 2020.

Akagi, S. K., Yokelson, R. J., Wiedinmyer, C., Alvarado, M. J., Reid, J. S., Karl, T., Crounse, J. D., and Wennberg, P. O.: Emission factors for open and domestic biomass burning for use in atmospheric models, Atmos. Chem. Phys., 11, 4039–4072, https://doi.org/10.5194/acp-11-4039-2011, 2011.

Ali, M. A., Bilal, M., Wang, Y., Nichol, J. E., Mhawish, A., Qiu, Z., de Leeuw, G., Zhang, Y., Zhan, Y., Liao, K., Almazroui, M., Dambul, R., Shahid, S., and Islam, M. N.: Accuracy assessment of CAMS and MERRA-2 reanalysis PM2.5 and PM10 concentrations over China, Atmos. Environ., 288, 119297, https://doi.org/10.1016/j.atmosenv.2022.119297, 2022.

Allen, R. G., Pereira, L. S., Raes, D., and Smith, M.: Crop evapotranspiration-Guidelines for computing crop water requirements - FAO Irrigation and drainage paper 56, FAO, Rome, available from: https://www.fao.org/4/X0490E/X0490E00.htm last access: 01/08/2024, 1998.

Andela, N., Morton, D. C., Giglio, L., Chen, Y., van der Werf, G. R., Kasibhatla, P. S., DeFries, R. S., Collatz, G. J., Hantson, S., Kloster, S., Bachelet, D., Forrest, M., Lasslop, G., Li, F., Mangeon, S., Melton, J. R., Yue, C., and Randerson, J. T.: A human-driven decline in global burned area, Science, 356, 1356-1362, https://doi.org/10.1126/science.aal4108, 2017.

Anderson, L. D., Dix, B., Schnell, J., Yokelson, R., Veefkind, J. P., Ahmadov, R., and de Gouw, J.: Analyzing the impact of evolving combustion conditions on the composition of wildfire emissions using satellite data, Geophys. Res. Lett., 50, e2023GL105811, https://doi.org/10.1029/2023GL105811, 2023.

Andreae, M. O.: Emission of trace gases and aerosols from biomass burning – an updated assessment, Atmos. Chem. Phys., 19, 8523–8546, https://doi.org/10.5194/acp-19-8523-2019, 2019.

Andreae, M. O. and Gelencsér, A.: Black carbon or brown carbon? The nature of light-absorbing carbonaceous aerosols, Atmos. Chem. Phys., 6, 3131–3148, https://doi.org/10.5194/acp-6-3131-2006, 2006.

Andreae, M. O. and Merlet, P.: Emission of trace gases and aerosols from biomass burning, Global Biogeochem. Cycles, 15, 955-966, https://doi.org/10.1029/2000GB001382, 2001.

Andreae, M. O., and Rosenfeld, D.: Aerosol–cloud–precipitation interactions. Part 1. The nature and sources of cloud-active aerosols, Earth-Sci. Rev., 89, 13-41, https://doi.org/10.1016/j.earscirev.2008.03.001, 2008.

Archibald, S.: Managing the human component of fire regimes: lessons from Africa, Philos. T. R. Soc. B., 371, 20150346, https://doi.org/10.1098/rstb.2015.0346, 2016.

Archibald, S., Lehmann, C. E. R., Belcher, C. M., Bond, W. J., Bradstock, R. A., Daniau, A-L., Dexter, K. G., Forrestel, E. J., Greve, M., He, T., Higgins, S. I., Hoffmann, W. A., Lamon, B. B., McGlinn, D. J., Moncrieff, G. R., Osborne, C. P., Pausas, J. G., Price, O., Ripley, B. S., Rogers, B. M., Schwilk, D. W., Simon, M. F., Turetsky, M. R., Van der Werf, G. R., and Zanne, A. E.: Biological and geophysical feedbacks with fire in the Earth system, Environ. Res. Lett., 13, 033003, https://doi.org/10.1088/1748-9326/aa9ead, 2018.

Atkinson, R.: Atmospheric chemistry of VOCs and NOx, Atmos. Environ., 34, 2063-2101, https://doi.org/10.1016/S1352-2310(99)00460-4, 2000.

Atwood, E. C., Englhart, S., Lorenz, E., Halle, W., Wiedemann, W., and Siegert, F.: Detection and Characterization of Low Temperature Peat Fires during the 2015 Fire Catastrophe in Indonesia Using a New High-Sensitivity Fire Monitoring Satellite Sensor (FireBird), PLoS One, 11, e0159410, https://doi.org/10.1371%2Fjournal.pone.0159410, 2016.

Aumann, H. H., Chahine, M. T., Gautier, C., Goldberg, M., Kalnay, E., McMillin, L., Revercomb, H., Rosenkranz, P. W., Smith, W. L., Staelin, D., Strow, L., and Susskind, J.: AIRS/AMSU/HSB on the Aqua mission: design, science objectives, data products, and processing systems, IEEE Trans. Geosci. Remote Sens., 41, 253-264, https://doi.org/10.1109/TGRS.2002.808356, 2003.

Babic, L., Braak, R., Dierssen, W., Kissi-Ameyaw, J., Kleipool, Q., Leloux, J., Loots, E., Ludewig, A., Rozenmeijer, N., Smeets, J., and Vacanti, G.: Algorithm theoretical basis document for the TROPOMI L01b data processor, Royal Netherlands Meteorological Institute, available from: https://sentiwiki.copernicus.eu/__attachments/1673595/S5P-KNMI-L01B-0009-SD%20-%20Sentinel-5P%20TROPOMI%20ATBD%20Level%2001B%20data%20processor%202022%20-%2010.0.0.pdf?inst-v=b245e836-25f8-4f0a-8ca4-ccb3ac15aa2a, last access: 31/07/2024, 2022.

Ballinger, T. J., Bigalke, S., Walsh, J. E., Brettschneider, B., Thoman, R. L., Bhatt, U. S., Hanna, E., Hanssen-Bauer, I., Kim, S.-J., Overland, J. E., and Wang, M.: NOAA Arctic Report Card 2023 : Surface Air Temperature, https://doi.org/10.25923/x3ta-6e63, 2023.

Balzter, H., Gerard, F. F., George, C. T., Rowland, C. S., Jupp, T. E., McCallum, I., Shvidenko, A., Nilsson, S., Sukhinin, A., Onuchin, A., and Schmullius, C.: Impact of the Arctic Oscillation pattern on interannual forest fire variability in Central Siberia, Geophys. Res. Lett., 32, L14709, https://doi.org/10.1029/2005GL022526, 2005.

Bao, F., Cheng, T., Li, Y., Gu, X., Guo, H., Wu, Y., Wang, Y., and Gao, J.: Retrieval of black carbon aerosol surface concentration using satellite remote sensing observations, Remote Sens. Environ., 226, 93-108, https://doi.org/10.1016/j.rse.2019.03.036, 2019.

Barnes, C., Boulanger, Y., Keeping, T., Gachon, P., Gillett, N., Boucher, J., Roberge, F., Kew, S., Haas, O., Heinrich, D., Vahlberg, M., Singh, R., Elbe, M., Sivanu, S., Arrighi, J., Van Aalst, M., Otto, F., Zachariah, M., Krikken, F., Wang, X., Erni, S., Pietropalo, E., Avis, A., Bisaillon, A., and Kimutai, J.: Climate change more than doubled the likelihood of extreme fire weather conditions in Eastern Canada, https://doi.org/10.25561/105981, 2023.

Baró, R., Palacios-Peña, L., Baklanov, A., Balzarini, A., Brunner, D., Forkel, R., Hirtl, M., Honzak, L., Pérez, J. L., Pirovano, G., San José, R., Schröder, W., Werhahn, J., Wolke, R., Žabkar, R., and Jiménez-Guerrero, P.: Regional effects of atmospheric aerosols on temperature: an evaluation of an ensemble of online coupled models, Atmos. Chem. Phys., 17, 9677–9696, https://doi.org/10.5194/acp-17-9677-2017, 2017a.

Baró, R., Lorente-Plazas, R., Montávez, J. P., and Jiménez-Guerrero, P.: Biomass burning aerosol impact on surface winds during the 2010 Russian heat wave, Geophys. Res. Lett., 44, 1088-1094, https://doi.org/10.1002/2016GL071484, 2017b.

Bartsch, A., Pointner, G., Nitze, I., Efimova, A., Jakober, D., Ley, S., Hogstrom, E., Grosse, G., and Schweitzer, P.: Expanding infrastructure and growing anthropogenic impacts along Arctic coasts, Environ. Res. Lett., 16, 115013, https://doi.org/10.1088/1748- 9326/ac3176, 2021.

Bechtold, M., De Lannoy, G. J. M., Koster, R. D., Reichle, R. H., Mahanama, S. P., Bleuten, W., Bourgault, M. A., Brümmer, C., Burdun, I., Desai, A. R., Devito, K., Grünwald, T., Grygoruk, M., Humphreys, E. R., Klatt, J., Kurbatova, J., Lohila, A., Munir, T. M., Nilsson, M. B., Price, J. S., Röhl, M., Schneider, A., and Tiemeyer, B.: PEAT-CLSM: A Specific Treatment of Peatland Hydrology in the NASA Catchment Land Surface Model, J. Adv. Mod. Earth Syst., 11, 2130-2162, https://doi.org/10.1029/2018MS001574, 2019.

Beer, R.: TES on the aura mission: scientific objectives, measurements, and analysis overview, IEEE Trans. Geosci. Remote Sens., 44, 1102-1105, https://doi.org/10.1109/TGRS.2005.863716, 2006.

Benscoter, B. W., Thompson, D. K., Waddington, J. M., Flannigan, M., Wotton, M., Groot, W. J., and Turetsky, M. R.: Interactive effects of vegetation, soil moisture and bulk density on depth of burning of thick organic soils, Int. J. Wildland Fire, 20, 1–12, https://doi.org/10.1071/WF08183, 2011.

Benscoter, B. W., and Wieder, R. K. Variability in organic matter lost by combustion in a boreal bog during the 2001 Chisholm fire, Can. J. For. Res., 33, 2509-2513, https://doi.org/10.1139/x03-162, 2003.

Berg, A., and Sheffield, J.: Climate Change and Drought: the Soil Moisture Perspective, Curr. Clim. Change Rep., 4, 180-191, https://doi.org/10.1007/s40641-018-0095-0, 2018.

Berner, L. T., Massey, R., Jantz, P., Forbes, B. C., Macias-Fauria, M., Myers-Smith, I., Kumpula, T., Gauthier, G., Andreu-Hayles, L., Gaglioti, B. V., Burns, P., Zetterberg, P., D'Arrigo, R., and Goetz, S. J.: Summer warming explains widespread but not uniform greening in the Arctic tundra biome, Nature Comms. 11, 4621, https://doi.org/10.1038/s41467-020-18479-5, 2020.

Bertrand, G., Ponçot, A., Pohl, B., Lhosmot, A., Steinmann, M., Johannet, A., Pinel, S., Caldirak, H., Artigue, G., Binet, P., Bertrand, C., Collin, L., Magnon, G., Gilbert, D., Laggoun-Deffarge, F., and Toussaint, M.-L.: Statistical hydrology for evaluating peatland water table sensitivity to simple environmental variables and climate changes application to the mid-latitude/altitude Frasne peatland (Jura Mountains, France), Sci. Tot. Environ., 754, 141931, https://doi.org/10.1016/j.scitotenv.2020.141931, 2021.

Bhatt, U. S., Walker, D. A., Raynolds, M. K., Bieniek, P. A., Epstein, H. E., Comiso, J. C., Pinzon, J. E., Tucker, C. J., Steele, M., and Ermold, W.: Changing seasonality of panarctic tundra vegetation in relationship to climatic variables, Environ. Res. Lett., 12, 055003, https://doi.org/10.1088/1748-9326/aa6b0b, 2017.

Biglake, S., and Walsh, J. E.: Future Changes of Snow in Alaska and the Arctic under Stabilized Global Warming Scenarios, Atmosphere, 13, 541, https://doi.org/10.3390/atmos13040541, 2022.

Bintanja, R.: The impact of Arctic warming on increased rainfall, Scientific Reports, 8, 16001, https://doi.org/10.1038/s41598-018-34450-3, 2018.

Bintanja, R., and Selten, F. M.: Future increases in Arctic precipitation linked to local evaporation and sea-ice retreat, Nature, 509, 479-482, https://doi.org/10.1038/nature13259, 2014.

Bintanja, R., and Andry, O.: Towards a rain-dominated Arctic, Nature, 7, 263-267, https://doi.org/10.1038/nclimate3240, 2017.

Black, R. R., Aurell, J., Holder, A., George, I. J., Gullett, B. K., Hays, M. D., Geron, C. D., and Tabor, D.: Characterization of gas and particle emissions from laboratory burns of peat, Atmos. Environ., 132, 49-57, https://doi.org/10.1016/j.atmosenv.2016.02.024, 2016.

Blackford, K. R., Kasoar, M., Burton, C., Prentice, C., and Voulgarakis, A.: INFERNO-peat v1.0.0 (v1.0.0), Zenodo [code], https://doi.org/10.5281/zenodo.10007362, 2023.

Blackford, K. R., Kasoar, M., Burton, C., Burke, E., Prentice, I. C., and Voulgarakis, A.: INFERNO-peat v1.0.0: a representation of northern high-latitude peat fires in the JULES-INFERNO global fire model, Geosci. Model Dev., 17, 3063–3079, https://doi.org/10.5194/gmd-17-3063-2024, 2024.

Bodah, B. W., Neckel, A., Maculan, L. S., Milanes, C. B., Korcelski, C., Ramírez, O., Mendez-Espinosa, J. F., Bodah, E. T., and Oliveira, M. L. S.: Sentinel-5P TROPOMI satellite application for NO2 and CO studies aiming at environmental valuation, J. Clean. Prod., 357, 131960, https://doi.org/10.1016/j.jclepro.2022.131960, 2022.

Boisvert-Marsh, L., Périé, C., and de Blois, S.: Shifting with climate? Evidence for recent changes in tree species distribution at high latitudes, Ecosphere, 5, 1-33, https://doi.org/10.1890/ES14-00111.1, 2014.

Bond, T. C., Streets, D. G., Yarber, K. F., Nelson, S. M., Woo, J.-H., and Klimont, Z.: A technology-based global inventory of black and organic carbon emissions from combustion, J. Geophys. Res.: Atmos., 109, D14203, https://doi.org/10.1029/2003JD003697, 2004.

Bond, T. C., Doherty, S. J., Fahey, D. W., Forster, P. M., Berntsen, T., DeAngelo, B. J., Flanner, M. G., Ghan, S., Karcher, B., Koch, D., Kinne, S., Kondo, Y., Quinn, P. K., Sarofim, M. C., Schultz, M. G., Shulz, M., Venkataraman, C., Zhang, H., Zhang, S., Bellouin, N., Guttikunda, S. K., Hopke, P. K., Jacobson, M. Z., Kaiser, J. W., Klimont, Z., Lohmann, U., Schwarz, J. P., Shindell, D., Storelvmo, T., Warren, S. G., and Zender, C. S.: Bounding the role of black carbon in the climate system: A scientific assessment, J. Geophys. Res.: Atmos, 118, 5380-5552, https://doi.org/10.1002/jgrd.50171, 2013.

Bondur, V. G., Gordo, K. A., Voronova, O. S., Zima, A. L., and Feoktistova, N. V.: Intense Wildfires in Russia over a 22-Year Period According to Satellite Data, Fire, 6, 99, https://doi.org/10.3390/fire6030099, 2023.

Borsdorff, T., Aan de Brugh, J., Hu, H., Aben, I., Hasekamp, O., and Landgraf, J.: Measuring carbon monoxide with TROPOMI: First results and a comparison with ECMWF-IFS analysis data, Geophysical Research Letters, 45, 2826–2832, https://doi.org/10.1002/2018GL077045, 2018.

Borsdorff, T., García Reynoso, A., Maldonado, G., Mar-Morales, B., Stremme, W., Grutter, M., and Landgraf, J.: Monitoring CO emissions of the metropolis Mexico City using TROPOMI CO

observations, Atmos. Chem. Phys., 20, 15761–15774, https://doi.org/10.5194/acp-20-15761-2020, 2020.

Bovensmann, H., Burrows, J.P., Buchwitz, M., Frerick, J., Noel, S., Rozanov, V.V., Chance, K.V., and Goede, A.P.H.: SCIAMACHY: Mission objectives and measurement modes, J. Atmos. Sci., 56, 127–150, https://doi.org/10.1175/1520-0469(1999)056%3C0127:SMOAMM%3E2.0.CO;2, 1999.

Bowman, D. M. J. S., Balch, J. K., Artaxo, P., Bond, W. J., Carlson, J. M., Cochrane, M. A., D'Antonio, C. M., DeFries, R. S., Doyle, J. C., Harrison, S. P., Johnston, F. H., Keeley, J. E., Krawchuk, M. A., Kull, C. A., Marston, J. B., Moritz, M. A., Prentice, I. C., Roos, C. I., Scott, A. C., Swetnam, T. W., Van der Werf, G. R., and Pyne, S. J., Fire in the Earth System, Science, 324, 481-484, https://doi.org/10.1126/science.1163886, 2009.

Bowman, D. M. J. S., Balch, J., Artaxo, P., Bond, W. J., Cochrane, M. A., D'Antonio, C. M., DeFries, R., Johnston, F. H., Keeley, J. E., Krawchuk, M. A., Kull, C. A., Mack, M., Moritz, M. A., Pyne, S., Roos, C. I., Scott, A. C., Sodhi, N. S., and Swetnam, T. W., The human dimension of fire regimes on Earth, J. Biogeog., 38, 2223-2236, https://doi.org/10.1111/j.1365-2699.2011.02595.x, 2011.

Box, J. E., Bhatt, U. S., Christensen, T. R., Derksen, C., Gerland, S., Granskog, M., Isaksen, K., Kohler, J., Mård, J., Meier, W. N., Mudryk, L., Romanovsky, V. E., Shiklomanov, A., Smith, S., Vanha-Majamaa, I., Wouters, B., and Yang, D.: Recent developments in Arctic climate observation indicators. In: AMAP Arctic Climate Change Update 2021: Key Trends and Impacts, Arctic Monitoring and Assessment Programme (AMAP), Tromso, Norway, 7-19, 2021.

Brook, R. D., Rajagopalan, S., Pope, C. A., III, Brook, J. R., Bhatnagar, A., Diez-Roux, A. V., Holguin, F., Hong, Y., Luepker, R. V., Mittleman, M. A., Peters, A., Siscovick, D., Smith, S. C., Jr., Whitsel, L., and Kaufman, J. D.: Particulate matter air pollution and cardiovascular disease: An update to the scientific statement from the American Heart Association, Circulation, 121, 2331-2378, https://doi.org/10.1161/cir.0b013e3181dbece1, 2010.

Brown, D. R. N., Jorgenson, M. T., Douglas, T. A., Romanovsky, V. E., Kielland, K., Hiemstra, C., Euskirchen, E. S., and Ruess, R. W.: Interactive effects of wildfire and climate on permafrost degradation in Alaskan lowland forests, J. Geophys. Res. Biogeosci., 120, 1619–1637, https://doi.org/10.1002/2015JG003033, 2015.

Bruhwiler, L., Parmentier, F-J. W., Crill, P., Leonard, M., and Palmer, P. I.: The Arctic Carbon Cycle and Its Response to Changing Climate, Curr. Clim. Change Rep., 7, 14-34, https://doi.org/10.1007/s40641-020-00169-5, 2021.

Buchwitz, M., de Beek, R., Bramstedt, K., Noël, S., Bovensmann, H., and Burrows, J. P.: Global carbon monoxide as retrieved from SCIAMACHY by WFM-DOAS, Atmos. Chem. Phys., 4, 1945–1960, https://doi.org/10.5194/acp-4-1945-2004, 2004.

Bunn, A. G., Goetz, S. J., Kimball, J. S., and Zhang, K.: Northern high-latitude ecosystems respond to climate change, Eos Trans. Am. Geophys. Union, 88, 333-335, https://doi.org/10.1029/2007EO340001, 2007.

Burke, E. J., Chadburn, S. E., and Ekici, A.: A vertical representation of soil carbon in the JULES land surface scheme (vn4.3_permafrost) with a focus on permafrost regions, Geosci. Model Dev., 10, 959–975, https://doi.org/10.5194/gmd-10-959-2017, 2017.

Burke, E. J., Zhang, Y., and Krinner, G.: Evaluating permafrost physics in the Coupled Model Intercomparison Project 6 (CMIP6) models and their sensitivity to climate change, The Cryosphere, 14, 3155–3174, https://doi.org/10.5194/tc-14-3155-2020, 2020.

Burrows, J. P., Weber, M., Buchwitz, M., Rozanov, V., Ladstätter-Weißenmayer, A., Richter, A., DeBeek, R., Hoogen, R., Bramstedt, K., Eichmann, K.-U., Eisinger, M., and Perner, D.: The Global Ozone Monitoring Experiment (GOME): Mission Concept and First Scientific Results, J. Atmos. Sci., 56, 151-175, https://doi.org/10.1175/1520-0469(1999)056%3C0151:TGOMEG%3E2.0.CO;2, 1999.

Burton, C., Betts, R., Cardoso, M., Feldpausch, T. R., Harper, A., Jones, C. D., Kelley, D. I., Robertson, E., and Wiltshire, A.: Representation of fire, land-use change and vegetation dynamics in the Joint UK Land Environment Simulator vn4.9 (JULES), Geosci. Model Dev., 12, 179–193, https://doi.org/10.5194/gmd12-179-2019, 2019.

Burton, C., Kelley, D. I., Jones, C. D., Betts, R. A., Cardoso, M., and Anderson, L.: South American fires and their impacts on ecosystems increase with continued emissions, Climate Res. Sustain., 1, e8, https://doi.org/10.1002/cli2.8, 2021.

Burton, C., Lampe, S., Kelley, D., Thiery, W., Hantson, S., Christidis, N., Gudmundsson, L., Forrest, M., Burke, E., Chang, J., Huang, H., Ito, A., Kou-Giesbrecht, S., Lasslop, G., Li, W., Nieradzik, L., Li, F., Chen, Y., Randerson, J., Reyer, C., and Mengel, M.: Global burned area increasingly explained by climate change, Nature [preprint], https://doi.org/10.21203/rs.3.rs-3168150/v1, in review, 2023.

Byrne, B., Liu, J., Bowman, K. W., Pascolini-Campbell, M., Chatterjee, A., Pandey, S., Miyazaki, K., van der Werf, G. R., Wunch, D., Wennberg, P. O., Roehl, C. M., and Sinha, S.: Carbon emissions from the 2023 Canadian wildfires, Nature, 633, 835-839, https://doi.org/10.1038/s41586-024-07878-z, 2024.

Cai, Z., You, Q., Wu, F., Chen, H. W., Chen, D., and Cohen, J.: Arctic Warming Revealed by Multiple CMIP6 Models: Evaluation of Historical Simulations and Quantification of Future Projection Uncertainties, J. Climate, 34, 4871-4892, https://doi.org/10.1175/JCLI-D-20-0791.1, 2021.

Calef, M. P., McGuire, A. D., and Chapin III, F. S.: Human Influences on Wildfire in Alaska from 1988 through 2005: An Analysis of the Spatial Patterns of Human Impacts, Earth Interact., 12, 1-17, https://doi.org/10.1175/2007EI220.1, 2008.

Callaghan, T. V., and Jonasson, S.: Arctic terrestrial ecosystems and environmental change, Philos. T. R. Soc. A., 352, 259-276, https://doi.org/10.1098/rsta.1995.0069, 1995.

Campos-Ruiz, R., Parisien, M-A., and Flannigan, M. D.: Temporal Patterns of Wildfire Activity in Areas of Contrasting Human Influence in the Canadian Boreal Forest, Forests, 9, 149, https://doi.org/10.3390/f9040159, 2018.

Carroll, M. J., Dennis, P., Pearce-Higgins, J. W., and Thomas, C. D.: Maintaining northern peatland ecosystems in a changing climate: effects of soil moisture, drainage and drain blocking on craneflies, Global Change Bio., 17, 2991-3001, https://doi.org/10.1111/j.1365-2486.2011.02416.x, 2011.

Cerosimo, A., Serio. C., and Masiello, G.: TROPOMI NO2 Tropospheric Column Data: Regridding to 1 km Grid-Resolution and Assessment of their Consistency with In-Situ Surface Observations, Remote Sens., 12, 2212, https://doi.org/10.3390/rs12142212, 2020.

Chadburn, S. E., Burke, E. J., Gallego-Sala, A. V., Smith, N. D., Bret-Harte, M. S., Charman, D. J., Drewer, J., Edgar, C. W., Euskirchen, E. S., Fortuniak, K., Gao, Y., Nakhavali, M., Pawlak, W., Schuur, E. A. G., and Westermann, S.: A new approach to simulate peat accumulation, degradation and stability in a global land surface scheme (JULES vn5.8_accumulate_soil) for northern and temperate peatlands, Geosci. Model Dev., 15, 1633– 1657, https://doi.org/10.5194/gmd-15-1633-2022, 2022.

Chakrabarty, R. K., Gyawali, M., Yatavelli, R. L. N., Pandey, A., Watts, A. C., Knue, J., Chen, L.-W. A., Pattison, R. R., Tsibart, A., Samburova, V., and Moosmüller, H.: Brown carbon aerosols from burning of boreal peatlands: microphysical properties, emission factors, and implications for direct radiative forcing, Atmos. Chem. Phys., 16, 3033–3040, https://doi.org/10.5194/acp-16-3033-2016, 2016.

Chambers, F. M., Beilman, D. W., and Yu, Z.: Methods for determining peat humification and for quantifying peat bulk density, organic matter and carbon content for palaeostudies of climate and peatland carbon dynamics, Mires and Peat, 7, 1-10, available from: http://www.mires-and-peat.net/pages/volumes/map07/map0707.php, last access: 30/07/2024, 2011.

Chan, K. L., Valks, P., Heue, K.-P., Lutz, R., Hedelt, P., Loyola, D., Pinardi, G., Van Roozendael, M., Hendrick, F., Wagner, T., Kumar, V., Bais, A., Piters, A., Irie, H., Takashima, H., Kanaya, Y., Choi, Y., Park, K., Chong, J., Cede, A., Frieß, U., Richter, A., Ma, J., Benavent, N., Holla, R., Postylyakov, O., Rivera Cárdenas, C., and Wenig, M.: Global Ozone Monitoring Experiment-2 (GOME-2) daily and monthly level-3 products of atmospheric trace gas columns, Earth Syst. Sci. Data, 15, 1831–1870, https://doi.org/10.5194/essd-15-1831-2023, 2023.

Chaudhari, R. R., Ahire, D. V., Ahire, V. D., Chkravarty, M., and Maity, S. Soil Bulk Density as related to Soil Texture, Organic Matter Content and available total Nutrients of Coimbatore Soil, Int. J. Sci. Res. Pub., 3, http://www.ijsrp.org/research-paper-0213.php?rp=P14721, 2018.

Chaudhary, N., Miller, P. A., and Smith, B.: Modelling Holocene peatland dynamics with an individual-based dynamic vegetation model, Biogeosciences, 14, 2571–2596, https://doi.org/10.5194/bg-14-2571-2017, 2017.

Chaudhary, N., Westermann, S., Lamba, S., Shurpali, N., Sannel, A. B. K., Schurgers, G., Miller, P. A., and Smith, B.: Modelling past and future peatland carbon dynamics across the pan-Arctic, Glob. Change Bio., 26, 4119-4133, https://doi.org/10.1111/gcb.15099, 2020.

Che, H., Segal-Rozenhaimer, M., Zhang, L., Dang, C., Zuidema, P., Sedlacek III, A. J., Zhang, X., and Flynn, C.: Seasonal variations in fire conditions are important drivers in the trend of aerosol optical properties over the south-eastern Atlantic, Atmos. Chem. Phys., 22, 8767–8785, https://doi.org/10.5194/acp-22-8767-2022, 2022.

Che Azmi, N. A., Apandi, N. M., and Rashid, A. S. A.: Carbon emissions from the peat fire problem – a review, Environ. Sci. Pollut. R., 2, 16948–16961, https://doi.org/10.1007/s11356-021-12886-x, 2021.

Chen, Y., Romps, D. M., Seeley. J. T., Veraverbeke, S., Riley, W. J., Mekonnen, Z. A., and Randerson, J. T.: Future increases in Arctic lightning and fire risk for permafrost carbon, Nat. Clim. Change, 11, 404–410, https://doi.org/10.1038/s41558-021-01011-y, 2021a.

Chen, D., Shevade, V., Baer, A., and Loboda, T. V.: Missing Burns in the High Northern Latitudes: The Case for Regionally Focused Burned Area Products, Remote Sens., 13, 4145, https://doi.org/10.3390/rs13204145, 2021b.

Chen, C., Peng, X., Frauenfeld, O. W., Zhao, Y., Yang, G., Tian, W., Li, X., Du, R., and Li, X.: Comprehensive Assessment of Seasonally Frozen Ground Changes in the Northern Hemisphere Based on Observations, J. Geophys. Res.: Atmos., 127, e2022JD037306, https://doi.org/10.1029/2022JD037306, 2022.

Chen, Y., Hall, J., van Wees, D., Andela, N., Hantson, S., Giglio, L., van der Werf, G. R., Morton, D. C., and Randerson, J. T.: Global Fire Emissions Database (GFED5) Burned Area (0.1), Zenodo [data set], https://doi.org/10.5281/zenodo.7668424, 2023a.

Chen, Y., Hall, J., van Wees, D., Andela, N., Hantson, S., Giglio, L., van der Werf, G. R., Morton, D. C., and Randerson, J. T.: Multi-decadal trends and variability in burned area from the fifth version of the Global Fire Emissions Database (GFED5), Earth Syst. Sci. Data, 15, 5227–5259, https://doi.org/10.5194/essd-15-5227-2023, 2023b.

Cho, Y., Yoon, J.-H., Jeong, J.-H., Kug, J.-S., Kim, B.-M., Kim, H., Park, R. J., and Kim, S.-W.: Precipitation-induced abrupt decrease of Siberian wildfire in summer 2022 under continued warming, Environ. Res. Lett., 19, 074037, https://doi.org/10.1088/1748-9326/ad5573, 2024.

Christensen, E. G., Fernandez-Anex, N., and Rein, G.: Influence of soil moisture conditions on the multidimensional spread of smouldering combustion in shallow layers, Combust. Flame, 214, 361–370, https://doi.org/10.1016/j.combustflame.2019.11.001, 2020.

Christensen, E. G., Hu, Y., Purnomo, D. M. J., and Rein, G.: Influence of wind and slope on multidimensional smouldering peat fires, Proc. Combust. Inst., 38, 5033-5041, https://doi.org/10.1016/j.proci.2020.06.128, 2021.

Christian, H. J. Blakeslee, R. J., Boccippio, D. J., Boeck, W. L., Buechler, D. E., Driscoll, K. T., Goodman, S. J., Hall, J. M., Koshak, W. J., Mach, D. M., and Stewart, M. F.: Global frequency and distribution of lightning as observed from space by the Optical Transient Detector, J. Geophys. Res.-Atmos., 108, 4005, https://doi.org/10.1029/2002jd002347, 2003.

Chuvieco, E.: Global Impacts of Fire, In: Chuvieco, E. (ed): Earth Observation of Wildland Fires in Mediterranean Ecosystems, Springer, 1-10, https://doi.org/10.1007/978-3-642-01754-4_1, 2009.

Chuvieco, E., Lizundia-Loiola, J., Pettinari, M. L., Ramo, R., Padilla, M., Tansey, K., Mouillot, F., Laurent, P., Storm, T., Heil, A., and Plummer, S.: Generation and analysis of a new global burned area product based on MODIS 250 m reflectance bands and thermal anomalies, Earth Syst. Sci. Data, 10, 2015–2031, https://doi.org/10.5194/essd-10-2015-2018, 2018.

Chuvieco, E., Mouillot, F., van der Werf, G. R., Miguel, J. S., Tanase, M., Koutsias, N., Garcia, M., Yebra, M., Padilla, M., Gotas, I., Heil, A., Hawbaker, T. J., and Giglio, L.: Historical background and current developments for mapping burned area from satellite Earth observation, Remote Sensing of Environment, 225, 45-64, https://doi.org/10.1016/j.rse.2019.02.013, 2019.

Chuvieco, E., Pettinari, M. L., Koutsias, N., Forkel, M., Hantson, S., and Turco, M.: Human and climate drivers of global biomass burning variability, Sci. Tot. Enviro., 779, 146361, https://doi.org/10.1016/j.scitotenv.2021.146361, 2021.

Clark, S. K., Ward, D. S., and Mahowald, N. M.: The sensitivity of global climate to the episodicity of fire aerosol emissions, J. Geophys. Res.: Atmos., 120, 11589-11607, https://doi.org/10.1002/2015JD024068, 2015.

Clerbaux, C., Boynard, A., Clarisse, L., George, M., Hadji-Lazaro, J., Herbin, H., Hurtmans, D., Pommier, M., Razavi, A., Turquety, S., Wespes, C., and Coheur, P.-F.: Monitoring of atmospheric composition using the thermal infrared IASI/MetOp sounder, Atmos. Chem. Phys., 9, 6041–6054, https://doi.org/10.5194/acp-9-6041-2009, 2009.

Conny, J. M., and Slater, J. F.: Black carbon and organic carbon in aerosol particles from crown fires in the Canadian boreal forest, Jour. Geophys. Res. Atmos., 107, AAC 4-1 - AAC 4-12, https://doi.org/10.1029/2001JD001528, 2002.

Coogan, S. C. P., Robinne, F-N., Jain, P., and Flannigan, M. D.: Scientists' warning on wildfire — a Canadian perspective, Can. J. For. Res., 49, 1015-1023, https://doi.org/10.1139/cjfr-2019-0094, 2019.

Coops, N. C., Hermosilla, T., Wulder, M. A., White, J. C., and Bolton, D. K.: A thirty year, fine-scale, characterization of area burned in Canadian forests shows evidence of regionally increasing trends in the last decade, PLoS ONE, 13, e0197218, https://doi.org/10.1371/journal.pone.0197218, 2018.

Curasi S., Melton, J., Arora, V., Humphreys, E., and Whaley, C. H.: Canada's wildfire future: climate change below a 2°C global target avoids large increases in burned area by the end of the century, npj Clim. Atmos. Sci. [preprint], https://doi.org/10.21203/rs.3.rs-4364877/v1, 2024.

Dadap, N. C., Cobb, A. R., Hoyt, A. M., Harvey, C. F., and Konings, A. G.: Satellite soil moisture observations predict burned area in Southeast Asian peatlands, Environ. Res. Lett., 14, 094014, https://doi.org/10.1088/1748-9326/ab3891, 2019.

Dargie, G. C., Lewis, S. L., Lawson, I. T., Mitchard, E. T. A., Page, S. E., Bocko, Y. E., and Ifo, S. A.: Age, extent and carbon storage of the central Congo Basin peatland complex, Nature, 543, 86-90, https://doi.org/10.1038/nature21048, 2017.

Davies, M. G., Gray, A., Rein, G., and Legg, C. J.: Peat consumption and carbon loss due to smouldering wildfire in a temperature peatland, Forest Ecol. Manage., 308, 169–177, https://doi.org/10.1016/j.foreco.2013.07.051, 2013.

Descals, A., Gaveau, D. L. A., Verger, A., Sheil, D., Naito, D., and Peñuelas, J.: Unprecedented fire activity above the Arctic Circle linked to rising temperatures, Science, 378, 532–537, https://doi.org/10.1126/science.abn9768, 2022

de Groot, W. J., Flannigan, M. D., and Cantin, A. S.: Climate change impacts on future boreal fire regimes, For. Ecol. Manag., 294, 35-44, https://doi.org/10.1016/j.foreco.2012.09.027, 2013.

de Vries, J., Voors, R., Mika, A., Otter, G., van der Valk, N., Aben, I., Hoogeveen, R., Gloudemans, A., Dobber, M., Veefkind, P., and Levelt, P.: TROPOMI, the solar backscatter satellite instrument for air quality and climate, heads towards detailed design, Proc. SPIE, 7474, 747409, https://doi.org/10.1117/12.830087, 2009.

Dockery, D. W., Pope, C. A., Xu, X., Spengler, J. D., Ware, J. H., Fay, M. E., Ferris, B. G., Jr., and Speizer, F. E.: An Association between Air Pollution and Mortality in Six U.S. Cities, N. Engl. J. Med., 329, 1753-1759, https://doi.org/10.1056/NEJM199312093292401, 1993.

Doerr, S. H., and Santin, C.: Global trends in wildfire and its impacts: perceptions versus realities in a changing world, Philos. T. R. Soc. B., 371, 20150345, http://dx.doi.org/10.1098/rstb.2015.0345, 2016.

Drummond, J. R., and Mand, G. S.: The Measurements of Pollution in the Troposphere (MOPITT) Instrument: Overall Performance and Calibration Requirements, J. Atmos. Oceanic Technol., 13, 314–320, https://doi.org/10.1175/1520-0426(1996)013<0314:TMOPIT>2.0.CO;2, 1996.

Drummond, J. R., Zou, J., Nichitiu, F., Kar, J., Deschambaut, R., and Hackett, J., A review of 9-year performance and operation of the MOPITT instrument, Adv. Space Res., 45, 760-774, https://doi.org/10.1016/j.asr.2009.11.019, 2010.

ECMWF, CAMS: Reanalysis data documentation, available from: https://confluence.ecmwf.int/display/CKB/CAMS%3A+Reanalysis+data+documentation ,last access: 31/07/2024, 2024.

EEA: Air quality in Europe — 2019 report, EEA Report No 10/2019. European Environment Agency, Copenhagen, https://doi.org/10.2800/822355, 2019.

Elmendorf, S. C., Henry, G. H. R., Hollister, R. D., Björk, R. G., Bjorkman, A. D., Callaghan, T. V., Siegwart Collier, L., Cooper, E. J., Cornelissen, J. H. C., Day, T. A., Fosaa, A. M., Gould, W. A., Grétarsdóttir, J., Harte, J., Hermanutz, L., Hik, D. S., Hofgaard, A., Jarrad, F., Jónsdóttir, I. S., Keuper, F., Klanderud, K., Klein, J. A., Koh, S., Kudo, G., Lang, S. I., Loewen, V., May, J. L., Mercado, J., Michelsen, A., Molau, U., Myers-Smith, I. H., Oberbauer, S. F., Pieper, S., Post, E., Rixen, C., Robinson, C. H., Schmidt, N. M., Shaver, G. R., Stenström, A., Tolvanen, A., Totland, Ø., Troxler, T., Wahren, C.-H., Webber, P. J., Welker, J. M., and Wookey, P. A. Global assessment of experimental climate warming on tundra vegetation: heterogeneity over space and time, Eco. Lett., 15, 164-175, https://doi.org/10.1111/j.1461-0248.2011.01716.x, 2011.

Ernakovich, J. G., Hopping, K. A., Berdanier, A. B., Simpson, R. T., Kachergis, E. J., Steltzer, H., and Wallenstein, M. D.: Predicted responses of arctic and alpine ecosystems to altered seasonality under climate change, Global Change Bio., 20, 3256-3269, https://doi.org/10.1111/gcb.12568, 2014.

ESA, global ozone monitoring experiment users manual, available from: https://Earth.esa.int/eogateway/documents/20142/37627/GOME-User-Manual.pdf, last access: 31/07/2024, 1995.

ESA, EnviSat AATSR Product Handbook, available from: https://Earth.esa.int/eogateway/documents/20142/37627/AATSR-product-handbook.pdf, last access: 31/07/2024, 2007.

Eskes, H. J., and Eichmann, K-U.: S5P Mission Performance Centre Nitrogen Dioxide [L2__NO2___] Readme, available from: https://sentinel.esa.int/documents/247904/3541451/Sentinel-5P-Nitrogen-Dioxide-Level-2-Product-Readme-File, last access: 31/07/2024, 2023.

Evangeliou, N., Kylling, A., Eckhardt, S., Myroniuk, V., Stebel, K., Paugam, R., Zibtsev, S., and Stohl, A.: Open fires in Greenland in summer 2017: transport, deposition and radiative effects of BC, OC and BrC emissions, Atmos. Chem. Phys., 19, 1393–1411, https://doi.org/10.5194/acp-19-1393-2019, 2019.

Farukh, M. A., and Hayasaka, H.: Active Forest Fire Occurrences in Severe Lightning Years in Alaska, J. Nat. Disaster Sci, 33, 71-84, https://doi.org/10.2328/jnds.33.71, 2012.

Fazel-Rastgar, F., and Sivakumar, V.: Weather pattern associated with climate change during Canadian Arctic wildfires: A case study in July 2019, Remote Sens. App.: Soc. Environ., 25, 100698, https://doi.org/10.1016/j.rsase.2022.100698, 2022.

Fewster, R. E., Morris, P. J., Ivanovic, R. F., Swindles, G. T., Peregon, A. M., and Smith, C. J.: Imminent loss of climate space for permafrost peatlands in Europe and Western Siberia, Nat. Clim. Change, 12, 373-379, https://doi.org/10.1038/s41558-022-01296-7, 2022.

Fiedler, S., Naik, V., O'Connor, F. M., Smith, C. J., Griffiths, P., Kramer, R. J., Takemura, T., Allen, R. J., Im, U., Kasoar, M., Modak, A., Turnock, S., Voulgarakis, A., Watson-Parris, D., Westervelt, D. M., Wilcox, L. J., Zhao, A., Collins, W. J., Schulz, M., Myhre, G., and Forster, P. M.: Interactions between atmospheric composition and climate change – progress in understanding and future opportunities from AerChemMIP, PDRMIP, and RFMIP, Geosci. Model Dev., 17, 2387–2417, https://doi.org/10.5194/gmd-17-2387-2024, 2024.

Field, R. D., van der Werf, G. R., Fanin, T., Fetzer, E. J., Fuller, R., Jethva, H., Levy, R., Livesey, N. J., Luo, M., Torres, O., and Worden, H. M., Indonesian fire activity and smoke pollution in 2015 show persistent nonlinear sensitivity to El Niño-induced drought, PNAS, 113, 9204-9209, https://doi.org/10.1073/pnas.1524888113, 2016.

Fisher, D., Wooster, M. J., Xu, W., Thomas, G., and Lestari, P.: Top-Down Estimation of Particulate Matter Emissions from Extreme Tropical Peatland Fires Using Geostationary Satellite Fire Radiative Power Observations, Sensors, 20, 7075, https://doi.org/10.3390/s20247075, 2020.

Flannigan. M. D., Logan, K. A., Amiro, B. D., Skinner, W. R., and Stocks, B. J.: Future Area Burned in Canada, Climatic Change, 72, 1-16, https://doi.org/10.1007/s10584-005-5935-y, 2005.

Frandsen, W. H.: Ignition probability of organic soils, Can. J. Forest Res., 27, 1471–1477, https://doi.org/10.1139/x97-106, 1997.

Friedlingstein, P., O'Sullivan, M., Jones, M. W., Andrew, R. M., Bakker, D. C. E., Hauck, J., Landschützer, P., Le Quéré, C., Luijkx, I. T., Peters, G. P., Peters, W., Pongratz, J., Schwingshackl, C., Sitch, S., Canadell, J. G., Ciais, P., Jackson, R. B., Alin, S. R., Anthoni, P., Barbero, L., Bates, N. R., Becker, M., Bellouin, N., Decharme, B., Bopp, L., Brasika, I. B. M., Cadule, P., Chamberlain, M. A., Chandra, N., Chau, T.-T.-T., Chevallier, F., Chini, L. P., Cronin, M., Dou, X., Enyo, K., Evans, W., Falk, S., Feely, R. A., Feng, L., Ford, D. J., Gasser, T., Ghattas, J., Gkritzalis, T., Grassi, G., Gregor, L., Gruber, N., Gürses, Ö., Harris, I., Hefner, M., Heinke, J., Houghton, R. A., Hurtt, G. C., Iida, Y., Ilyina, T., Jacobson, A. R., Jain, A., Jarníková, T., Jersild, A., Jiang, F., Jin, Z., Joos, F., Kato, E., Keeling, R. F., Kennedy, D., Klein Goldewijk, K., Knauer, J., Korsbakken, J. I., Körtzinger, A., Lan, X., Lefèvre, N., Li, H., Liu, J., Liu, Z., Ma, L., Marland, G., Mayot, N., McGuire, P. C., McKinley, G. A., Meyer, G., Morgan, E. J., Munro, D. R., Nakaoka, S.-I., Niwa, Y., O'Brien, K. M., Olsen, A., Omar, A. M., Ono, T., Paulsen, M., Pierrot, D., Pocock, K., Poulter, B., Powis, C. M., Rehder, G., Resplandy, L., Robertson, E., Rödenbeck, C., Rosan, T. M., Schwinger, J., Séférian, R., Smallman, T. L., Smith, S. M., Sospedra-Alfonso, R., Sun, Q., Sutton, A. J., Sweeney, C., Takao, S., Tans, P. P., Tian, H., Tilbrook, B., Tsujino, H., Tubiello, F., van der Werf, G. R., van Ooijen, E., Wanninkhof, R., Watanabe, M., Wimart-Rousseau, C., Yang, D., Yang, X., Yuan, W., Yue, X., Zaehle, S., Zeng, J., and Zheng, B.: Global Carbon Budget 2023, Earth Syst. Sci. Data, 15, 5301–5369, https://doi.org/10.5194/essd-15-5301-2023, 2023.

Frieler, K., Lange, S., Piontek, F., Reyer, C. P. O., Schewe, J., Warszawski, L., Zhao, F., Chini, L., Denvil, S., Emanuel, K., Geiger, T., Halladay, K., Hurtt, G., Mengel, M., Murakami, D., Ostberg, S., Popp, A., Riva, R., Stevanovic, M., Suzuki, T., Volkholz, J., Burke, E., Ciais, P., Ebi, K., Eddy, T. D., Elliott, J., Galbraith, E., Gosling, S. N., Hattermann, F., Hickler, T., Hinkel, J., Hof, C., Huber, V., Jägermeyr, J., Krysanova, V., Marcé, R., Müller Schmied, H., Mouratiadou, I., Pierson, D., Tittensor, D. P., Vautard, R., van Vliet, M., Biber, M. F., Betts, R. A., Bodirsky, B. L., Deryng, D., Frolking, S., Jones, C. D., Lotze, H. K., Lotze-Campen, H., Sahajpal, R., Thonicke, K., Tian, H., and Yamagata, Y.: Assessing the impacts of 1.5 °C global warming – simulation protocol of the Inter-Sectoral Impact Model Intercomparison Project (ISIMIP2b), Geosci. Model Dev., 10, 4321–4345, https://doi.org/10.5194/gmd-10-4321-2017, 2017.

Frolking, S., Talbot, J., Jones, M. C., Treat, C. C., Kauffman, J. B., Tuittila, E-S., and Roulet, N.: Peatlands in the Earth's 21st century climate system, Envir. Rev., 19, 371-396, https://doi.org/10.1139/a11-014, 2011.

Frolking, S. and Roulet, N. T.: Holocene radiative forcing impact of northern peatland carbon accumulation and methane emissions, Glob. Change Biol., 13, 1079–1088, https://doi.org/10.1111/j.1365-2486.2007.01339.x, 2007.

Fu, Y., Li, R., Huang, J., Bergeron, Y., Fu, Y., Wang, Y., and Gao, Z.: Satellite-Observed Impacts of Wildfires on Regional Atmosphere Composition and the Shortwave Radiative Forcing: A Multiple Case Study, J. Geophys. Res., 123, 8326-8343, https://doi.org/10.1029/2017JD027927, 2018.

Fuglestvedt, J. S., Berntsen, T. K., Isaksen, I. S. A., Mao, H., Liang, X-Z., and Wang, W-C.: Climatic forcing of nitrogen oxides through changes in tropospheric ozone and methane; global 3D model studies, Atmos. Environ., 33, 961-977, https://doi.org/10.1016/S1352-2310(98)00217-9, 1999.

Fujii, Y., Iriana, W., Oda, M., Puriwigati, A., Tohno, S., Lestari, P., Mizohata, A., and Huboyo, H. S.: Characteristics of carbonaceous aerosols emitted from peatland fire in Riau, Sumatra, Indonesia, Atmos. Enviro., 87, 164-169, https://doi.org/10.1016/j.atmosenv.2014.01.037, 2014.

Gaboriau, D. M., Asselin, H., Ali, A. A., Hély, C., and Girardin, M. P.: Drivers of extreme wildfire years in the 1965–2019 fire regime of the Tłı̨chǫ First Nation territory, Canada, Ecoscience, 29, 249-265, https://doi.org/10.1080/11956860.2022.2070342, 2022.

Gallego-Sala, A. V., and Prentice, I. C.: Blanket peat biome endangered by climate change, Nat. Clim. Change, 3, 152-155, https://doi.org/10.1038/nclimate1672, 2013.

Gallego-Sala, A. V., Charman, D. J., Brewer, S., Page, S. E., Prentice, I. C., Friedlingstein, P., Moreton, S., Amesbury, M. J., Beilman, D. W., Björck, S., Blyakharchuk, T., Bochicchio, C., Booth, R. K., Bunbury, J., Camill, P., Carless, D., Chimner, R. A., Clifford, M., Cressey, E., Courtney-Mustaphi, C., De Vleeschouwer, F., de Jong, R., Fialkiewicz-Koziel, B., Finkelstein, S. A., Garneau, M., Githumbi, E., Hribjlan, J., Holmquist, J., Hughes, P. D. M., Jones, C., Jones, M. C., Karofeld, E., Klein, E. S., Kokfelt, U., Korhola, A., Lacourse, T., Le Roux, G., Lamentowicz, M., Large, D., Lavoie, M., Loisel, J., Mackay, H., MacDonald, G. M., Makila, M., Magnan, G., Marchant, R., Marcisz, K., Martínez Cortizas, A., Massa, C., Mathijssen, P., Mauquoy, D., Mighall, T., Mitchell, F. J. G., Moss, P., Nichols, J., Oksanen, P. O., Orme, L., Packalen, M. S., Robinson, S., Roland, T. P., Sanderson, N. K., Sannel, A. B. K., Silva-Sánchez, N., Steinberg, N., Swindles, G. T., Turner, T. E., Uglow, J., Väliranta, M., van Bellen, S., van der Linden, M., van Geel, B., Wang, G., Yu, Z., Zaragoza-Castells, J., and Zhao, Y.: Latitudinal limits to the predicted increase of the peatland carbon sink with warming, Nature Clim. Change, 8, 907-913, https://doi.org/10.1038/s41558-018-0271-1, 2018.

García-Lázaro, J. R., Moreno-Ruiz, J. A., Riaño, D., and Arbelo, M.: Estimation of Burned Area in the Northeastern Siberian Boreal Forest from a Long-Term Data Record (LTDR) 1982–2015 Time Series, Remote Sens., 10, 940, https://doi.org/10.3390/rs10060940, 2018.

Gibson, C. M., Chasmer, L. E., Thompson, D. K., Quinton, W. L., Flannigan, M. D., and Olefeldt, D.: Wildfire as a major driver of recent permafrost thaw in boreal peatlands, Nature communications, 9, 3041, https://doi.org/10.1038/s41467-018-05457-1, 2018.

Giglio, L., Randerson, J. T., and van der Werf, G. R.: Analysis of daily, monthly, and annual burned area using the fourth-generation global fire emissions database (GFED4), J. Geophys. Res. Biogeosci., 118, 317-328, https://doi.org/10.1002/jgrg.20042, 2013.

Giglio, L., Boschetti, L., Roy, D. P., Humber, M. L., and Justice, C. O.: The Collection 6 MODIS burned area mapping algorithm and product, Remote Sensing of Environment, 217, 72-85, https://doi.org/10.1016/j.rse.2018.08.005, 2018.

Glushkov, I., Zhuravleva, I., McCarty, J. L., Komarova, A., Drozdovsky, A., Drozdovskaya, M., Lupachik, V., Yaroshenko, A., Stehman, S. V., and Prishchepov, A. V.: Spring fires in Russia: results from participatory burned area mapping with Sentinel-2 imagery, Environ. Res. Lett., 16, 125005, https://doi.org/10.1088/1748-9326/ac3287, 2021.

Goa, M., Xing, Z., Vollrath, C., Hugenholtz, C. H., and Barchyn, T. E.: Global observational coverage of onshore oil and gas methane sources with TROPOMI, Sci. Rep., 12, 16759, https://doi.org/10.1038/s41598-023-41914-8, 2023.

Goff, J. A., and Gratch, S.: Low-pressure properties of water from -160 to 212 °F, in Transactions of the American Society of Heating and Ventilating Engineers, pp 95-122, presented at the 52nd annual meeting of the American Society of Heating and Ventilating Engineers, New York, 1946.

Gogoi, M. M., Babu, S. S., Imasu, R., and Hashimoto, M.: Satellite (GOSAT-2 CAI-2) retrieval and surface (ARFINET) observations of aerosol black carbon over India, Atmos. Chem. Phys., 23, 8059–8079, https://doi.org/10.5194/acp-23-8059-2023, 2023.

Goldammer, J. G., Statheropoulos, M., and Andreae, M. O.: Chapter 1 Impacts of Vegetation Fire Emissions on the Environment, Human Health, and Security: A Global Perspective, in: Developments in Environmental Science, edited by: Bytnerowicz, A., Arbaugh, M. J., Riebau, A. R., and Andersen, C., Volume 8, 3-36, https://doi.org/10.1016/S1474-8177(08)00001-6, 2008.

Goldberg, D. L., Anenberg, S. C., Kerr, G. H., Mohegh, A., Lu, Z., and Streets, D. G.: TROPOMI NO2 in the United States: A Detailed Look at the Annual Averages, Weekly Cycles, Effects of Temperature, and Correlation With Surface NO2 Concentrations, Earth's Future, 9, e2020EF001665, https://doi.org/10.1029/2020EF001665, 2021.

Government of Canada: Carbon monoxide: main emission sources, available from: https://www.canada.ca/en/environment-climate-change/services/air-pollution/pollutants/common-contaminants/carbon-monoxide/main-emission-sources.html, last access: 01/08/2024, 2013.

Grace, J., Berninger, F., and Nagy, L.: Impacts of Climate Change on the Tree Line, Ann. Bot., 90, 537-544, https://doi.org/10.1093/aob/mcf222, 2002.

Griffin, D., Zhao, X., McLinden, C. A., Boersma, F., Bourassa, A., Dammers, E., Degenstein, D., Eskes, H., Fehr, L., Fioletov, V., Hayden, K., Kharol, S. K., Li, S.-M., Makar, P., Martin, R. V., Mihele, C., Mittermeier, R. L., Krotkov, N., Sneep, M., Lamsal, L. N., ter Linden, M., van Geffen, J., Veefkind, P., and Wolde, M.: High-resolution mapping of nitrogen dioxide with TROPOMI: First results and validation over the Canadian oil sands, Geophysical Research Letters, 46, 1049–1060, https://doi.org/10.1029/2018GL081095, 2019.

Griffin, D., McLinden, C. A., Dammers, E., Adams, C., Stockwell, C. E., Warneke, C., Bourgeois, I., Peischl, J., Ryerson, T. B., Zarzana, K. J., Rowe, J. P., Volkamer, R., Knote, C., Kille, N., Koenig, T. K., Lee, C. F., Rollins, D., Rickly, P. S., Chen, J., Fehr, L., Bourassa, A., Degenstein, D., Hayden, K., Mihele, C., Wren, S. N., Liggio, J., Akingunola, A., and Makar, P.: Biomass burning nitrogen dioxide emissions derived from space with TROPOMI: methodology and validation, Atmos. Meas. Tech., 14, 7929–7957, https://doi.org/10.5194/amt-14-7929-2021, 2021.

Grillakis, M., Voulgarakis, A., Rovithakis, A., Seiradakis, K. D., Koutroulis, A., Field, R. D., Kasoar, M., Papadopoulos, A., and Lazaridis, M., Climate drivers of global wildfire burned area, Enviro. Res. Lett., 17, 045021, https://doi.org/10.1088/1748-9326/ac5fa1, 2022.

Guimberteau, M., Zhu, D., Maignan, F., Huang, Y., Yue, C., Dantec-Nédélec, S., Ottlé, C., Jornet-Puig, A., Bastos, A., Laurent, P., Goll, D., Bowring, S., Chang, J., Guenet, B., Tifafi, M., Peng, S., Krinner, G., Ducharne, A., Wang, F., Wang, T., Wang, X., Wang, Y., Yin, Z., Lauerwald, R., Joetzjer, E., Qiu, C., Kim, H., and Ciais, P.: ORCHIDEE-MICT (v8.4.1), a land surface model for the high latitudes: model description and validation, Geosci. Model Dev., 11, 121–163, https://doi.org/10.5194/gmd-11-121-2018, 2018.

Haas, O., Prentice, I. C., and Harrison, S. P.: Global environmental controls on wildfire burnt area, size and intensity, Environ. Res. Lett., 17, 065004, https://doi.org/10.1088/1748-9326/ac6a69, 2022.

Hall, J. V., Loboda, T. V., Giglio, L., and McCarty, G. W.: A MODIS-based burned area assessment for Russian croplands: Mapping requirements and challenges, Remot. Sens. Environ., 184, 506-521, https://doi.org/10.1016/j.rse.2016.07.022, 2016.

Hall, R. J., Skakun, R. S., Metsaranta, J. M., Landry, R., Fraser, R. H., Raymond, D., Gartrell, M., Decker, V., and Little, J.: Generating annual estimations of forest fire disturbance in Canada: the

National Burned Area Composite, Int. J. Wildland Fire, 29, 878-891, https://doi.org/10.1071/WF19201, 2020.

Hantson, S., Padilla, M., Corti, D., and Chuvieco, E.: Strengths and weaknesses of MODIS hotspots to characterize global fire occurrence, Remote Sensing of Environment, 131, 152-159, https://doi.org/10.1016/j.rse.2012.12.004, 2013.

Hantson, S., Arneth, A., Harrison, S. P., Kelley, D. I., Prentice, I. C., Rabin, S. S., Archibald, S., Mouillot, F., Arnold, S. R., Artaxo, P., Bachelet, D., Ciais, P., Forrest, M., Friedlingstein, P., Hickler, T., Kaplan, J. O., Kloster, S., Knorr, W., Lasslop, G., Li, F., Mangeon, S., Melton, J. R., Meyn, A., Sitch, S., Spessa, A., van der Werf, G. R., Voulgarakis, A., and Yue, C.: The status and challenge of global fire modelling, Biogeosciences, 13, 3359–3375, https://doi.org/10.5194/bg-13-3359-2016, 2016.

Hantson, S., Kelley, D. I., Arneth, A., Harrison, S. P., Archibald, S., Bachelet, D., Forrest, M., Hickler, T., Lasslop, G., Li, F., Mangeon, S., Melton, J. R., Nieradzik, L., Rabin, S. S., Prentice, I. C., Sheehan, T., Sitch, S., Teckentrup, L., Voulgarakis, A., and Yue, C.: Quantitative assessment of fire and vegetation properties in simulations with fire-enabled vegetation models from the Fire Model Intercomparison Project, Geosci. Model Dev., 13, 3299– 3318, https://doi.org/10.5194/gmd-13-3299-2020, 2020.

Hao, W. M., Petkov, A., Nordgren, B. L., Corley, R. E., Silverstein, R. P., Urbanski, S. P., Evangeliou, N., Balkanski, Y., and Kinder, B. L.: Daily black carbon emissions from fires in northern Eurasia for 2002–2015, Geosci. Model Dev., 9, 4461–4474, https://doi.org/10.5194/gmd-9-4461-2016, 2016.

Hardy, C. C., Ottmar, R. D., Peterson, J. L., Core, J. E., and Seamon, P. (Eds): Smoke Management Guide for Prescribed and Wildland Fire 2001 Edition, National Wildfire Coordinating Group, available from: https://www.fs.usda.gov/pnw/pubs/journals/pnw_2001_ottmar001.pdf, last access: 01/08/2024, 2001.

Harsch, M. A., Hulme, P. E., McGlone, M. S., and Duncan, R. P.: Are treelines advancing? A global meta-analysis of treeline response to climate warming, Ecol. Lett., 12, 1040-1049, https://doi.org/10.1111/j.1461-0248.2009.01355.x, 2009.

Harvey, B. J., Cook, P., Shaffrey, L. C., and Schiemann, R.: The Response of the Northern Hemisphere Storm Tracks and Jet Streams to Climate Change in the CMIP3, CMIP5, and CMIP6 Climate Models, J. Geophys. Res.: Atmos., 125, e2020JD032701, https://doi.org/10.1029/2020JD032701, 2020.

Heil, A. and Goldammer, J.: Smoke-haze pollution: a review of the 1997 episode in Southeast Asia, Reg. Environ. Change, 2, 24–37, https://doi.org/10.1007/S101130100021, 2001.

Helbig, M., Waddington, J. M., Alekseychik, P., Amiro, B. D., Aurela, M., Barr, A. G., Black, T. A., Blanken, P. D., Carey, S. K., Chen, J., Chi, J., Desai, A. R., Dunn, A., Euskirchen, E. S., Flanagan, L. B., Forbrich, I., Friborg, T., Grelle, A., Harder, S., Heliasz, M., Humphreys, E. R., Ikawa, H., Isabelle, P.-E., Iwata, H., Jassal, R., Korkiakoski, M., Kurbatova, J., Kutzbach, L., Lindroth, A., Löfvenius, M. O., Lohila, A., Mammarella, I., Marsh, P., Maximov, T., Melton, J. R., Moore, P. A., Nadeau, D. F., Nicholls, E. M., Nilsson, M. B., Ohta, T., Peichl, M., Petrone, R. M., Petrov, R., Prokushkin, A., Quinton, W. L., Reed, D. E., Roulet, N. T., Runkle, B. R. K., Sonnentag, O., Strachan, I. B., Taillardat, P., Tuittila, E.-S., Tuovinen, J.-P., Turner, J., Ueyama, M., Varlagin, A., Wilmking, M., Wofsy, S. C., and Zyrianov, V.: Increasing contribution of peatlands to boreal evapotranspiration in a warming climate, Nat. Clim. Change, 10, 555-560, https://doi.org/10.1038/s41558-020-0763-7, 2020.

Hessilt, T. D., Abatzoglou, J. T., Chen, Y., Randerson, J. T., Scholten, R. C., van der Werf, G., and Veraverbeke, S.: Future increases in lightning ignition efficiency and wildfire occurrence expected from drier fuels in boreal forest ecosystems of western North America, Enviro. Res. Lett., 17, 054008, https://doi.org/10.1088/1748-9326/ac6311, 2022.

Hessilt, T. D., Rogers, B. M., Scholten, R. C., Potter, S., Janssen, T. A. J., and Veraverbeke, S.: Geographically divergent trends in snow disappearance timing and fire ignitions across boreal North America, Biogeosciences, 21, 109–129, https://doi.org/10.5194/bg-21-109-2024, 2024.

Hirano, T., Segah, H., Harada, T., Limin, S., June, T., Hirata, R., and Osaki, M. Carbon dioxide balance of a tropical peat swamp forest in Kalimantan, Indonesia, Glob. Change Bio., 13, 412-425, https://doi.org/10.1111/j.1365-2486.2006.01301.x, 2006.

Hokanson, K. J, Lukenbach, M. C, Devito, K. J., Kettridge, N, Petrone, R. M., and Waddington, J. M.: Groundwater connectivity controls peat burn severity in the boreal plains, Ecohydrol., 9, 574–584, https://doi.org/10.1002/eco.1657, 2016.

Holden, J., Shotbolt, L., Bonn, A., Burt, T. P., Chapman, P. J., Dougill, A. J., Fraser, E. D. G., Hubacek, K., Irvine, B., Kirkby, M. J., Reed, M. S., Prell, C., Stagl, S., Stringer, L. C., Turner, A., and Worrall, F.: Environmental change in moorland landscapes, Earth-Sci. Rev., 82, 75-100, https://doi.org/10.1016/j.earscirev.2007.01.003, 2007.

Holden, Z. A., Swanson, A., Luce, C. H., Jolly, W. M., Maneta, M., Oyler, J. W., Warren, D. A., Parsons, R., and Affleck, D.: Decreasing fire season precipitation increased recent western US forest wildfire activity, PNAS, 11, E8349-E8357, https://doi.org/10.1073/pnas.1802316115, 2018.

Holloway, J. E., Lewkowicz, A. G., Douglas, T. A., Li, X., Turetsky, M. R., Baltzer, J. L., and Jin, H. Impact of wildfire on permafrost landscapes: A review of recent advances and future prospects, Permafr. Periglac. Process., 31, 371-382, https://doi.org/10.1002/ppp.2048, 2020.

Horton, D. E., Johnson, N. C., Singh, D., Swain, D. L., Rajaratnam, B., and Diffenbaugh, N. S.: Contribution of changes in atmospheric circulation patterns to extreme temperature trends, Nature, 522, 465-469, https://doi.org/10.1038/nature14550, 2015.

Hu, F.S., Higuera, P.E., Duffy, P., Chipman, M.L., Rocha, A.V., Young, A.M., Kelly, R. and Dietze, M.C.: Arctic tundra fires: natural variability and responses to climate change, Front. Ecol. Environ., 13, 369-377, https://doi.org/10.1890/150063, 2015.

Hu, Y., Fernandez-Anez, N., and Smith, T. E. L., and Rein, G.: Review of emissions from smouldering peat fires and their contribution to regional haze episodes, Int. J. Wildland Fire, 27, 293–312, https://doi.org/10.1071/WF17084, 2018.

Hu, Y., Christensen, E., Restuccia, F., and Rein, G.: Transient gas and particle emissions from smouldering combustion of peat, P. Combust. Inst., 37, 4035–4042, https://doi.org/10.1016/j.proci.2018.06.008, 2019a.

Hu, Y., Christensen, E. G., Amin, H. M. F., Smith, T. E. L., and Rein, G.: Experimental study of moisture content effects on the transient gas and particle emissions from peat fires, Combust. Flame, 209, 408–417, https://doi.org/10.1016/j.combustflame.2019.07.046, 2019b.

Hu, Y., and Rein, G.: Development of gas signatures of smouldering peat wildfire from emission factors, Int. J. Wildland Fire, 31, 1014-1032, https://doi.org/10.1071/WF21093, 2022.

Huang, S., Siegert, F., Goldammer, J. G., and Sukhinin, A. I.: Satellite-derived 2003 wildfires in southern Siberia and their potential influence on carbon sequestration, Int. J. Remote Sens., 30, 1479–1492, https://doi.org/10.1080/01431160802541549, 2009.

Huang, X. and Rein, G.: Downward spread of smouldering peat fire: the role of moisture, density, and oxygen supply, Int. J. Wildland Fire, 26, 907–918, https://doi.org/10.1071/WF16198, 2017.

Huang, X. and Rein, G.: Upward-and-downward spread of smouldering peat fire, P. Combust. Inst., 37, 4025–4033, https://doi.org/10.1016/j.proci.2018.05.125, 2019.

Huang, Y., Ciais, P., Luo, Y., Zhu, D., Wang, Y., Qiu, C., Goll, D. S., Guenet, B., Makowski, D., De Graaf, I., Leifeld, J., Kwon, M. J., Hu, J., and Qu, L.: Tradeoff of CO2 and CH4 emissions from global peatlands under water-table drawdown, Nat. Clim. Change, 11, 618-622, https://doi.org/10.1038/s41558-021-01059-w, 2021.

Hugelius, G., Strauss, J., Zubrzycki, S., Harden, J. W., Schuur, E. A. G., Ping, C.-L., Schirrmeister, L., Grosse, G., Michaelson, G. J., Koven, C. D., O'Donnell, J. A., Elberling, B., Mishra, U., Camill, P., Yu, Z., Palmtag, J., and Kuhry, P.: Estimated stocks of circumpolar permafrost carbon with quantified

uncertainty ranges and identified data gaps, Biogeosciences, 11, 6573–6593, https://doi.org/10.5194/bg-11-6573-2014, 2014.

Hugelius, G., Loisel, J., Chadburn, S., Jackson, R. B., Jones, M., MacDonald, G., Marushchak, M., Olefeldt, D., Packalen, M., Siewert, M. B., Treat, C., Turetsky, M. R., Voigt, C., and Yu, Z.: Large stocks of peatland carbon and nitrogen are vulnerable to permafrost thaw, P. Natl. Acad. Sci. USA, 117, 20438–20446, https://doi.org/10.1073/pnas.1916387117, 2020a.

Hugelius, G., Loisel, J., Chadburn, S., Jackson, R. B., Jones, M., MacDonald, G., Marushchak, M., Olefeldt, D., Packalen, M., Siewert, M. B., Treat, C., Turetsky, M. R., Voigt, C., and Yu, Z.: Maps of northern peatland extent, depth, carbon storage and nitrogen storage, Dataset version 2, Bolin Centre Database [data set], https://doi.org/10.17043/hugelius-2020-peatland-2, 2020b.

Hung, W-T., Baker, B., Campbell, P., Tang, Y., and Jeong, G-R.: Estimations of CO and NO2 Emissions and the Fire Combustion Efficiency for Fire Activities over CONUS Using TROPOspheric Monitoring Instrument (TROPOMI) Measurements, MDPI Proceedings [preprint], 69, in review, 2022.

Hurtt, G., Chini, L. P., Frolking, S., Betts, R. A., Feddema, J., Fischer, G., Fisk, G., Hibbard, K., Houghton, R. A., Janetos, A., Jones, C. D., Kinderman, G., Kinoshita, T., Goldewijk, K. K., Riahi, K., Shevliakova, E., Smith, S., Stehfest, E., Thomson, A., Thornton, P., van Vuuren, D. P., and Wang, Y. P.: Harmonization of land-use scenarios for the period 1500–2100: 600 years of global gridded annual land-use transitions, wood harvest, and resulting secondary lands, Climate Change, 109, 117–161, https://doi.org/10.1007/s10584-011-0153-2, 2011.

Ialongo, I., Virta, H., Eskes, H., Hovila, J., and Douros, J.: Comparison of TROPOMI/Sentinel-5 Precursor NO2 observations with ground-based measurements in Helsinki, Atmos. Meas. Tech., 13, 205–218, https://doi.org/10.5194/amt-13-205-2020, 2020.

Ingram, R. C., Moore, P. A., Wilkinson, S., Petrone, R. M., and Waddington, J. M. Postfire Soil Carbon Accumulation Does Not Recover Boreal Peatland Combustion Loss in Some Hydrogeological Settings, J. Geophys. Res.: Biogeosci., 124, 775-788, https://doi.org/10.1029/2018JG004716, 2019.

Innes, R. J.: Fire regimes of Alaskan wet and mesic herbaceous systems. In: Fire Effects Information System, U.S. Department of Agriculture, Forest Service, Rocky Mountain Research Station, Missoula Fire Sciences Laboratory, available: www.fs.usda.gov/database/feis/fire_regimes/AK_wet_herbaceous/all.html, last access: 31/07/2024, 2015.

Inness, A., Ades, M., Agustí-Panareda, A., Barré, J., Benedictow, A., Blechschmidt, A.-M., Dominguez, J. J., Engelen, R., Eskes, H., Flemming, J., Huijnen, V., Jones, L., Kipling, Z., Massart,

S., Parrington, M., Peuch, V.-H., Razinger, M., Remy, S., Schulz, M., and Suttie, M.: The CAMS reanalysis of atmospheric composition, Atmos. Chem. Phys., 19, 3515–3556, https://doi.org/10.5194/acp-19-3515-2019, 2019.

IPCC, Climate Change 2013: The Physical Science Basis. Contribution of Working Group I to the Fifth Assessment Report of the Intergovernmental Panel on Climate Change, Cambridge University Press, Cambridge, United Kingdom and New York, NY, USA, available from: https://www.ipcc.ch/report/ar5/wg1/, last access: 29/07/2024, 2013.

Irannezhad, M., Liu, J., Ahmadi, B., and Chen, D. The dangers of Arctic zombie wildfires, Science, 369, 1171, https://doi.org/10.1126/science.abe1739, 2020.

Ise, T., Dunn, A. L., Wofsy, S. C., and Moorcroft, P. R.: High sensitivity of peat decomposition to climate change through water table feedback, Nat. Geoscience, 763-766, https://doi.org/10.1038/ngeo331, 2008.

ISIMIP Coordination Team, Sectoral Coordinators & Scientific Advisory Board, The Inter-sectoral Impact Model Intercomparison Project (ISIMIP): Mission and Implementation Document, 2018. Accessed: 25/03/24, available from: https://www.isimip.org/documents/355/MissionAndImplementation_12Sep2018.pdf

ISIMIP, ISIMIP2a Simulation protocol (extended version), available from: https://www.isimip.org/documents/647/ISIMIP2a_protocol_230302.pdf, last access: 30/07/2024, 2023.

ISIMIP, ISIMIP2b Simulation Protocol, available from: https://www.isimip.org/documents/564/ISIMIP2b_protocol_210131_noEnergy_IV_JS-1_IV_pmp-1.pdf, last access: 30/07/2024, 2021.

ISIMIP, ISIMIP3a simulation protocol, available from: https://protocol.isimip.org/#/ISIMIP3a/, last access: 30/07/2024, 2024.

ISIMIP, ISIMIP3b simulation protocol, available from: https://protocol.isimip.org/#/ISIMIP3b/, last access: 30/07/2024, 2024.

Ito, A., Nishina, K., and Noda, H. M.: Impacts of future climate change on the carbon budget of northern high-latitude terrestrial ecosystems: An analysis using ISI-MIP data, Polar Sci., 10, 346-355, https://doi.org/10.1016/j.polar.2015.11.002, 2016.

Jain, P., Castellanos-Acuna, D., Coogan, S. C. P., Abatzoglou, J. T., and Flannigan, M. D.: Observed increases in extreme fire weather driven by atmospheric humidity and temperature, Nature Clim. Change, 12, 63-70, https://doi.org/10.1038/s41558-021-01224-1, 2022.

Jeong, J. I., Park, R. J., and Youn, D.: Effects of Siberian forest fires on air quality in East Asia during May 2003, and its climate implication, Atmos. Environ., 42, 8910-8922, https://doi.org/10.1016/j.atmosenv.2008.08.037, 2008.

Jia, G., Shevliakova, E., Artaxo, P., De Noblet-Ducoudré, N., Houghton, R., House, J., Kitajima, K., Lennard, C., Popp, A., Sirin. A., Sukumar, R., and Verchot, L.: Land–climate interactions. In: Climate Change and Land: an IPCC special report on climate change, desertification, land degradation, sustainable land management, food security, and greenhouse gas fluxes in terrestrial ecosystem, edited by: Shukla, P.R., Skea, J., Calvo Buendia, E., Masson-Delmotte, V., Pörtner, H.-O., Roberts, D.C., Zhai, P., Slade, R., Connors, S., van Diemen, R., Ferrat, M., Haughey, E., Luz, S., Neogi, S., Pathak, M., Petzold, J., Portugal Pereira, J., Vyas, P., Huntley, E., Kissick, K., Belkacemi, M., and Malley, J., Cambridge University Press, 131-257, 2019.

Jiang, Y., Yang, X.-Q., Liu, X., Qian, Y., Zhang, K., Wang, M., Li, F., Wang, Y., and Lu, Z.: Impacts of Wildfire Aerosols on Global Energy Budget and Climate: The Role of Climate Feedbacks, J. Climate, 33, 3351-3366, https://doi.org/10.1175/JCLI-D-19-0572.1, 2020.

Jones, B. M., Grosse, G., Arp, C. D., Miller, E., Liu, L., Hayes, D. J., and Larsen, C. F. Recent Arctic tundra fire initiates widespread thermokarst development, Sci. Rep., 5, 15865, https://doi.org/10.1038/srep15865, 2015.

Jones, M. W., Abatzoglou, J. T., Veraverbeke, S., Andela, N., Lasslop, G., Forkel, M., Smith, A. J. P., Burton, C., Betts, R. A., van der Werf, G. R., Sitch, S., Canadell, J. G., Santín, C., Kolden, C., Doerr, S. H., and Le Quéré, C.: Global and Regional Trends and Drivers of Fire Under Climate Change, Rev. Geophys., 60, e2020RG000726, https://doi.org/10.1029/2020RG000726, 2022.

JULES collaboration: JULES code, Met Office Science Repository Service [code], https://code.metoffice.gov.uk/trac/jules, last access: 12 October 2023.

Kaiser, J. W., Heil, A., Andreae, M. O., Benedetti, A., Chubarova, N., Jones, L., Morcrette, J.-J., Razinger, M., Schultz, M. G., Suttie, M., and van der Werf, G. R.: Biomass burning emissions estimated with a global fire assimilation system based on observed fire radiative power, Biogeosciences, 9, 527–554, https://doi.org/10.5194/bg-9-527-2012, 2012.

Kajii, Y., Kato, S., Streets, D. G., Tsai, N.Y., Shvidenko, A., Nilsson, S., McCallum, I., Minko, N. P., Abushenko, N., Altyntsev, D., and Khodzer, T. V.: Boreal forest fires in Siberia in 1998: Estimation of area burned and emissions of pollutants by advanced very high resolution radiometer satellite data, J. Geophys. Res.-Atmos., 174, 4745, https://doi.org/10.1029/2001JD001078, 2002.

Kantzas, E., Lomas, M., and Quegan, S.: Fire at high latitudes: Data-model comparisons and their consequences, Global Biogeochem. Cy., 27, 677-691, https://doi.org/10.1002/gbc.20059, 2013.

Kaplan, J. O. and Lau, K. H-K.: The WWLLN Global Lightning Climatology and timeseries (WGLC) v2022.0.0, Zenodo [data set], https://doi.org/10.5281/zenodo.6007052, 2021.

Kaplan, J. O., Koch, A., and Lau, K. H.-K.: Estimated future global lightning strokes (2010-2100) v1.0.0., zenodo [dataset], https://doi.org/10.5281/zenodo.7511843, 2023.

Kasischke, E. S., Verbyla, D. L., Rupp, T. S., McGuire, A. D., Murphy, K. A., Jandt, R., Barnes, J. L., Hoy, E. E., Duffy, P. A., Calef, M., and Turetsky, M. R.: Alaska's changing fire regime — implications for the vulnerability of its boreal forests, Can. J. Forest Res., 40, 1313-1324, https://doi.org/10.1139/X10-098, 2010.

Keller, T., and Hakansson, I. Estimation of reference bulk density from soil particle size distribution and soil organic matter content, Geoderma, 154, 398-406, https://doi.org/10.1016/j.geoderma.2009.11.013, 2010.

Kelly, T. J., Baird, A. J., Roucoux, K. H., Baker, T. R., Honorio Coronado, E. N., Rios, M., and Lawson, I. T.: The high hydraulic conductivity of three wooded tropical peat swamps in northeast Peru: measurements and implications for hydrological function, Hydrol. Process., 28, 3373-3387, https://doi.org/10.1002/hyp.9884, 2014.

Kettridge, N., Turetsky, M. R., Sherwood, J. H., Thompson, D. K., Miller, C. A., Benscoter, B. W., Flannigan, M. D., Wotton, B. M., and Waddington, J. M.: Moderate drop in water table increases peatland vulnerability to post-fire regime shift, Sci. Rep.-UK, 5, 8063, https://doi.org/10.1038/srep08063, 2015.

Kettridge, N., Lukenbach, M. C., Hokanson, K. J., Devito, K. J., Petrone, R. M., Mendoza, C. A., and Waddington, J. M.: Severe wildfire exposes remnant peat carbon stocks to increased post-fire drying, Sci. Rep.-UK, 9, 3727, https://doi.org/10.1038/s41598-019-40033-7, 2019.

Kharuk, V. I., Ranson, K. J., Dvinskaya, M. L., and Im, S. T. Wildfires in northern Siberian larch dominated communities, Environ. Res. Lett., 6, 045208, http://dx.doi.org/10.1088/1748-9326/6/4/045208, 2011.

Kharuk, V. I., Ponomarev, E. I., Ivanova, G. A., Dvinskaya, M. L., Coogan, S. C. P., and Flannigan, M. D.: Wildfires in the Siberian taiga, Ambio, 50, 1953-1974, https://doi.org/10.1007/s13280-020-01490-x, 2021.

Kim, H. C., Lee, P., Judd, L., Pan, L., and Lefer, B.: OMI NO2 column densities over North American urban cities: the effect of satellite footprint resolution, Geosci. Model Dev., 9, 1111–1123, https://doi.org/10.5194/gmd-9-1111-2016, 2016.

Kirchmeier-Young, M. C., Gillett, N. P., Zwiers, F. W., Cannon, A. J., and Anslow, F. S.: Attribution of the Influence of Human-Induced Climate Change on an Extreme Fire Season, Earth's Future, 7, 2-10, https://doi.org/10.1029/2018EF001050, 2019.

Kirillina, K., Shvetsov, E. G., Protopopova, V. V., Thiesmeyer, L., and Yan, W.: Consideration of anthropogenic factors in boreal forest fire regime changes during rapid socio-economic development: case study of forestry districts with increasing burnt area in the Sakha Republic, Russia, Environ. Res. Lett., 15, 035009, https://doi.org/10.1088/1748-9326/ab6c6e, 2020.

Kloster, S., and Lasslop, G.: Historical and future fire occurrence (1850 to 2100) simulated in CMIP5 Earth System Models, Global and Planet. Change, 150, 58-69, https://doi.org/10.1016/j.gloplacha.2016.12.017, 2017.

Knorr, W., Kaminski, T., Arneth, A., and Weber, U.: Impact of human population density on fire frequency at the global scale, Biogeosciences, 11, 1085–1102, https://doi.org/10.5194/bg-11-1085-2014, 2014.

Knorr, W., Jiang, L., and Arneth, A.: Climate, CO2 and human population impacts on global wildfire emissions, Biogeosciences, 13, 267–282, https://doi.org/10.5194/bg-13-267-2016, 2016a.

Knorr, W., Jiang, L., and Arneth, A.: Demographic controls of future global fire risk, Nature Clim. Change, 6, 781-785, https://doi.org/10.1038/nclimate2999, 2016b.

Kochtubajda, B., Stewart, R. E., Flannigan, M. D., Bonsal, B. R., Cuell, C., and Mooney, C. J.: An Assessment of Surface and Atmospheric Conditions Associated with the Extreme 2014 Wildfire Season in Canada's Northwest Territories, Atmos.-Ocean, 57, 73-90, https://doi.org/10.1080/07055900.2019.1576023, 2019.

Koenigk, T., Berg, P., and Doscher, R.: Arctic climate change in an ensemble of regional CORDEX simulations, Polar Res., 34, 24603, http://dx.doi.org/10.3402/polar.v34.24603, 2015.

Koenigk, T., Key, J., and Vihma, T.: Climate Change in the Arctic. In: Physics and Chemistry of the Arctic Atmosphere, edited by: Kokhanovsky, A., and Tomasi, C., Springer Polar Sciences, Springer, https://doi.org/10.1007/978-3-030-33566-3_11, 2020.

Kohlenberg, A. J., Turetsky, M. R., Thompson, D. K., Branfireun, B. A., and Mitchell, C. P. J. Controls on boreal peat combustion and resulting emissions of carbon and mercury, Environ. Res. Lett., 13, 035005, https://doi.org/10.1088/1748-9326/aa9ea8, 2018.

Kolmonen, P., Sogacheva, L., Virtanen, T. H., de Leeuw, G., and Kulmala, M.: The ADV/ASV AATSR aerosol retrieval algorithm: current status and presentation of a full-mission AOD dataset, Int. J. Digit. Earth, 9, 545-561, https://doi.org/10.1080/17538947.2015.1111450, 2016.

Kondo, Y., Matsui, H., Moteki, N., Sahu, L., Takegawa, N., Kajino, M., Zhao, Y., Cubison, M. J., Jimenez, J. L., Vay, S., Diskin, G. S., Andersen, B., Wisthaler, A., Mikoviny, T., Fuelberg, H. E., Blake, D. R., Huey, G., Weinheimer, A. J., Knapp, D. J., and Brune, W. H.: Emissions of black carbon, organic, and inorganic aerosols from biomass burning in North America and Asia in 2008, J. Geophys. Res. Atmos., 116, D08204, https://doi.org/10.1029/2010JD015152, 2011.

Konovalov, I. B., Beekmann, M., Kuznetsova, I. N., Yurova, A., and Zvyagintsev, A. M.: Atmospheric impacts of the 2010 Russian wildfires: integrating modelling and measurements of an extreme air pollution episode in the Moscow region, Atmos. Chem. Phys., 11, 10031–10056, https://doi.org/10.5194/acp-11-10031-2011, 2011.

Konovalov, I. B., Berezin, E. V., Ciais, P., Broquet, G., Beekmann, M., Hadji-Lazaro, J., Clerbaux, C., Andreae, M. O., Kaiser, J. W., and Schulze, E.-D.: Constraining CO2 emissions from open biomass burning by satellite observations of co-emitted species: a method and its application to wildfires in Siberia, Atmos. Chem. Phys., 14, 10383–10410, https://doi.org/10.5194/acp-14-10383-2014, 2014.

Konovalov, I. B., Golovushkin, N. A., Beekmann, M., and Turquety, S.: Using Multi-Platform Satellite Observations to Study the Atmospheric Evolution of Brown Carbon in Siberian Biomass Burning Plumes, Remote Sens., 14, 2625, https://doi.org/10.3390/rs14112625, 2022.

Kopacz, M., Breeze, V., Kondragunta, S., Frost, G., Anenberg, S., Bruhwiler, L., Davis, S., da Silva, A., de Gouw, J., Duren, R., Flynn, L., Gaudel, A., Geigert, M., Goldman, G., Joiner, J., McDonald, B., Ott, L., Peuch, V.-H., Pusede, S. E., Stajner, I., Seftor, C., Sweeney, C., Valin, L. C., Wang, J., Whetstone, J., and Kalluri, S.: Global Atmospheric Composition Needs from Future Ultraviolet–Visible–Near-Infrared (UV–Vis–NIR) NOAA Satellite Instruments, Bull. Amer. Meteor. Soc., 104, E623–E630, https://doi.org/10.1175/BAMS-D-22-0266.1, 2023.

Koplitz, S. N., Mickley, L. J., Marlier, M. E., Buonocore, J. J., Kim, P. S., Liu, T., Sulprizio, M. P., DeFries, R. S., Jacob, D. J., Schwartz, J., Pongsiri, M., and Myers, S. S. Public health impacts of the severe haze in Equatorial Asia in September–October 2015: demonstration of a new framework for informing fire management strategies to reduce downwind smoke exposure, Environ. Res. Lett., 11, 094023, https://doi.org/10.1088/1748-9326/11/9/094023, 2016.

Koster, E., Koster, K., Berninger, F., Prokushkin, A., Aaltonen, H., Zhou, X., and Pumpanen, J.: Changes in fluxes of carbon dioxide and methane caused by fire in Siberian boreal forest with continuous permafrost, Journal of Environmental Management, 228, 405-415, https://doi.org/10.1016/j.jenvman.2018.09.051, 2018.

Krause, A., Kloster, S., Wilkenskjeld, S., and Paeth, H. The sensitivity of global wildfires to simulated past, present, and future lightning frequency, J. Geophys. Res.: Biogeosci., 119, 312-322, https://doi.org/10.1002/2013JG002502, 2014.

Kuhn-Régnier, A., Voulgarakis, A., Nowack, P., Forkel, M., Prentice, I. C., and Harrison, S. P.: The importance of antecedent vegetation and drought conditions as global drivers of burnt area, Biogeosciences, 18, 3861–3879, https://doi.org/10.5194/bg-18-3861-2021, 2021.

Kuze, A., Suto, H., Nakajima, M., and Hamazaki, T.: Thermal and near infrared sensor for carbon observation Fourier-transform spectrometer on the Greenhouse Gases Observing Satellite for greenhouse gases monitoring, App. Opt., 48, 671606733, https://doi.org/10.1364/AO.48.006716, 2009.

Lahteenoja, O., Flores, B., and Nelson, B.: Tropical Peat Accumulation in Central Amazonia. Wetlands 33, 495–503, https://doi.org/10.1007/s13157-013-0406-0, 2013.

Lama, S., Houweling, S., Boersma, K. F., Eskes, H., Aben, I., Denier van der Gon, H. A. C., Krol, M. C., Dolman, H., Borsdorff, T., and Lorente, A.: Quantifying burning efficiency in megacities using the NO2/CO ratio from the Tropospheric Monitoring Instrument (TROPOMI), Atmos. Chem. Phys., 20, 10295–10310, https://doi.org/10.5194/acp-20-10295-2020, 2020.

Lamsal, L. N., Martin, R. V., van Donkelaar, A., Steinbacher, M., Celarier, E. A., Bucsela, E., Dunlea, E. J., and Pinto, J. P.: Ground-level nitrogen dioxide concentrations inferred from the satellite-borne Ozone Monitoring Instrument, J. Geophys. Res., 113, D16308, https://doi.org/10.1029/2007JD009235, 2008.

Landgraf, J., aan de Brugh, J., Scheepmaker, R., Borsdorff, T., Hu, H., Houweling, S., Butz, A., Aben, I., and Hasekamp, O.: Carbon monoxide total column retrievals from TROPOMI shortwave infrared measurements, Atmos. Meas. Tech., 9, 4955–4975, https://doi.org/10.5194/amt-9-4955-2016, 2016.

Landgraf, J., Borsdorff, T., Langerock, B., and Keppens, A.: S5P Mission Performance Centre Carbon Monoxide [L2__CO____] Readme, available from: https://sentinel.esa.int/documents/247904/3541451/Sentinel-5P-Carbon-Monoxide-Level-2-Product-Readme-File, last access: 31/07/2024, 2023.

Lange, S.: ISIMIP3b bias adjustment fact sheet. Potsdam: Inter-Sectoral Impact Model Intercomparison Project, available from: https://www.isimip.org/documents/413/ISIMIP3b_bias_adjustment_fact_sheet_Gnsz7CO.pdf, last access: 30/07/2024, 2021.

Langmann, B., Duncan, B., Textor, C., Trentmann, J., and van der Werf, G. R.: Vegetation fire emissions and their impact on air pollution and climate, Atmos. Environ., 43, 107-116, https://doi.org/10.1016/j.atmosenv.2008.09.047, 2009.

Langner, A. and Siegert, F.: Spatiotemporal fire occurrence in Borneo over a period of 10 years, Glob. Change Biol., 15, 48–62, https://doi.org/10.1111/j.1365-2486.2008.01828.x, 2009.

Lasslop, G., Coppola, A. I., Voulgarakis, A., Yue, C., and Vereverbeke, S.: Influence of Fire on the Carbon Cycle and Climate, Curr. Clim. Change Rep., 5, 112–123, https://doi.org/10.1007/s40641-019-00128-9, 2019.

Laurent, P., Mouillot, F., Moreno, M. V., Yue, C., and Ciais, P.: Varying relationships between fire radiative power and fire size at a global scale, Biogeosciences, 16, 275–288, https://doi.org/10.5194/bg-16-275-2019, 2019.

Lavoue, D., and Stocks, B. J. Emissions of air pollutants by Canadian wildfires from 2000 to 2004, Int. J. wildland Fire, 20, 17-34, https://doi.org/10.1071/WF08114, 2011.

Lelieveld, J., Evans, J. S., Fnais, M., Giannadaki, D., and Pozzer, A.: The contribution of outdoor air pollution sources to premature mortality on a global scale, Nature, 525, 367-371, https://doi.org/10.1038/nature15371, 2015.

Lelieveld, J., Gromov, S., Pozzer, A., and Taraborrelli, D.: Global tropospheric hydroxyl distribution, budget and reactivity, Atmos. Chem. Phys., 16, 12477–12493, https://doi.org/10.5194/acp-16-12477-2016, 2016.

Leniham, J. M., Daly, C., Bachelet, D., and Neilson, R. P.: Simulating broad-scale fire severity in a dynamic global vegetation model, Northwest Sci., 72, 91-101, 1998.

Le Quéré, C., Andrew, R. M., Friedlingstein, P., Sitch, S., Hauck, J., Pongratz, J., Pickers, P. A., Korsbakken, J. I., Peters, G. P., Canadell, J. G., Arneth, A., Arora, V. K., Barbero, L., Bastos, A., Bopp, L., Chevallier, F., Chini, L. P., Ciais, P., Doney, S. C., Gkritzalis, T., Goll, D. S., Harris, I., Haverd, V., Hoffman, F. M., Hoppema, M., Houghton, R. A., Hurtt, G., Ilyina, T., Jain, A. K., Johannessen, T., Jones, C. D., Kato, E., Keeling, R. F., Goldewijk, K. K., Landschützer, P., Lefèvre, N., Lienert, S., Liu, Z., Lombardozzi, D., Metzl, N., Munro, D. R., Nabel, J. E. M. S., Nakaoka, S., Neill, C., Olsen, A., Ono, T., Patra, P., Peregon, A., Peters, W., Peylin, P., Pfeil, B., Pierrot, D., Poulter, B., Rehder, G., Resplandy, L., Robertson, E., Rocher, M., Rödenbeck, C., Schuster, U., Schwinger, J., Séférian, R., Skjelvan, I., Steinhoff, T., Sutton, A., Tans, P. P., Tian, H., Tilbrook, B., Tubiello, F. N., van der Laan-Luijkx, I. T., van der Werf, G. R., Viovy, N., Walker, A. P., Wiltshire, A. J., Wright, R., Zaehle, S., and Zheng, B.: Global Carbon Budget 2018, Earth Syst. Sci. Data, 10, 2141–2194, https://doi.org/10.5194/essd-10-2141-2018, 2018.

Levelt, P. F., van den Oord, G. H. J., Dobber, M. R., Malkki, A., Visser, H., de Vries, J., Stammes, P., Lundell, J. O.V., and Saari, H.: The ozone monitoring instrument, IEEE Trans. Geosci. Remote Sens., 44, 1093-1101, https://doi.org/10.1109/TGRS.2006.872333, 2006.

Levy, R. C., Mattoo, S., Munchak, L. A., Remer, L. A., Sayer, A. M., Patadia, F., and Hsu, N. C.: The Collection 6 MODIS aerosol products over land and ocean, Atmos. Meas. Tech., 6, 2989–3034, https://doi.org/10.5194/amt-6-2989-2013, 2013.

Li, F., Levis, S., and Ward, D. S.: Quantifying the role of fire in the Earth system – Part 1: Improved global fire modeling in the Community Earth System Model (CESM1), Biogeosciences, 10, 2293–2314, https://doi.org/10.5194/bg-10-2293-2013, 2013.

Li, F., Val Martin, M., Andreae, M. O., Arneth, A., Hantson, S., Kaiser, J. W., Lasslop, G., Yue, C., Bachelet, D., Forrest, M., Kluzek, E., Liu, X., Mangeon, S., Melton, J. R., Ward, D. S., Darmenov, A., Hickler, T., Ichoku, C., Magi, B. I., Sitch, S., van der Werf, G. R., Wiedinmyer, C., and Rabin, S. S.: Historical (1700–2012) global multi-model estimates of the fire emissions from the Fire Modeling Intercomparison Project (FireMIP), Atmos. Chem. Phys., 19, 12545–12567, https://doi.org/10.5194/acp-19-12545-2019, 2019.

Li, X. Y., Jin, H. J., Wang, H. W., Marchenko, S. S., Shan, W., Luo, D. L., He, R. X., Spektor, V., Huang, Y. D., Li, X. Y., and Jia, N.: Influences of forest fires on the permafrost environment: a review, advances in climate change research, 12, 48-65, https://doi.org/10.1016/j.accre.2021.01.001, 2021.

Lin, S., Sun, P., and Huang, X. Can peat fire support a flaming wildlife?, Int. J. Wildland Fire, 28, 601–613, https://doi.org/10.1071/WF19018, 2019.

Lin, S., Cheung, Y. K., Xiao, Y., and Huang, X.: Can rain suppress smoldering peat fire?, Sci. Tot. Enviro., 727, 138468, https://doi.org/10.1016/j.scitotenv.2020.138468, 2020.

Lin, S., Liu, Y., and Huang, X. Climate-induced Arctic-boreal peatland fire and carbon loss in the 21st century, Sci. Total Environ., 796, 148924, https://doi.org/10.1016/j.scitotenv.2021.148924, 2021.

Liu, L., Shawki, D., Voulgarakis, A., Kasoar, M., Samset, B. H., Myhre, G., Forster, P. M., Hodnebrog, Ø., Sillmann, J., Aalbergsjø, S. G., Boucher, O., Faluvegi, G., Iversen, T., Kirkevåg, A., Lamarque, J.-F., Olivié, D., Richardson, T., Shindell, D., and Takemura, T.: A PDRMIP Multimodel Study on the Impacts of Regional Aerosol Forcings on Global and Regional Precipitation, J. Climate, 31, 4429–4447, https://doi.org/10.1175/JCLI-D-17-0439.1, 2018.

Liu, T., Mickley, L. J., Marlier, M. E., DeFries, R. S., Khan, M. F., Latif, M. T., and Karambelas, A.: Diagnosing spatial biases and uncertainties in global fire emissions inventories: Indonesia as regional case study, Remot. Sens. Environ., 237, 111557, https://doi.org/10.1016/j.rse.2019.111557, 2020.

Loisel, J., Yu, Z., Beilman, D. W., Camill, P., Alm, J., Amesbury, M. J., Anderson, D., Andersson, S., Bochicchio, C., Barber, K., Belyea, L. R., Bunbury, J., Chambers, F. M., Charman, D. J., De Vleeschouwer, F., Fiałkiewicz-Kozieł, B., Finkelstein, S. A., Gałka, M., Garneau, M., Hammarlund, D., Hinchcliffe, W., Holmquist, J., Hughes, P., Jones, M. C., Klein, E. S., Kokfelt, U., Korhola, A.,

Kuhry, P., Lamarre, A., Lamentowicz, M., Large, D., Lavoie, M., MacDonald, G., Magnan, G., Makila, M., Mallon, G., Mathijssen, P., Mauquoy, D., McCarroll, J., Moore, T. R., Nichols, J., O'Reilly, B., Oksanen, P., Packalen, M., Peteet, D., Richard, P. J. H., Robinson, S., Ronkainen, T., Rundgren, M., Sannel, A. B. K., Tarnocai, C., Thom, T., Tuittila, E-S., Turetsky, M., Valiranta, M., van der Linden, M., van Geel, B., van Bellen, S., Vitt, D., Zhao, Y., and Zhou, W.: A database and synthesis of northern peatland soil properties and Holocene carbon and nitrogen accumulation, The Holocene, 24, 1028-1042, https://doi.org/10.1177/0959683614538073, 2014.

Loisel, J., Gallego-Sala, A. V, Amesbury, M. J., Magnan, G., Anshari, G., Beilman, D. W., Benavides, J. C., Blewett, J., Camill, P., Charman, D. J., Chawchai, S., Hedgpeth, A., Kleinen, T., Korhola, A., Large, D., Mansilla, C. A., Müller, J., van Bellen, S., West, J. B., Yu, Z., Bubier, J. L., Garneau, M., Moore, T., Sannel, A. B. K., Page, S., Väliranta, M., Bechtold, M., Brovkin, V., Cole, L. E. S., Chanton, J. P., Christensen, T. R., Davies, M. A., De Vleeschouwer, F., Finkelstein, S. A., Frolking, S., Gałka, M., Gandois, L., Girkin, N., Harris, L. I., Heinemeyer, A., Hoyt, A. M., Jones, M. C., Joos, F., Juutinen, S., Kaiser, K., Lacourse, T., Lamentowicz, M., Larmola, T., Leifeld, J., Lohila, A., Milner, A. M., Minkkinen, K., Moss, P., Naafs, B. D. A., Nichols, J., O'Donnell, J., Payne, R., Philben, M., Piilo, S., Quillet, A., Ratnayake, A. S., Roland, T. P., Sjögersten, S., Sonnentag, O., Swindles, G. T., Swinnen, W., Talbot, J., Treat, C., Valach, A. C., and Wu, J.: Expert assessment of future vulnerability of the global peatland carbon sink, Nat. Clim. Change, 11, 70–77, https://doi.org/10.1038/s41558-020-00944-0, 2021.

Loranty, M. M., and Goetz, S. J.: Shrub expansion and climate feedbacks in Arctic tundra, Environ. Res. Lett., 7, 011005, http://dx.doi.org/10.1088/1748-9326/7/1/011005, 2012.

Ludewig, A., Kleipool, Q., Bartstra, R., Landzaat, R., Leloux, J., Loots, E., Meijering, P., van der Plas, E., Rozemeijer, N., Vonk, F., and Veefkind, P.: In-flight calibration results of the TROPOMI payload on board the Sentinel-5 Precursor satellite, Atmos. Meas. Tech., 13, 3561–3580, https://doi.org/10.5194/amt-13-3561-2020, 2020.

Lukenbach, M. C., Hokanson, K. J., Moore, P. A., Devito, K. J., Kettridge, N, Thompson, D. K., Wotton, B. M., Petrone, R. M., and Waddington, J. M.: Hydrological controls on deep burning in a northern forested peatland, Hydrol. Process., 29, 4114–4124, https://doi.org/10.1002/hyp.10440, 2015.

Lund, M. T., Nordling, K., Gjelsvik, A. B., and Samset, B. H.: The influence of variability on fire weather conditions in high latitude regions under present and future global warming, Environ. Res. Commun., 5, 065016, https://doi.org/10.1088/2515-7620/acdfad, 2023.

Lutsch, E., Strong, K., Jones, D. B. A., Blumenstock, T., Conway, S., Fisher, J. A., Hannigan, J. W., Hase, F., Kasai, Y., Mahieu, E., Makarova, M., Morino, I., Nagahama, T., Notholt, J., Ortega, I., Palm, M., Poberovskii, A. V., Sussmann, R., and Warneke, T.: Detection and attribution of wildfire pollution

in the Arctic and northern midlatitudes using a network of Fourier-transform infrared spectrometers and GEOS-Chem, Atmos. Chem. Phys., 20, 12813–12851, https://doi.org/10.5194/acp-20-12813-2020, 2020.

Lyon, B., Barnston, A. G., Coffel, E., and Horton, R. M.: Projected increase in the spatial extent of contiguous US summer heat waves and associated attributes, Environ. Res. Lett., 14, 114029, https://doi.org/10.1088/1748-9326/ab4b41, 2019.

Mack, M. C., Schuur, E. A. G., Bret-Harte, M. S., Shaver, G. R., and Chapin III, F. S.: Ecosystem carbon storage in arctic tundra reduced by long-term nutrient fertilization, Nature, 431, 440-443, https://doi.org/10.1038/nature02887, 2004.

Mack, M. C., Bret-Harte, M. S., Hollingsworth, T. N., Jandt, R. R., Schuur, E. A. G., Shaver, G. R., and Verbylas, D. L.: Carbon loss from an unprecedented Arctic tundra wildfire, Nature, 475, 489–492, https://doi.org/10.1038/nature10283, 2011.

Madani, N., Parazoo, N. C., Kimball, J. S., Reichle, R. H., Chatterjee, A., Watts, J. D., and Saatchi, S.: The Impacts of Climate and Wildfire on Ecosystem Gross Primary Productivity in Alaska, J. Geophys. Res.: Biogeosci., 126, e2020JG006078, https://doi.org/10.1029/2020JG006078, 2021.

Magro, C., Nunes, L., Gonçalves, O. C., Neng, N. R., Nogueira, J. M. F., Castro Rego, F., and Vieira, P.: Atmospheric Trends of CO and CH4 from Extreme Wildfires in Portugal Using Sentinel-5P TROPOMI Level-2 Data, Fire, 4, 25, https://doi.org/10.3390/fire4020025, 2021.

Mangeon, S., Voulgarakis, A., Gilham, R., Harper, A., Sitch, S., and Folberth, G.: INFERNO: a fire and emissions scheme for the UK Met Office's Unified Model, Geosci. Model Dev., 9, 2685–2700, https://doi.org/10.5194/gmd-9-2685-2016, 2016.

Mann, M. E., Rahmstorf, S., Kornhuber, K., Steinman, B. A., Miller, S. K., and Coumou, D.: Influence of Anthropogenic Climate Change on Planetary Wave Resonance and Extreme Weather Events, Sci. Rep., 7, 45242, https://doi.org/10.1038/srep45242, 2017.

Martínez-Alonso, S., Deeter, M., Worden, H., Borsdorff, T., Aben, I., Commane, R., Daube, B., Francis, G., George, M., Landgraf, J., Mao, D., McKain, K., and Wofsy, S.: 1.5 years of TROPOMI CO measurements: comparisons to MOPITT and ATom, Atmos. Meas. Tech., 13, 4841–4864, https://doi.org/10.5194/amt-13-4841-2020, 2020.

Mathur, R.: Estimating the impact of the 2004 Alaskan forest fires on episodic particulate matter pollution over the eastern United States through assimilation of satellite-derived aerosol optical depths in a regional air quality model, J. Geophys. Res.: Atmos., 113, D17302, https://doi.org/10.1029/2007JD009767, 2008.

McCarty, J. L., Smith, T. E. L., and Turetsky, M. R. Arctic fires re-emerging, Nature Geoscience, 13, 658-660, https://doi.org/10.1038/s41561-020-00645-5, 2020.

McCarty, J. L., Aalto, J., Paunu, V.-V., Arnold, S. R., Eckhardt, S., Klimont, Z., Fain, J. J., Evangeliou, N., Venäläinen, A., Tchebakova, N. M., Parfenova, E. I., Kupiainen, K., Soja, A. J., Huang, L., and Wilson, S.: Reviews and syntheses: Arctic fire regimes and emissions in the 21st century, Biogeosciences, 18, 5053–5083, https://doi.org/10.5194/bg-18-5053-2021, 2021.

McCrystall, M. R., Stroeve, J., Serreze, M., Forbes, B. C., and Screen, J. A.: New climate models reveal faster and larger increases in Arctic precipitation than previously projected, Nature Commun., 12, 6765, https://doi.org/10.1038/s41467-021-27031-y, 2021.

Mebust, A. K. and Cohen, R. C.: Space-based observations of fire NO_x emission coefficients: a global biome-scale comparison, Atmos. Chem. Phys., 14, 2509–2524, https://doi.org/10.5194/acp-14-2509-2014, 2014.

Mekonnen, Z. A., Riley, W. J., Berner, L. T., Bouskill, N. J., Torn, M. S., Iwahana, G., Breen, A. L., Myers-Smith, I. H., García Criado, M., and Liu, Y.: Arctic tundra shrubification: a review of mechanisms and impacts on ecosystem carbon balance, Environ. Res. Lett., 16, 053001, https://doi.org/10.1088/1748-9326/abf28b, 2021.

Melton, J. R., Wania, R., Hodson, E. L., Poulter, B., Ringeval, B., Spahni, R., Bohn, T., Avis, C. A., Beerling, D. J., Chen, G., Eliseev, A. V., Denisov, S. N., Hopcroft, P. O., Lettenmaier, D. P., Riley, W. J., Singarayer, J. S., Subin, Z. M., Tian, H., Zürcher, S., Brovkin, V., van Bodegom, P. M., Kleinen, T., Yu, Z. C., and Kaplan, J. O.: Present state of global wetland extent and wetland methane modelling: conclusions from a model inter-comparison project (WETCHIMP), Biogeosci., 10, 753–788, https://doi.org/10.5194/bg-10-753-2013, 2013.

Melton, J. R., Chan, E., Millard, K., Fortier, M., Winton, R. S., Martín-López, J. M., Cadillo-Quiroz, H., Kidd, D., and Verchot, L. V.: A map of global peatland extent created using machine learning (Peat-ML), Geosci. Model Dev., 15, 4709–4738, https://doi.org/10.5194/gmd-15-4709-2022, 2022.

Melvin, A. M., Murray, J., Boehlert, B., Martinich, J. A., Rennels, L., and Rupp, T. S.: Estimating wildfire response costs in Alaska's changing climate, Clim. Change, 141, 783-795, https://doi.org/10.1007/s10584-017-1923-2, 2017.

Meredith, M., M. Sommerkorn, S. Cassotta, C. Derksen, A. Ekaykin, A. Hollowed, G. Kofinas, A. Mackintosh, J. Melbourne-Thomas, M.M.C. Muelbert, G. Ottersen, H. Pritchard, and E.A.G. Schuur: Polar Regions. In: Pörtner, H.-O., Roberts, D. C., Masson-Delmotte, V., Zhai, P., Tignor, M., Poloczanska, E., Mintenbeck, K., Alegría, A., Nicolai, M., Okem, A., Petzold, J., Rama, B., and Weyer, N. M. (eds), IPCC Special Report on the Ocean and Cryosphere in a Changing Climate,

Cambridge University Press, Cambridge, UK and New York, NY, USA, pp. 203–320. https://doi.org/10.1017/9781009157964.005, 2019.

Minschwaner, K., Manney, G. L., Livesey, N. J., Pumphrey, H. C., Pickett, H. M., Froidevaux, L., Lambert, A., Schwartz, M. J., Bernath, P. F., Walker, K. A., and Boone, C. D.: The photochemistry of carbon monoxide in the stratosphere and mesosphere evaluated from observations by the Microwave Limb Sounder on the Aura satellite, J. Geophys. Res., 115, D13303, https://doi.org/10.1029/2009JD012654, 2010.

Miranda, A. I., Borrego, C., Martins, H., Martins, V., Amorim, J. H., Valente, J., and Carvalho, A.: Forest Fire Emissions and Air Pollution in Southern Europe. In: Earth Observation of Wildland Fires in Mediterranean Ecosystems, edited by: Chuvieco, E., Springer, 171-187, http://dx.doi.org/10.1007/978-3-642-01754-4_12, 2009.

MNP LLP: Spring 2019 Wildfire Review, MNP LLP, Edmonton, Canada, available from: https://open.alberta.ca/dataset/5fa709d9-d70a-4176-a1b8-e097abafa9fe/resource/f42b9020-69e0-4d2c-984b-68ad33761f10/download/af-spring-2019-wildfire-review-final-report.pdf, last access: 01/08/2024, 2020.

Monks, S. A., Arnold, S. R., and Chipperfield, M. P.: Evidence for El Niño–Southern Oscillation (ENSO) influence on Arctic CO interannual variability through biomass burning emissions, Geophys. Res. Lett., 39, L14804, https://doi.org/10.1029/2012GL052512, 2012.

Moore, P. A., and Waddington, J. M.: Modelling Sphagnum moisture stress in response to projected 21st-century climate change, Hydrol. Proc., 29, 3966-3982, https://doi.org/10.1002/hyp.10484, 2015.

Moritz, M. A., Parisien, M.-A., Batllori, E., Krawchuk, M. A., Van Dorn, J., Ganz, D. J., and Hayhoe, K.: Climate change and disruptions to global fire activity, Ecosphere, 3, 1-22, https://doi.org/10.1890/ES11-00345.1, 2012.

Mortelmans, J., Felsberg, A., De Lannoy, G. J. M., Veraverbeke, S., Field, R. D., Andela, N., and Bechtold, M.: Improving the fire weather index system for peatlands using peat-specific hydrological input data, Nat. Hazards Earth Syst. Sci., 24, 445–464, https://doi.org/10.5194/nhess-24-445-2024, 2024.

Moss, R. H., Edmonds, J. A., Hibbard, K. A., Manning, M. R., Rose, S. K., van Vuuren, D. P., Carter, T. R., Emori, S., Kainuma, M., Kram, T., Meehl, G. A., Mitchell, J. F. B., Nakicenovic, N., Riahi, K., Smith, S. J., Stouffer, R. J., Thomson, A. M., Weyant, J. P., and Wilbanks, T. J. The next generation of scenarios for climate change research and assessment, Nature, 463, 747-756, https://doi.org/10.1038/nature08823, 2010.

Mouillot, F., Schultz, M. G., Yue, C., Cadule, P., Tansey, K., Ciasia, P., and Chuvieco, E.: Ten years of global burned area products from spaceborne remote sensing—A review: Analysis of user needs and recommendations for future developments, Int. J. Appl. Earth Obs., 26, 64-76, http://dx.doi.org/10.1016/j.jag.2013.05.014, 2014.

Mudryk, L., Santolaria-Otín, M., Krinner, G., Ménégoz, M., Derksen, C., Brutel-Vuilmet, C., Brady, M., and Essery, R.: Historical Northern Hemisphere snow cover trends and projected changes in the CMIP6 multi-model ensemble, The Cryosphere, 14, 2495–2514, https://doi.org/10.5194/tc-14-2495-2020, 2020.

Müller, J. and Joos, F.: Global peatland area and carbon dynamics from the Last Glacial Maximum to the present – a process-based model investigation, Biogeosci., 17, 5285–5308, https://doi.org/10.5194/bg-17-5285-2020, 2020.

Müller, J. and Joos, F.: Committed and projected future changes in global peatlands – continued transient model simulations since the Last Glacial Maximum, Biogeosci., 18, 3657–3687, https://doi.org/10.5194/bg-18-3657-2021, 2021.

Munro, R., Lang, R., Klaes, D., Poli, G., Retscher, C., Lindstrot, R., Huckle, R., Lacan, A., Grzegorski, M., Holdak, A., Kokhanovsky, A., Livschitz, J., and Eisinger, M.: The GOME-2 instrument on the Metop series of satellites: instrument design, calibration, and level 1 data processing – an overview, Atmos. Meas. Tech., 9, 1279–1301, https://doi.org/10.5194/amt-9-1279-2016, 2016.

Myers-Smith, I. H., Kerby, J. T., Phoenix, G. K., Bjerke, J. W., Epstein, H. E., Assmann, J. J., John, C., Andreu-Hayles, L., Angers-Blondin, S., Beck, P. S. A., Berner, L. T., Bhatt, U. S., Bjorkman, A. D., Blok, D., Bryn, A., Christiansen, C. T., Cornelissen, J. H. C., Cunliffe, A. M., Elmendorf, S. C., Forbes, B. C., Goetz, S. J., Hollister, R. D., de Jong, R., Loranty, M. M., Macias-Fauria, M., Maseyk, K., Normand, S., Olofsson, J., Parker, T. C., Parmentier, F.-J. W., Post, E., Schaepman-Strub, G., Stordal, F., Sullivan, P. F., Thomas, H. J. D., Tømmervik, H., Treharne, R., Tweedie, C. E., Walker, D. A., Wilmking, M., and Wipf, S.: Complexity revealed in the greening of the Arctic, Nature Clim. Change, 10, 106-117, https://doi.org/10.1038/s41558-019-0688-1, 2020.

Myhre, G., Shindell, D., Bréon, F.-M., Collins, W., Fuglestvedt, J., Huang, J., Koch, D., Lamarque, J.-F., Lee, D., Mendoza, B., Nakajima, T., Robock, A., Stephens, G., Takemura, T., and Zhang, H.: Anthropogenic and Natural Radiative Forcing, in Climate Change 2013: The Physical Science Basis. Contribution of Working Group I to the Fifth Assessment Report of the Intergovernmental Panel on Climate Change, edited by: Stocker, T. F., Qin, D., Plattner, G.-K., Tignor, M., Allen, S. K., Boschung, J., Nauels, A., Xia, Y., Bex, V., and Midgley, P. M., Cambridge University Press, Cambridge, United Kingdom and New York, NY, USA, 659–740, 2013.

Natole, M. Jr., Ying, Y., Buyantuev, A., Stessin, M., Buyantuev, V., and Lapenis, A.: Patterns of mega-forest fires in east Siberia will become less predictable with climate warming, Environ. Adv., 4, 100041, https://doi.org/10.1016/j.envadv.2021.100041, 2021.

Nabizadeh, E., Hassanzadeh, P., Yang, D., and Barnes, E. A.: Size of the Atmospheric Blocking Events: Scaling Law and Response to Climate Change, Geophys. Res. Lett., 46, 13488-13499, https://doi.org/10.1029/2019GL084863, 2019.

Nelson, K., Thompson, D., Hopkinson, C., Petrone, R., and Chasmer, L. Peatland-fire interactions: A review of wildland fire feedbacks and interactions in Canadian boreal peatlands. Sci. Tot. Environ. 769, 145212, https://doi.org/10.1016/j.scitotenv.2021.145212, 2021.

Nitzbon, J., Westermann, S., Langer, M., Martin, L. C. P., Strauss, J., Laboor, S., and Boike, J.: Fast response of cold ice-rich permafrost in northeast Siberia to a warming climate, Nat. Commun., 11, 2201, https://doi.org/10.1038/s41467-020-15725-8, 2020.

Nitze, I., Grosse, G., Jones, B. M., Romanovsky, V. E., and Boike, J.: Remote sensing quantifies widespread abundance of permafrost region disturbances across the Arctic and Subarctic, Nat. Commun., 9, 5423, https://doi.org/10.1038/s41467-018-07663-3, 2018.

Noble, A., Palmer, S. M., Glaves, D. J., Crowle, A., and Holden, J. Peatland vegetation change and establishment of re-introduced Sphagnum moss after prescribed burning, Biodivers. Conserv., 28, 939-952, https://doi.org/10.1007/s10531-019-01703-0, 2019.

Nossov, D. R., Jorgenson, M. T., Kielland, K., and Kanevskiy, M. Z.: Edaphic and microclimatic controls over permafrost response to fire in interior Alaska, Environ. Res. Lett., 8, 035013, https://doi.org/10.1088/1748-9326/8/3/035013, 2013.

Obu, J., Westermann, S., Bartsch, A., Berdnikov, N., Christiansen, H. H., Dashtseren, A., Delaloye, R., Elberling, B., Etzelmuller, B., Kholodov, A., Khomutov, A., Kaab, A., Leibman, M. O., Lewkowicz, A. G.,Panda, S. K., Romanovsky, V., Way, R. G., Westergaard-Nielsen, A., Wu, T., Yamkhin, J., and Zou, D.: Northern Hemisphere permafrost map based on TTOP modelling for 2000–2016 at 1 km2 scale, Earth-Science Reviews, 193, 299-316, https://doi.org/10.1016/j.earscirev.2019.04.023, 2019.

Oki, T., and Kanae, S.: Global Hydrological Cycles and World Water Resources, Science, 313, 1068-1072, https://doi.org/10.1126/science.1128845, 2006.

Olivier, J. G. J., van Aardenne, J. A., Dentener, F. J., Pagliari, V., Ganzeveld, L. N., and Peters, J. A. H. W.: Recent trends in global greenhouse gas emissions: regional trends 1970–2000 and spatial distribution of key sources in 2000, Environ. Sci., 2, 81-99, https://doi.org/10.1080/15693430500400345, 2005.

O'Neill, B. C., Kriegler, E., Riahi, K., Ebi, K. L., Hallegatte, S., Carter, T. R., Mathur, R., and van Vuuren, D. P.: A new scenario framework for climate change research: the concept of shared socioeconomic pathways, Climatic Change, 122, 387-400, https://doi.org/10.1007/s10584-013-0905-2, 2014.

O'Neill, B.C., Kriegler, E., Ebi, K. L., Kemp-Benedict, E., Riahi, K., Rothman, D. S., van Ruijven, B. J., van Vuuren, D. P., Birkmann, J., Kok, K., Levy, M., and Solecki, W.: The roads ahead: Narratives for shared socioeconomic pathways describing world futures in the 21st century, 42, 169-180, https://doi.org/10.1016/j.gloenvcha.2015.01.004, 2017.

O'Neill, B. C., Carter, T. R., Ebi, K., Harrison, P. A., Kemp-Benedict, E., Kok, K., Kriegler, E., Preston, B. L., Riahi, K., Sillmann, J., van Ruijven, B. J., van Vuuren, D., Carlisle, D., Conde, C., Fuglestvedt, J., Green, C., Hasegawa, T., Leininger, J., Monteith, S., and Pichs-Madruga, R.: Achievements and needs for the climate change scenario framework, Nature Clim. Change, 10, 1074-1084, https://doi.org/10.1038/s41558-020-00952-0, 2020.

Oris, F., Asselin, H., Ali, A. A., Finsinger, W., and Bergeron, Y.: Effect of increased fire activity on global warming in the boreal forest, Environ. Rev., 22, 206-219, http://dx.doi.org/10.1139/er-2013-0062, 2014.

Otón, G., Lizundia-Loiola, J., Pettinari, M. L., and Chuvieco, E.: Development of a consistent global long-term burned area product (1982–2018) based on AVHRRLTDR data, Int. J. Appl. Earth Obs., 103, 102473, https://doi.org/10.1016/j.jag.2021.102473, 2021.

Overland, J. E., Wang, M., Walsh, J. E., and Stroeve, J. C.: Future Arctic climate changes: Adaptation and mitigation time scales, Earth's Future, 2, 68-74, https://doi.org/10.1002/2013EF000162, 2013.

Page, S. E., Siegert, F., Rieley, J. O., Boehm, H.-D. V., Jaya, A., and Limin, S.: The amount of carbon released from peat and forest fires in Indonesia during 1997, Nature, 420, 61–65, https://doi.org/10.1038/nature01131, 2002.

Page, S. E., Rieley, J. O., and Banks, C. J.: Global and regional importance of the tropical peatland carbon pool, Glob. Change Bio., 17, 798-818, https://doi.org/10.1111/j.1365-2486.2010.02279.x, 2011.

Pan, S., Tian, H., Dangal, S. R. S., Yang, Q., Yang, J., Lu, C., Tao, B., Ren, W., and Ouyang, Z.: Responses of global terrestrial evapotranspiration to climate change and increasing atmospheric CO2 in the 21st century, Earth's Future, 3, 15-35, https://doi.org/10.1002/2014EF000263, 2014.

Panagos, P., Hiederer, R., Van Liedekerke, M., and Bampa, F.: Estimating soil organic carbon in Europe based on data collected through an European network, Ecol. Indic., 24, 439-450, https://doi.org/10.1016/j.ecolind.2012.07.020, 2013.

Panin, G.N., Solomonova, I.V. and Vyruchalkina, T.Y.: Climatic trends in the middle and high latitudes of the Northern Hemisphere, Water Resour., 36, 718–730, https://doi.org/10.1134/S0097807809060116, 2009.

Park, H., Jeong, S., Park, H., Labzovskii, L. D., and Bowman, K. W.: An assessment of emission characteristics of Northern Hemisphere cities using spaceborne observations of CO2, CO, and NO2, Remote Sens. Environ., 254, 112246, https://doi.org/10.1016/j.rse.2020.112246, 2021.

Parker, R. J., Boesch, H., Wooster, M. J., Moore, D. P., Webb, A. J., Gaveau, D., and Murdiyarso, D.: Atmospheric CH4 and CO2 enhancements and biomass burning emission ratios derived from satellite observations of the 2015 Indonesian fire plumes, Atmos. Chem. Phys., 16, 10111–10131, https://doi.org/10.5194/acp-16-10111-2016, 2016.

Parker, T. C., Thurstin, A. M., Raundrup, K., Subke, J-A., Wookey, P. A., and Hartley, I. P.: Shrub expansion in the Arctic may induce large-scale carbon losses due to changes in plant-soil interactions, Plant and Soil, 463, 643-651, https://doi.org/10.1007/s11104-021-04919-8, 2021.

Partain, J. L., Alden, S., Strader, H., Bhatt, U. S., Bieniek, P. A., Brettschneider, B. R., Walsh, J. E., Lader, R. T., Olsson, P. Q., Rupp, T. S., Thoman, R. L., York, A. D., and Ziel, R. H.: An Assessment of the Role of Anthropogenic Climate Change in the Alaska Fire Season of 2015, B. Am. Meteorol. Soc., 97, S14-S18, https://doi.org/10.1175/BAMS-D-16-0149.1, 2016.

Pastick, N. J., Duffy, P., Genet, H., Rupp, T. S., Wylie, B. K., Johnson, K. D., Jorgenson, M. T., Bliss, N., McGuire, A. D., Jafarov, E. E., and Knight, J. F.: Historical and projected trends in landscape drivers affecting carbon dynamics in Alaska, Ecol. App., 27, 1383-1402, https://doi.org/10.1002/eap.1538, 2017.

Pearson, R. G., Phillips, S. J., Loranty, M. M., Beck, P. S. A., Damoulas, T., Knight, S. J., and Goetz, S. J.: Shifts in Arctic vegetation and associated feedbacks under climate change, Nature Clim. Change, 3, 673-677, https://doi.org/10.1038/nclimate1858, 2013.

Pechony, O., and Shindell, D. T.: Fire parameterization on a global scale, J. Geophys. Res. Biogeosci., 114, D16115, https://doi.org/10.1029/2009JD011927, 2009.

Peiro, H. E., Kurt, A., and Crowell, S.: Combustion efficiency observed with CO and NO2 TROPOMI data: a first counties scale study during the 2020 fires of California, ESS Open Archive [preprint], https://doi.org/10.1002/essoar.10511087.1, 2022.

Perkins, O., Mateji, S., Erb, K., and Millington, J.: Towards a global behavioural model of anthropogenic fire: the spatiotemporal distribution of land-fire systems, Socio-Environ. Syst. Model, 4, 18130, https://doi.org/10.18174/sesmo.18130, 2022.

Pfister, G. G., Hess, P. G., Emmons, L. K., Rasch, P. J., and Vitt, F. M.: Impact of the summer 2004 Alaska fires on top of the atmosphere clear-sky radiation fluxes, J. Geophys. Res.: Atmos., 113, D02204, https://doi.org/10.1029/2007JD008797, 2008.

Poggio, L., de Sousa, L. M., Batjes, N. H., Heuvelink, G. B. M., Kempen, B., Ribeiro, E., and Rossiter, D.: SoilGrids 2.0: producing soil information for the globe with quantified spatial uncertainty, SOIL, 7, 217–240, https://doi.org/10.5194/soil-7-217-2021, 2021

Ponomarev, E. I., Kharuk, V. I., and Ranson, K. J.: Wildfires Dynamics in Siberian Larch Forests, Forests, 7, 125, https://doi.org/10.3390/f7060125, 2016.

Pope, C. A., III, Burnett, R. T., Thun, M. J., Calle, E. E., Krewski, D., Ito, K., and Thurston, G. D.: Lung Cancer, Cardiopulmonary Mortality, and Long-term Exposure to Fine Particulate Air Pollution, JAMA, 287, 1132-1141, https://doi.org/10.1001/jama.287.9.1132, 2002.

Popovicheva, O.B., Engling, G., Ku, I.T., Timofeev, M.A. and Shonija, N.K.: Aerosol Emissions from Long-lasting Smoldering of Boreal Peatlands: Chemical Composition, Markers, and Microstructure, Aerosol Air Qual. Res., 19, 484-503, https://doi.org/10.4209/aaqr.2018.08.0302, 2019.

Potter, C.: Ecosystem carbon emissions from 2015 forest fires in interior Alaska, Carbon Balance Manag., 13, 2, https://doi.org/10.1186/s13021-017-0090-0, 2018.

Potter, S., Cooperdock, S., Veraverbeke, S., Walker, X., Mack, M. C., Goetz, S. J., Baltzer, J., Bourgeau-Chavez, L., Burrell, A., Dieleman, C., French, N., Hantson, S., Hoy, E. E., Jenkins, L., Johnstone, J. F., Kane, E. S., Natali, S. M., Randerson, J. T., Turetsky, M. R., Whitman, E., Wiggins, E., and Rogers, B. M.: Burned area and carbon emissions across northwestern boreal North America from 2001–2019, Biogeosciences, 20, 2785– 2804, https://doi.org/10.5194/bg-20-2785-2023, 2023.

Poulter, B., Christensen, N. L., and Halpin, P. N.: Carbon emissions from a temperate peat fire and its relevance to interannual variability of trace atmospheric greenhouse gases, J. Geophys. Res., 111, D06301, https://doi.org/10.1029/2005JD006455, 2006.

Prat-Guitart, N., Rein, G., Hadden, R. M., Belcher, C. M., and Yearsley, J. M.: Effects of spatial heterogeneity in moisture content on the horizontal spread of peat fires, Sci. Tot. Environ., 572, 1422-1430, https://doi.org/10.1016/j.scitotenv.2016.02.145, 2016.

Prosperi, P., Bloise, M., Tubiello, F. N., Conchedda, G., Rossi, S., Boschetti, L., Salvatore, M., and Bernoux, M.: New estimates of greenhouse gas emissions from biomass burning and peat fires using MODIS Collection 6 burned areas, Clim. Change., 161, 415-432, https://doi.org/10.1007/s10584-020-02654-0, 2020.

Purnomo, D. M. J., Bonner, M., Moafi, S., and Rein, G.: Using cellular automata to simulate field-scale flaming and smouldering wildfires in tropical peatlands, Proc. Combust. Inst., 38, 5119– 5127, https://doi.org/10.1016/j.proci.2020.08.052, 2020.

Qian, H., Joseph, R., and Zeng, N.: Enhanced terrestrial carbon uptake in the Northern High Latitudes in the 21st century from the Coupled Carbon Cycle Climate Model Intercomparison Project model projections, Global Change Bio., 16, 641-656, https://doi.org/10.1111/j.1365-2486.2009.01989.x, 2010.

Qin, Y., Musa, D. N. S., Lin. S., and Huang, X.: Deep peat fire persistently smouldering for weeks: a laboratory demonstration, Int. J. Wildland Fire, 32, 86–98, https://doi.org/10.1071/WF22143, 2023.

Qiu, C., Zhu, D., Ciais, P., Guenet, B., Krinner, G., Peng, S., Aurela, M., Bernhofer, C., Brümmer, C., Bret-Harte, S., Chu, H., Chen, J., Desai, A. R., Dušek, J., Euskirchen, E. S., Fortuniak, K., Flanagan, L. B., Friborg, T., Grygoruk, M., Gogo, S., Grünwald, T., Hansen, B. U., Holl, D., Humphreys, E., Hurkuck, M., Kiely, G., Klatt, J., Kutzbach, L., Largeron, C., Laggoun-Défarge, F., Lund, M., Lafleur, P. M., Li, X., Mammarella, I., Merbold, L., Nilsson, M. B., Olejnik, J., Ottosson-Löfvenius, M., Oechel, W., Parmentier, F.-J. W., Peichl, M., Pirk, N., Peltola, O., Pawlak, W., Rasse, D., Rinne, J., Shaver, G., Schmid, H. P., Sottocornola, M., Steinbrecher, R., Sachs, T., Urbaniak, M., Zona, D., and Ziemblinska, K.: ORCHIDEE-PEAT (revision 4596), a model for northern peatland CO_2, water, and energy fluxes on daily to annual scales, Geosci. Model Dev., 11, 497–519, https://doi.org/10.5194/gmd-11-497-2018, 2018.

Qiu, C., Zhu, D., Ciais, P., Guenet, B., Peng, S., Krinner, G., Tootchi, A., Ducharne, A., and Hastie, A.: Modelling northern peatland area and carbon dynamics since the Holocene with the ORCHIDEE-PEAT land surface model (SVN r5488), Geosci. Model Dev., 12, 2961–2982, https://doi.org/10.5194/gmd-12-2961-2019, 2019.

Rabin, S. S., Melton, J. R., Lasslop, G., Bachelet, D., Forrest, M., Hantson, S., Kaplan, J. O., Li, F., Mangeon, S., Ward, D. S., Yue, C., Arora, V. K., Hickler, T., Kloster, S., Knorr, W., Nieradzik, L., Spessa, A., Folberth, G. A., Sheehan, T., Voulgarakis, A., Kelley, D. I., Prentice, I. C., Sitch, S., Harrison, S., and Arneth, A.: The Fire Modeling Intercomparison Project (FireMIP), phase 1: experimental and analytical protocols with detailed model descriptions, Geosci. Model Dev., 10, 1175–1197, https://doi.org/10.5194/gmd-10-1175-2017, 2017.

Ramonet, M., B. Langerock, T. Warneke, and H. J. Eskes, Validation report of the CAMS greenhouse gas global re-analysis, years 2003-2020, Copernicus Atmosphere Monitoring Service (CAMS) report, https://doi.org/10.24380/438c-4597, 2021.

Randerson, J. T., Liu, H., Flanner, M. G., Chambers, S. D., Jin, Y., Hess, P. G., Pfister, G., Mack, M. C., Treseder, K. K., Welp, L. R., Chapin, F. S., Harden, J. W., Goulden, M. L., Lyons, E., Neff, J. C.,

Schuur, E. A. G., and Zender, C. S.: The impact of boreal forest fire on climate warming, Science, 314, 1130-1132, https://doi.org/10.1126/science.1132075, 2006.

Randerson, J. T., Chen, Y., van der Werf, G. R., Rogers, B. M., and Morton, D. C.: Global burned area and biomass burning emissions from small fires, J. Geophys. Res. Biogeosci., 117, G04012, https://doi.org/10.1029/2012JG002128, 2012.

Rantanen, M., Karpechko, A. Y., Lipponen, A., Nordling, K., Hyvarinen, O., Ruosteenoja, K., Vihma, T., and Laaksonen, A.: The Arctic has warmed nearly four times faster than the globe since 1979, Nature Commun. Earth Environ., 3, 168, https://doi.org/10.1038/s43247-022-00498-3, 2022.

Rein, G., Cohen, S., and Simeoni, A. Carbon emissions from smouldering peat in shallow and strong fronts, Proc. Comb. Inst., 32, 2489-2496, https://doi.org/10.1016/j.proci.2008.07.008, 2009.

Rein, G.: Smouldering Fires and Natural Fuels, in: Fire Phenomena and the Earth System: An Interdisciplinary Guide to Fire Science, edited by: Belcher, C., Wiley and Sons, 15–33, https://doi.org/10.1002/9781118529539.ch2, 2013.

Rein, G.: Smouldering peat megafires: the largest fires on Earth, in: Coal and peat fires: a global perspective, Volume 4: Peat – Geology, Combustion, and Case Studies, edited by: Stracher, G. B., Prakash, A., and Rein, G., Elsevier Science, 1–11, https://doi.org/10.1016/C2010-0-68845-6, 2015.

Rein, G., and Huang, X.: Smouldering wildfires in peatlands, forests and the arctic: Challenges and perspectives, Curr. Opin. Environ. Sci. Health, 24, 100296, https://doi.org/10.1016/j.coesh.2021.100296, 2021.

Remer, L. A., Kaufman, Y. J., Tanré, D., Mattoo, S., Chu, D. A., Martins, J. V., Li, R.-R., Ichoku, C., Levy, R. C., Kleidman, R. G., Eck, T. F., Vermote, E., and Holben, B. N.: The MODIS Aerosol Algorithm, Products, and Validation, J. Atmos. Sci., 62, 947–973, https://doi.org/10.1175/JAS3385.1, 2005.

Rémy, S., Kipling, Z., Huijnen, V., Flemming, J., Nabat, P., Michou, M., Ades, M., Engelen, R., and Peuch, V.-H.: Description and evaluation of the tropospheric aerosol scheme in the Integrated Forecasting System (IFS-AER, cycle 47R1) of ECMWF, Geosci. Model Dev., 15, 4881–4912, https://doi.org/10.5194/gmd-15-4881-2022, 2022.

Riahi, K., van Vuuren, D.P., Kriegler, E., Edmonds, J., O'Neill, B., Fujimori, S., Bauer, N., Calvin, K., Dellink, R., Fricko, O., Lutz, W., Popp, A., Crespo Cuaresma, J., Leimbach, M., Kram, T., Rao, S., Emmerling, J., Hasegawa, T., Havlik, P., Humpenöder, F., Aleluia Da Silva, L., Smith, S.J., Stehfest, E., Bosetti, V., Eom, J., Gernaat, D., Masui, T., Rogelj, J., Strefler, J., Drouet, L., Krey, V., Luderer, G., Harmsen, M., Takahashi, K., Wise, M., Baumstark, L., Doelman, J., Kainuma, M., Klimont, Z., Marangoni, G., Moss, R., Lotze-Campen, H., Obersteiner, M., Tabeau, A., and Tavoni, M.: The

Shared Socioeconomic Pathways and their nergy, land use, and greenhouse gas emissions implications: An overview, Global Environmental Change, 42, 153-168, https://doi.org/10.1016/j.gloenvcha.2016.05.009, 2017.

Richardson, T. B., Forster, P. M., Andrews, T., Boucher, O., Faluvegi, G., Fläschner, D., Hodnebrog, Ø., Kasoar, M., Kirkevåg, A., Lamarque, J.-F., Myhre, G., Olivié, D., Samset, B. H., Shawki, D., Shindell, D., Takemura, T., and Voulgarakis, A.: Drivers of Precipitation Change: An Energetic Understanding, J. Climate, 31, 9641-9657, https://doi.org/10.1175/JCLI-D-17-0240.1, 2018.

Rocha, A. V., Loranty, M. M., Higuera, P. E., Mack, M. C., Hu, F. S., Jones, B. M., Breen, A. L., Rastetter, E. B., Goetz, S. J., and Shaver, G. R.: The footprint of Alaskan tundra fires during the past half-century: implications for surface properties and radiative forcing, Environ. Res. Lett., 7, 044039, https://doi.org/10.1088/1748-9326/7/4/044039, 2012.

Rosenzweig, C., Arnell, N. W., Ebi, K. L., Lotze-Campen, H., Raes, F., Rapley, C., Stafford Smith, M., Cramer, W., Frieler, K., Reyer, C. P. O., Schewe, J., van Vuuren, D., and Warszawski, L.: Assessing inter-sectoral climate change risks: the role of ISIMIP, Environ. Res. Lett., 12, 010301, https://doi.org/10.1088/1748-9326/12/1/010301, 2017.

Roteta, E., Bastarrika, A., Padilla, M., Storm, T., and Chuvieco, E.: Development of a Sentinel-2 burned area algorithm: Generation of a small fire database for sub-Saharan Africa, Remote Sens. Environ., 222, 1–17, https://doi.org/10.1016/j.rse.2018.12.011, 2019.

Rothermel, R. C.: A mathematical model for predicting fire spread in wildland fuels, Res. Pap. INT-115, Ogden, UT: U.S. Department of Agriculture, Intermountain Forest and Range Experiment Station, 40 pp., available from: https://research.fs.usda.gov/treesearch/32533, last access: 30/07/2024, 1972.

Roulet, N., Moore, T., Bubier, J., and Lafleur, P.: Northern fens: methane flux and climatic change, Tellus, 44, 100-105, https://doi.org/10.3402/tellusb.v44i2.15429, 1992.

Roulston, C., Paton-Walsh, C., Smith, T. E. L., Guérette, É.-A., Evers, S., Yule, C. M., Rein, G., and van der Werf, G. R. Fine Particle Emissions From Tropical Peat Fires Decrease Rapidly With Time Since Ignition, J. Geophys. Res.: Atmos., 123, 5607-5617, https://doi.org/10.1029/2017JD027827, 2018.

Rowe, J. P., Zarzana, K. J., Kille, N., Borsdorff, T., Goudar, M., Lee, C. F., Koenig, T. K., Romero-Alvarez, J., Campos, T., Knote, C., Theys, N., Landgraf, J., and Volkamer, R.: Carbon Monoxide in Optically Thick Wildfire Smoke: Evaluating TROPOMI Using CU Airborne SOF Column Observations, ACS Earth Space Chem., 6, 1799-1812, https://doi.org/10.1021/acsEarthspacechem.2c00048, 2022.

Salimi, S., Almuktar, S. A. A. A. N., and Scholz, M.: Impact of climate change on wetland ecosystems: A critical review of experimental wetlands, J. Environ. Manag., 286, 112160, https://doi.org/10.1016/j.jenvman.2021.112160, 2021.

Santoso, M. A., Huang, X., Prat-Guitart, N., Christensen, E., and Rein, G.: Smouldering fires and soil, in: Fire Effects on Soil Properies, edited by: Pereira, P., Mataix-Solera, J., Ubeda, X., Rein, G., and Ceradà, A., CSIRO Publishing, 203–216, https://doi.org/10.1071/9781486308149, 2019a.

Santoso, M. A., Christensen, E. G., Yang, J., and Rein, G. Review of the Transition From Smouldering to Flaming Combustion in Wildfires, Front. Mech. Eng., 5, 49, https://doi.org/10.3389/fmech.2019.00049, 2019b.

Santoso, M. A., Cui, W., Amin, H. M. F., Christensen, E. G., Nugroho, Y. S., and Rein, G.: Laboratory study on the suppression of smouldering peat wildfires: effects of flow rate and wetting agent, Int. J. Wildland Fire, 30, 378-390, https://doi.org/10.1071/WF20117, 2021.

Savenets, M., Dvoretska, I., Nadtochii, L., and Zhemera, N.: Comparison of TROPOMI NO2, CO, HCHO, and SO2 data against ground-level measurements in close proximity to large anthropogenic emission sources in the example of Ukraine, Meteorol. Appl., 29, e2108, https://doi.org/10.1002/met.2108, 2022.

Scholten, R. C., Jandt, R., Miller, E. A., Rogers, B. M., and Veraverbeke, S.: Overwintering fires in boreal forests, Nature, 593, 399-404, https://doi.org/10.1038/s41586-021-03437-y, 2021.

Scholten, R., C., Coumou, D., Luo, F., and Veraverbeke, S.: Early snowmelt and polar jet dynamics co-influence recent extreme Siberian fire seasons, Science, 378, 1005–1009, https://doi.org/10.1126/science.abn4419, 2022.

Schreier, S. F., Richter, A., Kaiser, J. W., and Burrows, J. P.: The empirical relationship between satellite-derived tropospheric NO_2 and fire radiative power and possible implications for fire emission rates of NO_x, Atmos. Chem. Phys., 14, 2447–2466, https://doi.org/10.5194/acp-14-2447-2014, 2014.

Schulte, M. L., McLaughlin, D. L., Wurster, F. C., Varner, J. M., Stewart, R. D., Aust, W. M., Jones, C. N., and Gile, B.: Short- and long-term hydrologic controls on smouldering fire in wetland soils, Int. J. Wildland Fire, 28, 177-186, https://doi.org/10.1071/WF18086, 2019.

Schuur, E. A. G., McGuire, A. D., Schadel, C., Grosse, G., Harden, J. W., Hayes, D. J., Hugelius, G., Koven, C. D., Kuhry, P., Lawrence, D. M., Natali, S. M., Olefeldt, D., Romanovsky, V. E., Schaefer, K., Turetsky, M. R., Treat, C. C., and Vonk, J. E.: Climate change and the permafrost carbon feedback, Nature, 520, 171-179, https://doi.org/10.1038/nature14338, 2015.

Serikova, S., Pokrovsky, O. S., Laudon, H., Krickov, I. V., Lim, A. G., Manasypov, R. M., and Karlsson, J.: High carbon emissions from thermokarst lakes of Western Siberia. Nature Commun., 10, 1552, https://doi.org/10.1038/s41467-019-09592-1, 2019.

Serreze, M. C., and Barry, R. G.: Processes and impacts of Arctic amplification: A research synthesis, Global Planet. Change, **77**, 85-96, https://doi.org/10.1016/j.gloplacha.2011.03.004, 2011.

Shaposhnikov, D., Revich, B., Bellander, T., Bedada, G. B., Bottai, M., Kharkova, T., Kvasha, E., Lezina, E., Lind, T., Semutnikova, E., and Pershagen, G.: Mortality Related to Air Pollution with the Moscow Heat Wave and Wildfire of 2010, Epidemiology, 25, 359–364, https://doi.org/10.1097/EDE.0000000000000090, 2014.

Sharma, A. R., Jain, P., Abatzoglou, J. T., and Flannigan, M.: Persistent Positive Anomalies in Geopotential Heights Promote Wildfires in Western North America. J. Climate, 35, 6469–6486, https://doi.org/10.1175/JCLI-D-21-0926.1, 2022.

Shulski, M., Wendler, G., Alden, S., and Larkin, N.: Alaska's exceptional 2004 fire season, In: Sixth Symposium on Fire and Forest Meteorology, 24th-27th October 2005, available from: https://ams.confex.com/ams/6FireJoint/techprogram/paper_97633.htm, last access: 01/08/2024, 2005.

Silva, S. J., and Arellano, A. F.: Characterizing Regional-Scale Combustion Using Satellite Retrievals of CO, NO2 and CO2, Remote Sens., 9, 744, https://doi.org/10.3390/rs9070744, 2017.

Silver, B., Arnold, S., Emmons, L., Reddington, C., and Conibear, L.: Health impacts of wildfire smoke in the Arctic, EGU General Assembly 2023, Vienna, Austria, 24–28 Apr 2023, EGU23- 9394, https://doi.org/10.5194/egusphere-egu23-9394, 2023.

Silver, B., Arnold, S. R., Reddington, C. L., Emmons, L. K., and Conibear, L.: Large transboundary health impact of Arctic wildfire smoke, Commun. Earth Environ. 5, 199, https://doi.org/10.1038/s43247-024-01361-3, 2024.

Sindelarova, K., Granier, C., Bouarar, I., Guenther, A., Tilmes, S., Stavrakou, T., Müller, J.-F., Kuhn, U., Stefani, P., and Knorr, W.: Global data set of biogenic VOC emissions calculated by the MEGAN model over the last 30 years, Atmos. Chem. Phys., 14, 9317–9341, https://doi.org/10.5194/acp-14-9317-2014, 2014.

Singh, H. B., Anderson, B. E., Brune, W. H., Cai, C., Cohen, R. C., Crawford, J. H., Cubison, M. J., Czech, E. P., Emmons, L., Fuelberg, H. E., Huey, G., Jacob, D. J., Jimenez, J. L., Kaduwela, A., Kondo, Y., Mao, J., Olson, J. R., Sachse, G. W., Vay, S. A., Weinheimer, A., and Wisthaler, A.: Pollution influences on atmospheric composition and chemistry at high northern latitudes: Boreal and California forest fire emissions, Atmos. Environ., 44, 4553-4564, https://doi.org/10.1016/j.atmosenv.2010.08.026, 2010.

Sirin, A. and Medvedeva, M.: Remote sensing mapping of peat-fireburnt areas: Identification among other wildfires, Remote Sens., 14, 194, https://doi.org/10.3390/rs14010194, 2022.

Sizov, O., Ezhova, E., Tsymbarovich, P., Soromotin, A., Prihod'ko, N., Petäjä, T., Zilitinkevich, S., Kulmala, M., Bäck, J., and Köster, K.: Fire and vegetation dynamics in northwest Siberia during the last 60 years based on high-resolution remote sensing, Biogeosciences, 18, 207–228, https://doi.org/10.5194/bg-18-207-2021, 2021.

Shaposhnikov, D., Revich, B., Bellander, T., Bedada, G. B., Bottai, M., Kharkova, T., Kvasha, E., Lezina, E., Lind, T., Semutnikova, E., and Pershagen, G. Mortality related to air pollution with the moscow heat wave and wildfire of 2010, Epidemiology, 25, 359-364, https://doi.org/10.1097/ede.0000000000000090, 2014.

Shindell, D. T., Faluvegi, G., Bauer, S. E., Koch, D. M., Unger, N., Menon, S., Miller, R. L., Schmidt, G. A., and Streets, D. G.: Climate response to projected changes in short-lived species under an A1B scenario from 2000–2050 in the GISS climate model, J. Geophys. Res.: Atmos., 112, D20103, https://doi.org/10.1029/2007JD008753, 2007.

Shindell, D. T., Faluvegi, G., Koch, D. M., Schmidt, G. A., Unger, N., and Bauer, S. E.: Improved Attribution of Climate Forcing to Emissions, Science, 326, 716-718, https://doi.org/10.1126/science.1174760, 2009.

Shindell, D. T., Voulgarakis, A., Faluvegi, G., and Milly, G.: Precipitation response to regional radiative forcing, Atmos. Chem. Phys., 12, 6969–6982, https://doi.org/10.5194/acp-12-6969-2012, 2012.

Smith, L.C., Beilman, D.W., Kremenetski, K.V., Sheng, Y., MacDonald, G.M., Lammers, R.B., Shiklomanov, A.I. and Lapshina, E.D.: Influence of permafrost on water storage in West Siberian peatlands revealed from a new database of soil properties, Permafrost and Peiglac. Process., 23, 69-79, https://doi.org/10.1002/ppp.735, 2012.

Smith, S. L., Riseborough, D. W., and Bonnaventure, P. P. Eighteen Year Record of Forest Fire Effects on Ground Thermal Regimes and Permafrost in the Central Mackenzie Valley, NWT, Canada, Permafrost and Peiglac. Process, 26, 289-303, https://doi.org/10.1002/ppp.1849, 2015.

Smith, C., Perkins, O., and Mistry, J.: Global decline in subsistence oriented and smallholder fire use, Nat. Sustain., 5, 542–551, https://doi.org/10.1038/s41893-022-00867-y, 2022a.

Smith, N. D., Burke, E. J., Schanke Aas, K., Althuizen, I. H. J., Boike, J., Christiansen, C. T., Etzelmüller, B., Friborg, T., Lee, H., Rumbold, H., Turton, R. H., Westermann, S., and Chadburn, S. E.: Explicitly modelling microtopography in permafrost landscapes in a land surface model (JULES

vn5.4_microtopography), Geosci. Model Dev., 15, 3603–3639, https://doi.org/10.5194/gmd-15-3603-2022, 2022b.

Sofan, P., Bruce, D., Jones, E., and Marsden, J.: Detection and Validation of Tropical Peatland Flaming and Smouldering Using Landsat-8 SWIR and TIRS Bands, Remote Sens., 11, 465, https://doi.org/10.3390/rs11040465, 2019.

Sofiev, M.: Chapter 21 - Wildland Fires: Monitoring, Plume Modelling, Impact on Atmospheric Composition and Climate. In: Developments in Environmental Science, edited by: Matyssek, R., Clarke, N., Cudlin, P., Mikkelsen, T. N., Ruovinen, J-P., Wieser, G., and Paoletti, E., Volume 13, 451-472, https://doi.org/10.1016/B978-0-08-098349-3.00021-9, 2013.

Spivakovsky, C. M., Logan, J. A., Montzka, S. A., Balkanski, Y. J., Foreman-Fowler, M., Jones, D. B. A., Horowitz, L. W., Fusco, A. C., Brenninkmeijer, C. A. M., Prather, M. J., Wofsy, S. C., and McElroy, M. B.: Three-dimensional climatological distribution of tropospheric OH: Update and evaluation, J. Geophys. Res., 105, 8931-8980, https://doi.org/10.1029/1999JD901006, 2000.

Stein, O., Schultz, M. G., Bouarar, I., Clark, H., Huijnen, V., Gaudel, A., George, M., and Clerbaux, C.: On the wintertime low bias of Northern Hemisphere carbon monoxide found in global model simulations, Atmos. Chem. Phys., 14, 9295–9316, https://doi.org/10.5194/acp-14-9295-2014, 2014.

Stocker, B. D., Spahni, R., and Joos, F.: DYPTOP: a cost-efficient TOPMODEL implementation to simulate sub-grid spatio-temporal dynamics of global wetlands and peatlands, Geosci. Model Dev., 7, 3089–3110, https://doi.org/10.5194/gmd-7-3089-2014, 2014.

Stocks, B. J., Mason, J. A., Todd, J. B., Bosch, E. M., Wotton, B. M., Amiro, B. D., Flannigan, M. D., Hirsch, K. G., Logan, K. A., Martell, D. L., and Skinner, W. R.: Large forest fires in Canada, 1959-1997, 108, 1849, https://doi.org/10.1029/2001JD000484, 2002.

Stockwell, C. E., Jayarathne, T., Cochrane, M. A., Ryan, K. C., Putra, E. I., Saharjo, B. H., Nurhayati, A. D., Albar, I., Blake, D. R., Simpson, I. J., Stone, E. A., and Yokelson, R. J.: Field measurements of trace gases and aerosols emitted by peat fires in Central Kalimantan, Indonesia, during the 2015 El Niño, Atmos. Chem. Phys., 16, 11711–11732, https://doi.org/10.5194/acp-16-11711-2016, 2016.

Stone, R. S., Anderson, G. P., Shettle, E. P., Andrews, E., Loukachine, K., Dutton, E. G., Schaaf, C., and Roman, M. O. III.: Radiative impact of boreal smoke in the Arctic: Observed and modelled, J. Geophys. Res.: Atmos., 113, D14S16, https://doi.org/10.1029/2007JD009657, 2008.

Stroppiana, D., Brivio, P. A., Grégoire, J.-M., Liousse, C., Guillaume, B., Granier, C., Mieville, A., Chin, M., and Pétron, G.: Comparison of global inventories of CO emissions from biomass burning derived from remotely sensed data, Atmos. Chem. Phys., 10, 12173–12189, https://doi.org/10.5194/acp-10-12173-2010, 2010.

Susskind, J., Barnet, C. D., and Blaisdell, J. M.: Retrieval of atmospheric and surface parameters from AIRS/AMSU/HSB data in the presence of clouds, IEEE Trans. Geosci. Remote Sens., 41, 390-409, https://doi.org/10.1109/TGRS.2002.808236, 2003.

Swindles, G. T., Morris, P. J., Mullan, D. J., Payne, R. J., Roland, T. P., Amesbury, M. J., Lamentowicz, M., Turner, T. E., GallegoSala, A., Sim, T., Barr, I. D., Blaauw, M., Blundell, A., Chambers, F. M., Charman, D. J., Feurdean, A., Galloway, J. M., Gałka, M., Green, S. M., Kajukało, K., Karofeld, E., Korhola, A., Lamentowicz, Ł., Langdon, P., Marcisz, K., Mauquoy, D., Mazei, Y. A., McKeown, M. M., Mitchell, E. A. D., Novenko, E., Plunkett, G., Roe, H. M., Schoning, K., Sillasoo, Ü., Tsyganov, A. N., van der Linden, M., Väliranta, M., and Warner, B.: Widespread drying of European peatlands in recent centuries, Nat. Geosci., 12, 922–928, https://doi.org/10.1038/s41561-019-0462-z, 2019.

Talucci, A. C., Loranty, M. M., and Alexander, H. D.: Siberian taiga and tundra fire regimes from 2001–2020, Environ. Res. Lett., 17, 025001, https://doi.org/10.1088/1748-9326/ac3f07, 2022.

Tape, K. D., Guistine, D. D., Ruess, R. W., Adams, L. G., and Clark, J. A.: Range Expansion of Moose in Arctic Alaska Linked to Warming and Increased Shrub Habitat, PLOS ONE, 11, e0160049, https://doi.org/10.1371/journal.pone.0152636, 2016.

Tarnocai, C.: The Impact of Climate Change on Canadian Peatlands. Can. Water Resour. J., 34, 453–466, https://doi.org/10.4296/cwrj3404453, 2009.

Teakles, A. D., So, R., Ainslie, B., Nissen, R., Schiller, C., Vingarzan, R., McKendry, I., Macdonald, A. M., Jaffe, D. A., Bertram, A. K., Strawbridge, K. B., Leaitch, W. R., Hanna, S., Toom, D., Baik, J., and Huang, L.: Impacts of the July 2012 Siberian fire plume on air quality in the Pacific Northwest, Atmos. Chem. Phys., 17, 2593–2611, https://doi.org/10.5194/acp17-2593-2017, 2017.

Teckentrup, L., Harrison, S. P., Hantson, S., Heil, A., Melton, J. R., Forrest, M., Li, F., Yue, C., Arneth, A., Hickler, T., Sitch, S., and Lasslop, G.: Response of simulated burned area to historical changes in environmental and anthropogenic factors: a comparison of seven fire models, Biogeosciences, 16, 3883–3910, https://doi.org/10.5194/bg-16-3883-2019, 2019.

Teixeira, J. C., Folberth, G. A., O'Connor, F. M., Unger, N., and Voulgarakis, A.: Coupling interactive fire with atmospheric composition and climate in the UK Earth System Model, Geosci. Model Dev., 14, 6515–6539, https://doi.org/10.5194/gmd-14-6515-2021, 2021.

Teixeira, J. C. M., Burton, C., Kelly, D. I., Folberth, G. A., O'Connor, F. M., Betts, R. A., and Voulgarakis, A.: Representing socio-economic factors in the INFERNO global fire model using the Human Development Index, Biogeosciences Discuss. [preprint], https://doi.org/10.5194/bg-2023-136, 2023.

Tian, H., Lu, C., Ciais, P., Michalak, A. M., Canadell, J. G., Saikawa, E., Huntzinger, D. N., Gurney, K. R., Sitch, S., Zhang, B., Yang, J., Bousquet, P., Bruhwiler, L., Chen, G., Dlugokencky, E., Friedlingstein, P., Melillo, J., Pan, S., Poulter, B., Prinn, R., Saunois, M., Schwalm, C. R., and Wofsy, S. C.: The terrestrial biosphere as a net source of greenhouse gases to the atmosphere, Nature, 531, 225-228, https://doi.org/10.1038/nature16946, 2016.

Tian, C., Yue, X., Zhu, J., Liao, H., Yang, Y., Lei, Y., Zhou, X., Zhou, H., Ma, Y., and Cao, Y.: Fire–climate interactions through the aerosol radiative effect in a global chemistry–climate–vegetation model, Atmos. Chem. Phys., 22, 12353–12366, https://doi.org/10.5194/acp-22-12353-2022, 2022.

Thoman, R. L., Moon, T. A., and Bruckenmiller, M. L.: Arctic Report Card 2023 https://doi.org/10.25923/5vfa-k694, 2023.

Thomas, J. L., Polashenski, C. M., Soja, A. J., Marelle, L., Casey, K. A., Choi, H. D., Raut, J-C., Wiedinmyer, C., Emmons, L. K., Fast, J. D., Pelon, J., Law, K. S., Flanner, M. G., and Dibb, J. E.: Quantifying black carbon deposition over the Greenland ice sheet from forest fires in Canada, Geophys. Res. Lett., 44, 7965– 7974, https://doi.org/10.1002/2017GL073701, 2017.

Thompson, D. K., Simpson, B. N., Whitman, E., Barber, Q. E., and Parisien, M.-A.: Peatland Hydrological Dynamics as A Driver of Landscape Connectivity and Fire Activity in the Boreal Plain of Canada, Forests, 10, 534, https://doi.org/10.3390/f10070534, 2019.

Thonicke, K., Venevsky, S., Sitch, S., and Cramer, W.: The Role of Fire Disturbance for Global Vegetation Dynamics: Coupling Fire into a Dynamic Global Vegetation Model, Glob. Ecol. Biogeogr., 10, 661-677, https://doi.org/10.1046/j.1466-822X.2001.00175.x, 2001.

Thonicke, K., Spessa, A., Prentice, I. C., Harrison, S. P., Dong, L., and Carmona-Moreno, C.: The influence of vegetation, fire spread and fire behaviour on biomass burning and trace gas emissions: results from a process-based model, Biogeosci., 7, 1991–2011, https://doi.org/10.5194/bg-7-1991-2010, 2010.

Thornhill, G. D., Collins, W. J., Kramer, R. J., Olivié, D., Skeie, R. B., O'Connor, F. M., Abraham, N. L., Checa-Garcia, R., Bauer, S. E., Deushi, M., Emmons, L. K., Forster, P. M., Horowitz, L. W., Johnson, B., Keeble, J., Lamarque, J.-F., Michou, M., Mills, M. J., Mulcahy, J. P., Myhre, G., Nabat, P., Naik, V., Oshima, N., Schulz, M., Smith, C. J., Takemura, T., Tilmes, S., Wu, T., Zeng, G., and Zhang, J.: Effective radiative forcing from emissions of reactive gases and aerosols – a multi-model comparison, Atmos. Chem. Phys., 21, 853–874, https://doi.org/10.5194/acp-21-853-2021, 2021.

Tomshin, O., and Solovyev, V.: Synoptic weather patterns during fire spread events in Siberia, Sci. Tot. Environ., 921, 171205, https://doi.org/10.1016/j.scitotenv.2024.171205, 2024.

Trettin, C. C., Laiho, R., Minkkinen, K., and Laine, J.: Influence of climate change factors on carbon dynamics in northern forested peatlands, Can. J. Soil Sci., 86, 296-280, https://doi.org/10.4141/S05-089, 2006.

Turetsky, M. R., and Wieder, R. K. A direct approach to quantifying organic matter lost as a result of peatland wildfire, Can. J. For. Res., 31, 363-366, https://doi.org/10.1139/x00-170, 2001.

Turetsky, M. R., Amiro, B., Bosch, E. and Bhatti, J.: Historical burn area in peatlands and its relationship to fire weather in western Canada, Glob. Biogeochem. Cycl., 18, GB4014, https://doi.org/10.1029/2004GB002222, 2004.

Turetsky, M. R., Donahue, W. F., and Benscoter, B. W.: Experimental drying intensifies burning and carbon losses in a northern peatland, Nat. Commun., 2, 514, https://doi.org/10.1038/ncomms1523, 2011a.

Turetsky, M. R., Kane, E. S., Harden, J. W., Ottmar, R. D, Manies, K. L., Hoy, E., and Kasischke, E. S.: Recent acceleration of biomass burning and carbon losses in Alaskan forests and peatlands, Nat. Geosci., 4, 27–31, https://doi.org/10.1038/NGEO1027, 2011b.

Turetsky, M. R., Benscoter, B., Page, S., Rein, G., van der Werf, G. R., and Watts, A.: Global vulnerability of peatlands to fire and carbon loss, Nat. Geosci., 8, 11–14, https://doi.org/10.1038/ngeo2325, 2015.

Turetsky, M. R., Abbott, B. W., Jones, M. C., Walter Anthony, K., Olefeldt, D., Schuur, E. A. G., Grosse, G., Kuhry, P., Hugelius, G., Koven, C., Lawrence, D. M., Gibson, C., Sannel, A. B. K., and McGuire, A. D.: Carbon release through abrupt permafrost thaw, Nature Geosci., 13, 138-143, https://doi.org/10.1038/s41561-019-0526-0, 2020.

Turquety, S., Logan, J. A., Jacob, D. J., Hudman, R. C., Leung, F. Y., Heald, C. L., Yantosca, R. M., Wu, S., Emmons, L. K., Edwards, D. P., and Sachse, G. W.: Inventory of boreal fire emissions for North America in 2004: Importance of peat burning and pyroconvective injection, J. Geophys. Res., 112, D12S03, https://doi.org/10.1029/2006JD007281, 2007.

UNEP: Global Peatlands Assessment – The State of the World's Peatlands: Evidence for action toward the conservation, restoration, and sustainable management of peatlands. Main Report, Global Peatlands Initiative, United Nations Environment Programme, Nairobi, https://doi.org/10.59117/20.500.11822/41222, 2022a.

UNEP: Spreading like Wildfire – The Rising Threat of Extraordinary Landscape Fires. A UNEP Rapid Response Assessment. Nairobi, available from: https://www.unep.org/resources/report/spreading-wildfire-rising-threat-extraordinary-landscape-fires, last access 29/07/2024, 2022b.

Urbanski, S.: Wildland fire emissions, carbon, and climate: Emission factors, Forest Ecol. Manage., 217, 51–60, https://doi.org/10.1016/j.foreco.2013.05.045, 2014.

van Vuuren, D. P., Edmonds, J., Kainuma, M., Riahi, K., Thomson, A., Hibbard, K., Hurtt, G. C., Kram, T., Krey, V., Lamarque, J.-F., Masui, T., Meinshausen, M., Nakicenovic, N., Smith, S. J., and Rose, S. K.: The representative concentration pathways: an overview, Clim. Change, 109, 5, https://doi.org/10.1007/s10584-011-0148-z, 2011.

van Vuuren, D. P., Kriegler, E., O'Niell, B.C., Ebi, K. L., Riahi, K., Carter, T. R., Edmonds, J., Hallegatter, S., Kram, T., Mathur, R., and Winkler, H.: A new scenario framework for Climate Change Research: scenario matrix architecture, Climatic Change, 122, 373-386, https://doi.org/10.1007/s10584-013-0906-1, 2014.

van Vuuren, D. P., Riahi, K., Calvin, K., Dellink, R., Emmerling, J., Fujimori, S., KC, S., Kriegler, E., and O'Neill, B.: The Shared Socio-economic Pathways: Trajectories for human development and global environmental change, Global Environmental Change, 42, 148-152, https://doi.org/10.1016/j.gloenvcha.2016.10.009, 2017.

van der Velde, I. R., van der Werf, G. R., Houweling, S., Eskes, H. J., Veefkind, J. P., Borsdorff, T., and Aben, I.: Biomass burning combustion efficiency observed from space using measurements of CO and NO2 by the TROPOspheric Monitoring Instrument (TROPOMI), Atmos. Chem. Phys., 21, 597–616, https://doi.org/10.5194/acp-21-597-2021, 2021.

van der Werf, G. R., Randerson, J. T., Giglio, L., Collatz, G. J., Mu, M., Kasibhatla, P. S., Morton, D. C., DeFries, R. S., Jin, Y., and van Leeuwen, T. T.: Global fire emissions and the contribution of deforestation, savanna, forest, agricultural, and peat fires (1997–2009), Atmos. Chem. Phys., 10, 11707–11735, https://doi.org/10.5194/acp-10-11707-2010, 2010.

van der Werf, G. R., Randerson, J. T., Giglio, L., van Leeuwen, T. T., Chen, Y., Rogers, B. M., Mu, M., van Marle, M. J. E., Morton, D. C., Collatz, G. J., Yokelson, R. J., and Kasibhatla, P. S.: Global fire emissions estimates during 1997–2016, Earth Syst. Sci. Data, 9, 697–720, https://doi.org/10.5194/essd-9-697-2017, 2017.

van Geffen, J. H. G. M., Eskes, H. J., Boersma, K. F., Maasakkers, J. D., and Veefkind, J. P.: TROPOMI ATBD of the total and tropospheric NO2 data products, issue 1.2.0 edn., s5P-KNMI-L2-0005-RP, available from: https://sentinel.esa.int/documents/247904/2476257/Sentinel-5P-TROPOMI-ATBD-NO2-data-products, last access: 01/08/2024, 2018.

van Geffen, J., Boersma, K. F., Eskes, H., Sneep, M., ter Linden, M., Zara, M., and Veefkind, J. P.: S5P TROPOMI NO2 slant column retrieval: method, stability, uncertainties and comparisons with OMI, Atmos. Meas. Tech., 13, 1315–1335, https://doi.org/10.5194/amt-13-1315-2020, 2020.

van Geffen, J., Eskes, H., Compernolle, S., Pinardi, G., Verhoelst, T., Lambert, J.-C., Sneep, M., ter Linden, M., Ludewig, A., Boersma, K. F., and Veefkind, J. P.: Sentinel-5P TROPOMI NO2 retrieval: impact of version v2.2 improvements and comparisons with OMI and ground-based data, Atmos. Meas. Tech., 15, 2037–2060, https://doi.org/10.5194/amt-15-2037-2022, 2022a.

Van Geffen, J. H. G. M., Eskes, H. J., Boersma, K. F., and Veefkind, J. P.: TROPOMI ATBD of the total and tropospheric NO2 data products, available from: https://sentinels.copernicus.eu/documents/247904/2476257/Sentinel-5P-TROPOMI-ATBD-NO2-data-products, last access: 31/07/2024, 2022b.

van Wees, D., van der Werf, G. R., Randerson, J. T., Rogers, B. M., Chen, Y., Veraverbeke, S., Giglio, L., and Morton, D. C.: Global biomass burning fuel consumption and emissions at 500 m spatial resolution based on the Global Fire Emissions Database (GFED), Geosci. Model Dev., 15, 8411–8437, https://doi.org/10.5194/gmd-15-8411-2022, 2022.

Veefkind, J. P., Aben, I., McMullan, K., Förster, H., de Vries, J., Otter, G., Claas, J., Eskes, H. J., de Haan, J. F., Kleipool, Q., van Weele, M., Hasekamp, O., Hoogeveen, R., Landgraf, J., Snel, R., Tol, P., Ingmann, P., Voors, R., Kruizinga, B., Vink, R., Visser, H., and Levelt, P. F. TROPOMI on the ESA Sentinel-5 Precursor: A GMES mission for global observations of the atmospheric composition for climate, air quality and ozone layer applications, Remote Sens. Environ., 120, 70-83, https://doi.org/10.1016/j.rse.2011.09.027, 2012.

Veraverbeke, S., Rogers, B. M., Goulden, M. L., Jandt, R. R., Miller, C. E., Wiggins, E. B., and Randerson, J. T.: Lightning as a major driver of recent large fire years in North American boreal forests, Nat. Clim. Change, 7, 529–534, https://doi.org/10.1038/NCLIMATE3329, 2017.

Veraverbeke, S., Delcourt, C. J. F., Kukavskaya, E., Mack, M., Walker, X., Hessilt, T., Rogers, B., and Scholten, R. C.: Direct and longer-term carbon emissions from arctic-boreal fires: A short review of recent advances, Curr. Opin. Environ. Sci. Health, 23, 100277, https://doi.org/10.1016/j.coesh.2021.100277, 2021.

Vidot, J., Landgraf, J., Hasekamp, O. P., Butz, A., Galli, A., Tol, P., and Aben, I.: Carbon monoxide from shortwave infrared reflectance measurements: A new retrieval approach for clear sky and partially cloudy atmospheres, Remot. Sens. Environ., 120, 255-266, https://doi.org/10.1016/j.rse.2011.09.032, 2012.

von Clarmann, T., Degenstein, D. A., Livesey, N. J., Bender, S., Braverman, A., Butz, A., Compernolle, S., Damadeo, R., Dueck, S., Eriksson, P., Funke, B., Johnson, M. C., Kasai, Y., Keppens, A., Kleinert, A., Kramarova, N. A., Laeng, A., Langerock, B., Payne, V. H., Rozanov, A., Sato, T. O., Schneider, M., Sheese, P., Sofieva, V., Stiller, G. P., von Savigny, C., and Zawada, D.:

Overview: Estimating and reporting uncertainties in remotely sensed atmospheric composition and temperature, Atmos. Meas. Tech., 13, 4393–4436, https://doi.org/10.5194/amt-13-4393-2020, 2020.

Voulgarakis, A. and Field, R. D.: Fire Influences on Atmospheric Composition, Air Quality and Climate, Curr. Pollut. Rep., 1, 70– 81, https://doi.org/10.1007/s40726-015-0007-z, 2015.

Voulgarakis, A., Marlier, M. E., Faluvegi, G., Shindell, D. T., Tsigaridis, K., and Mangeon, S.: Interannual variability of tropospheric trace gases and aerosols: The role of biomass burning emissions, J. Geophys. Res.-Atmos., 12, 7157–7173, https://doi.org/10.1002/2014JD022926, 2015.

Wagner, A., Bennouna, Y., Blechschmidt, A.-M., Brasseur, G., Chabrillat, S., Christophe, Y., Errera, Q., Eskes, H., Flemming, J., Hansen, K. M., Inness, A., Kapsomenakis, J., Langerock, B., Richter, A., Sudarchikova, N., Thouret, V., and Zerefos, C.: Comprehensive evaluation of the Copernicus Atmosphere Monitoring Service (CAMS) reanalysis against independent observations: Reactive gases, Elem. Sci. Anth., 9, 00171, https://doi.org/10.1525/elementa.2020.00171, 2021.

Walker, X. J., Baltzer, J. L., Cumming, S. G., Day, N. J., Ebert, C., Goetz, S., Johnstone, J. F., Potter, S., Rogers, B. M., Schuur, E. A. G., Turetsky, M. R., and Mack, M. C. Increasing wildfires threaten historic carbon sink of boreal forest soils, Nature, 572, 520-523, https://doi.org/10.1038/s41586-019-1474-y, 2019.

Walker, X. J., Baltzer, J. L., Bourgeau-Chaves, L. L., Day, N. J., de Groot, W. J., Dieleman, C., Hoy, E. E., Johnstone, J. F., Kane, E. S., Parisien, M. A., Potter, S., Rogers, B. M., Turetsky, M. R., Veraverbeke, S., Whitman, E., and Mack, M. C.: ABoVE: Synthesis of Burned and Unburned Forest Site Data, AK and Canada, 1983–2016, Oak Ridge, Tennessee, USA, ORNL DAAC [data set], https://doi.org/10.3334/ORNLDAAC/1744, 2020.

Walsh, J. E., Ballinger, T. J., Euskirchen, E. S., Hanna, E., Mard, J., Overland, J. E., Tangen, H., and Vihma, T.: Extreme weather and climate events in northern areas: A review, Earth-Sci. Rev., 209, 103324, https://doi.org/10.1016/j.earscirev.2020.103324, 2020.

Walsh, J. E., Bigalke, S., McAfee, S. A., Lader, R., Serreze, M. C., and Ballinger, T. J.L Precipitation, In: Arctic Report Card 2023, edited by: Thoman, R. L., Moon, T. A., Druckenmiller, M. L., https://doi.org/10.25923/hcm7-az41, 2023.

Wan, N., Xiong, X., Kluitenberg, G. J., Hutchinson, J. M. S., Aiken, R., Zhao, H., and Lin, X.: Estimation of biomass burning emission of NO_2 and CO from 2019–2020 Australia fires based on satellite observations, Atmos. Chem. Phys., 23, 711–724, https://doi.org/10.5194/acp-23-711-2023, 2023.

Wang, X., Thompson, D. K., Marshall, G. A., Tymstra, C., Carr, R., and Flannigan, M. D.: Increasing frequency of extreme fire weather in Canada with climate change, Climatic Change, 130, 573-586, https://doi.org/10.1007/s10584-015-1375-5, 2015.

Wang, X., Parisien, M.-A., Taylor, S. W., Candau, J.-N., Stralberg, D., Marshall, G. A., Little, J. M., and Flannigan, M. D.: Projected changes in daily fire spread across Canada over the next century, Environ. Res. Lett., 12, 025005, https://doi.org/0.1088/1748-9326/aa5835, 2017.

Wang, C., Wang, T., Wang, P., and Rakitin, V.: Comparison and Validation of TROPOMI and OMI NO2 Observations over China, Atmosphere, 11, 636, https://doi.org/10.3390/atmos11060636, 2020a.

Wang, Y., Ma, Y.-F., Eskes, H., Inness, A., Flemming, J., and Brasseur, G. P.: Evaluation of the CAMS global atmospheric trace gas reanalysis 2003–2016 using aircraft campaign observations, Atmos. Chem. Phys., 20, 4493–4521, https://doi.org/10.5194/acp-20-4493-2020, 2020b.

Wang, Y., and Hu, L.: A Theoretical Model of Soil Freezing Characteristic Curve Considering the Freezing of Adsorbed Water and Capillary Water, Water Resour. Res., 59, e2023WR034662, https://doi.org/10.1029/2023WR034662, 2023.

Ward, D. S., Kloster, S., Mahowald, N. M., Rogers, B. M., Randerson, J. T., and Hess, P. G.: The changing radiative forcing of fires: global model estimates for past, present and future, Atmos. Chem. Phys., 12, 10857–10886, https://doi.org/10.5194/acp-12-10857-2012, 2012.

Warszawski, L., Frieler, K., Huber, V., Piontek, F., Serdeczny, O., and Schewe, J.: The Inter-Sectoral Impact Model Intercomparison Project (ISI–MIP): Project framework, PNAS, 111, 3228-3232, http://www.pnas.org/cgi/doi/10.1073/pnas.1312330110, 2014

Wells, C. D., Kasoar, M., Bellouin, N., and Voulgarakis, A.: Local and remote climate impacts of future African aerosol emissions, Atmos. Chem. Phys., 23, 3575–3593, https://doi.org/10.5194/acp-23-3575-2023, 2023.

Wendler, G., Conner, J., Moore, B., Shulski, M., and Stuefer, M.: Climatology of Alaskan wildfires with special emphasis on the extreme year of 2004, Theor. Appl. Climatol., 104, 459–472, https://doi.org/10.1007/s00704-010-0357-9, 2011.

Wiedinmyer, C., Akagi, S. K., Yokelson, R. J., Emmons, L. K., Al-Saadi, J. A., Orlando, J. J., and Soja, A. J.: The Fire INventory from NCAR (FINN): a high resolution global model to estimate the emissions from open burning, Geosci. Model Dev., 4, 625–641, https://doi.org/10.5194/gmd-4-625-2011, 2011.

Wieder, R. K., Scott, K. D., Kamminga, K., Vile, M. A., Vitt, D. H., Bone, T., Xu, B., Benscoter, B. W., and Bhatti, J. S. Postfire carbon balance in boreal bogs of Alberta, Canada, Glob. Change Bio., 15, 63-81, https://doi.org/10.1111/j.1365-2486.2008.01756.x, 2009.

Wiggins, E. B., Andrews, A., Sweeney, C., Miller, J. B., Miller, C. E., Veraverbeke, S., Commane, R., Wofsy, S., Henderson, J. M., and Randerson, J. T.: Boreal forest fire CO and CH4 emission factors derived from tower observations in Alaska during the extreme fire season of 2015, Atmos. Chem. Phys., 21, 8557–8574, https://doi.org/10.5194/acp-21-8557-2021, 2021.

Wilkinson, S. L., Moore, P. A., Flannigan, M. D., Wotton, B. M., and Waddington, J. M.: Did enhanced afforestation cause high severity peat burn in the Fort McMurray Horse River wildfire, Environ. Res. Lett., 13, 014018, https://doi.org/10.1088/1748-9326/aaa136, 2018.

Wilkinson, S. L., Moore, P. A., and Waddington, J. M. Assessing Drivers of Cross-Scale Variability in Peat Smoldering Combustion Vulnerability in Forested Boreal Peatlands, Front. For. Glob. Change, 2, 84, https://doi.org/10.3389/ffgc.2019.00084, 2019.

Wilkinson, S. L., Tekatch, A. M., Markle, C. E., Moore, P. A., and Waddington, J. M. Shallow peat is most vulnerable to high peat burn severity during wildfire, Environ. Res. Lett., 15, 104032, https://doi.org/10.1088/1748-9326/aba7e8, 2020.

Wilkinson, S. L., Andersen, R., Moore, P. A., Davidson, S. J., Granath, G., and Waddington, J. M.: Wildfire and degradation accelerate northern peatland carbon release, Nat. Clim. Change, 13, 456–461, https://doi.org/10.1038/s41558-023-01657-w, 2023.

Winker, D. M., Hunt, W. H., and Hostetler, C. A.: Status and performance of the CALIOP lidar, Laser Radar Techn. Atmos. Sens., https://doi.org/10.1117/12.571955, 2004.

Winton, M.: Amplified Arctic climate change: what does surface albedo feedback have to do with it? Geophys. Res. Lett., 33, L03701, https://doi.org/10.1029/2005GL025244, 2006.

Woollings, T., Barriopedro, D., Methven, J., Son, S.-W., Martius, O., Harvey, B., Sillmann, J., Lupo, A. R., and Seneviratne, S.: Blocking and its Response to Climate Change, Curr. Clim. Change Rep., 4, 287-300, https://doi.org/10.1007/s40641-018-0108-z, 2018.

Wooster, M. J., Gaveau, D. L. A., Salim, M. A., Zhang, T., Xu, W., Green, D. C., Huijnen, V., Murdiyarso, D., Gunawan, D., Borchard, N., Schirrmann, M., Main, B., and Sepriando, A. New Tropical Peatland Gas and Particulate Emissions Factors Indicate 2015 Indonesian Fires Released Far More Particulate Matter (but Less Methane) than Current Inventories Imply, Remote Sens., 10, 495, https://doi.org/10.3390/rs10040495, 2018.

Wooster, M. J., Roberts, G. J., Giglio, L., Roy, D. P., Freeborn, P. H., Boschetti, L., Justice, C., Ichoku, C., Schroeder, W., Davies, D., Smith, A. M. S., Setzer, A., Csiszar, I., Strydom, T., Frost, P., Zhang, T., Xu, W., de Jong, M. C., Johnston, J. M., Ellison, L., Vadrevu, K., Sparks, A. M., Nguyen, H., McCarty, J., Tanpipat, V., Schmidt, C., and San-MIguel-Ayanz, J.: Satellite remote sensing of active fires: History and current status, applications and future requirements, Remote Sensing of Environment, 367, 113695, https://doi.org/10.1016/j.rse.2021.112694, 2021.

WHO: Health Aspects of Air Pollution with Particulate Matter, Ozone and Nitrogen Dioxide, World Health Organisation, Bonn, Germany, available from: https://apps.who.int/iris/handle/10665/107478, last access: 31/07/2024, 2003.

WHO: Air quality guidelines: global update 2005: particulate matter, ozone, nitrogen dioxide and sulfur dioxide, World Health Organisation, Copenhagen, ISBN 92 890 2192 6, 2006.

WHO: Ambient Air Pollution: A Global Assessment of Exposure and Burden of Disease, World Health Organisation, Geneva, available from: https://iris.who.int/bitstream/handle/10665/250141/9789241511353-eng.pdf?sequence=1, last access: 31/07/2024, 2016.

Worden, H. M., Deeter, M. N., Frankenberg, C., George, M., Nichitiu, F., Worden, J., Aben, I., Bowman, K. W., Clerbaux, C., Coheur, P. F., de Laat, A. T. J., Detweiler, R., Drummond, J. R., Edwards, D. P., Gille, J. C., Hurtmans, D., Luo, M., Martínez-Alonso, S., Massie, S., Pfister, G., and Warner, J. X.: Decadal record of satellite carbon monoxide observations, Atmos. Chem. Phys., 13, 837–850, https://doi.org/10.5194/acp-13-837-2013, 2013.

Wu, J.: Response of peatland development and carbon cycling to climate change: a dynamic system modeling approach, Environ. Earth Sci., 65, 141-151, https://doi.org/10.1007/s12665-011-1073-1, 2011.

Xu, J., Morris, P. J., Liu, J., and Holden, J.: PEATMAP: Refining estimates of global peatland distribution based on a meta-analysis, Catena, 160, 134–140, https://doi.org/10.1016/j.catena.2017.09.010, 2018.

Xu, L., Zhu, Q., Riley, W. J., Chen, Y., Wang, H., Ma, P.-L., and Randerson, J. T.: The Influence of Fire Aerosols on Surface Climate and Gross Primary Production in the Energy Exascale Earth System Model (E3SM), J. Climate, 34, 7219–7238, https://doi.org/10.1175/JCLI-D-21-0193.1, 2021.

Xu, W., Scholten, R. C., Hessilt, T. D., Liu, Y., and Veraverbeke, S.: Overwintering fires rising in eastern Siberia, Environ. Res. Lett., 17, 045005, https://doi.org/10.1088/1748-9326/ac59aa, 2022.

Yang, J., Tian, H., Tao, B., Ren, W., Kush, J., Liu, Y., and Wang, Y.: Spatial and temporal patterns of global burned area in response to anthropogenic and environmental factors: Reconstructing global fire

history for the 20th and early 21st centuries, J. Geophys. Res. Biogeosci., 119, 249-263, https://doi.org/10.1002/2013JG002532, 2014a.

Yang, K., Carn, S. A., Ge. C., Wang, J., and Dickerson, R. R.: Advancing measurements of tropospheric NO2 from space: New algorithm and first global results from OMPS, Geophys. Res. Lett., 41, 4777-4786, https://doi.org/10.1002/2014GL060136, 2014b.

Yang, J. and Chen, H.: Natural Downward Smouldering of Peat: Effects of Inorganic Content and Piled Bed Height, Fire Technol., 54, 1219–1247, https://doi.org/10.1007/s10694-018-0737-8, 2018.

Yang, X., Zhao, C., Zhao, W., Fan, H., and Yang, Y.: Characterisation of global fire activity and its spatiotemporal patterns for different land cover types from 2011 to 2020, Environmental Research, 227, 115746, https://doi.org/10.1016/j.envres.2023.115746, 2023.

Yarwood, G., Rao, S., Yocke, M., and Whitten, G.: Updates to the carbon bond chemical mechanism: CB05, Final report to the US EPA, EPA Report Number: RT-0400675, http://www.camx.com, last access: 31/07/2024, 2005.

Ye, H. Yang, D., Behrangi, A., Stuefer, S. L., Pan, X., Mekis, E., Dibike, Y., and Walsh, J. E.: Precipitation Characteristics and Changes, In: Arctic Hydrology, Permafrost and Ecosystems, edited by: D. Yang and D. L. Kane, Springer Nature, Switzerland, 25-59, https://doi.org/10.1007/978-3-030-50930-9, 2021.

Yokelson, R. J., Burling, I. R., Urbanski, S. P., Atlas, E. L., Adachi, K., Buseck, P. R., Wiedinmyer, C., Akagi, S. K., Toohey, D. W., and Wold, C. E.: Trace gas and particle emissions from open biomass burning in Mexico, Atmos. Chem. Phys., 11, 6787–6808, https://doi.org/10.5194/acp-11-6787-2011, 2011.

York, A., Bhatt, U. S., Gargulinski, E., Garbinski, Z., Jain, P., Soja, A., Thoman, R. L., and Ziel, R.: Wildland Fire in High Northern Latitudes, in: Arctic Report Card 2020, edited by: Thoman, R. L., Richter-Menge, J., and Druckenmiller, M. L., https://doi.org/10.25923/2gef-3964, 2020.

Yoshikawa, K., Bolton, W. R., Romanovsky, V. E., Fukuda, M., and Hinzman, L. D.: Impacts of wildfire on the permafrost in the boreal forests of interior Alaska, J. Geophys. Res., 18, 8148, https://doi.org/10.1029/2001JD000438, 2002.

Young, A. M., Higuera, P. E., Duffy, P. A., and Hu, F. S.: Climatic thresholds shape northern high-latitude fire regimes and imply vulnerability to future climate change, Ecography, 40, 506-617, https://doi.org/10.1111/ecog.02205, 2017.

Yu, Z., Loisel, J., Brosseau, D. P., Beilman, D. W., and Hunt, S. J.: Global peatland dynamics since the Last Glacial Maximum, Geophys. Res. Lett., 37, L13402, https://doi.org/10.1029/2010GL043584, 2010.

Yu, Z. C.: Northern peatland carbon stocks and dynamics: a review, Biogeosciences, 9, 4071–4085, https://doi.org/10.5194/bg-9-4071-2012, 2012.

Yu, L., and Zhong, S.: Trends in Arctic seasonal and extreme precipitation in recent decades, Theor. Appl. Climatol., 145, 1541-1559, https://doi.org/10.1007/s00704-021-03717-7, 2021.

Yue, C., Ciais, P., Cadule, P., Thonicke, K., Archibald, S., Poulter, B., Hao, W. M., Hantson, S., Mouillot, F., Friedlingstein, P., Maignan, F., and Viovy, N.: Modelling the role of fires in the terrestrial carbon balance by incorporating SPITFIRE into the global vegetation model ORCHIDEE – Part 1: simulating historical global burned area and fire regimes, Geosci. Model Dev., 7, 2747–2767, https://doi.org/10.5194/gmd-7-2747-2014, 2014.

Zhang, X., He, J., Zhang, J., Polyakov, I., Gerdes, R., Inoue, J., and Wu, P.: Enhanced poleward moisture transport and amplified northern high-latitude wetting trend, Nature Clim. Change, 3, 47-51, https://doi.org/10.1038/nclimate1631, 2013.

Zhang, Y., Wolfe, S. A., Morse, P. D., Olthof, I. and Fraser, R. H. Spatiotemporal impacts of wildfire and climate warming on permafrost across a subarctic region, Canada, J. Geophys. Res.: Earth Sci., 120, 2338-2356, https://doi.org/10.1002/2015JF003679, 2015.

Zhang, H., Piilo, S. R., Amesbury, M. J., Charman, D. J., Gallego-Sala, A. V., and Väliranta, M. M.: The role of climate change in regulating Arctic permafrost peatland hydrological and vegetation change over the last millennium, Quat. Sci. Rev., 182, 121-130, https://doi.org/10.1016/j.quascirev.2018.01.003, 2018.

Zhang, Z., Pan, Z., Pan, F., Zhang, J., Han, G., Huang, N., Wang, J., Pan, Y., Wang, Z., and Peng, R.: The Change Characteristics and Interactions of Soil Moisture and Temperature in the Farmland in Wuchuan County, Inner Mongolia, China, Atmosphere, 11, 503, https://doi.org/10.3390/atmos11050503, 2020.

Zhang, Y., Li, Z., Bai, K., Wei, Y., Xie, Y., Zhang, Y., Ou, Y., Cohen, J., Zhang, Y., Peng, Z., Zhang, X., Chen, C., Hong, J., Xu, H., Guang, J., Lv, Y., Li, K., and Li, D.: Satellite remote sensing of atmospheric particulate matter mass concentration: Advances, challenges, and perspectives, Fund. Res., 1, 240-258, https://doi.org/10.1016/j.fmre.2021.04.007, 2021.

Zhang, H., Väliranta, M., Swindles, G. T., Aquino-López, M. A., Mullan, D., Tan, N., Amesbury, M., Babeshko, K. V., Bao, K., Bobrov, A., Chernyshov, V., Davies, M. A., Diaconu, A. C., Feurdean, A., Finkelstein, S. A., Garneau, M., Guo, Z., Jones, M. C., Kay, M., Klein, E. S., Lamentowicz, M.,

Magnan, G., Marcisz, K., Mazei, N., Mazei, Y., Payne, R., Pelletier, N., Piilo, S. R., Pratte, S., Roland, T., Saldaev, D., Shotyk, W., Sim, T. G., Sloan, T. J., Słowinski, M., Talbot, J., Taylor, L., Tsyganov, A. N., Wetterich, S., Xing, W., and Zhao, Y.: Recent climate change has driven divergent hydrological shifts in high-latitude peatlands, Nat. Commun., 13, 4959, https://doi.org/10.1038/s41467-022-32711-4, 2022.

Zhang, Y., Mao, J., Ricciuto, D. M., Jin, M., Yu, Y., Shi, X., Wullschleger, S., Tang, R., and Liu, J.: Global fire modelling and control attributions based on the ensemble machine learning and satellite observations, Sci. Remote Sens., 7, 100088, https://doi.org/10.1016/j.srs.2023.100088, 2023.

Zhao, B. and Zhuang, Q.: Peatlands and their carbon dynamics in northern high latitudes from 1990 to 2300: a process-based biogeochemistry model analysis, Biogeosciences, 20, 251–270, https://doi.org/10.5194/bg-20-251-2023, 2023.

Zhuravleva, T. B., Kabanov, D. M., Nasrtdinov, I. M., Russkova, T. V., Sakerin, S. M., Smirnov, A., and Holben, B. N.: Radiative characteristics of aerosol during extreme fire event over Siberia in summer 2012, Atmos. Meas. Tech., 10, 179–198, https://doi.org/10.5194/amt-10-179-2017, 2017.

Zoltai, S. C.: Cyclic Development of Permafrost in the Peatlands of Northwestern Alberta, Canada, Arctic and Alpine Research, 25, 240-246, https://doi.org/10.2307/1551820, 1993.

Appendices

1. Supplementary information for Chapter 3

Table S1: Temporal correlation coefficients of BA over the 2010 to 2014 period, in INFERNO, and the two INFERNO-peat runs, with the three observational datasets.

Model	R (GFED4s)	R (GFED5)	R (fireCCILT11)
INFERNO	0.636	0.937	0.681
INFERNO-peat LIS-OTD	0.312	-0.184	0.241
INFERNO-peat WGLC	0.659	0.302	0.294

Table S2: Carbon emission averages, interannual variability and temporal correlations between models and observations over 2010 to 2014, broken down by subregion.

	Avg annual C emissions (Tg)	std	cv	R GFED4s	GFED500m	GFAS
Alaska						
INFERNO	3.849	0.343	0.089	0.648	0.577	0.916
INFERNO-peat LIS-OTD	0.374	0.096	0.644	0.572	0.915	0.374
INFERNO-peat WGLC	0.348	0.090	0.648	0.577	0.916	0.348
GFED4s	2.379	2.472	1.039		0.996	0.861
GFED 500m - total	4.901	4.358	0.889	0.996		0.811
GFAS	2.492	3.247	1.303	0.861	0.811	
Western Canada						
INFERNO	17.220	1.254	0.073	-0.255	-0.914	-0.037
INFERNO-peat LIS-OTD	83.674	16.411	0.196	0.221	-0.414	0.329
INFERNO-peat WGLC	28.956	4.848	0.167	0.824	0.142	0.849
GFED4s	70.783	39.125	0.553		0.444	0.972
GFED 500m - total	78.128	27.395	0.351	0.444		0.227
GFAS	99.386	39.053	0.393	0.972	0.227	
Eastern Canada						
INFERNO	7.123	0.232	0.033	0.188	0.297	-0.004
INFERNO-peat LIS-OTD	26.517	6.531	0.246	0.111	-0.066	0.344
INFERNO-peat WGLC	9.922	1.353	0.136	0.067	-0.091	0.275
GFED4s	7.132	10.618	1.489		0.978	0.969
GFED 500m - total	23.005	30.573	1.329	0.978		0.900
GFAS	9.243	12.037	1.302	0.969	0.900	
Fennoscandia						
INFERNO	12.489	1.697	0.136	-0.273	-0.242	-0.420
INFERNO-peat LIS-OTD	23.020	4.132	0.180	-0.539	-0.470	-0.673
INFERNO-peat WGLC	15.485	4.214	0.272	-0.191	-0.217	-0.363
GFED4s	2.496	2.853	1.143		0.986	0.980
GFED 500m - total	2.219	1.985	0.895	0.986		0.968
GFAS	15.987	29.518	1.846	0.980	0.968	
Western Russia						

INFERNO	13.982	3.695	0.264	0.986	0.990	0.991
INFERNO-peat LIS-OTD	23.993	5.293	0.221	0.598	0.496	0.498
INFERNO-peat WGLC	15.689	3.537	0.225	0.993	0.969	0.988
GFED4s	2.865	1.748	0.610		0.972	0.986
GFED 500m - total	5.148	5.208	1.012	0.972		0.996
GFAS	1.338	1.244	0.930	0.986	0.996	
Central Russia						
INFERNO	22.682	3.388	0.149	0.990	0.920	0.959
INFERNO-peat LIS-OTD	118.036	40.404	0.342	0.408	0.668	0.501
INFERNO-peat WGLC	40.372	11.273	0.279	0.543	0.746	0.659
GFED4s	46.484	34.675	0.746		0.935	0.986
GFED 500m - total	77.258	63.823	0.826	0.935		0.969
GFAS	40.114	38.351	0.956	0.986	0.969	
Eastern Russia						
INFERNO	18.371	1.154	0.063	0.421	0.329	0.045
INFERNO-peat LIS-OTD	23.498	1.329	0.057	0.807	0.584	0.631
INFERNO-peat WGLC	19.189	1.092	0.057	0.650	0.459	0.260
GFED4s	78.207	30.153	0.386		0.893	0.808
GFED 500m - total	148.959	48.600	0.326	0.893		0.918
GFAS	135.688	66.059	0.487	0.808	0.918	



Figure S1: Carbon emissions timeseries graphs comparing aboveground burning from INFERNO and the GFED500m aboveground product, and belowground burning from the peat only INFERNO-peat runs and the

GFED500m belowground product. Results are broken down by subregion, from 2001 to 2014. Note that the WGLC INFERNO-peat runs are only for 2010 to 2014. Dashed lines indicate observations and solid lines represent models.

2. Supplementary information for Chapter 4

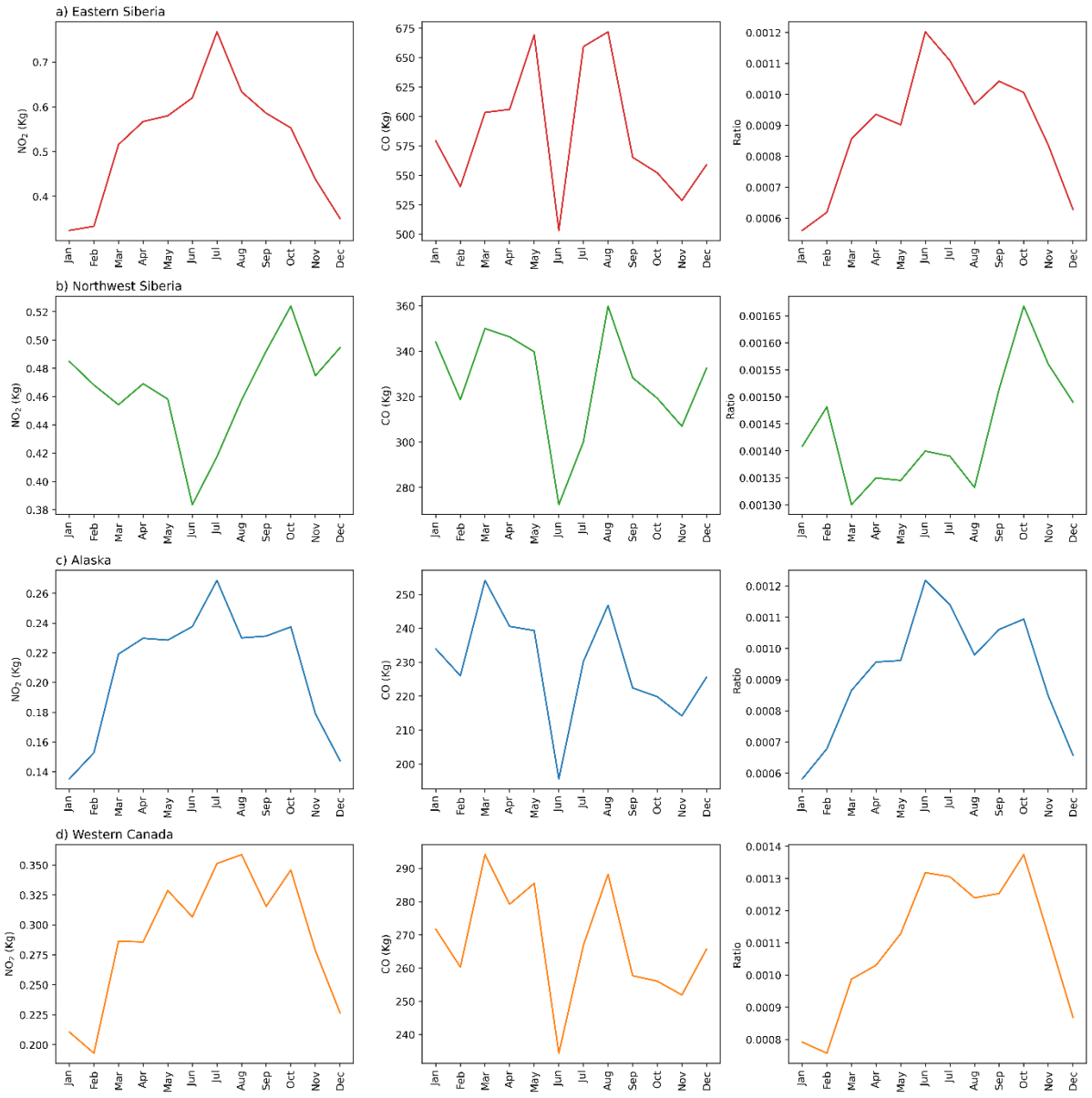


Figure S2: Seasonality of NO_2, CO and the NO_2:CO ratio averaged over the monthly data from 2018-2021 for CAMS reanalysis in eastern Siberia (a), northwest Siberia (b), Alaska (c), and western Canada (d).

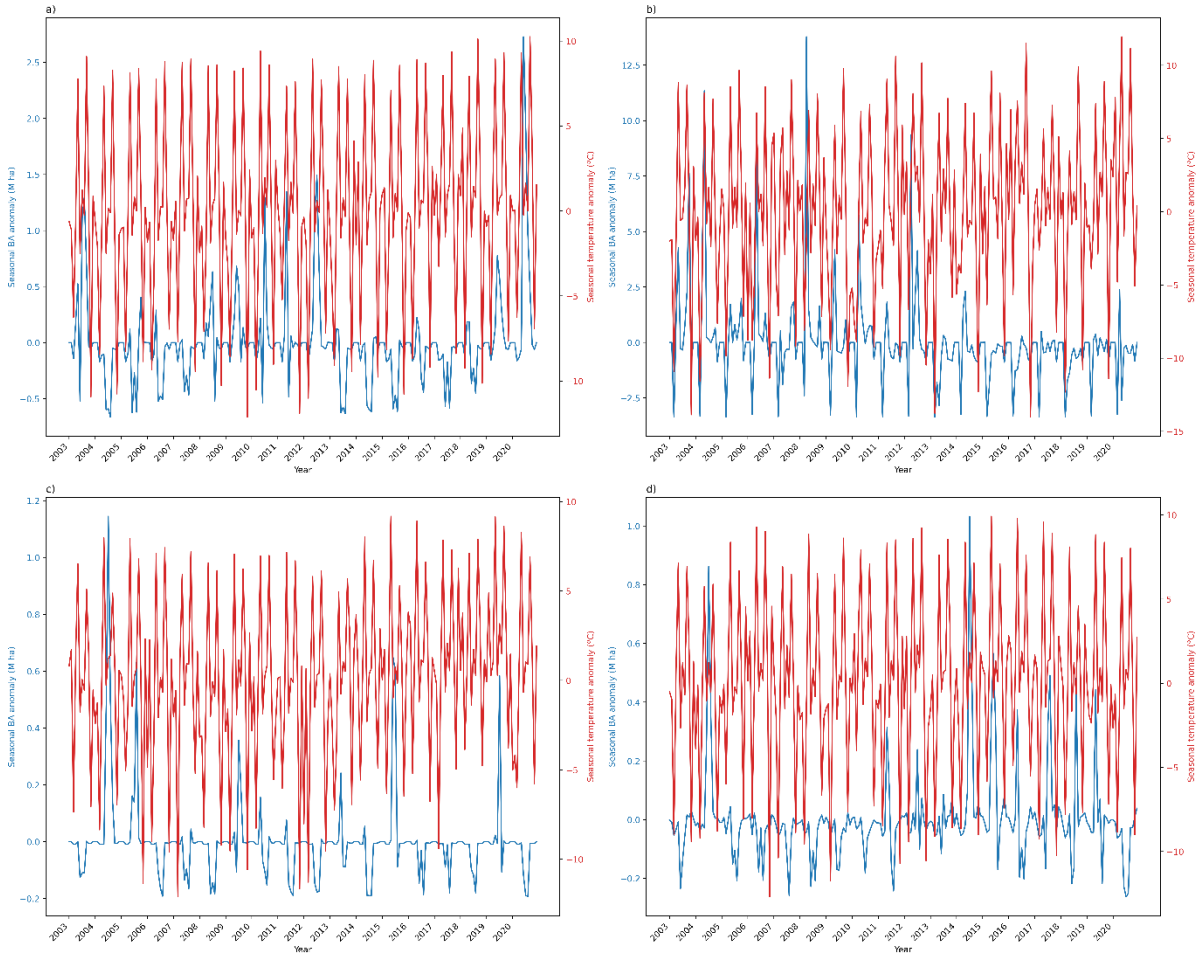


Figure S3: Monthly burnt area and temperature anomalies from 2003 to 2020 in a) eastern Siberia, b) northwest Siberia, c) Alaska, and d) western Canada.

Table S3: Monthly changes in BA, peat BA, peat percentage of BA, TROPOMI NO2, TROPOMI CO and TROPOMI NO2:CO between 2019 and 2020 in each subregion. Highlighted cells indicate months where we see >1 M ha change in peat BA (green), or >5% change in peat fire percentage (purple).

Month	Change BA	Change peat BA	Change peat %	Change NO_2	Change CO	Change ratio
Eastern Siberia						
Jan	0.000	0.000	0.000	-0.002	1.160	-0.00003
Feb	0.000	0.000	0.000	-0.002	2.137	-0.00002
Mar	-0.005	-0.001	2.081	-0.005	1.792	-0.00002
Apr	-0.086	-0.003	1.583	-0.003	9.099	-0.00001
May	-0.189	-0.014	0.597	-0.006	1.708	-0.00003
Jun	1.953	0.217	1.023	0.013	5.167	0.00007
Jul	1.378	0.164	2.060	0.012	8.537	0.00005
Aug	0.703	0.073	1.752	0.000	-53.338	0.00004
Sep	0.427	0.013	-5.939	0.008	2.963	0.00004
Oct	0.037	0.003	0.321	0.002	20.480	0.00000
Nov	-0.001	0.000	0.000	0.002	3.608	0.00002
Dec	0.000	0.000	0.000	0.004	0.830	0.00007
Northwest Siberia						
Jan	0.000	0.000	0.000	0.004	-0.830	0.00009
Feb	0.000	0.000	0.000	0.003	0.966	0.00002
Mar	0.058	0.001	-0.073	-0.009	1.026	-0.00006
Apr	2.247	0.223	3.139	0.008	9.015	0.00005

May	-2.990	-0.073	3.433	0.003	3.230	0.00002
Jun	0.342	0.003	-5.208	0.008	3.374	0.00007
Jul	-0.349	0.040	8.235	-0.002	-3.826	-0.00001
Aug	-0.425	0.032	12.698	0.001	-14.473	0.00004
Sep	-0.076	0.006	2.182	0.004	2.872	0.00002
Oct	-0.223	-0.011	-0.660	-0.008	13.006	-0.00011
Nov	0.016	0.001	2.352	-0.004	-1.078	-0.00005
Dec	-0.001	0.000	-27.463	-0.005	3.002	-0.00024
Alaska						
Jan	0.000	0.000	0.000	-0.001	-3.020	-0.00003
Feb	0.000	0.000	0.000	-0.001	2.577	-0.00002
Mar	0.000	0.000	-3.171	-0.004	3.526	-0.00005
Apr	0.000	0.000	-9.313	-0.002	1.343	-0.00002
May	-0.026	0.000	6.693	-0.001	6.520	-0.00002
Jun	-0.111	-0.001	10.791	-0.002	-2.971	-0.00003
Jul	-0.772	-0.060	0.639	-0.001	-5.409	0.00000
Aug	-0.087	-0.009	-4.127	0.001	-10.816	0.00003
Sep	-0.008	-0.001	-6.854	-0.001	-3.413	-0.00001
Oct	0.000	0.000	-4.032	-0.003	7.951	-0.00005
Nov	0.000	0.000	0.000	0.003	4.712	0.00005
Dec	0.000	0.000	0.000	-0.005	0.970	-0.00052
Western Canada						
Jan	0.008	0.001	-0.116	0.008	-1.960	0.00018
Feb	0.012	0.001	5.747	-0.002	-1.508	-0.00002
Mar	-0.019	-0.001	-4.770	-0.005	3.772	-0.00005
Apr	-0.012	-0.001	-2.668	-0.001	2.583	-0.00001
May	-0.473	-0.084	-8.817	-0.003	2.203	-0.00003
Jun	-0.219	-0.037	-1.516	0.000	-2.957	0.00001
Jul	-0.332	-0.045	0.391	-0.002	-5.951	-0.00002
Aug	-0.034	-0.008	-9.912	0.004	-21.354	0.00009
Sep	-0.042	0.001	8.158	0.000	-6.461	0.00001
Oct	-0.033	-0.001	0.493	-0.001	10.674	-0.00003
Nov	0.022	0.003	0.855	0.008	3.817	0.00014
Dec	0.039	0.009	8.307	-0.005	-1.163	-0.00017

Table S4: Annual peat BA (M ha) estimated from GFED5 and modelled by INFERNO-peat, and the annual CAMS NO2:CO ratio in a) eastern Siberia, b) northwest Siberia, c) Alaska, and d) western Canada.

Year	GFED5 peat BA (M ha)	INFERNO-peat peat BA (M ha)	CAMS NO_2:CO
a) Eastern Siberia			
2003	0.575	0.276	0.00074
2004	0.028	0.336	0.00072
2005	0.128	0.233	0.00073
2006	0.084	0.377	0.00071
2007	0.103	0.307	0.00077
2008	0.223	0.449	0.00078
2009	0.348	0.292	0.00083
2010	0.438	0.390	0.00086
2011	0.170	0.346	0.00086
2012	0.382	0.433	0.00081
2013	0.084	0.170	0.00081
2014	0.053	0.199	0.00087
b) Northwest Siberia			

2003	0.941	7.640	0.00139
2004	1.535	6.799	0.00134
2005	1.024	4.966	0.00134
2006	1.292	5.735	0.00125
2007	0.495	5.985	0.00129
2008	1.221	9.091	0.00129
2009	0.946	6.317	0.00138
2010	0.919	6.690	0.00129
2011	0.948	4.315	0.00145
2012	2.687	9.564	0.00135
2013	0.928	11.350	0.00130
2014	0.689	7.079	0.00138
c) Alaska			
2003	0.019	0.029	0.00074
2004	0.155	0.029	0.00090
2005	0.125	0.023	0.00088
2006	0.013	0.021	0.00076
2007	0.022	0.014	0.00088
2008	0.006	0.017	0.00081
2009	0.072	0.034	0.00094
2010	0.033	0.016	0.00089
2011	0.010	0.021	0.00093
2012	0.007	0.022	0.00081
2013	0.042	0.055	0.00087
2014	0.009	0.024	0.00090
d) Western Canada			
2003	0.116	3.206	0.00098
2004	0.269	4.861	0.00103
2005	0.106	2.003	0.00098
2006	0.082	3.006	0.00097
2007	0.125	3.251	0.00104
2008	0.084	2.963	0.00102
2009	0.041	2.589	0.00105
2010	0.067	1.923	0.00110
2011	0.182	2.505	0.00115
2012	0.343	3.942	0.00104
2013	0.202	3.340	0.00104
2014	0.580	3.568	0.00122